

See discussions, stats, and author profiles for this publication at: <https://www.researchgate.net/publication/361840404>

An Accurate Skin Lesion Classification Using Fused Pigmented Deep Feature Extraction Method

Chapter · July 2022

DOI: 10.1007/978-981-19-2057-8_3

CITATIONS
4

READS
638

5 authors, including:



Rabia Javed
Universiti Teknologi Malaysia

16 PUBLICATIONS 398 CITATIONS

[SEE PROFILE](#)



Mohd Shafry Mohd Rahim
Universiti Teknologi Malaysia

188 PUBLICATIONS 2,877 CITATIONS

[SEE PROFILE](#)



Mazhar Javed Awan
University of Management and Technology (Pakistan)

59 PUBLICATIONS 2,065 CITATIONS

[SEE PROFILE](#)

Tanzila Saba
Amjad Rehman
Sudipta Roy *Editors*

Prognostic Models in Healthcare: AI and Statistical Approaches

Studies in Big Data

Volume 109

Series Editor

Janusz Kacprzyk, Polish Academy of Sciences, Warsaw, Poland

The series “Studies in Big Data” (SBD) publishes new developments and advances in the various areas of Big Data- quickly and with a high quality. The intent is to cover the theory, research, development, and applications of Big Data, as embedded in the fields of engineering, computer science, physics, economics and life sciences. The books of the series refer to the analysis and understanding of large, complex, and/or distributed data sets generated from recent digital sources coming from sensors or other physical instruments as well as simulations, crowd sourcing, social networks or other internet transactions, such as emails or video click streams and other. The series contains monographs, lecture notes and edited volumes in Big Data spanning the areas of computational intelligence including neural networks, evolutionary computation, soft computing, fuzzy systems, as well as artificial intelligence, data mining, modern statistics and Operations research, as well as self-organizing systems. Of particular value to both the contributors and the readership are the short publication timeframe and the world-wide distribution, which enable both wide and rapid dissemination of research output.

The books of this series are reviewed in a single blind peer review process.

Indexed by SCOPUS, EI Compendex, SCIMAGO and zbMATH.

All books published in the series are submitted for consideration in Web of Science.

Tanzila Saba · Amjad Rehman · Sudipta Roy
Editors

Prognostic Models in Healthcare: AI and Statistical Approaches



Springer

Editors

Tanzila Saba
Artificial Intelligence and Data Analytics
Lab
College of Computer and Information
Sciences
Prince Sultan University
Riyadh, Saudi Arabia

Amjad Rehman
Artificial Intelligence and Data Analytics
Lab
College of Computer and Information
Sciences
Prince Sultan University
Riyadh, Saudi Arabia

Sudipta Roy
Artificial Intelligence and Data Science
Jio Institute
Ulwe, Navi Mumbai, India

ISSN 2197-6503
Studies in Big Data
ISBN 978-981-19-2056-1
<https://doi.org/10.1007/978-981-19-2057-8>

ISSN 2197-6511 (electronic)
ISBN 978-981-19-2057-8 (eBook)

© The Editor(s) (if applicable) and The Author(s), under exclusive license to Springer Nature Singapore Pte Ltd. 2022

This work is subject to copyright. All rights are solely and exclusively licensed by the Publisher, whether the whole or part of the material is concerned, specifically the rights of translation, reprinting, reuse of illustrations, recitation, broadcasting, reproduction on microfilms or in any other physical way, and transmission or information storage and retrieval, electronic adaptation, computer software, or by similar or dissimilar methodology now known or hereafter developed.

The use of general descriptive names, registered names, trademarks, service marks, etc. in this publication does not imply, even in the absence of a specific statement, that such names are exempt from the relevant protective laws and regulations and therefore free for general use.

The publisher, the authors and the editors are safe to assume that the advice and information in this book are believed to be true and accurate at the date of publication. Neither the publisher nor the authors or the editors give a warranty, expressed or implied, with respect to the material contained herein or for any errors or omissions that may have been made. The publisher remains neutral with regard to jurisdictional claims in published maps and institutional affiliations.

This Springer imprint is published by the registered company Springer Nature Singapore Pte Ltd.
The registered company address is: 152 Beach Road, #21-01/04 Gateway East, Singapore 189721,
Singapore

Preface

Medical imaging issues are so complex owing to high importance of correct diagnosis and treatment of diseases in healthcare systems. Recent research efforts have been devoted to processing and analyzing medical images to extract meaningful information such as volume, shape, motion of organs, to detect abnormalities, and to quantify changes in follow-up studies. Medical image analysis is diverse, and the large amount of information introduced through the hybrid systems requires next generation of image quantification that need to be addressed. This book addresses the issues and describes current advanced method in interactive medical image analysis.

The book is organized in 18 chapters.

The chapter “[Segmentation of White Blood Cells in Acute Myeloid Leukemia Microscopic Images: A Review](#)” presents state-of-the-art computer-aided diagnosis (CAD) systems as an accurate diagnostic tool for AML and assist pathologists during the diagnosis process. Segmentation of WBC is the first step toward developing an accurate CAD system for AML. To date, WBC segmentation has several challenges due to several reasons such as different staining conditions, complex nature of microscopic blood images, and morphological diversity of WBCs. Current WBC segmentation techniques vary from conventional image processing methods to advanced machine learning and deep learning methods. This chapter discusses current segmentation methods as well as the potential solutions for improving automated WBC segmentation accuracy.

The chapter “[Computer Vision-Based Prognostic Modelling of COVID-19 from Medical Imaging](#)” examines prognostic models for COVID-19 patients’ survival prediction based on clinical data and lung/lesion radiometric characteristics retrieved from chest imaging. While it seems that there are various early indicators of prognosis, we will discuss prognostic models or scoring systems that are useful exclusively to individuals who have received confirmation of their cancer diagnosis. A summary of some of the research work and strategies based on machine learning and computer vision that have been applied for the identification of COVID-19 have been presented in this chapter. Some strategies based on preprocessing, segmentation, handmade features, deep features, and classification have been discussed, as well as some other techniques.

The chapter “[An Accurate Skin Lesion Classification Using Fused Pigmented Deep Feature Extraction Method](#)” handles challenge for skin lesion classification for low contrast and over-segmented images. According to the literature surveyed, available hand-crafted features could not generate better results when the skin lesion images contain low contrast, under and over-segmented images. The hand-crafted features for skin lesions did not discriminate well between the two significantly different densities. The pigmented network feature vector and deep feature vector have been fused using a parallel fusion method to increase classification accuracy. This optimized fused feature vector has been fed to machine learning classifiers that accurately classify the dermoscopic images into two categories as benign and malignant melanoma. The statistical performance measures were used to assess the proposed fused feature vector on three skin lesion datasets (ISBI 2016, ISIC 2017, and PH2). The proposed fused feature vector accurately classified the skin lesion with the highest accuracy of 99.8% for the ISBI 2016, an accuracy of 99.3% for the ISIC 2017 dataset, 98.6% for the PH2 dataset.

The chapter “[COVID-19 Prediction, Diagnosis and Prevention Through Computer Vision](#)” presents various computer vision (CV) technologies along with other artificial intelligence (AI) subsets have significant potential to fight in frontline of this turbulent war. Normally radiologists and other clinicians are using reverse transcript polymerase chain reaction (RT-PCR) for diagnosing COVID-19, which requires strict examination environment and a set of resources. Further, this method is also prone to false-negative errors. One of the potential solutions for effective and fast screening of doubtful cases is the intervention of computer vision-based support decision systems in healthcare. CT-scans, X-rays, and ultra-sound images are being widely used for detection, segmentation, and classification of COVID-19. Computer vision is using these modalities and is providing the fast, optimal diagnosis at the early stage controlling mortality rate. Computer vision-based surveillance technologies are also being used for monitoring physical distance, detecting people with or without face masks, screening infected persons, measuring their temperature, tracing body movements, and detecting hand washing. In addition to these, it is also assisting in production of vaccine and contributing in administrative tasks and clinical management. This chapter presents an extensive study of some computer vision-based technologies for detection, diagnosis, prediction, and prevention of COVID. Our main goal here is to draw a bigger picture and provide the role of computer vision in fight against COVID-19 pandemic.

The chapter “[Health Monitoring Methods in Heart Diseases Based on Data Mining Approach: A Directional Review](#)” explores data mining techniques for identifying and diagnosing diseases, categorizing patients in disease management, and finding patterns to diagnose patients more quickly and prevent complications. Increasing the accuracy of diagnosis, reducing costs, and reducing human resources in the medical sector have been proven by researchers as the benefits of introducing data mining in medical analysis. Heart disease is evaluated to make the study more comprehensive, including fetal health diagnosis, arrhythmias, and machine learning data mining angiography. Attempts are made to introduce the relevant database in each disease and to evaluate the desired methods in health monitoring.

The chapter “[Machine Learning-Based Brain Diseases Diagnosing in Electroencephalogram Signals, Alzheimer’s, and Parkinson’s](#)” emphasizes that brain monitoring tools are used to detect these diseases early. An inexpensive and useful tool, as well as low-risk brain signals, are electroencephalograms. In order to analyze brain signals, the use of machine learning-based methods has been able to show its superiority. In order to diagnose Alzheimer’s and Parkinson’s in machine learning, there are preprocessing steps, feature extraction, feature selection, classification, and evaluation. Since electroencephalogram data have high repetition and correlation in different channels recorded on the head, feature extraction techniques will be of great importance. Feature selection methods seek to select the most effective features to classify and identify disease status. Finally, the selected features will be categorized using different categories. In this chapter, a complete overview of the stages of diagnosis of these diseases with the help of machine learning will be provided.

The chapter “[Skin Lesion Detection Using Recent Machine Learning Approaches](#)” states skin cancer is the highest popular form of cancer. Sunlight, ultraviolet rays, moles, and many other reasons cause skin cancer. Skin cancer can be treated if it is diagnosed at the premature stage. Manually diagnosing skin cancer is a time-consuming procedure, requiring a lot of human power while it is a grueling procedure. Various approaches for automatically detecting skin cancer have now been developed in recent years as technology has improved. In this chapter, skin lesion detection steps like preprocessing (to remove noise from images), segmentation (to get skin lesion location), feature extraction, feature selection, and classification methods have been discussed in detail. Furthermore, limitation and gaps in the domain of skin lesions are also discussed that provide help for the researchers.

The chapter “[Improving Monitoring and Controlling Parameters for Alzheimer’s Patients Based on IoMT](#)” states that currently the Internet has become an integral part of people’s lives. With the spread of the Internet, and the diversity of Internet applications, a new type of Internet use called the Internet of Things (IoT) has emerged. In the Internet of Things, information is collected, managed, and communicated in the daily life of man through the Internet. In this chapter, an improved method, low power and lossy network, is proposed to control and monitor the Alzheimer’s patient in the cloud robot on the Internet of Things in smart homes. In the proposed method with load balancing in the routing protocol in LLN networks based on RPL is presented. The proposed method improves the structure of the pair-to-pair (P2P) path. Data packets are sent as RPL sorted and irregular. Paths sent in P2P mode have been improved to reduce computational overhead and balance load on the network. Elimination of control messages and load balancing in routing are among the advantages of the proposed method.

The chapter “[A Novel Method for Lung Segmentation of Chest with Convolutional Neural Network](#)” states that medical images have made a high impact on medicine, diagnosis, and treatment. The most important part of image processing is image segmentation. This chapter presents a novel X-ray of lungs segmentation method using the U-Net model. First, we construct the U-Net which combine the lungs and mask. Then, we convert to problem of positive and negative TB lungs into the segmentation of lungs and extract the lungs by subtracting the chest from

the radiography. In experiment, the proposed model achieves 97.62% on the public dataset of collection by Shenzhen Hospital, China, and Montgomery County X-ray Set.

The chapter “[Leukemia Detection Using Machine and Deep Learning Through Microscopic Images—A Review](#)” presents that there are numerous studies for the detection of acute leukemia, but there are only a few studies to detect chronic leukemia. Additionally, microscopic-based methods can be used to analyze microscopic smear images and detect the incidence of leukemia automatically and quickly. It also discusses the benefits, drawbacks, and limitations of a variety of traditional artificial intelligence-based approaches for detecting leukemia, such as machine learning and deep learning. Hence, this chapter aims to review the existing literature in the field of medical image processing of blood smear images, with a focus on automated leukemia detection. The analysis of various studies shows that deep learning techniques provide the best results compared to machine learning techniques. Hence, the major drawback in recent studies is that most of the research has been done on locally available datasets.

The chapter “[A Review on Machine Learning-Based WBCs Analysis in Blood Smear Images: Key Challenges, Datasets, and Future Directions](#)” presents that manual detection, counting, and classification of WBCs are very slow, challenging, and boring task due to complex overlapping and morphological uneven structure. In this chapter, we provide a concise analysis of available ML techniques to use these techniques for leucocytes analysis in microscopic images. The main aim of this chapter is to identify high-performance and suitable ML algorithms for WBCs analysis using blood microscopic smear images. In the proposed review study, the recent and most relevant research papers are collected from IEEE, Science Direct, Springer, and Web of Science (WoS) with the following keywords: “leucocytes detection” or “leucocytes classification.” This study gives an extensive review of MIA, but the research focuses more on the ML-based leucocytes/WBCs analysis in smear images. These techniques include traditional machine learning (TML), deep learning (DL), convolutional neural network (CNN) models, hybrid learning, and attention learning-based techniques to analyze medical image modalities to detect and classify cells in smear images.

The chapter “[Automatic Detection of Liver Cancer Using Artificial Intelligence and Imaging Techniques—A Review](#)” is a systematic review that evaluates several types of researches and advanced technologies that can help to diagnose liver cancer automatically. Through this review of 26 relevant articles, the following syntheses of liver cancer detection techniques have been produced: a) the use of machine learning (ML) and deep learning (DL) methods and b) the use of classical imaging technologies. Finally, it is found that the latest deep learning (DL) classifiers are capable of detecting liver cancer accurately, fastly, and reliably. However, a major problem with existing relevant articles is that there is a lack of publicly available datasets for the detection of liver cancer and the drawback of these datasets is that almost all have few images. Hence, further research should be performed on large publicly available datasets to improve the complexity of computation for reliable

diagnosis of liver cancer. As a result, it serves mankind much better in efficiency and cost-effectiveness.

The chapter “[Spot Filtering Adaptive Thresholding \(SFAT\) Method for Early Pigment Spot Detection on Iris Surface](#)” states that iris pigment spot is a discrete pigmentation on the iris surface and can detect eye cancer. There are two types of iris spots, freckles and nevi. While freckles are usually harmless, nevi distort the stromal layer, and therefore, its existence is considered high potential for Uveal Melanoma, a type of cancer that can cause blindness. The features used to detect the Uveal Melanoma are size, shape, number of existences, spot of existence, and the color of the pigment spot on the iris surface. In image processing, feature extraction method typically extracts size, shape, and color. However, it is still challenging to produce an accurate extraction result for iris pigment spot. In this study, a threshold intensity value of color is identified as the pigment spot feature used in the feature extraction process.

The chapter “[A Big Survey on Biometrics for Human Identification](#)” emphases that biometric authentication systems developed in recent years are better than other traditional authentication methods such as passwords or signatures. All human biological traits are unique as biometrics such as fingerprints, palms, irises, palm blood vessels and fingerprint blood vessels, and other biometrics. Biometric identification systems basically have a complex structure that consists of different parts. Biometric-based authentication systems and authentication methods, along with other authentication systems, can improve the security aspects of authentication systems. Identification methods and tools are used in many important and essential applications such as surveillance processes, security investigations, fraud detection technologies, and access controls. Biometric-based identification methods in machine learning consist mainly of preprocessing, feature extraction, feature selection, classification, and finally evaluation. These systems can also be based on one biometric or based on several biometrics together.

The chapter “[Computer-Aided Diagnosis of Pneumothorax Through X-Ray Images Using Deep Learning—A Review](#)” emphases on automated diagnosis of pneumothorax in health surveillance is difficult for radiologists. Early detection of a pneumothorax is crucial for improving treatment outcomes and patient survival. In the medical field, the identification of pneumothorax through image processing is a tricky task. Recently, a rise of interest has been noticed in employing deep learning algorithms to aid pneumothorax detection. Nowadays, different medical Imaging tools are available to detect specific diseases. Chest radiographs are widely used to diagnose pneumothorax. Detection of pneumothorax at early stages can overcome the treatment difficulties. This chapter evaluates several innovative technologies and research that could help detect pneumothorax automatically. Artificial intelligence (AI) provides a significant result for automated pneumothorax (PTX) detection. Research has been done to see pneumothorax disease automatically through the chest radiograph. This article abstracts previous articles for detecting PTX from CXRs through machine and deep learning and also discusses different publicly available datasets. This study provides a detailed overview and discusses the existing literature’s goodness and limitation.

In chapter “[ML and DL Architectures Comparisons for the Classification of COVID-19 Using Chest X-ray Images](#),” automated and AI-based prediction models for COVID- 19 are the main attraction for the scientist hoping to support some good medical decisions at this difficult time. However, mostly classical image processing methods have been implemented to detect COVID cases resultant in low accuracy. In this chapter, multiple naïve machine and deep learning architectures are implied to evaluate the performance of the models for the classification of COVID-19 using a dataset comprising of chest X-ray images of, i.e., COVID-19 patients and normal (non-infected) individuals. The analysis looks at three machine learning architectures including logistic regression, decision tree (DT) classifier, and support vector machine (SVM), and four deep learning architectures, namely convolutional neural networks (CNNs), VGG19, ResNet50, and AlexNet. The dataset has been divided into train, test, and validation set, and the same data have been used for the training, testing, and validation of all the architectures. The result analysis shows that AlexNet provides the best performance out of all the architectures. It can be seen that the AlexNet model achieved 98.05% accuracy (ACC), 97.40% recall, 98.03% F1 score, 98.68% precision, and 98.05% area under the curve (AUC) score.

The chapter “[Data Mining in Medical Laboratory Service Improves Disease Surveillance and Quality Healthcare](#)” examines origin, basic principles, advantages and disadvantages, uses and challenges of data mining in relation to Medical Laboratory Information Management System (MLIMS) while looking at data management from hard to soft copies, possible applications, ethico-legal perspectives, implications of data mining, disease surveillance, and data mining toward quality improvement as used in medical laboratories. It is evident that most of decisions taken in health care and public health are based on information provided by data mining from medical laboratory services based on the diseases of interest. Data mining in medical laboratory services is a tool that aids in monitoring trends in the diagnosis of cancer, HIV, COVID-19, malaria, diabetes, and other diseases based on various parameters of assessment with all demographic variables well documented and analyzed. The interested Agencies or Ministries may apply data mining techniques based on medical laboratory results to find trends in disease outbreaks or deaths, per hospital, state, region, or country through which policies could be formulated and implemented toward surveillance and quality healthcare improvement.

The chapter “[Deep Learning-Based Lung Infection Detection Using Radiology Modalities and Comparisons on Benchmark Datasets in COVID-19 Pandemic](#)” presents deep learning techniques for microscopic COVID-19 infection diagnosis, prevention and treatment on public datasets. Additionally, a general CAD architecture for COVID-19 detection is presented and each stage is discussed in detail. Based on radiology images analysis, several lungs treatment strategies for COVID-19 infected patients are suggested. Finally, evidence-based methodologies and modalities were explored in the analysis and findings, leading to a conclusion and possible future healthcare planning.

The editors are very thankful to all the members of Springer (India) Private Limited, especially Aninda Bose, for the given opportunity to edit this book.

Riyadh, Saudi Arabia
Riyadh, Saudi Arabia
Navi Mumbai, India

Dr. Tanzila Saba
Dr. Amjad Rehman
Dr. Sudipta Roy

Contents

Segmentation of White Blood Cells in Acute Myeloid Leukemia Microscopic Images: A Review	1
Tusneem A. Elhassan, Mohd Shafry Mohd Rahim, Tan Tian Swee, Siti Z. Mohd Hashim, and Mahmoud Aljurf	
Computer Vision-Based Prognostic Modelling of COVID-19 from Medical Imaging	25
Abdul Muiz Fayyaz, Mahyar Kolivand, Jaber Alyami, Sudipta Roy, and Amjad Rehman	
An Accurate Skin Lesion Classification Using Fused Pigmented Deep Feature Extraction Method	47
Rabia Javed, Mohd Shafry Mohd Rahim, Tanzila Saba, Gul Sahar, and Mazhar Javed Awan	
COVID-19 Prediction, Diagnosis and Prevention Through Computer Vision	79
Sajid Iqbal, Hareem Ayesha, Muhammad Farooq Khan Niazi, Noor Ayesha, and Khawaja Tehseen Ahmad	
Health Monitoring Methods in Heart Diseases Based on Data Mining Approach: A Directional Review	115
Majid Harouni, Mohsen Karimi, Afroz Nasr, Helia Mahmoudi, and Zakieh Arab Najafabadi	
Machine Learning-Based Brain Diseases Diagnosing in Electroencephalogram Signals, Alzheimer's, and Parkinson's	161
Nakisa Tavakoli, Zahra Karimi, Somayeh AsadiJouzani, Nastaran Azizi, Sara Rezakhani, and Atefeh Tobeiha	
Skin Lesion Detection Using Recent Machine Learning Approaches	193
Ihtishaam ul haq, Javeria Amin, Muhammad Sharif, and Muhammad Almas Anjum	

Improving Monitoring and Controlling Parameters for Alzheimer's Patients Based on IoMT	213
Mohsen Karimi, Majid Harouni, Elaheh Izadi Jazi, Afroz Nasr, and Nastaran Azizi	
A Novel Method for Lung Segmentation of Chest with Convolutional Neural Network	239
Muhammad Awais Malik, Mazhar Javed Awan, Muhammad Rehan Saleem, Amjad Rehman, and Jaber Alyami	
Leukemia Detection Using Machine and Deep Learning Through Microscopic Images—A Review	261
Qurat Ul Ain, Shahzad Akbar, Sahar Gull, Muzammil Hussain, and Noor Ayesha	
A Review on Machine Learning-Based WBCs Analysis in Blood Smear Images: Key Challenges, Datasets, and Future Directions	293
Siraj Khan, Muhammad Sajjad, Naveed Abbas, and Amjad Rehman	
Automatic Detection of Liver Cancer Using Artificial Intelligence and Imaging Techniques—A Review	315
Zunaira Naqvi, Shahzad Akbar, Syed Ale Hassan, Aima Khalid, and Muhammad Jawad Bashir	
Spot Filtering Adaptive Thresholding (SFAT) Method for Early Pigment Spot Detection on Iris Surface	347
Mohamad Faizal Ab Jabal, Suhardi Hamid, Nur Zuraifah Syazrah Othman, and Mohd Shafry Mohd Rahim	
A Big Survey on Biometrics for Human Identification	371
Zahra Karimi, Somayeh Arab Najafabadi, Aliakbar Rabbani Nezhad, and Farnaz Ahmadi	
Computer-Aided Diagnosis of Pneumothorax Through X-Ray Images Using Deep Learning—A Review	403
Farwa Urooj, Shahzad Akbar, Syed Ale Hassan, Saba Firdous, and Muhammad Jawad Bashir	
ML and DL Architectures Comparisons for the Classification of COVID-19 Using Chest X-Ray Images	433
Erum Afzal, Tanzila Saba, Haris Ali, Adnan Karim, and Kashif Javed	
Data Mining in Medical Laboratory Service Improves Disease Surveillance and Quality Healthcare	459
Uchejeso Mark Obeta, Obiora Reginald Ejinaka, and Nkereuwem Sunday Etukudoh	

Deep Learning-Based Lung Infection Detection Using Radiology Modalities and Comparisons on Benchmark Datasets in COVID-19 Pandemic	483
Jaber Alyami	

Editors and Contributors

About the Editors

Prof. Tanzila Saba earned her Ph.D. in document information security and management from the Faculty of Computing, Universiti Teknologi Malaysia (UTM), Malaysia, in 2012. She won the best student award in the Faculty of Computing UTM for 2012. Currently, she serves as Research Professor and Associate Chair of the Information Systems Department in the College of Computer and Information Sciences, Prince Sultan University, Riyadh, KSA. Her primary research focus in recent years is medical imaging, pattern recognition, data mining, MRI analysis, and soft computing. She led more than 15 research-funded projects. She has above two hundred research publications that have around 10,000 plus citations with h-index 63. Her most publications are in biomedical research published in ISI/SCIE indexed. Due to her excellent research achievement, she is included in Marquis Who's Who (S & T) 2012. She is Editor and Reviewer of reputed journals and on the panel of TPC of international conferences. She has full command of various subjects and taught several courses at the graduate and postgraduate levels. On the accreditation side, she is a skilled lady with ABET & NCAAA quality assurance. She is Senior Member of IEEE. Dr. Tanzila is Leader of Artificial Intelligence & Data Analytics Research Lab at PSU and Active Professional Member of ACM, AIS, and IAENG organizations. She is PSU WiDS (Women in Data Science) Ambassador at Stanford University.

Dr. Amjad Rehman is Senior Researcher in the Artificial Intelligence & Data Analytics Lab CCIS, Prince Sultan University, Riyadh, Saudi Arabia. He received his Ph.D. & postdoc from Faculty of Computing Universiti Teknologi Malaysia with a specialization in Forensic Documents Analysis and Security with honor in 2010 and 2011, respectively. He received rector award for 2010 best student in the university. Currently, he is PI in several funded projects and also completed projects funded from MOHE, Malaysia, and Saudi Arabia. His keen interests are in data mining, health

informatics, and pattern recognition. He is Author of more than 200 ISI journal papers and conferences and is Senior Member of IEEE.

Dr. Sudipta Roy is working as Assistant Professor in Artificial Intelligence & Data Science department at JIO institute, Navi Mumbai. Prior to that, he was Postdoctoral Research Associate at Washington University in St. Louis, MO, USA. He has received his Ph.D. in Computer Science & Engineering from the Department of Computer Science and Engineering, University of Calcutta. He is Author of more than 50 publications in refereed international journals and conferences including IEEE, Springer, Elsevier, and many others. He has authored/edited four books and many chapters. He holds a US patent in medical image processing and filed an Indian patent in the smart agricultural system. He has served as Regular Reviewer of many international journals including IEEE, Springer, Elsevier, IET, and many others, and international conferences. He has served as International Advisory Committee Member and Program Committee Member of INDIACom-2020, AICAE-2019, INDIACom-2019, CAAI 2018, ICAITA-2018, ICSESS-2018, INDIACom-2018, ISICO-2017, AICE-2017, and many more conferences. Currently, he is serving as Associate Editor of *IEEE Access* (IEEE), *International Journal of Computer Vision and Image Processing* (IJCVIP-IGI Global), and *Topic Editor of Journal of Imaging* (MDPI). In recognition of his exceptional contributions to the IEEE access journal as Associate Editor, the IEEE Access Editorial Board and Editorial Office honored him as Outstanding Associate Editor of 2020. He has more than five years of experience in teaching and research. His fields of research interests are biomedical image analysis, image processing, steganography, artificial intelligence, big data analysis, machine learning, and big data technologies.

Contributors

Ab Jabal Mohamad Faizal Fakulti Sains Komputer dan Matematik, Universiti Teknologi MARA, Cawangan Johor Kampus Pasir Gudang, Masai, Johor, Malaysia

Abbas Naveed Digital Image Processing Lab, Department of Computer Science, Islamia College University Peshawar KPK, Peshawar, Pakistan

Afzal Erum National University of Sciences and Technology, Islamabad, Pakistan

Ahmadi Farnaz Department of Electrical Engineering, Tabriz University, Azerbaijan, Iran

Akbar Shahzad Riphah College of Computing, Riphah International University, Faisalabad Campus, Faisalabad, Pakistan

Ali Haris National University of Sciences and Technology, Islamabad, Pakistan

Aljurf Mahmoud King Faisal Specialist Hospital and Research Center, Riyadh, Saudi Arabia

Almas Anjum Muhammad National University of Technology (NEUTCH), Islamabad, Pakistan

Alyami Jaber Department of Diagnostic Radiology, Faculty of Applied Medical Sciences, King Abdulaziz University, Jeddah, Saudi Arabia;
Imaging Unit, King Fahd Medical Research Center, King Abdulaziz University, Jeddah, Saudi Arabia;
Smart Medical Imaging Research Group, King Abdulaziz University, Jeddah, Saudi Arabia

Amin Javeria Department of Computer Science, University of Wah, Wah Cantt, Pakistan

Arab Najafabadi Zakieh Department of Engineering, South of Tehran Branch, Islamic Azad University, Tehran, Iran

AsadiJouzani Somayeh School of Electrical and Computer Engineering, University of Tehran, Tehran, Iran

Awan Mazhar Javed Department of Software Engineering, School of System and Technology, Lahore, Pakistan;
Department of Computer Sciences, Karakoram International University, Gilgit-Baltistan, Pakistan

Ayesha Hareem Department of Computer Science, Bahauddin Zakariya University, Multan, Pakistan

Ayesha Noor School of Clinical Medicine, Zhengzhou University, Zhengzhou, Henan, PR China

Azizi Nastaran Sepahan Institute of Higher Education, Science and Technology, Isfahan, Iran

Bashir Muhammad Jawad School of Electrical Engineering and Computer Science, National University of Science and Technology (NUST), Islamabad, Pakistan

Ejinaka Obiora Reginald Department of Medical Laboratory Management, Federal School of Medical Laboratory Science, Jos, Nigeria

Elhassan Tusneem A. School of Computing, Faculty of Engineering, Universiti Teknologi Malaysia, Johor Bahru, Malaysia

Etukudoh Nkereuwem Sunday Department of Medical Laboratory Management, Federal School of Medical Laboratory Science, Jos, Nigeria

Farooq Khan Niazi Muhammad Consultant Radiologist, Diagnostic Imaging Department King Salman North West Armed Forces Hospital (NWAFH), Tabuk, Saudi Arabia

Firdous Saba Riphah College of Computing, Riphah International University, Faisalabad Campus, Faisalabad, Pakistan

Gull Sahar Riphah College of Computing, Riphah International University, Faisalabad Campus, Faisalabad, Pakistan

Hamid Suhardi Fakulti Sains Komputer dan Matematik, Universiti Teknologi MARA, Cawangan Kedah, Merbok, Kedah, Malaysia

Harouni Majid Department of Computer Engineering, Doalatabad Branch, Islamic Azad University, Isfahan, Iran

Hashim Siti Z. Mohd Department of Data Science, Universiti Malaysia Kelantan, Kota Bharu, Malaysia

Hassan Syed Ale Riphah College of Computing, Riphah International University, Faisalabad Campus, Faisalabad, Pakistan

Hussain Muzammil School of Systems and Technology, University of Management and Technology, Lahore, Pakistan

Iqbal Sajid Department of Computer Science, Bahauddin Zakariya University, Multan, Pakistan

Javed Kashif National University of Sciences and Technology, Islamabad, Pakistan

Javed Rabia School of Computing, Faculty of Engineering, Universiti Teknologi Malaysia, Skudai, Johor Bahru, CO, Malaysia;

Department of Computer Science, Lahore College for Women University, Lahore, CO, Pakistan

Jazi Elaheh Izadi Department of Computer Engineering, Ferdowsi University of Mashhad, Mashhad, Iran

Karim Adnan National University of Sciences and Technology, Islamabad, Pakistan

Karimi Mohsen Department of Bioelectronics and Biomedical Engineering, School of Advanced Technologies in Medicine, Isfahan University of Medical Sciences, Isfahan, Iran

Karimi Zahra Department of Bioelectronics and Biomedical Engineering, School of Advanced Technologies in Medicine, Isfahan University of Medical Sciences, Isfahan, Iran

Khalid Aima Riphah Collage of Computing, Riphah International University, Faisalabad, Pakistan

Khan Siraj Digital Image Processing Lab, Department of Computer Science, Islamia College University Peshawar KPK, Peshawar, Pakistan

Kolivand Mahyar Department of Medicine, University of Liverpool, Liverpool, UK;

School of Computing and Digital Technologies, Staffordshire University, Staffordshire, UK

Mahmoudi Helia MD, MPH Candidate in Family Medicine, Department of Community Medicine, Medical University of Isfahan, Isfahan, Iran

Malik Muhammad Awais Department of Software Engineering, School of System and Technology, Lahore, Pakistan

Muiz Fayyaz Abdul Department of Computer Science, University of Wah, Wah, Pakistan

Naaqvi Zunaira Riphah Collage of Computing, Riphah International University, Faisalabad, Pakistan

Najafabadi Somayeh Arab Department of Computer Engineering, Islamic Azad University, Najafabad Branch, Isfahan, Iran

Nasr Afroz Department of Computer Engineering, Isfahan (Khorasgan) Branch, Islamic Azad University, Isfahan, Iran

Nezhad Aliakbar Rabbani Department of Electrical Engineering, Isfahan University of Technology, Isfahan, Iran

Obeta Uchejeso Mark Department of Medical Laboratory Management, Federal School of Medical Laboratory Science, Jos, Nigeria

Othman Nur Zuraifah Syazrah School of Computing, Faculty of Engineering, University Technology Malaysia, Skudai, Johor, Malaysia

Qurat Ul Ain Riphah College of Computing, Riphah International University, Faisalabad Campus, Faisalabad, Pakistan

Rahim Mohd Shafry Mohd School of Computing, Faculty of Engineering, University Technology Malaysia, Skudai, Johor Bahru, Malaysia

Rehman Amjad Artificial Intelligence and Data Analytics Lab (AIDA), CCIS Prince Sultan University, Riyadh, Saudi Arabia

Rezakhani Sara Department of Electrical Engineering, Najaf Abad Branch, Islamic Azad University, Isfahan, Iran

Roy Sudipta Artificial Intelligence & Data Science, Jio Institute, Navi Mumbai, India

Saba Tanzila Artificial Intelligence and Data Analytics Lab CCIS, Prince Sultan University, Riyadh, Saudi Arabia;

College of Computing and Information Sciences, Prince Sultan University, Riyadh, CO, Saudi Arabia

Sahar Gul Department of Software Engineering, University of Management and Technology, Lahore, Pakistan

Sajjad Muhammad Digital Image Processing Lab, Department of Computer Science, Islamia College University Peshawar KPK, Peshawar, Pakistan

Saleem Muhammad Rehan Department of Computer Science, School of System and Technology, Lahore, Pakistan

Sharif Muhammad Department of Computer Science, COMSATS University Islamabad, Wah Campus, Pakistan

Swee Tan Tian Bioinspired Device and Tissue Engineering Research Group, Faculty of Engineering, School of Biomedical Engineering and Health Sciences, Universiti Teknologi Malaysia, Skudai, Johor, Malaysia

Tavakoli Nakisa Department of Computer Engineering, Farsan Branch, Islamic Azad University, Farsan, Iran

Tehseen Ahmad Khawaja Department of Computer Science, Bahauddin Zakariya University, Multan, Pakistan

Tobeiha Atefeh Department of Electrical Engineering, Najaf Abad Branch, Islamic Azad University, Isfahan, Iran

ul haq Intishaam Department of Computer Science, COMSATS University Islamabad, Wah Campus, Pakistan

Urooj Farwa Riphah College of Computing, Riphah International University, Faisalabad Campus, Faisalabad, Pakistan

Segmentation of White Blood Cells in Acute Myeloid Leukemia Microscopic Images: A Review



Tusneem A. Elhassan, Mohd Shafry Mohd Rahim, Tan Tian Swee,
Siti Z. Mohd Hashim, and Mahmoud Aljurf

Abstract Acute Myeloid Leukemia (AML) is a fast-growing leukemia caused by the rapid proliferation of immature myeloid cells. AML is a life-threatening disease if left untreated. Therefore, early detection of AML is crucial, maximizes the cure opportunities, and saves patients' lives. Initial AML diagnosis is done by expert pathologists where blood smear images are utilized to detect abnormalities in WBCs. However, manual detection of AML is subjective and prone to errors. On the contrary, computer-aided diagnosis (CAD) systems can be an accurate diagnostic tool for AML and assist pathologists during the diagnosis process. Segmentation of White Blood Cells is the first step toward developing an accurate CAD system for AML. To date, WBC segmentation has several challenges due to several reasons such as different staining conditions, complex nature of microscopic blood images, and morphological diversity of WBCs. Current WBC segmentation techniques vary from conventional image processing methods to advanced machine learning and deep learning methods. This chapter discusses current segmentation methods as well as the potential solutions for improving automated WBC segmentation accuracy.

T. A. Elhassan · M. S. M. Rahim (✉)

School of Computing, Faculty of Engineering, Universiti Teknologi Malaysia, Johor Bahru, Malaysia

e-mail: shafry@utm.my

T. A. Elhassan

e-mail: amtusneem@graduate.utm.my

T. T. Swee

Bioinspired Device and Tissue Engineering Research Group, Faculty of Engineering, School of Biomedical Engineering and Health Sciences, Universiti Teknologi Malaysia, 81300 Skudai, Johor, Malaysia

e-mail: tantswee@biomedical.utm.my

S. Z. M. Hashim

Department of Data Science, Universiti Malaysia Kelantan, Kota Bharu, Malaysia
e-mail: sitizaiton@umk.edu.my

M. Aljurf

King Faisal Specialist Hospital and Research Center, Riyadh, Saudi Arabia
e-mail: maljurf@kfshrc.edu.sa

Keywords While blood cells · Segmentation · Acute myeloid leukemia · Computer-aided diagnosis (CAD)

1 Introduction

Segmentation is the process of partitioning the image space into non-overlapping regions where each region can be characterized by unique features. White blood cell (WBC) segmentation is the process of dividing the blood image into two regions, namely WBCs and other blood components. WBC segmentation is a curtail step in the automatic diagnosis of leukemia. More precisely, it is a prerequisite step for other image processing tasks, including feature extraction, WBC classification, and WBC counting. Segmentation is further used for nucleus and cytoplasm segmentation which has an important role in situations where the nucleus: cytoplasm ratio is a key factor in diagnosis process [1]. To date, WBC segmentation has been performed manually by pathologists or using quantitative methods. However, advanced qualitative methods utilizing advance image processing and pattern recognition is not yet implemented [2]. This makes the process subject to human error and produces inaccurate results. The process is tedious, time-consuming, and subject to inter- and intra-class variation among pathologists. Only 76.6% of cases showed agreement between pathologists during the leukemia diagnosis [3]. Therefore, accurate segmentation techniques for WBCs and their regions using computer-aided systems are needed. These systems can implement advanced image processing and pattern recognition methods, such as deep learning, to extract complex features of WBC and its regions with minimal human intervention. Several methods have been proposed to detect and segment the WBCs and their nuclei and cytoplasm. Nevertheless, automated WBC segmentation is a difficult task and encompasses several challenges due to the noisy nature of microscopic images. Irregular boundaries and textural similarities between WBCs and other blood components are some of the challenges that make it difficult to differentiate between WBCs and other blood components [4–6]. Moreover, WBCs have a complex structure in term of shapes, textures, and colors [7–9]. Section 3 summarizes different segmentation methods implemented in WBC segmentation including its nucleus and cytoplasm.

This chapter is organized as follows: Section 2 presents an overview of AML; Section 3 discusses some of the challenges facing automated segmentation methods; Section 4 introduces the publicly available datasets on AML WBC segmentation; Section 5 describes the different types of automated WBC segmentation methods presented in the literature. Section 6 discusses WBC limitations and future solutions. Finally, the topic is summarized in Sect. 7.

2 Acute Myeloid Leukemia

2.1 An Overview

Leukemia is a blood cancer that originates from cells that normally develop into different types of blood cells. Usually, it develops from immature white blood cells called leukocytes, but some types of leukemia can develop from other blood cells. Leukemia can be divided into two types: acute and chronic. Acute leukemia is a fast-growing cancer that is fatal if left untreated, while chronic leukemia is a slow-growing cancer that patients can live with for a long time.

Acute leukemia can be divided into ALL, which originates from lymphocytes, and AML, which develops from myelocytes. In both cases, acute leukemia starts in the bone marrow, where leukemic cells (i.e., blasts) proliferate and replace normal blood cells. They can also spread to other organs in the body. Early detection of acute leukemia is crucial to ensure that appropriate treatment modalities are provided to save patients' lives [10].

2.2 AML Subtypes

AML has several subtypes, and it is important to classify them to understand patients' prognosis and the appropriate treatment modality (e.g., Acute Promyelocytic Leukemia (APL) is treated by a different type of drug than other subtypes). Classification is based on the level of cell maturation at the time of diagnosis. Two systems have been used for classification: the French–American–British (FAB) classification system and the World Health Organization (WHO) classification system.

FAB System

The FAB classification system was developed by seven hematologists who formed an international cooperative group. It is based on the morphological features of leukemic cells identified under a microscope after staining and the type of cells from which leukemia develops (Table 1).

Subtypes M0–M5 all start in immature forms of white blood cells. However, M6 starts in very immature forms of red blood cells, while M7 starts in immature forms of cells that make platelets.

WHO Classification

The WHO system considers various factors that can affect AML prognosis, mainly based on cytogenetics. The following are WHO AML classes based on genetics abnormalities [11, 12]:

- AML with a translocation between chromosomes 8 and 21 [$t(8;21)$].
- AML with a translocation or inversion in chromosome 16 [$t(16;16)$ or $inv(16)$].

Table 1 AML FAB classification system

FAB subtype	Name
M0	Undifferentiated acute myeloblastic leukemia
M1	Acute myeloblastic leukemia with minimal maturation
M2	Acute myeloblastic leukemia with maturation
M3	Acute promyelocytic leukemia
M4	Acute myelomonocytic leukemia
M4 eos	Acute myelomonocytic leukemia with eosinophilia
M5	Acute monocytic leukemia
M6	Acute erythroid leukemia
M7	Acute megakaryoblastic leukemia

- APL with the PML-RARA fusion gene.
- AML with a translocation between chromosomes 9 and 11 [t (9;11)].
- AML with a translocation between chromosomes 6 and 9 [t (6;9)].
- AML with a translocation or inversion in chromosome 3 [t (3;3) or inv (3)].
- AML (megakaryoblast) with translocation between chromosomes 1 and 22 [t (1;22)].
- AML with the BCR-ABL1 (BCR-ABL) fusion gene.
- AML with mutated NPM1 gene.
- AML with biallelic mutations of the CEBPA gene (that is, mutations in both copies of the gene).
- AML with a mutated RUNX1 gene.

2.3 Diagnosis of AML

Leukemia diagnosis starts by looking at abnormal white cells, red cells, and platelets counts in a blood sample using a CBC test. If there is evidence of abnormal cells in blood samples, a blood smear is furtherly examined to determine the percentage of blast cells. However, a percentage of more than 20% is considered as evidence of leukemia. Differentiation-based classification methods involving flow cytometry are used to determine the subtype of myeloid leukemia where different patterns of antigen acquisition exist (Fig. 1).

2.4 Morphology of Acute Leukemia

Morphological differences of WBC in acute leukemia are based on two factors: the cell line and the level of cell differentiation (i.e., maturation) [13].

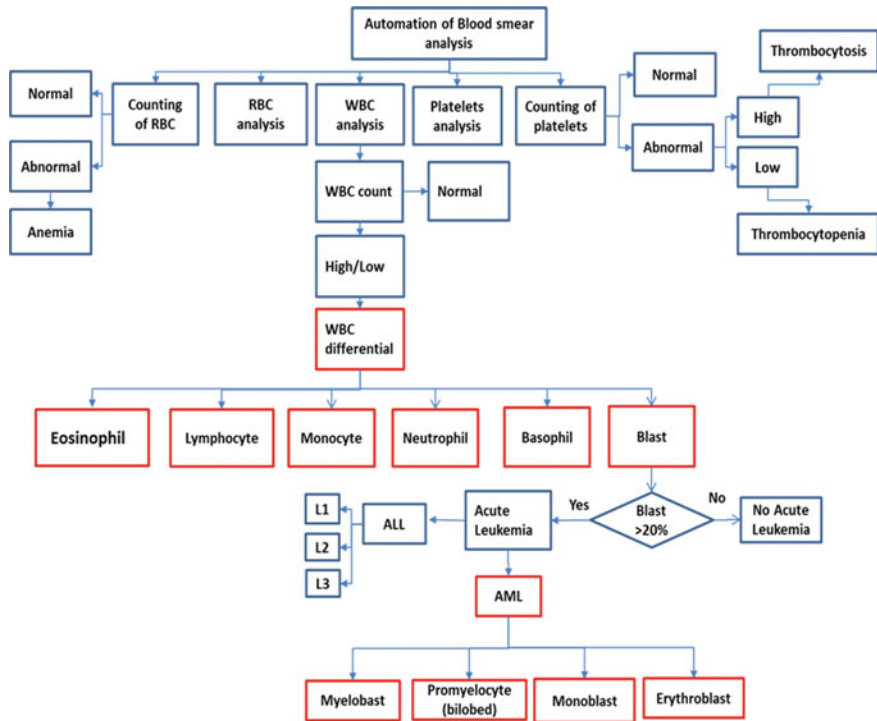


Fig. 1 Diagnosis of AML based on blood smear analysis

Based on FAB system, acute leukemia is classified into myeloid (AML) and lymphoblastic (ALL) which can only be utilized for untreated patients. This is because treatments such as chemotherapy can change the nature of normal and leukemic cells [14]. ALL is classified into three different subtypes (L1, L2, and L3), while AML is divided into eight subtypes (M0, M1, M2, M3, M4, M5, M6, and M7).

Types of WBCs Presented in AML

There are several types of cells in AML blood smears. These cells are divided into immature and mature cells:

Mature Cells

- **Lymphocyte:** These are rounded cells, containing a single, large round nucleus and a clear cytoplasm. It is classified into two types: *B* and *T* cells.
- **Neutrophil:** This type of cells has an irregularly shaped nucleus that contains multiple lobes and dotted granular cytoplasm. Neutrophil can be further classified into two types:

- (a) Neutrophil (banded): The banded neuropil cell is derived from metamyelocytes. It called “banded” because all the nuclear sections of the nucleus are the same width (band).
- (b) Neutrophil (segmented): segmented neutrophils represent the final stage in the lineage that starts with myeloblasts, forming gradually, without any clear transition or further cell divisions, by increasing the contraction of their nuclei. The nuclear segments are connected only by narrow chromatin bridges, which should be no thicker than one-third of the average diameter of the nucleus. The chromatin in each segment forms coarse bands or patches and is denser than the chromatin in band neutrophils. The cytoplasm of segmented neutrophilic granulocytes varies after staining from nearly colorless to soft pink or violet. The abundant granules are often barely visible dots.

Immature Cells

Blasts

- Erythroblasts: Nucleated cells derived from red marrow or red blood cells.
- Monoblasts: Progenitor cells that are differentiated from myeloid stem cell. They are presented in bone marrow rather than in normal peripheral blood. Later, they mature into monocytes.
- Promyelocytes (bilobed): these cells are characterized by the presence of bilobed nuclei that have been likened to butterfly wings. Usually, the cells present abundant cytoplasmic granules; numerous Auer rods and some ermed faggot cells. However, some cases do not have obvious cytoplasmic granules, may have basophilic cytoplasm, and have folded bilobed nuclei that may be mistaken for monocytes.
- Myeloblasts: Myeloblasts are the least mature cells in the granulocyte lineage. Mononuclear, round-to-ovoid cells may be distinguished from proerythroblasts by the finer, “grainy” reticular structure of their nuclei and the faintly basophilic cytoplasm. On first impression, they may look like large or even small lymphocytes (micro myeloblasts), but the delicate structure of their nuclei always distinguishes from micro myeloblasts. The cytoplasm contains azurophilic granules.

Non-blasts

- Promyelocytes: Promyelocytes are the product of myeloblast division and usually grow larger than their progenitor cells. During maturation, their nuclei show an increasingly coarse chromatin structure. The nucleus is eccentric; the lighter zone over its bay-like indentation corresponds to the Golgi apparatus. The wide layer of basophilic cytoplasm contains copious large azurophilic granules containing peroxidases, hydrolases, and other enzymes. These granulations also exist scattered all around the nucleus, as may be seen by focusing on different planes of the preparation using the micrometer adjustment on the microscope.

Non-blasts (Semi-mature Cells)

- Metamyelocytes: Metamyelocytes (young granulocytes) are derived from the final myelocyte. They show further maturation of the nucleus with an increasing number of stripes and points of density that give the nuclei a spotted appearance. The nuclei slowly take on a kidney bean shape and have some plasticity.
- Myelocytes: Myelocytes are the direct product of promyelocyte mitosis and are always clearly smaller than their progenitors. They are characterized with an ovoid nucleus with a banded structure; the cytoplasm is becoming lighter with maturation and sometimes acquiring a pink tinge. A special type of granules, which no longer stain red like the granules in promyelocytes (“specific granules,” peroxidase-negative), are evenly distributed in the cytoplasm. Myelocyte morphology is wide-ranging because myelocytes cover three different varieties of dividing cells [15].

AML blood smear samples include normal and abnormal WBCs. Figure 2 illustrates different types of WBCs presented in the blood smear sample. Table 2 presents the five normal types of WBCs and their relative percentages in the blood.

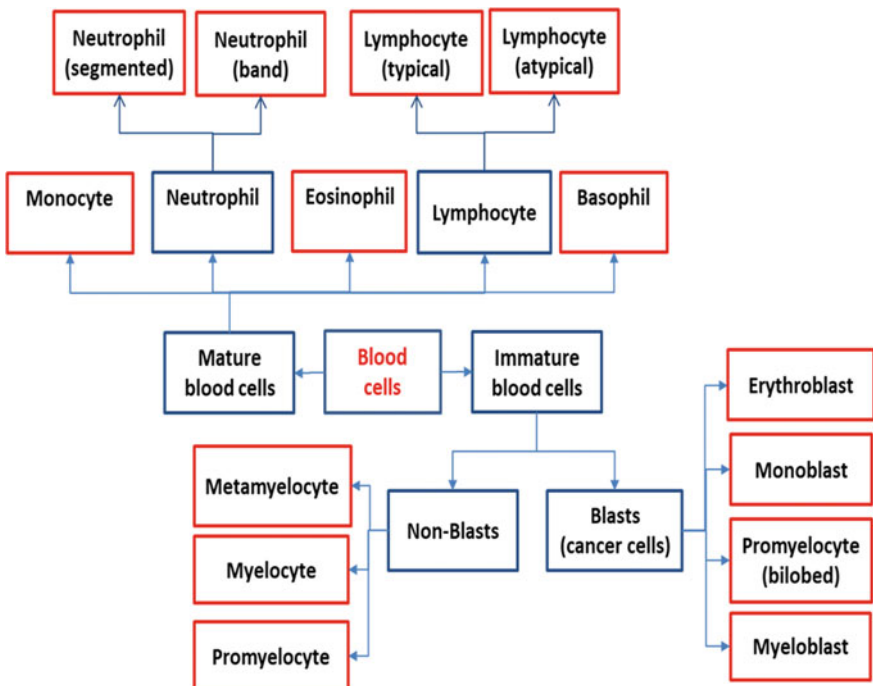
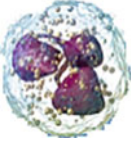
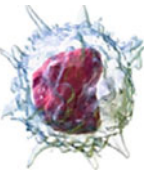
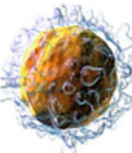
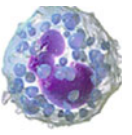


Fig. 2 Classification of WBCs presented in the AML blood smear samples

Table 2 Different types of white blood cells

Cell image	Name of the cell	Percentage in the blood (%)
	Neutrophils	50–70
	Monocytes	3–8
	Lymphocytes	24–45
	Eosinophils	2–4
	Basophils	0.5–1

3 Challenges of WBC Segmentation

WBC segmentation faces several challenges, including differences in the staining processes, illumination variation, complex WBC structure, and the similarities in color and texture between different components of the blood image [7–9].

- Staining variation: Different staining techniques have various effects on the degree of WBC staining. Some parts show different degrees of staining compared to other parts. For example, the nucleus is presented with darker colors compared to the cytoplasm. Moreover, some parts of the nucleus show darker colors compared to other nucleus parts. Different degrees of staining make it difficult to differentiate between the boundaries of the nucleus, cytoplasm, and WBC [6].
- Illumination variation: Illumination methods used by different types of microscopes vary, and they result in different color distributions for the nucleus and

cytoplasm. Moreover, the utilization of new technologies such multicolor light-emitting diodes (LEDs), which allow for multiple color illumination sources, make it difficult to discern between these WBC and other blood components [3, 16]. Imbalanced illumination affects the contrast between cell boundaries, and the background exhibits difficulties in differentiating between nucleus and cytoplasm boundaries [17].

- Complex structure of WBC: WBCs comprise diverse morphological variations in terms of shapes, colors, textures, sizes, and nucleus to cytoplasm ratios. Furthermore, during different WBC maturation stages, a single type of WBC exhibits variation in terms of shapes, sizes, and cytoplasm characteristics, which makes it difficult to differentiate between various WBC components and between WBC and other blood components, such as RBCs.
- Complex microscopic image background: The blood smear image background is relatively complex due to the presence of overlapping objects such as WBCs and RBCs. This problem makes it difficult for segmentation algorithms to achieve accurate results. Moreover, these algorithms must apply WBC segmentation in two separate steps. The first is to differentiate between WBCs and RBCs, and the second is to apply the subsequent segmentation algorithm [18].
- Texture and color similarities: Some types of WBCs, such as neutrophils and monoblasts, exhibit similarities in their cytoplasm and image background color and texture; this makes it difficult to differentiate between these regions [19].

4 Datasets

Most of datasets available on AML and utilized by several research papers are private datasets and were used for the purpose of AML classification. The only publicly available dataset for AML classification of WBCs is the (AML_Cytomorphology_LMU) dataset, which was published by Matek et al. in 2019 [20]. However, this dataset is annotated for WBC classification and not for WBC segmentation. The dataset is a single-cell morphological dataset of 18,365 WBCs obtained from 100 patients with AML and 100 non-malignant controls at Munich University Hospital between 2014 and 2017. The dataset consisted of 15 different types of single-cell images labeled by expert pathologists. Four of these were leukemic cells, and the other 11 were normal blood cells. Among the 11 types, seven were mature leukocytes and four were immature. Cancerous and noncancerous WBCs were classified by expert pathologists based on standard morphological classifications. To our knowledge, there are no datasets on AML annotated for segmentation purposes.

5 Current Automated Segmentation Methods

Computer-aided WBC segmentation methods can be categorized into two types: conventional methods and machine/deep learning-based methods. Conventional methods include edge detection-based, color-based, thresholding-based, clustering-based, region-based methods, and partial differential equations (PDEs) [21].

5.1 Conventional Methods

Edge Detection Techniques

Edge detection methods use special type of filters that are applied to the digital images to identify points with discontinuities which are the points with sharp changes in image intensity. These points represent pixels with high gradients, that is, pixels with sharp changes in intensity in specific direction. The gradient direction is represented by the gradient vector angle while the magnitude is represented by the degree of change in pixel intensity. A higher degree of change indicates a strong edge while minimal changes indicate weak edges [22]. Gradient- and Laplacian-based edge detection are the most common types of edge detection methods in WBC segmentation.

(a) The gradient method

The gradient method detects edges by looking for the maximum and minimum points in the first derivative of the image. A pixel location is declared an edge location if the value of the gradient exceeds a specific threshold. As mentioned before, edges will have higher pixel intensity values than the surrounding pixels. However, gradient-based algorithms such as the Prewitt and Sobel filters have the major drawback of being sensitive to noise.

(b) The Laplacian method

The Laplacian method searches for zero crossings in the second derivative of the image to find edges. Zero crossing occurs when the first derivative is at a maximum.

Edge detection methods are simple and works well for images with high contrast and clear separated regions. However, they do not perform well in complex applications where images have no clear boundaries between regions. Moreover, some of these methods, such as the Laplace algorithm, have fixed characteristics in all directions, which make them sensitive to some edges while ignoring the others. Furthermore, these methods are sensitive to noise, which results in false edge detection, missing true edges, and producing thin or thick lines (Table 4).

Several studies utilized edge detection methods for WBC segmentation and achieved good results [23–26].

Color-Based Methods

These methods utilize the characteristics of different colors and their components to highlight specific regions in the image [27]. Mathematically, a color space is represented by a matrix of two or more dimensions. RGB (red, green, blue), HSI (hue H, saturation S, and luminance), CMYK (cyan, magenta, yellow, and black), and CIE Lab (Commission Internationale de l'Eclairage) are examples of different color systems. RGB color space is the color model utilized in blood smear images. It is an additive color space where all colors can be obtained from the three primary colors: red, green, and blue. However, one limitation of RGB is that it cannot simulate human visual perception of colors [28]. Moreover, a direct connection to a particular RGB value is difficult. Therefore, it usually transforms to other color spaces, such as HSI, CMYK, and Lab. In WBC segmentation, the R and G bands are suitable for WBC nucleus detection [29].

Pixel color information is useful in identifying WBCs and their different parts, including nuclei and cytoplasm. However, selecting the right color space is curtail for accurate WBC detection [30]. Following are the main color spaces applied in segmenting of WBCs and their regions:

(a) The HSI color space

HSI is a color space of three components, hue (H), saturation (S), and luminance (I). The main advantage of this color space is that it is close to humans' color perception. The H and S components are closely related to human color perception. The I component has no color information. Converting the RGB to HSI color space helps with WBC and nucleus detection. Specifically, extracting the H-channel helps in WBC localization while S-channel helps in nucleus localization [31].

(b) CMYK color space

CMYK is a subtractive color system commonly used in printing where C denotes cyan, M denotes magenta, Y denotes yellow, and K denotes black color. Converting an RGB image to CMYK helps highlight the entire WBC including nucleus and cytoplasm. For example, extracting the Y-channel helps highlight the entire WBC including nucleus and cytoplasm, while C-, M-, and K-channels help with nucleus detection.

(c) YCbCr color space

In YCbCr, Y refers the luma component, while Cb and Cr refer to the blue-difference and red-difference chroma components, respectively. It helps highlight the WBC nucleus with less noise compared to other color spaces.

(d) The Lab color space

Like HIS, the Lab color space was developed based on the human vision system. L represents lightness, and a and b represent the four main colors of human vision: red,

green, blue, and yellow. It is mainly based on minimizing the correlation between different color components.

Several researchers have used color-based methods in the segmentation of WBCs and their regions [8, 21, 31–34].

Safuan et al. [29] has utilized RGB, CMYK, HSI, and YCbCr color spaces for segmentation of WBC and their different regions. They applied color correction using the Lab color space by subtracting the mean and standard deviation from each component to obtain a color corrected image. They then used the corrected image with different single-color components and combinations of colors components using the abovementioned color spaces to segment WBCs using Otsu threshold algorithm. They extracted the individual bands including R, G, B, C, M, Y, K, H, S, and I, to compare their performance in highlighting different parts of WBCs. They also performed different subtraction of individual color components to improve the performance. They found that the R-, G-, S-C-, M-, and K-color components perform well in highlighting the nucleus. However, the S- and G-color components achieved the best results in nucleus segmentation, with less noise and better contrast compared to other color components. They further subtracted different components such S-G, C-G, and S-G, of these, S-G achieved the best performance. In contrast, Y- and H- showed good performance in highlighting the entire WBC including the cytoplasm. They also found that the B-color component performed well in highlighting RBCs only. Furthermore, they subtracted Y- and H- and obtained better results with less noise and disappearance of RBC regions. The method was evaluated based on WBC counting accuracy, and they found that S-component and S-C achieved the best results, at 96.92% and 96.56% for the S-component and S-C, respectively.

Several studies have utilized the CMYK color space in combination with other techniques for segmentation of WBCs and their regions. Tavakoli et al. [35] developed a new WBC classification method based on nucleus segmentation and part of the cytoplasm. They utilized the CMYK and HSI color spaces for color transformation and then calculated a soft map for nucleus segmentation. Shape and color features were then extracted, and SVM classifier was then utilized. They achieved 96.75% accuracy using the dice similarity index. Table 3 summarizes the use of different color spaces in WBC, nucleus, and cytoplasm segmentation. Thresholding- and clustering-based methods are the most common methods used in combination with color-based methods [36, 37].

Thresholding Based Methods

Image thresholding is the process through which the gray-scale image is transformed into a binary image. In this process, each pixel is replaced by a black or white pixel based on a selected threshold value T using the following equation:

$$I(x, y) = \begin{cases} 0 & \text{if } I(x, y) < T \\ 1 & \text{if } I(x, y) \geq T \end{cases} \quad (1)$$

Thresholding methods have been classified into five groups [38]:

Table 3 Advantages and disadvantages of applying different color spaces channels on segmentation of WBCs and their regions (nucleus and cytoplasm) using thresholding and clustering algorithms

Color space/channel	WBCs	Nucleus	Cytoplasm	RBCs	Advantages	Limitations
<i>RGB</i>						
R		Yes	–	–	<ul style="list-style-type: none"> • WBC nucleus localization • Result does not include RBCs 	<ul style="list-style-type: none"> • Not able to localize the cytoplasm
G		Yes	–	–	<ul style="list-style-type: none"> • WBC nucleus localization • Result does not include RBCs 	<ul style="list-style-type: none"> • Not able to localize the cytoplasm
B		Yes	–	Yes	<ul style="list-style-type: none"> • WBC nucleus localization 	<ul style="list-style-type: none"> • Results includes RBCs
<i>CIE lab</i>						
L*	–	–	–	–	–	–
a*	–	Y	–	–	<ul style="list-style-type: none"> • Highlights the nucleus with light color 	<ul style="list-style-type: none"> • It is commonly used with clustering algorithm such as <i>k</i>-means and fuzzy <i>C</i>-means
b*	–	Y	–	–	<ul style="list-style-type: none"> • Highlights the nucleus with dark color 	
<i>CMYK</i>						
C	–	Yes	–	–	<ul style="list-style-type: none"> • The best performance in nucleus localization 	<ul style="list-style-type: none"> • Not able to localize cytoplasm or entire WBC
M	–	Yes	–	–	<ul style="list-style-type: none"> • WBC nucleus localization • Result does not include RBCs 	<ul style="list-style-type: none"> • Not able to localize the cytoplasm
Y	Yes	–	–	Yes	<ul style="list-style-type: none"> • WBC localization (nucleus and cytoplasm) 	<ul style="list-style-type: none"> • Results includes RBCs
K	–	Yes	–	–	<ul style="list-style-type: none"> • WBC nucleus localization • Result does not include RBCs 	<ul style="list-style-type: none"> • Not able to localize the cytoplasm

(continued)

Table 3 (continued)

Color space/channel	WBCs	Nucleus	Cytoplasm	RBCs	Advantages	Limitations
<i>HSI</i>						
H	Yes	–	–	Yes	• WBC localization (nucleus and cytoplasm)	• Results includes RBCs
S	–	Yes	–	–	• Best performance in nucleus segmentation	• Not able to localize the cytoplasm
I	Yes	–	–	Yes	• WBC nucleus localization	• Results includes RBCs

Histogram-Based Thresholding

Histogram-based methods select the threshold value according to the histogram's peaks, valleys, and curvatures.

Clustering-Based Thresholding

In these methods, the gray-level image is divided into two clusters background versus foreground (object). It also uses a mixture of two Gaussian two distributions to divide the image space in two clusters. The Otsu thresholding algorithm is an example of this kind of method.

Entropy-Based Thresholding

In this method, the entropy of the image probability distribution is calculated. The optimal threshold that maximizes the entropy of the image foreground and background is selected for image segmentation.

Object Attribute-Based Thresholding

This method applies similarity measures between the gray-level image and the binarized images to find the optimal threshold. Gray-level moments and fuzzy measures are some examples of applied similarity measures.

Locally Adaptive Thresholding

The threshold is calculated using local parameters such as image intensity range, variance, or surface-fitting in the neighborhood.

Several studies used thresholding methods for WBC segmentation and achieved positive results [30, 31, 39–42]. Li et al. [31] applied the dual-threshold method for WBC segmentation. In their method, the Otsu threshold was applied, where greyscale images and HSV-H-component images were used to generate a WBC segmentation mask. Threshold segmentation was utilized to extract the image background

Table 4 Summary of conventional image segmentation process advantages and limitations

Methods	Advantages	Limitations
Edge detection methods	<ul style="list-style-type: none"> The process is close to nature human segmentation process 	<ul style="list-style-type: none"> Works well with Images Good Contrast Sensitive to noise
Thresholding methods	<ul style="list-style-type: none"> Simple and fast Does not require image special information 	<ul style="list-style-type: none"> Sensitive to noise Selection of threshold is curtail Automatic selection of threshold works well for images with good contracts Does not work with images of smooth boundaries
Region based methods	<ul style="list-style-type: none"> Generates clear boundaries between regions Forms well separates regions 	<ul style="list-style-type: none"> Computationally expensive Sensitive to noise Subject to over-segmentation
Color-based methods	<ul style="list-style-type: none"> Ability to exploit the color variation between different cell components in the segmentation process The hue component from the HSI color spaces is not sensitive to noise 	<ul style="list-style-type: none"> Poor performance in presence of shades and lights Unable to differentiate between regions with color similarities such as WBC cytoplasm
Cluster-based methods	<ul style="list-style-type: none"> Simplicity 	<ul style="list-style-type: none"> Works well with small data size Computationally expensive for large data
PDE-based methods	<ul style="list-style-type: none"> Ability to utilize regularization techniques into their models Ability to solve PDEs using finite difference methods (FDM) Ability to link between PDEs and the level set framework for implementing finite difference methods Ability to extend the PDE framework from 2-D to 3-D or even higher dimensions 	<ul style="list-style-type: none"> Numerical computations are expensive Complexity depends on operator size Gives good results with images of good contrasts

and RBCs from the greyscale and H-component images, respectively. Their method achieved 97.85% accuracy.

Clustering-Based Methods

This Clustering algorithm partitions the pixels space into two clusters based on the Euclidean distance between pixels. The clusters are created based on the objective function, which minimizes the sum of the squared error between the pixels and the cluster centroid. Some examples of clustering algorithms are the k -means and fuzzy C-means.

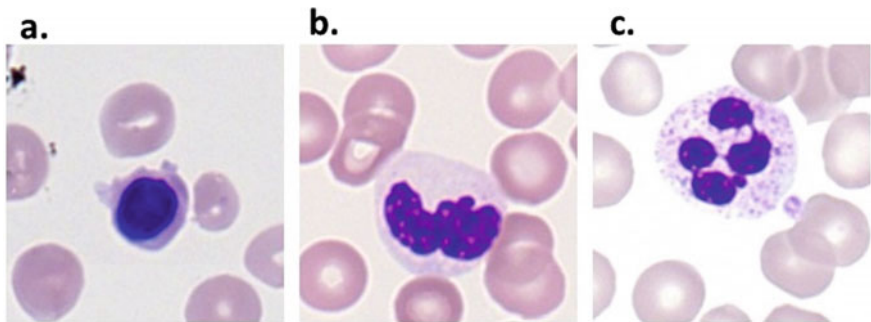


Fig. 3 Examples of challenging WBC segmentation tasks: **a** color similarities between WBC and cytoplasm, **b** light cytoplasm color with smooth texture, **c** light cytoplasm color

Image segmentation using thresholding methods has several limitations and requires special settings, such as uniform light distribution. Therefore, to achieve accurate segmentation results several pre-processing techniques such as color correction and color space transformation were used. Thresholding techniques also showed several limitations in terms of the segmentation of WBC and its different regions. For example, applying simple thresholding fails in segmenting WBCs because of the difficulties in differentiating between WBCs and RBCs due to color similarities (Fig. 3).

Several studies have applied clustering algorithms such as k -means, mean shift clustering, and Fuzzy C -means in WBC segmentation with positive results [43–48].

Region-Based Methods

Region-growing algorithm is an example of the thresholding algorithms that divide the image into separate mutually exclusive regions. Watershed algorithm is another example of region-based methods which is used to overcome the problem of overlapping WBCs. Several researchers utilized region-based methods in combination with other segmentation method for WBC segmentation [26, 40, 42, 47, 49–55].

PDE-Based Methods

These methods are based on solving PDE equation to find the evolution of a given curve in the image which mostly implemented using active contour algorithms also known as snakes [56, 57].

Several studies utilized contour-based and level set algorithms for WBC segmentation [34, 58–65]. Rad et al. [66] were able to overcome the problem of manual contour initialization by developing an automatic region-based initial contour to be used with the level set function. The proposed method achieved an overall accuracy of 96%. Moreover, the proposed method was tested using two external datasets and achieved the best results. Table 4 summarizes the advantages and disadvantages of using conventional image segmentation methods in WBC segmentation.

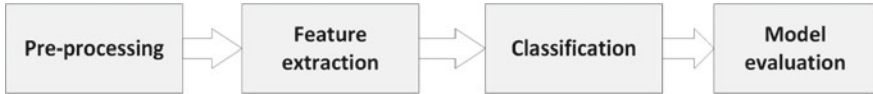


Fig. 4 Pixel-based classification phases

5.2 Pixel-Based Classification Methods

Pixel-based classification also known as semantic segmentation is the process of classifying each pixel in the image into a specific label. This process can be divided into four phases, pre-processing, feature extraction, classification, and model evaluation (Fig. 4).

Pixel-based classification can be divided into two types based on feature extraction method: (a) classifier-based hand-crafted features and (b) classifiers based on deep learning features. Flowing is a description of each phase:

Pre-processing

The pre-processing phase involves with noise reduction, rescaling using normalization and standardization techniques. Pre-processing is an important step to facilitate efficient learning process. Rescaling is a crucial step for learning algorithms to avoid overfitting and to learn significant information [67].

Feature Extraction

In this process, pixel-level features are extracted and linked to the corresponding pixel labels to prepare the dataset for the next classification stage. Feature extraction techniques can be divided into two categories: hand-crafted features and deep learning-based features.

Hand-crafted features are low-level features calculated from image data using human pre-defined rules and are used with traditional machine learning algorithms. Texture, edge contour, statistical, and color features are examples of hand-crafted features. More advanced hand-crafted feature extraction methods include histogram-oriented gradient (HOG) [68], invariant feature transform (SIFT) [69], and bag of words (BoW) [70].

On the contrary, deep learning-based features are high-level features learned from image data using complex operations such as convolutional operations. Convolution neural network (CNN) is considered the state-of-the-art feature extraction method for images classification, both at the pixel and image levels. It is characterized by its excellent performance and its ability to extract hidden and complex patterns without using the traditional image processing pipeline [71]. CNN models can work as feature extractors or classifiers. CNN feature extractors can be further classified into two types:

(a) Feature extraction using transfer learning

Transfer learning utilizes weights that are learned by other models using a huge number of images after fine-tuning to new data. In this approach, features are extracted from specific layers of the network and then used for model training. This method is useful in situations where the datasets are small and for weight initialization [72].

(b) Feature extraction using end-to-end models

In this approach, the feature extraction model consists of a set of a fully trainable multi-layer architecture. In these architectures, the first layers are involved with low-level feature extraction while the last layers are involved with the high-level feature extraction. It consists of several types of layers including convolutional, pooling, normalization, and dropout, with each type of layer responsible for specific task. In end-to-end approach, the layers are learned simultaneously, which results in robust and reliable features that are considered the most advantage of CNN. Another advantage of CNN-based models is weight sharing, which reduces the size of the network and simplifies the training process [73]. Figures 5 and 6 illustrate different types of WBC hand-crafted and deep learning-based features, respectively.

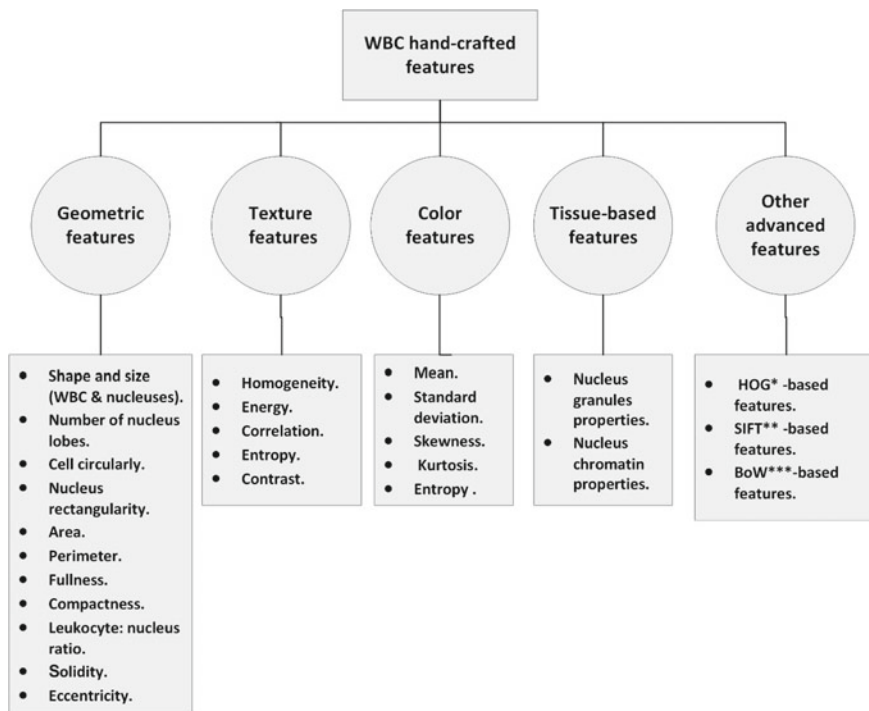
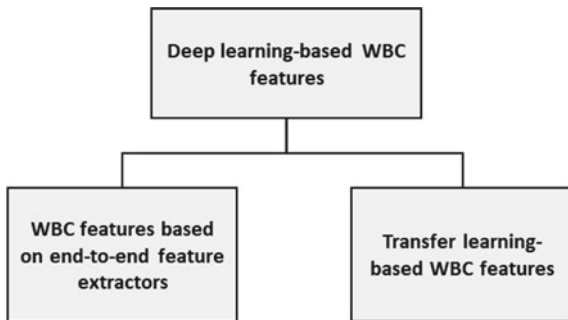


Fig. 5 WBC hand-crafted features

Fig. 6 Type of WBC deep learning-based features



Recently, several researchers have used deep learning models for WBC segmentation and achieved excellent results [74–76]. Roy et al. [76] proposed a WBC segmentation system using the DeepLabv3+ architecture and ResNet-50 and achieved 96.1% segmentation accuracy. Banik et al. [75] proposed a CNN-based WBC classification model based on nucleus segmentation. The model achieved segmentation accuracy of 96%. Lu et al. [74] developed a WBC segmentation model based on multiscale feature fusion using feature encoder with residual blocks. The model was evaluated using several normal WBC datasets, including neutrophils, eosinophils, basophils, monocytes, and lymphocytes. The system achieved excellent results compared to other segmentation methods.

Classification

Classification process utilizes the extracted features as inputs and applies classification algorithms to categorize each pixel into specified labels. Examples of these algorithms include support vector machine (SVM), k -nearest neighbors (KNN), multi-layer perceptron (MLP), or Naïve Bayes. However, in deep learning frameworks the classification process is presented with simple or multiple fully connected layers (FCL). The strength of deep learning models lies in feature extraction. However, the classification part is equivalent to the MLP model used in traditional machine learning methods. Figure 7 summarizes different methods used for WBC segmentation.

Model Evaluation

The pixel-based classification model can be evaluated using several metrics such as sensitivity, specificity, precision, F -score, and overall accuracy. However, the quality of the segmented WBCs can be measured by comparing the segmented image to a ground truth image using similarity measurements, such as the Jaccard index known as (IoU) dice index. The ground truth image is obtained by an expert pathologist and serves as a benchmark.

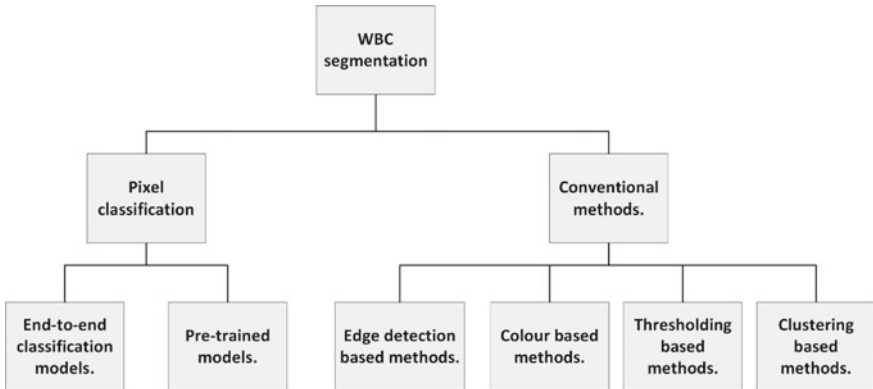


Fig. 7 WBC deep learning-based features

6 Limitations and Future Work

Despite advances in the field of WBC segmentation and pattern recognition, several researches have revealed several limitations. One of the main limitations is the limited number of datasets that include images with their corresponding ground truth. Most published works have utilized private datasets that cannot be used for benchmarking. Datasets with ground truths are important to test the accuracy of newly proposed segmentation methods and benchmark with existing methods. Moreover, the ground truths available in the literature are not generated by pathologists. However, obtaining pathologist-generated ground truth for large number of images is another challenge. WBC segmentation methods, especially those based in deep learning are computationally expensive, and much computer power is needed to train deep learning models. Another limitation is that this type of model needs a large amount of data especially in the case of end-to-end models, where no pre-trained models are used. Furthermore, model modification is expensive and requires model re-training. In addition to the abovementioned limitations, these models are difficult to validate the complex structures. Therefore, future work should focus on developing benchmark datasets to promote research development and to facilitate the validation of newly proposed methods. Additionally, new methods that are invariant to illumination, light, and different staining processes should be developed to overcome problems with inter-microscopic variation. Research should also focus on utilizing of high-performance computation (HPC) to efficiently utilize huge number of images with less computation time. This is especially important in the development of new robust end-to-end segmentation systems, which are considered crucial for developing hematological CAD systems.

7 Conclusion

In this chapter, we attempted to review automated WBC segmentation methods applied in Acute Myeloid leukemia blood smear microscopic images. Complex structure of smear images, morphological diversity of WBCs, staining and illumination variation, and complex image background are the main challenges presented in automatic WBC segmentation. Segmentation methods have been classified into methods using traditional image processing techniques and methods using machine learning including deep learning. Deep learning methods have been further classified into transfer learning methods and end-to-end methods. Generalization and segmentation accuracy were the main limitations of traditional image processing techniques. However, the state-of-the-art deep learning methods overcome most of the shortcomings exhibited by tradition methods specially in feature extraction area. One of the main limitations of the WBC segmentation in AML is the lack of public datasets where most of published research utilized private datasets which make it difficult to evaluate and benchmark new segmentation methods. Generation of WBC ground truths for WBC requires annotation to be done by expert pathologists which is expensive and time-consuming especially for deep learning that requires huge amount of data. In my opinion, new datasets should be published with a limited random pre-selected images to be served as ground truth to reduce the manual annotation overhead.

References

1. Abbas, N., Mohamad, D., Abdullah, A.H., Saba, T., Al-Rodhaan, M., Al-Dhelaan, A.: Nuclei segmentation of leukocytes in blood smear digital images. *Pak. J. Pharm. Sci.* **28**(5), 1801–1806 (2015)
2. Rehman, A., Abbas, N., Saba, T., Rahman, S.I.U., Mehmood, Z., Kolivand, H.: Classification of acute lymphoblastic leukemia using deep learning. *Microsc. Res. Tech.* **81**(11), 1310–1317 (2018)
3. Bigorra, L., et al.: Feature analysis and automatic identification of leukemic lineage blast cells and reactive lymphoid cells from peripheral blood cell images. *J. Clin. Lab. Anal.* **31**(2), e22024 (2017)
4. Walker, H.K., Hall, W.D., Hurst, J.W.: *Clinical Methods: The History, Physical, and Laboratory Examinations*. Boston (1990)
5. Choi, J.W., et al.: White blood cell differential count of maturation stages in bone marrow smear using dual-stage convolutional neural networks. *PLoS ONE* **12**(12), e0189259–e0189259 (2017)
6. Rehman, A., Abbas, N., Saba, T., Mahmood, T., Kolivand, H.: Rouleaux red blood cells splitting in microscopic thin blood smear images via local maxima, circles drawing, and mapping with original RBCs. *Microsc. Res. Tech.* **81**(7), 737–744 (2018)
7. Iqbal, S., Khan, M.U.G., Saba, T., Mehmood, Z., Javaid, N., Rehman, A., Abbasi, R.: Deep learning model integrating features and novel classifiers fusion for brain tumor segmentation. *Microsc. Res. Tech.* **82**(8), 1302–1315 (2019). <https://doi.org/10.1002/jemt.23281>
8. Nawaz, M., Mehmood, Z., Nazir, T., Naqvi, R.A., Rehman, A., Iqbal, M., Saba, T.: Skin cancer detection from dermoscopic images using deep learning and fuzzy k-means clustering. *Microsc. Res. Tech.* **85**(1), 339–351 (2022)

9. Lung, J.W.J., Salam, M.S.H., Rehman, A., Rahim, M.S.M., Saba, T.: Fuzzy phoneme classification using multi-speaker vocal tract length normalization. *IETE Tech. Rev.* **31**(2), 128–136 (2014). <https://doi.org/10.1080/02564602.2014.892669>
10. Vardiman, J.W.: The World Health Organization (WHO) classification of tumors of the hematopoietic and lymphoid tissues: an overview with emphasis on the myeloid neoplasms. *Chem. Biol. Interact.* **184**(1–2), 16–20 (2010)
11. Vardiman, J.W.: The World Health Organization (WHO) classification of tumors of the hematopoietic and lymphoid tissues: an overview with emphasis on the myeloid neoplasms. *Chem. Biol. Interact.* **184**(1), 16–20 (2010)
12. Arber, D.A., et al.: The 2016 revision to the World Health Organization classification of myeloid neoplasms and acute leukemia. *Blood* **127**(20), 2391–2405 (2016)
13. Ladines-Castro, W., et al.: Morphology of leukaemias. *Rev. Méd. Hosp. Gen. Méx.* **79**(2), 107–113 (2016)
14. Bennett, J. M., Marie-Therese Daniel, D.C., Flandrin, G., Galton, D.A.G., Gralnick, H.R., Sultan, C.: Proposals for the classification of the acute Leukaemias French-American-British (FAB) co-operative group. *Br. J. Hematol.* **33**(4) (1976)
15. Thieml, H.D., Haferlach, T.: Color Atlas of Hematology. Thieme (2004)
16. Makkapati, V.V., Pathangay, V.: Adaptive color illumination for microscopes. In: 2011 National Conference on Communications (NCC) (2011)
17. Sadeghian, F., et al.: A framework for white blood cell segmentation in microscopic blood images using digital image processing. *Biol. Proced. Online* **11**(1), 196 (2009)
18. Miao, H., Xiao, C.: Simultaneous segmentation of leukocyte and erythrocyte in microscopic images using a marker-controlled Watershed algorithm. *Comput. Math. Methods Med.* **2018**, 7235795 (2018)
19. Elhassan, T.A., et al.: Feature extraction of white blood cells using CMYK-moment localization and deep learning in acute myeloid leukemia blood smear microscopic images. *IEEE Access* (2022)
20. Matek, C., et al.: A single-cell morphological dataset of Leukocytes from AML patients and non-malignant controls. In: 2019: The Cancer Imaging Archive
21. Kumar, P.R., et al.: Segmentation of white blood cells using image segmentation algorithms. In: 2020 5th International Conference on Computing, Communication and Security (ICCCS) (2020)
22. Jadooki, S., Mohamad, D., Saba, T., Almazyad, A.S., Rehman, A.: Fused features mining for depth-based hand gesture recognition to classify blind human communication. *Neural Comput. Appl.* **28**(11), 3285–3294 (2017)
23. Fatonah, N.S., Tjandrasa, H., Faticah, C.: Identification of acute lymphoblastic leukemia subtypes in touching cells based on enhanced edge detection. *Int. J. Intell. Eng. Syst.* **13**(4), 204–215 (2020)
24. Sadeghian, F., et al., A framework for white blood cell segmentation in microscopic blood images using digital image processing. *Biol. Proced. Online* **11**(1), 196–206 (2009)
25. Liao, Q., Deng, Y.: An accurate segmentation method for white blood cell images. In: Proceedings IEEE International Symposium on Biomedical Imaging. IEEE (2002)
26. Joshi, M.D., et al.: White blood cells segmentation and classification to detect acute leukemia. *Int. J. Emerg. Trends Technol. Comput. Sci. (IJETTCS)* **2**(3), 147–151 (2013)
27. Zhang, C., et al.: White blood cell segmentation by color-space-based k -means clustering. *Sensors (Basel, Switz.)* **14**(9), 16128–16147 (2014)
28. Ibraheem, N., et al.: Understanding color models: a review. *ARPN J. Sci. Technol.* **2** (2012)
29. Safuan, S.N.M., et al., White blood cell counting analysis of blood smear images using various segmentation strategies. *AIP Conf. Proc.* **1883**(1), 020018 (2017)
30. Duan, J., Yu, L.: A WBC segmentation method based on HSI color space. In: 2011 4th IEEE International Conference on Broadband Network and Multimedia Technology. IEEE (2011)
31. Li, Y., et al.: Segmentation of white blood cell from acute lymphoblastic Leukemia images using dual-threshold method. *Comput. Math. Methods Med.* **2016**, 9514707 (2016)

32. Sundara, S.M., Aarthi, R.: Segmentation and evaluation of white blood cells using segmentation algorithms. In: 2019 3rd International Conference on Trends in Electronics and Informatics (ICOEI). IEEE (2019)
33. Mohapatra, S., et al.: Unsupervised blood microscopic image segmentation and leukemia detection using color based clustering. *Int. J. Comput. Inf. Syst. Ind. Manag. Appl.* **4**, 477–485 (2012)
34. Angkoso, C.V., Purnama, I.K.E., Purnomo, M.H.: Automatic white blood cell segmentation based on color segmentation and active contour model. In: 2018 International Conference on Intelligent Autonomous Systems (ICoIAS). IEEE (2018)
35. Tavakoli, S., et al.: New segmentation and feature extraction algorithm for classification of white blood cells in peripheral smear images. *Sci. Rep.* **11**(1), 19428 (2021)
36. Cao, H., Liu, H., Song, E.: A novel algorithm for segmentation of leukocytes in peripheral blood. *Biomed. Signal Process. Control* **45**, 10–21 (2018)
37. Sarrafzadeh, O., Dehnavi, A.M.: Nucleus and cytoplasm segmentation in microscopic images using K -means clustering and region growing. *Adv. Biomed. Res.* **4**, 174 (2015)
38. Carabias, D.M.: Analysis of Image Thresholding Methods for Their Application to Augmented Reality Environments (2012)
39. Mohammed, Z.F., Abdulla, A.A.: Thresholding-based white blood cells segmentation from microscopic blood images. *UHD J. Sci. Technol.* **4**(1), 9–17 (2020)
40. Salem, N., et al.: A comparative study of white blood cells segmentation using Otsu threshold and watershed transformation. *J. Biomed. Eng. Med. Imag.* **3**(3), 15 (2016)
41. Dorini, L.B., Minetto, R., Leite, N.J.: White blood cell segmentation using morphological operators and scale-space analysis. In: XX Brazilian Symposium on Computer Graphics and Image Processing (SIBGRAPI 2007). IEEE (2007)
42. Mohammed, E.A., et al.: Chronic lymphocytic leukemia cell segmentation from microscopic blood images using watershed algorithm and optimal thresholding. In: 2013 26th IEEE Canadian Conference on Electrical and Computer Engineering (CCECE). IEEE (2013)
43. Zhang, C., et al.: White blood cell segmentation by color-space-based k -means clustering. *Sensors* **14**(9), 16128–16147 (2014)
44. Jiang, K., Liao, Q.-M., Xiong, Y.J.S.C.: A novel white blood cell segmentation scheme based on feature space clustering. *Soft Comput.* **10**(1), 12–19 (2006)
45. Ko, B.C., Gim, J.-W., Nam, J.-Y.J.M.: Automatic white blood cell segmentation using stepwise merging rules and gradient vector flow snake. *Micron* **42**(7), 695–705 (2011)
46. Salem, N.M.: Segmentation of white blood cells from microscopic images using K -means clustering. In: 2014 31st National Radio Science Conference (NRSC). IEEE (2014)
47. Liu, Z., et al.: Segmentation of white blood cells through nucleus mark watershed operations and mean shift clustering. *Sensors* **15**(9), 22561–22586 (2015)
48. Zheng, X., et al.: Fast and robust segmentation of white blood cell images by self-supervised learning. *Micron* **107**, 55–71 (2018)
49. Tulsani, H., Saxena, S., Yadav, N.J.I.: Segmentation using morphological watershed transformation for counting blood cells. *IJCAIT* **2**(3), 28–36 (2013)
50. Faticah, C., et al.: Overlapping white blood cell segmentation and counting on microscopic blood cell images. *Int. J. Smart Sens. Intell. Syst.* **7**(3) (2014)
51. Cao, F., et al.: A novel segmentation algorithm for nucleus in white blood cells based on low-rank representation. *Neural Comput. Appl.* **28**(1), 503–511 (2017)
52. Sarrafzadeh, O., Dehnavi, A.M.: Nucleus and cytoplasm segmentation in microscopic images using K -means clustering and region growing. *Adv. Biomed. Res.* **4** (2015)
53. Jiang, K., Liao, Q.-M., Dai, S.-Y.: A novel white blood cell segmentation scheme using scale-space filtering and watershed clustering. In: Proceedings of the 2003 International Conference on Machine Learning and Cybernetics (IEEE Cat. No. 03EX693). IEEE (2003)
54. Ghane, N., et al.: Segmentation of white blood cells from microscopic images using a novel combination of K -means clustering and modified watershed algorithm. *J. Med. Sig. Sens.* **7**(2), 92 (2017)

55. Miao, H., Xiao, C.: Simultaneous segmentation of leukocyte and erythrocyte in microscopic images using a marker-controlled watershed algorithm. *Comput. Math. Methods Med.* (2018)
56. Kass, M., Witkin, A., Terzopoulos, D.: Snakes: active contour models. *Int. J. Comput. Vis.* **1**(4), 321–331 (1988)
57. Jiang, X., Zhang, R., Nie, S.: Image segmentation based on PDEs model: a survey. In: 2009 3rd International Conference on Bioinformatics and Biomedical Engineering (2009)
58. Khamael, A.-D., et al.: Evaluation and benchmarking of level set-based three forces via geometric active contours for segmentation of white blood cell nuclei shape. *Comput. Biol. Med.* **116**, 103568 (2020)
59. Al-Dulaimi, K., et al.: White blood cell nuclei segmentation using level set methods and geometric active contours. In: 2016 International Conference on Digital Image Computing: Techniques and Applications (DICTA). IEEE (2016)
60. Chinnathambi, K., et al.: Robust segmentation of cancer affected white blood cells using modified level set algorithm. *Int. J. Simul. Syst. Sci. Technol.* **14**(9) (2014)
61. Marzuki, N.I.C., Mahmood, N.H., Razak, M.A.A.: Segmentation of white blood cell nucleus using active contour. *J. Teknol.* **74**(6) (2015)
62. Mukherjee, D.P., Ray, N., Acton, S.T.: Level set analysis for leukocyte detection and tracking. *IEEE Trans. Image Process.* **13**(4), 562–572 (2004)
63. Eom, S., et al.: Leukocyte segmentation in blood smear images using region-based active contours. In: International Conference on Advanced Concepts for Intelligent Vision Systems. Springer (2006)
64. Wenhua, Q., et al.: White Blood Cell Nucleus Segmentation Based on Canny Level Set. *IEEE Trans. Image Process.* **180**(10), 85 (2014)
65. Zamani, F., Safabakhsh, R.: An unsupervised GVF snake approach for white blood cell segmentation based on nucleus. In: 2006 8th International Conference on Signal Processing. IEEE (2006)
66. Rad, A.E., et al.: Morphological region-based initial contour algorithm for level set methods in image segmentation. *Multimed. Tools Appl.* **76**(2), 2185–2201 (2017)
67. Rawat, J., et al.: Classification of acute lymphoblastic leukaemia using hybrid hierarchical classifiers. *Multimed. Tools Appl.* **76**(18), 19057–19085 (2017)
68. Sternberg, S.R.: Method and Apparatus for Pattern Recognition and Detection (1983)
69. Lowe, D.G.: Distinctive image features from scale-invariant keypoints. *Int. J. Comput. Vision* **60**(2), 91–110 (2004)
70. Sivic, J., Zisserman, A.: Efficient visual search of videos cast as text retrieval. *IEEE Trans. Pattern Anal. Mach. Intell.* **31**(4), 591–606 (2009)
71. Hegde, R.B., et al.: Feature extraction using traditional image processing and convolutional neural network methods to classify white blood cells: a study. *Aust. Phys. Eng. Sci. Med.* **42**(2), 627–638 (2019)
72. Barman, R., et al.: Transfer Learning for Small Dataset (2019)
73. Alzubaidi, L., et al.: Review of deep learning: concepts, CNN architectures, challenges, applications, future directions. *J. Big Data* **8**(1), 53 (2021)
74. Lu, Y., et al.: WBC-net: a white blood cell segmentation network based on UNet++ and ResNet. *Appl. Soft Comput.* **101**, 107006 (2021)
75. Banik, P.P., Saha, R., Kim, K.-D.: An automatic nucleus segmentation and CNN model based classification method of white blood cell. *Expert Syst. Appl.* **149**, 113211 (2020)
76. Roy, R.M., Ameer, P.M.: Segmentation of leukocyte by semantic segmentation model: a deep learning approach. *Biomed. Sig. Process. Control* **65**, 102385 (2021)

Computer Vision-Based Prognostic Modelling of COVID-19 from Medical Imaging



Abdul Muiz Fayyaz , Mahyar Kolivand, Jaber Alyami, Sudipta Roy, and Amjad Rehman 

Abstract COVID19 is a respiratory illness that is extremely infectious and is spreading at an alarming rate at the moment. Chest radiography images play an important part in the automated diagnosis of COVID19, which is accomplished via the use of several machine learning approaches. This chapter examines prognostic models for COVID-19 patients' survival prediction based on clinical data and lung/lesion radiometric characteristics retrieved from chest imaging. While it seems that there are various early indicators of prognosis, we will discuss prognostic models or scoring systems that are useful exclusively to individuals who have received confirmation of their cancer diagnosis. A summary of some of the research work and strategies based on machine learning and computer vision that have been applied for the identification of COVID19 have been presented in this chapter. Some strategies based on pre-processing, segmentation, handmade features, deep features, and classification have been discussed, as well as some other techniques. Apart from that, a few relevant datasets have been provided, along with a few research gaps and challenges in the respective sector that have been identified, all of which will be useful for future study efforts.

A. Muiz Fayyaz

Department of Computer Science, University of Wah, Wah, Pakistan

M. Kolivand

Department of Medicine, University of Liverpool, Liverpool, UK

e-mail: M.Kolivand@student.Liverpool.ac.uk

School of Computing and Digital Technologies, Staffordshire University, Staffordshire, UK

J. Alyami

Department of Diagnostic Radiology, Faculty of Applied Medical Science, King Abdulaziz, Jeddah 21589, Saudi Arabia

Imaging Unit, King Fahad Medical Research Centre, King Abdulaziz, Jeddah 21589, Saudi Arabia

S. Roy

Artificial Intelligence & Data Science, Jio Institute, Navi Mumbai 410206, India

A. Rehman ()

Artificial Intelligence & Data Analytics Lab (AIDA), CCIS Prince Sultan University, Riyadh, Saudi Arabia

e-mail: arkhan@psu.edu.sa

Keywords Brain tumor · Deep learning and Transfer learning · Healthcare · Health risks · Public health

1 Introduction

The Coronavirus (COVID-19) is among the most dangerous and lethal infections on the globe. COVID-19 has had a huge influence on world health and continues to be a major global concern due to the rapid increase in the number of infected individuals and deaths resulting from the disease [1, 2]. As a result, it spreads like wildfire from one person to another. It initially appeared in Wuhan, China, in December 2019 [3, 4]. The virus that causes the sickness is a member of a group of viruses that cause respiratory dysfunction and are a significant threat to public health [5, 6]. SARS and MERS are two illnesses that are closely linked to COVID-19. The most common symptoms of COVID-19 include fatigue, breathing problems, fever, difficulty moving body parts, headache, and weakness. COVID-19 is a virus that affects the respiratory system [7]. To avoid the transmission of infection, the accurate diagnosis of COVID-19 is essential for treatment and determines which patients need to isolate. Because of the recent spread of COVID-19, successful identification is still a challenging task [8]. The use of reverse transcription-polymerase chain reaction (RT-PCR) test kits as the primary diagnostic approach for COVID-19 is now available.

Nonetheless, it takes several hours to complete the final results. Parallel to this, chest x-rays, CT scans, and other biomarkers are now increasingly being examined by several nations to aid in the diagnosis of the condition, as previously stated [9, 10]. Chest X-rays, ultrasounds, and computed tomography (CT) scans are important tools in evaluating and diagnosing individuals with severe SARS symptoms [11].

The worldwide health organizations collaborated to limit the most recent epidemic by isolating people who were ill from the rest of the population [12]. To identify infected persons, health authorities use RT-PCR tests, which include the extraction of RNA from the virus from a nasal swab taken from the ill person and then the visual interpretation of the findings [13]. On the other hand, this test is subject to several restrictions that must be taken into account [14]. Because of the epidemic's early beginnings and a large number of affected people, it was not possible to conduct a significant number of laboratory tests. This test is not recommended for beginners because of the length of time required to complete and provide the results [15]. Probably, members of the medical staff who took part in the test got infected with the virus, which is exceedingly contagious [16]. Several studies have also demonstrated that the RT-PCR test commonly generates false-positive results due to data processing and quality control difficulties, among other things [17–19].

Even though certain viruses and bacteria can cause pneumonia, analyzing a large number of chest X-ray images to diagnose and differentiate between subtle COVID-19 infected viral pneumonia and other non-COVID-19 infected communal pneumonia can be time-consuming for general radiologists in hospitals [20]. Aside from

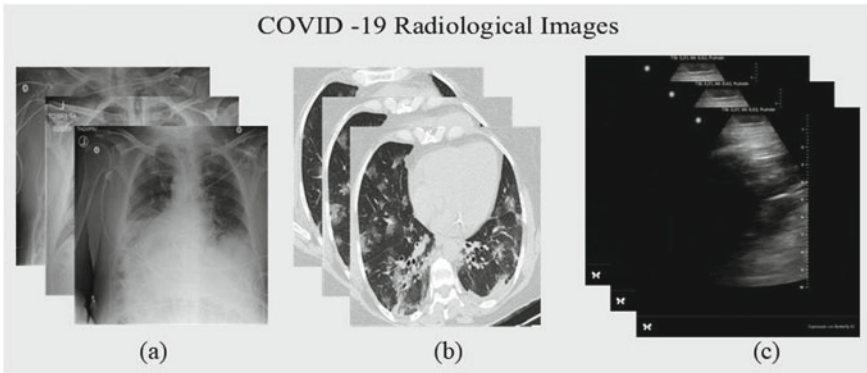


Fig. 1 COVID-19 **a** Chest X-ray, **b** CT-Scans, and **c** Ultrasounds images

that, it seems that COVID-19 and other kinds of pneumonia have several characteristics. As a result, radiologists are confronted with a disease detection problem in this epidemic [21]. Infection rates are rising, which is very harmful since it negatively impacts the body's immune system, which is critical for battling diseases in the human body. Different imaging modalities, such as chest X-rays, CT scans, and ultrasounds, are used to evaluate the COVID-19 [22, 23]. Figure 1 illustrates several representative COVID-19-infected chest X-rays, CT scans, and ultrasound images.

1.1 Motivation

The Coronavirus (COVID-19) is one of the most dangerous viruses known to exist in the natural world, and it has been linked to many deaths. It spreads very quickly from one person to another, and it is contagious. In recent years, COVID-19 has emerged as a worldwide pandemic illness spreading from person to person at an alarmingly fast pace. It first appeared in Wuhan, China, in December of this year and has since spread. The virus is a member of a group of viruses that have been linked to the development of respiratory disorders in the past. Any methodological elements include SARS and MERS, which are considered a serious threat to public health and should be avoided. COVID-19 is characterized by various symptoms, including weakness, respiratory issues, fever, mobility problems, headaches, and tiredness. To enhance such algorithms for COVID identification, researchers were greatly supported by the fast development of image processing and machine learning modules in recent years. The extraction, selection, and optimization of robust functions are the first steps in the problem's analysis, and they are the first stage in the problem's analysis.

Furthermore, the suggested approach, which is based on prognostic modelling, should be sufficiently resilient to achieve better overall performance. A large number of academics presented a variety of methodologies and algorithms for recognizing,

segmenting, and categorizing COVID-19. Some limitations remain with the strategies that were offered to lessen the risk factor. The difficulties addressed in the present study serve as the foundation for choosing optimum deep features to improve performance, accuracy, and efficiency in segmentation and classification analysis and classification.

1.2 *Applications*

When it comes to real-time applications, the identification and analysis of COVID utilizing machine learning are critical. As a result, chest X-ray and computed tomography (CT) scans are critical in the detection, segmentation, and classification of COVID compared to normal and pneumonia. With automated detection in combination with bedside ultrasonography, it has shown to be very effective in reducing the risk of healthcare professionals coming into touch with or exposing the patient to potentially dangerous chemicals. Patients are relieved of the need to rush to the hospital when their illness can be identified in the comfort of their own homes, hence eliminating the need for them to do so in the first place. As a consequence, radiologists who have access to a fully automated CAD system are more effective in diagnosing COVID-19. Both in terms of illness diagnostic speed and in terms of computing accuracy, it is possible to implement this technique.

2 Prognostic Modeling Based Key Phases for Analysis COVID-19

In their attempts to classify COVID-19, several researchers have employed a variety of methodologies, including pre-processing [24], segmentation [25], features extraction [26], features selection [27], features fusion [28], and classification [29]. In this part, we will go through numerous strategies that have been provided in this research, as seen in Fig. 2. The procedures required for automated COVID-19 identification and classification as shown in Fig. 2, which shows the sequence of stages.

2.1 *Pre-processing*

Pre-processing is the initial step of image processing, during which we apply different algorithms to the images to remove noise or extraneous information [30]. Several pre-processing approaches are being utilized to remove useless information from medical images, and these strategies include [31]. Images of a resolution ranging from 148×61 pixels to 1637×1225 pixels were used in the study procedure under



Fig. 2 The procedures required for automated COVID-19 identification and classification

consideration, presenting a substantial challenge for deep learning researchers. Using a linear interpolation approach, each slice of the U-Net [32] segmentation network was scaled to meet the required dimension of the input layer of the network. The goal size for the regular perturbation technique was 512×512 pixels. Although the pixel array measurements and CT window designs may vary, the suggested technique provides a low degree of segmentation error despite the aforesaid variances in these parameters. A reliable pre-processing approach for transforming various resolution chest images into the same resolution chest images is suggested, and the resulting images are then submitted to U-net for further processing [33]. They utilized two different pre-processing approaches to reduce the brightness of certain areas in the chest images, which they found to be effective. A bilateral low pass filtering and equalization of histograms are used in this approach to get the desired result. Convolutional neural networks are trained on the output filtered image, which is then convolved with the original image to produce a pseudocolour image for use in training. The researchers' findings reveal that their pre-processing technique boosts accuracy from 88 to 94.5%, on average. In the pre-processing phase, there are several

processes to do. These procedures include image enhancement, image scaling, colour space transformation, and image filtering, among others.

For improving the pre-processing filter block, which is ultimately utilized for deep network training, a loss function is presented. The system was trained using the publicly available dataset Covidx, which resulted in an accuracy of 97.48% when tested. When dealing with large datasets with a variety of dimensions, CSS (Column Subset Selection) is an excellent approach to use. It can choose a small amount of data from a large number of datasets [34]. It was necessary to apply the column subset selection approach as a pre-processing step to find the COVID-19 from chest radiography images. CSS allows researchers to minimize the quantity of the datasets they have access to, resulting in more effective results [35]. Deep learning algorithms perform well for images with a certain resolution, but they do not perform well for images with a large variation in the number of pixels in each image. This is accomplished by using the adaptive variation approach to express the deep pixel-level information. They refined a deep model and produced results that surpassed those obtained by prior efforts [36]. When there is significant penetration of distortion in a chest ultrasound image, it can include noise and unusable content. Many researchers have sought to reduce noise via the use of different ways as a consequence of this [37]. During the development of COVID-19, the N-CLAHE method was employed to increase the accuracy of ultrasound images. The findings revealed that COVID, pneumonia, and conventional chest ultrasonography images could be distinguished more accurately. In radiography, N-CLAHE is a technique for increasing the colour accuracy of radiographic images [38].

Segmentation

Segmentation is the second and most important stage in the identification of COVID-19 after pre-processing. It is also the most time-consuming. Using this process, a single image is divided into smaller parts, which are referred to as segments. Given the time-consuming and error-prone nature of human segmentation, a variety of semi-automatic and fully automated procedures are used to assure accurate identification. Object identification, medical imaging, content-based image processing, autonomous traffic control systems, and recognition jobs, to name a few of the most common applications segmented, are among the most popular segmented applications. Segmentation is a technique that is often used in medical imaging to distinguish polluted areas from healthy ones. Techniques such as edge-based segmentation, cluster-based segmentation, region-based segmentation, instance segmentation, graph-based segmentation, threshold-based segmentation, colour-based segmentation, deep-learning-based segmentation, and others are addressed in this area.

When it comes to the assessment and quantification of COVID-19, segmentation is a critical step in the image processing and analysis process. It is used to describe areas of interest (ROIs) in chest X-ray or CT images, such as the liver, lobes, bronchopulmonary segments, and afflicted regions or lesions, among other things. Segmented areas might be used for diagnostics and other purposes, such as removing hand-crafted or self-learned functionality [39]. The fact that there are several approaches

for medical image segmentation has resulted in just a few tests being undertaken and evaluated on an image of a COVID-19 lesion to determine how well they can segment the lesion exactly. It is shown in this study how to reduce over segmented regions in images for segmentation by using an upgraded image-dependent multi-level image thresholding strategy, which can be found here [40]. An array of extraction techniques for contaminated segments from a CTSI were developed in this work, which used a variety of image orientations, including coronal and axial, to do so. This study also suggests a method for determining the lung infection rate based on the number of infected individuals and the number of lung regions [41].

It is also proposed that dice loss for segmentation and COPLE-Net, a COVID segmentation network, be used as components of a stable system. COPLE-Net is capable of performing segmentation tasks on a wide range of files, including those with noise, variable scales, and varying orientations, among others. The data indicated that the suggested model is more efficient than the existing one [42]. To prepare for COVID-19, we used a variety of data augmentation methods for a small sample of CT scans. This approach generates a large number of randomly distributed and frequently occurring image patches, which are then used to train the U-Net architecture. They created a segmentation algorithm that was validated 20 times and that accurately segments COVID-19 infection from chest CT images while avoiding overfitting the data. Their goal of reaching a 0.95 dice coefficient was met with success. Specifically, they were interested in examining the comparability of characteristics acquired by non-covid lesions. Transfer learning methodologies were applied in four different ways. According to their findings, non-covid lesions allow for the development of a more stable model for the distinction of COVID-19 in CT images, resulting in better outcomes with less training time [43]. For segmentation of the COVID-19 area in X-ray images of the lungs, we employed semi-supervised segmentation of the region. The ground reality values were obtained via the usage of DenseNet201 activation maps. They employed DeepLabv3 for semantic segmentation after properly configuring the learning rate and epochs, and the results were much better than previously available studies in the literature [44].

2.2 *Features Extraction*

A fundamental stage in image processing is feature extraction involves obtaining important characteristics from images that may then be used for recognition and categorization. To acquire typical applications, feature extraction is a method that is used. When it comes to computer vision (CV) and machine learning, feature extraction is very important (ML). It is necessary to extract features from images to do classification. The following sorts of features are used: Handcrafted features, Advanced Deep feature sets, Morphological-based features, Texture-based features, and Instance-based features. Furthermore, in this literature, we primarily cover two kinds of extracted features for classification, which are called Handcrafted feature extraction and Deep CNN-based feature extraction, respectively.

2.2.1 Handcrafted Features

Many difficulties, such as angle, occlusion, illumination, and size, are manually corrected by the human eye in the case of handmade features, as a balance between accuracy and productivity was achieved via the development of these elements. Local Ternary Patterns (LTP), Local Phase Quantization (LPQ), Grey, Local Binary Patterns (LBP), SURF [45, 46], KAZE [47, 48], MSER [49–52], HOG [53, 54], PHOG [50], Harris [55], FAST [56], GOG [57], SFTA [58, 59] and the Level Co-Occurrence Matrix (GLCM) [60] are well-known handmade functions that have become popular. This section will discuss how to conduct COVID-19 research utilizing a variety of methodologies that include handmade elements [6].

To understand COVID-19, they investigated a variety of multi-resolution properties. They employed transforms such as the Shearlet, Wavelet, and Contourlet transform to create the groupings in their analysis. As a result of using entropy in the function extraction process, they attained an accuracy of 99.92%. It has been argued that FUSI-CAD is the confluence of handcrafted and deep-element components [61]. This was accomplished via the use of a textual handmade feature known as the discrete wavelet transform (DGT) and a handcrafted mathematical feature known as the grey-level co-occurrence matrix (GLCM). After combining these characteristics with automated features and comparing their model to the CT Dataset, they were able to achieve a 99% accuracy rate. According to their methodology, both its sensitivity and accuracy are 99%, which indicates that it is a reliable model [62]. The reason for the difficulty in identification was investigated, and it was determined that it was caused by function generalization. They suggest a model that mixes handmade characteristics with some automated features to get a more comprehensive generalization of features. According to their results, their technique exceeds other approaches in terms of performance.

Using x-ray images, Hussain et al. [63] COVID-19 have a variety of textural elements that have been recovered. They classified these features using a variety of artificial intelligence methods and attained an accuracy rate of 79.52%. Ozturk et al. [64] It has been established that the quantity of data available for COVID-19 is inadequate to train CNN models adequately, leading to the usage of handmade features for detection by the researchers. They were able to extract a variety of characteristics from chest x-ray and CT images, including GLCM, GLRLM, DFTA, and LBGCM. These characteristics were pooled, and principal component analysis (PCA) was applied to minimize the number of characteristics. They put their model through its paces using a dataset gathered locally and discovered that it was 86.54% accurate.

Kang et al. [65] Using CT scans, we extracted a variety of handmade features and employed latent representation to reflect the properties of the individual features, so assuring class separation. They give labels depending on the presence of COVID-19 infection as well as other pneumonia, allowing for even more precise identification. The model developed by the researchers is trustworthy, resistant to overfitting, and outperforms other strategies in the real world. Elazir et al. [66] detection of COVID-19 was accomplished by using orthogonal momentum characteristics extracted from

chest x-ray images. They proposed FrMeMs, a new function descriptor for extracting COVID19 characteristics that were developed by them. A strategy for increasing the performance of numerical operations was also proposed by the authors. In addition to this, a technique for feature reduction is also proposed in this article. It is estimated that they are accurate to within 0.1% of the true value.

2.2.2 Deep Features

Deep features, which were initially defined in 2006, are automatically retrieved features from deep convolutional layers. Because of the way it is designed, it has a layered structure with several levels that are all connected. Each layer completes its feature extraction procedure and transfers the results to another layer that is linked to it through a communication channel. In the medical literature, the use of deep features in medical imaging is rather widespread. VGG-16/VGG-19 [67, 68], AlexNet [67, 69, 70], GoogleNet [32, 71, 72], following are just a few instances of CNN models, which are often trained using the ImageNet dataset.

According to Ankita et al. [73] TB, and pneumonia are with 95% accuracy. Furthermore, they were able to classify COVID-19 and pneumonia from these images using DenseNet-161, which had a 98.9% accuracy rate when it came to classification. Afterwards, they assessed the COVID-19 according to severity, assigning it to one of three categories: moderate, severe, or critical, based on the patient's condition. They were able to determine severity with 76% accuracy when they used the ResNet-18 network. Narin et al. [44], x-ray images were utilized to develop several different deep models. Their dataset consisted of COVID, pneumonia (both bacterial and viral), and stable X-ray images, which were divided into four categories. During the creation of their work, they included images from three separate databases. Dr. Joseph Cohen has made his work available to the public via a GitHub repository. Both the first and second images are from the publicly accessible dataset "ChestX-ray." Finally, "Chest X-Ray Images (Pneumonia)," an open-source dataset from Kaggle, was utilized to complete the analysis. Among all pre-trained networks, Resnet50 has the highest accuracy of 99.7%, according to their testing, which puts it ahead of the competition.

Roberts et al. [74], according to the argument, the current procedures employed on the POCUS dataset, which comprises LUS images, are not stable and cannot be examined visually since they are not steady. As a consequence, using the same dataset, they suggested a deep learning system that was more stable and explainable. Deep models are often trained via the use of analytical risk reduction techniques (ERM). Islam et al. [75], an approach for identifying x-ray images that incorporates deep models and long-term short memory has been presented (LTSM). To extract features from 4575 images from diverse sources, deep CNN models were utilized. In the next step, they classified the data using LSTM, which was built on the characteristics that had been retrieved. They were able to obtain an accuracy rate of 99.4%. Roy et al. [76], a new collection of ultrasound images acquired from Italian clinics and properly annotated for illness intensity levels was provided by the contributors. Within the total

of 58,924 LUS frames in this collection, 5684 of them are labelled. Covid-positive individuals constituted 495 out of 35 patients who had ultrasound video clips taken. To improve the classification and identification of B-lines in LUS images, CsNet, a current deep shallow network, has been suggested. The ultrasound clips obtained from the 400 participants were utilized for training the CsNet neural network. They were successful in achieving an AUC of 0.97 [77].

CoroDet is a novel binary, two, and three classification-based architecture with 22 layers of binary, two, and three classifications. They point out that their model outperforms the results of existing classification algorithms in terms of efficiency and that it may thus assist medical specialists in resolving the problem of test kit scarcity. Specifically, they conducted studies on three different data forms: two binary classes containing healthy images and one with covid images, three classes containing both healthy and covid pneumonia, and four classes that contained images of viral and bacterial pneumonia, as well as covid and healthy images. For binary, two-class, and four-class classifications, accuracy rates of 99.1%, 94.2%, and 91.2%, respectively, are reached [78]. COVIDagnosis Net is an optimized variation of the SqueezeNet Deep Neural Network developed by SqueezeNet. With the addition of Bayesian optimization, the SqueezeNet has been exactly fine-tuned to identify covid-19. Across the board, they earned 98.26% accuracy [79]. To support related tasks, an upgraded COVID-CXNET infrastructure built on a pre-trained CXNet was proposed. They processed their data via a vast public archive as well as on a variety of publicly available databases. The biggest x-ray imaging collection accessible for covid-19 has been combined, according to the researchers. They achieved a precision of 96.72% [80]. An enhanced COVID-CXNET architecture based on a pre-trained CXNet has been suggested to handle related activities. A massive public archive, as well as several publicly accessible databases, were used to process their data. According to the researchers, they have integrated the largest x-ray image collection available for use with covid-19. It took them 96.72% of the time to reach accuracy [81, 82].

2.3 Feature Selection Techniques

A significant amount of work must be invested in deciding which features are the most beneficial. By choosing just a subset of the original features, the algorithm's efficiency and accuracy are not affected; instead, poor, noisy, and volatile features are removed or cut out when selecting acceptable features, and the algorithm's efficiency and accuracy are not jeopardized. The result is that neural networks are used to deal with both high and low relevance of attributes, and generalization has been improved as a result of this. There are five primary kinds of feature selection approaches, which are referred to as Non-Linear Method [83], Filter-Based Method [41], Wrapper Method [84], and Embedded Method [84]. The linear method may include the PCA, LDA [85], and MCIA [86] algorithms. The non-linear method includes the GA [87, 88], PSO [89], Atom [89], and LEM. The filter method contains mRMR [90], CFS [4]. The

wrapper method comprises like Boruta [91] and Jackstraw [3]. And the embedded method like LASSO [92], Elastic [93], Ridge.

The Hyper Learning Binary Dragonfly Algorithm (HLBDA) is a unique algorithm for finding the best subset of characteristics for a particular classification task that is discussed here. An improved variant of the Binary Dragonfly Algorithm (BDA), the Hyper Learning Dragonfly Algorithm (HLBDA), employs a hyper learning method to aid the algorithm in escaping local optima and improving searching behaviour [94]. The suggested approach is applied to a dataset of coronavirus illness (COVID-19), which is included. The findings reveal that HLBDA is better in terms of enhancing classification accuracy while simultaneously decreasing the number of chosen characteristics. Automatic X-ray and CT image diagnostic and detection technologies have emerged. This work used three CNN models and three classes of X-ray images to develop a high-performance detection system (COVID-19, Normal, Pneumonia). Among the feature selection approaches, the PSO and ACO algorithms' results were compared. The findings were achieved using SVM and a k-NN classifier with tenfold cross-validation. The SVM method without feature selection has the greatest overall accuracy of 99.83%. The SVM + PSO approach obtained 99.86% performance after feature selection [95].

2.4 Classification

To identify which category of an item belongs to which class, classification must be performed. The use of Boltzmann machines and convolutional neural networks as autoencoders and decoders in automated classification is essential for achieving high accuracy in the process. The use of deep learning-based techniques for image and object identification and classification is addressed in detail [96]. Since the disease's development, a large number of studies have employed classifier-based approaches to identify COVID-19 using a variety of imaging modalities, including CT images, ultrasound images, and chest x-ray images. Several studies had shown that ultrasonic images performed much better than other imaging modalities when it came to categorization [97].

Based on an adaptive lead random forest classifier, a feature selection strategy for discriminating covid-19 images from pneumonia images was presented. Given the limited amount of data available for covid imaging, the covid CT and pneumonia CT characteristics are startlingly comparable. It was proposed as a consequence that adaptive characteristics should be used instead of location-specific features since location-specific features would not be able to distinguish between covid and pneumonia with sufficient accuracy. A total of 1495 verified COVID-19 images were obtained from several area hospitals, with 1027 of those images being pneumonia-related. According to the data, this strategy outperforms the other four benchmark approaches in terms of producing better outcomes [31]. The [98] convolutional support vector machine (CSVM) classifier combines the support vector machine (SVM) classifier with convolutional neural networks (CSVM). Smaller datasets are

described in more detail, which increases the accuracy of the results. CSVM should be used for the grouping of COVID-19. They put their model through its paces on CT scans and discovered that it was 94.03% accurate [99]. It was suggested to use decision trees to build a deep classifier. Three different tree classifiers, each with a unique attribute, make up this classifier system. To discriminate between stable and contaminated X-ray images, the first tree uses binary classification. Two trees discriminate between tuberculosis and natural chest x-ray images, while a third tree distinguishes between stable chest x-ray images and covid-19 contaminated chest x-ray images, with the second tree distinguishing between tuberculosis and natural chest x-ray images. They were successful in achieving a 95% accuracy rate. Furthermore, they suggested that this model may be used to assess suspected individuals before to doing PCR investigations on them [100].

A multi-task learning model, a deep learning algorithm, and a multi-layer perceptron were all utilized in the research. Various forms of data are included into MTL to increase performance and generalization. To differentiate between COVID and non-COVID lesions and to segment the infected and non-infected regions of the lesions, the authors employed MTL to discriminate between the two types of lesions [101]. Experts in ultrasonography from across the globe were consulted to corroborate their categorization results. They started from the ground up and compared it to eight other well-known deep models to define covid-19 using LUS images, which they found to be lacking [102]. They found, on the other hand, that Xception surpasses all other models, and they confirmed their results with human experts. They employed several classifiers to make the identification. Besides that, they demonstrated their results using Grad-Cam to better explain their findings. A second step is to rebuild the image to improve feature representation. LUS images are tough to assess by a human specialist since they are quite comparable to COVID or non-COVID images as well. Given the seriousness of the COVID-19 situation, we cannot rely only on computers to solve the problem. It follows as a result that the veracity of the categorization results is critical in the diagnostic procedure.

The use of an unsupervised technique was suggested for the localization of pleural lines in the LUS. Their suggested technique is based on the Markov model, and they used the Viterbi algorithm to put it into practice. Following the process of localization, they utilized an SVM classifier for supervised classification, which they trained themselves. The recommended technique will reveal the status of a person's lung health based on the state of the pleural lines that have been drawn. When the data gathered by Italian hospitals is combined, an average accuracy of 94% is attained on a national scale [103]. In the YOLO target identification system, the DenseNet model was utilized as a classifier for the COVID-19 x-ray dataset, which was trained using the DenseNet model. When dealing with two-class data, they acquired an accuracy of 98.08%, and when dealing with three-class data, they obtained an accuracy of 87.02% [104]. To illustrate that owing to the disease's novelty, there is less information accessible, hospitals must share patient information, but they must place a high priority on data security. The authors use federated learning, which assists hospitals in collecting practice data, and then disseminate the learnt model across a public network utilizing blockchain technology, which maintains the confidentiality

Table 1 A summary of public databases

References	Type	Dataset size
Cohen et al. [106]	CT + X-Ray images	125 images
Hussain et al. [78]	X-ray images	2843 images
Born et al. [107]	Ultrasound images	235 images
Horry et al. [108]	Ultrasound images	235 images
Shan et al. [109]	CT images	249 images
Kumar et al. [110]	CT Images	340,006 images
Ma et al. [111]	CT images	20 annotated images
Yang et al. [112]	CT Images	225 images
Wu et al. [7]	CT Images	453 images

of patient information. Using the most recent data from hospitals, they evaluated multiple deep models and determined that the capsule network classifier surpassed the competition. They also offer CC-19, a new dataset for novel coronaviruses that has 34,006 CT scans from 89 different persons and is intended to aid in the detection of novel coronaviruses [105].

3 Dataset's Description

It is necessary to have image datasets to run the learning algorithms and models, which are subsequently employed for covid-19 categorization. These datasets may be gathered from the chests of infected individuals in several ways and a variety of modalities. Since the disorder is new, only a limited amount of the evidence is publicly available. When compared to other imaging modalities, the lung ultrasound dataset is far less extensive. It is more probable that the model will be overfitted when there are fewer dataset images available, resulting in inaccurate classification conclusions when there are fewer data images available. For categorization reasons, several studies employed locally gathered data, while others used data augmentation procedures to increase the amount of data available (Table 1).

4 Performance Evaluation Measures

The examination of COVID-19 results is a crucial activity that assists in the diagnosis and treatment of illnesses and disorders. The legitimacy of the offered models is verified via the use of quality tests. The confusion matrix, which is comprised of four possible outcomes, is the most often used technique of assessing findings in the scientific community [98, 113]. TP represents a positive instance of test data

Table 2 Performance evaluation metrics

Performance measures	Evaluation
Accuracy	$\frac{TP+TN}{TP+TN+FP+FN}$
Precision	$\frac{TP}{TP+FP}$
Sensitivity/recall	$\frac{TP}{TP+FN}$
Specificity	$\frac{TN}{TN+FP}$
F1-score	$\frac{2 \times \text{precision} \times \text{sensitivity}}{\text{precision} + \text{sensitivity}}$

that has been successfully classified by a selected classifier; if the positive instance of test data has not been correctly classified, it is labelled False negative (FN). As an example, if the negative instance is correctly identified as negative, it is referred to as True negative (TN), as opposed to False positive (FP), which is the opposite of True negative (FP). The suggested system's performance will be assessed in terms of specificity, sensitivity, precision, and accuracy, among other characteristics. Precision is defined as the proportion of accurately labelled predicted values to the total number of pixels in Table 2. As stated by the Statistical Computing Centre, precision is the number of properly predicted values divided by the total number of positive anticipated values [18, 114]. A measure of sensitivity is the proportion of true positives in a set of measured data, while specificity is the proportion of genuine negatives. The F1 score is calculated as the harmonic mean of accuracy and sensitivity ratings, or as the biased total of the two evaluations [13, 115]. In addition, there is a ROC parameter that is extensively utilized. When calculating AUC, it is helpful to see the relationship between sensitivity and false-positive rate as a graph. Several important performance metrics used in the assessment of the COVID classification are included in Table 2, along with their mathematical formulations, as follows:

5 Conclusion

Chest radiography images play a significant role in the automated diagnosis of covid-19, which is performed via a variety of machine learning algorithms. This research will investigate prognostic models for COVID-19 patients' survival prediction based on clinical data and lung/lesion radiomic features acquired from chest imaging to improve survival prognosis. However, although it seems that there are a variety of early signs of prognosis, we will examine prognostic models or scoring systems that are only beneficial to those who have gotten confirmation of their cancer diagnosis. This article describes some of the research work and methodologies based on machine learning and computer vision that have been employed for the detection of covid-19 and a discussion of the future directions of the field. Some tactics based on pre-processing, segmentation, handcrafted features, deep features, classification, and some other approaches have been described, as well as some additional techniques not before mentioned. The report also includes some valuable data sets and a list of

research gaps and issues in the relevant industry that have been discovered, all of which will be beneficial for future research efforts.

Funding No specific funding received for this research.

Declaration Authors declare no conflict for this research.

References

1. Khan, M.A., Kadry, S., Zhang, Y.D., Akram, T., Sharif, M., Rehman, A., Saba, T.: Prediction of COVID-19-pneumonia based on selected deep features and one class kernel extreme learning machine. *Comput. Electr. Eng.* **90**, 106960 (2021)
2. Saba, T., Khan, A.R. (eds.): Intelligent Computing Applications for COVID-19: Predictions, Diagnosis, and Prevention. CRC Press (2021)
3. Khan, M.Z., Khan, M.U.G., Saba, T., Razzak, I., Rehman, A., Bahaj, S.A.: Hot-spot zone detection to tackle COVID19 spread by fusing the traditional machine learning and deep learning approaches of computer vision. *IEEE Access* **9**, 100040–100049 (2021)
4. Amin, J., Anjum, M.A., Sharif, M., Saba, T., Tariq, U.: An intelligence design for detection and classification of COVID19 using fusion of classical and convolutional neural network and improved microscopic features selection approach. *Microsc. Res. Tech.* (2021). <https://doi.org/10.1002/jemt.23779>
5. Haimed, A.M.A., Saba, T., Albasha, A., Rehman, A., Kolivand, M.: Viral reverse engineering using Artificial Intelligence and big data COVID-19 infection with long short-term memory (LSTM). *Environ. Technol. Innov.* **22**, 1–20 (2021)
6. Saba, T., Abunadi, I., Shahzad, M.N., Khan, A.R.: Machine learning techniques to detect and forecast the daily total COVID-19 infected and deaths cases under different lockdown types. *Microsc. Res. Tech.* **84**(7), 1462–1474 (2021)
7. Wang, W., et al.: Detection of SARS-CoV-2 in different types of clinical specimens. *JAMA* **323**(18), 1843–1844 (2020)
8. Rehman, A., Sadad, T., Saba, T., Hussain A., Tariq, U.: Real-time diagnosis system of COVID-19 using X-ray images and deep learning. *IEEE IT Prof.* **23**(4), 57–62 (2021). <https://doi.org/10.1109/MITP.2020.3042379>
9. Iqbal, S., Khan, M.U.G., Saba, T., Mehmood, Z., Javaid, N., Rehman, A., Abbasi, R.: Deep learning model integrating features and novel classifiers fusion for brain tumor segmentation. *Microsc. Res. Tech.* **82**(8), 1302–1315 (2019). <https://doi.org/10.1002/jemt.23281>
10. Nawaz, M., Mehmood, Z., Nazir, T., Naqvi, R.A., Rehman, A., Iqbal, M., Saba, T.: Skin cancer detection from dermoscopic images using deep learning and fuzzy k-means clustering. *Microsc. Res. Tech.* **85**(1), 339–351 (2022)
11. Bhattacharyya, A., Bhaik, D., Kumar, S., Thakur, P., Sharma, R., Pachori, R.B.: A deep learning based approach for automatic detection of COVID-19 cases using chest X-ray images. *Biomed. Signal Process. Control* **71**, 103182 (2022)
12. Rehman, A., Khan, M.A., Saba, T., Mehmood, Z., Tariq, U., Ayesha, N.: Microscopic brain tumor detection and classification using 3D CNN and feature selection architecture. *Microsc. Res. Tech.* **84**(1), 133–149 (2021a). <https://doi.org/10.1002/jemt.23597>
13. Jamal, A., Hazim Alkawaz, M., Rehman, A., Saba, T.: Retinal imaging analysis based on vessel detection. *Microsc. Res. Tech.* **80**(7), 799–811 (2017)
14. Chakraborty, S., Paul, S., Hasan, K.: A Transfer learning-based approach with deep CNN for COVID-19-and pneumonia-affected chest X-ray image classification. *SN Comput. Sci.* **3**(1), 1–10 (2022)

15. Chen, D., et al.: Can chest CT features distinguish patients with negative from those with positive initial RT-PCR results for coronavirus disease (COVID-19)? *Am. J. Roentgenol.* **216**(1), 66–70 (2021)
16. Malhotra, A., et al.: Multi-task driven explainable diagnosis of COVID-19 using chest X-ray images. *Pattern Recogn.* **122**, 108243 (2022)
17. Iftikhar, S., Fatima, K., Rehman, A., Almazyad, A.S., Saba, T.: An evolution based hybrid approach for heart diseases classification and associated risk factors identification. *Biomed. Res.* **28**(8), 3451–3455 (2017)
18. Saba, T., Haseeb, K., Ahmed, I., Rehman, A.: Secure and energy-efficient framework using internet of medical things for e-healthcare. *J. Infect. Public Health* **13**(10), 1567–1575 (2020)
19. Sadad, T., Munir, A., Saba, T., Hussain, A.: Fuzzy C-means and region growing based classification of tumor from mammograms using hybrid texture feature. *J. Comput. Sci.* **29**, 34–45 (2018)
20. Rashid, M., Khan, M.A., Alhaisoni, M., Wang, S.H., Naqvi, S.R., Rehman, A., Saba, T.: A sustainable deep learning framework for object recognition using multi-layers deep features fusion and selection. *Sustainability* **12**(12), 5037 (2020)
21. Rehman, A., Saba, T., Tariq, U., Ayesha, N.: Deep learning-based COVID-19 detection using CT and X-ray images: current analytics and comparisons. *IT Professional* **23**(3), 63–68 (2021)
22. Saba, T., Rehman, A., Mehmood, Z., Kolivand, H., Sharif, M.: Image enhancement and segmentation techniques for detection of knee joint diseases: a survey. *Curr. Med. Imaging Rev.* **14**(5), 704–715 (2018a). <https://doi.org/10.2174/1573405613666170912164546>
23. Yousaf, K., Mehmood, Z., Saba, T., Rehman, A., Munshi, A.M., Alharbey, R., Rashid, M.: Mobile-health applications for the efficient delivery of health care facility to people with dementia (PwD) and support to their carers: A survey. *Biomed. Res. Int.* **2019**, 1–26 (2019)
24. Rahim, M.S.M., Norouzi, A., Rehman, A., Saba, T.: 3D bones segmentation based on CT images visualization. *Biomed. Res.* **28**(8), 3641–3644 (2017)
25. Abbas, N., Saba, T., Mohamad, D., Rehman, A., Almazyad, A.S., Al-Ghamdi, J.S.: Machine aided malaria parasitemia detection in Giemsa-stained thin blood smears. *Neural Comput. Appl.* **29**(3), 803–818 (2018)
26. Khan, M.A., Sharif, M.I., Raza, M., Anjum, A., Saba, T., Shad, S.A.: Skin lesion segmentation and classification: A unified framework of deep neural network features fusion and selection. *Expert Syst. e12497* (2019)
27. Saba, T., Bokhari, S.T.F., Sharif, M., Yasmin, M., Raza, M.: Fundus image classification methods for the detection of glaucoma: A review. *Microsc. Res. Tech.* (2018). <https://doi.org/10.1002/jemt.23094>
28. Mitchell, H.B.: *Image Fusion: Theories, Techniques and Applications*. Springer Science & Business Media (2010)
29. Nazir, M., Khan, M.A., Saba, T., Rehman, A.: Brain tumor detection from MRI images using multi-level wavelets. In: 2019 International Conference on Computer and Information Sciences (ICCIS), pp. 1–5. IEEE (2019, Apr)
30. Hall, E.L., Kruger, R.P., Dwyer, S.J., Hall, D.L., McLaren, R.W., Lodwick, G.S.: A survey of pre-processing and feature extraction techniques for radiographic images. *IEEE Trans. Comput.* **100**(9), 1032–1044 (1971)
31. Mughal, B., Muhammad, N., Sharif, M., Rehman, A., Saba, T.: Removal of pectoral muscle based on topographic map and shape-shifting silhouette. *BMC Cancer* **18**(1), 1–14 (2018)
32. Ullah, H., Saba, T., Islam, N., Abbas, N., Rehman, A., Mehmood, Z., Anjum, A.: An ensemble classification of exudates in color fundus images using an evolutionary algorithm based optimal features selection. *Microsc. Res. Tech.* **82**(4), 361–372 (2019). <https://doi.org/10.1002/jemt.23178>
33. Javed, R., Rahim, M.S.M., Saba, T., Rehman, A.: A comparative study of features selection for skin lesion detection from dermoscopic images. *Netw. Model. Anal. Health Inform. Bioinform.* **9**(1), 1–13 (2020)
34. Rehman, A., Abbas, N., Saba, T., Mehmood, Z., Mahmood, T., Ahmed, K.T.: Microscopic malaria parasitemia diagnosis and grading on benchmark datasets. *Microsc. Res. Tech.* **81**(9), 1042–1058 (2018). <https://doi.org/10.1002/jemt.23071>

35. Saba, T.: Automated lung nodule detection and classification based on multiple classifiers voting. *Microsc. Res. Tech.* **82**(9), 1601–1609 (2019)
36. Amin, J., Sharif, M., Raza, M., Saba, T., Rehman, A.: Brain tumor classification: Feature fusion. In: 2019 International Conference on Computer and Information Sciences (ICCIS), pp. 1–6. IEEE (2019)
37. Ramzan, F., Khan, M.U.G., Iqbal, S., Saba, T., Rehman, A.: Volumetric segmentation of brain regions from MRI scans using 3D convolutional neural networks. *IEEE Access* **8**, 103697–103709 (2020)
38. Perveen, S., Shahbaz, M., Saba, T., Keshavjee, K., Rehman, A., Guergachi, A.: Handling irregularly sampled longitudinal data and prognostic modeling of diabetes using machine learning technique. *IEEE Access* **8**, 21875–21885 (2020)
39. Rehman, A.: Ulcer recognition based on 6-layers deep convolutional neural network. In: Proceedings of the 2020 9th International Conference on Software and Information Engineering (ICSIE), pp. 97–101. Cairo Egypt (2020)
40. Oulefki, A., Agaian, S., Trongtirakul, T., Laouar, A.K.: Automatic COVID-19 lung infected region segmentation and measurement using CT-scans images. *Pattern Recogn.* **114**, 107747 (2021)
41. Rehman, A.: Light microscopic iris classification using ensemble multi-class support vector machine. *Microsc. Res. Tech.* **84**(5), 982–991 (2021)
42. Wang, G., et al.: A noise-robust framework for automatic segmentation of COVID-19 pneumonia lesions from CT images. *IEEE Trans. Med. Imaging* **39**(8), 2653–2663 (2020)
43. Wang, Y., et al.: Does non-COVID-19 lung lesion help? Investigating transferability in COVID-19 CT image segmentation. *Comput. Methods Programs Biomed.* **202**, 106004 (2021)
44. Rehman, A., Abbas, N., Saba, T., Rahman, S.I.U., Mehmood, Z., Kolivand, H.: Classification of acute lymphoblastic Leukemia using deep learning. *Microsc. Res. Tech.* **81**(11), 1310–1317 (2018)
45. Meethongjan, K., Dzulkifli, M., Rehman, A., Altameem, A., Saba, T.: An intelligent fused approach for face recognition. *J. Intell. Syst.* **22**(2), 197–212 (2013). <https://doi.org/10.1515/jisy-2013-0010>
46. Saba, T.: Pixel intensity based cumulative features for moving object tracking (MOT) in darkness. *3D Res.* **7**(10), 1–6 (2016)
47. Alkawaz, M.H., Sulong, G., Saba, T., Rehman, A.: Detection of copy-move image forgery based on discrete cosine transform. *Neural Comput. Appl.* (2016). <https://doi.org/10.1007/s00521-016-2663-3>
48. Alsayyh, M.A.M.Y., Mohamad, D., Saba, T., Rehman, A., AlGhamdi, J.S.: A Novel fused image compression technique using DFT, DWT, and DCT. *J. Inf. Hiding Multimedia Signal Process.* **8**(2), 261–271 (2017)
49. Saba, T., Mohamed, A.S., El-Affendi, M., Amin, J., Sharif, M.: Brain tumor detection using fusion of hand crafted and deep learning features. *Cogn. Syst. Res.* **59**, 221–230 (2020)
50. Saba, T., Sameh, A., Khan, F., Shad, S.A., Sharif, M.: Lung nodule detection based on ensemble of hand crafted and deep features. *J. Med. Syst.* **43**(12), 332 (2019)
51. Khan, M.A., Sharif, M., Akram, T., Raza, M., Saba, T., Rehman, A.: Hand-crafted and deep convolutional neural network features fusion and selection strategy: An application to intelligent human action recognition. *Appl. Soft Comput.* **87**, 105986 (2020). <https://doi.org/10.1016/j.asoc.2019.105986>
52. Sharif, M., Naz, F., Yasmin, M., Shahid, M.A., Rehman, A.: Face recognition: A survey. *J. Eng. Sci. Technol. Rev.* **10**(2), 166–177 (2017)
53. Saba, T., Khan, M.A., Rehman, A., Marie-Sainte, S.L.: Region extraction and classification of skin cancer: A heterogeneous framework of deep CNN features fusion and reduction. *J. Med. Syst.* **43**(9), 289 (2019)
54. Saba, T., Khan, S.U., Islam, N., Abbas, N., Rehman, A., Javaid, N., Anjum, A.: Cloud-based decision support system for the detection and classification of malignant cells in breast cancer using breast cytology images. *Microsc. Res. Tech.* **82**(6), 775–785 (2019)

55. Saba, T.: Computer vision for microscopic skin cancer diagnosis using handcrafted and non-handcrafted features. *Microsc. Res. Tech.* **84**(6), 1272–1283 (2021)
56. Sadad, T., Rehman, A., Munir, A., Saba, T., Tariq, U., Ayesha, N., Abbasi, R.: Brain tumor detection and multi-classification using advanced deep learning techniques. *Microsc. Res. Tech.* **84**(6), 1296–1308 (2021)
57. Khan, A.R., Khan, S., Harouni, M., Abbasi, R., Iqbal, S., Mehmood, Z.: Brain tumor segmentation using K-means clustering and deep learning with synthetic data augmentation for classification. *Microsc. Res. Tech.* **84**(7), 1389–1399 (2021). <https://doi.org/10.1002/jemt.23694>
58. Hasan, M.J., Uddin, J., Pinku, S.N.: A novel modified SFTA approach for feature extraction. In: 2016 3rd International Conference on Electrical Engineering and Information Communication Technology (ICEEICT), pp. 1–5. IEEE (2016)
59. Hasan, M., Khan, N.K., Hridi, N.A., Ontora, F.T.: A novel parallel feature extraction method using HGAPSO and GLCO based SFTA. BRAC University (2016)
60. Gadkari, D.: Image Quality Analysis Using GLCM (2004)
61. Javed, R., Shafry, M., Saba, T., Fati, S.M., Rehman, A., et al.: Statistical histogram decision based contrast categorization of skin lesion datasets dermoscopic images. *Comput. Mater. Continua* **67**(2), 2337–2352 (2021)
62. Das, R., Arshad, M., Manjhi, P., Thepade, S.D.: Covid-19 Identification with chest X-ray images merging handcrafted and automated features for enhanced feature generalization. In: 2020 5th International Conference on Computing, Communication and Security (ICCCS), pp. 1–6 IEEE (2020)
63. Hussain, L., et al.: Machine-learning classification of texture features of portable chest X-ray accurately classifies COVID-19 lung infection. *Biomed. Eng. Online* **19**(1), 1–18 (2020)
64. Özтурk, Ş., Özkaraya, U., Barstuğan, M.: Classification of coronavirus (COVID-19) from X-ray and CT images using shrunken features. *Int. J. Imaging Syst. Technol.* **31**(1), 5–15 (2021)
65. Kang, H., et al.: Diagnosis of coronavirus disease 2019 (covid-19) with structured latent multi-view representation learning. *IEEE Trans. Med. Imaging* **39**(8), 2606–2614 (2020)
66. Elaziz, M.A., Hosny, K.M., Salah, A., Darwish, M.M., Lu, S., Sahlol, A.T.: New machine learning method for image-based diagnosis of COVID-19. *PLoS ONE* **15**(6), e0235187 (2020)
67. Sadad, T., Rehman, A., Hussain, A., Abbasi, A.A., Khan, M.Q.: A review on multi-organs cancer detection using advanced machine learning techniques. *Curr. Med. Imaging* **17**(6), 686–694 (2021)
68. Rehman, A., Yar, H., Ayesha, N., Sadad, T.: Dermoscopy cancer detection and classification using geometric feature based on resource constraints device (Jetson Nano). In: 2020 13th International Conference on Developments in eSystems Engineering (DeSE). IEEE, pp. 412–417 (2020, Dec)
69. Krizhevsky, A., Sutskever, I., Hinton, G.E.: ImageNet classification with deep convolutional neural networks. *Commun. ACM* **60**(6), 84–90 (2017)
70. Iqbal, S., Khan, M.U.G., Saba, T., Rehman, A.: Computer-assisted brain tumor type discrimination using magnetic resonance imaging features. *Biomed. Eng. Lett.* **8**(1), 5–28 (2018)
71. Zhou, B., Lapedriza, A., Khosla, A., Oliva, A., Torralba, A.: Places: A 10 million image database for scene recognition. *IEEE Trans. Pattern Anal. Mach. Intell.* **40**(6), 1452–1464 (2017)
72. Szegedy, C. et al.: Going deeper with convolutions. In: Proceedings of the IEEE Conference on Computer Vision and Pattern Recognition, pp. 1–9 (2015)
73. Rehman, A., Abbas, N., Saba, T., Mahmood, T., Kolivand, H.: Rouleaux red blood cells splitting in microscopic thin blood smear images via local maxima, circles drawing, and mapping with original RBCs. *Microsc. Res. Tech.* **81**(7), 737–744 (2018)
74. Roberts, J., Tsiligiannis, T.: Ultrasound diagnosis of COVID-19: Robustness and explainability. [arXiv:2012.01145](https://arxiv.org/abs/2012.01145) [cs, eess], 30 Nov 2020 (2020)
75. Islam, M.Z., Islam, M.M., Asraf, A.: A combined deep CNN-LSTM network for the detection of novel coronavirus (COVID-19) using X-ray images. (In en): Informatics in Medicine Unlocked, vol. 20, p. 100412, 2020 (2020). <https://doi.org/10.1016/j.imu.2020.100412>

76. Roy, S. et al.: Deep learning for classification and localization of COVID-19 markers in point-of-care lung ultrasound. *IEEE Trans. Med. Imaging* **39**(8), 2676–2687, Aug 2020 (2020). <https://doi.org/10.1109/TMI.2020.2994459>
77. Balloescu, C. et al.: Automated lung ultrasound B-line assessment using a deep learning algorithm. *IEEE Trans. Ultrason. Ferroelectr. Freq. Control* **67**(11), 2312–2320, Nov 2020 (2020). <https://doi.org/10.1109/TUFFC.2020.3002249>
78. Hussain, E. et al.: CoroDet: A Deep Learning Based Classification for COVID-19 Detection Using Chest X-ray Images, vol. 142, p. 110495 (2021)
79. Ucar, F., Korkmaz, D.: COVIDagnosis-Net: Deep Bayes-SqueezeNet based diagnosis of the coronavirus disease 2019 (COVID-19) from X-ray images. (In en), *Medical Hypotheses*, vol. 140, p. 109761, July, 2020 (2020). <https://doi.org/10.1016/j.mehy.2020.109761>
80. Haghani, A., Majdabadi, M.M., Choi, Y., Deivalakshmi, S., Ko, S.: COVID-CXNet: Detecting COVID-19 in Frontal Chest X-ray Images Using Deep Learning. *arXiv:2006.13807* [cs, eess], 28 July 2020 (2020)
81. Wang, Z., Liu, Q., Dou, Q.: Contrastive Cross-Site Learning With Redesigned Net for COVID-19 CT Classification. *IEEE J. Biomed. Health Inf.* **24**(10), 2806–2813, Oct 2020 (2020). <https://doi.org/10.1109/JBHI.2020.3023246>
82. Khan, A.I., Shah, J.L., Bhat, M.M.: CoroNet: A deep neural network for detection and diagnosis of COVID-19 from chest x-ray images. (In en), *Computer Methods and Programs in Biomedicine*, vol. 196, p. 105581, Nov 2020 (2020). <https://doi.org/10.1016/j.cmpb.2020.105581>
83. Saleem, S., Usman, M., Saba, T., Abunadi, I., Rehman, A., et al.: Efficient facial recognition authentication using edge and density variant sketch generator. *CMC-Comput. Mater. Continua* **70**(1), 505–521 (2022)
84. Hassan, S.A., Akbar, S., Rehman, A., Saba, T., Kolivand, H., Bahaj, S.A.: Recent developments in detection of central serous retinopathy through imaging and artificial intelligence techniques—A review, *IEEE Access* (2021)
85. Iqbal, S., Siddiqui, G.F., Rehman, A., Hussain, L., Saba, T., Tariq, U., Abbasi, A.A.: Prostate cancer detection using deep learning and traditional techniques. *IEEE Access* **9**, 27085–27100 (2021)
86. Meng, C., Kuster, B., Culhane, A.C., Gholami, A.M.: A multivariate approach to the integration of multi-omics datasets. *BMC Bioinf.* **15**(1), 1–13 (2014)
87. Too, J., Abdullah, A.R.: A new and fast rival genetic algorithm for feature selection. *J. Supercomput.* **77**(3), 2844–2874 (2021)
88. Too, J., Abdullah, A.R., Mohd Saad, N., Tee, W.: Emg feature selection and classification using a pbest-guide binary particle swarm optimization. *Computation* **7**(1), 12 (2019)
89. Shahzad, M.N., Ali, H., Saba, T., Rehman, A., Kolivand, H., Bahaj, S.A.: Identifying patients with PTSD utilizing resting-state fMRI data and neural network approach. *IEEE Access* **9**, 107941–107954 (2021)
90. De Jay, N., Papillon-Cavanagh, S., Olsen, C., El-Hachem, N., Bontempi, G., Haibe-Kains, B.: mRMRe: an R package for parallelized mRMR ensemble feature selection. *Bioinformatics* **29**(18), 2365–2368 (2013)
91. Amin, J., Anjum, M.A., Sharif, M., Rehman, A., Saba, T., Zahra, R.: Microscopic segmentation and classification of COVID-19 infection with ensemble convolutional neural network. *Microsc. Res. Tech.* (2021). <https://doi.org/10.1002/jemt.23913>
92. Fonti, V., Belitsser, E.: Feature selection using lasso. *VU Amsterdam Res. Paper Bus. Anal.* **30**, 1–25 (2017)
93. Sajjad, M., Ramzan, F., Khan, M.U.G., Rehman, A., Kolivand, M., Fati, S.M., Bahaj, S.A.: Deep convolutional generative adversarial network for Alzheimer's disease classification using positron emission tomography (PET) and synthetic data augmentation. *Microsc. Res. Tech.* **84**(12), 3023–3034 (2021)
94. Yousaf, K., Mehmood, Z., Awan, I.A., Saba, T., Alharbey, R., Qadah, T., Alridge, M.A.: A comprehensive study of mobile-health based assistive technology for the healthcare of dementia and Alzheimer's disease (AD). *Health Care Manag. Sci.* 1–23 (2019)

95. Durbhaka, G.K., Selvaraj, B., Mittal, M., Saba, T., Rehman, A., Goyal, L.M.: Swarm-LSTM: Condition monitoring of gearbox fault diagnosis based on hybrid LSTM deep neural network optimized by swarm intelligence algorithms. *CMC-Comput. Mater. Continua* **66**(2), 2041–2059 (2021)
96. Husham, A., Hazim Alkawaz, M., Saba, T., Rehman, A., Saleh Alghamdi, J.: Automated nuclei segmentation of malignant using level sets. *Microsc. Res. Tech.* **79**(10), 993–997 (2016)
97. Mughal, B., Sharif, M., Muhammad, N., Saba, T.: A novel classification scheme to decline the mortality rate among women due to breast tumor. *Microsc. Res. Tech.* **81**(2), 171–180 (2018)
98. Fahad, H.M., Ghani Khan, M.U., Saba, T., Rehman, A., Iqbal, S.: Microscopic abnormality classification of cardiac murmurs using ANFIS and HMM. *Microsc. Res. Tech.* **81**(5), 449–457 (2018)
99. Özkaya, U., Öztürk, Ş., Budak, S., Melgani, F., Polat, K.: Classification of COVID-19 in Chest CT Images using Convolutional Support Vector Machines. [arXiv:2011.05746](https://arxiv.org/abs/2011.05746) [cs, eess], 11 Nov 2020 (2020)
100. Yoo, S.H., et al.: Deep learning-based decision-tree classifier for COVID-19 diagnosis from chest X-ray imaging. *Front. Med.* **7**, 427 (14 July 2020) <https://doi.org/10.3389/fmed.2020.00427>
101. Amyar, A., Modzelewski, R., Li, H., Ruan, S.: Multi-task deep learning based CT imaging analysis for COVID-19 pneumonia: Classification and segmentation. *Comput. Biol. Med.* **126**, 104037 (2020)
102. Arntfield, R. et al.: Development of a deep learning classifier to accurately distinguish COVID-19 from look-a-like pathology on lung ultrasound. *Respir. Med.*, preprint (15 Oct 2020). Accessed: 01 Dec 2020, 17:08:42
103. Carrer, L., et al., Automatic pleural line extraction and COVID-19 scoring from lung ultrasound data. *IEEE Trans. Ultrason. Ferroelectr. Freq. Control.* **67**(11), 2207–2217, Nov 2020 (2020) <https://doi.org/10.1109/TUFFC.2020.3005512>
104. Ozturk, T., Talo, M., Yildirim, E.A., Baloglu, U.B., Yildirim, O., Rajendra Acharya, U.: Automated detection of COVID-19 cases using deep neural networks with X-ray images. (In en), *Computers in Biology and Medicine*, vol. 121, p. 103792, June 2020 (2020). <https://doi.org/10.1016/j.combiomed.2020.103792>
105. Kumar, R., et al.: Blockchain-Federated-Learning and Deep Learning Models for COVID-19 Detection Using CT Imaging. [arXiv:2007.06537](https://arxiv.org/abs/2007.06537) [cs, eess], 10 July 2020 (2020)
106. Cohen, J.P., Morrison, P., Dao, L.: COVID-19 Image Data Collection. [arXiv:2003.11597](https://arxiv.org/abs/2003.11597) [cs, eess, q-bio], 25 Mar 2020 (2020)
107. Born, J., et al.: POCOVID-Net: Automatic Detection of COVID-19 from a New Lung Ultrasound Imaging Dataset (POCUS) (2020)
108. Horry, M.J., et al.: COVID-19 Detection through transfer learning using multimodal imaging data. *IEEE Access* **8**, 149808–149824 (2020). <https://doi.org/10.1109/ACCESS.2020.3016780>
109. Shan, F., et al.: Lung Infection Quantification of COVID-19 in CT Images with Deep Learning (2020)
110. Kumar, R. et al.: Blockchain-Federated-Learning and deep Learning Models for COVID-19 Detection Using CT imaging (2020)
111. Ma, J., et al.: Towards Data-Efficient Learning: A Benchmark for COVID-19 CT Lung and Infection Segmentation (2020)
112. X. Yang, X. He, J. Zhao, Y. Zhang, S. Zhang, P. Xie, COVID-CT-Dataset: A CT Scan Dataset about COVID-19. [arXiv:2003.13865](https://arxiv.org/abs/2003.13865) [cs, eess, stat], 17 June 2020 (2020)
113. Ahmad, A.M., Sulong, G., Rehman, A., Alkawaz, M.H., Saba, T.: Data hiding based on improved exploiting modification direction method and Huffman coding. *J. Intell. Syst.* **23**(4), 451–459 (2014)
114. Khan, S.A., Nazir, M., Khan, M.A., Saba, T., Javed, K., Rehman, A., et al.: Lungs nodule detection framework from computed tomography images using support vector machine. *Microsc. Res. Tech.* **82**(8), 1256–1266 (2019)

115. Soleimanizadeh, S., Mohamad, D., Saba, T., Rehman, A.: Recognition of partially occluded objects based on the three different color spaces (RGB, YCbCr, HSV). *3D Res.* **6**(3), 1–10 (2015)

An Accurate Skin Lesion Classification Using Fused Pigmented Deep Feature Extraction Method



Rabia Javed, Mohd Shafry Mohd Rahim, Tanzila Saba, Gul Sahar, and Mazhar Javed Awan

Abstract Melanoma is one of the riskiest diseases that extensively influence the quality of life and can be dangerous or even fatal. Skin lesion classification methods faced challenges in varying scenarios. The available hand-crafted features could not generate better results when the skin lesion images contain low contrast, under and over-segmented images. The hand-crafted features for skin lesions did not discriminate well between the two significantly different densities. The pigmented network feature vector and deep feature vector have been fused using a parallel fusion method to increase classification accuracy. This optimized fused feature vector has been fed to machine learning classifiers that accurately classify the dermoscopic images into two categories as benign and malignant melanoma. The statistical performance measures were used to assess the proposed fused feature vector on three skin lesion datasets (ISBI 2016, ISIC 2017, and PH2). The proposed fused feature vector accurately classified the skin lesion with the highest accuracy of 99.8% for the ISBI 2016, an

R. Javed (✉) · M. Shafry Mohd Rahim

School of Computing, Faculty of Engineering, Universiti Teknologi Malaysia, 81310 Skudai, Johor Bahru, CO, Malaysia

e-mail: javed.rabia@graduate.utm.my

M. Shafry Mohd Rahim

e-mail: shafry@utm.my

R. Javed

Department of Computer Science, Lahore College for Women University, Lahore 54000, CO, Pakistan

T. Saba

College of Computing and Information Sciences, Prince Sultan University, Riyadh 11586, CO, Saudi Arabia

G. Sahar

Department of Software Engineering, University of Management and Technology, Lahore, Pakistan

e-mail: gulsahar@kiu.edu.pk

M. Javed Awan

Department of Computer Sciences, Karakoram International University, Gilgit-Baltistan 15100, Pakistan

e-mail: mazhar.awan@umt.edu.pk

accuracy of 99.3% for the ISIC 2017 dataset, 98.6% for the PH2 dataset. Moreover, a comparative analysis has been conducted between the proposed methods and the current methods. In the conclusion, the objectives of this research feature extraction methods performed better than existing methods.

Keywords Deep network · Pigmented network features · Lesion classification · Health risks and Health care

1 Introduction

The classification of skin lesions plays a crucial role in the diagnosis of various local and gene-related medical conditions in dermoscopy. The estimation of these biomarkers provides contain insights while concurrently detecting cancerous cells and classifying the lesion as either benign or malignant. Skin cancer is one of the deadliest diseases for human beings. For physicians, the investigation of these lesions is time-consuming due to the high similarity between melanoma and benign lesions. The automated classification of skin lesions will assist in saving efforts, time spent, and human lives. The accurate detection of melanoma and high classification rates are essential in the early detection of skin cancer. Without computer-based assistance, the clinical diagnosis accuracy for melanoma detection was reported to be between 65 and 80% [1]. The use of dermoscopic images improved skin lesions diagnostic accuracy by 49% [2]. However, the visual differences between melanoma and benign skin lesion can be very subtle, making it difficult to distinguish between the two cases, even for trained medical experts. Figure 1 shows samples of dermoscopic images of benign and malignant melanoma. For the reasons described above, an intelligent medical imaging-based skin lesion diagnosis system can be a welcome tool to assist a physician in the classification of skin lesion. In this research, there is a lesions classification problem, namely: determining whether a dermoscopic image contained a melanoma skin lesion or a benign lesion. Among the most significant challenges for lesion classification after the segmentation process was to choose the most minor and most prominent feature sets, which provide tremendous output in terms of accuracy, complexity, and performance. Generally, melanoma diagnosis performance is directly proportional to the meaningful feature's extraction from the dermoscopic image. The characteristics of a mole/lesion that appear in the skin are utilized to distinguish between benign and melanoma cells. A mole has various features such as shape, color, texture/pattern, border, and others. Thus, myriad lesion features can be extracted from the dermoscopic image. Therefore, the features are crucially essential to differentiate between benign and malignant melanoma. Various features such as hand-crafted, pattern, clinical and deep learning were used to increase the accuracy of melanoma detection. All these features can classify the lesion, but their accuracy is not very promising. Furthermore, current feature extraction methods may be influenced by background complications and are dependent on lesion size and color when extracting lesion features. Although several of the existing studies have joined the

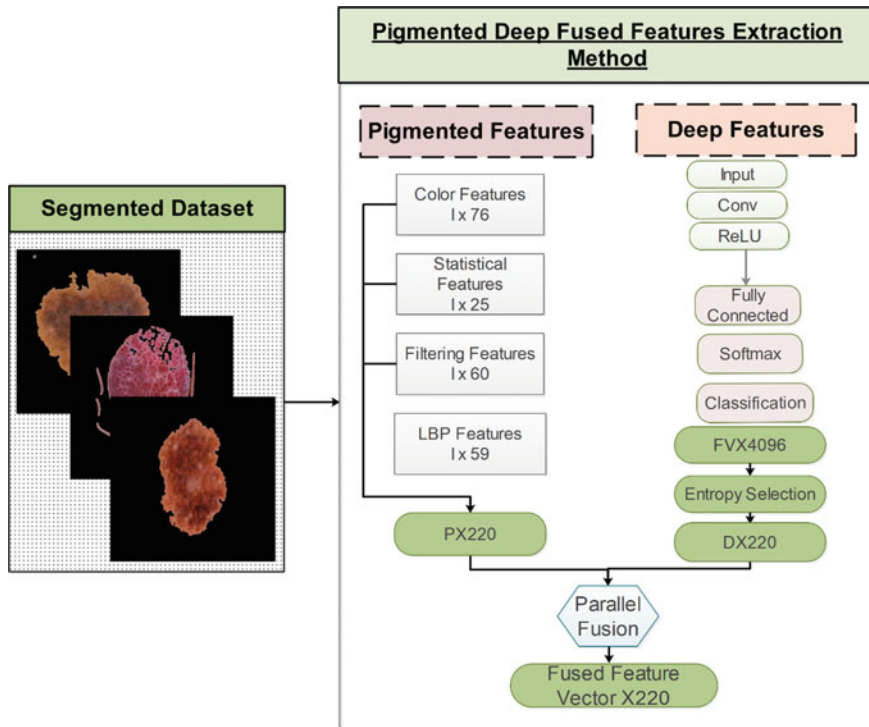


Fig. 1 An overall process of the proposed method (PDFFEM)

different features to increase lesion classification accuracy, these feature extraction methods are still restricted to spatial data and quantization properties. This paper describes the proposed method of lesion features extraction, namely the ‘pigmented deep fused features extraction method (PDFFEM)’ to overcome the limitations of existing methods. Numerous dermoscopic features were used for skin lesion classification, but pigmented network features were selected because these are more specific for lesion classification that segregates the lesions into melanoma and benign.

This article comprises several subsections where Sect. 2 presents the literature of lesion features extraction methods. Section 3 describes the proposed method of lesion features extraction, followed by Sect. 3 explaining the skin lesion classification. Section 4 presents the experimental results of three datasets in detail, which are the ISBI 2016, the ISIC 2017 and the PH2. Section 5 describes the evaluation and discussion of the results of the proposed and existing methods and lastly, a summary of this study is given in Sect. 6 under ‘Discussion’.

2 Literature Review

In the digital image processing field of study, the majority of researchers have addressed the hand-crafted image features such as color, shape, texture, and border for the diagnosis of melanoma [3, 4]. Typically, hand-crafted image features work efficiently on small-scale datasets [5]. In the past, hand-crafted features gave minimal aspects of the lesion, and it was noted that these features required a very complex computational model. Furthermore, hand-crafted image features have several harmful elements; for example, these extracted features are low-level features that are not suitable for the accurate detection of the lesion's characteristics. Conversely, it is noted that minor existing works address deep learning features and dermoscopic features [6, 7]. The computational power of deep learning algorithms is very advanced and deals with a large dataset [8]. Hence, this situation demanded a more efficient feature extraction method. Consequently, the beneficial potential of the deep learning method is evident, and there is the prospect to create feature fusion with dermoscopic image features to improve classification performance. However, there is no established and effective list or collection of features for skin lesion segmentation and melanoma categorization in the literature. Diverse data sets include a variety of pictures as a consequence of the fact that distinct features produced inconsistent findings in other datasets. A comparison of hand-crafted features versus deep learning was conducted in 2016. The experiment demonstrated that hand-crafted features outperformed deep learning features in terms of accuracy, but only on a limited number of datasets [9]. Additionally, the authors found that high-level features (asymmetric, border, color, and texture) yielded more accurate findings, with a sensitivity of 92% and specificity of 95% on 206 datasets, compared to low-level features (again, the dataset is limited) [10]. In 2017, comparison study was conducted to examine the most delicate features list, as well as 36 colors and 14 shape features tests, using 250 classifications, which was time demanding and required a significant amount of processing power [11]. Numerous studies on automated skin lesion identification feature sets have been conducted [12, 13].

Thus far, various features were used for melanoma detection, but in literature, there is a dearth of work found on dermoscopic features. The deep learning method did not achieve satisfactory accuracy using the dermoscopic features [14]. They had presented a CNN-based technique for dermoscopic feature extraction. Their deep learning methodology achieved 84.4% accuracy for the dermoscopic features extraction task. Different clinical methods can be used for dermoscopic feature extraction, such as ABCD rules, 7-checkpoint, etc. Due to the reasons, there is a need to improve accuracy by proposing certain new methods or trying out another existing method. Moreover, in another research reported in [15], authors used the fully convolutional network to detect dermoscopic features. Their proposed method achieved 89.3% accuracy on the ISIC 2017 dataset. The pigmented network features are beneficial for detecting the lesion and segregating them into benign and melanoma through identification and classification, as shown in Table 1. In most dermoscopic images, the lesion contains a pigmented network [16]. In instances when the pigmented network

Table 1 Pigmented features for Benign and Melanoma

Pigmented features	Benign (Typical)	Melanoma (Atypical)	Extraction method
Color	Light-to-dark-brown	Black Brown Gray	Histogram based features Color asymmetry Statistical measures
Texture	Uniformly spaced network holes Thin network lines (global pattern)	Irregular holes Thick lines	Statistical model-based Filter-based
Shape	Distributed regularly	Irregularly	Asymmetry index Statistical geometrical measures Border features

is spread over in the skin area, this type of lesion is primarily considered benign. Conversely, if the pigmented network is present in one area only or the center of the lesion, it is perceived as melanoma. The standard dermoscopic features achieved the highest sensitivity of 94% only. Moreover, for the early detection of melanoma, these features are not powerful [17, 18].

According to researchers work on detection of pigmented networks and classification into the present and absent [19], as shown in Table 1, moreover, the authors had used the ten texture features to detect the atypical pigmented network (APN) sourced from the dermoscopic images [20]. They achieved a 95.4% average accuracy on 106 dermoscopy images, indicating that is a remarkable technique for the detection of the atypical, pigmented network. Conversely, the problem of categorization between the pigmented network and the non-pigmented network was not resolved. However, the authors classified the pigmented network into two classes; ‘pigmented network or non-pigmented’ without performing any pre-processing and segmentation and achieved an accuracy of 83.64% [21]. The proposed method had extracted 23 features that contain six color features, spectral features, and seventeen statistical texture features from a dataset of 220 images.

The pigmented network classification was also performed by [22] using the Laplacian of the Gaussian filter (cyclic texture features). The proposed method obtained a 94.3% accuracy through the evaluation of the 500 images [22]. In a different study by [23], they had combined morphological methods for the detection of pigment networks. The suggested technique was verified by 40 images and accomplished an 85% accuracy. The results of this work were very motivating, but the number of images used for testing is significantly less, and it was not promising to estimate the strength of the technique sufficiently. From the study by [24], they had proposed a method for hair and pigment network detection through extracting color and spectral features. The validation was performed on 734 images, and no evidence is provided on achieved results. The work achieved the advantage of remarkable work on the detection of hair. Some of the existing feature extraction methods based on pigmented network features are discussed in Table 2.

Table 2 Existing methods on pigmented network features

Reference	Features	Accuracy (%)	Dataset	Purpose	Issue
[20]	Texture (10)	95.4	106 images	Atypical pigment network analysis	Less no. of images
[21]	Spectral texture and statistical texture features (17)	83.6	220 images	Pigmented network classification	Accuracy needs improvement Fail case: low contrast images
[22]	Cyclic texture features	94.3	500 images	Pigment network	–
[23]	Texture	85	40 images	Detection of pigmented network	Less no. of images

Several pigmented network features have been proposed [25]. Such features were also utilized for the classification of the pigmented network and classified as absent or present. Numerous solutions have been proposed for feature extraction and selection of pigmented skin lesions to represent them according to a particular clinical criterion. Such features may be used for the segmentation process to provide dermatologists with a computer-aided diagnosis of pigmented skin lesions.

3 Research Methodology

The proposed lesion feature extraction in this study consisted of a combined method employed for the extraction of extract the pigmented and deep lesion features. A method of statistical filter color-based local binary pattern (FSCLBP) based was implemented to extract the pigmented features. In contrast, the AlexNet deep learning model method was carried out to extract the deep features. The proposed method for lesion feature extraction consisted of two steps. In the first step, the proposed pigmented network and deep learning methods are implemented for the lesion feature extraction. In the second step, the parallel fusion method is implemented for these two extracted features pigmented network features and deep features (AlexNet Features). The overall procedure of feature extraction for the lesion classification is illustrated in Fig. 1.

3.1 Pigmented Features

The pigmented network skin lesion images contain different types of features such as the color (light to dark), shape (distributive or irregular), and texture (holes and lines) for benign lesion, as shown in Fig. 2. However, this color changes from dark

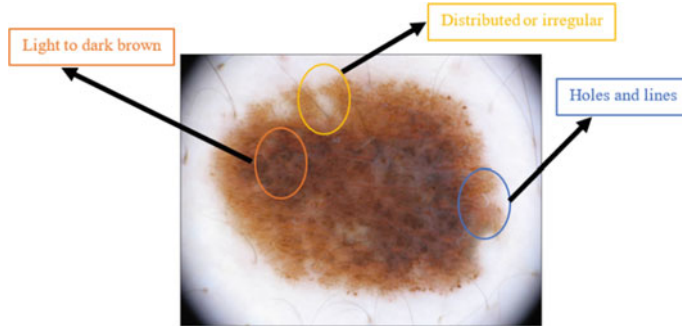


Fig. 2 Pigmented network features of skin image

into gray, the lines are thicker, and the shape is irregular if the lesion is melanoma. For the extraction of these complex features of lesions, different feature extraction methods were implemented.

In the proposed method for pigmented network features extraction, there are four types of feature methods, which are filtering-based features, color features, local binary pattern (LBP), and statistical features were used. These pigmented features were extracted after the visualization of the pigmented lesion images, as shown in Fig. 3.

The pigmented lesions images were chosen because they are overwhelmingly present in both datasets. The pigmented network has a distinct texture to it. The texture features that specify the characteristic nature of holes and lines are extracted. The pigmented lesion contains black, blue, gray, brown, and blue colors. The details of these extracted features are explained as the following:

1. Start
2. Select image from dataset until end.

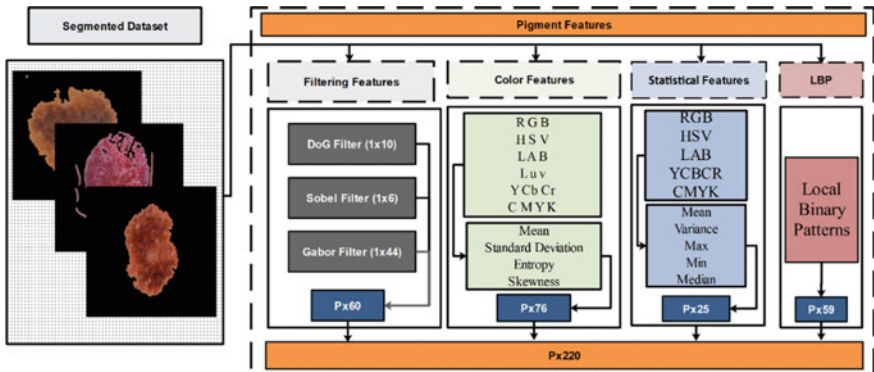


Fig. 3 The proposed pigmented network feature extraction method

- a. Extract Filtering Features (60) by Applying
 - i. DoG Filter (1×10)
 - ii. Sobel Filter (1×6)
 - iii. Gabor Filter (1×44)
 - b. Extract Color Features [76 (19×4)]
 - i. Separate Each Channel from RGB, HSV, LAB, LUV, YCbCr, CMYK.
 - ii. Calculate Mean, Standard Deviation, Entropy, Skewness for each channel.
 - c. Extract Statistical Features [25 (5×5)]
 - i. Calculate Mean, Variance, Maximum, Minimum, and Median from RGB, HSV, LAB, YCbCr, CMYK
 - d. Extract LBP Features (59)
 - i. Extract Local Binary Pattern
 - e. Add All Features into Single row of Matrix (1×220)
3. Go to Step 2
- (a) End

Filtering Based Features

According to the requirement of pigmented network features, three types of filters were selected for this purpose, close to pigmented lesion features. These are differences between the Gaussians (DoG), Sobel filter, and Gabor filter. The details of each filter are given as the following:

The Difference of Gaussian (DoG) Filter

The DoG is a low-pass filter that enhances the visibility of boundaries and additional details existing in the dermoscopic image. The current study utilized a Gaussian filter with (10,15) and with (10,20) and took their difference to obtain the DoG image, and hence, the DoG features were calculated by extracting the histogram of the DoG image. The 10 number of features was the output obtained as shown in Table 3. The DoG filter steps are explained as the following.

- i. Filter1 = fspecial (10,15)
- ii. Filter2 = fspecial (10,20)
- iii. Difference Image = Filter2-Filter1
- iv. DoG Features = Histogram (Different Image).

Gabor Filter

Firstly, the Gabor filters were applied over the segmented image, obtaining a set of blurred images. The motivation to carry out this filtering was to eliminate part of the existing noise. Gabor features were extracted by taking each row's absolute and then were applied to the down sample of rows and columns. Normalization was performed by taking the mean and standard deviation. The 44 numbers of features were the output vectors as shown in Table 3. Typically, GABORFEATURES extracts

Table 3 Features list

S/N	Filtering features (60)			Statistical features (25)			Color features (70)			LBP (59)		
	DoG (10)	Sobel (6)	Gabor (44)	Color space	Channel	Value	Feature	Color space	Channel			
1	0.010	228.947	1.730	CMYK	Mean	24.510	Mean	RGB	R	225.749		
2	0.010	457.895	1.730		Variance	0.026		G	G	210.619		
3	0.010	457.895	1.729		Min	1.000		B	B	201.856		
4	0.010	457.895	1.729		Max	124.098		HSV	H	0.195		
5	0.010	457.895	1.727		Median	17.000			S	0.128		
6	0.010	228.947	1.727		Mean	152.361			V	0.892		
7	0.010	—	1.725		Variance	0.028		LAB	L	85.237		
8	0.010	—	1.724		Min	1.000			A	3.989		
9	0.010	—	1.724		Max	123.809			B	6.372		
10	0.010	—	1.720		Median	135.000		LUV	L	92.215		
11	—	—	1.719	LAB	Mean	31.866	YCbCr		U	-1.835		
12	—	—	1.714		Variance	0.010			V	4.341		
13	—	—	1.713		Min	1.000			Y	199.904		
14	—	—	1.713		Max	0.851		Cb	Cb	121.905		
15	—	—	1.710		Median	8.210		Cr	Cr	135.273		
S/N												
Filtering features (60)												
S/N	DoG (10)	Sobel (6)	Gabor (44)	Color space	Channel	Value	Feature	Color space	Channel	Value	LBP (59)	
	—	—	1.709	HSV	Mean	0.405	CMYK	C	11.909	0.007		
16	—	—	1.707		Variance	0.010		M	20.082	0.001		
17								N				
S/N												
Filtering features (60)												
S/N	DoG (10)	Sobel (6)	Gabor (44)	Color space	Channel	Value	Feature	Color space	Channel	Value	DoG (10)	
	—	—	1.707				CMYK	C	11.909	0.007		

(continued)

Table 3 (continued)

S/N	Filtering features (60)			Statistical features (25)			Color features (70)			LBP (59)
	DoG (10)	Sobel (6)	Gabor (44)	Color space	Channel	Value	Feature	Color space	Channel	
18	-	-	1.704	Min	0.367			Y	33.712	0.116
19	-	-	1.702	Max	0.099			K	22.436	0.017
20	-	-	1.690	median	0.158	SVD	RGB	R	32.788	0.132
21	-	-	1.687	RGB	Mean	212.741		G	34.630	0.006
22	-	-	1.680	Variance	0.023			B	38.123	0.123
23	-	-	1.664	Min	1.000	HSV	H		0.273	0.018
24	-	-	1.653	Max	132.695			S	0.114	0.123
25	-	-	1.650	median	221.000			V	0.127	0.005
26	-	-	1.632	-	-	LAB	L		13.029	0.092
27	-	-	1.624	-	-		A		5.047	0.111
28	-	-	1.600	-	-		B		6.437	0.168
29	-	-	1.588	-	-	LUV	L		12.687	0.149
30	-	-	1.550	-	-		U		71.773	0.086
31	-	-	1.510	-	-		V		6.228	0.096
32	-	-	1.470	-	-	YCbCr	Y		28.823	0.144
33	-	-	1.467	-	-		Cb		5.899	0.138
34	-	-	1.460	-	-		Cr		7.105	0.242
35	-	-	1.458	-	-	CMYK	C		21.892	0.078
36	-	-	1.044	-	-		M		27.480	0.380
37	-	-	1.024	-	-		Y		29.395	0.067
38	-	-	0.997	-	-		K		30.533	0.219

the Gabor features of an input image. It creates a column vector consisting of the Gabor features of the input image. In the current study, the feature vectors were normalized to zero mean and unit variance. Here, the 44 features were selected out of 160 features. The Gabor filter steps are explained as the following:

```
% r: rows down sampling
% c: columns down sampling
GaborAbsolute = abs(gaborResult{i,j})
GaborAbsolute = downsample(GaborAbsolute,r)
GaborAbsolute = downsample(GaborAbsolute,c)
GaborAbsolute = (GaborAbsolute - mean (GaborAbsolute))/std
GaborFeature = [GaborFeature; GaborAbsolute]
```

Sobel Filter

Conventionally, the Sobel operator is usually utilized for lines and boundaries extraction, to color it tracks the dark to the light range. Sobel features are extracted based on the segmented dermoscopic image gradient by taking the histogram's magnitude. The six (6) features were the output as shown in Table 3. The steps for Sobel filter features extraction are as the following:

- i. Magnitude of Gradient = gradient (Gray Image)
- ii. Feature Pixel Values = histogram (Magnitude of Gradient)
- iii. Sobel Features = Gradient (Feature Pixel Values).

Color Features

In this research study, the color spaces such as RGB, HSV, Lab, Luv, YCbCr, CMYK were used, where all channels were separated from each color space, and the Mean, Standard Deviation, Entropy, and Skewness for each channel were then calculated. The following color transformations were applied to RGB: HSV (3 channels), LAB (3 channels), Luv (3 channels), YCbCr (3 channels), and CMYK (4 channels). After splitting each channel for each color space, a total of 16 channels were obtained. The mean, standard deviation, entropy, and skewness for each channel were then calculated. Each channel's mean was calculated by arithmetic mean or an average of all the color channels of these three-color spaces, as shown in Eq. 1.

$$\bar{r} = \frac{\sum r}{n} \quad (1)$$

After that, each channel's standard deviation was calculated, in which the difference was taken for each color channel as illustrated in the equation, where \sum means “sum of”, r is a value in the data set, \bar{r} is the mean of the data set, and N is the number of data points in the population as shown in Eq. 2.

$$\sigma = \sqrt{\frac{\sum_{i=1}^N (r_i - \bar{r})^2}{N}} \quad (2)$$

Entropy was calculated for each channel as described in Eq. 3.

$$Et = \sum r * \log(r) \quad (3)$$

Skewness for each channel was calculated for checking the symmetry or normal distribution of each color channel as explained in the equation, where i is the observations, \bar{r} is the mean, n is the total number of observations, y is the variance, and r contains the histogram for the channel skewness for each channel was calculated as shown in Eq. 4:

$$\text{Skew} = \sqrt{\frac{\sum_{i=1}^N (r_i - \bar{r})}{(n - 1)y^2}} \quad (4)$$

The concatenation operation was performed on all features that were then converted into a row vector to obtain the color features. Hence, the 70 number of features was the output vector.

Local Binary Pattern (LBP)

The LBP was used to extract the uniform local binary patterns from a grayscale image I and returns the features in a 1-by-N vector. LBP features encode local texture information and can be used for many tasks, including classification, detection, and recognition. Hence, the 59 number features were obtained.

Statistical Features

Statistical features were calculated by calculating the Mean, Variance, Max, Min, Median for RGB HSV, Lab, YCbCr, and CMYK color spaces, and hence a feature set of 1×25 was the output. The following color transformations were applied: RGB, HSV, LAB, YCbCr, and CMYK. Then, the following statistical measures were calculated: Mean, Variance, Max, Min, and Median. Hence, the number of 25 features was extracted from the statistical features. After the extraction of all these pigmented network features, these features were then combined, and the final feature vector was obtained [25]. From Table 3, the filtering features are 60, with 76 being color features, 59 being LBP features, and 25 being statistical features. The total pigmented feature vector (PFV) was 220 after combining all these features as shown in Eq. 5.

$$P = (\text{Filtering} + \text{Color} + \text{LBP} + \text{Statistical}) \quad (5)$$

3.2 AlexNet Features

The pigmented lesion image features were extracted using the pigmented network features. The remaining features for the other images that existed in the datasets were extracted by AlterNet. The deep features were chosen because they are more dynamic features. Deep residual network (AlexNet) is a straightforward and clean framework in comparison to other frameworks: ResNet, OverFeat, and VGG. In addition, in terms of time computational, AlexNet gave the best solution as compared to other CNN architecture. The AlexNet deep learning architecture as defined by [26] comprised five superficial layers in which three layers are fully connected, the fourth one is rectified linear units (ReLUs), and the last is dropout max-pooling. The detailed process of AlexNet features extraction is shown in Fig. 4.

The AlexNet was trained on the ImageNet dataset that consisted of 1000 classes. The stock network layers were pre-trained on the ImageNet dataset. These pre-trained models were trained according to the ImageNet dataset. That is the reason why the extracted features were not specific to skin lesion features. Thus, in the proposed customized AlexNet, the last three layers were removed. Moreover, the modified three new layers were padded according to lesion classes. Here, in this research, there are two classes for lesion classification that are benign and melanoma. In customized AlexNet, transfer learning was applied to train the model according to skin lesion classes.

AlexNet Layers Structure

The RGB dermoscopic image was fed into the network as an input, as shown in Fig. 5. The size of the input image was 227×227 . The three separate channels (3) of RGB are passed to the network. The neural network AlexNet consisted of five convolutional layers (Conv-1 to Conv-5), two fully connected layers (FC6, FC7),

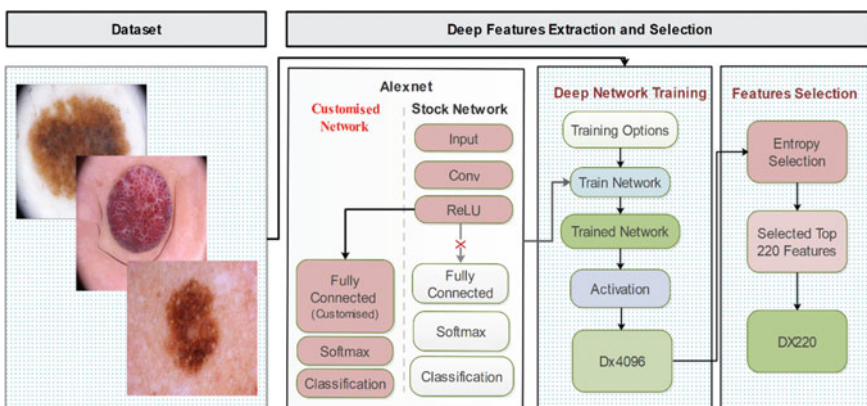


Fig. 4 Customized AlexNet features extraction

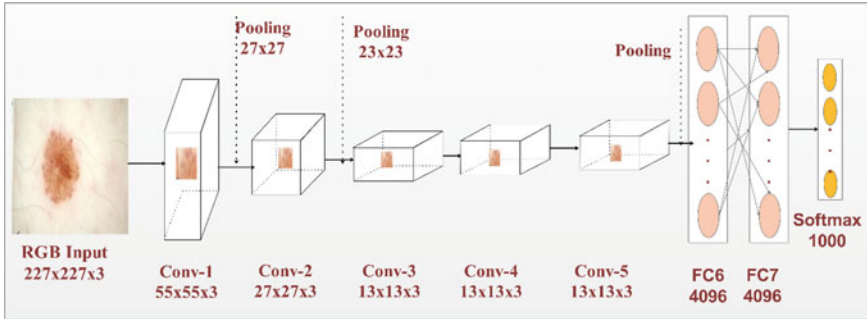


Fig. 5 Layer structure of AlexNet model

and one output layer. This layered architecture works the same as the pre-trained AlexNet network proposed by [26].

Transfer Learning

The AlexNet network was used in this current research for feature extraction without any changes. However, for this research, transfer learning was performed on AlexNet. After the FC layers, the pre-trained network was modified by adding two skin lesion classes: benign and melanoma instead of the ImageNet classes. The ratio 70:30 was used for the transfer learning process on the skin lesion dataset in which 70% dataset was used for training and 30% dataset was utilized for testing.

4 Optimized Feature Selection

After the deep feature extraction, it is crucial to select the optimized features and remove redundancy from the feature vector $D = 1 \times 1000$. For that purpose, the entropy-based selection was applied in this study for the best feature selection, from which the top 220 features were selected. The reason for limiting the number of features to 220 was that these features must be combined with pigmented network features. A total of 220 features were extracted using the pigmented network.

5 Parallel Fusion

Following the extraction of two feature vectors, the following step was taken. The first was a pigmented feature vector, and the second was an AlexNet feature vector that will be aggregated into a single feature vector. There are two types of feature fusion methods that are commonly used: serial-based fusion and parallel-based fusion methods. Serial-based fusion used concatenation operation, and parallel-based fusion

used addition operation for fusing the extracted feature vectors. Both have their advantages and limitations [27]. Perhaps parallel-based fusion approaches will be utilized for feature fusion of pigmented network features and AlexNet features. Here, in this research, parallel fusion was applied for combining both the feature vectors. The pigmented network and AlexNet features both have an equal number of a feature that is 220. The reason for keeping both feature vectors similar in size is that it will be easy to fuse these vectors using parallel-based fusion. Otherwise, if these feature vectors are not in equal size, then the zeroes are set to balance the vector. Thus, for avoiding placing the zeroes, both feature's vectors size is kept fixed. The resultant feature vector after the fusion is the same in size as $PDFF \times 220$.

6 Fused Feature Vector

The fusion method is formulated as: Let $S1$, $S2$, and $S3$ be known as lesion classes: melanoma, atypical nevi, and benign. Suppose $\mathcal{F} = \{\mathcal{C} \mid \mathcal{C} \in SK\}$ as denoting the test class of images. Given that two extracted feature sets $P = \{\rho \mid \rho \in Sp\}$, and $D = \{\beta \mid \beta \in Sd\}$, where ρ and β are two feature vectors: pigmented network and deep AlexNet. After the fusion of these two feature sets P and D , a new single feature set (F) is generated with the PD , where d is the dimension of the extracted set of features as shown in Eq. 6.

$$F(PD) = (\rho_1, \rho_2, \dots, \rho_d)(\beta_1, \beta_2, \dots, \beta_d) \quad (6)$$

The dimension (d) of these two extracted feature vectors is $P = 1 \times 220$, and $D = 1 \times 220$. Then, the pigmented deep fused features are defined as in Eq. 7.

$$PDFE = (\rho d + \beta d \mid \rho \in P, \beta \in D) \quad (7)$$

7 Skin Lesion Classification

Skin lesion classification is the last step for the identification and categorization of skin lesion. In this research, the two main classes: melanoma and benign, were classified by applying the various machine learning classifiers. The different machine learning classifiers were giving different accuracies on three different datasets. It is well known that the skin lesion classification methods are based typically on feature extraction. The proposed feature vector has been accurately classifying the skin lesion images. The ISBI 2016 and ISIC 2017 datasets contain two classes benign and melanoma, but the PH2 dataset contains three classes atypical nevus, common nevus, and melanoma. All these classes have been classified accurately. The classifier categorizes the skin lesion image efficiently and achieves an accuracy of 99.8% on

the ISBI 2017 dataset and 99.3% on the ISIC 2017 dataset, 98.6% on the PH2 dataset. Furthermore, the detailed results are shown in the below section.

8 Experimental Results and Analysis

This section presents the evaluation of the experimental results that were done for the proposed fused feature vector validation. Various performance measures were used for the evaluation of the proposed method. Moreover, to prove the validation of the proposed method, a comparison was performed with state-of-the-art methods. The detailed summary of the experimental results, analysis, and discussions on implementing the proposed method for the two types of feature extraction and their fusion are discussed in this section. For that, the various experiments were conducted using three feature's vectors on three skin lesion datasets. The proposed research method's performance was benchmarked against the recent techniques on skin lesion classification of dermoscopic images in the field literature to date.

8.1 *Experimental Setup*

This section presents the experimental results and the proposed research method's analysis using three publicly available skin lesion datasets: ISBI 2016, ISIC 2017, and PH2.

8.2 *Experimental Results*

The skin lesion datasets were randomly divided into three sets for training, testing, and validation. The training dataset was 70%, and the validation and testing dataset comprise 30% of the total images. The training and testing process was accomplished by using a tenfold cross-validation method. The six performance evaluation matrices: Precision, Sensitivity (Sen), Specificity (Spec), the area under the curve (AUC), false-negative rate (FNR), and Accuracy were used for the validity of classification results. Moreover, the overall classifier training time was also calculated. The proposed fused feature vector was used to input the machine learning classifiers to categorize these two classes, such as benign and melanoma. The dermatologists classified each image in the datasets as either benign or melanoma with the ground-truth labels. The extracted feature vectors and the fused features vector were classified through different types of machine learning classifiers such as decision trees (DT), discriminant analysis (LDA), support vector machine (SVM), k-nearest neighbor (KNN), and ensemble methods. The experiment was performed on two extracted feature vectors (pigmented network feature and deep feature) and one fused features vector to check

the validity of these three feature vectors. Firstly, the extracted pigmented network features vector was feed to machine learning classifiers, and their results were calculated. Secondly, the classification results of the deep features vector were measured. Lastly, the proposed fused features vector was also submitted to the classifiers, and their results were also calculated. These experiments were performed on three skin lesion datasets: ISBI 2016, ISICI 2017 and PH2 datasets. The detailed extracted results of the three feature vectors on each dataset are explained in the following subsection.

Experimental Results of ISBI 2016 Dataset

The ISBI 2016 dataset contains two classes, namely benign and melanoma. A total of 1273 dermoscopic images containing 1025 benign images and 248 melanoma images were involved in this research study. As can be seen, the dataset has unbalanced classes that reduced the performance of classifiers. The image augmentation was performed on the ISBI 2016 dataset to balance the classes by rotating the images into four intervals with viewpoints of 90°, 180°, and 270°. The whole dataset was divided into two parts for the experiments: one for the testing dataset and another for the training dataset. The testing dataset involved 891 images, and 382 images have been contained in the testing dataset, as shown in Table 4.

Two extracted feature vectors and the proposed fused features vector performance results were compared, as shown in Table 5. These three feature's vectors were fed individually into the machine learning classifiers such as support vector machine (SVM), naive Bayes, Complex Tree (CT), W-KNN, linear discriminant analysis (LDA), Ensemble Boosted Tree (EBT), Ensemble Subspace Discriminant Analysis (ESDA), Linear Regression (LR). After the performance analysis of these classifiers, the best results were obtained from the Quadratic SVM classifier. The seven statistical performance measures were calculated, including execution time, precision, sensitivity, specificity, false-negative rate (FNR), the area under the curve (AUC), and accuracy. The best-achieved classification time 3.91 s was taken by deep features after that pigmented network feature takes the 5.16 s to complete classification, and in the last, the fused feature vector obtained the 5.18 s. The highest accuracy, 99.8%, achieved by the fused feature vector and the second-best 99.7% accuracy were gained by deep features. The pigmented network features gave the 80.5%, which individually was not very promising, but after fusion of the pigmented network features and deep features, the accuracy was slightly increased.

Table 4 ISBI 2016 dataset division

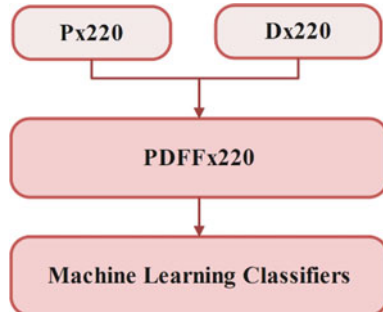
No. of classes	Skin lesion category	Dermoscopic images	Training dataset	Testing dataset
1	Benign (Non-Melanoma)	1025	–	–
2	Melanoma	248	–	–
Total		1273	891	382

Table 5 Proposed fused feature vector results on dataset ISBI 2016

Dataset: ISBI 2016	Extracted features		Fused feature vector (s)	Training time (s)	Performance measures (%)			
	Pigmented	Deep			Precision	Sen	Spec	AUC
Quadratic-SVM	✓		5.16	68.5	62.5	0.75	19.5	80.5
		✓	3.91	99	99	99.0	1.00	0.3
		✓	5.18	99.5	100	1.00	0.2	99.8

* The bold results of quadratic-SVM show the best accuracy

Fig. 6 Pigmented deep fused feature



The graphical representation of classification results is shown in Fig. 6. Some images have illustrated the demonstration of the lesion classification into benign lesion and melanoma lesion as shown in Fig. 7.

Experimental Result of ISIC 2017 Dataset

The ISIC 2017 (International Skin Imaging Collaboration) contains two types of image data clinical (100 images) and dermoscopic contact non-polarized (4000 images). These images have a resolution of 296 by 1456. The collection contains 2000 images of benign (non-melanoma) and 2000 images of melanoma. The image augmentation was not applied in the ISIC 2017 dataset because classes have a balanced number of images. The training dataset contains a total amount of images of 2800 of which 1400 are benign, and 1400 are melanoma images, as shown in Table 6. The testing dataset has 600 benign and 600 melanoma images.

Similar to the ISBI 2016 dataset, two extracted feature vectors and the proposed fused features vector performance results were compared with each other, as shown in Table 7. These three feature's vectors were fed individually into the machine learning classifiers such as support vector machine (SVM), naive Bayes, complex tree (CT), W-KNN, linear discriminant analysis (LDA), ensemble boosted tree (EBT), ensemble subspace discriminant analysis (ESDA), and linear regression (LR). After the performance analysis of these classifiers, the best results were obtained from the Quadratic SVM classifier. The seven statistical performance measures were calculated, including execution time, precision, sensitivity, specificity, false-negative rate (FNR), the area under the curve (AUC), and accuracy. The best-achieved classification time of 2.84 s was taken by a fused feature vector, which was followed by the pigmented network features which took the 7.63 s to complete the classification, and lastly, by, the deep features vector which took the 10.7 s. The highest accuracy of 99.3% was achieved by the fused features vector, and the second-best 91.9% accuracy was demonstrated by the pigmented network. The deep features demonstrated an accuracy of 89.3%, which was not very promising. However, after the fusion of the pigmented network features and deep features, the accuracy was greatly increased.

Similar to the ISBI 2016 dataset, the graphical representation of classification results on dataset ISIC 2017 is shown in Fig. 7 of the classification results on ISIC

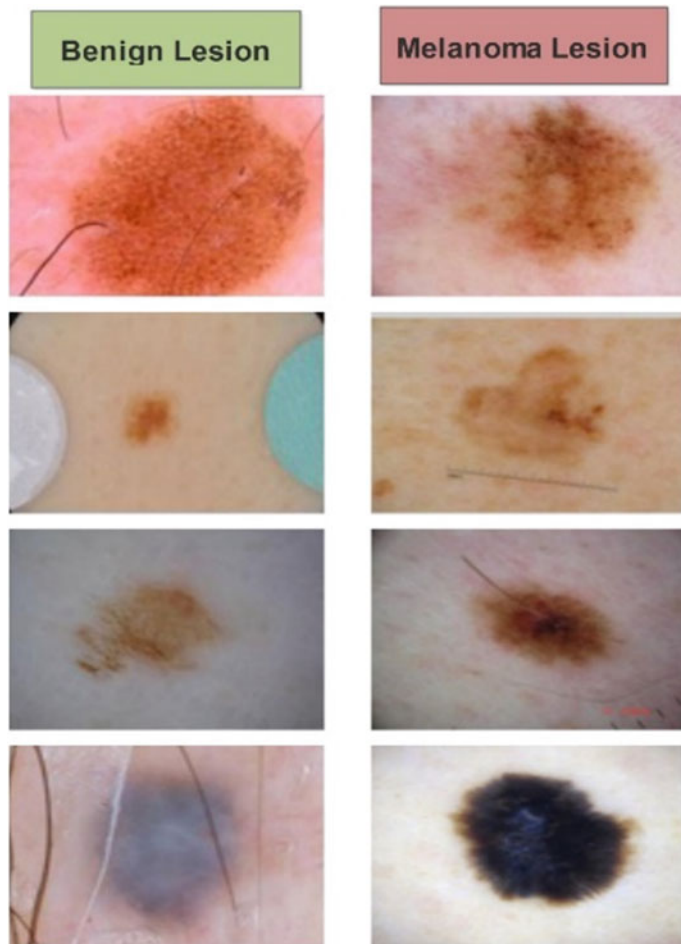


Fig. 7 Classification results on ISBI 2016 dataset

Table 6 ISIC 2017 dataset division

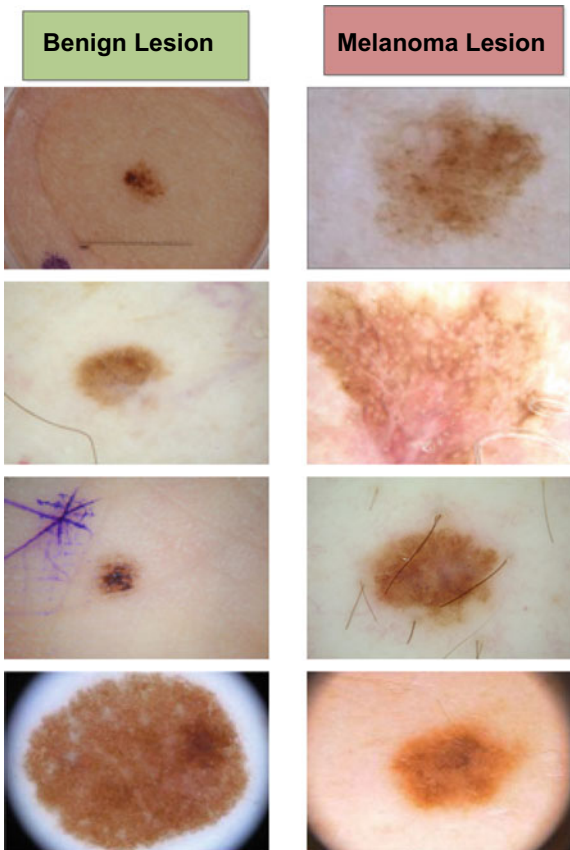
No. of classes	Skin lesion category	Dermoscopic images	Training dataset	Testing dataset
1	Benign (Non-Melanoma)	2000	1400	600
2	Melanoma	2000	1400	600
Total		4000	2800	1200

Table 7 Proposed fused feature vector results on dataset ISIC 2017

Dataset: ISIC 2017 Classifier	Extracted features		Fused feature vector (s)	Training time (s)	Performance measures (%)					
	Pigmented	Deep			Precision	Sen	Spec	AUC	FNR	Accuracy
Quadratic-SVM	✓		7.63	91	91	91	0.97	8.1	91.9	
		✓	10.7	92.5	82.5	82.5	0.94	10.7	89.3	
		✓	2.84	98.5	99	99	1.00	0.7	99.3	

* The bold results of quadratic-SVM show the best accuracy

Fig. 8 Classification results on ISIC 2017 dataset



2017 Dataset. Some images presented in Fig. 7 have illustrated benign lesion and melanoma lesion (Fig. 8).

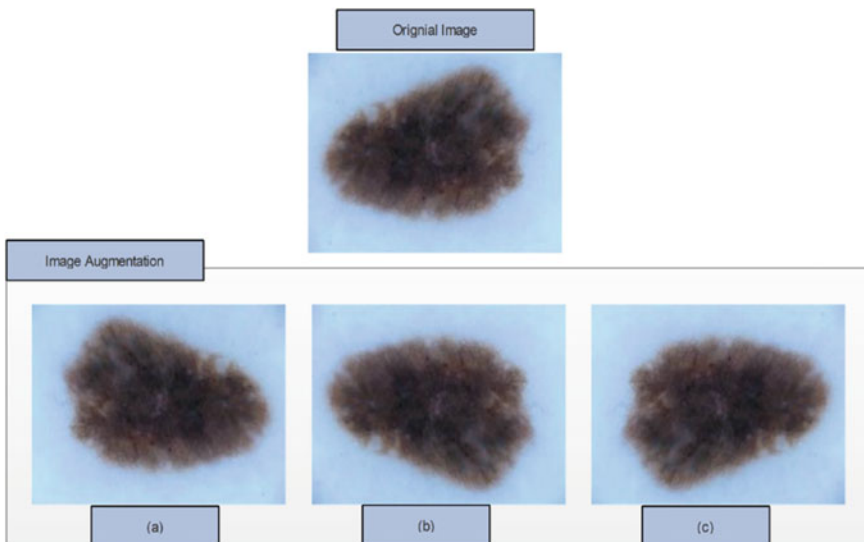
Experimental Results of PH2 Dataset

In the PH2 dataset, a total of 200 images are accessible. The resolution of 8-bit images is 768 by 660. In the PH2, there are two categories, such as benign (Atypical nevi and Common nevi) and melanoma. The detailed dataset division is shown in Table 8. The training dataset holds 180 images, and the testing dataset holds 60 images. In training, the dataset contains very few melanoma images.

The image augmentation was applied only on the training dataset by rotating images into four intervals with viewpoints of 0° , 90° , 180° , and 270° as illustrated graphically in Fig. 9. Subsequently, the training dataset was increased to 180 images. The PH2 dataset includes medical annotation of all the images, namely medical segmentation of the lesion, clinical and histological diagnosis, and the assessment of several dermoscopic criteria (colors, pigment network, dots/globules, streaks, regression areas, blue-whitish veil). The benchmark PH2 dataset contains a very small

Table 8 PH2 dataset division

No. of classes	Skin lesion category	Dermoscopic images	Training dataset	Testing dataset
1	Atypical Nevi (Non-melanoma)	80	–	–
2	Common Nevi (Non-melanoma)	80	–	–
3	Melanoma	40	–	–
Total		200	180	60

**Fig. 9** Image augmentation on dataset PH2

amount of dermoscopic images, but the researchers also utilized this dataset to test or train and evaluate their methods.

The two extracted feature vectors and fused features vector were fed into a different number of classifiers. The quadratic-SVM classifier showed the best accuracy of 98.6%, on the fused features vector. The other parameters for the fused features vector showed the following results such as Training Time of 2.36 s, Precision 97.3%, Sen 96.3%, Spec 96.3%, AUC 1.00%, and FNR 2.9%. The pigmented network features showed an accuracy of 77.4% that was individually not very satisfactory. The deep features work better than pigmented network features and obtained a 96.9% accuracy. These fused features vector results were comparatively better than the other two features individually with an accuracy of 98.6%. The detailed classification results of the PH2 dataset in terms of their performance measures are presented in Table 9.

Table 9 Proposed fused feature vector results on dataset PH2

Dataset: PH2	Extracted features		Fused feature vector	Training time (s)	Performance measures (%)			
	Pigmented	Deep			Precision	Sen	Spec	AUC
Quadratic-SVM	✓			10.3	77.0	77.6	0.84	22.6
		✓		6.46	97.3	96.3	0.96	1.00
			✓	2.36	97.3	96.3	1.00	2.9
								98.6

* The bold results of quadratic-SVM show the best accuracy

As can be observed, PH2 has three classes: atypical nevus, common nevus, and melanoma, as shown in the classification results in Fig. 10. Like the other two datasets ISBI 2016, and ISIC 2017, it can be classified into two classes only, namely benign and melanoma.

The proposed fused feature vector analysis was performed, and a comparison was made between the accuracies achieved on these three datasets on the Quadratic-SVM classifier. As shown in Fig. 11, the highest accuracy achieved was 99.8% on the ISBI 2016 dataset by Fused Feature Vector as shown in the green bar of the bar chart. Secondly, the fused features vector has also shown performed efficiently on the dataset ISIC 2017 by achieving a 99.3% accuracy. The proposed fused features vector also executed well on the PH2 dataset by gaining 98.9% accuracy. As it can be seen

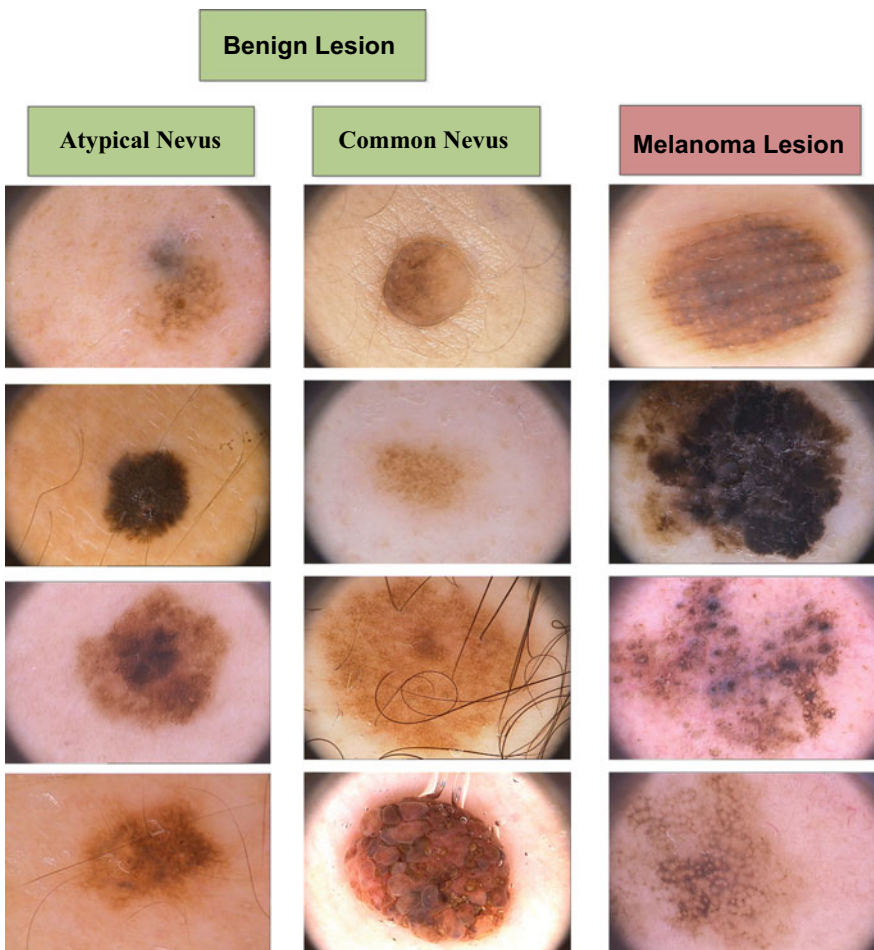


Fig. 10 Classification results on PH2 dataset

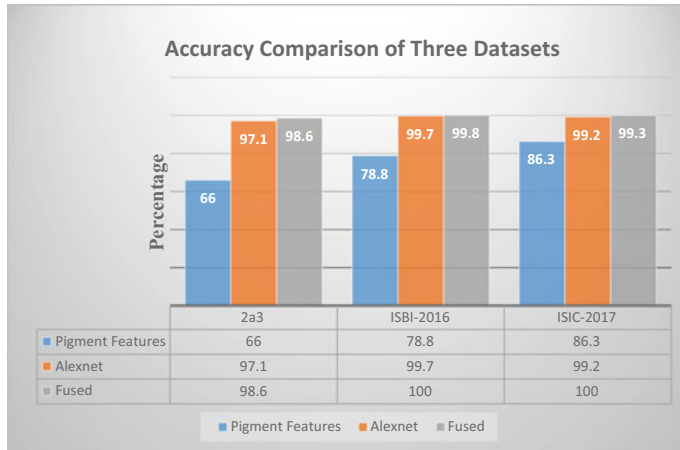


Fig. 11 Analysis and comparison of accuracy with three skin lesion dataset

individually, the pigmented and AlexNet features are also performed efficiently, but by fusing these two features (pigmented and AlexNet) the proposed feature vector gains promising accuracy as compared to existing methods [29].

9 Evaluation and Discussion

In this section, a comprehensive discussion is conducted by comparing the state-of-the-art methods. A comparative analysis was performed with three skin lesion datasets to evaluate the proposed method against the state-of-the-art methods (ISBI 2016, ISIC 2017, and PH2). For each dataset, a separate comparison was performed in terms of accuracy, sensitivity, and specificity. The proposed method was associated with the relevant state-of-the-art methods that used ISBI 2016 dataset. For the dataset ISBI 2016 achieved the lowest accuracy in comparison with the other methods, demonstrating the accuracy of 85.5% [28] as shown in Table 10. In another study reported in [1] has obtained a slightly higher accuracy than reported in [4] with an accuracy of 90.2% as indicated in Table 10. The color and DCNN features were fused in [2]. In Table 10, their fused vector gained 92.1% accuracy by the multi-class SVM classifier.

The deep learning Inception V3 CNN pre-trained model was utilized for feature extraction [3]. For feature fusion, they used the hamming distance-based fusion method and achieved 95.1% accuracy. A different study in [29] fused the ABCDE, and shape features using serial-based fusion and achieved 99.2% accuracy on the M-SVM classifier, which is the highest in comparison with all the existing methods. In this study, the proposed pigmented and deep feature fusion was obtained by a parallel fusion-based method. The machine learning classifier Quadratic-SVM gave 99.8%

Table 10 Proposed method comparison with state-of-the-art methods using ISBI 2016 dataset

Related studies	Year	Accuracy (%)	Sensitivity (%)	Specificity (%)
[28]	2017	85.5	50.7	94.1
[29]	2018	99.2	99.2	99.4
[1]	2019	90.2	90.5	99.2
[3]	2019	95.1	95.0	95.0
[2]	2019	92.1	92.0	90.0
Proposed PDFF Method	2020	99.8	99.5	100

Accuracy is the proportion of the correctly detected area over the GT (ground truth). It is the proportion of correct predictions over the total number of predictions

Sensitivity: A higher value close to 1.0 of Sensitivity shows a good execution in segmentation which means that all the lesions were effectively separated

Specificity signals TN of the non-lesions if specificity is higher, which means the competency of a method in the segmentation of the lesions

accuracy on this fused feature vector. However, all these existing methods efficiently classified the skin lesion, but their accuracy was not as promising compared to the proposed method, as shown in Table 10.

The proposed method was associated with the relevant state-of-the-art methods that used ISIC 2017 dataset. Li and Shen [14] achieved the lowest accuracy than the other existing methods with 85.7% accuracy on ISIC 2017 dataset. The deep learning Inception V3 CNN pre-trained model was utilized for feature extraction [3]. For feature fusion, they used the hamming distance-based fusion method and achieved 94.8% accuracy. Javed et al. [1] method have a slightly higher accuracy than reported in [3] with 95.5%. The color and DCNN features were fused in [2]. Their fused vector gains 96.5% accuracy by the multi-class SVM classifier. In this study, the proposed pigmented and deep feature fusion was obtained by a parallel fusion-based method. The machine learning classifier Quadratic-SVM gave 99.3% accuracy on this fused feature vector. However, all these existing methods efficiently classified the skin lesion, but their accuracy was not as promising or scored a high accuracy in comparison to the proposed method, as shown in Table 11.

Table 11 Proposed method comparison with state-of-the-art methods using ISIC 2017 dataset

Related studies	Year	Accuracy (%)	Sensitivity (%)	Specificity (%)
[14]	2018	85.7	49.0	96.1
[31]	2019	94.8	94.5	98
[33]	2019	96.5	96.5	97.0
[30]	2019	95.5	95.5	95.0
Proposed PDFF Method	2020	99.3	99	99

Accuracy is the proportion of the correctly detected area over the GT (ground truth). It is the proportion of correct predictions over the total number of predictions

The proposed method was associated with the relevant state-of-the-art methods that used the PH2 dataset. For dataset PH2, the authors achieved the lowermost accuracy likened to the other methods with 86% accuracy [34]. In another study, the SIFT features were used and gained 92.0% accuracy [35]. In addition to this, the shape, color, and texture features were extracted and obtained 97.0% accuracy [36]. The researchers were achieved equal accuracy of 97.5%. with serial-based fusion for hand-crafted features (color, texture, and shape) fusion. Furthermore, the authors fused the hand-crafted features (ABCDE and shape) using serial-based fusion [29]. The deep learning Inception V3 CNN pre-trained model was utilized for high-level feature extraction [31]. For feature fusion, they used the hamming distance-based fusion method and achieved 94.8% accuracy.

In this study, the proposed fusion of pigmented network features vector and deep features vector was obtained by a parallel fusion-based method. The machine learning classifier Quadratic-SVM gave 98.6% accuracy on this fused feature vector son the PH2 dataset. However, all these exiting methods had efficiently classified the skin lesion, but their accuracies were not promising as compared to the proposed method, as shown in Table 12.

The proposed fused features vector worked efficiently in comparison with individual extracted features (pigmented and deep features). Moreover, the proposed fused feature vector performance results were quite promising. It can be the observer through the comparison made with the performance made by other state-art-methods as shown in Fig. 12.

The proposed fused feature vector had classified the skin lesion accurately with the highest accuracy of 99.8% on ISBI 2016 dataset as can be seen in Fig. 12. The existing method highest accuracy is 99.2% on ISBI 2016 dataset using ABCDE features by [29] as indicated in Fig. 12 and Table 12. This current research study on “Skin Lesion Classification Based on Fused Saliency Map Segmentation Using

Table 12 Proposed method comparison with state-of-the-art methods using PH2 dataset

Related studies	Year	Accuracy (%)	Sensitivity (%)	Specificity (%)
[35]	2016	92.0	87.5	93.1
[36]	2017	97.0	96.0	97.0
[37]	2018	97.5	97.7	96.7
[34]	2018	86.0	78.9	93.2
[29]	2018	97.5	96.3	99.5
[31]	2019	98.4	98.2	98.5
Proposed PDFF Method	2020	98.6	96.3	96.3

Accuracy is the proportion of the correctly detected area over the GT (ground truth). It is the proportion of correct predictions over the total number of predictions

Sensitivity: A higher value close to 1.0 of Sensitivity shows a good execution in segmentation which means that all the lesions were effectively separated

Specificity signals TN of the non-lesions if specificity is higher, which means the competency of a method in the segmentation of the lesions

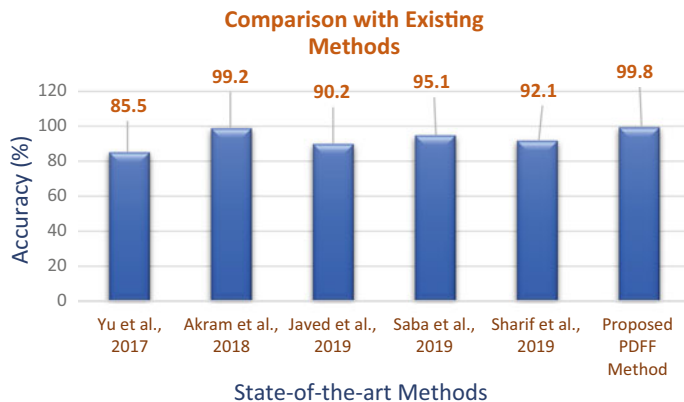


Fig. 12 Comparison of the proposed method with state-of-the-art methods for ISBI 2016 dataset

Pigmented and Deep Features” provides a new perspective on skin lesion segmentation and classification methods. A combination of pigmented network features and deep learning feature extraction methods has been proposed to resolve the limitations of the current skin lesion feature extraction methods that were easily affected by a background complication and is limited to spatial information. In the proposed feature extraction method, the pigmented network features were extracted and fused with AlexNet deep network. Machine learning classifiers were used for the classification of skin lesion. The fused feature vector was fed into the machine learning classifiers. The results of this current research revealed that the proposed method had successfully increased the lesion classification accuracy, which was otherwise restricted on low contrast images. The experimental evaluation of the proposed method for skin lesion classification shows their effectiveness in analyzing images containing low contrast, under, and over-segmented images. Subsequently, based on the evaluated performance results of the proposed fused features vector on three skin lesion datasets, the proposed fused features reported the best accuracy instead of using only one type of features vector individually. The ISBI 2016 dataset achieved the best accuracy of 99.8% on the proposed fused feature vector that performed better than previously proposed methods.

10 Conclusion

The significance of the proposed fused feature extraction method is that it has the capability of improving the accuracy of lesion classification. The pigmented network and deep features have been extracted from the segmented image. The pigmented feature was also important in accurately classifying the lesion. Deep learning features are more discriminatory, particularly in skin lesion classification. As a result, a customized AlexNet deep neural network was developed to retrieve robust features

while avoiding the deep network's computational complexity. Moreover, the entropy features selection method was used to select the efficient features list. The pigmented features and deep features were fused. This fused feature vector provided accurate categorization of benign and melanoma images. After comparing the proposed classification results of this current study to the existing methods, the classification results were also favorable to prove its accuracy and efficiency.

Acknowledgements This work is supported by Artificial Intelligence and Data Analytics (AIDA) Lab Prince Sultan University Riyadh, Saudi Arabia. The authors are thankful for the support. Also, this work is supported by the School of Computing, Faculty of Engineering, Universiti Teknologi Malaysia, 81310 Skudai, Johor Bahru, Malaysia. Moreover, the first author is also grateful for the support of the Department of Computer Science, Lahore College for Women University, Jail Road, Lahore 54,000, Pakistan.

References

1. Javed, R., Shafry, M., Saba, T., Fati, S.M., Rehman, A., et al.: Statistical histogram decision based contrast categorization of skin lesion datasets dermoscopic images. *Computers. Mater. Continua.* **67**(2), 2337–2352 (2021)
2. Khan, M.A., Sharif, M.I., Raza, M., Anjum, A., Saba, T., Shad, S.A.: Skin lesion segmentation and classification: A unified framework of deep neural network features fusion and selection. *Expert Syst. e12497* (2019)
3. Saba, T., Khan, M.A., Rehman, A., Marie-Sainte, S.L.: Region extraction and classification of skin cancer: A heterogeneous framework of deep CNN features fusion and reduction. *J. Med. Syst.* **43**(9), 289 (2019)
4. Yuan, Y., Chao, M., Lo, Y.: Automatic Skin Lesion Segmentation Using Deep Fully Convolutional Networks with Jaccard Distance, vol. 0062, no. c, pp. 1–11 (2017). <https://doi.org/10.1109/TMI.2017.2695227>
5. Khan, S., Yong, S.P.: A comparison of deep learning and hand crafted features in medical image modality classification. In: 2016 3rd International Conference on Computer and Information Sciences (ICCOINS), pp. 633–638 (2016). <https://doi.org/10.1109/ICCOINS.2016.7783289>
6. Saba, T., Khan, S.U., Islam, N., Abbas, N., Rehman, A., Javaid, N., Anjum, A.: Cloud-based decision support system for the detection and classification of malignant cells in breast cancer using breast cytology images. *Microsc. Res. Tech.* **82**(6), 775–785 (2019)
7. Codella, N.C.F. et al.: Skin lesion analysis toward melanoma detection: A challenge at the 2017 International symposium on biomedical imaging (ISBI), hosted by the international skin imaging collaboration (ISIC). In: 2018 IEEE 15th International Symposium on Biomedical Imaging (ISBI 2018), vol. 2018-April, no. Isbi, pp. 168–172 (2018). <https://doi.org/10.1109/ISBI.2018.8363547>
8. Deng, J., Dong, W., Socher, R., Li, L.-J., Li, K., Fei-Fei, L.: ImageNet: A large-scale hierarchical image database. In: 2009 IEEE Conference on Computer Vision and Pattern Recognition, pp. 248–255 (2009). <https://doi.org/10.1109/CVPRW.2009.5206848>
9. Shoieb, D.A., Youssef, S.M., Aly, W.M.: Computer-Aided Model for Skin Diagnosis Using Deep Learning, vol. 4, no. 2, pp. 122–129 (2016). <https://doi.org/10.18178/joig.4.2.122-129>
10. Saba, T., Al-Zahrani, S., Rehman, A.: Expert system for offline clinical guidelines and treatment. *Life Sci. J.* **9**(4), 2639–2658 (2012)
11. Husham, A., Alkawaz, M.H., Saba, T., Rehman, A., Alghamdi, J.S.: Automated nuclei segmentation of malignant using level sets. *Microsc. Res. Tech.* **79**(10), 993–997 (2016). <https://doi.org/10.1002/jemt.22733>

12. Saba, T., Sameh, A., Khan, F., Shad, S.A., Sharif, M.: Lung nodule detection based on ensemble of hand crafted and deep features. *J. Med. Syst.* **43**(12), 332 (2019)
13. Afza, F., Khan, M.A., Sharif, M., Saba, T., Rehman, A., Javed, M.Y.: Skin lesion classification: An optimized framework of optimal color features selection. In: 2020 2nd International Conference on Computer and Information Sciences (ICCIS), pp. 1–6. IEEE (2020, Oct)
14. Dutta, K., Roy, S., Whitehead, T.D., Luo, J., Jha, A.K., Li, S., Quirk, J.D., Shoghi, K.I.: Deep learning segmentation of triple-negative breast cancer (TNBC) patient derived tumor xenograft (PDX) and sensitivity of radiomic pipeline to tumor probability boundary. *Cancers* **13**(15), 3795 (2021). <https://doi.org/10.3390/cancers13153795>
15. Patel, B., Dhayal, K., Roy, S., Shah, R.: Computerized skin cancer lesion identification using the combination of clustering and entropy. *Int. Conf. Big Data Anal. Comput. Intell. (ICBDAC)* **2017**, 46–51 (2017). <https://doi.org/10.1109/ICBDAC1.2017.8070807>
16. Anantha, M., Moss, R.H., Stoecker, W.V.: Detection of pigment network in dermatoscopy images using texture analysis. *Comput. Med. Imaging Graph.* **28**(5), 225–234 (2004). <https://doi.org/10.1016/j.compmedimag.2004.04.002>
17. Iftikhar, S., Fatima, K., Rehman, A., Almazyad, A.S., Saba, T.: An evolution based hybrid approach for heart diseases classification and associated risk factors identification. *Biomed. Res.* **28**(8), 3451–3455 (2017)
18. Lung, J.W.J., Salam, M.S.H., Rehman, A., Rahim, M.S.M., Saba, T.: Fuzzy phoneme classification using multi-speaker vocal tract length normalization. *IETE Tech. Rev.* **31** (2), 128–136 (2014). <https://doi.org/10.1080/02564602.2014.892669>
19. Skrøvseth, S.O. et al.: A computer aided diagnostic system for malignant melanomas. In: 2010 3rd International Symposium on Applied Sciences in Biomedical and Communication Technologies (ISABEL 2010), pp. 1–5 (2010). <https://doi.org/10.1109/ISABEL.2010.5702825>
20. Shrestha, B., et al.: Detection of atypical texture features in early malignant melanoma. *Ski. Res. Technol.* **16**(1), 60–65 (2010). <https://doi.org/10.1111/j.1600-0846.2009.00402.x>
21. García Arroyo, J.L., García Zapirain, B.: Detection of pigment network in dermoscopy images using supervised machine learning and structural analysis. *Comput. Biol. Med.* **44**(1), 144–157 (2014). <https://doi.org/10.1016/j.combiomed.2013.11.002>
22. Sadeghi, M., Razmara, M., Lee, T.K., Atkins, M.S.: A novel method for detection of pigment network in dermoscopic images using graphs. *Comput. Med. Imaging Graph.* **35**(2), 137–143 (2011). <https://doi.org/10.1016/j.compmedimag.2010.07.002>
23. Xiao, F., Chiang, I.J., Wong, J.M., Tsai, Y.H., Huang, K.C., Liao, C.C.: Automatic measurement of midline shift on deformed brains using multiresolution binary level set method and Hough transform. *Comput. Biol. Med.* **41**(9), 756–762 (2011). <https://doi.org/10.1016/j.combiomed.2011.06.011>
24. Wighton, P., Lee, T.K., Lui, H., McLean, D.I., Atkins, M.S.: Generalizing common tasks in automated skin lesion diagnosis. *IEEE Trans. Inf. Technol. Biomed.* (2011). <https://doi.org/10.1109/TITB.2011.2150758>
25. Javed, R., Saba, T., Shafry, M., Rahim, M.: An intelligent saliency segmentation technique and classification of low contrast skin lesion dermoscopic images based on histogram decision. In: 2019 12th International Conference on Developments in eSystems Engineering (DeSE), pp. 164–169 (2020)
26. Javed, R., Rahim, M.S.M., Saba, T., Rashid, M.: Region-based active contour JSEG fusion technique for skin lesion segmentation from dermoscopic images. *Biomed. Res.* **30**(6), 1–10 (2019)
27. Saba, T., Javed, R., Shafry, M., Rehman, A., Bahaj, S.A.: IoMT enabled melanoma detection using improved region growing lesion boundary extraction. *CMC-Comput. Mater. Continua* **71**(3), 6219–6237 (2022)
28. Yu, L., Chen, H., Dou, Q., Qin, J., Heng, P.-A.: Automated melanoma recognition in dermoscopy images via very deep residual networks. *OP Conf. Ser. Mater. Sci. Eng.* **561**(1), 994–1004 (2017). <https://doi.org/10.1088/1757-899X/561/1/012107>
29. Akram, T., Khan, M.A., Sharif, M., Yasmin, M.: Skin lesion segmentation and recognition using multichannel saliency estimation and M-SVM on selected serially fused features. *J. Ambient Intell. Humaniz. Comput.* (2018). <https://doi.org/10.1007/s12652-018-1051-5>

30. Khan, A., Javed, M.Y., Sharif, M., Saba, T., Rehman, A.: Multi-model deep neural network based features extraction and optimal selection approach for skin lesion classification. In: 2019 International Conference on Computer and Information Sciences (ICCIS), pp. 1–7 (2019). <https://doi.org/10.1109/ICCISSci.2019.8716400>
31. Nawaz, M., Mehmood, Z., Nazir, T., Naqvi, R.A., Rehman, A., Iqbal, M., Saba, T.: Skin cancer detection from dermoscopic images using deep learning and fuzzy k-means clustering. *Microsc. research and technique*, **85**(1), 339–351 (2022)
32. Khan, M.A., Sharif, M.I., Raza, M., Anjum, A., Saba, T., Shad, S.A.: Skin lesion segmentation and classification: A unified framework of deep neural network features fusion and selection. *Expert Syst. (October)*, 1–21 (2019). <https://doi.org/10.1111/exsy.12497>
33. Adjed, F., Gardezi, S.J.S., Ababsa, F., Faye, I., Dass, S.C.: Fusion of structural and textural features for melanoma recognition. *IET Comput. Vis.* **12**(2), 185–195 (2018). <https://doi.org/10.1049/iet-cvi.2017.0193>
34. Bi, L., Kim, J., Ahn, E., Feng, D., Fulham, M.: Automatic melanoma detection via multi-scale lesion-biased representation and joint reverse classification. In: 2016 IEEE 13th International Symposium on Biomedical Imaging (ISBI), vol. 2016-June, pp. 1055–1058. (2016). <https://doi.org/10.1109/ISBI.2016.7493447>
35. Satheesha, T.Y., Satyanarayana, D., Prasad, M.N.G., Dhruve, K.D.: Melanoma is skin deep: A 3D reconstruction technique for computerized dermoscopic skin lesion classification. *IEEE J. Transl. Eng. Heal. Med.* **5**(December), 2017 (2016). <https://doi.org/10.1109/JTEHM.2017.2648797>
36. Nasir, M. Attique Khan, M., Sharif, M., Lali, I.U., Saba, T., Iqbal, T.: An improved strategy for skin lesion detection and classification using uniform segmentation and feature selection based approach. *Microsc. Res. Tech. (October 2017)* (2018). <https://doi.org/10.1002/jemt.23009>

COVID-19 Prediction, Diagnosis and Prevention Through Computer Vision



Sajid Iqbal **Hareem Ayesha** **Muhammad Farooq Khan Niazi**,
Noor Ayesha, and **Khawaja Tehseen Ahmad**

Abstract Recent Corona Virus Disease (COVID) outbreak, caused by severe acute respiratory syndrome coronavirus 2 (SARS-CoV2), has been posing a big threat to global health since December 2019. In response, research community from all over the world has shifted all their efforts to contribute in this global war by providing crucial solutions. Various computer vision (CV) technologies along with other artificial intelligence (AI) subsets have significant potential to fight in frontline of this turbulent war. Normally radiologists and other clinicians are using reverse transcript polymerase chain reaction (RT-PCR) for diagnosing COVID-19, which requires strict examination environment and a set of resources. Further, this method is also prone to false negative errors. One of the potential solutions for effective and fast screening of doubtful cases is the intervention of computer vision-based support decision systems in healthcare. CT-scans, X-rays and ultrasound images are being widely used for detection, segmentation and classification of COVID-19. Computer vision is using these modalities and is providing the fast, optimal diagnosis at the early-stage controlling mortality rate. Computer vision-based surveillance technologies are also being used for monitoring physical distance, detecting people with or without face masks, screening infected persons, measuring their temperature, tracing body movements and detecting hand washing. In addition to these, it is also assisting in production of vaccine and contributing in administrative tasks and clinical management. This chapter presents an extensive study of some computer vision-based technologies for detection, diagnosis, prediction and prevention of COVID. Our main goal here is to draw a bigger picture and provide the role of computer vision in fight against COVID-19 pandemic.

S. Iqbal · H. Ayesha · K. Tehseen Ahmad

Department of Computer Science, Bahauddin Zakariya University, Multan, Pakistan

e-mail: Sajid.iqbal@bzu.edu.pk

M. Farooq Khan Niazi

Consultant Radiologist, Diagnostic Imaging Department King Salman North West Armed Forces Hospital (NWAFH), Tabuk, Saudi Arabia

N. Ayesha

School of Clinical Medicine, Zhengzhou University, Zhengzhou, Henan, PR China

Keywords Computer vision · COVID-19 · Coronavirus · Review · Diagnosis · Detection · Classification · Control · Prevention · Prognosis

1 Overview of COVID-19 Pandemic

1.1 Potential Origin

Coronaviruses (CoV) are a big family of zoonotic viruses because they contaminate from animals to humans [1]. First severe outbreak of CoV was due to Severe Acute Respiratory Syndrome Coronavirus (SARS-CoV) which occurred in 2003 and originated from musk cats [1]. Second known epidemic of severe illness is Middle East Respiratory Syndrome coronavirus (MERS-CoV) that was occurred in Saudi Arabia in 2012. It was contaminated from dromedary to humans. Current third outbreak of coronavirus is called Severe Acute Respiratory Syndrome Coronavirus 2 (SARS-CoV2) because it is genetically similar to SARS-CoV. The first case of this attack appeared in December 2019, in Wuhan, Hubei province, China. Initially, it was predicted to be contaminated from bats and pangolins to humans [2].

1.2 Replication

SARS-CoV2's original source is still not confirmed; however its human to human transmission ability is strongly evidenced. This novel virus spreads through respiratory transmission from human to human and from contact with already infected patients and surface through use of nose, eye or mouth. Its transmission through air is seemed to be more dominant source of COVID-19 spread [3]. Despite immense efforts including enforcement of globally quarantine and travel restrictions to hold the virus within China, it circulated globally. World Health Organization (WHO) declared this outbreak a global pandemic on March 11, 2020, and spectrum of infection caused by this coronavirus is now known as Coronavirus Disease 2019 (COVID-19).

1.3 Symptoms

Most common signs of COVID-19 include dry cough, fever and tiredness. Less common symptoms include aches, pain, sore throat, nasal congestion, diarrhea, headache, sneezing, loss of taste and smell, pain in muscles and rashes on skin. Serious indicators include shortness in breath, pressure or pain in chest, difficulty in speaking and moving and bilateral lung infiltrates [1, 4]. In most severe cases, patients infected with COVID-19 suffer from pneumonia, severe acute respiratory syndrome

(SARS), septic shock, multi-organ failure, heart and kidney injury, pulmonary edema, acute respiratory distress syndrome (ARDS) and death [5, 6]. It is also seen in some cases where no symptoms are detectable (asymptomatic) imposing a bigger health challenge because disease can be transmitted to other humans. It has been determined that older persons and those who have already been having medical problems like chronic respiratory, cancer, diabetes and heart disease are more vulnerable to COVID-19 [1].

1.4 Threat to Global Health

Due to its high spread rate and communicable nature, COVID-19 is catching globally. As of September 20, 2021, based on John Hopkins dashboard [7], there are 228,557,439 confirmed cases of COVID-19 worldwide with USA reporting the highest number of confirmed cases (42,087,485) followed by India (33,478,419), Brazil (21,239,783), UK (7,464,791), Russia (7,170,069), France (7,043,875) and Turkey (6,847,229) on the seventh position. The number of worldwide reported deaths is 4,692,079 with USA reporting highest number of deaths (673,765) followed by Brazil (590,752), India (445,133), Mexico (271,503), Peru (199,066), Russia (194,671), Indonesia (140,468) and UK (135,539) on the eighth position (Fig. 1). It is estimated that the actual number of patients is higher than reported cases.

2 Contributions of This Work

This work contributes to research in following ways:

- A comprehensive review has been made about the computer vision and its application for the detection and diagnosis of COVID-19, and for controlling its spread.
- The work provides an overview of the disease and its effects on global society

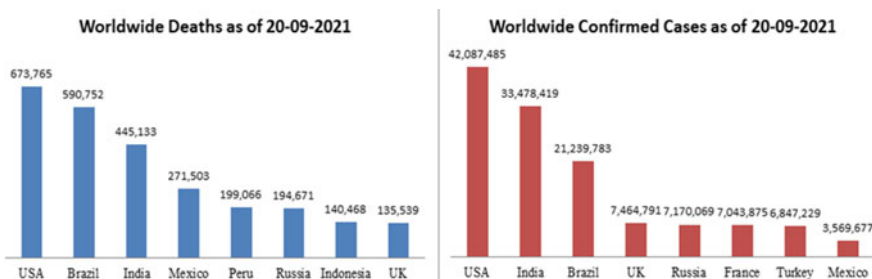


Fig. 1 Worldwide confirmed cases of COVID-19 and deaths

- A list of datasets available for COVID study has been provided
- Future challenges and research directions are provided for the interested researchers.

3 Diagnosis of COVID-19

As SARS-CoV2 is contagious in nature, the diagnosis of COVID-19 at early stage is essential to hold the virus. This, however, is not easy because the virus can remain quiet in humans approximately five days before showing any signs [8]. Even with symptoms, it is difficult to distinguish COVID-19 from common influenza.

3.1 *Etiological Tests*

At present, the gold standard for diagnosing COVID-19 is reverse transcription polymerase chain reaction (RT-PCR) in which a swab is taken from patient's throat or nose and then sent to machine to check the existence of virus. But this method has faults such as its sensitivity and specificity which are up to 70% and 95% respectively [9, 10]. Many factors can affect the results including but not limited to disease severity, types of collected resources, method to collect and handle the resources and duration of symptoms [11]. For example, if transportation of swab from patient to testing machine takes too long, the germ may die and result of infected person may be declared as negative. Also, this test is complicated and slow as it consumes almost 2–3 h. Moreover, it demands experts for adequate diagnosis and monitoring the COVID-19 progression. Thus, requirement of strict environment and lack of expensive resources for testing result in ineffective diagnosis of suspected patients. Furthermore, RT-PCR only identifies the presence of viral-RNA and cannot verify that the virus is active or transmissible [12]. In some cases it has been shown that RT-PCR also gives false negatives [13].

3.2 *Serological Tests*

Another way of COVID-19 early detection is testing of antibody produced as an immune response from body infected by COVID-19 [14]. This method is cheap, produces results in less time, almost 15 min, and requires a modest laboratory to carry out the test [15]. However, accuracy of this test is limited by the timing of test administration. The average maturation period of virus is 5.2 days [8]; however, antibodies are not detectable before tenth day of infection and more significantly, before fourteenth day onwards. This diagnosis is therefore not appropriate for early detection. Moreover, this test is susceptible to both false negatives and false positives

for cases with minor symptoms. Yet, this method can be carried out when RT-PCR is not available or in cases that has been symptomatic for fourteen or more days and RT-PCR is negative.

3.3 Imaging Tests

Diagnosis through medical images has gained significance, given the constraints of time and unavailability of resources for etiological tests. Computed tomography (CT) scans, chest X-rays, ultrasound and magnetic resonance imaging (MRI) are some imaging modalities used for clinical diagnosis of COVID-19.

CT Scans. Most of COVID-19 cases have similar characteristics on CT scans and chest X-ray images including bilateral distribution of patchy shadowing and ground-glass opacities (GGO) [16]. Normally, pneumonia produces fluid in the lung which keeps building up and manifests itself as opacities. In COVID-19 infected patient, these opacities look like ground glass pointed by arrow in Fig. 2b and majority of them appear along the periphery of lung. Findings of COVID-19 CT images, however, vary with patient's immunity level, age, disease level, underlying diseases and drug inter-mediation at diagnosis time [17]. Along with exposing harmful radiations, another major drawback of CT scans is that these images present low specificity and higher sensitivity [18]. Therefore, many scientific societies do not recommend the use of CT images as first-line tool to diagnose COVID-19 due to its similarity with features of other pulmonary diseases [19].

Chest X-Rays. Although chest X-rays present less sensitivity than CT images especially in early detection of COVID-19 (Fig. 3), these images can be used to assess and monitor COVID-19 progression. Therefore, chest X-rays are used as first-line tool for COVID-19 diagnosis. This imaging modality is also more affordable than CT and commonly used. But, these also expose the patient to harmful ionizing radiations like CT images, and therefore, it is not recommended for adults and pregnant women.

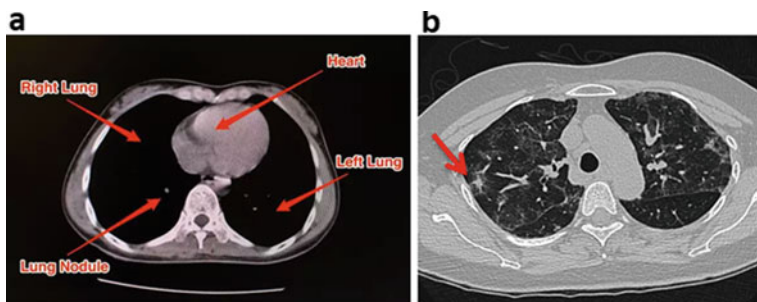


Fig. 2 **a** CT scan of a normal person's lung; **b** COVID-19 positive CT taken from open source dataset [19] (irregular opacities-arrow)

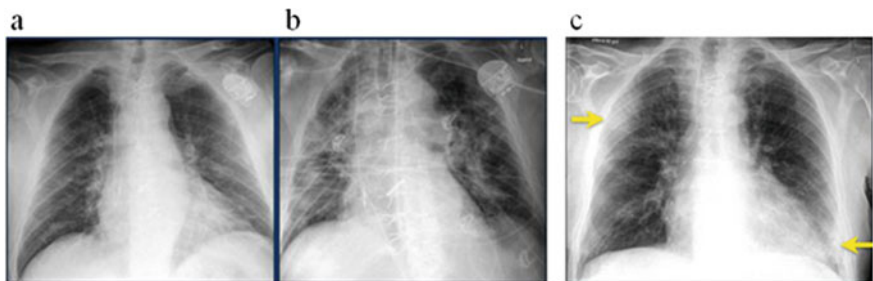


Fig. 3 **a** Chest X-Ray of a normal person; **b** Bi-lateral consolidations in Chest X-Ray of COVID-19 patient; **c** Consolidations in the left lower lobe and right upper lobe (arrows) and GGO (images taken from open source dataset [19])

Another problem with use of CT scans and chest X-rays for diagnosing COVID-19 is, there is often need to transfer the patients to CT rooms along with CT and X-ray machines. This requires extensive cleaning of machinery after each use.

Ultrasound. Other alternative of CT scans is image acquisition through ultrasound (Fig. 4). This method is cost-effective, portable and non-invasive with minimal radiation risks. Lung ultrasound is being used for initial bed screening of suspected cases and detection, diagnosis and monitoring of confirmed patients [20–22]. Although ultrasound gives good sensitivity score, its specificity score is low; common findings are consolidations, B-lines and sub-pleural thickening [23]. Additionally, it requires experts and proper guidelines for carrying out test and to manage patients.

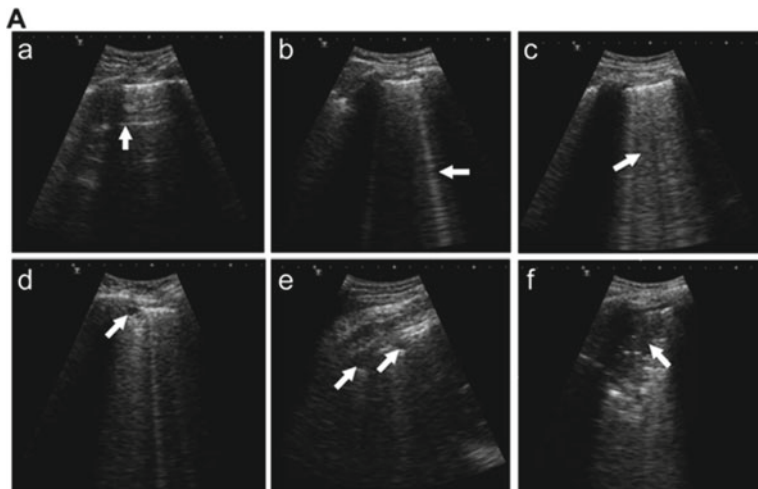


Fig. 4 COVID-19 findings (arrows) in lung ultrasound images from open source dataset [24]; **a** A-lines; **b** Single B-lines; **c** Confluent B-lines; **d** Sub-pleural consolidations; **e** Substantial consolidations; **f** Consolidation with air bronchogram



Fig. 5 Images taken from [28]. **a** Axial CT scan and **b** PET-CT fusion images (multiple largely peripheral GGO within the left upper lobe (arrow); more delicate GGO in the right upper lobe with increased FDG uptake (arrow))

PET. Positron emission tomography (PET) is another non-invasive imaging modality to identify and monitor pulmonary and inflammatory diseases. As compared with previous modalities, it is not being used for primary diagnosis of COVID-19 (Fig. 5). However, it has been reported for early and accidental COVID-19 detection in infected but asymptomatic cases [25]. Integration of PET with CT and flourine-18 fluorodeoxyglucose (^{18}F -FDG), a commonly used imaging agent, ^{18}F -FDG PET/CT delivers structural, functional and molecular information of SARS-CoV-2 [26] and is also used for managing patients and healthcare workers. ^{18}F -FDG PET/CT is more sensitive than other imaging modalities, but it is not being widely used for COVID-19 diagnosis due to its poor specificity, complicated and costly scanning process, low worldwide availability and associated risks of infection spread [27].

MRI. MRI is another non-ionizing imaging modality with ability to characterize properties of soft tissues. This method is not recommended as first-line for COVID-19 diagnosis because it is not relevant to evaluation of lung infection. Moreover, it is relatively costly and requires longer time for scanning than CT scans and ultrasound. But, it contributes in defining spine and brain targets of confirmed cases of COVID-19. SARS-CoV-2 mainly distributes in the lung but its infection also damages vessels, heart, liver, kidney and other organs [24]. Due to outstanding performance for envisioning functional and structural properties of different soft organs, MRI can be used as to better understand the nature of infection by assessing the vulnerability of different organs (Fig. 6). Moreover, for patients such as older adults and pregnant women, who must be avoided from radiation, non-invasive MRI imaging is a practical alternative.

4 Workflow of Image-Based COVID-19 Diagnosis

Conventional workflow of image-based diagnosis of COVID-19 consists of mainly three steps [30]:

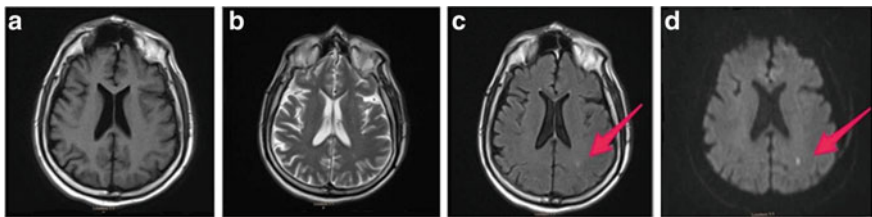


Fig. 6 Images taken from [29] **a** and **b** Normal Brain MRI scans; **c** and **d** an infarct spot and a cerebrovascular manifestation due to limited blood circulation in acute stroke, indicated by red arrow respectively

- (1) Pre-test preparation
- (2) Image acquisition
- (3) Disease diagnosis.

In first step, each patient is instructed and a technician assists him to pose on screening bed according to specified guidelines such as feet-first versus head-first and prone versus spine in CT. After that, target body part is visually identified on patient and relative position of screening machine is manually adjusted. In image acquisition phase, images such as CT scan and ultrasound are attained with machines whose parameters are already adjusted by radiologists grounded on body shapes of patients. In final step, acquired imaging modality is transferred to picture archiving and communication systems (PACS) for consequent examination and diagnosis [30].

Along with individual drawbacks of each imaging modality described in previous section, there are some risks associated with current conventional in-contact diagnosis method itself. First this method is highly dependent on human labor and is time consuming. Moreover, in image acquisition phase, there is inevitable contact between patients and technicians which causes high risks of virus spread if patient is declared to be infected. Scanning machine is also likely to have droplets distributed by patient. So, an extensive cleanup of machine is needed after each case. Therefore, a contactless automated procedure is required for efficient and accurate diagnosis and to control the viral spread. Here comes computer vision as a rescue which plays a major role in providing rapid solutions for automatic disease's early detection, prediction, diagnosis, prognosis and prevention.

5 Computer Vision

Computer vision (CV) is a subfield of artificial intelligence (AI) that enables the systems and computers to mimic human sight without the intervention of explicit human programming. It assists systems to visualize, understand and derive significant information from visual data such as digital images and videos and make decisions and recommendations based on derived information. CV-based tasks range from low level such as edge detection to high level such as interpreting complete scene. It

highly relies on huge volume of data to be trained on and applies pattern recognition algorithms to detect, localize, segment and classify the objects. This process is further augmented by deep learning (DL) which helps in recognizing more complex patterns and neural networks (NN); in this context, it makes the job easier by auto-feature extraction. Moreover, availability of large volume of labeled visual data and high-speed GPUs has advanced the research in computer vision field. Some other uses of computer vision include self-driving car, face recognition, security surveillance, manufacturing, gaming, optical character recognition, robotics and healthcare.

5.1 Applications of CV in Healthcare

With the availability of large volume of digital data, computer vision (CV) technology along with other artificial intelligence (AI) methods such as DL, image processing (IP), expert systems (ES) and NN is revolutionizing healthcare industry by solving several complex health problems. It has the potential to assist medical professionals for fast and accurate diagnosis and to save lives. Major applications of CV in healthcare are given as follows:

Medical Imaging Analysis. In medical industry, computer vision's most salient and widely explored application is the deep analysis of different imaging modalities, i.e., X-rays, positron emission tomography (PET), computed tomography (CT-scans), ultrasound and magnetic resonance imaging (MRI). Various computer vision models are being trained on these medical images to perform different image analysis tasks which assist medical experts in efficient and effective clinical decision making [31]. Some major medical imaging analysis tasks performed for disease diagnosis include:

- *Image classification:* A medical image is classified into two (normal or abnormal) or more classes where an abnormal image is further assigned a label from different disease classes, i.e., tumor types. In medical imaging, image classification is a fundamental task of CV and plays a crucial role in computer-aided diagnosis [32–34].
- *Object detection and localization:* Object detection refers to identifying the abnormal regions and organs and localization refers to highlighting the position of detected areas by drawing a bounding box around them [35–37]. This task aims to detect the earliest marks of abnormalities and referred as computer aided detection.
- *Image segmentation:* It is the process of partitioning an image into segments that share similar characteristics and assigning a unique color or label to each segment. In medical imaging, segmentation is mostly performed to determine the size of abnormality in a computer aided detection system [38, 39]. It automatically identifies and labels the regions of an image, i.e., lung or abnormality such as lesions and cancer.
- *Radiology Report Generation:* In this technique, a radiology report consisting of single or multiple natural language sentences is generated against an image

which explains the finding of an image such that which part is normal and which is abnormal. This is more challenging task than image classification, detection and segmentation [40, 41].

Surgery. Refining and advancement in DL has supported CV to accurately use medical imaging analysis techniques to analyze inter-operative videos, to memorize past surgical actions and to accurately identify surgical steps and instruments during a variety of surgical procedures. Similar to teaching a medical student the steps of operations, researchers are developing algorithms and teaching computers to automatically detect the surgical phase at a given point of time with accuracy comparable to physical surgeons [42, 43]. Commercial and research entities are also developing CV-based robotic surgical systems which use mechanical arms and camera attached with surgical instrument for tracking [44, 45]. Surgeons operate through controlling the mechanical arm via a console positioned adjacent to operating table. The console provides the surgeon with a magnified, high definition, 3D view of surgery. Some real-world applications of CV are Gauss Surgical (<https://www.gausssurgical.com/>) and RSIP Vision (<https://rsipvision.com/orthopedics/>). Former is a US-based company that offers CV-based system called Triton which monitors the blood loss during surgery and latter is a California-based company that provides CV-based solutions for accurate navigation during orthopedic surgery, respectively.

Patient's Monitoring. Another application of CV is monitoring of critical patients from a remote location [46]. Patient's monitoring systems are mostly used in intensive care units (ICUs) where patients need more attention than normal wards and require 24-h observation to provide them medical aid in the moment of need. These systems offer additional care with the help of different CV-based software tools to analyze patient's vital signs, values and trends [47]. Monitoring systems are also being used in clinical observations to analyze abnormal activities such that bed climbing, unbalanced walk and body movements [48]. Instead of demanding more staff for monitoring the patient's activities, CV-based surveillance systems are assisting in collecting details of patient's movements and activities for better assessment.

In addition, CV can also assist in remote monitoring of patients who prefer home-based rehabilitation after an illness [16]. Medical professionals deliver required therapy to patients and monitor their progress remotely using CV-based video-assisted systems. These systems can also monitor elderly patients because of their non-intrusive nature. One such application is fall detection system that analyzes the rate of change in movement with respect to floor point and assists elderly patients by alarming them about objects that can cause the fall [49]. The computer vision methods can also be used to analyze the changing situation of patients suffering from COVID.

Automatic Lab Tests. Computer vision is also being used to develop blood analyzer that either takes image of blood sample as an input or accepts comprehensible data in the form of an image of a slide holding a film of blood [50]. Trained experts acquire these images using a special-designed cameras attached to a microscope.

Then based on image processing and CV technologies, system processes the image and automatically identifies the precise irregularities in blood samples [51].

Clinical Trials. Clinical trial is the most expensive stage of drug development because of time and effort needed to find the appropriate candidates. The candidates have to symbolize many races, ages, ethnicities and genders. Moreover, they have to be comprehensively examined before taking part in the trials. This is a costly and time-consuming process. Here comes CV as a rescue and helps to choose appropriate candidate and monitor the effect of medicine [52]. One example of such application is AI Cure (<https://aicure.com/>); a US-based company whose objective is to reduce risks of clinical trials. AI Cure software monitors the candidate as they go under prescribed treatment and assists the doctors and clinicians to predict and understand the patient's adherence to treatment.

Some other applications of CV in healthcare include screening of critical cases from a queue of patients [53], remote radiation therapy [54] and improving administrative procedures for example automatic searching and interpreting patients' health records [55].

6 Role of Computer Vision in COVID-19 Pandemic

Recent Corona Virus Disease (COVID) outbreak caused by SARS-CoV2 has been posing a big threat to global health since December 2019. In response, research community from all over the world has shifted all their efforts to contribute in this global war by providing crucial solutions. Since various computer vision (CV) applications are already revolutionizing healthcare industry by solving several complex health problems. Therefore, computer vision has also significant potential to fight in frontline of this turbulent war. During current rapid spread of pandemic, when there is urgent need to control this spread and identify positive cases, computer vision is playing a major role by providing rapid solutions for COVID-19 early detection, prediction, diagnosis, prognosis and prevention.

6.1 Computer Vision for COVID-19 Diagnosis

Conventional in-contact COVID-19 diagnostic methods include reverse transcription polymerase chain reaction (RT-PCR), tests through antibodies and different imaging modalities. But these all methods have demerits such as false negatives and false positives, time-consuming, lack of resources, etc., as described previously in Sect. 2. An alternative is CV-based diagnosis that is a rapid, cost-effective, efficient diagnostic method with large-scale availability. In this computer-aided diagnostic method, images of different modalities are given as an input to the system that has the ability to classify suspicious cases, detect infection and segment the infected area.

CV-Empowered Imaging Workflow. Existing scanning machines are equipped with cameras used to monitor the patients. These machines can support contactless diagnosis workflow for example, and technician can observe the patient from control room with the help of video stream from the camera. But, this is still challenging for technician because camera provides only over-head view of the patient and other parameters for scanning such that scan range cannot be determined. In this situation, CV automates this process [56–58] by identifying shape and pose of patient via visual sensors such as time-of-flight (TOF) pressure, RGB or thermal imaging and optimal parameters of scanning are calculated [59]. One such typical parameter is the range of scan that defines the start and end positions of scan. Another key parameter is ISO-centering that refers to alignment of patient's body area such that its center overlaps with the center of scanner. It has been shown that such automated imaging workflow improves the efficiency of scanning and reduces excessive exposure to radiation [60, 61].

During COVID-19 pandemic, various contactless imaging methods are developed, such that utilizing cameras on the device [62] or in the scanning room [63, 64] and to CV-empowered mobile CT platforms utilizing AI technologies [65, 66]. An example of such platform is shown in Fig. 7. It mainly consists of two fully isolated rooms; scanning room and control room, each with its own entrance to evade needless interaction between patients and technicians. After going into scanning room, patients are guided through audio and visual prompts to pose on the scanning bed. Technicians monitor patients through the window and live video captured by camera mounted in the ceiling of scanning room and correct the patient's pose when necessary. When patient is seemed ready, his 3D pose and fully reconstructed mesh are recovered

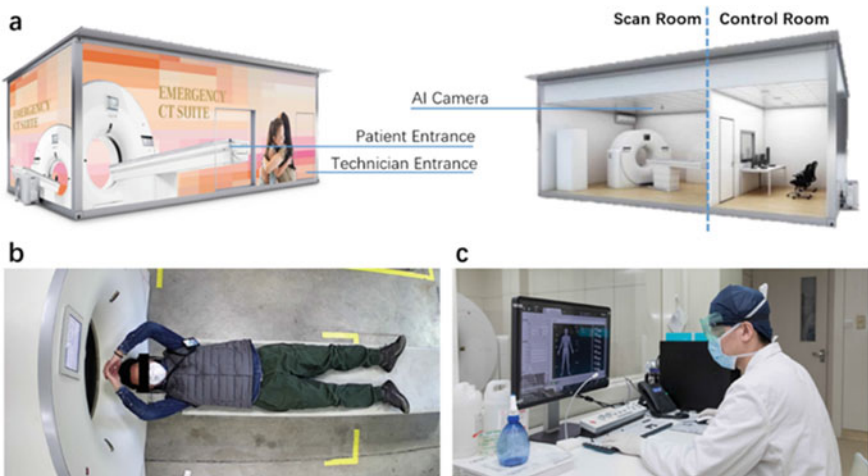


Fig. 7 **a** A mobile scanning room equipped with CV-empowered image acquisition workflow; **b** An image captured by camera to monitor patient; **c** Patient's positioning and scanning operated remotely by technician

through a motion analysis algorithm. Based on this 3D mesh, scan range and center-line of body's target area are determined as scanning parameters. Once these parameters are verified and adjusted by technician, scanning bed will be automatically adjusted to ISO-center and entered into CT scan gantry for image acquisition that will be further used for screening purpose.

Segmentation of COVID-19. After image acquisition, the segmentation of image is a fundamental step in the processing and analysis of image for COVID-19 assessment. Image segmentation defines region of interest (ROI) such as lobes, lung, bronchopulmonary areas and infected/abnormal lesions or regions in the CT image or chest X-ray. This segmented area is further utilized for features extraction and diagnosis. CT-scans offer high-quality three-dimensional images for COVID-19 detection. Although chest X-ray is most widely used imaging modality but projection of ribs onto soft tissues in 2-dimensional confounds the image contrast [30]. This makes segmentation of X-ray images more challenging as compared to CT images.

In terms of ROI in CT images, segmentation is considered essential process for COVID-19 diagnosis because it provides correct quantification information for assessment of COVID-19 progression in follow-up, detailed prediction of infection severity and visualization of lung lesions spread using percentage of interest (POI) [30]. These methods can be generally categorized into two groups. First group contains lung region-based methods which aim to segment lung areas, i.e., entire lung and lobes from background areas in CT image or X-ray. Second category contains lung lesions-based methods in which metal, lung lesions or motion artifacts are separated from other lung areas. Because lung nodules or lesions could be tiny with a variety of textures and shapes, identifying them is a challenging process. Popular DL-based segmentation models used for COVID-19 detection include U-Net [67], U-Net++ [68], and V-Net [69]. U-Net is used for segmentation of both lung lesions and lung regions for COVID-19 detection. U-Net is a fully convolutional neural network having U-shape architecture with symmetric encoding and decoding layers. Layers on same level are connected through shortcut connections providing better comprehensive contextures and visual information. Various variants of U-Net have also been proposed by researchers that gave reasonable results in COVID-19 applications [70–75]. Authors in [76] used U-Net to distinguish COVID-19 from normal pneumonia on chest CT scans with the help of lung segmentation. Another AI-based work presented a method for fast diagnosis of COVID-19 [77] which accepts CT scans as an input and performs segmentation that further goes into classification model. Researchers in [2] used V-Net to perform segmentation of COVID-19 infected regions of lungs. Another network called InfNet aimed the segmentation of COVID-19 lung infection and is developed by [78]. The authors used two staged approach to resolve the multi-segmentation issue. In the first stage, overall lung lesion is segmented and then forwarded to the second stage that further distinguishes into consolidation lesion (Fig. 8).

Classification of COVID-19. In the classification problem, CV is being used to classify COVID-19 images (chest X-ray, CT scans, etc.) into various classes (Fig. 9). Some researches separated COVID-19 cases from non-COVID-19 indi-

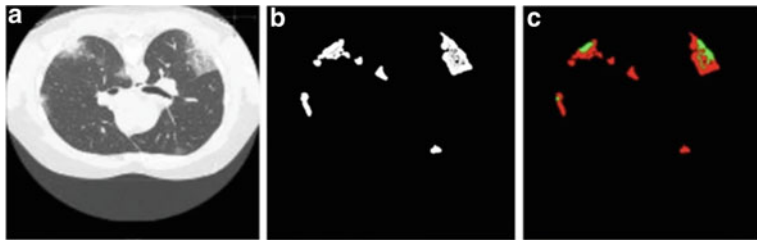


Fig. 8 **a** A sample lung CT scan from open source Med-seg dataset [79]. **b** Overall segmented lung lesion. **c** Segmented GGO in red and segmented consolidation in green)

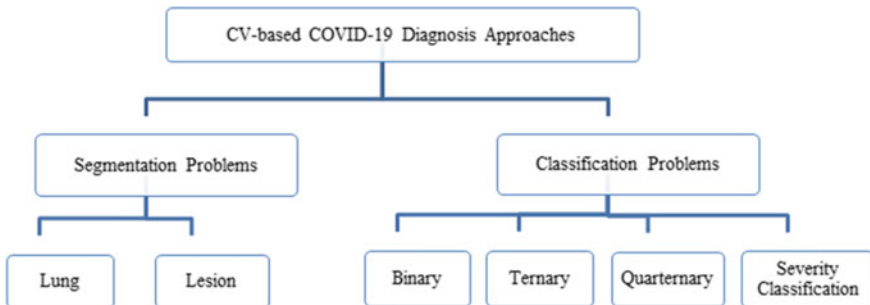


Fig. 9 CV-based COVID-19 diagnosis approaches

viduals either having common pneumonia or non-pneumonia subjects. This task is referred as binary classification problem. Another mostly explored method is multi-classification (ternary, quaternary or quandary) of images to detect COVID-19. Classes included in ternary classification problem are COVID-19 cases, no pneumonia/no infection and pneumonia (bacterial or any other non-COVID-19 infection). In quaternary classification problem, images are classified into normal, no pneumonia, bacterial infection and COVID-19 cases. In other multi-classification problems (i.e., quandary/five or greater), images are classified into COVID-19, pneumonia, viral infection, bacterial infection and normal. In the following section, proposed work by research community to perform different classification problems related to COVID-19 is presented.

COVID-19 Detection as Binary Classification Problem—COVID-19 and Common Pneumonia Types. Authors in [80] proposed and evaluated a transfer learning-based approach by using the VGG-16 model. They developed two models; in the first model, chest X-rays are classified into a healthy case and a patient with common pulmonary disease. In case the X-ray is classified as common pulmonary disease, X-ray is fed into a second model designed to detect whether the pulmonary disease is COVID-19. Their model showed 96% accuracy for the classification between normal and common pulmonary disease cases and 98% accuracy for the detection of COVID-19. A binary classifier to discriminate CT scans between COVID-19

cases and non-COVID-19 cases is presented in [81]. Authors used attention mechanism for screening COVID-19 and showed 97.9% accuracy. Another pre-trained ResNet-based model for the classification of COVID-19 infection from non-COVID pneumonia from CT images was proposed in [82]. They replaced the input layer of neural network with wavelet transform layer. The output image of the transform layer is used as an input to the next layer of ResNet and all layers of ResNet were re-trained. They also used heat maps to visualize the area of interest being focused by the convolutional neural network in the final classification stage. Their classification model obtained 92.2% accuracy. Another binary classification model called DarkCovidNet for COVID-19 detection is proposed in [83]. Their model is based on DarkNet neural network [84] that has remarkable results in object detection tasks. Their presented model classified X-rays into COVID-19 and no findings and produced 98.8% accuracy. They also verified their model by sharing the outputs of presented model with expert radiologists who confirmed model's robustness. Moreover, they acquired heat maps of the final output of their model which visually depicted the areas of images emphasized by model. These heat maps were also given to radiologists to evaluate and interpret the model. In [85], authors used transfer learning and trained Inception-V3 on chest X-rays to detect COVID-19. Their model discriminated between COVID-19 cases and other pneumonia cases. They also generated attention heat maps of each output of the model and provided to two expert radiologists for ensuring the interoperability and robustness of the proposed model. A binary classifier for COVID-19 diagnosis proposed in [86] is based on Res2Net model [87]. They modified the last layer of Res2Net as a fully connected layer with two nodes to output the probabilities of two classes, i.e., positive or negative case. Authors in [88] trained eight different neural networks on both chest X-rays and CT scans and compared the results of binary classification. Besides, they also used local interpretable model-agnostic explanations (LIME) to explain and demonstrate the model's interoperability. Some other studies presenting models for COVID-19 detection as a binary classification task are proposed in [89–92].

COVID-19 Detection as Ternary Classification Problem—Normal, Pneumonia and COVID-19. A multi-class classifier aimed to discriminate CT scans between three classes (COVID-19 cases, general pneumonia and non-pneumonia cases) is presented in [80]. Authors used attention mechanism for screening COVID-19 and showed 94.3% accuracy. Another CV-based model called DarkCovidNet for COVID-19 detection is proposed in [82]. Their model is based on DarkNet neural network [83] that has remarkable results in object detection tasks. Their presented model classified X-rays into three classes: COVID-19, pneumonia and no findings and produced 87.02% accuracy. They also verified their model by sharing the outputs of presented model with expert radiologists who confirmed model's robustness. Moreover, they acquired heat maps of the final output of their model which visually depicted the areas of images emphasized by model. These heat maps were also given to radiologist to evaluate and interpret the model. In [84], authors used transfer learning and trained Inception-V3 on chest X-rays to detect COVID-19. Their model classified images into COVID-19 cases, pneumonia and normal cases. They also generated attention heat maps of each output of the model and provided to two expert radiologists

for ensuring the interoperability and robustness of the proposed model. Transfer learning is used in [91] where authors trained ChexNet on chest X-rays and performed ternary classification to detect COVID-19 detection. Their model obtained 93.71% accuracy. An architecture used for COVID-19 diagnosis called COVIDagnosis-Net is developed by [93]. Their model is based on SqueezeNet neural network [94] and aimed to classify the X-rays into normal, pneumonia and COVID-19 cases. In [95], authors used auto-encoder-based approach to first detect the abnormal region in X-ray and then used deep learning-based model to classify the chest X-rays into normal, non-COVID pneumonia and COVID-19 classes. Researchers in [96] first segmented the abnormal region in CT images using V-Net model and then segmented patches are fed into a ResNet-18-based model which classifies images into normal, influenza-A and COVID-19 cases. Their model produced 86.7% accuracy. Some other studies presenting models for COVID-19 detection as a ternary classification task are proposed in [76, 97–99].

COVID-19 Detection as Quaternary Classification Problem—Normal, Viral Pneumonia/Tuberculosis, Bacterial Pneumonia and COVID-19. In [84], authors used transfer learning and trained Inception-V3 on chest x-rays to detect COVID-19. Their model classified images into COVID-19 cases, viral pneumonia cases, bacterial pneumonia cases and normal. They also generated attention heat maps of each output of the model and provided to two expert radiologists for ensuring the interoperability and robustness of the proposed model. A patch-based model is proposed in [100], in which firstly lung areas in chest X-rays are segmented using DenseNet-103 model. The segmented images are fed into a ResNet-18-based classification model using a patch-by-patch training and prediction. Images are classified into four classes: COVID-19, normal, bacterial pneumonia and tuberculosis. Authors in [101] also detected COVID-19 using quaternary classification of chest X-rays among normal, COVID-19, bacterial infection and non-COVID viral infection. A novel model referred as Domain Extension Transfer Learning (DETL) is presented in [102]. They fine-tuned pre-trained convolutional neural networks including AlexNet-8, VGGNet-16 and ResNet-50 and classified chest X-rays into four classes: normal, COVID-19 cases, pneumonia and other diseases. Some other studies presenting models for COVID-19 detection as a quaternary classification task are proposed in [4, 103, 104].

6.2 Computer Vision for COVID-19 Prognosis and Severity Assessment

Once the suspected individuals of COVID-19 are confirmed, it is essential to monitor the disease severity and progression. Automatic artificial intelligence-based computer vision techniques play vital role in this situation and are being used for disease progression monitoring. Imaging findings of patients suffering from COVID-19 have correlation with the disease severity. For example, by comparing chest CT

scans of COVID-19 patient with disease severity exposed a higher rate of occurrence of linear opacities, consolidations, bronchial wall thickening, and crazy-paving patterns than in non-COVID patients. Authors in [105] proposed a severity assessment model using frontal chest X-rays of COVID-19 patients. They used pre-trained DenseNet model to extract features from X-rays and build a severity assessment model. Their prediction model was based on two parameters: the degree of lung involvement and the degree of opacity for each lung. A mobile-based COVID-19 severity assessment applications are proposed in [106, 107]. Another CV-based severity classification algorithm is built by [108]. Their model is named as Convolutionary Siamese Neural Network (CSNN) which generates a score of pulmonary X-ray severity (PXS) of COVID-19 patient. They argued that their proposed model could also assist to forecast whether a patient will need intubation or not before dying. Authors in [109] designed a clinically valuable CV-based tool based on U-Net for lung segmentation and quantified pulmonary opacity in ten days and obtained human level training performance on CT images. Authors in [110] used region-based lung ultrasound videos along with other medical information such as symptoms, age and medical history and proposed a COVID-19 severity assessment model. Another CV-based model for severity classification of COVID-19 is proposed in [111]. They decomposed 3D CT images into multi-view slices which reduced the model's complexity. They also integrated other metadata of patient along with CT slices and classified images into four stages of severity (Fig. 10): early stage which shows GGO, progressive stage which displays an increase in both crazy-paving shapes, peak stage which indicates consolidation and absorption stage which displays gradual reduction in consolidation.

Another study developed an accurate, rapid and machine-agnostic model which segments and quantifies COVID-19 disease severity [112]. To enlarge the size of the training dataset, they designed a CT scan simulator by using multiple CT images from single COVID-19 patient taken at different time points, then decomposed 3D segmentation and presented a 2D segmentation model based on symmetry attributes

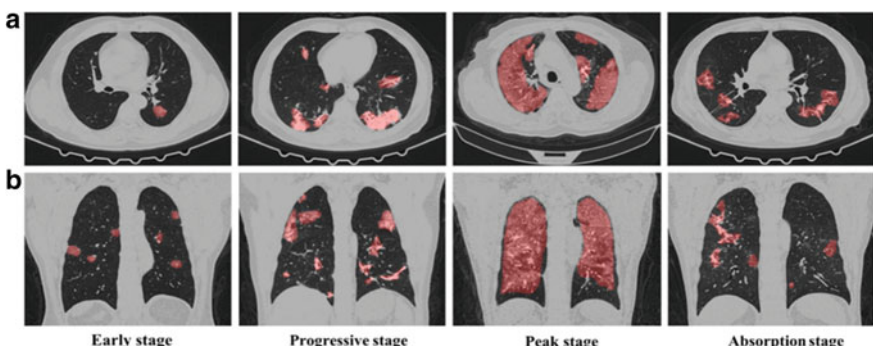


Fig. 10 Examples of 4 clinical of COVID-19 disease on CT scans of four patients. **a** Transverse scans. **b** Reconstructed coronal scans. Areas in red are lesion areas segmented by [111]

of lungs and other tissues. This decomposition reduced the model parameters. They evaluated their model on multi-machine and multinational data and achieved significant performance on segmentation and quantification of infected region. Researchers in [113] developed deep learning-based model for the detection and quantification of abnormalities (consolidations and GGO) in CT images of COVID-19 patients. In [114] a framework containing of segmentation of the pulmonary vessels and the lung, and detection of pneumonia is used for the quantification of lesion volume, lung volume, lesion fraction and average lesion thickness of the entire lung, left lung, right lung, and every lobe, which were then utilized to assess the severity of COVID-19. Some other studies presenting models for COVID-19 severity assessment and quantification are proposed in [115–118].

6.3 Computer Vision for COVID-19 Prevention

While the whole world is struggling hard to find the effective medicine of COVID-19, government of each country is also adopting preventing strategies such as imposing lockdown, travel restrictions, social distancing, quarantine and self-isolation of suspected and infected persons, closing public areas, ensuring masked faces, temperature screening and regularly hand washing. However, these large-scale strategies are not so efficient and have presented serious challenges in countries of weak infrastructure and health systems, and lacking in funding and health surveillance facilities. Moreover, the adherence and implementation of these restrictions have great impact on political and social norms and on economy. These tactics are therefore opposite to long-term human practices. Computer vision has the potential to provide non-intrusive and automatic solutions to control the COVID-19 pandemic and is being utilized in several ways to mitigate the spread of coronavirus. Some CV-based approaches to prevent the coronavirus spread are given in the subsequent sections.

Social Distance Monitoring. Social distance monitoring implicates reducing physical contact between persons by imposing acceptable physical distance among them in public spaces, normally two meters and usually minimizing public get-togethers. These strategies are most effective for breaking the chain of COVID-19 transmission by reducing the infection rate and size of pandemic peak (Fig. 11). Social distancing also decreases the load on health organizations and reduces mortality rate by guaranteeing that the number of infected patients does not exceed the public healthcare capability [119]. Many governments have employed various strategies to ensure social distancing such as closing public areas, border control, travel constraints and warning people to maintain distance (1.5–2 m) from each other. However, these tactics are opposite to long-term human practices. Hence, non-intrusive and automated solution may be useful for facilitating social distance monitoring in current COVID-19 pandemic.

Computer vision has the ability to provide such well-suited and potential solutions for observing social distance obedience. Recent rapid advancement in the AI and its

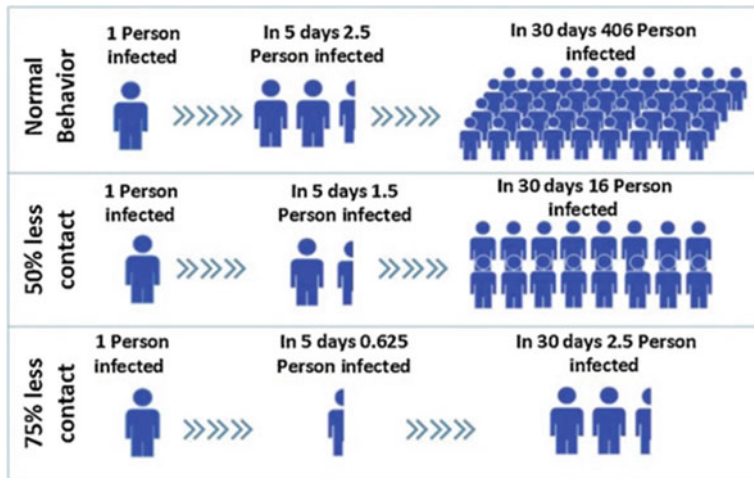


Fig. 11 Prominence of social distancing

domains such as deep learning and pattern recognition and CV based algorithms have been directed to the designing of many object detection models. This capability can be utilized to enable, encourage and enforce social distancing such as detecting crowd and recognizing people in public places through real-time imaging captured by surveillance cameras (Fig. 12). For example, the authorities can be informed to take proper actions if the number of citizens does not obey social distancing rules (e.g., no gathering of more than 10 people). Researchers are utilizing CV and providing effective solutions to monitor social distancing by using side or frontal perspectives of individuals. Authors in [120] offered a framework to detect people and also presented the Deepsort method to track the identified people by using bounding boxes and allocated IDs information. An automatic drone-based framework to monitor social distancing is developed by [121]. Authors in [122, 123] presented model to detect people in crowded conditions. Their frameworks are intended to detect those persons



Fig. 12 **a** Human detection to recognize the number of persons in the public area; **b** Face recognition of the isolated person without and with mask

who do not obey the rules of social distance (i.e., 1.5–2 m space between them). The proposed model will calculate the distance between each pair among the crowd and red mark the person who is getting closer than an allowable limit. In [124, 125], researchers used over-head perspective of people to detect human and used Euclidean distance measure to track human who crosses the social distance limit (Fig. 13).

Masked Face Detection. Although SARS-CoV2's original source is still not confirmed, its human to human transmission ability is strongly evidenced. This novel coronavirus spreads through respiratory transmission from human to human and from contact with already infected patients and surface through use of nose, eye or mouth. Its transmission through air (by sneeze and cough of infected person) is seemed to be more dominant source of COVID-19 spread [3]. Hence, health organizations are strongly advising the usage of face masks if person is having respiratory symptoms or taking care of infected people. Masked face can cut the COVID-19 spread as masks prevent the virus to enter the body through mouth and eyes [126]. Moreover several public service providers want the customers to wear masks while using the service. CV has the capability of automatic and contactless face detection that can be utilized in this pandemic situation to detect the masks wearing especially in high crowded areas [127–130]. Authors in [131] presented a CV-based model to detect the violation of wearing face masks among construction labor force to guarantee their safety on project during pandemic. In [132], authors proposed face masks detection model trained on the images captured from videos of surveillance cameras. Masked face detection systems can also be used as a reminder if a person is not wearing mask. For example, cameras outside of the public building can detect the person with and without mask and send warning message (i.e., audio or beep sound) to the person who is not wearing mask and intends to enter the building [133]. Model proposed in [134] aims to reflect the masked face conditions (Fig. 14).

Recognition and Monitoring of Quarantined Persons. Moreover, the diseased person or other people who had physical interaction with the infected person must be quarantined to control the spread of the virus. For example, people returning back from highly infected regions or countries are often requested to be self-isolated or quarantined for minimum 14 days. Due to the shortage of facilities, government of



Fig. 13 Social distance monitoring [124]



Fig.14 Detection of face mask wearing condition; correct face mask (Green bounding boxes); No face mask (Red bounding boxes); face with an improper face mask (Blue bounding boxes)

most countries is self-isolating infected people at home. This requirement can be enforced with the help of CV's capability of face detection by analyzing the real-time images or videos from surveillance cameras. Contactless CV-based systems can be used for screening of infected people in a short period of time. These systems not only make rapid and remote detection of positive cases but also require minimal personnel. Because people are instructed to wear mask in public areas, images with masks and without masks are taken to build the training dataset. Then a face detection system is trained over these both type of images that learns from images and analyzes the images from videos or images captured from surveillance cameras to identify quarantined person's appearance. If the infected persons are spotted in public, the authorities can be informed to take proper actions. CV can also trace the path of infected persons and alert the other people who had been closer to infected people on their way. CV-based algorithms for motion detection and monitoring can also be used in hospitals to alert the authorities if a person intends to go out of the room.

Detection and Monitoring of COVID-19 Symptoms. As the airborne transmission of coronavirus from symptomatic cases is confirmed by medical professionals, it can also spread from asymptomatic patients and prior to signs onset [135]. The most common symptomatic signs include fever (88%), dry cough (68%), tiredness (38%), dyspnea (19%), arthralgia or myalgia (15%), inflamed throat (14%) and headache (14%). Less common signs include vomiting (5%) and diarrhea (4%) [136]. Detection of these symptoms from people and alerting them and authorities would be helpful to cut down the coronavirus spread. Contactless CV-based systems can have the capability to measure symptoms and signs of COVID-19 and can be used for screening of infected people in a short period of time (Fig. 15). These systems not only make rapid and remote detection of suspicious cases but also require minimal personnel. For example infrared/thermal imaging technology and CV-based motion recognition software are being used to detect and evaluate abnormal respiratory patterns of public. This has been proved a promising method for additional validation of the suspected cases of COVID-19 [137, 138]. Fusion of thermal imaging with CV is being utilized globally for mass fever screening at public places (i.e., malls, buildings, hospitals, offices, airports and so on) [139–141]. A similar complete CV-based system is proposed by [142]. They used thermal and normal RGB cameras to identify fever patients and prevent COVID-19 spread. CV's ability to detect human pose and behavior is also playing a vital role in detecting COVID-19 symptoms for instance detection of coughing and sneezing people and ensuring hand washing



Fig. 15 Thermal image of an individual talking on mobile phone. **a** After 1 min of conversation; **b** After 15 min of conversation. Temperature of the circled area is increased from 30.56 to 35.15 °C and Temperature of the ear region (arrow) is increased from 33.35 to 34.82 °C [143]. Similar system can be developed for coronavirus related fever screening. **c** Human pose detection

by estimating human behavior and body movements from videos of surveillance cameras [119]. Another application is pandemic drones incorporated with visual images and sensory cameras to detect infected persons.

Vision-guided Robots. Another CV-based approach to control and mitigate the COVID-19 spread is use of vision-guided robots especially in hospitals where nurses, doctors and other healthcare workers are bearing greater risk of infection. Shortage of personal protective equipment (PPE) is one of the basic reasons increasing the risk of infection for the healthcare staffs [144]. Here, robotic technology incorporated with CV algorithms and thermal sensors can be used in several routines to lower the transmission of infection. These routines include but not limited to the daily inspections on patient's mental and physical conditions, delivery of food, medicine, or other essential stuffs, operating the medical equipment, and extensive cleaning of the high-touch surfaces [145, 146]. An example is a semi-automatic swab robot developed to perform swabs tests of patients [147]. A remote camera is armed on the swab robot, which assists the medical professionals to carry out the sampling with a perfect vision without being close in contact with the patient (Fig. 16a, b). Many fever screening robots have also been employed at the entrance of many hospitals in China (Fig. 16c). Another telerobotic system is proposed by [144] that targets to block virus transmission by minimizing the chance of interaction between the

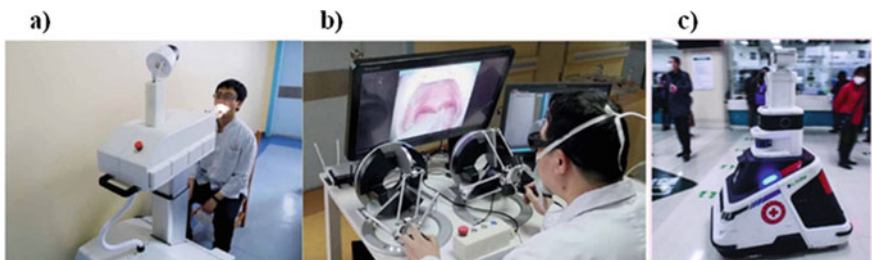


Fig. 16 **a** A semi-automatic swab robot; **b** Remote monitoring of swab test; **c** A Fever monitoring robot at a hospital in Shenyang, China

healthcare staff and COVID-19 patients. The proposed robotic system can assist or even replace the medical staffs to take care of patients in the isolation ward. To enforce social distancing in hotels, CV-based robots have been proved as an effective approach against COVID-19. Such robots are being adopted to protect both guests and service labor [148]. Some strategies are employed to potentially substitute face-to-face service, including facial scan check-ins, robot delivery, robot receptionists, and robot gatekeeper assistants, etc.

7 Challenges of Using Computer Vision for COVID-19 Diagnosis

At present, research community is facing the several challenges in CV-based COVID-19 diagnosis such as scarcity, legislation, noisy, ambiguous and diverse data, lack of large-scale training data, class imbalance problem in the available training data, lack of knowledge in the intersection of medicine and computer science and data security and privacy issues. These challenges are described as follows:

- *Lack of large-scale training dataset:* Most CV-based systems rely on high volume of annotated training data to design a robust system for COVID-19 diagnosis. These data may include medical imaging modalities and numerous biological data. As, research on COVID-19 is very new, the insufficiency of standard training data is major challenge for CV-based diagnosis of this novel virus.
- *Massive ambiguous and noisy data:* As the data have been collected from a variety of resources, the available annotated datasets of COVID-19 patients are incomplete, ambiguous and noisy. For example, images might be taken with different angles and in different color and light intensities. Moreover, in some cases, images are annotated incorrectly [149]. To training of a CV-based model on such diverse, massive and low quality data becomes very complex because it requires many issues to be resolved such as removing data redundancy and noise from images. The accuracy and applicability of CV-based systems are limited due to this problem.
- *Problem of model overfitting:* Because of training of model on small scale of annotated data, the generalization ability of a CV-based model suffers that causes overfitting of the model. This leads to accurate prediction of COVID-19 disease in the training phase but failing to give accurate results in the testing time. So these systems are not widely applicable in real-world applications [150].
- *Data imbalance between classes:* Class imbalance in the available annotated data is another problem for designing a CV-based COVID-19 diagnosis system. COVID-19 related labeled data are far less than other general lung diseases. Furthermore, data of negative cases are also greater than the images having positive class [149]. Imbalanced data raises biasness during the training step.
- *Lack of knowledge in the intersection of medicine and computer science:* Many CV-based diagnosis systems are designed in computer science field, but the

applications of CV in COVID-19 pandemic require full cooperation in medical imaging, computer science, virology, bioinformatics and many other fields. Therefore, it is critical to coordinate the supportive work of research communities of different disciplines and incorporate the knowledge of various subjects to jointly fight the COVID-19 battle.

- *Legal challenges for clinicians:* Defining legal responsibilities associated with contrary outputs of CV-based diagnosis systems is controversial [151]. CV-based COVID-19 diagnosis systems may lack in explainability, privacy concerns and generalizability. Moreover, these systems may mistakenly predict healthy person as positive case of COVID-19 or classify infected individual as a negative case making clinician accountable for mistakes. Consequently, medical professionals hesitate to use these systems in their practices [149].
- *Human rights protection and data privacy concerns:* While developing the dataset, patient's privacy issue arises. As CV-based models highly rely on massive amount of training data, to collect this data, we need to look patient's genome, electronic health records (EHRs), blood samples and family history. However, most of the patients feel uncomfortable sharing such intimate information to a potentially hackable database. How to successfully protect patient's personal information during data acquisition and CV-based data processing is a worth noting challenge.

8 Imaging Datasets of COVID-19

As computer vision systems are based on deep learning, these models require a huge amount of training data to give best testing performance. Therefore, physicians and researchers have been exchanging information, but still researchers are facing difficulties in collecting datasets due to lock down restrictions. However, some datasets proposed by research community gave exceptional results in the detection of COVID-19 infection. A list of some publically available imaging datasets in this domain is given in Table 1.

9 Conclusion

Recent Corona Virus Disease (COVID) outbreak caused by SARS-CoV2 has been posing a big threat to global health since December 2019. In response, research community from all over the world has shifted all their efforts to contribute in this global war by providing crucial solutions. In this chapter, we presented an extensive study of computer vision-based technologies for detection, diagnosis, prediction and prevention of COVID. Various computer vision (CV) technologies along with other artificial intelligence (AI) subsets are being used to fight in frontline of this turbulent war. Among all wonderful applications of computer vision, automated early diagnosis of COVID-19 is major and the most needed application. CT scans,

Table 1 Open source COVID-19 datasets

References	Description	Dataset source
[19]	CT images and chest X-rays up to 373 images	https://github.com/ieee8023/covid-che stxray-dataset
[152]	3616 COVID positive, 10,192 Normal, 1345 viral Pneumonia and 6012 lung opacity x-ray images	https://www.kaggle.com/tawsifurr ahman/covid19-radiography-database
[98]	13,975 chest X-rays (8066 normal, 5538 pneumonia and 358 COVID positive images)	https://github.com/lindawangg/COV ID-Net
[153]	238 chest X-rays (58 COVID positive, 127 no findings and 53 inconclusive images)	https://github.com/agchung/Actualmed-COVID-chestxray-dataset
[154]	55 chest X-rays (35 COVID positive, 3 no findings and 15 inconclusive images)	https://github.com/agchung/Figure1-COVID-chestxray-dataset
[155]	620 chest X-rays(310 COVID positive and 310 COVID negative images)	https://data.mendeley.com/datasets/2fx z4px6d8/4
[156]	9544 chest X-rays (5500 COVID negative and 4044 COVID positive images) and 8055 CT scans (2628 COVID negative and 5427 COVID positive scans)	https://data.mendeley.com/datasets/8h6 5ywd2jr/3
[157]	115 chest X-rays and CT scans	https://sirm.org/category/senza-categoria/covid-19/
[158]	59 Chest radiography images (CT scans and X-rays)	https://www.bsti.org.uk/training-and-education/covid-19-bsti-imaging-database/
[159]	773 Chest radiography images (485 pneumonia, 153 normal and 135 COVID positive images)	https://radiopaedia.org/articles/normal-chest-imaging-examples?lang=gb
[160]	812 CT images (349 COVID positive and 453 COVID negative images)	https://github.com/UCSD-AI4H/COV ID-CT
[79]	100 axial CT images from more than 40 COVID positive patients	http://medicalsegmentation.com/covid19/
[161]	7377 chest X-rays and 6687 CT images	https://bimcv.cipf.es/bimcv-projects/bimcv-COVID19/
[162]	~ 200 Lung ultrasound videos and ~ 60 images	https://github.com/jannisborn/covid19_ultrasound
[163]	5000 images with masked faces and 90,000 face images of same individuals without masks	https://github.com/X-zhangyang/Real-World-Masked-Face-Dataset

X-rays and ultrasound images are being widely used for early detection, segmentation and classification of COVID-19. These diagnosis systems are replacing the requirements of traditional test called reverse transcript polymerase chain reaction (RT-PCR), which requires strict examination environment and many resources and is also prone to false negative errors. Intervention of computer vision-based support decision systems in healthcare is reducing these medication errors and controlling mortality rate. Computer vision-based surveillance technologies are also being used for monitoring physical distance, detecting people with or without face masks, screening infected persons, measuring their temperature, tracing body movements and detecting hand washing. Some other applications of computer vision for COVID-19 prevention and control include pandemic drones, vision-guided robots and germ scanning. In addition to these, computer vision is also assisting in production of vaccine, and contributing in administrative tasks and clinical management such as classifying critically ill patients and providing them immediate treatment. Despite of wide use of CV in COVID-19 pandemic, research community is still facing the several challenges such as scarcity, legislation, noisy, ambiguous and diverse data, lack of large-scale training data, class imbalance problem in the available training data, lack of knowledge in the intersection of medicine and computer science and data security and privacy issues.

Acknowledgements We are thankful to the publishers of open source datasets [19, 24, 28, 29, 81].

Disclosure Statement No potential conflict of interest was reported by the authors.

References

1. World Health Organization: Coronavirus Disease (COVID-19). Available at: <https://www.who.int/health-topics/coronavirus> (23 Jan 2020)
2. Khan, M.A., Kadry, S., Zhang, Y.D., Akram, T., Sharif, M., Rehman, A., Saba, T.: Prediction of COVID-19-pneumonia based on selected deep features and one class kernel extreme learning machine. *Comput. Electr. Eng.* **90**, 106960 (2021)
3. Zhang, R., Li, Y., Zhang, A.L., Wang, Y., Molina, M.J.: Identifying airborne transmission as the dominant route for the spread of COVID-19. *Proc. Natl. Acad. Sci.* **117**(26), 14857–14863 (2020)
4. Haimed, A.M.A., Saba, T., Albasha, A., Rehman, A., Kolivand, M.: Viral reverse engineering using Artificial Intelligence and big data COVID-19 infection with Long Short-term Memory (LSTM). *Environ. Technol. Innov.* **22**(1–20), 101531 (2021)
5. Rehman, A., Sadad, T., Saba, T., Hussain A., Tariq, U.: Real-time diagnosis system of COVID-19 using X-ray images and deep learning. *IEEE IT Professional* **23** (4):57–62 (2021). <https://doi.org/10.1109/MITP.2020.3042379>
6. Rothan, H.A., Byrareddy, S.N.: The epidemiology and pathogenesis of coronavirus disease (COVID-19) outbreak. *J. Autoimmun.* **1**(109), 102433 (2020)
7. <https://coronavirus.jhu.edu/map.html> (20 Sept 2021)
8. Dawood, S., Dawood, A., Alaskar, H., Saba, T.: COVID-19 artificial intelligence based surveillance applications in the kingdom of Saudi Arabia. In: 2021 1st International Conference on Artificial Intelligence and Data Analytics (CAIDA), pp. 200–205. IEEE (2021, Apr)

9. Watson, J., Whiting, P.F., Brush, J.E.: Interpreting a covid-19 test result. *BMJ* **12**, 369 (2020)
10. Rehman, A., Saba, T., Tariq, U., Ayesha, N.: Deep learning-based COVID-19 detection using CT and X-ray images: Current analytics and comparisons. *IT Professional* **23**(3), 63–68 (2021)
11. Saba, T., Abunadi, I., Shahzad, M.N., Khan, A.R.: Machine learning techniques to detect and forecast the daily total COVID-19 infected and deaths cases under different lockdown types. *Microsc. Res. Tech.* **84**(7), 1462–1474 (2021)
12. Joynt, G.M., Wu, W.K.: Understanding COVID-19: What does viral RNA load really mean? *Lancet. Infect. Dis* **20**(6), 635–636 (2020)
13. Zhang, J.J., Cao, Y.Y., Dong, X., Wang, B.C., Liao, M.Y., Lin, J., Yan, Y.Q., Akdis, C.A., Gao, Y.D.: Distinct characteristics of COVID—19 patients with initial rRT—PCR—positive and rRT—PCR—negative results for SARS—CoV—2. *Allergy* (1 July 2020)
14. Guo, L., Ren, L., Yang, S., Xiao, M., Chang, D., Yang, F., Dela Cruz, C.S., Wang, Y., Wu, C., Xiao, Y., Zhang, L.: Profiling early humoral response to diagnose novel coronavirus disease (COVID-19). *Clin. Infect. Dis.* **71**(15), 778–785 (2020)
15. Rahman, S., Sarker, S., Al Miraj, M.A., Nihal, R.A., Haque, A.N., Al, N.A.: Deep learning-driven automated detection of COVID-19 from radiography images: A comparative analysis. *Cogn. Comput.* **2**, 1–30 (2021)
16. Ramzan, F., Khan, M.U.G., Iqbal, S., Saba, T., Rehman, A.: Volumetric segmentation of brain regions from MRI scans using 3D convolutional neural networks. *IEEE Access* **8**, 103697–103709 (2020)
17. Iqbal, S., Khan, M.U.G., Saba, T., Mehmood, Z., Javaid, N., Rehman, A., Abbasi, R.: Deep learning model integrating features and novel classifiers fusion for brain tumor segmentation. *Microsc. Res. Tech.* **82**(8), 1302–1315 (2019). <https://doi.org/10.1002/jemt.23281>
18. Kovács, A., Palásti, P., Veréb, D., Bozsik, B., Palkó, A., Kincses, Z.T.: The sensitivity and specificity of chest CT in the diagnosis of COVID-19. *Eur. Radiol.* **31**(5), 2819–2824 (2021)
19. Khan, A.R., Khan, S., Harouni, M., Abbasi, R., Iqbal, S., Mehmood, Z.: Brain tumor segmentation using K-means clustering and deep learning with synthetic data augmentation for classification. *Microsc. Res. Tech.* **84**(7), 1389–1399 (2021)
20. Nouvenne, A., Zani, M.D., Milanese, G., Parise, A., Baciarello, M., Bignami, E.G., Odone, A., Sverzellati, N., Meschi, T., Ticinesi, A.: Lung ultrasound in COVID-19 pneumonia: Correlations with chest CT on hospital admission. *Respiration* **99**(7), 617–624 (2020)
21. Colombi, D., Petrini, M., Maffi, G., Villani, G.D., Bodini, F.C., Morelli, N., Milanese, G., Silva, M., Sverzellati, N., Michieletti, E.: Comparison of admission chest computed tomography and lung ultrasound performance for diagnosis of COVID-19 pneumonia in populations with different disease prevalence. *Eur. J. Radiol.* **1**(133), 109344 (2020)
22. Smargiassi, A., Soldati, G., Borghetti, A., Scoppettuolo, G., Tamburrini, E., Testa, A.C., Moro, F., Natale, L., Larici, A.R., Buonsenso, D., Valentini, P.: Lung ultrasonography for early management of patients with respiratory symptoms during COVID-19 pandemic. *J. Ultrasound* **7**, 1–8 (2020)
23. Sofia, S., Boccatonda, A., Montanari, M., Spampinato, M., D’ardes, D., Cocco, G., Accogli, E., Cipollone, F., Schiavone, C.: Thoracic ultrasound and SARS-COVID-19: A pictorial essay. *J. Ultrasound* **23**(2), 217–221 (2020)
24. Rehman, A., Khan, M. A., Saba, T., Mehmood, Z., Tariq, U., Ayesha, N.: Microscopic brain tumor detection and classification using 3D CNN and feature selection architecture. *Microsc. Res. Tech.* **84** (1), 133–149 (2021).<https://doi.org/10.1002/jemt.23597>
25. Jamal, A., Hazim Alkawaz, M., Rehman, A., Saba, T.: Retinal imaging analysis based on vessel detection. *Microsc. Res. Tech.* **80**(7), 799–811 (2017)
26. Iftikhar, S., Fatima, K., Rehman, A., Almazyad, A.S., Saba, T.: An evolution based hybrid approach for heart diseases classification and associated risk factors identification. *Biomed. Res.* **28**(8), 3451–3455 (2017)
27. Treglia, G.: The role of 18 F-FDG PET for COVID-19 infection: Myth versus reality. *Clin. Transl. Imaging* **8**(3), 125–126 (2020)
28. Franceschi, A.M., Clifton, M., Ahmed, O., Matthews, R., Franceschi, D.: Incidental PET/CT findings of suspected COVID-19 in a region of high prevalence. *Cureus* **12** (8) (2020 Aug)

29. Espinosa, P.S., Rizvi, Z., Sharma, P., Hindi, F., Filatov, A.: Neurological complications of coronavirus disease (COVID-19): Encephalopathy, MRI brain and cerebrospinal fluid findings: Case 2. *Cureus* **12** (5) (2020 May)
30. Shi, F., Wang, J., Shi, J., Wu, Z., Wang, Q., Tang, Z., He, K., Shi, Y., Shen, D.: Review of artificial intelligence techniques in imaging data acquisition, segmentation, and diagnosis for COVID-19. *IEEE Rev. Biomed. Eng.* **16**(14), 4–15 (2020)
31. Sadad, T., Munir, A., Saba, T., Hussain, A.: Fuzzy C-means and region growing based classification of tumor from mammograms using hybrid texture feature. *J. Comput. Sci.* **29**, 34–45 (2018)
32. Saba, T., Rehman, A., Mehmood, Z., Kolivand, H., Sharif, M.: Image enhancement and segmentation techniques for detection of knee joint diseases: A survey. *Curr. Med. Imaging Rev.* **14**(5), 704–715 (2018)
33. Tariq, M., Iqbal, S., Ayesha, H., Abbas, I., Ahmad, K.T., Niazi, M.F.: Medical image based breast cancer diagnosis: State of the art and future directions. *Expert Syst. Appl.* **1**(167), 114095 (2021)
34. Yousaf, K., Mehmood, Z., Saba, T., Rehman, A., Munshi, A.M., Alharbey, R., Rashid, M.: Mobile-health applications for the efficient delivery of health care facility to people with dementia (PwD) and support to their carers: A survey. *Biomed. Res. Int.* **2019**, 1–26 (2019)
35. Rahim, M.S.M., Norouzi, A., Rehman, A., Saba, T.: 3D bones segmentation based on CT images visualization. *Biomed. Res.* **28**(8), 3641–3644 (2017)
36. Abbas, N., Saba, T., Mohamad, D., Rehman, A., Almazyad, A.S., Al-Ghamdi, J.S.: Machine aided malaria parasitemia detection in Giemsa-stained thin blood smears. *Neural Comput. Appl.* **29**(3), 803–818 (2018)
37. Khan, M.A., Sharif, M.I., Raza, M., Anjum, A., Saba, T., Shad, S.A.: Skin lesion segmentation and classification: A unified framework of deep neural network features fusion and selection. *Expert Syst. e12497* (2019)
38. Saba, T., Bokhari, S.T.F., Sharif, M., Yasmin, M., Raza, M.: Fundus image classification methods for the detection of glaucoma: A review. *Microsc. Res. Tech.* (2018). <https://doi.org/10.1002/jemt.23094>
39. Nazir, M., Khan, M. A., Saba, T., Rehman, A.: Brain tumor detection from MRI images using multi-level wavelets. In: *2019 International Conference on Computer and Information Sciences (ICCIS)*, pp. 1–5. IEEE (2019, Apr)
40. Ayesha, H., Iqbal, S., Tariq, M., Abrar, M., Sanaullah, M., Abbas, I., Rehman, A., Niazi, M.F., Hussain, S.: Automatic medical image interpretation: State of the art and future directions. *Pattern. Recogn.* **29**, 107856 (2021)
41. Ullah, H., Saba, T., Islam, N., Abbas, N., Rehman, A., Mehmood, Z., Anjum, A.: An ensemble classification of exudates in color fundus images using an evolutionary algorithm based optimal features selection. *Microsc. Res. Tech.* **82**(4), 361–372 (2019)
42. Javed, R., Rahim, M.S.M., Saba, T., Rehman, A.: A comparative study of features selection for skin lesion detection from dermoscopic images. *Netw. Model. Anal. Health Inf. Bioinform.* **9**(1), 1–13 (2020)
43. Rehman, A., Abbas, N., Saba, T., Mehmood, Z., Mahmood, T., Ahmed, K.T.: Microscopic malaria parasitemia diagnosis and grading on benchmark datasets. *Microsc. Res. Tech.* **81**(9), 1042–1058 (2018)
44. Sharif, M., Attique, M., Tahir, M.Z., Yasmim, M., Saba, T., Tanik, U.J.: A Machine learning method with threshold based parallel feature fusion and feature selection for automated gait recognition. *J. Organ. End User Comput. (JOEUC)* **32**(2), 67–92 (2020)
45. Mehmood, A., Khan, M.A., Sharif, M., Khan, S.A., Shaheen, M., Saba, T., et al.: Prosperous human gait recognition: An end-to-end system based on pre-trained CNN features selection. *Multimedia Tools Appl.* 1–21 (2020). <https://doi.org/10.1007/s11042-020-08928-0>
46. Rehman, A., Saba, T.: An intelligent model for visual scene analysis and compression. *Int. Arab J. Inf. Technol.* **10**(13), 126–136 (2013)
47. Sharif, M., Khan, M.A., Akram, T., Javed, M.Y., Saba, T., Rehman, A.: A framework of human detection and action recognition based on uniform segmentation and combination

- of Euclidean distance and joint entropy-based features selection. *EURASIP J. Image Video Process.* **2017** (1), 89, 1–18 (2017)
- 48. Amin, J., Sharif, M., Raza, M., Saba, T., Rehman, A.: Brain tumor classification: Feature fusion. In: 2019 International Conference on Computer and Information Sciences (ICCIS), pp. 1–6. IEEE (2019)
 - 49. Saba, T.: Automated lung nodule detection and classification based on multiple classifiers voting. *Microsc. Res. Tech.* **82**(9), 1601–1609 (2019)
 - 50. Rehman, A., Abbas, N., Saba, T., Rahman, S.I.U., Mehmood, Z., Kolivand, H.: Classification of acute lymphoblastic Leukemia using deep learning. *Microsc. Res. Tech.* **81**(11), 1310–1317 (2018)
 - 51. Garcia-Martinez, A., Vicente-Samper, J.M., Sabater-Navarro, J.M.: Automatic detection of surgical haemorrhage using computer vision. *Artif. Intell. Med.* **1**(78), 55–60 (2017)
 - 52. Delso, G., Cirillo, D., Kaggie, J.D., Valencia, A., Metser, U., Veit-Haibach, P.: How to design AI-driven clinical trials in nuclear medicine. In: Seminars in Nuclear Medicine, vol. 51, no. 2, pp. 112–119. WB Saunders (1 Mar 2021)
 - 53. Fernandes, K., Cardoso, J.S., Fernandes, J.: Automated methods for the decision support of cervical cancer screening using digital colposcopies. *IEEE Access* **22**(6), 33910–33927 (2018)
 - 54. Gu, Y., Pandit, S., Sarraee, E., Nordahl, T., Ellis, T., Betke, M.: Home-based physical therapy with an interactive computer vision system. In: Proceedings of the IEEE/CVF International Conference on Computer Vision Workshops 2019, pp. 0–0.
 - 55. KR, S., Shankar, S.P., Parakh, S.D.: Computer vision in healthcare management system through mobile communication. *Ilkogretim Online* **20** (5) (1 Sept 2021)
 - 56. Singh, V., Ma, K., Tamer soy, B., Chang, Y.J., Wimmer, A., O'Donnell, T., Chen, T.: Darwin: Deformable patient avatar representation with deep image network. In: International Conference on Medical Image Computing and Computer-Assisted Intervention, pp. 497–504. Springer, Cham (10 Sept 2017)
 - 57. Meethongjan, K., Dzulkifli, M., Rehman, A., Altameem, A., Saba, T.: An intelligent fused approach for face recognition. *J. Intell. Syst.* **22**(2), 197–212 (2013)
 - 58. Li, J., Udayasankar, U.K., Toth, T.L., Seamans, J., Small, W.C., Kalra, M.K.: Automatic patient centering for MDCT: Effect on radiation dose. *Am. J. Roentgenol.* **188**(2), 547–552 (2007)
 - 59. Casas, L., Navab, N., Demirci, S.: Patient 3D body pose estimation from pressure imaging. *Int. J. Comput. Assist. Radiol. Surg.* **14**(3), 517–524 (2019)
 - 60. Wang, Y., Lu, X., Zhang, Y., Zhang, X., Wang, K., Liu, J., Li, X., Hu, R., Meng, X., Dou, S., Hao, H.: Precise pulmonary scanning and reducing medical radiation exposure by developing a clinically applicable intelligent CT system: Toward improving patient care. *EBioMedicine* **1**(54), 102724 (2020)
 - 61. Booij, R., Budde, R.P., Dijkshoorn, M.L., van Straten, M.: Accuracy of automated patient positioning in CT using a 3D camera for body contour detection. *Eur. Radiol.* **29**(4), 2079–2088 (2019)
 - 62. United Imaging Sends Out More than 100 CT Scanners and X-ray Machines to Aid Diagnosis of the Coronavirus (2020) [online]. Available: <https://www.itnonline.com/content/united-imaging-sends-out-more-100-ct-scanners-and-x-ray-machines-aid-diagnosis-coronavirus>
 - 63. Lee, J.H., Kim, D.I., Cho, M.K. (Inventors); Samsung Electronics Co Ltd. (Assignee): Computed tomography apparatus and method of controlling X-ray by using the same. United States patent US 9,655,584, 23 May 2017
 - 64. Forthmann, P., Pfleiderer, G. (Inventors); Koninklijke Philips NV (Assignee): Augmented display device for use in a medical imaging laboratory. United States patent US 10,412,377, 10 Sept 2019.
 - 65. United Imaging's Emergency Radiology Departments Support Mobile Cabin Hospitals, Facilitate 5G Remote Diagnosis (2020) [Online]. Available: <https://www.prnewswire.com/news-releases/united-imaging-s-emergency-radiology-departments-support-mobile-cabin-hospitals-facilitate-5g-remote-diagnosis-301010528.html>

66. Prehospital CT scans possible with mobile stroke unit (2020) [Online]. Available: <https://www.ems1.com/ems-products/ambulances/articles/prehospital-ct-scans-possible-with-mobile-stroke-unit-4JKu37U2neG4k68j/>
67. Ronneberger, O., Fischer, P., Brox, T.: U-net: Convolutional networks for biomedical image segmentation. In: International Conference on Medical Image Computing and Computer-Assisted Intervention 5 Oct 2015, pp. 234–241. Springer, Cham
68. Zhou, Z., Siddiquee, M.M., Tajbakhsh, N., Liang, J.: Unet++: A nested u-net architecture for medical image segmentation. In: Deep learning in medical image analysis and multimodal learning for clinical decision support 20 Sept 2018, pp. 3–11. Springer, Cham
69. Milletari, F., Navab, N., Ahmadi, S.A.: V-net: Fully convolutional neural networks for volumetric medical image segmentation. In: 2016 Fourth International Conference on 3D Vision (3DV) 25 Oct 2016, pp. 565–571. IEEE
70. Zheng, C., Deng, X., Fu, Q., Zhou, Q., Feng, J., Ma, H., Liu, W., Wang, X.: Deep learning-based detection for COVID-19 from chest CT using weak label. MedRxiv (1 Jan 2020)
71. Cao, Y., Xu, Z., Feng, J., Jin, C., Han, X., Wu, H., Shi, H.: Longitudinal assessment of COVID-19 using a deep learning-based quantitative CT pipeline: Illustration of two cases. Radiol. Cardiothorac. Imaging **2** (2):e200082 (23 Mar 2020)
72. Huang, L., Han, R., Ai, T., Yu, P., Kang, H., Tao, Q., Xia, L.: Serial quantitative chest CT assessment of COVID-19: A deep learning approach. Radiol. Cardiothorac. Imaging (30 Mar 2020) **2** (2), e200075
73. Saeedizadeh, N., Minaee, S., Kafieh, R., Yazdani, S., Sonka, M.: COVID TV-Unet: Segmenting COVID-19 chest CT images using connectivity imposed Unet. Comput. Methods Programs Biomed. Update **1**(1), 100007 (2021)
74. Xu, X., Wen, Y., Zhao, L., Zhang, Y., Zhao, Y., Tang, Z., Yang, Z., Chen, C.Y.: CARes-UNet: Content-aware residual UNet for lesion segmentation of COVID-19 from chest CT images. Med. Phys. **48**(11), 7127–7140 (2021)
75. Saood, A., Hatem, I.: COVID-19 lung CT image segmentation using deep learning methods: UNET versus SegNET
76. Li, L., Qin, L., Xu, Z., Yin, Y., Wang, X., Kong, B., Bai, J., Lu, Y., Fang, Z., Song, Q., Cao, K.: Artificial intelligence distinguishes COVID-19 from community acquired pneumonia on chest CT. Radiology (19 Mar 2020)
77. Rehman, A., Abbas, N., Saba, T., Mahmood, T., Kolivand, H.: Rouleaux red blood cells splitting in microscopic thin blood smear images via local maxima, circles drawing, and mapping with original RBCs. Microsc. Res. Tech. **81**(7), 737–744 (2018)
78. Fan, D.P., Zhou, T., Ji, G.P., Zhou, Y., Chen, G., Fu, H., Shen, J., Shao, L.: Inf-net: Automatic covid-19 lung infection segmentation from CT images. IEEE Trans. Med. Imaging **39**(8), 2626–2637 (2020)
79. COVID-19 CT segmentation dataset: Accessed Jan 2022 (2020). Available at: <http://medicalsegmentation.com/covid19/>
80. Brunese, L., Mercaldo, F., Reginelli, A., Santone, A.: Explainable deep learning for pulmonary disease and coronavirus COVID-19 detection from X-rays. Comput. Methods Programs Biomed. **1**(196), 105608 (2020)
81. Han, Z., Wei, B., Hong, Y., Li, T., Cong, J., Zhu, X., Wei, H., Zhang, W.: Accurate screening of COVID-19 using attention-based deep 3D multiple instance learning. IEEE Trans. Med. Imaging **39**(8), 2584–2594 (2020)
82. Matsuyama, E.: A deep learning interpretable model for novel coronavirus disease (COVID-19) screening with chest CT images. J. Biomed. Sci. Eng. **13**(07), 140 (2020)
83. Ozturk, T., Talo, M., Yildirim, E.A., Baloglu, U.B., Yildirim, O., Acharya, U.R.: Automated detection of COVID-19 cases using deep neural networks with X-ray images. Comput. Biol. Med. **1**(121), 103792 (2020)
84. Redmon, J., Farhadi, A.: YOLO9000: better, faster, stronger. In: Proceedings of the IEEE Conference on Computer Vision and Pattern Recognition, pp. 7263–7271 (2017)
85. Tsiknakis, N., Trivizakis, E., Vassalou, E.E., Papadakis, G.Z., Spandidos, D.A., Tsatsakis, A., Sánchez-García, J., López-González, R., Papanikolaou, N., Karantanas, A.H., Marias, K.:

- Interpretable artificial intelligence framework for COVID-19 screening on chest X-rays. *Exp. Ther. Med.* **20**(2), 727–735 (2020)
- 86. Wu, Y.H., Gao, S.H., Mei, J., Xu, J., Fan, D.P., Zhang, R.G., Cheng, M.M.: Jcs: An explainable covid-19 diagnosis system by joint classification and segmentation. *IEEE Trans. Image Process.* **18**(30), 3113–3126 (2021)
 - 87. Gao, S., Cheng, M.M., Zhao, K., Zhang, X.Y., Yang, M.H., Torr, P.H.: Res2net: A new multi-scale backbone architecture. *IEEE Trans. Pattern Anal. Mach. Intell.* (30 Aug 2019)
 - 88. Ahsan, M.M., Gupta, K.D., Islam, M.M., Sen, S., Rahman, M., Hossain, M.S.: Study of different deep learning approach with explainable ai for screening patients with COVID-19 symptoms: Using CT scan and chest x-ray image dataset. arXiv preprint [arXiv:2007.12525](https://arxiv.org/abs/2007.12525) (24 July 2020)
 - 89. Angelov, P., Soares, E.: Explainable-by-design approach for covid-19 classification via CT-scan. medRxiv (1 Jan 2020)
 - 90. Jaiswal, A.K., Tiwari, P., Rathi, V.K., Qian, J., Pandey, H.M., Albuquerque, V.H.: Covidpen: A novel covid-19 detection model using chest x-rays and CT scans. Medrxiv (1 Jan 2020)
 - 91. Sarker, L., Islam, M.M., Hannan, T., Ahmed, Z.: COVID-DenseNet: A deep learning architecture to detect COVID-19 from chest radiology images
 - 92. Sharma, V., Dyreson, C.: COVID-19 screening using residual attention network an artificial intelligence approach. In: *2020 19th IEEE International Conference on Machine Learning and Applications (ICMLA)*, 14 Dec 2020). IEEE, pp. 1354–1361
 - 93. Ucar, F., Korkmaz, D.: COVIDagnosis-net: Deep Bayes-SqueezeNet based diagnosis of the coronavirus disease 2019 (COVID-19) from X-ray images. *Med. Hypotheses* **1**(140), 109761 (2020)
 - 94. Iandola, F.N., Han, S., Moskewicz, M.W., Ashraf, K., Dally, W.J., Keutzer, K.: SqueezeNet: AlexNet-level accuracy with 50x fewer parameters and < 0.5 MB model size. arXiv preprint [arXiv:1602.07360](https://arxiv.org/abs/1602.07360) (24 Feb 2016)
 - 95. Khobahi, S., Agarwal, C., Soltanianian, M.: Coronet: A deep network architecture for semi-supervised task-based identification of covid-19 from chest x-ray images. MedRxiv (1 Jan 2020)
 - 96. Xu, X., Jiang, X., Ma, C., Du, P., Li, X., Lv, S., Yu, L., Ni, Q., Chen, Y., Su, J., Lang, G.: A deep learning system to screen novel coronavirus disease 2019 pneumonia. *Engineering* **6**(10), 1122–1129 (2020)
 - 97. Zokaeinikoo, M., Kazemian, P., Mitra, P., Kumara, S.: AIDCOV: an interpretable artificial intelligence model for detection of COVID-19 from chest radiography images. *ACM Trans. Manag. Inf. Syst. (TMIS)* **12**(4), 1–20 (2021)
 - 98. Wang, L., Lin, Z.Q., Wong, A.: Covid-net: A tailored deep convolutional neural network design for detection of covid-19 cases from chest x-ray images. *Sci. Rep.* **10**(1), 1–2 (2020)
 - 99. Song, Y., Zheng, S., Li, L., Zhang, X., Zhang, X., Huang, Z., Chen, J., Wang, R., Zhao, H., Chong, Y., Shen, J.: Deep learning enables accurate diagnosis of novel coronavirus (COVID-19) with CT images. *IEEE/ACM Trans. Comput. Biol. Bioinf.* **18**(6), 2775–2780 (2021)
 - 100. Oh, Y., Park, S., Ye, J.C.: Deep learning covid-19 features on CXR using limited training data sets. *IEEE Trans. Med. Imaging* **39**(8), 2688–2700 (2020)
 - 101. Ibrahim, A.U., Ozsoz, M., Serte, S., Al-Turjman, F., Yakoi, P.S.: Pneumonia classification using deep learning from chest X-ray images during COVID-19. *Cogn. Comput.* **4**, 1–3 (2021)
 - 102. Dagli, Y., Choksi, S., Sudipta, R.: Prediction of two year survival among patients of non-small cell lung cancer. In: Peter, J., Fernandes, S., Eduardo Thomaz, C., Viriri, S. (eds.) *Computer Aided Intervention and Diagnostics in Clinical and Medical Images. Lecture Notes in Computational Vision and Biomechanics*, vol. 31, pp. 169–177. Springer, Cham (2019)
 - 103. Hussain, E., Hasan, M., Rahman, M.A., Lee, I., Tamanna, T., Parvez, M.Z.: CoroDet: A deep learning based classification for COVID-19 detection using chest X-ray images. *Chaos, Solitons Fractals* **1**(142), 110495 (2021)
 - 104. Ghoshal, B., Tucker, A.: Estimating uncertainty and interpretability in deep learning for coronavirus (COVID-19) detection. arXiv preprint [arXiv:2003.10769](https://arxiv.org/abs/2003.10769) (22 Mar 2020)

105. Cohen, J.P., Dao, L., Roth, K., Morrison, P., Bengio, Y., Abbasi, A.F., Shen, B., Mahsa, H.K., Ghassemi, M., Li, H., Duong, T.: Predicting covid-19 pneumonia severity on chest x-ray with deep learning. *Cureus* **12** (7) (July 2020)
106. App Determines COVID-19 Disease Severity Using Artificial Intelligence, *Biomarkers* (2020) [Online]. Available: <https://www.sciencedaily.com/releases/2020/06/200603132529.htm>
107. Using Artificial Intelligence to Determine CIVID-19 Severity (2020) [Online]. Available: <https://www.healtheuropa.eu/using-artificial-intelligence-to-determine-covid-19-severity/100501/>
108. AI can assess COVID-19 severity on chest x-rays (2020) [Online]. Available: <https://www.auntninnie.com/index.aspx?sec=ser&sub=def&pag=dis&ItemID=129674>
109. Anastasopoulos, C., Weikert, T., Yang, S., Abdulkadir, A., Schmülling, L., Bühler, C., Paciolla, F., Sexauer, R., Cyriac, J., Nesić, I., Twerenbold, R.: Development and clinical implementation of tailored image analysis tools for COVID-19 in the midst of the pandemic: The synergetic effect of an open, clinically embedded software development platform and machine learning. *Eur. J. Radiol.* **1**(131), 109233 (2020)
110. Xue, W., Cao, C., Liu, J., Duan, Y., Cao, H., Wang, J., Tao, X., Chen, Z., Wu, M., Zhang, J., Sun, H.: Modality alignment contrastive learning for severity assessment of COVID-19 from lung ultrasound and clinical information. *Med. Image Anal.* **1**(69), 101975 (2021)
111. Li, Z., Zhao, S., Chen, Y., Luo, F., Kang, Z., Cai, S., Zhao, W., Liu, J., Zhao, D., Li, Y.: A deep-learning-based framework for severity assessment of COVID-19 with CT images. *Expert Syst. Appl.* **15**(185), 115616 (2021)
112. Zhou, L., Li, Z., Zhou, J., Li, H., Chen, Y., Huang, Y., Xie, D., Zhao, L., Fan, M., Hashmi, S., Abdelkareem, F.: A rapid, accurate and machine-agnostic segmentation and quantification method for CT-based COVID-19 diagnosis. *IEEE Trans. Med. Imaging* **39**(8), 2638–2652 (2020)
113. Chaganti, S., Grenier, P., Balachandran, A., Chabin, G., Cohen, S., Flohr, T., Georgescu, B., Grbic, S., Liu, S., Mellot, F., Murray, N.: Automated quantification of CT patterns associated with COVID-19 from chest CT. *Radiol. Artif. Intell.* **2** (4), e200048 (29 July 2020)
114. Shen, C., Yu, N., Cai, S., Zhou, J., Sheng, J., Liu, K., Zhou, H., Guo, Y., Niu, G.: Quantitative computed tomography analysis for stratifying the severity of coronavirus disease 2019. *J. Pharm. Anal.* **10**(2), 123–129 (2020)
115. Gozes, O., Frid-Adar, M., Sagie, N., Zhang, H., Ji, W., Greenspan, H.: Coronavirus detection and analysis on chest CT with deep learning. *arXiv preprint arXiv:2004.02640* (6 Apr 2020)
116. He, K., Zhao, W., Xie, X., Ji, W., Liu, M., Tang, Z., Shi, Y., Shi, F., Gao, Y., Liu, J., Zhang, J.: Synergistic learning of lung lobe segmentation and hierarchical multi-instance classification for automated severity assessment of COVID-19 in CT images. *Pattern Recogn.* **1**(113), 107828 (2021)
117. Zhang, K., Liu, X., Shen, J., Li, Z., Sang, Y., Wu, X., Zha, Y., Liang, W., Wang, C., Wang, K., Ye, L.: Clinically applicable AI system for accurate diagnosis, quantitative measurements, and prognosis of COVID-19 pneumonia using computed tomography. *Cell* **181**(6), 1423–1433 (2020)
118. Zhu, X., Song, B., Shi, F., Chen, Y., Hu, R., Gan, J., Zhang, W., Li, M., Wang, L., Gao, Y., Shan, F.: Joint prediction and time estimation of COVID-19 developing severe symptoms using chest CT scan. *Med. Image Anal.* **1**(67), 101824 (2021)
119. Nguyen, C.T., Saputra, Y.M., Van Huynh, N., Nguyen, N.T., Khoa, T.V., Tuan, B.M., Nguyen, D.N., Hoang, D.T., Vu, T.X., Dutkiewicz, E., Chatzinotas, S.: Enabling and emerging technologies for social distancing: a comprehensive survey and open problems. *arXiv preprint arXiv:2005.02816* (1 May 2020)
120. Punn, N.S., Sonbhadra, S.K., Agarwal, S., Rai, G.: Monitoring COVID-19 social distancing with person detection and tracking via fine-tuned YOLO v3 and deepsort techniques. *arXiv preprint arXiv:2005.01385* (4 May 2020)
121. Jain, R., Gupta, M., Garg, K., Gupta, A.: Robotics and Drone-Based Solution for the Impact of COVID-19 Worldwide Using AI and IoT. *Emerging Technologies for Battling Covid-19: Applications and Innovations*, 139–156 (2021)

122. Sathyamoorthy, A.J., Patel, U., Savle, Y.A., Paul, M., Manocha, D.: COVID-robot: Monitoring social distancing constraints in crowded scenarios. arXiv preprint [arXiv:2008.06585](https://arxiv.org/abs/2008.06585) (14 Aug 2020)
123. Ansari, M.A., Singh, D.K.: Monitoring social distancing through human detection for preventing/reducing COVID spread. *Int. J. Inf. Technol.* **13**(3), 1255–1264 (2021)
124. Degadwala, S., Vyas, D., Dave, H., Mahajan, A.: Visual social distance alert system using computer vision & deep learning. In: 2020 4th International Conference on Electronics, Communication and Aerospace Technology (ICECA), pp. 1512–1516. IEEE (5 Nov 2020)
125. Ahmed, I., Ahmad, M., Jeon, G.: Social distance monitoring framework using deep learning architecture to control infection transmission of COVID-19 pandemic. *Sustain. Cities Soc.* **1**(69), 102777 (2021)
126. Leung, N.H., Chu, D.K., Shiu, E.Y., Chan, K.H., McDevitt, J.J., Hau, B.J., Yen, H.L., Li, Y., Ip, D.K., Peiris, J.M., Seto, W.H.: Respiratory virus shedding in exhaled breath and efficacy of face masks. *Nat. Med.* **26**(5), 676–680 (2020)
127. Abboah-Offei, M., Salifu, Y., Adewale, B., Bayuo, J., Ofosu-Poku, R., Opare-Lokko, E.B.: A rapid review of the use of face mask in preventing the spread of COVID-19. *Int. J. Nursing Stud. Adv.* **1**(3), 100013 (2021)
128. Oumina, A., El Makhfi, N., Hamdi, M.: Control the covid-19 pandemic: Face mask detection using transfer learning. In: 2020 IEEE 2nd International Conference on Electronics, Control, Optimization and Computer Science (ICECOCS), pp. 1–5. IEEE (2 Dec 2020)
129. Mangla, M., Sayyad, A., Mohanty, S.N.: An AI and computer vision-based face mask recognition and detection system. In: 2021 2nd International Conference on Secure Cyber Computing and Communications (ICSCCC), pp. 170–174. IEEE (21 May 2021)
130. Suganthalakshmi, R., Hafeeza, A., Abinaya, P., Devi, A.G.: Covid-19 facemask detection with deep learning and computer vision. *Int. J. Eng. Res. Tech. (IJERT) ICRADL* (2021)
131. Razavi, M., Alikhani, H., Janfaza, V., Sadeghi, B., Alikhani, E.: An automatic system to monitor the physical distance and face mask wearing of construction workers in covid-19 pandemic. *SN Comput. Sci.* **3**(1), 1–8 (2022)
132. Draughon, G.T., Sun, P., Lynch, J.P.: Implementation of a computer vision framework for tracking and visualizing face mask usage in urban environments. In: 2020 IEEE International Smart Cities Conference (ISC2), pp. 1–8. IEEE (2020)
133. Bornstein, A.: Personal Face Mask Detection with Custom Vision and Tensorflow.js. Medium (22 Mar 2020). Accessed: 21 Nov 2021 (2021) [Online]. Available: <https://medium.com/microsoftazure/corona-face-mask-detection-with-custom-vision-and-tensorflow-js-86e5fff84373>
134. Zhang, J., Han, F., Chun, Y., Chen, W.: A novel detection framework about conditions of wearing face mask for helping control the spread of COVID-19. *IEEE Access* **17**(9), 42975–42984 (2021)
135. Chen, J.: Pathogenicity and transmissibility of 2019-nCoV—a quick overview and comparison with other emerging viruses. *Microbes Infect.* **22**(2), 69–71 (2020)
136. Perpetuini, D., Filippini, C., Cardone, D., Merla, A.: An overview of thermal infrared imaging-based screenings during pandemic emergencies. *Int. J. Environ. Res. Public Health* **18**(6), 3286 (2021)
137. Mestha, L.K., Shilla, E., Bernal, E.A., Pennington, G.S., Madhu, H.J. (Inventors); Xerox Corp (Assignee).: Breathing pattern identification for respiratory function assessment. United States patent US 10,219,739, 5 Mar 2019
138. Huang, C., Xu, X., Cai, Y., Ge, Q., Zeng, G., Li, X., Zhang, W., Ji, C., Yang, L.: Mining the characteristics of COVID-19 patients in China: Analysis of social media posts. *J. Med. Internet Res.* **22**(5), e19087 (2020)
139. Ghassemi, P., Pfeifer, T.J., Casamento, J.P., Simpson, R., Wang, Q.: Best practices for standardized performance testing of infrared thermographs intended for fever screening. *PLoS ONE* **13**(9), e0203302 (2018)
140. Nuertey, B.D., Ekremet, K., Haidallah, A.R., Mumuni, K., Addai, J., Attibu, R.I., Damah, M.C., Duorinna, E., Seidu, A.S., Adongo, V.C., Adatsi, R.K.: Performance of COVID-19

- associated symptoms and temperature checking as a screening tool for SARS-CoV-2 infection. *PLoS ONE* **16**(9), e0257450 (2021)
- 141. Somboonkaew, A., Prempree, P., Vuttivong, S., Wetcharungsri, J., Porntheeraphat, S., Chanhorn, S., Pongsoon, P., Amarit, R., Intaravanne, Y., Chaitavon, K., Sumriddetchkajorn, S.: Mobile-platform for automatic fever screening system based on infrared forehead temperature. In: 2017 Opto-Electronics and Communications Conference (OECC) and Photonics Global Conference (PGC), pp. 1–4 (31 July 2017). IEEE
 - 142. Tan, W., Liu, J.: Application of face recognition in tracing COVID-19 fever patients and close contacts. In: 2020 19th IEEE International Conference on Machine Learning and Applications (ICMLA), pp. 1112–1116. IEEE (14 Dec 2020)
 - 143. Lahiri, B.B., Bagavathiappan, S., Jayakumar, T., Philip, J.: Medical applications of infrared thermography: A review. *Infrared Phys. Technol.* **55**(4), 221–235 (2012)
 - 144. Yang, G., Lv, H., Zhang, Z., Yang, L., Deng, J., You, S., Du, J., Yang, H.: Keep healthcare workers safe: Application of teleoperated robot in isolation ward for COVID-19 prevention and control. *Chin. J. Mech. Eng.* **33**(1), 1–4 (2020)
 - 145. Wang, X.V., Wang, L.: A literature survey of the robotic technologies during the COVID-19 pandemic. *J. Manuf. Syst.* (13 Feb 2021)
 - 146. Di Lallo, A., Murphy, R., Krieger, A., Zhu, J., Taylor, R.H., Su, H.: Medical robots for infectious diseases: Lessons and challenges from the COVID-19 pandemic. *IEEE Robot. Autom. Mag.* **28**(1), 18–27 (2021)
 - 147. Li, S.Q., Guo, W.L., Liu, H., Wang, T., Zhou, Y.Y., Yu, T., Wang, C.Y., Yang, Y.M., Zhong, N.S., Zhang, N.F., Li, S.Y.: Clinical application of an intelligent oropharyngeal swab robot: Implication for the COVID-19 pandemic. *Eur. Resp. J.* **56** (2) (1 Aug 2020)
 - 148. Jiang, Y., Wen, J.: Effects of COVID-19 on hotel marketing and management: A perspective article. *Int. J. Contemp. Hospitality Manage.* (23 June 2020)
 - 149. Chen, J., Li, K., Zhang, Z., Li, K., Yu, P.S.: A survey on applications of artificial intelligence in fighting against COVID-19. *ACM Comput. Surv (CSUR)* **54**(8), 1–32 (2021)
 - 150. Khemasuwan, D., Colt, H.G.: Applications and challenges of AI-based algorithms in the COVID-19 pandemic. *BMJ Innov.* **7** (2) (1 Apr 2021)
 - 151. Price, W.N., Gerke, S., Cohen, I.G.: Potential liability for physicians using artificial intelligence. *JAMA* **322**(18), 1765–1766 (2019)
 - 152. Chowdhury, M.E., Rahman, T., Khandakar, A., Mazhar, R., Kadir, M.A., Mahbub, Z.B., Islam, K.R., Khan, M.S., Iqbal, A., Al Emadi, N., Reaz, M.B.: Can AI help in screening viral and COVID-19 pneumonia? *IEEE Access*. **20**(8), 132665–132676 (2020)
 - 153. Chung, A.: COVID CA. Chest x-ray data initiative (2020). <https://github.com/agchung/Actualmed-COVID-chestxray-dataset>
 - 154. Chung, A.: Figure 1 COVID-19 chest x-ray dataset initiative. Retrieved April. 17, 2020 (2020)
 - 155. Alqudah, A.M., Qazan, S.: Augmented COVID-19 X-ray Images Dataset, Mendeley Data, V4 (2020). <https://doi.org/10.17632/2fxz4px6d8.4>
 - 156. El-Shafai, W., Abd El-Samie, F.: Extensive COVID-19 X-Ray and CT chest images dataset. Mendeley Data, V3
 - 157. SRIM. COVID-19 database. Society of Medical and Interventional Radiology. Accessed January 2022. Available at: <https://sirm.org/category/senza-categoria/covid-19/>
 - 158. BSTI. COVID-19 British Society of Thoracic Imaging Database. Accessed January 2022. Available at: <https://www.bsti.org.uk/training-and-education/covid-19-bsti-imaging-database/>
 - 159. Radiopaedia: (2020). Accessed January 2022. Available at: <https://radiopaedia.org/articles/normal-chest-imaging-examples?lang=gb>
 - 160. Yang, X., He, X., Zhao, J., Zhang, Y., Zhang, S., Xie, P.: COVID-CT-dataset: A CT scan dataset about COVID-19. *arXiv preprint arXiv:2003.13865* (30 Mar 2020)
 - 161. BIMCV COVID-19. BIMCV Medical Imaging Databank of the Valencia Region. Accessed January 2022. Available at: <https://bimcv.cipf.es/bimcv-projects/bimcv-COVID19/>
 - 162. Born, J., Brändle, G., Cossio, M., Disdier, M., Goulet, J., Roulin, J., Wiedemann, N.: POCOVID-Net: Automatic detection of COVID-19 from a new lung ultrasound imaging dataset (POCUS). *arXiv preprint arXiv:2004.12084* (25 Apr 2020)

163. Wang, Z., Wang, G., Huang, B., Xiong, Z., Hong, Q., Wu, H., Yi, P., Jiang, K., Wang, N., Pei, Y., Chen, H.: Masked face recognition dataset and application. arXiv preprint [arXiv:2003.09093](https://arxiv.org/abs/2003.09093) (20 Mar 2020)

Health Monitoring Methods in Heart Diseases Based on Data Mining Approach: A Directional Review



Majid Harouni , Mohsen Karimi , Afroz Nasr , Helia Mahmoudi , and Zakeh Arab Najafabadi

Abstract Health monitoring in humans is very important. This monitoring can be done in different people from embryonic period to adulthood. A healthy fetal will lead to a healthy baby. For this purpose, health assessment methods are used from the fetal to adulthood. One of the most common methods of assessing health at different times is to use clinical signs and data. Measuring heart rate, blood pressure, temperature, and other symptoms can help monitor health. However, there are usually errors in human predictions. Data mining is a technique for identifying and diagnosing diseases, categorizing patients in disease management, and finding patterns to diagnose patients more quickly and prevent complications. It could be a great help. Increasing the accuracy of diagnosis, reducing costs, and reducing human resources in the medical sector have been proven by researchers as the benefits of introducing data mining in medical analysis. In this paper, data mining methods will be introduced to diagnose and monitor health in individuals with various heart diseases. Heart disease will be evaluated to make the study more comprehensive, including fetal health diagnosis, arrhythmias, and machine learning data mining angiography. Attempts are made to introduce the relevant database in each disease and to evaluate the desired methods in health monitoring.

M. Harouni

Department of Computer Engineering, Doalatabad Branch, Islamic Azad University, Isfahan, Iran

M. Karimi ()

Department of Bioelectronics and Biomedical Engineering, School of Advanced Technologies in Medicine, Isfahan, University of Medical Sciences, Isfahan, Iran

e-mail: mohsen.karimi25@gmail.com

A. Nasr

Department of Computer Engineering, Isfahan (Khorasgan) Branch, Islamic Azad University, Isfahan, Iran

H. Mahmoudi

MD, MPH Candidate in Family Medicine, Department of Community Medicine, Medical University of Isfahan, Isfahan, Iran

Z. Arab Najafabadi

Department of Engineering, South of Tehran Branch, Islamic Azad University, Tehran, Iran
e-mail: z.arab@resident.mui.ac.ir

Keywords Health monitoring · Data mining · Heart · Arrhythmia · Fetal · Angiography

1 Introduction

Around the world, most people living in cities are less physically active. The world's population is growing, and most people are living longer than in the past. At the same time, people are eating more unhealthy and bulky foods than in the past. Therefore, improper combination (low physical activity and use of unhealthy foods) has led to an uncontrollable increase in the prevalence of heart disease in the world. Heart disease is a chronic and sometimes hazardous disease that results from a heart malfunction in the body. An estimate in 2005 found that 30 million people worldwide had a variety of heart conditions. It is predicted that by 2025 the number of people with heart disease will reach more than 333 million [1].

The mechanical activity of the human heart originates from electrical stimuli inside the heart. Depolarization is an activation of a certain part of the heart (atrium or ventricle) results in mechanical contraction of that same part. Repolarization (atrial or ventricular) results in mechanical rest of the heart cavities. Electrocardiogram or ECG data recorders record electrical activity of the heart muscle through millivolts in sensors attached to human skin [2]. Both atria contract during normal heart activity, followed by contraction, and both ventricles contract. Atrial fibrillation results from atrial contraction, which is plotted as a P-wave on an electrocardiogram. Ventricular contraction or ventricular contraction is also associated with QRS. During the ventricular contraction that sends the heart to other body parts, the QRS composition appears to be more intense than the gentle P-wave. After ventricular contraction due to ventricular repolarization, both ventricles return to rest. A T-wave represents this ventricular polarization or mechanical relaxation. Polarization or atrial relaxation appears to be buried under the stronger QRS compound [3]. A Dutch researcher named Willem Einthoven first assigned the letters PQRST to different electrocardiogram waveform deviations as shown in Fig. 1.

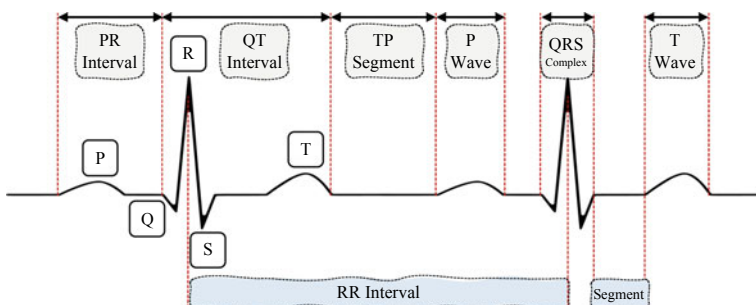


Fig. 1 Heart signal and its waves

Monitoring and controlling the heart's function as a vital element in the body is essential. Cardiac activity is recorded and monitored using an ECG. ECG recording of cardiac signals is a non-invasive method of recording, monitoring, and controlling heart function. In order to monitor cardiac function and diagnose cardiac arrhythmias, the use of long-term recording of these signals is recommended for at least a 24-h interval [4]. ECGs usually have certain shapes in healthy people. Any changes or abnormalities in heart function can be seen on the ECG. These abnormalities are known as cardiac arrhythmias. An electrocardiogram is a physiological non-stationary ECG signal. The ECG is not just for examining patterns created and heartbeats. It can also be used to check for irregular heart activity [5]. The use of ECG signals has challenges such as not seeing the signs of cardiac arrhythmia in the period when the ECG signal is recorded [6], changing the morphological characteristics of cardiac signals such as amplitude, period, multiple peaks, and compression QRS in different people. These characteristics depend on parameters and factors such as age, gender, physical condition, living conditions, and even mental condition. Deciding and presenting a generalized solution or even a standard for a community of people is difficult or even impossible [6]. Non-stationary ECG signal, different ECG for a person in different conditions such as walking, running, resting, and sleeping [7], difficulty in analyzing ECG data, due to the high volume and high number of recorded data And the creation of diagnostic error, the presence of repetitive data in ECG signals [8], the effect of noise, dummy effects, different moods in individuals on heart function, and ECG morphology [8] have been observed.

Careful monitoring of fetal health based on information available before delivery is crucial and significantly impacts fetal health monitoring. The fetal is dependent on the mother for oxygen exchange and carbon dioxide in the placenta, which depends on the adequate concentration of gases in the mother's blood, the amount of blood in the uterus, placental exchange, and gas transfer to the fetal. Deficiency in any of the above factors can lead to hypoxia in fetal tissues (hypoxia) which, despite compensatory mechanisms, may lead to abnormal increases in blood acid levels (acidosis) [9]. One of the most important factors in diagnosing fetal health and the mainstay of prenatal fetal health assessment is fetal heart rate (FHR) monitoring. Commonly monitored items include fetal core heart rate, periodic changes, and non-periodic changes. The main purpose of heart rate monitoring is to assess stress or diagnose possible fetal heart disease, which can prevent fetal death. In addition, if there is a system that can predict the following condition according to the current condition of the fetal, it can prevent problems such as miscarriage or serious injuries. Also, in fetal heart monitoring and assessing the heart rate, sometimes the mother's uterine contractions are examined to some extent, which provides good information to specialists in identifying possible diseases. One of the useful tools for monitoring in this area is the use of a cardiotocography (CTG) device.

Some observations are seen from disease states, some observations are seen from health states, and some observations are seen in both hidden states of health and disease. The probability of observations can be estimated approximately based on the statistics received from hospitals and samples. The basal heart rate of the fetal, if there is any possible disease, is 110–160 beats per minute. If this rate exceeds 160,

the fetal will be in tachycardia, and if it is less than 110, the fetal heart will be in bradycardia. Acceleration and decline are part of the changes in the fetal heart. In fact, an increase of 15–20 beats per minute above the basal rate for 15 s is said to accelerate, which of course indicates the health of peripheral neurotransmitters and healthy myocardium. Also, the decrease in heart rate compared to the basal heart rate is called a decrease, which is divided into three categories: (1) premature decrease, (2) late decrease, and (3) variable decrease. Baseline variability, called B.b.v., indicates the health of the nerve pathway from the medial cortex and vagus nerve to the cardiac conduction system. The normal range of B.b.v is about 6–25 beats per minute. B.b.v levels are less than two indicators of a fetal health problem. Excessive changes or more than 25 beats per minute, also called B.b.v mutations, indicate premature fetal hypoxia, which is itself dangerous. So, the fetal can be in one of the moderate B.b.v and abnormal B.b.v. Also, the shape of the fetal ECG should not have a sinusoidal pattern. An example of the signals recorded on paper from the cardiotocography device is shown in Fig. 2.

It seems that in order to monitor cardiac signals and cardiotocographic data in the fetus for a long time, using traditional methods or even the use of manpower is difficult and sometimes impossible. For this purpose, the use of machine learning-based methods has been proposed [10]. Machine learning is a science that has many subsets. One of these subsets is data mining, and one of the subsets is classification data mining. The classification of data causes the machine to learn in such a way that after training the machine, by entering new data, the machine can identify which category or class this data belongs to. This method is also called predictor. In fact, in such cases, our test data may be so large that it is beyond human computing power, in which case, with proper machine learning, time and energy can be saved and information can be classified in a fraction of a second [11].

In the classification of cardiac signals, five modes are commonly defined to detect arrhythmias. Natural N, ventricular V, supraventricular S, natural and ventricular combination F, and unknown bits Q [12] are presented. In recent years, several

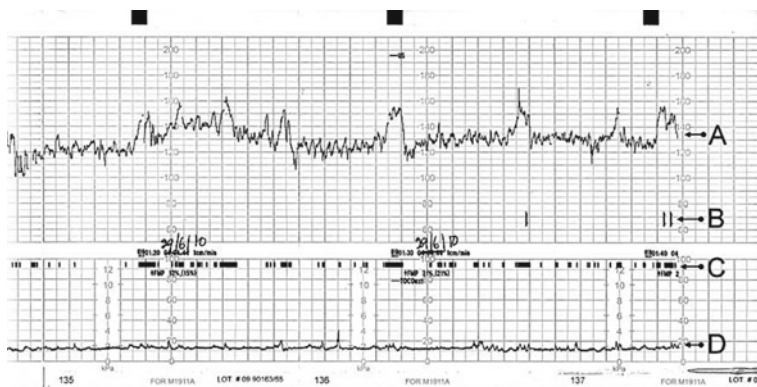


Fig. 2 A sample of the signal recorded from the fetus by a cardiotocography device

methods have been proposed to diagnose types of artemia based on machine learning. Methods based on machine learning or pattern recognition consist mainly of preprocessing, feature extraction, feature selection, and classification. In these methods, ECG signals are first amplified for different types of noise and artificial effects [13]. Then a variety of properties such as time domain properties, frequency domain properties, and multi-precision properties are extracted: Among the time domain properties can be morphological properties such as PQPST which includes P-wave, QRS complex, and T-wave [14] extract. Features such as wavelet transform [15], higher-order HOS statistical moments [16], Hermite basis function [17], and hidden Markov models [18] are extracted. After extracting the attribute, selecting the attribute is used. Because ECG signals have high correlations as well as higher dimensions, they contain duplicate information. In order to reduce the dimension as well as remove duplicate information, methods based on dimension reduction and feature selection are used. One of the most common methods of reducing the principal component of PCA analysis is independent component analysis [19]. Although dimensionality eliminates duplicate information, it does not in itself mean selecting the most informed features for classification training. Finally, the selected features or reduced dimension will be used to classify the training. The most common classifications used are support vector machine (SVM), artificial neural networks (ANNs), and k-nearest neighborhood (KNN) [20].

The main problem with the former methods of automatic fetal health diagnosis is the lack of a solution with a degree of confidence in the performance of the output produced at the appropriate level. Sometimes different interpretations of tachograph signals can be made, and therefore, it is necessary to perform a statistically accurate analysis of the input data [21]. Therefore, it requires the use of self-signal analysis techniques and machine learning. Accordingly, intelligent methods of diagnosing this disease have become one of the hot topics in the medical field [22].

The use of pattern recognition and machine learning algorithms can be introduced as a tool for intelligent detection of this category [23, 24]. As mentioned, intelligent diagnosis of fetal health as one of the preventive factors among physicians has been a big challenge, because the physician must either confirm the results of testing and sampling of the fetus and perform the final analysis or one who performs accurate calculations. Nowadays, doctors can deal with this disease by diagnosing it early. In order to automatically detect fetal health, researchers have recently decided to use the field of artificial intelligence and soft computing.

The main purpose of this paper is to provide a comprehensive overview of the application of machine learning and data mining methods in the diagnosis of heart disease in adults and to monitor the condition of the fetal heart using cardiotocographic data in the fetus. Various studies have been conducted in recent years to monitor health in this area based on machine learning. This paper will examine the proposed methods in detail and comprehensively. The contribution of this paper can be described as follows:

- Evaluation and introduction of cardiac arrhythmias
- Complete introduction of cardiac signals and cardiotocographic data in the fetus

- Introduction of a database in the field of cardiac arrhythmia and cardiotocography
- Evaluation of steps in data mining and machine learning methods in the diagnosis of arrhythmias and fetal disease
- Review of the latest research in the diagnosis of machine-based heart disease.

This paper is composed of the following sections. Section 2 introduces the types of cardiac arrhythmias. Recorded electrocardiographic signals from the heart will also be provided. In this section, fetal diseases and cardiotocographic data are introduced. In Sect. 3, methods based on machine learning and data mining in disease diagnosis will be examined. In Sect. 4, research conducted by researchers in previous years based on machine learning and data mining methods will be reviewed. Finally, in Sect. 5, the conclusion of the paper is presented.

2 Heart Disease

Heart disease is one of the most common causes of death. They account for more than 31% of the causes of death. Also, more than 80% of the cause of cardiac death is related to cardiac arrhythmias [25]. One of the common and effective ways to diagnose cardiac arrhythmias is the use of electrocardiogram or ECG signals. ECG records the electrical activity of the heart over a medium period of time with electrodes placed on the skin at various locations. Recording the electrical activity potentials of the heart with different electrodes and at different angles can show the state of an unhealthy heart in changes in heart waveform. Using ECG waveforms, physicians can identify a variety of diseases for the purpose of blood supply to tissues [26], heart attacks, and shock. Diagnosing a cardiac arrhythmia can be both a good help for the doctor and can help normal people stay healthy. Figure 3 shows an example

Fig. 3 ECG recording system in 12 channels [27]

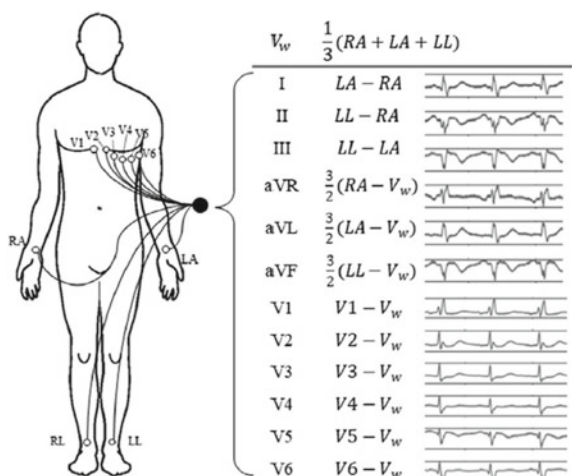
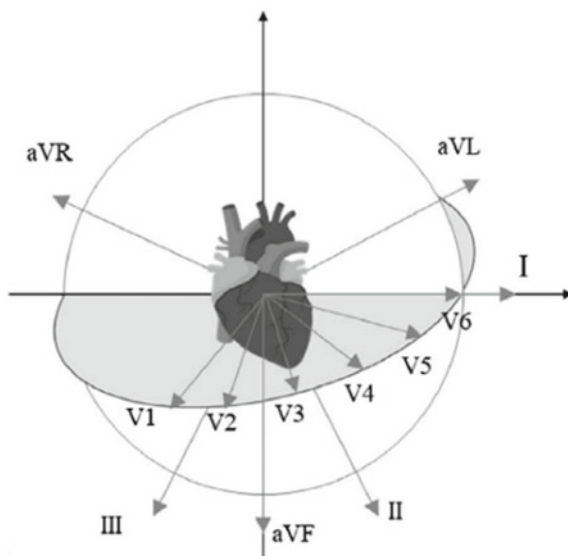


Fig. 4 Registration of potential difference between electrodes [27]



of recording cardiac signals. In this figure, the spatial distribution of the electrodes, which includes 10 electrodes in the 12-lead system. In this system, there are three sloping leads, three additional sloping leads, and six leads located on the chest. There is also a carbon lead known as the Wilson center lead.

Figure 4 shows the potential difference between different electrodes placed on the skin, which records and displays the electrical activity of the heart in 12 leads.

In studies, the diagnosis and identification of arrhythmias have been extensively studied. One of the free and public databases available is MIT-BIH [28], where heart rate analyzes are performed. Heart rate and heart rate analysis are performed in five normal classes, supraventricular (ventricular) SVEB, ventricular heart rate VEB, heart rate integration, and unknown beats, in which the waveforms are completely different. Because the electrocardiogram records the mechanical activity of the heart muscle, the contraction and contraction of the heart muscle are recorded as a waveform. Where there are important points P, Q, R, S, and T. There are also important intervals QT, TS, which include points Q and T for QT and S and T for the interval TS. Also, three QRS points in a row form the QRS complex. Figure 5 shows these concepts. The presence of cardiac arrhythmias causes changes in the ECG waveform that this deformation and recognition of these deformations make it possible to identify the disease [29].

- **Cardiac arrhythmia**

Anything that disrupts the electrical impulses that cause the heart to contract causes a heart arrhythmia. A healthy human heart should beat 60–100 times a minute at rest. The more athletic a person is and the healthier his body, the lower his resting heart rate per minute. Olympic champions, for example, have a heart

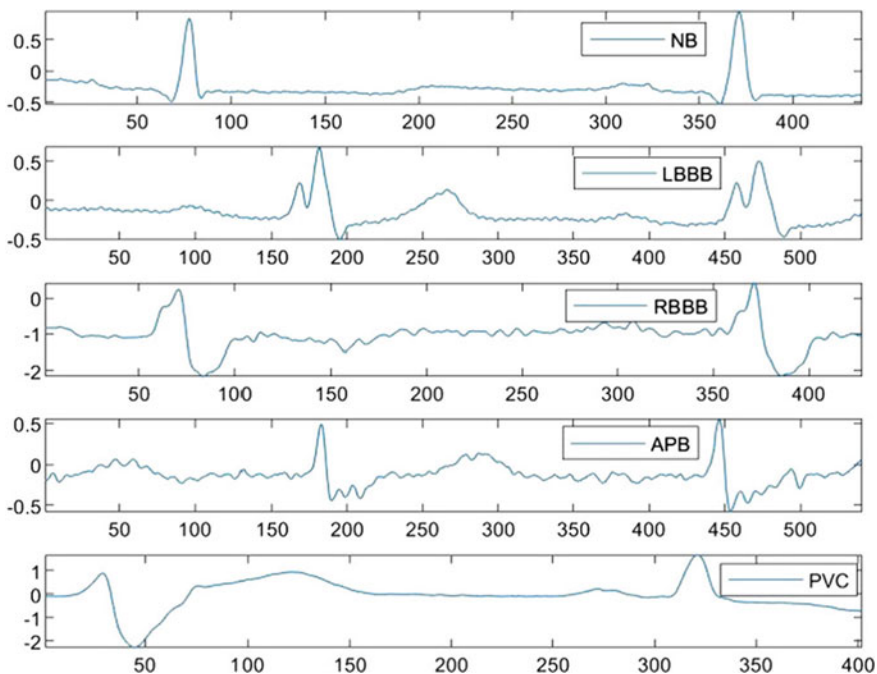


Fig. 5 Types of cardiac arrhythmias [29]

rate of less than 60 beats per minute, which is because their hearts are more efficient [30].

- **Shockability and non-shockability**

The heart muscle is a dynamic system that can have a regular or regular or even irregular rhythm. Irregular heart muscle function, or briefly, irregular heart function, is seen ventricular fibrillation in VF [31]. VF cardiac contraction is the leading cause of many cardiac deaths [32]. If the heart does not contract, VF can cause death in less than a few minutes. In this case, with the help of implantable cardioverter/defibrillator (ICD) or automatic external defibrillator (AED), the person can be shocked. These devices make important and vital decisions by detecting the shock or non-shock of the heart signal. In other words, the equipment must accurately detect the functional state of the heart: shock or non-shock. If the heart is in a state of shock, it should receive a rapid response from the dilator or defibrillator. Proper performance and response of the defibrillator are very important. Many existing devices operate on ECG cardiac signals based on winding path analysis, peak analysis, and thresholding on designed filters or existing mid-pass filters [32]. In the event of a shock, the ECG signals are completely different. In other words, each time a shocking signal occurs, the ECG produces a completely different and, of course, completely random form.

This completely random form of ECG signal has made shock detection difficult and difficult [33].

Challenges of ECG monitoring

Cardiac signals vary from person to person. Although the same standard and morphology are defined for cardiac signals, there are still many differences in these signals. Even in a person, the signals are still different due to his various mental and physical states. By creating a cardiac artemia, these patterns are still different. By creating a cardiac artemia, these patterns are still different. These signals have a high volume, which creates a high computational complexity. There is duplicate data. This duplicate data complicates final processes such as classification.

Monitoring the function of the heart as a vital element in the body is essential. Cardiac activity is recorded and monitored using an ECG. ECGs usually have certain shapes in healthy people. An electrocardiogram is a physiological non-stationary ECG signal. The ECG is not only used to check for patterns in the heart, but can also be used to check for abnormal heart activity [5]. But using ECG signals has its challenges. Some of these challenges are:

Symptoms of cardiac arrhythmia may not be seen during the period when the ECG signal is recorded [6].

1. The morphological characteristics of cardiac signals such as amplitude, period, multiple peaks, and QRS compression vary from person to person. These characteristics depend on parameters and factors such as age, gender, physical condition, living conditions, and even mental condition. Deciding and presenting a generalized solution or even a standard for a community of people is difficult or even impossible [6].
2. As stated, the ECG signal is not stationary. An ECG varies from person to person, depending on the situation. In other words, people have different ECGs in different postures such as walking, running, resting, and sleeping [7].
3. Analysis of ECG data is difficult due to the large volume and large number of recorded data. High volume of data causes diagnostic error. ECG signals also contain duplicate data [8].
4. Noise, artificial effects, and different moods in individuals affect the morphology and function of the ECG heart [8].

The challenges posed to the ECG signal are expressed in healthy individuals. Now when VF occurs and the heart function is completely random, the challenge is even greater. In VF mode, the heart vibrates instead of pumping blood. In this case, the function of the heart, and therefore, the ECG will be completely random [34].

Fetal Electrocardiographs

Direct fetal ECG signal is extracted from the fetal heart with a special electrode (a more common type of coil) that is inserted into the uterus and attached to the fetus after passing through the amniotic fluid. The corresponding signal amplitude is about 1 mV, which can be amplified and recorded with good quality (internal monitoring) [35]. If the fetal ECG is obtained from the external surface of the mother's body,

it is in the range of 200–500 mV and will be accompanied by the mother's ECG and the signal resulting from contractions of the uterine and abdominal muscles and other intra-abdominal movements of the mother and fetus. FECG is available during certain periods of pregnancy and is usually the best time to do so after 12 weeks of gestation. When receiving FECG, the mother should be completely relaxed and also the city noise should be removed with proper technique and filtering. FECG contains valuable information from the fetal heart, but obtaining it requires special tools and high expertise [36].

Embryo monitoring

The extraordinary invention of electrical fetal monitoring in the world of obstetrics and gynecology made the diagnosis of fetal distress no longer hypothetical. With accurate information, it is possible to definitively diagnose fetal distress and prevent fetal death. Of course, permanent monitoring is preferable to cross-sectional monitoring. Currently, the two monitoring methods that will be mentioned are widely used, but the methods of fetal evaluation are constantly changing and show that the effectiveness of these methods is not completely satisfactory [37]. This monitoring includes external [37] and internal [38].

Fetal heart patterns

Lack of proper naming or contracting in fetal heart patterns can be problematic. Transverse or longitudinal recording of the waves greatly alters the appearance of the fetal heartbeat. The recommended scaling factors are 30 beats per centimeter vertically. To record fetal heart patterns, the paper must move at a speed of three centimeters per minute. Changes in the fetal heart at a rate of less than one centimeter per minute show false and useless results [39].

Basic fetal heart activity

Basic heart activity is the activity of the heart away from the acceleration or lack of acceleration caused by uterine contractions. In basic heart activity, the characteristics of velocity, heart rate variability, and fetal arrhythmia are defined[40].

Fetal Cardiac arrhythmia

It occurs as a bradycardia, tachycardia, or more commonly as a sudden spearhead. Arrhythmia recording is possible using series electrodes (in internal monitor) [41]. The use of only one lead or electrode in this method greatly limits the interpretation of the findings. Most supraventricular arrhythmias are not significant unless they are concomitant with hydrops-induced heart failure. Many arrhythmias disappear immediately after birth, although some are associated with cardiac structural abnormalities that can be detected by ultrasound during pregnancy. During pregnancy, fetal arrhythmias can be controlled by prescribing digoxin, verapamil, and other drugs to the mother. Except for extrasystole, ventricular arrhythmias are uncommon in the fetus. Arrhythmias interfere with the interpretation of heartbeats during childbirth [42].

Prolonged fetal electrocardiography

Fetal heart monitoring is completed using signals taken from the mother's abdomen, which is a non-invasive technique that allows the fetus to be evaluated and monitored for long periods of time, with appropriate processing of the received signals. Impact-to-shock information about fetal FECG electrocardiography is obtained from signals from the mother's abdomen. The P-wave can also be detected after processing ventricular signals and averaging from the FECG.

The signals received from the mother's abdomen not only contain the desired signals, such as the heart of the fetal ECG or FECG, but also other signals. Signals whose amplitude is much higher than the signal coming from the fetal heart. This is mainly the case with muscle noise. When FECG is detected, MECG is an important source of confusion. The R-wave peak in the maternal electrocardiogram is 7 times the R-wave peak in the FECG. Other annoying signals that get the most attention include baseline noise, signals from muscle contractions (mother's abdomen or other muscles), and signals from uterine contractions, especially during labor. After removing all these additional signals, the FECG is still impregnated with electrical noise and the signal-to-noise ratio (SNR) is weak. Several methods have been proposed to improve and increase the signal strength received from the fetal heart. The purpose of these methods is to detect the fetal heartbeat correctly [43].

3 Machine Learning Methods

A large amount of data is generated daily. The explosive growth of data volumes is the result of the mechanization of societies as well as the development of more powerful tools for data collection and storage. One of the basic needs is the analysis of this large amount of data [44]. Any technique that gives us new insights into data can be considered data mining [45]. In short, data mining has served as a bridge between computer science, statistics, artificial intelligence, modeling, machine learning, and visual representation [46]. It can be said that in data mining, by combining database theories, machine learning, and artificial intelligence, as well as statistical science, provide a new field of application. Data mining is one of the recent advances in the data utilization industry. In essence, data mining is a set of different techniques that enable a person to move beyond ordinary data processing and to explore information in the mass of data and to gain secret knowledge or its selection [47]. Machine learning involves algorithms that discover patterns or models in data under acceptable computational constraints. Another definition is that data mining is a type of technique for identifying information or decision-making knowledge from data pieces, so that by extracting them, in the areas of decision-making, forecasting, forecasting and estimates to be used [48]. Important approaches to data mining and machine learning are divided into supervised, semi-supervisory, semi-supervisory, and reinforcement learning groups.

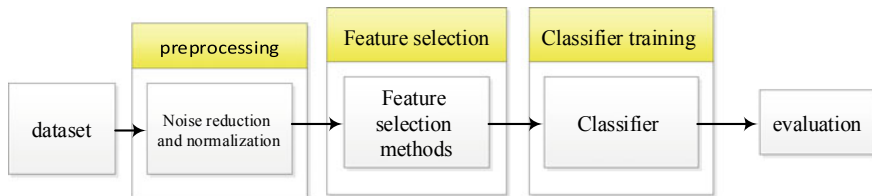


Fig. 6 Data mining steps in supervisory learning

Supervised learning: This type of learning, although not common in nature, is the most common type of learning in the educational system of human societies. In this type of learning, the presence of an observer, or an expert, or data containing knowledge is necessary [49].

Unsupervised Learning: It is one of the most difficult types of learning to be found in many creatures and in different parts of human life. In this type of learning, there is no need for the presence of an expert or observer [50].

Semi-supervised learning: This type of learning is a combination of learning with observer and learning without observer, which in addition to using the experiences provided by the observer, the possibility of using unsupervised approaches has also been considered [51].

Reinforcement learning: In reinforcement learning, implicit measurements for indirect learning are used to determine the rightness or wrongness of learning. In fact, the stored knowledge is weakened or strengthened by penalty or reward signals[52].

In a supervised learning process in machine learning, in order to explore the database and classify it, there are stages of preprocessing, feature extraction, feature selection, classification, and evaluation [53]. Figure 6 shows a block diagram of the process of identifying and classifying in a machine learning database.

Raw data in databases often has problems such as noise, bias, drastic changes in dynamic range, and sampling. Using raw or raw data will undermine subsequent designs. Preprocessing also involves more complex conversions that are used to reduce the size of the data. In short, data preprocessing involves all the conversions that take place on raw data, makes them easier for later processing, such as use in classification, and makes it more effective [54]. There are various tools and methods for preprocessing, such as normalization, which converts data into new data with the appropriate range or distribution. Bleaching is used to decouple data. Dimension reduction is used to remove duplicate, extra or irrelevant data for categorization [55].

Recently, the available data, both in number of samples and in dimensions, has increased dramatically in many machine learning applications. Based on knowledge acquisition, it is very important and necessary to study how to use this large-scale data. The sheer amount of large data has posed a significant challenge to machine learning methods. Due to the existence of noisy, irrelevant, and extra data, learning algorithms not only slow down a lot and reduce the efficiency of learning methods, but also lead to difficulty in interpreting the model. Although preprocessing methods

are somewhat effective, they do not have the necessary efficiency to improve the final result [56]. At this point, feature selection will be an efficient option. Feature selection is able to select a small subset of related features from the main features by removing noisy, irrelevant, and extra features [57].

The exact definition of a feature selection depends on the context in which it is used. But the most widely used definition is that feature selection is the selection of a subset of features with the best result of the classification function [58]. The logic for this definition is that additional unrelated feature or unrelated features often have similar noise in the data, which causes the classifier to be mistaken and the classifier function to be degraded. Deleting such features causes the resulting features to have the same or higher classification function than the total features. As a direct result, fewer features are required for storage, thus speeding up the classification process. In addition, reducing the number of features helps the expert to focus on a subset of the relevant features, which gives them a better view of the process described by the data [59]. In general, feature selection helps to better understand the data, reduce computational requirements, reduce the detrimental effect of dimensions, and improve predicted performance. Feature selection focuses on selecting a subset of input variables that can effectively describe the input data and reduce the effects of noise and irrelevant variables, while providing well-predicted results[60]. Feature selection methods have been able to optimally increase classifier efficiency by selecting a subset of features. Although attribute selection methods have been able to improve the performance of classifiers, in today's world, multiple databases are generated for different purposes. The methods presented in feature selection may not be very efficient and effective in categorizing this data. It seems that the introduction of new methods in feature selection is necessary to improve the performance of the classifier.

Frequently used classifiers in data classification in monitoring methods such as support vector machine (SVM) [45, 61], K-nearest neighbor (KNN) [62], random forest (RF) [63], artificial neural networks (ANNs) [64], and traditional methods are used. But challenges such as lack of convergence in education, sensitivity to outdated data, poor performance in big data due to correlation, and duplication of features have led to a greater tendency to use feature selection [65]. In data mining with so many features, it is very difficult to choose a suitable feature selection method. In practice, the type of feature selection depends on the application. Feature selection can improve the accuracy of detecting and detecting an error in an industrial or medical process. Although there are several methods for selecting a feature, one method for selecting a feature may not be suitable for all applications. Each process, depending on the application, requires an appropriate method of feature selection. Numerous categories have been proposed for the various methods offered in feature selection. These categories are 1- Classification based on data labels, 2- Classification based on the relationship between learning models, 3- Classification based on search strategies [66], which is presented in Fig. 7 of this classification.

Based on the availability of data tags, feature selection methods are classified into three groups, which are regulatory, semi-regulatory, and non-regulatory[67]. In feature selection monitoring methods, all data are labeled. However, in selecting the

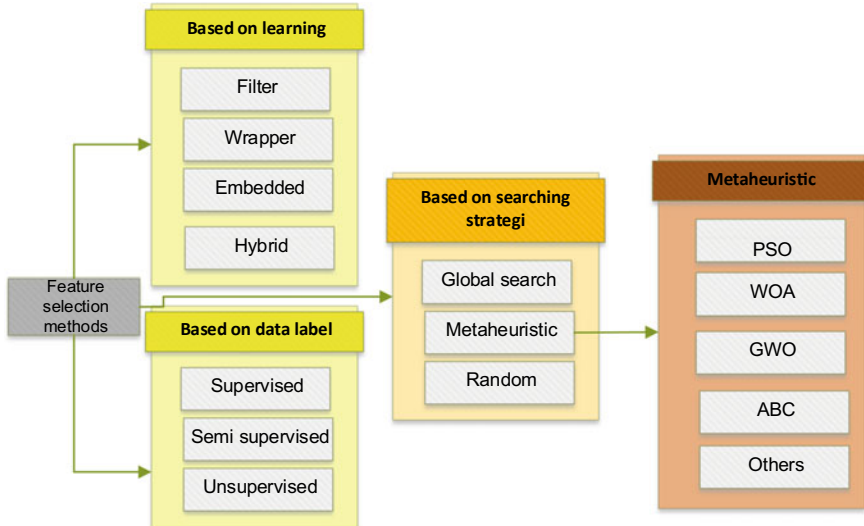


Fig. 7 Classification of feature selection methods

non-monitoring feature, none of the primary data is labeled. But in semi-regulatory methods, some data are labeled, while others are not labeled. It should be noted that real-world data is more than the third type. It seems that semi-regulatory methods can be of great importance [51].

Feature selection algorithms are divided into four groups based on the relationship and different evaluations between learning models: filter, wrapper, permutation, and hybrid-based methods. Filter-based methods use statistical information of properties. As a result, these methods do not require any learning model. These methods are fast and efficient, and at the same time, they are computationally light [69]. Wrapper-based methods select a subset of features based on a learning algorithm. The type of features selected depends a lot on the type of learning algorithm. These methods are more effective and better than filter-based methods, but they are computationally complex [69]. The placement methods select the selected set based on the placement of the features in a learning algorithm. The selected subset of features is selected based on the built-in category. In this model, there is a deeper relationship between the learning model and the selected features. These methods are used for high-dimensional data, and although they have good efficiency, they are very complex [69]. They use a balanced combination of filter and wrapper-based methods to select the optimal subset of features. Hybrid-based methods take advantage of both types of feature selection methods, while trying not to cover the weaknesses of the two methods. Filter-based methods reduce the correlation between features and, in turn, improve the correlation between features and class labels. Filter-based methods are divided into two categories [69]. Many feature selection algorithms based on search strategy for feature selection are provided. Based on search strategies, feature selection and its methods

are divided into three categories: complete, randomized, and evolutionary methods [70].

Complete search methods include searching for the best subset of features in the entire 2^n search space, n is the number of features. As a result, it is almost impossible to identify the best subset, especially if the data volume is high or the data is large, it cannot select the best subset at a reasonable time. In a randomized search, in a limited space of the entire feature space, the best subset is searched, and the dimensions of the selected subset depend on the stop criterion such as maximum repetition, or cost function. Although the interaction between the convergence speed and the optimization of the search algorithm is done by using parameter settings, the algorithms used have the ability to get stuck in the global minimum. In meta-exploration feature selection algorithms, a set is added or subtracted to a subset of selected features. These methods are very computationally suitable, and many such researches have been presented so far. Methods based on PSO particle optimization algorithm [71], bee colony optimization BCA [72], ant colony optimization [73] ACO, and gray wolf optimization algorithm GWO [74]. The ability to search these algorithms globally has caused a lot of Note, however, that there is still the possibility of learning at local minimums in these types of algorithms.

Signal processing

Feature extraction means converting primary data (with all variables) into a dataset with fewer variables. The goal of feature extraction is to obtain the features that contain the most separable information. This may be done to reduce the number of measurements, which leads to lower costs, or it may be done to remove extra and irrelevant information that will lead to less complex separations [75]. In feature extraction, all variables are used to transfer data (conversational or nonlinear) to the feature space with smaller dimensions. Therefore, the goal is to replace the original data with less variable data [76]. Feature extraction can be done for several reasons.

- To reduce the bandwidth of the input data (which leads to improved speed).
- To provide a suitable set of features for a separator (which leads to improved classifier performance, especially for simpler separators).
- To reduce duplicate information.
- To find new meaningful features that describe the data (which leads to a better understanding of the data production process).
- For displaying data in smaller dimensions (ideally, in two dimensions) with the least loss of information (where the data is better seen and the relationships and structures in the data can be better identified) [77].

After preprocessing the cardiac signals, there is a feature extraction step from these signals. This step is one of the most important and challenging steps of a pattern recognition and recognition system. Be entropy is a family of signal processing tools that is capable of producing unique signal properties.

Entropy

Entropy in information theory is a numerical measure of the amount of information or randomness of a random variable. To put it more precisely, the entropy of a random variable is the mathematical expectation of the amount of information obtained from its observation. In simpler terms, the higher the entropy of a random variable, the greater the ambiguity about that random variable. Therefore, by observing the definite result of that random variable, more information is obtained. Naturally, there is an expectation from any function suitable for measuring the amount of information in an observation, including that the information obtained from an observation is a negative value. The information obtained from observing a definite event (i.e., with a probability of one) is zero, and most importantly, the information obtained from observing each of them is clear. It can be shown that the only function that implements the above three properties is the negative function of the logarithm of probability. In general, in engineering sciences, entropy is a measure of the degree of ambiguity or disorder [78]. Entropy is defined as Eq. (1).

$$H(x) = E[I(x)] = E[-\log(P(x))] \quad (1)$$

In this equation, H is entropy of random variable x, E is mathematical expectation, and P(x) is probability density function.

Approximate entropy

The approximate entropy ApEN similar epochs in a time series such as data related to biological signals. The more repetitive patterns the time series, such as biological signals, have the lower the approximate entropy ApEN. On the other hand, the more predictable the patterns, the higher the ApEN value. So ApEN will measure the ability to not predict changes in a range and different beats. ApEN will be calculated based on Eq. 2.

$$\text{ApEN}(d, R, L) = \frac{1}{N - d + 1} \sum_{i=1}^{L-d+1} \log C_i^d(R) - \frac{1}{L - d} \sum_{i=1}^{L-d+1} \log C_i^{d+1}(R) \quad (2)$$

$$C_i^d = \frac{1}{L - d + 1} \sum_{i,j=1}^{L-d+1} \phi(R - x_i - x_j) \quad (3)$$

In the above equation, d is the placement dimension, R is the similarity criterion, L is the data wavelength, ϕ is the step function.

Sample entropy

Sample entropy is a standard measure that works similar to approximate entropy, except that it measures the complexity of the signal. Larger entropy values of the *SamEn* sample indicate a lower regularity in the time series, and vice versa

$$s(d, R, L) = -\ln \left[\phi'^d(R)/\phi'^{d+1}(R) \right] \quad (4)$$

$$\phi'^m(R) = (L - d + 1) \sum_{i=1}^{L-d+1} A_i'(R) \quad (5)$$

In the above equation, d is placement dimensions, R is the criterion of similarity. As in ApEN, it will be used in SamEN. Studies have shown that the SamEN and ApEN entropy criteria are good tools for understanding the dynamics and physiology of brain systems and therefore will be used in this study [79].

Recurrence period density entropy

Recurrence period density entropy RPDE return period is a useful criterion for describing a range that repeats a series of identical sequences. It is therefore similar to the linear correlation criterion except that RPDE measures repetition in the system phase space instead of the time domain, resulting in a more reliable measure based on the dynamics of the underlying system that produces the signal. Is, offers.

The basic premise is that biological signals consist of a definite (nonlinear) component and a random component, and this method attempts to explain the random component. This measurement criterion is based on the concept of recursive method, which can be considered as a generalization of periodicity. Based on the analysis of the time index difference $d(i) = n_{i+1} - n_i$, between points in a reconstructed fuzzy space, it is possible to detect the behavior of fundamental dynamics. Considering periodicity as the simplest type of chaotic behavior as the most complex, entropy (H) is a period density function f(d) as a measure of the degree of complexity.

$$H = - \sum_{d=1}^N f(d) \ln f(d) \quad (6)$$

where $f(d)$ is created by normalizing the $d(i)$ series histogram.

In order to calculate $f(d)$, first the histogram function $d(i)$ is calculated and then normalized. The normalized histogram function is called the period density function. When the entropy is zero, it represents only a nonzero value of $f(d)$ of a periodic circuit. An increase in H is an increase in the various periods d shown along the path, or equivalently, the noise caused by random changes in the values of $d(i)$. For an incremental combination of definite dynamics with correlated noise, noise decreases the gain of $f(d)$ function peaks by increasing variance [80].

Permutation entropy

Permutation entropy is the general order structure of a time series that provides a measure of the quantitative complexity of a dynamic time series [81]. The calculation of the permutation entropy depends very much on the choice of m. The permutation entropy is presented by Bandt and Pompe [82]. To improve it, they have used symbolization methods. Suppose that a time series x exists such that

$$X = \{x_1, x_2, \dots, x_N\} \quad (7)$$

The embedding process will be used to generate a number of $N - (m - 1)L$ vectors called $X_{N-(m-1)L}, \dots, X_2, X_1$. Each X_t will be defined as Eq. (8)

$$X_t = [x_t, x_{t+\tau}, \dots, x_{t+(m-1)L}] \quad (8)$$

In Eq. (8), m has an embedded dimension or an embedded dimension that has a delay of L . The X_t vector can be arranged ascending or descending. If X_t is sorted in ascending order, Eq. (9) will be created.

$$x_{t+(j_1-1)L} \leq x_{t+(j_2-1)L} \leq \dots \leq x_{t+(j_m-1)L} \quad (9)$$

We can now calculate the order event of the π_i pattern, which we denote by $C(\pi_i)$. can be defined:

$$p(\pi) = \frac{C(\pi)}{(N - (m - 1)L)} \quad (10)$$

$$PE = - \sum_{m=1}^{m!} p(\pi) \ln p(\pi) \quad (11)$$

The largest value of permutation entropy (PE) will be the value of $\log(m!)$ which means that this time series is completely random. The minimum PE value will also be zero, indicating that the time series is well-defined and regular. The permutation entropy represents the local order structure of a time series. As a result, it shows the complexity of a dynamic signal or time series. The calculation of permutation entropy is highly dependent on the determination of m . If m is too small (e.g., less than 3), this scheme may not work properly because there may be only a small number of specified cases for EEG recording. On the other hand, larger values of m are very important for determining the obvious differences between a completely random and definite dynamic state. A condition must be met for any possible order pattern to be usable, or in other words any possible order pattern of embedding dimensions m in the signal of length N . Equations (12) and (13)

$$m! < N - (m - 1)L \quad (12)$$

$$N \gg m! + (m - 1)L \quad (13)$$

As a result, the value of m should be chosen in such a way as to avoid down-sampling. So it seems that $N \gg m! + (m - 1)L$. In [84], the selection condition m is defined in such a way that low sampling is avoided and the changes made in the desired signal can be measured based on it.

Shannon entropy

Shannon entropy indicates uncertainty in the random process or random values. The value of ShEn is defined as follows in Eq. 14:

$$\text{ShEn}(X) = - \sum_i P_i \log P_i \quad (14)$$

In this relation, P_i is the probability of any possible value of X occurring [83].

Statistical features

Extracting the frequency band from a motion signal limits the frequency range, but does not change the volume and length of the data. However, according to the sparse display, the data volume wavelet transform is reduced (although not significantly). Therefore, it is necessary to extract a set of features from each frequency sub-band as a representative. Properties should be selected in such a way that both their calculation is appropriate in terms of computational volume, and they make a significant difference for a multi-class problem [84].

For this purpose, a set of statistical, temporal, and frequency characteristics that are very important and common in signal processing were used, which are as follows:

1. Frequency average, 2. Medium frequency, 3. High-to-low frequency ratio, 4. Absolute average of data, 5. The absolute mean slope of the data, 6. Average spectral range, 7. The middle of the spectral range, 8. Modified absolute mean of data, 9. Modified absolute mean of 2 data, 10. Window length, 11. of Lyapunov exponent.

Classification

In processes, a classifier structure is used to provide an automated algorithm for classifying the classes of a problem, which are based on a set of mathematical or linguistic rules. The extracted properties are used as the input of a classifier structure, and the output of this structure is the class label given to each of the properties. In machine-based methods, neural network-based methods have received more attention. This attention has grown due to advances in the hardware industry [85]. Therefore, in this study, the structure of neural networks will be examined to predict human activity. Neural network-based models in predicting human activity are categorized as follows.

1. Multilayer feedforward neural networks MLFNN
2. Convolutional neural networks CNN
3. Radial base neural networks RBFNN
4. Wavelet neural networks WNN
5. Recurrent neural networks RNN and long short-term memory LSTM
6. Fuzzy neural networks FNN

In the following, these networks will be briefly examined.

Table 1 Neural network terms

Expertion	Definition and description
Training	The process of setting model parameters to minimize the cost function in a database is called training. In the neural network, the training process is called adjusting the weights of the neural network
Testing	The process of evaluating the model is taught in the relevant database. Regulatory training is the process of training an algorithm in machine learning that has a database output. In other words, it has a label
Unsupervised learning	The training process of a machine learning algorithm with unlabeled data is called unsupervised training
Feedforward neural network	A neural network in which information changes in only one direction from the input layers to the output layer
Backward forward neural network	A regulatory training and learning process optimizing the minimum gradient in neural network training. At each training step, an error or difference between the output and the target values is obtained, and the weights are updated from the output layer to the input layer. This process will continue until the error is reduced to the minimum desired value
Fine-tuning	The process of fine-tuning the parameters of a neural network model in order to achieve a better result

Definition of neural network terms

The terms used in neural networks to predict activity are shown in Table 1.

Multilayer feedforward neural networks

The MLFNN method is a reliable method for predicting human activity. However, the output of the neural network may not be the desired value in the prediction, in which case evolutionary algorithms are used. Another solution is to increase the number of layers of forward feeding neural network. In this case, a deep structure is created. In the MLFNN network, there is an input layer, an output layer, and finally one or more hidden layers. Each layer in this network has a number of neurons, also called units. These neurons are connected by weighted links. These links and weights transfer information from one layer to another. MLFNN is perhaps the most common type of neural network used by many machine learning users. MLFNN can estimate the function of nonlinear functions. In order to train this neural network, backward propagation is one of the effective training methods. The neural networks that use this method are called BPNNs. If there are more than two hidden layers, this network can be called a deep network [86]. Figures 8 and 9 show these two structures.

Radial base neural networks

These networks (RBFNN) have three layers, including an input layer, an output layer, and a hidden layer that use Radial basis function RBF as activity functions. RBFs are

Fig. 8 Three-layer perceptron neural network [86]

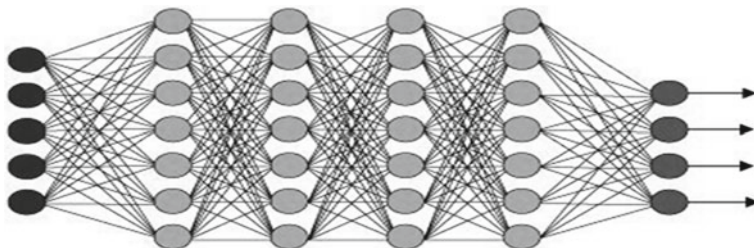
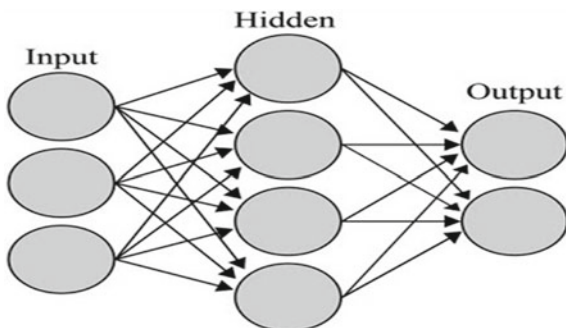


Fig. 9 Deep perceptron neural network [87]

functions with real values that output based on a type of distance, such as Euclidean, express from a center or input. Among RBFs, the Gaussian function is the most widely used. There are usually two steps to training RBFNNs.

1. Non-supervised Training 2. Supervised Training

In the first step, the input values are the parameters of the radial functions, including the center and the radius or bandwidth (standard deviation), which are performed separately for each neuron in the hidden layer. This step can be done non-supervised like clustering methods so that the input samples belong to different clusters. The number of clusters is a design parameter and is determined by the number of neurons in the hidden layer [88]. By performing clustering, cluster centers are calculated based on the distance between the samples and the centers themselves.

In supervised learning, the weight of the hidden layers and the output layers are obtained using the hidden layer outputs and the resulting outputs. The training in RBFNN is done using a linear model considering a goal function such as least squares. Because the generalizability and learning speed of these networks are high, they are used in many studies that do time series prediction. One of the most common radial base networks of RBFNN is the General regression neural network GRNNs that make predictions based on mathematical statistics. Figure 10 shows an RBFNN neural network [89].

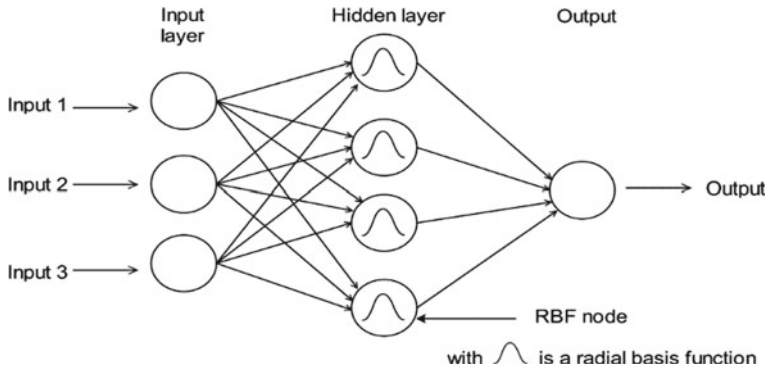


Fig. 10 RBFNN neural network [89]

Wavelet neural networks

A Wavelet Neural Network (WNN) is a combination of wavelet theory and an ANN. These networks are essentially an MLFNN neural network that uses a wavelet function instead of the usual activity functions such as sigmoid. A wavelet function is a function that has a mean of zero. Zero mean indicates that signal evaluation is performed in two modes of time and frequency [90]. Figure 11 shows the structure of a WNN. The advantages of this model include the ability to analyze multiple comparisons and the ability to learn NN tutorial in approximating the weight of complex patterns. WNNs have shown good results in predicting time series. WNNs, like RBFNNs, are more generalizable than MLFNNs. Also, setting WNN parameters is easier and more convenient than MLFNN and RBFNN [91].

Time-Delayed Neural Networks TDNN

TDNN neural networks are similar to a multilayer neural network, except that delayed or shifted input layers make such neural networks more successful in modeling and recognizing dynamic temporal states. An example of a neural network is shown in

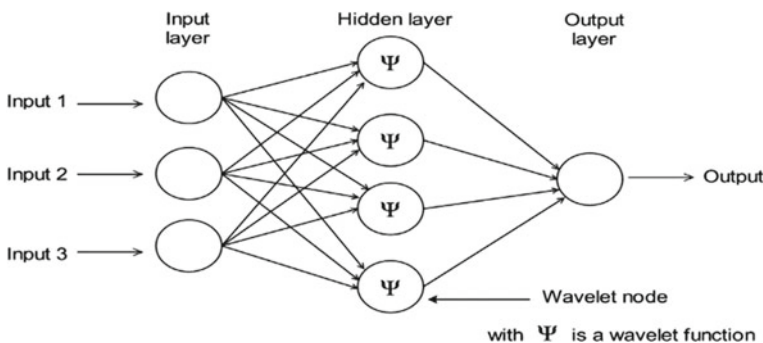


Fig. 11 Structure of a WNN [90]

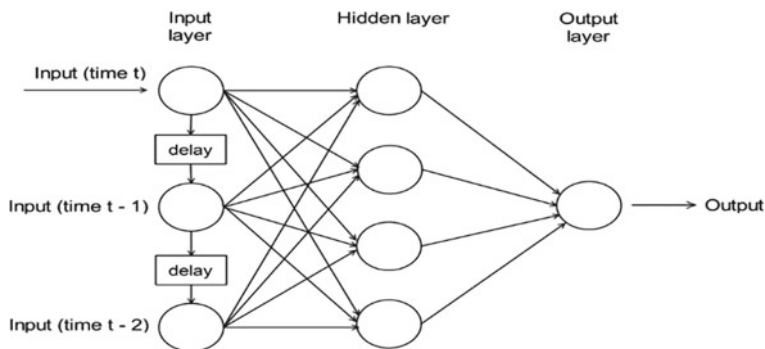


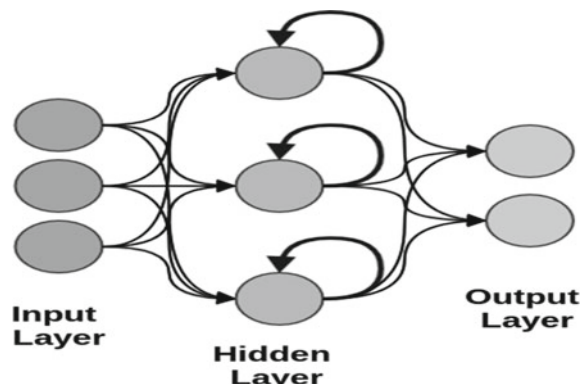
Fig. 12 TDNN neural networks

Fig. 12. Hidden layer neurons receive input values at time t with a delay of $t - 1$ or t . This delay can be applied to other layers as well. When a delay is applied to neurons in subsequent layers, the TDNN uses the input states or the output generated in the previous states. In this case, the model includes feedback connections and can be considered as RNN, but in general, TDNN can be considered as a specific RNN mode. TDNN can be used to show the correlation between past and future values in a forward feeding model. The delay in TDNN in the training process is estimated. Therefore, TDNN has less adjustment parameter than RNN [92].

Recurrent neural networks

Recursive neural networks are widely used in RNN time series. Compared to FFNN forward neural networks, there is a connection from the output or from the power supply to the input (previous step). Figure 13 shows this structure. In the most common type of RNN, the network output is connected to the input. This feedback can be considered as memory [93].

Fig. 13 Recurrent neural networks [93]



Long short-term memory

RNN networks cannot handle long-term dependencies properly. To overcome this weakness, LSTM is introduced. This model uses a gateway mechanism that determines how and even when to upgrade memory. An LSTM network typically consists of a cell, an inlet valve, and an outlet valve. The cell represents memory, the input hatch represents new information that can be stored in memory and indicates the information that needs to be erased from memory. Finally, the output port shows how memory is used in the LSTM output [94] (Fig. 14).

MIT-BIT Dataset

The MIT-BIH dataset contains information on 18 patients (15 males and 3 females). They range in age from 17 to 82 years. These figures were obtained straight from the hospitals. The Holter device is used to determine the ratio of such signals. The sample rate is set at 256 Hz. The parameters for this database are shown in Table 2 [96]. Table 2 shows the specifications of this database [96].

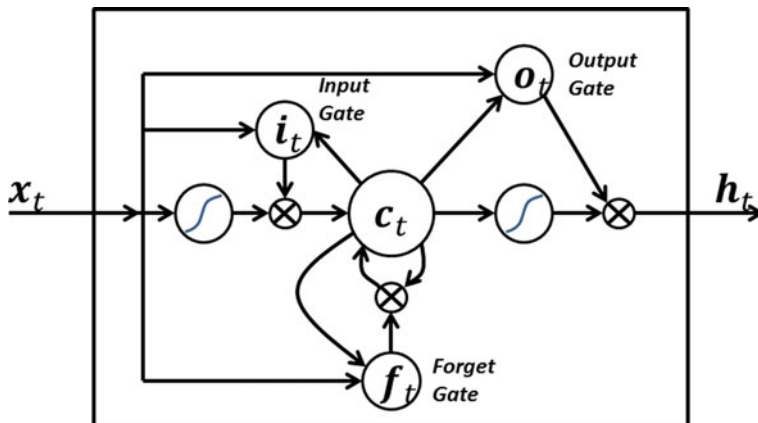


Fig. 14 Long short-term memory [95]

Table 2 MIT-BIH database specifications

Type of arrhythmia	Class MIT-BIH	Beam MIT-BIH
Natural (N)	N-L-R-e-j	Normal beat LBBB RBBB Atrial escape beat
Supraventricular ectopic beat (SVBE)		Nodal premature
Ventricular ectopic beat (VEB)	a-J-s-V	Nodal
Fusion beat (F)	E-F-P-f-U	Fusion
Unknown beat (Q)		

GTC Database

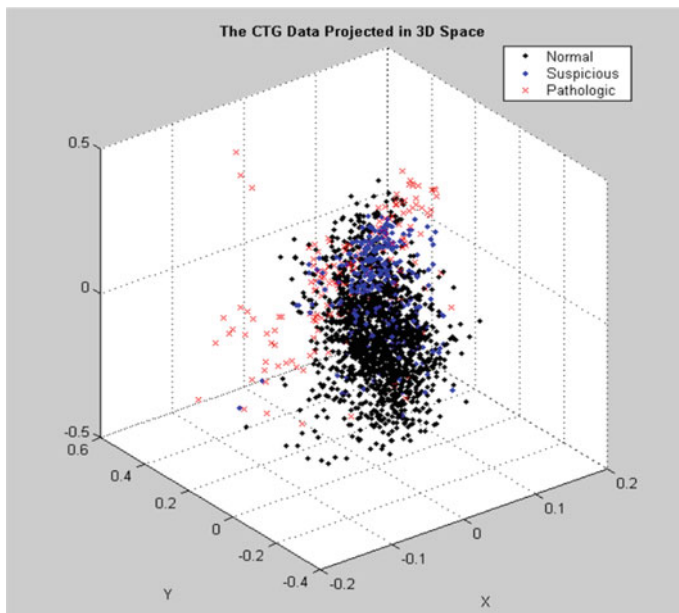
The CTG database contains 23 features and has 2126 registered items. All features are numerical and data classification will be classified into three modes: normal, suspicious, and pathological. This database includes fetal heart rate (FHR) and uterine contractions (UC) on these data. These modes are used to assess the health of the fetus during pregnancy as well as at birth. These features are shown in Table 3. Table 4 shows the description of the classification modes. Figure 15 shows the three-dimensional distribution of CTG data with feature modes. This figure shows the natural CTG data in black, the suspicious data in red, and the pathology data in green. The 3D display of this data can be seen on the mentioned site. In this figure, the red color of the pathology data, the black color of the suspicious data, and the blue color of the normal data.

Table 3 Information about the desired features

Number	Abbreviation	Description
1	LB-FHR	Baseline (beats per minute)
2	AC-#	# of accelerations per second
3	FM-#	# of fetal movements per second
4	VC-#	# of uterine contractions per second
5	DL-#	# of light decelerations per second
6	DS-#	# of severe decelerations per second
7	DP-#	# of prolonged decelerations per second
8	ASTV	Percentage of time with abnormal short-term variability
9	MSTV	Mean value of short-term variability
10	ALTV	Percentage of time with abnormal long-term variability
11	MLTV	Mean value of long-term variability
12	Width	Width of FHR histogram
13	Min	Minimum of FHR histogram
14	Max	Maximum of FHR histogram
15	Nmax-#	# of histogram peaks
16	NZreo-#	# of histogram zeros
17	Mode	Histogram mode
18	Median	Histogram mean
19	Mean	Histogram median
20	Variance	Histogram variance
21	Tendency	Histogram tendency
22	CLASS-FGR	Pattern class code (1 to 10)
23	NSP	Fetal state class code (Normal = 1; Suspect = 2; Pathologic = 3)

Table 4 Explanation of classification scenarios

Class information	Description
N	All selected features are normal
S	All selected features are in unreliable mode, and other unselected features are in unreliable mode
P	Selected attributes are in two or more unreliable states and at least 2 or more attributes are in unreliable states

**Fig. 15** Three-dimensional distribution of CTG data

Heart diseases database

The database contains 303 cases of heart disease at the University Hospital of Zurich, Switzerland. There are 75 attributes in this database. This database is one of the standard databases for diagnosing heart disease.

Kosar Database

Also, for further evaluation, the proposed method was simulated on a dataset collected from individuals who underwent coronary angiography in Kosar Hospital in Shiraz in September 2013. In this database, 152 of these people were randomly selected and a questionnaire containing demographic information of the disease, diagnostic tests, and angiographic results in the file was completed for them. In this database, 13 diagnostic factors for this disease were considered, which were divided into two

categories: continuous and discrete. This is done after consulting with specialist doctors. Continuous variables include age (100/year), creatinine (10/n), total cholesterol (1000/n), triglycerides (1000/n), discharge fraction (100/n). Discrete variables include gender (female = 1, male = 0), smoking (yes = 1, no = 0), history of high blood pressure = 1, no = 0), history of diabetes = 1, no = 0), family history of heart disease = 1, no = 0), history of heart attack, no = .), exercise test result (normal, abnormal = 1), and echo result (normal, abnormal = 1) (Ayat 2017a). Table 5 summarizes these variables or input properties [97].

Evaluation criteria

For evaluation of the classification method, after a proper preprocessing of the data, feature extraction and selection, the selected features are then used to classify the types of classifiers. Finally, it will be analyzed using a variety of evaluation criteria. The three criteria for evaluating accuracy, sensitivity, and precision [98], which are introduced to measure the accuracy in diagnosing the performance of the proposed system, are calculated according to Eqs. 15–17 and will be used to evaluate the system [99].

$$\text{Precision} = \frac{N_{\text{TP}}}{N_{\text{TP}} + N_{\text{FP}}} \quad (15)$$

$$\text{Sensitivity} = \frac{N_{\text{TP}}}{N_{\text{TP}} + N_{\text{FN}}} \quad (16)$$

Table 5 Kosar database specifications

Feature	Type of feature		Value
	Continue	Discrete	
Age (100/year)	■		(100 / year)
Creatine	■		(10 / number)
Total cholesterol	■		(1000 / number)
triglyceride	■		(1000 / number)
Drainage deduction	■		(100 / number)
Gender		■	(Female = 1, male = 0)
Being a smoker		■	(Yes = 1, No = 0)
History of high blood pressure		■	(Yes = 1, No = 0)
History of diabetes		■	(Yes = 1, No = 0)
Family history of heart disease		■	(Yes = 1, No = 0)
Has a history of heart attack		■	(Yes = 1, No = 0)
Test result		■	(Normal = 0, abnormal = 1)
Echo result		■	(Normal = 0, abnormal = 1)

$$\text{Accuracy} = \frac{N_{\text{TP}} + N_{\text{TN}}}{N_{\text{TP}} + N_{\text{FP}} + N_{\text{TN}} + N_{\text{FN}}} \quad (17)$$

N_{TP} is number of true positive, N_{FP} is false positive, N_{TN} is true negative, N_{FN} is false negative.

4 Literature Review

So far, different algorithms have been proposed to classify cardiac arrhythmias and diagnose fetal disease from cardiotocographic data. Some of these studies will be reviewed later.

Heart disease literature review

A group of proposed algorithms operate in the time domain. The problem with these algorithms is that they use the ECG signal itself without extracting features from it to classify cardiac arrhythmias. This results in high time costs and moderate accuracy of these methods. Given the above, it can be concluded that feature extraction from the ECG signal is an important step in the classification of cardiac arrhythmias.

Various methods are used to extract features from the ECG signal. These include discrete Fourier transform DFT [100], discrete cosine transformation DCT [101], higher-order statistical methods such as second-, third-, and fourth-order moments [102]. Discrete wavelet transform is also used in various researches to extract features from ECG signal. Wavelet transform is a useful technique for analyzing signal frequency time. Wavelet transform can accurately estimate rapid signal changes.

In [103], three classifications of neural networks, decision trees, and Naive Bayes have been used in the diagnosis and prediction of heart disease. In this study, in addition to ECG signals, clinical features such as gender, age, blood pressure, and blood sugar have been used. In other words, in addition to the features of T.S.R.Q.P in the cardiac signal, clinical information has also been used in the diagnosis of cardiac arrhythmia. Although the combination of these features has been able to improve identification accuracy by up to 96%, it sometimes seems that clinical data may not be available to improve classification performance.

In [104], support vector machine classification and frequency domain characteristics have been used to diagnose cardiomyopathy and cardiovascular disease. In other words, three normal (healthy) states and these two diseases have been diagnosed with the help of frequency domain characteristics. The software used is Tangara, and the section validation method has been used for evaluation. The accuracy of the method used is 94%.

In [105] noted that it is the cause of death from heart disease and has designed a remote ECG recording system to reduce the rate of death due to heart disease, which aims to detect cardiac arrhythmias early. In the designed system, ECG data are classified using decision tree (DT) and random forest (RF). The designed system can serve up to sixty patients simultaneously. The accuracy of diagnosing the disease

in the decision tree classification is 97% and in the random forest is about 99%. Although the accuracy of the proposed method is high and the ability to provide services to sixty people at the same time, the design and use of this device are very difficult due to the high computational complexity.

In [106], neural networks have been used as a classifier to classify and identify cardiac arteries. In order to reduce the effect of the above training, the reduced dimension of the extracted features has been used in the proposed method. The proposed method is simulated on the MIT database and 97% accuracy is obtained. The proposed method does not seem to be particularly innovative and uses only a neural network to classify the data.

In [107] to extract, the heartbeat feature has its own characteristics. The extracted features are classified using support vector machine (SVM) classifier and ANN. The accuracy of the proposed method is reported to be 90%, but a comprehensive model for diagnosing arrhythmias cannot be presented and found in research.

[97] has suggested the early diagnosis of coronary heart disease using modern methods of artificial intelligence. In the present study, angiographic results are classified into two categories: normal and abnormal using artificial intelligence methods. The proposed method was simulated on a dataset of 152 patients undergoing coronary angiography using a combination of neural-fuzzy network and genetic algorithm. In the implementation, 85% of the data were used for neural-fuzzy network training and the remaining 15% for the test phase. The use of genetic algorithms has been used to improve the neural-fuzzy network training process. This improved the speed of this simulation. Also, the high index obtained confirms the proper functioning of the proposed system in the classification and diagnosis of people with coronary heart disease.

In [108], the hidden Markov and spark model in ECG signal analysis is presented. In the proposed method, the HHM hidden Markov model is combined with the Apache spark to increase the speed of signal analysis. Although the speed of signal processing for the classification and diagnosis of cardiac arrhythmias has increased, the low accuracy of the proposed 79% method makes it difficult to apply scientifically.

In [109], a deep DNN neural network with an in-depth training algorithm is proposed to classify the features extracted from ECG signals. Although in the case of healthy and diseased two classes, where the type of disease has not been determined, 99% of the identification accuracy has been obtained, because it is a two-class classification, it cannot identify other cardiac arteries.

[110] used Apache spark features to detect cardiac arrhythmias. The main challenge in diagnosing cardiac arrhythmias is the irregularities in the ECG signal, which is very important for diagnosing the condition. In this study, the Spark Scala tool was used to extract features and classifications that were designed to identify artemia. The extracted features were classified using a random forest classifier and a decision tree, with 97% accuracy for the random forest (RF) classifier and 98% for the decision tree. In this study, ready-made tools have been used to determine the type of cardiac arrhythmia in which no particular innovation is seen.

In [111], a new intelligent online method for the diagnosis of cardiac artemia is presented. The proposed method includes preprocessing steps of feature extraction

and classification. The middle filter is used to remove the noise, and then the PQRT and S waves are extracted above the values of each wave. Is. Different diseases and different arrhythmias have been identified in six classes with 96% accuracy. Although the proposed method claims to have a high speed, the speed of this method can be improved by selecting a feature.

In [112], artificial neural networks have been used to diagnose three types of cardiac artemia, lung disease, and liver disease. The neural network used is a multi-layer perceptron network with a training algorithm for forward feeding and then error propagation, as a result of which patient and healthy diagnosis are separated and identified. Identification of heart patients in three diseases, liver in 4 cases and in lung patients in two cases of diagnosis and diagnosis has been done that the accuracy of the presented method is 96%. It should be noted that the neural network designed to diagnose heart patients used ECGs and pulmonary and liver patients used CT images. Features of the fast Fourier transform frequency domain were used to extract the feature.

Reference [113] used the spectrum obtained by Fourier transform short-term STFT along with convolutional neural networks to investigate the classification of cardiac arrhythmias. In the method presented in this research, the ECG time signal in five heart beam modes called normal and normal beat NOR, left beat black beat and LBBB right band black band RBBB, PVC, and APC are transmitted to the spectral domain by Fourier transform of STFT short version. Then, five types of arrhythmias in a 2D-CNN 2D cannulation neural network are distinguished by these features. 99% has been reported for the proposed method, but until this desired accuracy is achieved, several parameters such as the type of window used in STFT, the number of pool layers in CNN, and the dimensions of the convolution filter in clinical CNN should be adjusted correctly. These settings make it difficult to use this method in practice.

Reference [114] proposed a non-regulatory method for detecting cardiac arrhythmias in a 12-channel ECG signal based on tensor wavelet transform and 2D Gaussian spectral clustering (high dimensions of ECG data and signals and large number of variables are among the challenges of ECG signal classification). In this research, to overcome this challenge, discrete wavelet transform has been used to obtain a tensor wavelet. Two-dimensional Gaussian is used. The accuracy of the proposed method is 96%, which in comparison with the heavy processing cost required, does not seem to be a good number.

Reference [115] used the DEA differential evolutionary algorithm to optimize the weights of traditional ELM and showed the improvement of ELM in the arrhythmia classification using cardiac signals. Feature extraction was performed by discrete wavelet transform in PR period, QT period, ST period, and QRs wave. These features are then entered into the ELM, and the number of hidden layer neurons as well as the number of hidden layers are optimized using the DEA algorithm. The accuracy of the proposed method is reported to be 97.5%. Although the optimization performed on the ELM was optimally performed by an evolutionary algorithm, it seems that the extractor did not provide a suitable feature for detecting cardiac arrhythmias,

and using the appropriate feature extractors, the accuracy of the best numbers can be achieved.

In [96], cardiac artemia has also been diagnosed as a structural event based on statistical moments and the matrix. In the proposed method, the combination of statistical moments as morphological features and matrix properties of all structural events along with the features extracted from discrete Fourier transform has been able to provide a high accuracy of 96% in the diagnosis of cardiac artemia. While each of the extracted features alone hardly has 90% detection accuracy. The proposed combination, which is a linear combination, has been able to provide good accuracy. However, the length of the feature vector for each patient is large enough for the overfitting phenomenon to occur. It seems that using feature selection methods can improve accuracy and even prevent the phenomenon of over-training.

Reference [116] provide a method for identifying and classifying heart disease data. In the proposed method, they improve the PSO particle swarm optimization algorithm and then classify it with possible classifications including generalized trees, multilayer neural networks, support vector machines, and possible neural networks. Feature selection in the proposed method is non-supervisory, but to show the superiority of the proposed method, which was basically based on improving the performance of PSO, it was also compared with the selection of the principal component analysis (PCA) feature. Although the results show the superiority of the proposed method, it seems that the number of parameters to be adjusted in the improved PSO algorithm must be changed a lot to achieve good efficiency.

In [117] both in feature extraction and in feature selection, the combination of classifiers in cardiac base classification has been used to diagnose the disease. The main theory of this paper is based on the idea that suitable features for each class are interconnected and must be extracted from the data by a combination of feature extractors. SVM is also used in combining output classifications. In the proposed method, features are extracted by the combination that has the highest correlation with the SVM classifier that is used in combination. The results of the proposed method in comparison with the single feature extractor mode and the single feature selector show the superiority of the combined mode. But the volume of calculations has increased dramatically.

In [118], deep group neural networks have used clinical data to predict and diagnose heart disease. In the proposed method, although the volume of processes has increased relatively, the sensitivity of the calculations as well as the results of the correlation table show the superiority of this method)

In [119], convolutional features are used for classification and it is also compared with nonlinear features. In this study, it has been proven that if nonlinear features are combined with convolutional features, the accuracy and sensitivity efficiency will increase significantly. The results also show that the nonlinear property of the sample entropy and the fractal estimated from the signal have been able to show better results. The proposed system in which the three-class mode was investigated and the sensitivity obtained for this case was a figure equivalent to 87%, which was more in line with reality.

For further evaluation and comparison of the presented methods, all the researches presented in Table 6 are compared.

In the presented researches, machine-based methods have been used in the diagnosis of heart diseases and arrhythmias. Frequency domain characteristics and location domain characteristics were extracted, and then the type of arrhythmia was diagnosed and identified using a classifier. However, the low accuracy of some methods and at the same time in others low speed has caused the need for fast methods and of course with high accuracy. In this research, entropy-based features will be used to improve accuracy, and feature-based selection methods will be used to improve classification and identification speed [120, 121]. Feature-based methods: In addition to reduce the dimension in the feature matrix, it will select the features that have the greatest impact on detection.

Fetal Heart disease literature review

Reference [122] have proposed a new method for diagnosing fetal health based on the multi-objective genetic algorithm optimization method. This method, called multi-objective genetic algorithm MOGA, selects the most efficient features using the proposed algorithm and classifies them with the help of support vector machine classifications, random forest as well as neural network. Although the results are acceptable, the diagnosis of fetal health has been made only in healthy and sick cases. Also, in case of suspicion, the investigation has not been carried out.

Reference [123] have presented a method of identifying and classifying fetal disease. In the proposed method, they improve the PSO particle swarm optimization algorithm and then classify it with possible classifications including generalized trees, multilayer neural networks, and support vector machines and possible neural networks. Feature selection in the proposed method is non-supervisory, but to show the superiority of the proposed method, which was basically based on improving the performance of PSO, it was also compared with the selection of the principal component analysis (PCA) feature. Although the results show the superiority of the proposed method, it seems that the number of parameters to be adjusted in the improved PSO algorithm must be changed a lot to achieve good efficiency.

In [124] both in feature extraction and in feature selection, the combination of classifiers has been used. The main theory of this paper is based on the idea that suitable features for each class are interconnected and must be extracted from the data by a combination of feature extractors. SVM is also used in combining output classifications. In the proposed method, features are extracted by the combination that has the highest correlation with the SVM classifier that is used in combination. The results of the proposed method in comparison with the single feature extractor mode and the single feature selector show the superiority of the combined mode. But the volume of calculations has increased dramatically.

In [99], deep ensemble neural networks have used FHR signals to predict and identify the fetus. In the proposed method, although the volume of processes has increased relatively, the sensitivity of the calculations as well as the results of the correlation table show the superiority of this method.

Table 6 Comparison of literature review in Heart disease

No	Researcher	Proposed method	Demerit	Merit
1	Palaniappan and Awang [103]	Use a combination of classifications, a combination of clinical data, and an ECG signal	Low speed, unavailability of clinical data for data mining	High accuracy, combination of clinical data and signal in diagnosis
2	Rajkumar [104]	Support vector machine classification and frequency domain characteristics for the diagnosis of cardiomyopathy and cardiovascular disease	Low accuracy	
3	Ma'Sum [105]	Design of a remote ECG recording system designed to detect early cardiac arrhythmias using decision tree (DT) and random forest (RF)	High complexity, unusability in practice	High detection speed, simplicity of the proposed method
4	Li et al. [107]	Extract heartbeat feature and classification with support vector machine (SVM) and ANN classification neural network		
5	Ayat et al. [97]	Combination of neural fuzzy network and genetic algorithm	Low accuracy, lack of a model for identifying arrhythmias in other data in other people	High accuracy, good speed
6	Celesti et al. [109]	Use of DNN deep neural network with in-depth training algorithm to classify features extracted from ECG signals	Lack of diagnosis of arrhythmia, classified into healthy and sick	High detection speed
7	Lassoued and Ketata [106]	Classification and identification of cardiac arrhythmias using neural networks as classifiers to reduce the effect of higher education	Lack of diagnosis of arrhythmia, classified into healthy and sick	High detection speed

(continued)

Table 6 (continued)

No	Researcher	Proposed method	Demerit	Merit
8	Brien et al. [108]	Provide Markov and spark concealed model in ECG signal analysis and combination with Apache spark	Low speed	Proper identification accuracy
9	Alarsan and Younes [110]	Use the Apache spark feature to detect cardiac arrhythmias	Very low accuracy, so that practical use has become impossible	High detection speed
10	Khan et al. [111]	Provide a method with morphological features and discrete wavelet transform, backup vector machine classifier	Low speed, computational complexity	Proper identification accuracy
11	Nayeem et al. [112]	Using a multilayer neural network with a pre-procedure and post-fault propagation training algorithm	Computational complexity	Excellent detection accuracy, high speed
12	Huang et al. [113]	Use of the spectrum obtained by Fourier transform short-time STFT along with convolutional neural networks	Low diagnostic accuracy, over-training occurs in the neural network	
13	He et al. [114]	Presentation of a non-regulatory method in the diagnosis of cardiac arrhythmia in a 12-channel ECG signal based on tensor wavelet transform and 2D Gaussian spectral clustering	High number of regulatory parameters to detect the type of arrhythmia	High accuracy
14	Diker et al. [115]	Use of DEA Differential Evolution Algorithm to Optimize Traditional ELM Ultimate Learning Machine Weights	High computational complexity	High accuracy

(continued)

Table 6 (continued)

No	Researcher	Proposed method	Demerit	Merit
15	Nascimento [96]	Diagnosis of cardiac artemia based on a combination of statistical moments and matrix is also a structural event	Lack of extractor providing a suitable feature for identification, low speed	Improve the speed of signal analysis, increase the speed of detection

In [125], this possibility is provided by using techniques based on machine learning to enable the existence of any pathological disorder in the fetus. In this study, information was collected from the UCI dataset for 2126 people. These data consist of 21 features and have reached a sensitivity of more than 99% for two-class analysis without using the feature selection technique. They removed data suspected of pathological risk from the dataset, resulting in two-class analysis. They have also used several popular classifiers such as neural networks, k-nearest neighborhood, support vector machine, and some unsupervised methods to separate outputs.

In [126] using a combination of machine learning methods, they suggested identifying disease status or fetal health. Combined methods were a set of techniques including decision trees, support vector machines, neural networks, neural networks, and incremental gradients.

In [127], the base linear functions are used to estimate the condition of the fetus. These functions show better results compared to nonlinear properties as well as fractal properties. Nonlinear properties and their chronological order have also been investigated using signal analysis as well as size. The results showed that non-interconnected and nonlinear functions and fractals as well as main lines provide the best information for classification.

In [128], the feature extraction technique based on the combined Keymin's method as well as the support vector machine classifier reached a sensitivity of 90%, which apparently the classes were examined as one against all.

Reference [129] which categorized the data through the decision tree and was able to achieve a sensitivity of 95%. Of course, the amount of information processed in this area has increased over time due to the high volume of features. Data is retrieved from the UCI dataset.

In [130], the spectral power of the ability to change the FHR in relation to fetal blood pH has been used. Normalized spectral power as well as the amount and magnitude of spectral power were measured in low-frequency as well as high-frequency bands. The results showed that the normalized low frequencies as well as the normalized high frequencies are very efficient for comparing and calculating the pH of fetal scalp blood.

Reference [131] used techniques such as particle swarm optimization method used of feature selection.

In [132], convolutional features are used for classification and it is also compared with nonlinear features. In this study, it has been proven that if nonlinear features

are combined with convolutional features, the accuracy and sensitivity efficiency will increase significantly. The results also show that the nonlinear property of the sample entropy and the fractal estimated from the signal have been able to show better results. The proposed system in which the three-class mode was investigated, and the sensitivity obtained for this case was a figure equivalent to 70%, which was more in line with reality.

In [133] fuzzy systems and neural networks, they attempted to build an algorithm whose final sensitivity of their work is equal to 96%, which, of course, must be determined. This method is like one against all or classification of all is equal to all or multi-class mode to detect this issue.

In [134] on the prediction, this disease was performed using Infis classifier (adaptive fuzzy neural network) and for two classes of data, the sensitivity was 96%.

In [135], the aim was to identify possible harm and its presence to the fetus. They suggested using a neural network for this purpose to classify correctly. The sensitivity in their work for classification reached 93%.

Reference [136] used a support vector machine with minimal squares optimized by the particle swarm algorithm. Evaluation was done by splitting the data by K-fold method, and finally, the sensitivity was 91.6% for the total cases (96% for the first class, 70% for the suspected class of disease, and finally 75% for the case). Pathological is obtained.

In [136], a system-based method is proposed to estimate FHR parameters and uterine pressure. Extraction of nonlinear features in FHR analysis has been able to increase the sensitivity of classification and identification of disease. Nonlinear methods such as approximation entropy and sample entropy have also been investigated in this study.

In [9], discrete violet conversion has been used to estimate parameters of FHR and uterine pressure. The classification used was LR-SVM. Although the discrete violet feature extractor has multi-resolution capability and is highly compatible with the dynamic properties of FHR signals in feature extraction, the classifier used in the feature separation has not been able to do the job well and the results are unsatisfactory.

Table 7 summarizes the research conducted with the advantages and disadvantages of each.

Numerous studies have been conducted to diagnose fetal health, although they have achieved good results, increased the sensitivity and accuracy of the diagnosis, and reduced the computational complexity remain challenges. Feature selection methods are very helpful in improving the function of segregation and identification of fetal disease. Deep group neural network methods have used FHR signals to predict and identify the fetus. Deep neural networks. Although they have proven their effectiveness in other methods based on machine learning, they are not safe from a major drawback. Deep neural network training requires a large set of datasets, and more in topics related to large datasets are used. The use of a combination of deep neural networks in the diagnosis of fetal health, although it has been able to show good results, it seems that this method cannot be economically viable. Because the

Table 7 Fetal heat disease literature review

No	References	Proposed method	Demerit	Merit
1	[124]	Extract attributes and select attributes from group classifiers, use SVM group classifiers	Significant increase in computing volume	Suitable sensitivity, high accuracy
2	[123]	Use the improved PSO algorithm, then classify with a variety of classifications including generalized trees, multilayer neural networks, and support vector machines and possible neural networks	Computational complexity, increased processing time	Non-regulatory feature selection, non-regulatory clustering
3	[99]	Deep group neural networks	Increasing the number of adjustable parameters in the PSO algorithm	High accuracy and sensitivity
4	[126]	Combining machine learning methods including decision tree, support vector machines, neural network, neural networks, and incremental gradient	Computational complexity, increased processing time	Improve the accuracy and sensitivity of calculations
5	[127]	Use the main linear functions to estimate the condition of the fetus	Lack of coordination between the categories used	Create the best information for categorization by main lines
6	[130]	Techniques based on machine learning and two-class analysis	Nonlinear were fractal functions	Use of non-regulatory methods for classification, low computational complexity
7	[129]	Use the decision tree to categorize data	Low sensitivity and accuracy	Sensitivity equivalent to 95%, increased processed information
8	[132]	Use convolutional features for classification, combining with nonlinear features including fractals	Increase processing time	Increased sensitivity and accuracy due to the combination of methods, increased privacy in calculations
9	[133]	Fuzzy systems and neural networks	High computational complexity, generality of the proposed method	Proper sensitivity

(continued)

Table 7 (continued)

No	References	Proposed method	Demerit	Merit
10	[134]	Prediction of this disease using Infis classifier (adaptive fuzzy neural network)	One is against all, or classifying all against all, or multi-class mode to detect this	Proper sensitivity and accuracy
11	[136]	Proposed support vector machine with minimum squares optimized by particle swarm algorithm. Evaluation by dividing the data by K-fold method	Classification of two classes of data	High-processing speed and good sensitivity
12	[135]	Recognition of possible damage and its existence for the fetus by neural network method	Discrepancies in the findings, so that all three classes of disease are not identified with high efficiency	Simplicity of the proposed method while high efficiency
13	[130]		Lack of significant innovation in the proposed method	Proper sensitivity obtained, use of high frequency
14	[136]	Use of spectral power ability to change the FHR associated with high-frequency fetal blood pH	Dependence of the algorithm on high-frequency parameters	Increase the sensitivity of classification and identification
15	[9]	Estimation of FHR parameters and uterine pressure by system-based method and extraction of nonlinear features in FHR analysis	Nonlinearity of the proposed method	The discrete violet feature extractor has multi-resolution capability and is highly compatible with the dynamic property of FHR signals in feature extraction

use of these networks, especially in group mode, requires high-processing systems as well as large datasets, it is very important to provide an efficient method that can work with ordinary hardware systems or even mid-range processors. Also, in this study, the health of the fetus has been separated and identified in both healthy and unhealthy cases, and the suspected case has not been investigated at all.

5 Conclusion

With changes in people's lifestyles, reduced physical activity and, of course, obesity, heart disease and fetal heart disease have become among the deadliest diseases in

recent decades. Since the health and life of individuals depend to a large extent on the health of heart function and the diagnosis of arrhythmias and dysfunction at the level of the heart should be done in a short time and also with high accuracy and precision, offering new methods with high efficiency in diagnosis of arrhythmias and heart disease seems necessary. This study was conducted with a comprehensive review approach to the diagnosis of heart disease based on machine learning. Optimal use of data mining methods based on machine learning has been able to diagnose heart disease with high accuracy. However, there are challenges in this area. This research has well-introduced these challenges. It has also introduced useful and efficient solutions based on research in this field.

Conflicts of Interest No conflicts of interest to report for this research.

References

1. Iqbal, S., Khan, M.U.G., Saba, T., Mehmood, Z., Javaid, N., Rehman, A., Abbasi, R.: Deep learning model integrating features and novel classifiers fusion for brain tumor segmentation. *Microsc. Res. Tech.* **82**(8), 1302–1315 (2019). <https://doi.org/10.1002/jemt.23281>
2. Abdou, A.D., Ngom, N.F., Niang, O. (eds.): *Electrocardiograms Patterns Analysis Using Artificial Neural Network and Non-Linear Regression*. CARI (2018)
3. Khan, M.G.: *Rapid ECG Interpretation*. Springer Science & Business Media (2008)
4. Nawaz, M., Mehmood, Z., Nazir, T., Naqvi, R.A., Rehman, A., Iqbal, M., Saba, T.: Skin cancer detection from dermoscopic images using deep learning and fuzzy k-means clustering. *Microsc. Res. Tech.* **85**(1), 339–351 (2022)
5. Iftikhar, S., Fatima, K., Rehman, A., Almazyad, A.S., Saba, T.: An evolution based hybrid approach for heart diseases classification and associated risk factors identification. *Biomed. Res.* **28**(8), 3451–3455 (2017)
6. Fahad, H.M., Khan, M.U.G., Saba, T., Rehman, A., Iqbal, S.: Microscopic abnormality classification of cardiac murmurs using ANFIS and HMM. *Microsc Res Tech*. **81**(5), 449–457 (2018). <https://doi.org/10.1002/jemt.22998>
7. Velic, M., Padavic, I., Car, S. (eds.): *Computer aided ECG analysis—State of the Art and Upcoming Challenges*. Eurocon 2013. IEEE (2013)
8. Bhirud, B., Pachghare, V. (eds.): *Arrhythmia detection using ECG signal: A survey*. In: *Proceeding of International Conference on Computational Science and Applications*. Springer (2020)
9. Alfirevic, Z., Gyte, G.M., Cuthbert, A., Devane, D.: Continuous cardiotocography (CTG) as a form of electronic fetal monitoring (EFM) for fetal assessment during labour. *Cochrane Database of Systematic Reviews* (2) (2017)
10. Rashid, M., Khan, M.A., Alhaisoni, M., Wang, S.H., Naqvi, S.R., Rehman, A., Saba, T.: A sustainable deep learning framework for object recognition using multi-layers deep features fusion and selection. *Sustainability* **12**(12), 5037 (2020)
11. Sharif, U., Mehmood, Z., Mahmood, T., Javid, M.A., Rehman, A., Saba, T.: Scene analysis and search using local features and support vector machine for effective content-based image retrieval. *Artif. Intell. Rev.* **52**(2), 901–925 (2019)
12. Chaudhuri, S., Pawar, T.D., Duttagupta, S.: *Review of ECG Analysis. Ambulation Analysis in Wearable ECG*. Springer, pp. 15–26 (2009)
13. Celin, S., Vasanth, K.: ECG signal classification using various machine learning techniques. *J. Med. Syst.* **42**(12), 1–11 (2018)

14. do Vale Madeiro, J.P., Marques, J.A.L., Han, T., Pedrosa, R.C.: Evaluation of mathematical models for QRS feature extraction and QRS morphology classification in ECG signals. *Measurement* **156**, 107580 (2020)
15. Yang, H., Kan, C., Liu, G., Chen, Y.: Spatiotemporal differentiation of myocardial infarctions. *IEEE Trans. Autom. Sci. Eng.* **10**(4), 938–947 (2013)
16. Zhou, S., Tan, B.: Electrocardiogram soft computing using hybrid deep learning CNN-ELM. *Appl. Soft Comput.* **86**, 105778 (2020)
17. De Lannoy, G., François, D., Delbeke, J., Verleysen, M.: Weighted conditional random fields for supervised interpatient heartbeat classification. *IEEE Trans. Biomed. Eng.* **59**(1), 241–247 (2011)
18. Chang, P.-C., Lin, J.-J., Hsieh, J.-C., Weng, J.: Myocardial infarction classification with multi-lead ECG using hidden Markov models and Gaussian mixture models. *Appl. Soft Comput.* **12**(10), 3165–3175 (2012)
19. Gupta, V., Mittal, M.: KNN and PCA classifier with autoregressive modelling during different ECG signal interpretation. *Proc. Comput. Sci.* **125**, 18–24 (2018)
20. Berkaya, S.K., Uysal, A.K., Gunal, E.S., Ergin, S., Gunal, S., Gulmezoglu, M.B.: A survey on ECG analysis. *Biomed. Signal Process. Control* **43**, 216–235 (2018)
21. Grissa, D., Comte, B., Pétéra, M., Pujos-Guillot, E., Napoli, A.: A hybrid and exploratory approach to knowledge discovery in metabolomic data. *Discrete Appl. Math.* (2019)
22. Nohuddin, P., Zainol, Z., Lee, A.S.H., Nordin, I.: A case study in knowledge acquisition for logistic cargo distribution data mining framework. *Int. J. Adv. Appl. Sci.* **5**(1), 8–14 (2018)
23. Kamath, R., Kamat, R.: Modeling fetal morphologic patterns through cardiotocography data: Decision tree-based approach. *J. Pharmacy Res.* **12**(10) (2018)
24. Rehman, A., Harouni, M., Karimi, M., Saba, T., Bahaj, S.A., Awan, M.J.: Microscopic retinal blood vessels detection and segmentation using support vector machine and K-nearest neighbors. *Microsc. Res. Tech.*
25. Rehman, A., Khan, M.A., Saba, T., Mehmood, Z., Tariq, U., Ayesha, N.: Microscopic brain tumor detection and classification using 3D CNN and feature selection architecture. *Microsc. Res. Tech.* **84**(1), 133–149 (2021). <https://doi.org/10.1002/jemt.23597>
26. Gusev, M., Stojmenski, A., Guseva, A. (eds.): ECGalert: A heart attack alerting system. In: International Conference on ICT Innovations. Springer (2017)
27. Yao, Q., Wang, R., Fan, X., Liu, J., Li, Y.: Multi-class Arrhythmia detection from 12-lead varied-length ECG using attention-based time-incremental convolutional neural network. *Inf. Fusion* **53**, 174–182 (2020)
28. Ullah, H., Saba, T., Islam, N., Abbas, N., Rehman, A., Mehmood, Z., Anjum, A.: An ensemble classification of exudates in color fundus images using an evolutionary algorithm based optimal features selection. *Microsc. Res. Tech.* **82**(4), 361–372 (2019). <https://doi.org/10.1002/jemt.23178>
29. Jamal, A., Hazim Alkawaz, M., Rehman, A., Saba, T.: Retinal imaging analysis based on vessel detection. *Microsc. Res. Tech.* **80**(7), 799–811 (2017)
30. Rantanen, J.M., Riahi, S., Schmidt, E.B., Johansen, M.B., Søgaard, P., Christensen, J.H.: Arrhythmias in patients on maintenance dialysis: A cross-sectional study. *Am. J. Kidney Dis.* **75**(2), 214–224 (2020)
31. Lung, J.W.J., Salam, M.S.H., Rehman, A., Rahim, M.S.M., Saba, T.: Fuzzy phoneme classification using multi-speaker vocal tract length normalization. *IETE Tech. Rev.* **31**(2), 128–136 (2014). <https://doi.org/10.1080/02564602.2014.892669>
32. Panigrahy, D., Sahu, P., Albu, F.: Detection of ventricular fibrillation rhythm by using boosted support vector machine with an optimal variable combination. *Comput. Electr. Eng.* **91**, 107035 (2021)
33. Kesmia, M., Boughaba, S., Jacquier, S.: New approach of controlling cardiac alternans. *Discr. Continuous Dyn. Syst. B.* **23**(2), 975 (2018)
34. Saba, T., Haseeb, K., Ahmed, I., Rehman, A.: Secure and energy-efficient framework using Internet of medical things for e-healthcare. *J. Infect. Public Health* **13**(10), 1567–1575 (2020)

35. Wei, W., Zhan, G., Wang, X., Zhang, P., Yan, Y. (eds.): A novel method for automatic heart murmur diagnosis using phonocardiogram. In: Proceedings of the 2019 International Conference on Artificial Intelligence and Advanced Manufacturing (2019)
36. Sadad, T., Munir, A., Saba, T., Hussain, A.: Fuzzy C-means and region growing based classification of tumor from mammograms using hybrid texture feature. *J. Comput. Sci.* **29**, 34–45 (2018)
37. Chandraharan, E.: Intrapartum fetal monitoring. *Evidence Based Labor and Delivery Management* **75** (2019)
38. Jabeen, S., Mehmood, Z., Mahmood, T., Saba, T., Rehman, A., Mahmood, M.T.: An effective content-based image retrieval technique for image visual representation based on the bag-of-visual-words model. *PLoS ONE* **13**(4), e0194526 (2018)
39. Saba, T., Rehman, A., Mehmood, Z., Kolivand, H., Sharif, M.: Image enhancement and segmentation techniques for detection of knee joint diseases: a survey. *Curr. Med. Imaging Rev.* **14**(5), 704–715 (2018a). <https://doi.org/10.2174/1573405613666170912164546>
40. Jezewski, J., Wrobel, J., Matonia, A., Horoba, K., Martinek, R., Kupka, T., et al.: Is abdominal fetal electrocardiography an alternative to doppler ultrasound for FHR variability evaluation? *Front. Physiol.* **8**, 305 (2017)
41. Pavel, M.S.R., Islam, M.R., Siddiqee, A.M. (eds.) Fetal arrhythmia detection using fetal ECG signal. In: 2019 IEEE International Conference on Telecommunications and Photonics (ICTP) IEEE (2019)
42. Gao, X.: Non-invasive detection and compression of fetal electrocardiogram. In: Interpreting Cardiac Electrograms-From Skin to Endocardium, InTechOpen. 53–74 (2017)
43. Khan, M.A., Kadry, S., Zhang, Y.D., Akram, T., Sharif, M., Rehman, A., Saba, T.: Prediction of COVID-19-pneumonia based on selected deep features and one class kernel extreme learning machine. *Comput. Electr. Eng.* **90**, 106960 (2021)
44. Ghazal, M.M., Hammad, A.: Application of knowledge discovery in database (KDD) techniques in cost overrun of construction projects. *Int. J. Constr. Manage.* 1–15 (2020)
45. Khan, A.R., Doosti, F., Karimi, M., Harouni, M., Tariq, U., Fati, S.M., et al.: Authentication through gender classification from iris images using support vector machine. *Microsc. Res. Tech.* (2021)
46. Yousaf, K., Mehmood, Z., Saba, T., Rehman, A., Munshi, A.M., Alharbey, R., Rashid, M.: Mobile-health applications for the efficient delivery of health care facility to people with dementia (PwD) and support to their carers: A survey. *Biomed. Res. Int.* **2019**, 1–26 (2019)
47. AlNuaimi, N., Masud, M.M., Serhani, M.A., Zaki, N.: Streaming feature selection algorithms for big data: A survey. *Appl. Comput. Inf.* (2020)
48. Raman, A.: Secondary Data Analysis: Lessons and Perspective of a Research Parasite (2021)
49. Rahim, M.S.M., Norouzi, A., Rehman, A., Saba, T.: 3D bones segmentation based on CT images visualization. *Biomed. Res.* **28**(8), 3641–3644 (2017)
50. Cai, J., Luo, J., Wang, S., Yang, S.: Feature selection in machine learning: A new perspective. *Neurocomputing* **300**, 70–79 (2018)
51. Sheikhpour, R., Sarram, M.A., Gharaghani, S., Chahooki, M.A.Z.: A survey on semi-supervised feature selection methods. *Pattern Recogn.* **64**, 141–158 (2017)
52. Abbas, N., Saba, T., Mohamad, D., Rehman, A., Almazyad, A.S., Al-Ghamdi, J.S.: Machine aided malaria parasitemia detection in Giemsa-stained thin blood smears. *Neural Comput. Appl.* **29**(3), 803–818 (2018)
53. Aryanmehr, S., Karimi, M., Boroujeni, F.Z. (eds.): CVBL IRIS gender classification database image processing and biometric research, computer vision and biometric laboratory (CVBL). In: 2018 IEEE 3rd International Conference on Image, Vision and Computing (ICIVC). IEEE (2018)
54. Khan, M.A., Sharif, M.I., Raza, M., Anjum, A., Saba, T., Shad, S.A.: Skin lesion segmentation and classification: A unified framework of deep neural network features fusion and selection. *Expert Syst. e12497*
55. Alasadi, S.A., Bhaya, W.S.: Review of data preprocessing techniques in data mining. *J. Eng. Appl. Sci.* **12**(16), 4102–4107 (2017)

56. Li, C.: Preprocessing Methods and Pipelines of Data Mining: An Overview. arXiv preprint arXiv:190608510 (2019)
57. Saba, T., Bokhari, S.T.F., Sharif, M., Yasmin, M., Raza, M.: Fundus image classification methods for the detection of glaucoma: A review. *Microsc. Res. Tech.* (2018). <https://doi.org/10.1002/jemt.23094>
58. Urbanowicz, R.J., Meeker, M., La Cava, W., Olson, R.S., Moore, J.H.: Relief-based feature selection: Introduction and review. *J. Biomed. Inf.* (2018)
59. Li, J., Cheng, K., Wang, S., Morstatter, F., Trevino, R.P., Tang, J., et al.: Feature selection: A data perspective. *ACM Comput. Surv. (CSUR)*. **50**(6), 94 (2018)
60. Nazir, M., Khan, M.A., Saba, T., Rehman, A.: Brain tumor detection from MRI images using multi-level wavelets. In: 2019 International Conference on Computer and Information Sciences (ICCIS), pp. 1–5. IEEE (2019, Apr)
61. Li, C., Lin, S., Xu, F., Liu, D., Liu, J.: Short-term wind power prediction based on data mining technology and improved support vector machine method: A case study in Northwest China. *J. Clean. Prod.* **205**, 909–922 (2018)
62. Javed, R., Rahim, M.S.M., Saba, T., Rehman, A.: A comparative study of features selection for skin lesion detection from dermoscopic images. *Netw. Model. Anal. Health Inf. Bioinf.* **9**(1), 1–13 (2020)
63. Touw, W.G., Bayjanov, J.R., Overmars, L., Backus, L., Boekhorst, J., Wels, M., et al.: Data mining in the life sciences with random forest: A walk in the park or lost in the jungle? *Brief. Bioinform.* **14**(3), 315–326 (2013)
64. Rehman, A., Abbas, N., Saba, T., Mehmood, Z., Mahmood, T., Ahmed, K.T.: Microscopic malaria parasitemia diagnosis and grading on benchmark datasets. *Microsc. Res. Tech.* **81**(9), 1042–1058 (2018). <https://doi.org/10.1002/jemt.23071>
65. Saba, T.: Automated lung nodule detection and classification based on multiple classifiers voting. *Microsc. Res. Tech.* **82**(9), 1601–1609 (2019)
66. Rakhamatulin, I.: Review of EEG feature selection by neural networks. *Int. J. Sci. Bus.* **4**(9), 101–112 (2020)
67. Amin, J., Sharif, M., Raza, M., Saba, T., Rehman, A.: Brain tumor classification: Feature fusion. In: 2019 International Conference on Computer and Information Sciences (ICCIS), pp. 1–6. IEEE
68. Guan, D., Yuan, W., Lee, Y.-K., Najeebulah, K., Rasel, M.K.: A review of ensemble learning based feature selection. *IETE Tech. Rev. 2014*; **31**(3), 190–198 (2019)
69. Ramzan, F., Khan, M.U.G., Iqbal, S., Saba, T., Rehman, A.: Volumetric segmentation of brain regions from MRI scans using 3D convolutional neural networks. *IEEE Access* **8**, 103697–103709 (2020)
70. Rostami, M., Forouzandeh, S., Berahmand, K., Soltani, M.: Integration of multi-objective PSO based feature selection and node centrality for medical datasets. *Genomics* **112**(6), 4370–4384 (2020)
71. Andrushia, A.D., Patricia, A.T.: Artificial bee colony optimization (ABC) for grape leaves disease detection. *Evol. Syst.* **11**(1), 105–117 (2020)
72. Aurangzeb, K., Haider, I., Khan, M.A., Saba, T., Javed, K., Iqbal, T., et al.: Human behavior analysis based on multi-types features fusion and Von Nauman entropy based features reduction. *J. Med. Imaging Health Inf.* **9**(4), 662–669 (2019)
73. Perveen, S., Shahbaz, M., Saba, T., Keshavjee, K., Rehman, A., Guergachi, A.: Handling irregularly sampled longitudinal data and prognostic modeling of diabetes using machine learning technique. *IEEE Access* **8**, 21875–21885 (2020)
74. Karimi, M., Harouni, M., Rafieipour S.: Automated Medical Image Analysis in Digital Mammography. *Artificial Intelligence and Internet of Things: CRC Press*, pp. 85–116 (2021)
75. Harouni, M., Karimi, M., Rafieipour, S.: Precise Segmentation Techniques in Various Medical Images. *Artificial Intelligence and Internet of Things: Applications in Smart Healthcare*, p. 117 (2021)
76. Raza, M., Sharif, M., Yasmin, M., Khan, M.A., Saba, T., Fernandes, S.L.: Appearance based pedestrians' gender recognition by employing stacked auto encoders in deep learning. *Futur. Gener. Comput. Syst.* **88**, 28–39 (2018)

77. Khan, M.A., Zhang, Y.D., Alhussen, M., Kadry, S., Wang, S.H., Saba, T., Iqbal, T.: A fused heterogeneous deep neural network and robust feature selection framework for human actions recognition. *Arab. J. Sci. Eng.* 1–16 (2021)
78. Aslam, A., Ahmad, N., Saba, T., Almazyad, A.S., Rehman, A., Anjum, A., Khan, A.: Decision support system for risk assessment and management strategies in distributed software development. *IEEE Access* **5**, 20349–20373 (2017)
79. Mehmood, A., Khan, M.A., Sharif, M., Khan, S.A., Shaheen, M., Saba, T., et al.: Prosperous human gait recognition: An end-to-end system based on pre-trained CNN features selection. *Multimedia Tools Appl.* 1–21. <https://doi.org/10.1007/s11042-020-08928-0>
80. Arunkumar, N., Ram Kumar, K., Venkataraman, V.: Automatic detection of epileptic seizures using permutation entropy, Tsallis entropy and Kolmogorov complexity. *J. Med. Imaging Health Inf.* **6**(2), 526–531 (2016)
81. Bandt, C., Pompe, B.: Permutation entropy: A natural complexity measure for time series. *Phys. Rev. Lett.* **88**(17), 174102 (2002)
82. Phung, D.Q., Tran, D., Ma, W., Nguyen, P., Pham, T. (eds.): Using Shannon entropy as EEG signal feature for fast person identification. *ESANN* (2014)
83. Figueiredo, J., Santos, C.P., Moreno, J.C.: Automatic recognition of gait patterns in human motor disorders using machine learning: A review. *Med. Eng. Phys.* **53**, 1–12 (2018)
84. Saba, T., Khan, M.A., Rehman, A., Marie-Sainte, S.L.: Region extraction and classification of skin cancer: A heterogeneous framework of deep CNN features fusion and reduction. *J. Med. Syst.* **43**(9), 289 (2019)
85. Hussain, N., Khan, M.A., Sharif, M., Khan, S.A., Albesher, A.A., Saba, T., Armaghan, A.: A deep neural network and classical features based scheme for objects recognition: An application for machine inspection. *Multimed Tools Appl.* (2020). <https://doi.org/10.1007/s11042-020-08852-3>
86. Pienaar, S.W., Malekian, R. (eds.): Human activity recognition using LSTM-RNN deep neural network architecture. In: 2019 IEEE 2nd Wireless Africa Conference (WAC). IEEE (2019)
87. Khan, A.R., Khan, S., Harouni, M., Abbasi, R., Iqbal, S., Mehmood, Z.: Brain tumor segmentation using K-means clustering and deep learning with synthetic data augmentation for classification. *Microsc. Res. Tech.* (2021)
88. Khan, M.A., Sharif, M., Akram, T., Raza, M., Saba, T., Rehman, A.: Hand-crafted and deep convolutional neural network features fusion and selection strategy: An application to intelligent human action recognition. *Appl. Soft Comput.* **87**, 10598 (2020)
89. Adeel, A., Khan, M.A., Akram, T., Sharif, A., Yasmin, M., Saba, T., Javed, K.: Entropy-controlled deep features selection framework for grape leaf diseases recognition. *Expert Syst.* (2020)
90. Adnan, M.M., Rahim, M.S.M., Rehman, A., Mehmood, Z., Saba, T., Naqvi, R.A.: Automatic image annotation based on deep learning models: a systematic review and future challenges. *IEEE Access* **9**, 50253–50264 (2021)
91. Bashardoost, M., Rahim, M.S.M., Saba, T., Rehman, A.: Replacement attack: A new zero text watermarking attack. *3D Res.* **8**(1), 8 (2017)
92. Ordóñez, F.J., Roggen, D.: Deep convolutional and LSTM recurrent neural networks for multimodal wearable activity recognition. *Sensors* **16**(1), 115 (2016)
93. Afza, F., Khan, M.A., Sharif, M., Saba, T., Rehman, A., Javed, M.Y.: Skin lesion classification: An optimized framework of optimal color features selection. In: 2020 2nd International Conference on Computer and Information Sciences (ICCIS), pp. 1–6. IEEE (2020, Oct)
94. Amin, J., Sharif, M., Yasmin, M., Saba, T., Raza, M.: Use of machine intelligence to conduct analysis of human brain data for detection of abnormalities in its cognitive functions. *Multimedia Tools Appl.* **79**(15), 10955–10973 (2020)
95. Nascimento, N.M.M., Marinho, L.B., Peixoto, S.A., do Vale Madeiro, J.P., de Albuquerque, V.H.C., Rebouças Filho, P.P.: Heart arrhythmia classification based on statistical moments and structural co-occurrence. *Circ. Syst. Signal Process.* **39**(2), 631–650 (2020)
96. Ayat, S.: Classification of angiographic results by combining neural-fuzzy network and genetic algorithm. *J. Knowl. Health Basic Med. Sci.* **12**(2), 1–8 (2017)

97. Harouni, M., Baghmaleki, H.Y.: Color image segmentation metrics. *Encycl. Image Process.* **95** (2018)
98. Kalsum, T., Mehmood, Z., Kulsoom, F., Chaudhry, H.N., Khan, A.R., Rashid, M., Saba, T.: Localization and classification of human facial emotions using local intensity order pattern and shape-based texture features. *J. Intell. Fuzzy Syst.* **40**(5), 9311–9331 (2021)
99. Lin, C.-H.: Frequency-domain features for ECG beat discrimination using grey relational analysis-based classifier. *Comput. Math. Appl.* **55**(4), 680–690 (2008)
100. Martis, R.J., Acharya, U.R., Lim, C.M., Suri, J.S.: Characterization of ECG beats from cardiac arrhythmia using discrete cosine transform in PCA framework. *Knowl. Based Syst.* **45**, 76–82 (2013)
101. Afkhami, R.G., Azarnia, G., Tinati, M.A.: Cardiac arrhythmia classification using statistical and mixture modeling features of ECG signals. *Pattern Recogn. Lett.* **70**, 45–51 (2016)
102. Palaniappan, S., Awang, R. (eds.): Intelligent heart disease prediction system using data mining techniques. In: 2008 IEEE/ACS International Conference on Computer Systems and Applications. IEEE (2008)
103. Rajkumar, A., Reena, G.S.: Diagnosis of heart disease using datamining algorithm. *Global J. Comp. Sci. Technol.* **10**(10), 38–43 (2010)
104. Ma'Sum, M.A., Jatmiko, W., Suhartanto, H. (eds.): Enhanced tele ECG system using Hadoop framework to deal with big data processing. In: 2016 International Workshop on Big Data and Information Security (IWBUS). IEEE (2016)
105. Sharif, M., Attique, M., Tahir, M.Z., Yasmim, M., Saba, T., Tanik, U.J.: A machine learning method with threshold based parallel feature fusion and feature selection for automated gait recognition. *J. Organ. End User Comput. (JOEUC)* **32**(2), 67–92 (2020)
106. Saba, T., Rehman, A., AlGhamdi, J.S.: Weather forecasting based on hybrid neural model. *Appl. Water Sci.* **7**(7), 3869–3874 (2017)
107. O'Brien, J.: Using Hidden Markov Models and Spark to Mine ECG Data. (2019)
108. Celesti, F., Celesti, A., Carnevale, L., Galletta, A., Campo, S., Romano, A., et al. (eds.): Big data analytics in genomics: The point on deep learning solutions. In: 2017 IEEE Symposium on Computers and Communications (ISCC). IEEE (2017)
109. Alarsan, F.I., Younes, M.: Analysis and classification of heart diseases using heartbeat features and machine learning algorithms. *J. Big Data* **6**(1), 1–15 (2019)
110. Khan, R.U., Hussain, T., Quddus, H., Haider, A., Adnan, A., Mehmood, Z., (eds.): An intelligent real-time heart diseases diagnosis algorithm. In: 2019 2nd International Conference on Computing, Mathematics and Engineering Technologies (iCoMET). IEEE (2019)
111. Nayeem, M.O.G., Wan, M.N., Hasan, M.K.: Prediction of disease level using multilayer perceptron of artificial neural network for patient monitoring. *Int. J. Soft Comput. Eng. (IJSCe)* (2015)
112. Huang, J., Chen, B., Yao, B., He, W.: ECG arrhythmia classification using STFT-based spectrogram and convolutional neural network. *IEEE Access* **7**, 92871–92880 (2019)
113. He, H., Tan, Y., Xing, J.: Unsupervised classification of 12-lead ECG signals using wavelet tensor decomposition and two-dimensional Gaussian spectral clustering. *Knowl. Based Syst.* **163**, 392–403 (2019)
114. Diker, A., Avci, E., Tanyildizi, E., Gedikpinar, M.: A novel ECG signal classification method using DEA-ELM. *Med. Hypotheses* **136**, 109515 (2020)
115. Thiagaraj, M., Suseendran, G.: Enhanced Prediction of Heart Disease Using Particle Swarm Optimization and Rough Sets with Transductive Support Vector Machines Classifier. *Data Management, Analytics and Innovation*. Springer, pp. 141–152 (2020)
116. Tama, B.A., Im, S., Lee, S.: Improving an intelligent detection system for coronary heart disease using a two-tier classifier ensemble. *BioMed Res. Int.* **2020** (2020)
117. Baccouche, A., Garcia-Zapirain, B., Castillo Olea, C., Elmaghriby, A.: Ensemble deep learning models for heart disease classification: A case study from Mexico. *Information* **11**(4), 207 (2020)
118. Dutta, A., Batabyal, T., Basu, M., Acton, S.T.: An efficient convolutional neural network for coronary heart disease prediction. *Expert Syst. Appl.* **113408** (2020)

119. Habibi, N., Harouni, M.: Estimation of re-hospitalization risk of diabetic patients based on radial base function (RBF) neural network method combined with colonial competition optimization algorithm. *Majlesi J. Electr. Eng.* **12**(1), 109–116 (2018)
120. Rehman, A., Harouni, M., Karchegani, N.H.S., Saba, T., Bahaj, S.A., Roy, S.: Identity verification using palm print microscopic images based on median robust extended local binary pattern features and k-nearest neighbor classifier. *Microsc. Res. Tech.* (2021)
121. Husham, A., Alkawaz, M.H., Saba, T., Rehman, A., Alghamdi, J.S.: Automated nuclei segmentation of malignant using level sets. *Microsc. Res. Tech.* **79**(10), 993–997 (2016). <https://doi.org/10.1002/jemt.22733>.
122. Agrawal, K., Mohan, H. (eds.): Cardiotocography analysis for fetal state classification using machine learning algorithms. In: 2019 International Conference on Computer Communication and Informatics (ICCCI). IEEE (2019)
123. Silwattananusarn, T., Kanarkard, W., Tuamsuk, K.: Enhanced classification accuracy for cardiotocogram data with ensemble feature selection and classifier ensemble. *J. Comput. Commun.* **4**(04), 20 (2016)
124. Jagannathan, D.: Comparative study between various classification algorithms for classification of cardiotocogram data. *Int. J. Sci. Res. Comput. Sci. Eng. Inf. Technol.* **2**(4), 651–657 (2017)
125. Batra, A., Chandra, A., Matoria, V. (eds.): Cardiotocography analysis using conjunction of machine learning algorithms. In: 2017 International Conference on Machine Vision and Information Technology (CMVIT). IEEE (2017)
126. Kabir, M.F., Ludwig, S.A.: Enhancing the performance of classification using super learning. *Data-Enabled Disc. Appl.* **3**(1), 5 (2019)
127. Chamidah, N., Wasito, I. (eds.): Fetal state classification from cardiotocography based on feature extraction using hybrid K-Means and support vector machine. In: 2015 International Conference on Advanced Computer Science and Information Systems (ICACSIS). IEEE (2015)
128. Shah, S.A.A., Aziz, W., Arif, M., Nadeem, M.S.A. (eds.): Decision trees based classification of cardiotocograms using bagging approach. In: 2015 13th International Conference on Frontiers of Information Technology (FIT). IEEE (2015)
129. Sahin, H., Subasi, A.: Classification of the cardiotocogram data for anticipation of fetal risks using machine learning techniques. *Appl. Soft Comput.* **33**, 231–238 (2015)
130. Inbarani, H.H., Banu, P.N., Azar, A.T.: Feature selection using swarm-based relative reduct technique for fetal heart rate. *Neural Comput. Appl.* **25**(3–4), 793–806 (2014)
131. Georgoulas, G., Spilka, J., Karvelis, P., Chudáček, V., Stylios, C., Lhotská, L. (eds.): A three class treatment of the FHR classification problem using latent class analysis labeling. In: 2014 36th Annual International Conference of the IEEE Engineering in Medicine and Biology Society. IEEE (2014)
132. Das, S., Roy, K., Saha, C.K. (eds.): Fuzzy membership estimation using ANN: A case study in CTG analysis. In: Proceedings of the 3rd International Conference on Frontiers of Intelligent Computing: Theory and Applications (FICTA) 2014. Springer (2015)
133. Ocak, H., Ertunc, H.M.: Prediction of fetal state from the cardiotocogram recordings using adaptive neuro-fuzzy inference systems. *Neural Comput. Appl.* **23**(6), 1583–1589 (2013)
134. Tomáš, P., Krohova, J., Dohnalek, P., Gajdoš, P. (eds.): Classification of cardiotocography records by random forest. In: 2013 36th International Conference on Telecommunications and Signal Processing (TSP). IEEE (2013)
135. Yilmaz, E., Kılıkçıer, Ç.: Determination of fetal state from cardiotocogram using LS-SVM with particle swarm optimization and binary decision tree. *Comput. Math. Methods Med.* **2013** (2013)
136. Westerhuis, M.E., Visser, G.H., Moons, K.G., Van Beek, E., Benders, M.J., Bijvoet, S.M., et al.: Cardiotocography plus ST analysis of fetal electrocardiogram compared with cardiotocography only for intrapartum monitoring: A randomized controlled trial. *Obstet. Gynecol.* **115**(6), 1173–1180 (2010)

Machine Learning-Based Brain Diseases Diagnosing in Electroencephalogram Signals, Alzheimer's, and Parkinson's



Nakisa Tavakoli^{ID}, Zahra Karimi^{ID}, Somayeh AsadiJouzani^{ID}, Nastaran Azizi^{ID}, Sara Rezakhani^{ID}, and Atefeh Tobeiha^{ID}

Abstract Brain dysfunction is very common in old age and even in middle-aged people. Alzheimer's and Parkinson's diseases are among the most common diseases due to brain dysfunction. In Alzheimer's disease, a person gradually loses his mental abilities. Although it is normal for people to become a little forgetful as they get older, this memory disorder gradually progresses, posing great challenges. In order to prevent the spread of Alzheimer's disease, early detection will be very helpful. Parkinson's is another disease that will increase in prevalence as life expectancy increases. Brain monitoring tools are used to detect these diseases early. An inexpensive and useful tool and low-risk brain signals are electroencephalograms. In order to analyze brain signals, the use of machine learning-based methods has been able to show its superiority. In order to diagnose Alzheimer's and Parkinson's in machine learning, there are preprocessing steps, feature extraction, feature selection, classification, and evaluation. Since electroencephalogram data have high repetition and correlation in different channels recorded on the head, feature extraction techniques will be of great importance. Feature selection methods seek to select the most effective features to classify and identify disease status. Finally, the selected features will be categorized using different categories. In this chapter, a complete overview of the stages of diagnosis of these diseases with the help of machine learning will be provided.

N. Tavakoli (✉)

Department of Computer Engineering, Farsan Branch, Islamic Azad University, Farsan, Iran
e-mail: Nakisatavakoli@gmail.com

Z. Karimi

Department of Bioelectronics and Biomedical Engineering, School of Advanced Technologies in Medicine, Isfahan University of Medical Sciences, Isfahan, Iran

S. AsadiJouzani

School of Electrical and Computer Engineering, University of Tehran, Tehran, Iran

N. Azizi

Sepahan Institute of Higher Education, Science and Technology, Isfahan, Iran

S. Rezakhani · A. Tobeiha

Department of Electrical Engineering, Najaf Abad Branch, Islamic Azad University, Isfahan, Iran

Keywords Alzheimer · Parkinson · Electroencephalogram · Machine learning · Feature extraction and selection

1 Introduction

Alzheimer's disease is a progressive disease that begins and progresses with mild symptoms. Researchers believe that Alzheimer's-related brain changes begin at the age of 20 or even earlier with mild symptoms. The disease has several stages, including: 1-Cognitively normal CN, 2-Significant memory concern SMC, 3-Early memory cognitive impairment EMCI disorder, 4-Diagnosis of MCI memory disorder, 5-Late mild cognitive impairment LMCI, and finally, 6-Alzheimer's disease AD [1]. Cognitively normal CN are people who have symptoms of life expectancy, depression, and dementia. In SMC, people have normal cognitive activity but sometimes have memory problems. People with long-term memory problems have more problems, and in LMCI, MCI, and EMCI, brain activity and memory are deteriorating day by day, making it difficult for patients to perform daily activities [2]. In recent years, the rise of Alzheimer's disease and the need to identify and diagnose it has led researchers to work seriously on this disease. Different conditions of the disease and identifying different conditions of the disease from the beginning to the onset of Alzheimer's disease is a very challenging process. Numerous studies have been performed to diagnose and classify different conditions of Alzheimer's disease. Identification and classification of different conditions and stages of the disease were performed on structural magnetic resonance imaging SMRI, Functional MRI, Positron emission tomography PET images, CT scan images, and EEG signals. MCI is usually associated with decreased levels of consciousness, such as poor memory function or poor thinking, which increases with age. About 20% of people over the age of 60 suffer from MCI. Although the symptoms of the disease are seen in people, patients can hardly go about their daily lives. Recent research has shown that if MCI is detected in the early stages can be returned to normal with treatment [3].

Around the world, most people living in cities are less physically active. The world's population is growing, and most people are living longer than in the past. Therefore, improper combination (low physical activity and use of unhealthy foods) has led to an uncontrollable increase in the prevalence of various diseases in the world. One of these diseases is Parkinson's disease, which will increase with increasing life expectancy [4]. The prevalence of Parkinson's disease in Iran is about two per thousand people, and this rate increases tenfold for people over 65 and reaches two per hundred people. According to 2020 statistics, there are about 211,000 people with Parkinson's disease in Iran [5]. According to the latest statistics published by the World Health Organization in 2017, the number of deaths due to Parkinson's disease among Iranians is 297 or 0.09 total deaths, and in this regard, Iran is ranked 145th in the world. However, the results of the latest studies have shown that Parkinson's disease will grow by one-fifth in the next 7 years, and by 2040, the incidence of it will double [6].

The extent of the parts involved in this disease causes the affected person to show a range of motor and non-motor problems. In addition to the six main characteristics, some other movement problems such as speech disorder, swallowing disorder, and micrograph are also observed in the affected people. Patients with Parkinson's also have some non-motor problems, such as sleep disorders, depression and anxiety, psychosis, autoimmune disorders (sympathetic and parasympathetic), sexual problems, urinary disorders, dementia, and anxiety [7]. This disease causes movement disorders of the (Hypokinetic) type, disrupts all speech infrastructures including vocalization, production, and (Prosody), and causes paralytic speech paralysis in the individual. Among the features of paralyzed speech (Hypokinetic Dysarthria) can be reduced volume and pitch (Variable rate) and wheezing and breathless sound [8].

A process of identifying brain diseases such as Alzheimer's and Parkinson's in machine learning involves preprocessing, feature extraction and feature selection, classification, and finally evaluation. Extracting features to train classifications and to differentiate between healthy and diseased people, and then finding the difference between brain hallucinations is a key step in these systems [9]. One of the methods to study the differentiation of two states (healthy and diseased) to be examined by different characteristics. Different methods are proposed for extracting features in the EEG. A number of studies have focused on extracting and evaluating EEG frequency domain properties to analyze these signals. This is while other studies on the extraction of space or time characteristics of EEG signals are analyzed [10]. One of the aims of this study is to investigate the changes in frequency and non-frequency characteristics in sick and healthy people and to evaluate them. To determine the best feature to diagnose amnesia and Alzheimer's disease, spatial or temporal domain characteristics in EEG signals such as entropy and approximate entropy, and various statistical properties such as variance and approximate entropy can be helpful in this regard. Frequency properties such as entropy of the power spectrum, Power spectral entropy (PSE), and Gravity Frequency (GF) can also be considered [11–13]. Discrete Fourier transform characteristics and subtypes, such as fast and short Fourier transform, and multi-layered violet conversion properties that convert EEG signal to different sub-bands can also help in this separation. It can be stated that in most studies performed on the extraction of features from EEG by methods such as descriptors or Low-Level Descriptors (Pitch), Teaser, Linear Prediction Cepstral Coefficients, Perceptual Linear Prediction (MFCCs), Frequency domain transformations (wavelet, Gabor, etc.), Fourier-based transformations, types of neural networks such as convolutional neural networks (CNN) and Long short-term memory (LSTM) and other methods has been used [14].

The exact definition of a feature selection depends on the context in which it is used. But the most widely used definition is that feature selection is the selection of a subset of features with the best result of the classification function [15, 16]. The rationale for this definition is that additional or irrelevant features often have similar noise in the data, which causes the classifier to be mistaken and the classification function to be degraded. Eliminating such features causes the resulting features to have the same or higher classification function than the whole features [17]. As a direct result, fewer features are required for data storage, and the classification process

is accelerated. In addition, reducing the number of features helps the expert to focus on a subset of the relevant features, which gives them a better view of the process described by the data [18, 19]. Feature selection helps to better understand the data, reduce computational requirements, reduce the detrimental effect of dimensions, and improve predicted performance [20]. Feature selection focuses on selecting a subset of input variables that can effectively describe the input data and reduce the effects of noise and irrelevant variables, while still providing well-predicted results [21].

Brain EEG signals vary greatly from person to person, whether healthy or with Alzheimer's or Parkinson's disease. In addition, in different bands of EEG signal, each of them shows several features that actually make the diagnosis of the disease difficult. Diagnosis of the band from which early detection of MCI or Parkinson's can be performed, as well as the best characteristics based on which the disease can be identified from normal and healthy people. This is another challenge that researchers have conducted numerous studies to address. In the detection, after removing the artifacts, and improving the signal quality, the sub-bands in the EEG signal, which include gamma, beta, alpha, theta, and delta bands, are extracted, then several properties are extracted, and a suitable method is selected using a suitable method. Appropriate characteristics are extracted from the band to diagnose the disease and diagnosed with the help of classification, such as support vector machine, or K nearest neighborhood. By obtaining the results, the best band with the most information to diagnose Alzheimer's is selected and, with the help of statistical analysis, the superiority of the obtained band will be proved.

Parkinson's and Alzheimer's diseases are progressive neurological and cerebral diseases. This disease is caused by a deficiency of some dopaminergic neurons, advanced state of the disease motor symptoms, and function disorders. These symptoms are accompanied by tremors resting gesture changes. Brain signals (EEGs) are a non-invasive, powerful, and relatively inexpensive method of controlling and monitoring brain function. The EEG records excellent information about brain activity and function. In Parkinson's disease (PD), the interaction and function of neurons is easily recorded by EEG. EEG Signals have a good time resolution when this spatial resolution records high information about the functioning of the brain. The use of artificial intelligence and machine learning has been used in the diagnosis of many diseases. The efficiency and effectiveness of machine learning methods have been proven in these studies. Different studies have been presented for diagnosis (PD) and AD. In this regard, a review of the research will be done. The innovations of this chapter can be listed as follows:

- A review of methods based on all stages of machine learning in the diagnosis of AD and PD
- Full introduction of EEG and its capabilities in diagnosing diseases
- A comprehensive overview of methods for extracting features from EEG brain signals
- Introduction of related databases.

In order to achieve the goals of the chapter, the following sections have been considered. Section 2 introduces the types of PA and AD diseases. EEG electroencephalogram signals will also be introduced. In Sect. 3, PA and AD machine learning methods will be examined. In Sect. 4, research conducted by researchers in previous years will be reviewed. Finally, in Sect. 5, the conclusion of the chapter is presented.

2 PA and AD Diseases

Alzheimer disease AD is a neurological disorder in people that negatively affects memory and cognitive ability. Alzheimer's disease is a progressive and irreversible brain disease that slowly destroys memory and thinking power, and even deprives a person of the ability to do simple things. Alzheimer's disease starts slowly. The disease primarily affects the parts of the brain that control memory and language. Alzheimer's is a progressive disease. This means that over time, more parts of the brain are damaged. When this happens, more symptoms are seen and the disease worsens. Alzheimer's disease is a deadly disease that ultimately affects all aspects of a person's life [22].

Alzheimer's disease specialists believe that Alzheimer's occurs due to overproduction of β or Amyloid $A\beta$ starch as well as high protein tau Phosphorylation of tau [8]. The underlying cause of Alzheimer's disease is still unknown and, in some cases, genetic. With age, some of the mental and physical abilities of people decrease because the brain, like other parts of the body, changes, decays, and wears out, and if we do not do something to maintain and care for it, it may decline and go to destruction. Alzheimer's is the most common type of "dementia." It is one of the most common problems in old age and is more likely to develop from the age of 60–65, but not every elderly person will develop Alzheimer [11].

Dementia is a general term for neurological and memory-related diseases. Alzheimer's is a common type of dementia. According to the Global Alzheimer's Report in 2015, more than 50 million people suffer from dementia, of which 70–80% are related to Alzheimer's disease [12]. It is estimated that by 2050, more than 132 million people worldwide will have Alzheimer's disease. In other words, one person gets Alzheimer's disease every three seconds around the world. Also, according to global Alzheimer's statistics in 2018, the financial damage to Alzheimer's patients is estimated at more than \$ 818 billion. This cost will reach more than one thousand billion dollars by 2020, and it is even predicted that by 2030 it will be two thousand billion dollars. 3% of people with Alzheimer's disease have an age range of 65–74 years, % of people aged 75–84 years, and other people over 85 years old [23].

2.1 Types of Alzheimer's

Usually, the first signs of Alzheimer's cognitive impairment are memory problems. Some people with memory problems have a condition called mild cognitive impairment (MCI). In MCI, people have more memory problems than their healthy peers, but their symptoms are not severe enough to interfere with their daily lives. Motor and olfactory problems are also related to (MCI). Elderly people with MCI are at higher risk for Alzheimer's, but not all of them have Alzheimer's. Some may even improve and return to a normal cognitive state. The first symptoms of Alzheimer's vary from person to person. In many people, loss of non-memory aspects of cognition such as word recall, visual/spatial problems, impaired reasoning, or judgment may be an early signal of the early stages of Alzheimer's disease. Researchers are studying biomarkers (biological signs of the disease found in images of the brain, cerebrospinal fluid, and blood) to find a way to diagnose early-stage MCI brain changes and people with normal cognitive ability who are at higher risk for Alzheimer's. Recent research suggests that early diagnosis may be possible, but more research is needed before these early detection techniques can be used in the day-to-day performance of a healthcare team.

2.2 Parkinson's Disease

Human knowledge about Parkinson's disease has evolved over time, leading to advances in the treatment of the disease and hope for the future. Parkinson's disease was first published by Dr. James Parkinson in an 1817 book entitled *Essay on Shaking Palsy*. This disease was known as tremor paralysis for many years, and in medical terms, it was called agitated paralysis. It was later named Parkinson's disease to commemorate the services of Dr. James Parkinson as the first person to describe the disease [24]. He featured the disease to features such as resting tremors, decreased muscle strength, and unsteady posture. Tre'tiakoff then described the destruction of the Substantia Nigra in the disease. Jean-Martin Charcot, a French neurologist, was instrumental in improving and expanding the initial description of the disease and in disseminating international information about Parkinson's disease. He distinguished Parkinson's disease from MS and other disorders characterized by tremor and identified cases that were later classified as Parkinsonism Plus syndromes. In 2000, a Swedish scientist named Carlson won the Nobel Prize for his studies on dopamine and its effects on Parkinson's disease. He explained that in Parkinson's, dopamine levels decrease and cause a person to lose movement. Early treatments for Parkinson's disease were based on experimental observations, and anticholinergic drugs have been used since the nineteenth century. The discovery of dopaminergic defects in Parkinson's disease led to the first human experiments with levodopa. In addition, important anatomical, biochemical, and physiological studies have established other

therapeutic targets for Parkinson's disease, enabling physicians to develop a set of treatments aimed at improving function for this incurable disease [25].

2.3 Brief Description of the Disease

Body movements are regulated by a part of the brain called the Basal Ganglia. The cells of this section need a proper balance of dopamine and acetylcholine. These two substances are involved in the transmission of nerve impulses. Parkinson's disease is the result of the loss or weakening of dopamine-producing nerve cells in the midbrain. Parkinsonism is a syndrome that can be diagnosed by a combination of the following six symptoms: resting tremor, Bradykinesia, lack of postural reflexes, curved posture, and locking. The most common type is primary Parkinson's, which is called Parkinson's disease. The common denominator of almost all disorders associated with clinical Parkinsonism is the loss of neurons in the substantia nigra, especially dopaminergic neurons. When 80% of the black matter nerve cells are damaged or destroyed, the person will experience constant tremors. Previously, the disease was thought to be caused solely by the gradual degradation of dopamine-containing neurons in the Pars Compacta black matter part of the nucleus, but more recent studies have shown that in addition to black matter, Lewy Bodies are also found in different areas of the brainstem, such as Olfactory Bulb, Dorsal Motor nucleus of the Vagus, Raphe Nuclei, Locus Coeruleus, and Reticular Formation.

The extent of the parts involved in this disease causes the affected person to show a range of motor and non-motor problems. In addition to the six main characteristics, some other movement problems such as speech disorder, swallowing disorder, and micrograph are also observed in the affected people. Patients with Parkinson's also have some immobile problems, including sleep disorders, depression and anxiety, psychosis, Hypokinetic disorders, sexual problems, urinary disorders, dementia, and anxiety. This disease causes movement disorders of the hypokinetic type and disrupts all the infrastructures involved in speech, including vocalization, production, Prosody, and Hypokinetic Dysarthria in the person. Slowly, among the features of paralytic paralysis are reduced volume and pitch or variable rate and hoarse voice [24].

2.4 Nervous System

The nervous system is the body's most important communication system that monitors the actions of other body systems. In a general division, the nervous system is divided into two main parts: the central nervous system (CNS), which is located inside the skull and the vertebral canal, and includes the brain and spinal cord, and the lateral or peripheral nervous system (PNS) (Fig. 1). The lateral nervous system

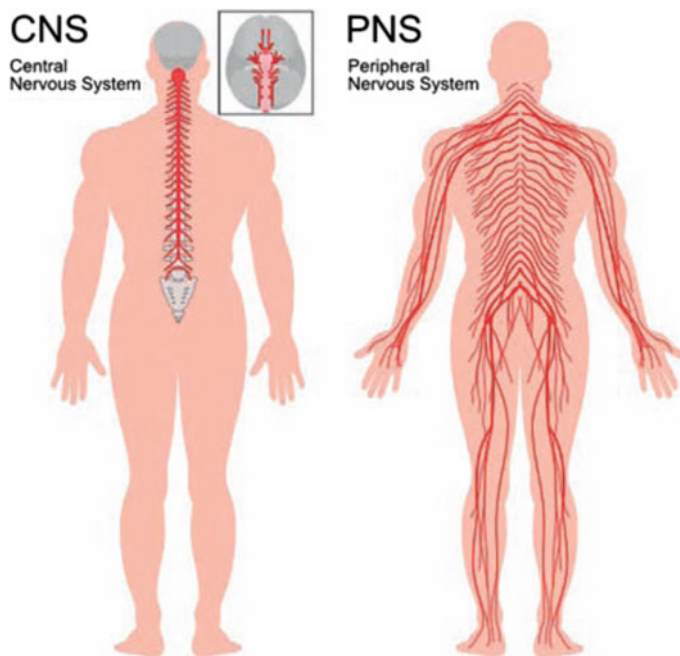


Fig. 1 The human nervous system

is composed of nerve fibers or axons and is responsible for transmitting the neural message from the environment to the CNS or vice versa [26].

The nervous system is made up of special tissue that includes two types of cells: neurons or neurones and non-neurons or neuroglia. Nerve cells, which are the most complex cells in the body, are the descriptive and functional unit of the nervous system, and their number in the nervous system is about 16 billion. These cells consist of three main parts of the cell body: axons and dendrites (Fig. 2) [13].

The cell body consists of the nucleus and the cytoplasm. In the cytoplasm, there are subtle fibers called nerve fibers or neurofibers that are responsible for transmitting nerve messages. Dendrites are short appendages that carry nerve messages to the cell body. An axon is a long, single appendage that carries nerve messages out of a cell body and can vary in length from one millimeter to one meter. The function of non-neuronal cells is to nourish, repair, and protect neurons. These cells have no role in transmitting neural messages. Functionally, nerve cells can be divided into two categories:

Sensory or Afferent neuron: The function of these neurons, also known as sensory nerves, is to transmit nerve messages from the environment (skin and sensory organs) to the CNS [15].

Motor or Efferent neuron: The function of these neurons, also known as motor or motor nerves, is to transmit nerve messages from the CNS to the organs [15].

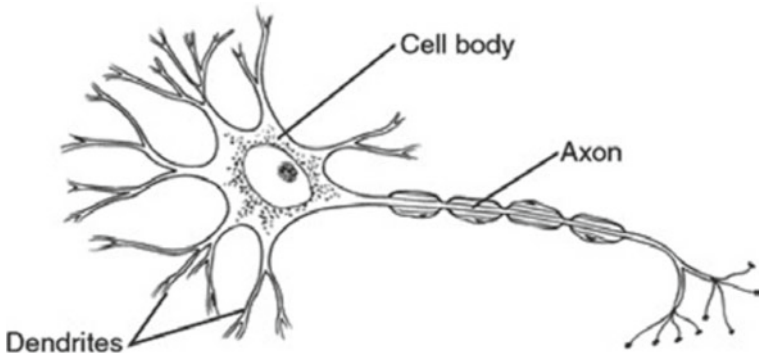


Fig. 2 Microscopic image of a human nerve cell

2.5 Exchange of Information with the Nervous System

The function of neural connections is to exchange information with the nervous system, which can be bilateral. Communication and information transmission within the nervous system is done through electrical signals. In fact, this communication is basically through the rate and pattern of electrical signals, which is called “action potential” (hereinafter referred to as AP, as well as through the number or distance of these action potentials per unit time that encodes information in the nervous system [15]. Most of the nervous system information processing is done by these same APs and their spatial time patterns. Thus, information can be transmitted to the nervous system by providing APs, or conversely, the number, rate, or pattern of these APs can be obtained and used to retrieve information from the nervous system and exchange information with the nervous system. It is done at different levels. At the level of the lateral nerves, the recording of efferent signals can be used to control the movement of a mechanical prosthesis. On the contrary, sensor feedback from force sensors and touch sensors, etc., can be used to stimulate afferent nerve fibers inside the user’s remaining limb. In addition, the exchange of information can take place at the level of the central nervous system, which can be with the brain or with the spinal cord. At this level, stimulation can affect the organs and signal recording can be used to learn and obtain information about the status of this system [27].

The function of the lateral nervous system, hereinafter referred to as the PNS, is to transmit information from the CNS to the peripheral organs and vice versa. Communication with the lateral nerves is important because it can enhance motor function or extract sensory information and use it to perform precise prostheses. In such cases, the lateral nerves are intact and can be used to drive drivers that improve the ability of the lateral nerves to initiate muscle and limb contractions. The ability to stimulate the lateral nerves to have optimal motor outputs is one of the most important reasons for using PNS interfacing. These connections to the nervous system are typically made by recording and stimulation electrodes [28].

2.6 Electrical Connection with the Nervous System

When excited nerve cells in the membrane, ion currents are produced that cause a change in voltage between inside and outside the cell. In the excitation phase, the electrode converts the electric current into ionic currents inside the axons. These ionic currents activate the ion channels of excitable cells and cause the depolarized cell to produce AP. In the electrode recording phase, the changes due to the movement of ions are converted into electrons (electric current). Depending on where the signals are recorded, the measurement of neural activity can be divided into two categories:

- Intracellular registration, which records AP from individual cells. The signals recorded in this type of recording are about tens of millivolts. Although these types of signals are accurate and have almost no noise, the disadvantage of this type of recording is that access to individual cells requires very sharp electrodes with very high accuracy, which requires complex processes in electrode fabrication. In addition, the chances of damaging the cells are very high. In fact, this type of recorder is not suitable for long-term implantable technologies and is only suitable for in vitro measurements due to cell destruction and death after a few hours of recording [29].
- Extracellular registration, which records AP from a large number of nerve cells. APs recorded in this way are called “sensory APs” and range in size from a few tens to a few hundred microvolts in the 300 Hz frequency range up to a maximum of 10 KHz. The incidence rate of these APs varies from 10 to 120 per second Is [29].

2.7 Electroencephalogram

EEG, Electroencephalography or EEG, records the electrical activity of the brain by placing superficial electrodes on the head in a non-invasive way. In general, in an EEG system, the electrical effect of the activity of brain neurons is transmitted to the device through electrodes mounted on the head, and after amplifying and removing the noise, it is recorded and displayed as a time signal. The recorded signal can be analyzed directly or after computer processing by a physician or neurologist.

With the help of electroencephalography, it is possible to determine the amount of that activity and the insufficiency of the affected areas of the brain in various brain activities. As a result, the study and analysis of the signal recorded through electroencephalography has an effective role in a wide range of diagnostic and research applications, such as the following:

1. Diagnosing cerebral brain injury and determining its location
2. Investigation of epileptic seizures
3. Diagnosis of mental disorders
4. Study sleep and study its disorders
5. Observing and analyzing the brain's responses to sensory stimuli

Table 1 Specifications of the frequency band in the EEG signal

Features	Frequency	Sub-bands
Seen in infants, deep sleep and in some brain diseases	Between 0.5 and 3.5 Hz	Delta Sub-band
Seen in the parietal and temporal regions of the brain, and in children, seen in adults who are depressed or under stress	Between 4 and 7 Hz	Theta sub-band
Seeing in normal people and in a state of consciousness with closed eyes, recording in a relaxed state, being in the back area	Between 8 and 13 Hz	Alpha sub-band
Seeing in a relaxed state and reducing anxiety	Between 12 and 15 Hz	SMR wave
Being seen in intense brain activity in the forehead and parietal areas, being seen while thinking and thinking	Beta 1 band: between 14 and 30 Hz Beta (gamma) 2 band: between 30 and 50 Hz Intermediate beta band: between 16 and 20 Hz	Beta sub-band
Being seen in cognitive activities such as intense and focused attention, stimulation of the disease	Between 30 and 50 Hz	Gamma sub-band

6. Research related to Brain–Computer Interface Systems (BCI).

Brain signal recordings of patients are usually made in the waking state. However, depending on the test, the person may be asked to keep their eyes open or closed. In the open eye, sometimes the patient's sensitivity to light stimulation is measured through a flashing light (photik) [30].

An EEG brain signal is a dynamic set that changes with any physical or non-physical change. The sensitivity of these signals is such that they change even with blinking. In order to analyze these signals more accurately, they are divided into different sub-bands based on different frequencies. The main EEG signal is usually in the frequency range of 0.5–50 Hz [31]. In the proposed classification, the created and known sub-bands are Delta sub-bands, their beta sub-bands, SMR sub-band, beta sub-band, and finally gamma sub-band. Table 1 shows the specifications of these sub-bands. Figure 3 also shows these sub-bands.

3 Machine Learning

EEG electroencephalogram is a method of monitoring the brain, in other words, measuring voltage changes in the activity of brain neurons, which directly shows its activity. An electroencephalogram records the spontaneous and unwanted electronic

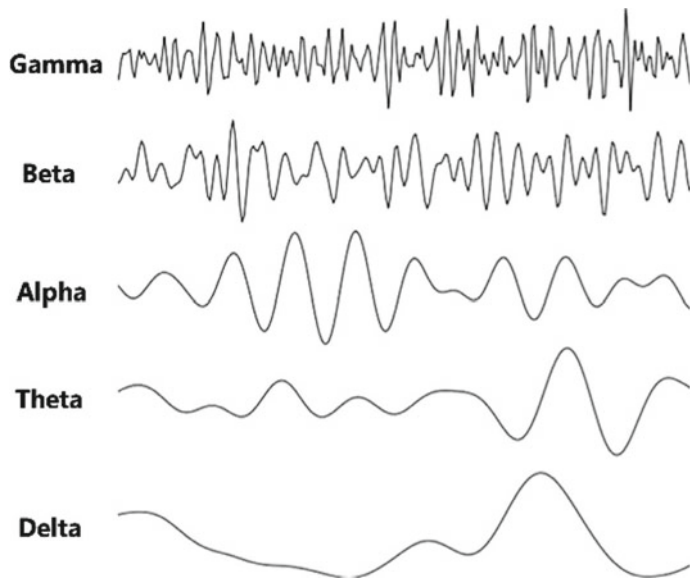


Fig. 3 Sub-bands extracted from EEG signal [32]

activity of the brain. In other words, EEG can be considered as a measure of the function of more than one hundred million brain neurons [33]. It is a good tool for analyzing brain activity and function. In addition to being able to show the health of brain function, it can also be used in many cases, such as diagnosing disease [34].

Extracting useful and appropriate information from EEG signals is essential. There are usually several patterns in the EEG brain signal of people in different situations. These different patterns are not seen throughout the brain, but may occur in specific areas of the brain [35]. One way to diagnose the disease with EEG signals is to use machine-based methods. Machine learning-based methods as a technique for identifying, diagnosing, classifying disease, and finding patterns for recognizing the type and state of emotion can be crucial. Increasing the accuracy of diagnosis, reducing costs, and reducing the cost of human resources in the areas of applying the results in identifying the disease have been proven by the benefits of introducing machine learning in analysis by researchers [32]. Figure 4 shows the block diagram of machine learning-based methods in diagnosing the proposed disease.

The proposed methods in diagnosing disease based on machine learning mainly consist of preprocessing, feature extraction, feature selection, classification, and finally evaluation. Human disease is characterized by the use of EEG signals and conventional descriptors in this field, such as short-time Fourier transform and discrete wavelet transform. It is very important to use methods with low computational cost in order to extract the feature [36].

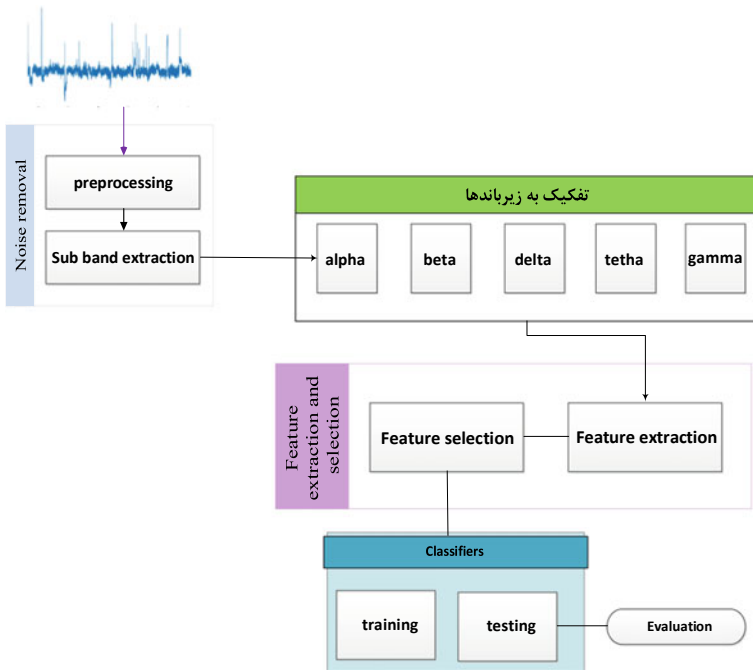


Fig. 4 Block diagram of the proposed method

3.1 Preprocessing

There are usually unwanted events in the recording of brain signals, which affect the EEG. An unwanted event is artifacts. There are ocular or muscular artifacts in the processing of brain signals. This type is caused by the test subject blinking or moving the limb involuntarily. The received signals, which contain useful and important information, are affected by this artifact. Numerous studies have been performed to identify the artifact and remove it from the signal and remove it from the EEG signal [37]. In order to remove these artifacts in the preprocessing stage on this EEG signal, processes such as filtering are used [38]. These artifacts include blinking, eye movement, tooth clenching, head movement, and drinking water. Detection of the artifact, in other words, removal of the artifact from the EEG, is inevitable. In the preprocessing stage, this important point is observed in research [39]. The bands of the EEG spectrum (delta, theta, alpha, beta, and gamma) are highly interdependent. This dependency produces similar properties. Some of these cases are obtained from the analytical methods resulting from the results [40]. Due to the performance, there are correlations between specific oscillation frequencies. There are no definite boundaries in various bands in the EEG spectrum and the methods for determining them are still debated. For example, the high dependence of the alpha and beta bands

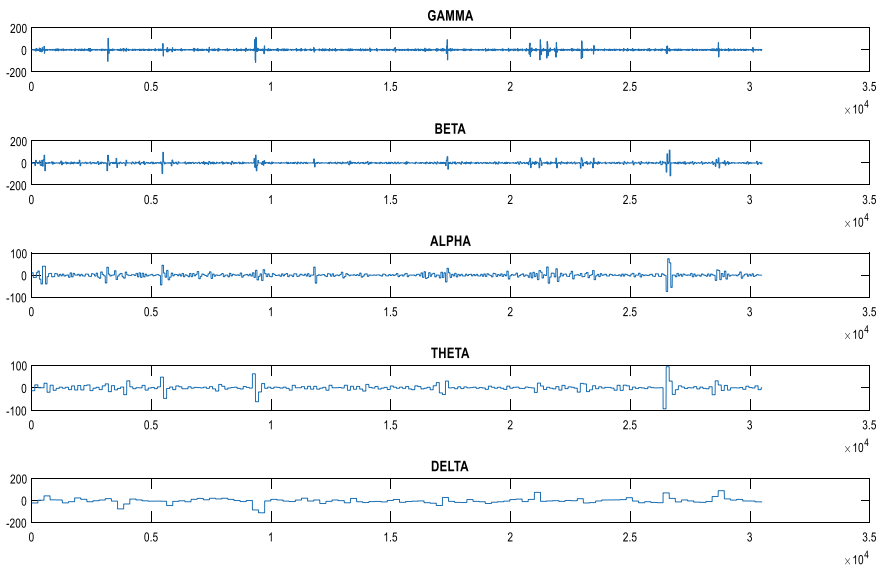


Fig. 5 Delta, theta, alpha, beta, and gamma sub-bands in the EEG

observed in the data may be due to blurred bandwidth or interpersonal variability. Figure 5 shows an example of EEG sub-bands.

3.2 Feature Extraction

The exact definition of a feature extraction problem depends on its context. But the most widely used definition is that feature extraction is the selection of a subset of features with the best result of the classification function [15, 20]. The rationale for this definition is that additional or irrelevant information in the data, including the signal of an image, often contains noise or similar information in the data, which causes the classifier function to be erroneous. Eliminating such features causes the resulting features to perform better or similar or higher in classification than the total features [41, 42]. As a direct result, fewer and more efficient features are required for storage, and thus, the classification process is accelerated [43]. In addition, reducing the number of features helps the expert system to focus on a subset of the relevant features, which gives it a better view of the process described by the data [18].

The purpose of feature extraction is to obtain the characteristics that contain the most separable information [17]. In feature extraction, all variables are used to transfer data (conversational or nonlinear) to the feature space with smaller dimensions. To reduce the bandwidth of the input data (which leads to improved speed) [21], the following benefits can be enumerated for feature extraction.

- Reduce the amount of space required for data storage
- Reduce computational time in data processing.
- Duplicate, unrelated data, and noise are removed.
- Improving data quality
- Algorithms that are inefficient on high-volume data can be used [43].
- Improves processing accuracy. Design machine learning processes will be improved.
- Pattern recognition processes such as clustering and classification will be improved [44].

Among the properties that can be extracted from brain signals are statistical properties in the time domain, discrete Fourier transform properties in the frequency domain, and multi-precision properties such as discrete wavelet transform.

3.3 A Set of Statistical Features

The set of statistical features that are extracted from brain signals for identification has received much attention from researchers [45]. These characteristics and statistical parameters are as follows: mean, variance, mode, median, stiffness, curvature (statistical third torque) (fourth statistical torque), minimum and maximum, Range. Other statistical parameters such as coefficient of variation (CV) as the ratio of SD standard deviation to the mean of the samples [42, 46, 47]. In a way, the scatter of data related to the mean of the statistical population is also defined. First and third quartiles (Q_1, Q_3), which indicate the density and compactness of the data, are also in this category. Quarter range, the IQR, also shows the deviation between the first and third quarters [48]. Table 2 shows the statistical characteristics.

3.4 Mathematical Transformations

In a general view, the purpose of applying a mathematical conversion to a signal is to obtain additional information that is not available in the original raw signal. In most processing approaches in engineering, the primary raw signal is the desired signal in the time domain [49]. The Fourier transform only indicates whether the frequency f is present in the signal, but it does not provide any information about the time interval corresponding to the occurrence of that frequency. Fourier transform is weak in analyzing unstable signals. The simplest idea that comes to mind is that a short part of an unstable signal can be assumed to be static. In the following, the most important available conversions will be introduced [50].

- **Fourier transform**
- Fourier Invariance and deformation instability.

Table 2 Statistical features

Description	Statistical feature	Number
The average of the values within the desired area of the signal	Average	1
The variance of the values within the desired area of the signal	Variance	2
Standard deviation of the values within the desired area of the signal	Standard deviation	3
Maximum values within the desired area of the signal	maximum	4
Min wax values within the desired area of the signal	minimum	5
Maximum and minimum difference	Area	6
The first, second, and third quarters in the values within the desired area of the signal	skewness	7
Intermediate levels of values within the target area of the signal	Middle	8
The highest repetition of the values within the desired area of the signal	Fashion	9
Peak in the statistical graph of the values within the desired area of the signal	Curve elongation	10
Skewness in the statistical graph of the values within the desired area of the signal	kurtosis	11
The entropy of the values within the desired region of the signal	entropy	12
As the ratio of SD standard deviation to the mean of the samples. Shows the scatter of data related to the mean of the statistical population	Coefficient of variation	13
Data density and compactness	First and third quarters (Q_1, Q_3),	14

Assume that the $\hat{x}(w) = \int x(u)e^{-iwu}du$ Fourier transform is a signal. If so, the February conversion would be. The absolute value of the $\hat{x}_c(w) = e^{-icw}\hat{x}(w)$ Fourier transform to the Fourier transform is stable because

$$|\hat{x}_c(w)| = |\hat{x}(w)| \quad (1)$$

A stability spectrometer of this conversion ϕ in the window in alternating periods T With $\int \phi(u)du = 1$. Records that are defined by Eq. (2).

$$|\hat{x}(t, w)| = \left| \int x(u)\phi(u-t)e^{-iwu}du \right| \quad (2)$$

In the event that $|c| \ll T$ Well, then we will

$$|\hat{x}_c(t, w)| \approx |\hat{x}(t, w)| \quad (3)$$

However, immutability is not a sufficient condition for time-shift. Assume that x is a transmitted and modified signal, that is $x_T(t)x(t-T)(t)$, $|T'(t)| < 1$. that is a function relative to stable changes if $\Phi(x)$ its Euclidean form, that is, $\|\Phi(x) - \Phi(x_T)\|$, is small enough at the time of change. The size of the deformation is measured with the $\sup_t |T'(t)|$ function. If this value is not zero, the net conversion is performed without change. Sustainability is usually defined by the Lipschitz continuity condition. In the sense that there is a value of $C > 0$ for $x(t)$ that $\sup_t |T'(t)| < 1$

$$\|\Phi(x) - \Phi(x_T)\| \leq C \sup_t |T'(t)| \|x\| \quad (4)$$

The constant C is a measure of stability.

The Lipschitz correlation criterion shows the overall linear variation with $\Phi(x)$. In fact, Lipschitz or the desired cohesion criteria can be derived anywhere. In fact, $\Phi(x) - \Phi(x_T)$ can be estimated with a linear operator, provided that $\sup_t |T'(t)|$ is small enough. In other words, a family of changes and shapes is produced in linear space. In the conversion space, no change in (stability to change) is created by transferring to the linear space.

The absolute value of Fourier $\Phi(x) = |\hat{x}|$ is not stable to changes because it changes a lot at high frequencies with small changes. For example, suppose there is a small delay $T(t) = \epsilon t$ where $0 < \epsilon \ll 1$. Since $T'(t) = \epsilon$, the Lipschitz continuity condition in Eq. (4) is defined as Eq. (5).

$$\|\hat{x} - |\hat{x}_T|\| \leq C \in \|x\| \quad (5)$$

Fourier transform $x_T(t) = x((1 - \epsilon)t)$ means $\hat{x}_T(w) = (1 - \epsilon)^{-1}\hat{x}((1 - \epsilon)^{-1}w)$. Transmission latency in frequency components is measured at frequency w_0 with $\epsilon |w_0|$. In a harmonic signal $x(t) = g(t) \sum_n a_n ((1 - \epsilon)t)$ in this case, the Fourier transform is calculated as (6)

$$\hat{x}(w) = \sum_n \frac{\alpha_n}{2} (\hat{g}(w - n\xi) + \hat{g}(w + n\xi)) \quad (6)$$

After time-warping, each part $\hat{g}(w \pm n\xi)$ is calculated with the value ($\epsilon n\xi$). If ϵ is very small, it $\epsilon n\xi$ will be larger than the latent band at high frequencies \hat{g} . As a result, the harmonics of $\hat{g}(w(1 - \epsilon)^{-1} - n\xi)$ from \hat{x}_T will not overlap with the harmonics of $\hat{g}(w(1 - \epsilon)^{-1} - n\xi)$ and \hat{x} . The Euclidean distance between $|\hat{x}_T|$ and $|\hat{x}|$ will not increase in proportion to ϵ . This proves that the condition for the stability of changes in Eq. (5) is not a condition for every $C > 0$ proof. The correlation $Rx(u) = \int x(t)x^*(t-u)dt$ with respect to changes is stable and the instability of changes for the absolute constraint of Fourier transform will be as follows [51].

$$\hat{R}r(w) = |\hat{x}(w)|^2 so \|Rx - Rx_T\| = (2\pi)^{-1} \left\| |\hat{x}|^2 - |\hat{x}_T|^2 \right\| \quad (7)$$

- **Stability to Mel frequency changes and filter banks**

Mel frequency spectroscopy calculates the average energy spectra with Mel-scale filters ψ_λ . The λ is average frequency of each $\hat{\psi}_\lambda(w)$ will be in relation (8).

$$Mx(t, \lambda) = \frac{1}{2} \int |\hat{x}(t, w)|^2 |\hat{\psi}_\lambda(w)|^2 dw \quad (8)$$

Intermediate filters $\hat{\psi}_\lambda$ have a fixed frequency value Q at high frequency. This frequency in the center supports λ width $\frac{\lambda}{Q}$. At low frequencies, instead of a constant value of Q the bandwidth will be $\hat{\psi}_\lambda$ equal to $\frac{2\pi}{T}$. Mean Mel frequencies cause the instability of large-magnitude changes in high frequency latency. If $x_T(t) = x((1-\epsilon)t)$, you can see the frequency components of w_0 transmitted with $\in |w_0|$. The higher the $|w_0|$, the greater the transfer. Although the $\hat{\psi}_\lambda(w)$ Mel-scale filter covers the frequency. And will have $\lambda/Q \sim |w_0|/Q$ bandwidth. As a result, the error associated with averaging $|\hat{\psi}|^2$ will be $\in Q$. After averaging the Mel frequency, the relative frequencies x_T, x will overlap at all frequencies, so we can write:

$$\|M_x(t, \lambda) - M_T x(t, \lambda)\| \leq C_\epsilon \|x\| \quad (9)$$

In this case, C is a constant value proportional to Q . This value is not dependent on x, ϵ . In contrast to Eq. (2), the Mel frequency spectrum of Eq. (8) satisfies the condition of the stability of the change in Lipschitz. Mell frequency averaging provides time-wrapping stability, but there is a loss of information. It is proved that this frequency average is equivalent to the average output of the filter bank, which creates a method to overcome data loss. Since $\hat{x}(t, w)$ in relation (2) the Fourier transform $x_t(u) = x(u)\phi(u-t)$ is performed with the condition of the Plancherel formula.

$$\begin{aligned} Mx(t, \lambda) & \frac{1}{2\pi} \int |\hat{x}_t(w)|^2 |\hat{\psi}_\lambda(w)|^2 dw \\ &= \int |\hat{x}_t * \psi_\lambda(v)|^2 dv \\ &= \int |x_t^* \psi_\lambda(v)|^2 dv \end{aligned} \quad (10)$$

If $\lambda \gg Q/T$ in this case, $\phi(t)$ will be almost constant to support $\psi_\lambda(t)$. Therefore:

$$\phi(u-t)\psi_\lambda(v-u) \approx \phi(v-t)\psi_\lambda(v-u) \quad (11)$$

$$\begin{aligned} Mx(t, \lambda) & \approx \int \left| \int x(u)\psi_\lambda(v-u) du \right|^2 |\phi(v-t)|^2 dv \\ &= |x * \psi_\lambda|_*^2 |\phi^2|(t) \end{aligned} \quad (12)$$

In other words, the average frequency of the spectrum will be approximately $|x * \psi_\lambda|_*^2 |\phi^2|$ at the time of averaging. In this regard, window ϕ is a pass-through filter. This filter is invariant locally to time changes [52].

- Wavelet transform and absolute magnitude

Q Fixed filter bank is used to calculate wavelet transform. Wavelet transform properties and its absolute magnitude are used to calculate scatter wavelet transform. A wavelet transform $\{\psi_\lambda\}$ is a transient filter. Suppose $\hat{\psi}(0) = 0$ mixed wavelets with a second-order phase of $\hat{\psi}(w) \approx 0$ to $w < 0$, and for every $\lambda > 0$ a dilated wavelet transform with a central frequency of λ is written as relation (13).

$$\begin{aligned}\hat{\psi}_\lambda(w) &= \hat{\psi}_\lambda(w) = \hat{\psi}\left(\frac{w}{\lambda}\right) \\ \psi_\lambda(t) &= \lambda \psi(\lambda t)\end{aligned}\quad (13)$$

The center frequency $\hat{\psi}$ is normalized to 1. Q is the number of filters required per octave. That is $\lambda = 2^{k/Q}$, the $K \in \mathbb{Z}$ bandwidth is $\hat{\psi}$ of the order to cover the entire frequency axis Q^{-1} with wavelet filters.. The function focuses $\psi_\lambda(w)$ on the value λ with the bandwidth $\frac{\lambda}{Q}$. In this case, the amount of energy $\psi_\lambda(t)$ around zero of an intervals $2\pi Q/\lambda$ should be less than T . It is ψ_λ defined based on Eq. (12). This value is set to $\lambda \geq \frac{2\pi Q}{T}$. $[0, 2\pi Q/T]$ For smaller intervals, the $\lambda < \frac{2\pi Q}{T}$ frequency is covered with filters approximately equal to $\hat{\psi}_\lambda$. The bandwidth of these filters is $2n/T$. To simplify, these low-pass filters are called wavelets. The expression Λ is used to represent a network of wavelets with a central frequency of λ . The wavelet transform of a signal is x , convolution x with a low-pass filter ϕ in bandwidth $2\pi/T$. Convolution is also at high frequencies ψ_λ for values $\lambda \in \Lambda$.

$$w_x = (x * \phi(t), x * \psi_\lambda(t))_{t \in R, \lambda \in \Lambda} \quad (14)$$

Indices and meanings of T are used as the basis for wavelet transform. Because it is repetitive enough. The wavelet ψ and ϕ the down-pass filter is designed to cover the filters at all relevant axis frequencies. In other words:

$$A(w) = |\hat{\phi}(w)|^2 + \frac{1}{2} \sum_{\lambda \in \Lambda} (|\hat{\psi}_\lambda(w)|^2 + |\hat{\psi}_\lambda(-w)|^2) \quad (15)$$

$$1 - \alpha \leq A(w) \leq 1 \text{ with } \alpha < 1 \quad (16)$$

This condition is such that the W wavelet transform is a stable and unchanging operator. Multiply Eq. (16) by $|\hat{x}(w)|^2$ use the Plancherel Equation.

$$(1 - \alpha) \|x\|^2 \leq \|Wx\|^2 \leq \|x\|^2 \quad (17)$$

In relation (17) $\|x\|^2 = \int |x(t)^2 dt|$ and W_x , the square is the sum of all the squares of the coefficients. In other words:

$$\|Wx\|^2 = \int |x * \phi(t)^2 dt| + \sum_{\lambda \in \Lambda} \int |x * \psi_\lambda(t)^2 dt| \quad (18)$$

The upper part of Equation (17) means that W is a contractionary operator. The lower part of this relation shows that W is a stable inverse. It will also retrieve X , W inverse overnight from Eq. (18).

$$x(t) = (x * \phi * \bar{\phi}(t) + \sum_{\lambda \in \Lambda} \text{Real}((x * \bar{\psi}_\lambda(t))) \quad (18)$$

Recovery filters are defined as relation (19).

$$\hat{\phi}(w) = \frac{\hat{\phi} * (w)}{A(w)}, \hat{\psi}_\lambda(w) = \frac{\hat{\psi}_\lambda^*(w)}{A(w)} \quad (19)$$

In this regard, $z*$ is the conjugate complex of $z \in C$. If is a value in relation (16) $\alpha = 0$, W is a tight operator, in this case $\bar{\phi}(t) = \phi(-t)$, $\bar{\psi}_\lambda(t) = \psi_\lambda^*(-t)$. By defining an analytical wavelet with octave resolution Q and $\bar{\psi}(t) = e^{it\theta}(t)$, we can have $\hat{\psi}(w) = \hat{\theta}(w - 1)$ this is a low-pass filter transfer function in this regard Q^{-1} . The bandwidth of this filter $\hat{\theta}(-1) \neq 0$ is of the order:

$$\begin{aligned} \hat{\psi}(w) &= \hat{\theta}(w - 1) - \hat{\theta}(w)\hat{\theta}(-1)/\hat{\theta}(0) \\ \hat{\psi}(0) &= 0 \end{aligned} \quad (20)$$

If θ it has a Gaussian distribution, ψ is called a Morlet wavelet. The Morelet analytic wavelet is very small but $|\hat{\psi}(w)|$ is larger than zero. Figure 3 shows Morlet, $\hat{\psi}_\lambda$ wavelets that $Q = 8$. In this case, the wavelet transform is obtained by selection ψ . This part is the real part of the wavelet that creates the persuasive bases like the cube spline. Based on Eq. (12), the mel frequency spectrum is approximated using nonlinear wavelet transform absolute value operators. In this case, the complex part of all wavelet coefficients is calculated as Eq. (21).

$$|w|x = (x * \varphi(t),) - |x * \psi_\lambda(t)|)_{t \in R, \lambda \in \Lambda} \quad (21)$$

Given the absolute value, the wavelet coefficients can be considered as Hilbert cap demodulation. Demodulation is used to separate carriers, and demodulation is used to place carriers and coatings. However, absolute value wavelength operators eliminate the mixed phase. But it does not delete any information from the signal because it holds the time changes of the signal.

A signal cannot be reconstructed from the absolute value of the Fourier transform but can be reconstructed from the absolute value of the wavelet transform. The

following time variable is sampled. In wavelet conversion, it can have more coefficients than the original signal. These coefficients are very repetitive and have a high frequency coverage. In many wavelet families, it can be proved that $|w|$ is a reversible operator whose inverse is continuous. Operator $|w|$ is a contractile operator, in other words W is contractile and complex. So that $\|a| - |b\| \leq |a - b|$ for each value is $(a, b) \in C^2$ because:

$$\||w|x - |W|x'\|_2 \leq \|Wx - Wx'\|_2 \leq \|x - x'\|^2 \quad (22)$$

Which is a tight frame operator such that:

$$\||w|x\| = \|Wx\| = \|x\| \quad (23)$$

Which $|x|$ is a soft signal [53].

3.5 Feature Selection

Dimension reduction is done in two ways: feature selection and feature extraction. In selecting a feature from the existing dataset and features, the desired features are selected. As a result, some features can be lost. In feature extraction, no feature is lost, but from the original data, based on the use of multiple methods, the desired properties are extracted. The comparison Table 3 shows the methods of feature extraction and feature selection [17].

Feature selection methods are used to select features from feature matrix, and these features are classified in four group as wrapper-based feature selection, filter-based feature selection correlation, embedded based feature selection, and hybrid-based feature selection.

Filter-based: filter-based feature selection algorithm begins with selecting a feature or for a subset of features with all the features in the database. They then use statistical criteria to select each feature to evaluate the desired features for the purpose of

Table 3 Comparison of feature extraction and feature selection

Advantages	Disadvantages	The main objective	Method
Maintain all features, consider the relationship between features	Data analysis with large volume is not useful and in the extracted properties, there are duplicate and unrelated values	Summarize data by using a linear combination of features in the data	Feature extraction
Maintain data structure and goals	The structure of the networks is not covered	Select related properties based on defined criteria	Feature selection

selection or purpose. Including Statistical Criteria can be Pearson coefficient [28]. Linear discriminant analysis (LDA), chi-squares, mutual information (MI), or other methods are used. All these statistical methods depend on the change feature in the database. Pearson coefficient methods and mutual information are among the most common statistical methods in the field of filtering. Filter methods: filter-based methods are used to select features from characteristics such as information gain, stability, dependence, correlation, and distance criterion.

Wrapper-based methods: Wrapper-based methods are known as black box methods. These methods have no information about the features. And the type of features selected are selected based on the learning methods. In other words, the features are selected based on the estimation of accuracy in the learning methods. Based on the accuracy obtained in the learning use, the features are selected. Wrapper-based methods have higher complexity but very high recent relative to filter-based methods that can be referred to the methods of selection hierarchical feature go forward, selection, hierarchical feature backwards, and methods based on evolutionary algorithms.

Embedded methods: Embedded methods for selecting a feature use learning-based method. Embedded methods work on a learning, compositional, and group basis. The use of group learning methods reduces the cost of computation. It also improves the accuracy of the classification. It should be noted that even by adding a feature to the feature set in question, the computational cost in this method does not increase. In the embedded methods, feature selection, and evaluation [54], learning is done simultaneously, while in the wrapper methods, the feature selection process is done after learning. Simultaneous performance of learning is done in these methods.

Hybrid methods: Hybrid methods are used based on the type of strategy feature selection, the combination of filters and rappers. The purpose of hybrid methods is to overcome weaknesses in any of the methods and to strengthen the existing strengths. In other words, the combination of the wrapper method with the filter covers the weaknesses of the wrapper method with the filter method and vice versa. Table 4 shows a comparison of these methods.

Challenges of Feature Selection: Although there are many benefits to defining a feature, it will bring with it challenges. For example, it is possible that the feature selection method, which reduces the features, complicates the classification operation and the classification can give a good result. Also, the existence of unbalanced data in classes in the database can cause problem selection. Unbalanced data are data that have several properties in one class that are different from other classes.

Today, the role of data mining and knowledge discovery is very important in digital software. In data mining, data is processed, and knowledge is extracted and identified from data processing. Today, data is not produced in different dimensions and types. The size of the data, the complexity, and even the diversity are evolving day by day. A large database in addition to Holding High number of features also have a very large number of events. On the contrary, the increase in the volume of data has made machine learning and data mining algorithms difficult. Increase the volume

Table 4 Comparison methods of selection feature based on type of learning

Strengths	Weaknesses	Feature selection methods
<ul style="list-style-type: none"> • Computationally effective and light • Independent of learning methods • Faster than other methods is like a wrapper • The correlation between the features is taken into account 	<ul style="list-style-type: none"> • Correlation between classifications is not considered • Causes more overfitting in classification 	Filter-based
<ul style="list-style-type: none"> • Correlation between features and tags is considered • Dependence between classifications is considered • It has higher accuracy than filter methods • Can be used in small data 	<ul style="list-style-type: none"> • They are computationally complex • The evaluation of the selected features is done repeatedly • The feature selection for classification at the beginning is random • Create more fit in the category • Overflow in search 	wrapper-based
<ul style="list-style-type: none"> • Computationally, they are relatively lighter than the wrapper method • They have a higher accuracy than the wrapper and filter method 	<ul style="list-style-type: none"> • In terms of computational cost, they are more complex than the filter method • Not suitable for high dimensions in data 	Embedded-based

data caused. Pattern identification, classification, and other data mining processes can be problematic. Large data databases usually contain duplicate and unrelated data. On the contrary, unrelated and repetitive features will also impair data mining performance. To overcome these challenges, methods of reduction in data have been proposed. In reducing data, repeat and unrelated filter. Reduced Dimension data usually have the least repetitive, irrelevant, and even noise characteristics.

4 Literature Review

4.1 Epilepsy

Ahmadvou et al. [55] used different fractal dimension-based methods called KATZ and Higuchi methods to detect Alzheimer's in EEG signals. In the proposed method, after removing the noise with a filter, the fractal dimension properties were extracted and then the relevant identification was performed using SVM classification. The accuracy of the proposed method is reported to be 99%. The proposed method uses only the fractal dimension, but does not discuss which sub-band has the most information about amnesia.

Bruna et al. [56] presented an entropy-based method for distinguishing MCI from AD and normal state in signal Magnetoencephalography MEG. The authors conclude that the amount of entropy in people with MCI in the anterior region is higher than in healthy people. Using a reduction in entropy, the accuracy of MCI diagnosis of AD from AD and healthy individuals was reported to be %65. In the proposed method based on entropy, only the distinction between signal recording regions in Alzheimer's diagnosis is presented. The accuracy provided is very low, and it seems that the use of more features can improve the accuracy of identification.

Sankari et al. [57] proposed a convergent wavelet model for the diagnosis of Alzheimer's disease in healthy individuals using EEG signals. The results show that a decrease in the amount of convergent wavelet is seen in the central anterior region in the delta band of Alzheimer's patients. The accuracy of Alzheimer's disease detection in this method is %86. Although in the proposed method the differentiating region of the EEG signal as well as the corresponding band is determined, the accuracy of the proposed method is very low.

Ahmadolou et al. [58] in another study in 2014 proposed two new criteria for brain network complexity in diagnosing people with MCI and AD and healthy people with MEG signals. The achieved accuracy is reported to be %97. The proposed criteria are efficiency complexity of the EC and the IC Index complexity. The results show that the amount of EC can differentiate healthy people from people with MCI.

Houmani et al. [59] presented iteration-based entropy (EE) for people with Alzheimer's disease on EEG signals. The accuracy obtained is reported to be %83, and it is also claimed that this value is improved by using Shannon entropy. The accuracy obtained is very poor. Also, the area of EEG signal recording and band effective in identifying and distinguishing AD patients from healthy individuals has not been determined.

Amezquita and Sanchez [60] developed a new method for identifying healthy individuals with Alzheimer's disease (AD) using EEG signals, using Sternberg's task of the master combination of combined experimental analysis, permutation entropy, and improved, enhanced probabilistic EPNN probability as the feature used. The accuracy obtained is reported to be 98.4%.

Mammone et al. [61] presented the Shift Non-Adjustment Index or PDI to classify and identify MCI individuals from AD. Relevant features are extracted from EEG signals. The results of the proposed method show that the amount of PDI in the delta and theta bands is high in MCI patients and if this amount is increased, the risk of converting MCI to AD will be high. The accuracy of identification in the proposed method is reported to be 91%.

Mamun et al. [62] have proposed another measure called the 12PJD permutation jacquard distance to determine the internal changes in the electrical connections of the brain. The proposed PJD criterion evaluates longitudinal changes in four MCI patients with AD. The results show that the amount of PJD in the delta and theta bands of people who have changed from MCI to AD is higher than healthy people or even MCI people.

Amezquita and Sanchez [3] have introduced a new method based on signal processing called multiple signal classification and experimental wavelet transform

MUSIC-EWT. In addition to the experimental wavelet transform properties, the proposed method uses other features such as fractal dimension properties, turbulence theory, and probabilistic neural network model to be able to predict MCI. In the proposed method, although several features have been extracted for identification, %90 of the obtained identification accuracy has been reported. Computational complexity of the method presented above [3].

In 2021, Ramos used the LSTM Deep Learning and Long-Term Memory Model to detect Parkinson's (EEG) signals. In the simulations as well as various performances in the proposed method, %99 accuracy indicates the superiority of the proposed method. In the proposed method, he has used the database in UCI and based on the features extracted from this database, and he has taught deep learning and LSTM models with the relevant training data. Finally, it evaluated the accuracy with the test data [63].

4.2 *Parkinson's Disease*

In 2021, Sharma et al. used a deep neural network-based classification method. The properties extracted in the proposed method are classified both by the support vector machine classifier and by the soft classifier. Finally, they are weighed against the evaluation criteria. The results obtained in the classification (SVM) in the accuracy criterion of 83% and in the soft classification are 87% [64].

In 2020, Oliveira et al. diagnosed (PD) using relative partial directed (PDC) features. The extracted features are classified by a Benign neural network and a Bayesian classifier. The accuracy of the proposed method is reported to be %91. Although in the proposed method, noise and artifacts are removed using preprocessing methods, it seems that the extracted features are not well separable [4].

Byeon et al. [65] states that mild cognitive impairment begins with (MCI). To identify the disease in its early stages, an improved randomized forest-based method has been proposed. The proposed method used random forest prediction (MCI) to diagnose Parkinson's. The proposed method is compared with the split tree as well as the regression. The obtained results indicate the superiority of the proposed method.

In 2020, Anjoum et al. used Linear-predictive-coding EEG algorithm in spectral properties for diagnosis (PD). In the proposed methods, spectral properties are extracted from different bands in the signal (EEG) and then linearly predicted coding, the most effective properties are selected and classified by a 5-fold classifier. The accuracy of the proposed method is reported to be %93. Although the linear prediction coding method is strong in feature selection, it seems that the classifier used does not have a high capability in classification [66].

In 2020, Kaya et al. Minimum Redundancy Maximum Relevance (mRMR) in a SVM classifier. They used the LOSO method as a cross-validation technique for their model to prevent Bias deviations. In a Leave One Subject Out (LOSO) (LOSO), all

of a person's audio samples that fit the test sample will be removed from the rest of the data. Their approach has achieved %92.75 classification accuracy [67].

In 2019, Bhurane et al. used the Self-similarity features to diagnose Parkinson's disease from EEGs. In the proposed method, similar properties between the two channels, correlation coefficients, and prediction coefficients are extracted from both channels. They are then categorized using the vector machine classification. Also, the feature selection method based on scoring and principal component analysis is used to select the most effective features. The accuracy of the proposed method is reported to be 98%. In the proposed method, although the properties of the time domain are extracted and conversion-based methods are no longer needed, but since the uncertainty (EEG) is very high, it seems that this method is very sensitive to noise. In the presence of noise, the performance of this method is very challenging [68].

In 2019, Wang et al. focused on monitoring the progression of Parkinson's disease by feature extraction using signal processing techniques and used a large database of 6000 samples from 42 patients in the early stages of Parkinson's disease. They attempted to estimate the disease in the early stages using linear and nonlinear regression. Their results are 7.5 points with different clinical estimates. These three main datasets are publicly available in the field of Parkinson's disease research [69].

In 2018, Biagioni presented an intelligent workflow to diagnose Parkinson's disease. In this chapter, the support vector machine classifier is improved by the forging bacterium optimization algorithm. The proposed method is compared with other methods in which classification (SVM) is combined with particle swarm optimization (PSO) as well as relief feature selection. The results show the superiority of the proposed method. Kai explicitly states that SVM is one of the most widely used classifications in identifying patients with PD. In classification (SVM), a compromise can be made between minimizing training set error and maximizing margin in order to achieve optimal generalizability while avoiding overfitting [70].

In 2017, Hassan et al. presented a hybrid method in which multiple methods are used in preprocessing and feature extraction. Then, several classifications have been used and with the proposed combination, they have reached %95 accuracy in the prediction. %95 accuracy has been achieved [71].

In 2017, Fayyazifar [72] proposed a way to fill the gap between feature selection and classification of duplicate data. The proposed system uses fewer features for classification and has a higher recognition rate than other methods. As a result, in addition to reducing the computational load, the complexity of the forecasting system is also reduced. In these two proposed methods, first the genetic algorithm is applied to reduce the feature vector size and select the optimal feature set. AdaBoost and Bagging methods are then used to classify the input data into healthy and diseased categories. In the first method, after applying AdaBoost, the feature vector size is reduced from 22 to seven features and the recognition rate is 98.28%. In the second method, after selecting 10 features (as optimal features) with genetic algorithm, the recognition rate was 96.55%. The genetic algorithm is then re-applied to the optimal feature vector obtained from the previous experiment to reduce the number of features

if possible. Finally, by generalizing the genetic algorithm for 15 times, using only six characteristics, they have achieved the same 96.55% accuracy.

5 Conclusion

With the advancement of technology, especially in the health industry, human life expectancy has increased, and the population of the elderly community is expanding day by day. Alzheimer's and Parkinson's are among the diseases that seriously threaten this population. Early detection of these diseases can help doctors to treat them. EEG is one of the cheapest and most reliable methods for diagnosing these diseases. Several methods have been proposed to diagnose the disease in machine-based EEG. Machine learning methods include preprocessing, feature extraction and selection, classification, and evaluation. This chapter presents the different sections of the diagnosis of these diseases. It also provides an overview of the latest research in this area.

Conflicts of Interest

There is no conflicts of interest in this chapter.

References

1. Ramzan, F., Khan, M.U.G., Rehmat, A., Iqbal, S., Saba, T., Rehman, A., Mehmood, Z.: A deep learning approach for automated diagnosis and multi-class classification of alzheimer's disease stages using resting-state fMRI and residual neural networks. *J. Med. Syst.* **44**(2), 37 (2020)
2. Sajjad, M., Ramzan, F., Khan, M.U.G., Rehman, A., Kolivand, M., Fati, S.M., Bahaj, S.A.: Deep convolutional generative adversarial network for Alzheimer's disease classification using positron emission tomography (PET) and synthetic data augmentation. *Microsc. Res. Tech.* **84**(12), 3023–3034 (2021). <https://doi.org/10.1002/jemt.23861>
3. Amezquita-Sanchez, J.P., Mammone, N., Morabito, F.C., Marino, S., Adeli, H.: A novel methodology for automated differential diagnosis of mild cognitive impairment and the Alzheimer's disease using EEG signals. *J. Neurosci. Methods* **322**, 88–95 (2019)
4. Yousaf, K., Mehmood, Z., Awan, I.A., Saba, T., Alharbey, R., Qadah, T., & Alridge, M.A.: A comprehensive study of mobile-health based assistive technology for the healthcare of dementia and Alzheimer's disease (AD). *Health Care Manage. Sci.* 1–23 (2019)
5. Abbas, N., Saba, T., Mohamad, D., Rehman, A., Almazyad, A.S., Al-Ghamdi, J.S.: Machine aided malaria parasitemia detection in Giemsa-stained thin blood smears. *Neural Comput. Appl.* **29**(3), 803–818 (2018)
6. Amin, J., Sharif, M., Raza, M., Saba, T., Rehman, A.: Brain Tumor classification: feature fusion. In: 2019 International Conference on Computer and Information Sciences (ICCIS), pp. 1–6. IEEE (2019)
7. Iqbal, S., Khan, M.U.G., Saba, T., Mehmood, Z., Javaid, N., Rehman, A., Abbasi, R.: Deep learning model integrating features and novel classifiers fusion for brain tumor segmentation. *Microsc. Res. Tech.* **82**(8), 1302–1315 (2019). <https://doi.org/10.1002/jemt.23281>
8. Khan, M.A., Kadry, S., Zhang, Y.D., Akram, T., Sharif, M., Rehman, A., Saba, T.: Prediction of COVID-19-pneumonia based on selected deep features and one class kernel extreme learning machine. *Comput. Electr. Eng.* **90**, 106960 (2021)

9. Khan, A.R., Khan, S., Harouni, M., Abbasi, R., Iqbal, S., Mehmood, Z.: Brain tumor segmentation using K-means clustering and deep learning with synthetic data augmentation for classification. *Microsc. Res. Tech.* (2021)
10. Zou, B., Liu, Y., Guo, M., Wang, Y.: EEG-based assessment of stereoscopic 3D visual fatigue caused by vergence-accommodation conflict. *J. Disp. Technol.* **11**(12), 1076–1083 (2015)
11. Khan, M.A., Sharif, M.I., Raza, M., Anjum, A., Saba, T., Shad, S.A.: Skin lesion segmentation and classification: a unified framework of deep neural network features fusion and selection. *Expert Syst. e12497* (2019)
12. Javed, R., Rahim, M.S.M., Saba, T., Rehman, A.: A comparative study of features selection for skin lesion detection from dermoscopic images. *Netw. Model. Anal. Health Inf. Bioinf.* **9**(1), 1–13 (2020)
13. Jamal, A., Hazim Alkawaz, M., Rehman, A., Saba, T.: Retinal imaging analysis based on vessel detection. *Microsc. Res. Tech.* **80**(7), 799–811 (2017)
14. Perveen, S., Shahbaz, M., Saba, T., Keshavjee, K., Rehman, A., Guergachi, A.: Handling irregularly sampled longitudinal data and prognostic modeling of diabetes using machine learning technique. *IEEE Access* **8**, 21875–21885 (2020)
15. Nazir, M., Khan, M.A., Saba, T., Rehman, A.: Brain tumor detection from MRI images using multi-level wavelets. In: 2019 International Conference on Computer and Information Sciences (ICCIS), pp. 1–5. IEEE (2019)
16. Aryamehr, S., Karimi, M., Boroujeni, F.Z. (eds.): CVBL IRIS gender classification database image processing and biometric research, computer vision and biometric laboratory (CVBL). In: 2018 IEEE 3rd International Conference on Image, Vision and Computing (ICIVC). IEEE (2018)
17. Khan, A.R., Doosti, F., Karimi, M., Harouni, M., Tariq, U., Fati, S.M., et al.: Authentication through gender classification from iris images using support vector machine. *Microsc. Res. Tech.* (2021)
18. Li, J., Cheng, K., Wang, S., Morstatter, F., Trevino, R.P., Tang, J., et al.: Feature selection: a data perspective. *ACM Comput. Surv. (CSUR)* **50**(6), 94 (2018)
19. Rehman, A., Harouni, M., Karimi, M., Saba, T., Bahaj, S.A., Awan, M.J.: Microscopic retinal blood vessels detection and segmentation using support vector machine and K-nearest neighbors. *Microsc. Res. Tech.*
20. Raftarai, A., Mahounaki, R.R., Harouni, M., Karimi, M., Olghoran, S.K.: Predictive models of hospital readmission rate using the improved AdaBoost in COVID-19. In: Intelligent Computing Applications for COVID-19, pp. 67–86. CRC Press (2021)
21. Meethongjan, K., Dzulkifli, M., Rehman, A., Altameem, A., Saba, T.: An intelligent fused approach for face recognition. *J. Intell. Syst.* **22**(2), 197–212 (2013). <https://doi.org/10.1515/jisy-2013-0010>
22. Lung, J.W.J., Salam, M.S.H., Rehman, A., Rahim, M.S.M., Saba, T.: Fuzzy phoneme classification using multi-speaker vocal tract length normalization, *IETE Tech. Rev.* **31**(2), 128–136 (2014). <https://doi.org/10.1080/02564602.2014.892669>
23. As, A.: 2018 Alzheimer's disease facts and figures. *Alzheimers Dement.* **14**(3), 367–429 (2018)
24. Putri, F.T., Ariyanto, M., Caesarendra, W., Ismail, R., Pambudi, K.A., Pasmanasari, E.D.: Low cost Parkinson's disease early detection and classification based on voice and electromyography signal, pp. 397–426. Springer, Computational Intelligence for Pattern Recognition (2018)
25. Goetz, C.G.: The history of Parkinson's disease: early clinical descriptions and neurological therapies. *Cold Spring Harb. Perspect. Med.* **1**(1), a008862 (2011)
26. Ramzan, F., Khan, M.U.G., Iqbal, S., Saba, T., Rehman, A.: Volumetric segmentation of brain regions from MRI scans using 3D convolutional neural networks. *IEEE Access* **8**, 103697–103709 (2020)
27. Nawaz, M., Mehmood, Z., Nazir, T., Naqvi, R.A., Rehman, A., Iqbal, M., Saba, T.: Skin cancer detection from dermoscopic images using deep learning and fuzzy k-means clustering. *Microsc. Res. Tech.* **85**(1), 339–351 (2022)
28. Durand, D., McCallum, G., Qiu, C.: Interfacing with the peripheral nervous system (pns) using targeted fascicular interface device. Google Patents (2019)

29. Guo, T., Chen, L., Tran, K., Ghelich, P., Guo, Y.-S., Nolta, N., et al.: Extracellular single-unit recordings from peripheral nerve axons in vitro by a novel multichannel microelectrode array. *Sens. Actuators, B Chem.* **315**, 128111 (2020)
30. Badura, A., Maśłowska, A., Myśliwiec, A., Piętka, E.: Multimodal signal analysis for pain recognition in physiotherapy using wavelet scattering transform. *Sensors* **21**(4), 1311 (2021)
31. Dabas, H., Sethi, C., Dua, C., Dalawat, M., Sethia, D. (eds.): Emotion classification using EEG signals. In: Proceedings of the 2018 2nd International Conference on Computer Science and Artificial Intelligence (2018)
32. Zhang, J., Yin, Z., Chen, P., Nichele, S.: Emotion recognition using multi-modal data and machine learning techniques: a tutorial and review. *Information Fusion* **59**, 103–126 (2020)
33. San-Segundo, R., Gil-Martín, M., D'Haro-Enríquez, L.F., Pardo, J.M.: Classification of epileptic EEG recordings using signal transforms and convolutional neural networks. *Comput. Biol. Med.* **109**, 148–158 (2019)
34. Bagheri, M., Power, S.D.: EEG-based detection of mental workload level and stress: the effect of variation in each state on classification of the other. *J. Neural Eng.* (2020)
35. Martínez-Tejada, L.A., Maruyama, Y., Yoshimura, N., Koike, Y.: Analysis of personality and EEG features in emotion recognition using machine learning techniques to classify arousal and valence labels. *Mach. Learn. Knowl. Extr.* **2**(2), 99–124 (2020)
36. Singh, A., Kingsbury, N.: Multi-resolution dual-tree wavelet scattering network for signal classification. arXiv preprint arXiv:170203345 (2017)
37. Sheela, P., Puthankattil, S.D.: A hybrid method for artifact removal of visual evoked EEG. *J. Neurosci. Methods* **336**, 108638 (2020)
38. Bera, A., Das, N., Chakraborty, M. (eds.): Optimal filtering of single channel EEG data using linear filters. In: 2020 Sixth International Conference on Bio Signals, Images, and Instrumentation (ICBSII). IEEE (2020)
39. Subha, D.P., Joseph, P.K., Acharya, R., Lim, C.M.: EEG signal analysis: a survey. *J. Med. Syst.* **34**(2), 195–212 (2010)
40. de Munck, J.C., Gonçalves, S.I., Mammoliti, R., Heethaar, R.M., Da Silva, F.L.: Interactions between different EEG frequency bands and their effect on alpha-fMRI correlations. *Neuroimage* **47**(1), 69–76 (2009)
41. Ramírez-Gallego, S., Mouríño-Talín, H., Martínez-Rego, D., Bolón-Canedo, V., Benítez, J.M., Alonso-Betanzos, A., et al.: An information theory-based feature selection framework for big data under apache spark. *IEEE Trans. Syst. Man Cybern. Syst.* **48**(9), 1441–1453 (2018)
42. Rehman, A., Harouni, M., Karchegani, N.H.S., Saba, T., Bahaj, S.A., Roy, S.: Identity verification using palm print microscopic images based on median robust extended local binary pattern features and k-nearest neighbor classifier. *Microsc. Res. Tech.* (2021)
43. Karimi, M., Harouni, M., Nasr, A., Tavakoli, N.: Automatic lung infection segmentation of Covid-19 in CT scan images. In: Intelligent Computing Applications for COVID-19, pp. 235–53. CRC Press (2021)
44. Wan-Hui, W., Yu-Hui, Q., Guang-Yuan, L. (eds.): Electrocardiography recording, feature extraction and classification for emotion recognition. In: 2009 WRI World Congress on Computer Science and Information Engineering. IEEE (2009)
45. Harouni, M., Karimi, M., Rafieipour, S.: Precise segmentation techniques in various medical images. *Artif. Intell. Internet of Things Appl. Smart Healthc.* 117 (2021)
46. Habibi, N., Harouni, M.: Estimation of re-hospitalization risk of diabetic patients based on radial base function (RBF) neural network method combined with colonial competition optimization algorithm. *Majlesi J. Electr. Eng.* **12**(1), 109–116 (2018)
47. Mohammadi Dashti, M., Harouni, M.: Smile and laugh expressions detection based on local minimum key points. *Signal Data Process.* **15**(2), 69–88 (2018)
48. Sinha, N., Babu, D. (eds.): Statistical feature analysis for EEG baseline classification: Eyes Open vs Eyes Closed. In: 2016 IEEE Region 10 Conference (TENCON). IEEE (2016)
49. Karimi, M., Harouni, M., Rafieipour, S.: Automated Medical Image Analysis in Digital Mammography, pp. 85–116. CRC Press, Artificial Intelligence and Internet of Things (2021)

50. Vincent, L., El-Hajj, C., Mathias, R., Grégoire, L., Joakim, A., Mathieu, L.: Time–frequency scattering accurately models auditory similarities between instrumental playing techniques. *EURASIP J. Audio Speech Music Process.* **2021**(1), (2021)
51. Rehman, A., Khan, M.A., Saba, T., Mehmood, Z., Tariq, U., Ayesh, N.: Microscopic brain tumor detection and classification using 3D CNN and feature selection architecture. *Microsc. Res. Tech.* **84**(1), 133–149 (2021). <https://doi.org/10.1002/jemt.23597>
52. Rehman, A., Abbas, N., Saba, T., Mehmood, Z., Mahmood, T., Ahmed, K.T.: Microscopic malaria parasitemia diagnosis and grading on benchmark datasets. *Microsc. Res. Tech.* **81**(9), 1042–1058 (2018). <https://doi.org/10.1002/jemt.23071>
53. Rehman, A., Saba, T.: Performance analysis of character segmentation approach for cursive script recognition on benchmark database, *Digit. Signal Process.* **21**(3), 486–490 (2011). <https://doi.org/10.1016/j.dsp.2011.01.016>
54. Harouni, M., Baghmaleki, H.Y.: Color image segmentation metrics. *Encycl. Image Process.* **95** (2018)
55. Ahmadlou, M., Adeli, H., Adeli, A.: Fractality and a wavelet-chaos-methodology for EEG-based diagnosis of Alzheimer disease. *Alzheimer Dis. Assoc. Disord.* **25**(1), 85–92 (2011)
56. Bruña, R., Poza, J., Gomez, C., Garcia, M., Fernandez, A., Hornero, R.: Analysis of spontaneous MEG activity in mild cognitive impairment and Alzheimer’s disease using spectral entropies and statistical complexity measures. *J. Neural Eng.* **9**(3), 036007 (2012)
57. Sankari, Z., Adeli, H., Adeli, A.: Wavelet coherence model for diagnosis of Alzheimer disease. *Clin. EEG Neurosci.* **43**(4), 268–278 (2012)
58. Ahmadlou, M., Adeli, A., Bajo, R., Adeli, H.: Complexity of functional connectivity networks in mild cognitive impairment subjects during a working memory task. *Clin. Neurophysiol.* **125**(4), 694–702 (2014)
59. Houmani, N., Dreyfus, G., Vialatte, F.B.: Epoch-based entropy for early screening of Alzheimer’s disease. *Int. J. Neural Syst.* **25**(08), 1550032 (2015)
60. Amezquita-Sanchez, J.P., Adeli, A., Adeli, H.: A new methodology for automated diagnosis of mild cognitive impairment (MCI) using magnetoencephalography (MEG). *Behav. Brain Res.* **305**, 174–180 (2016)
61. Mammone, N., Bonanno, L., Salvo, S.D., Marino, S., Bramanti, P., Bramanti, A., et al.: Permutation disalignment index as an indirect, EEG-based, measure of brain connectivity in MCI and AD patients. *Int. J. Neural Syst.* **27**(05), 1750020 (2017)
62. Mammone, N., Ieracitano, C., Adeli, H., Bramanti, A., Morabito, F.C.: Permutation Jaccard distance-based hierarchical clustering to estimate EEG network density modifications in MCI subjects. *IEEE Trans. Neural Netw. Learn. Syst.* **29**(10), 5122–5135 (2018)
63. Ramos, A.A., Machado, L.: A comprehensive meta-analysis on short-term and working memory dysfunction in Parkinson’s disease. *Neuropsychol. Rev.* 1–24 (2021)
64. Sharma, G., Parashar, A., Joshi, A.M.: DepHNN: A novel hybrid neural network for electroencephalogram (EEG)-based screening of depression. *Biomed. Signal Process. Control* **66**, 102393 (2021)
65. Byeon, H.: Is the Random forest algorithm suitable for predicting Parkinson’s disease with mild cognitive impairment out of Parkinson’s disease with normal cognition? *Int. J. Environ. Res. Public Health* **17**(7), 2594 (2020)
66. Anjum, M.F., Dasgupta, S., Mudumbai, R., Singh, A., Cavanagh, J.F., Narayanan, N.S.: Linear predictive coding distinguishes spectral EEG features of Parkinson’s disease. *Parkinsonism Relat. Disord.* **79**, 79–85 (2020)
67. Kaya, D.: The mRMR-CNN based influential support decision system approach to classify EEG signals. *Measurement* **156**, 107602 (2020)
68. Bhurane, A.A., Dhok, S., Sharma, M., Yuvaraj, R., Murugappan, M., Acharya, U.R.: Diagnosis of Parkinson’s disease from electroencephalography signals using linear and self-similarity features. *Expert Syst. e12472* (2019)
69. Wang, S.-H., Zhang, Y.-D., Yang, M., Liu, B., Ramirez, J., Gorri, J.M.: Unilateral sensorineural hearing loss identification based on double-density dual-tree complex wavelet transform and multinomial logistic regression. *Integr. Comput.-Aided Eng.* **26**(4), 411–426 (2019)

70. Biagioli, M.C., Sharma, K., Migdadi, H.A., Cucca, A.: Non-invasive neuromodulation therapies for Parkinson's disease. In: Parkinson's Disease-Understanding Pathophysiology and Developing Therapeutic Strategies. IntechOpen (2018)
71. Hassan, A.R., Bhuiyan, M.I.H.: Automated identification of sleep states from EEG signals by means of ensemble empirical mode decomposition and random under sampling boosting. *Comput. Methods Programs Biomed.* **140**, 201–210 (2017)
72. Fayyazifar, N., Samadiani, N. (eds.): Parkinson's disease detection using ensemble techniques and genetic algorithm. In: 2017 Artificial Intelligence and Signal Processing Conference (AISP). IEEE (2017)

Skin Lesion Detection Using Recent Machine Learning Approaches



Ihtishaam ul haq, Javeria Amin, Muhammad Sharif,
and Muhammad Almas Anjum

Abstract Traditional and deep learning approaches act a significant performance in the medical fields. They have been used to identify various illnesses on the early stage. Countless death rates were recorded in the last two decades due to cancer. Out of these cases, skin cancer was the highest popular form of cancer. Sunlight, ultraviolet rays, moles, and many other reasons cause skin cancer. Skin cancer can be treated if it is diagnosed at the premature stage. Manually diagnosing skin cancer is a time-consuming procedure, requiring a lot of human power while it is a grueling procedure. Various approaches for automatically detecting skin cancer have now been developed in recent years as technology has improved. In this chapter skin lesion detection steps like preprocessing (to remove noise from images), segmentation (to get skin lesion location), feature extraction, feature selection, and classification methods have been discussed in detail. Furthermore limitation, gaps in the domain of skin lesions are also discussed that provide help for the researchers.

Keywords Skin lesion detection · Preprocessing · Hand-crafted feature extraction and selection · Deep feature extraction · Machine learning · Deep learning · Classification

1 Introduction

Skin cancer has become the ultimate dangerous disease in all continents. It is one out of every five tumors [1]. Out of all types of skin cancer, melanoma is common. It penetrates our body rapidly and is curable if identified in the initial stages [2]. Early

I. ul haq · M. Sharif (✉)

Department of Computer Science, COMSATS University Islamabad, Wah Campus, Pakistan
e-mail: sharif@ciitwah.edu.pk

J. Amin

Department of Computer Science, University of Wah, Wah Cantt, Pakistan
e-mail: javeria.amin@uow.edu.pk

M. Almas Anjum

National University of Technology (NEUTCH), Islamabad, Pakistan

prediction is a necessity because it leads to increased survival. The 5-year initial stage viability rate of Aggressive melanoma is 94% relative to 5-year survival. It spread to too many other parts of the human body [3]. So according to the medical records, any of the skin patients with ten or more dysplastic nevi have a twelve-time chance. Several test devices are made for melanoma detection to emulate the experience of dermatologists by finding. Cases of skin lesions are on the rise every day and are a significant source of the growing burden of disease. Skin lesions are the fifth source of the global disease burden [4]. The conventional way of identifying melanoma is long-term intrusive and painful. Computerized systems may use to overcome this situation. Which are depicted in Fig. 1.

Skin cancer is a rapidly increasing disease all over the world according to the WHO reports. Therefore, in this chapter, the following are the important questions discussed for the comprehensive examination:

- i. Which are the most common and effective methods in traditional and machine learning that use for skin lesion detection?
- ii. Which are the benchmark datasets being available for skin lesion detection and what are their characteristics?

The chapter organization as follows. Section 2 gives an overview of image pre-processing techniques. The vital step in skin cancer classification is segmentation that is expressed in Sect. 3. A detailed overview of the hand-crafted feature extraction and selection methods is marked out in Sect. 4. Deep feature extraction methods are discussed in Sect. 5. Different classification techniques that give the best results are elaborated in Sect. 6. Section 7 has the information about available benchmark datasets. Challenges in skin lesion detection are discussed in Sect. 8. Lastly, Sect. 9 is described the chapter summary.

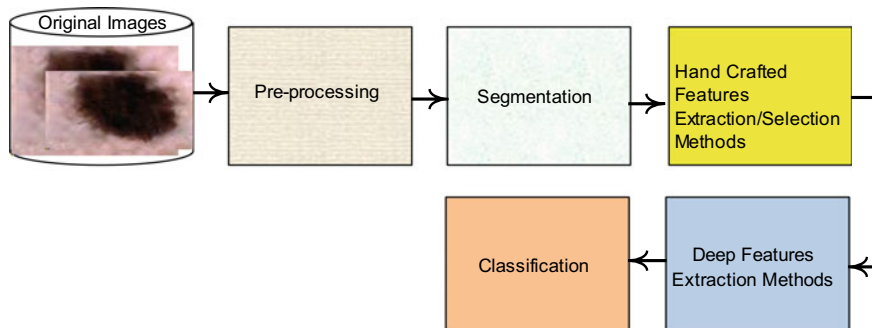


Fig. 1 General steps for skin lesion detection [5]

2 Preprocessing

The first and vital goal of preprocessing stage is to eliminate artifacts that diminish the computer-aided system accuracy. Lesion spots and surrounding skin are in proper order. Therefore, lesion detection is a crucial problem for an expert dermatologist. Skin images include particular objects such as black background, dermoscopic gel, black mole, black frames, and the hair on the skin [6]. Other artefacts such as the eyes, blood vessels, and skin folds can affect the detection of skin lesions [7]. To reduce these artifacts preprocessing is necessary. Many researchers used dull razor for hair removal. It is online available for research purposes [8]. Such artifacts create a border detection barrier and result in loss of accuracy and higher computational costs. So, few techniques are compulsory to eliminate these objects to improve the effectiveness of classification and segmentation. Something that generates an obstacle in border detection has to be identified and also substituted. Different researchers use different approaches like contrast adjustment [9], filtering [10], color quantization [11], image resizing, hair removal, and cropping [12]. The median filter [13–16] is the most effective approach used to remove artifacts in dermoscopic images. It has been broadly used in digital image processing (DIP). It removes the noise but preserves the edges [17]. It is a non-linear method of smoothing. Slide the mask (3×3 or 5×5) on the whole image and median value set in the center pixel. For the elimination of black frames, various researchers have suggested and adopted specific strategies [18]. Ellipse and circular shapes have been used to delimit for the deletion of black frames in skin images. Hair is another undesirable artefact that finds in skin images. Abbas et al. proposed a technique to remove hairs from the image [19]. They used morphological edge-based methods on grayscale images, with the first derivative of Gaussian for hair removal. This technique had applied on a hundred pitchers and 93% accuracy was achieved. Many researchers used dull razor for hair removal. It is online available for research purposes. Dull razor identifies the hair's presence and uses a morphological closing operation. Then it removes the hair by using an adaptive median filter. Thick hairs are removed with a median filter, while thin hairs remove by dull razor from skin images. Smoothing the picture with a versatile filter named a peer group filter (PGF), average filter, median filter, Gaussian filter, and anisotropic diffusion filter (ADF) is the simplest way to eliminate these objects. One of the huge drawbacks of these filters is that they were designed for scalar images in the first place. For vector images, marginal filtering is a technique that involves applying a scalar filter to every channel separately and afterward combining their effects. Despite its pace, the performance of this scheme contains color objects. Filters that handle pixels as vectors are an alternative approach [20]. Choosing a mask size relative to image size is another notable feature that allows you to play with the tradeoff between image smoothing and edge blurring. And if you take care of all of the above, there is no guarantee that you will end up with a picture clean of objects. Using specialized strategies for each artifact class is an alternative technique for artifact removal. Many approaches have been proposed; only a handful have combined various aspects of objects, and none have included all cases of artifacts.

That is the reasoning behind it. In [21], they changed the RGB color into L*a*b color to differentiate the skin lesion and mole. To get a grayscale image, subtract the L channel from a and b, then apply averaging filtering to remove the hairs. After this, enhance the contrast of images. In [22], they smooth the images by utilizing a median filter that is changed the pixel value according to neighboring pixel median values. This method removes the tiny unwanted details while thick hairs eliminate using the efficient model dull razor. Lastly, emphasized the border by singular value decomposition. Hameed et al. [23] utilized a Gaussian filter for noise removal, while a dull razor is used for hair removal from the images. Hameed et al. [24] resized the image in $227 \times 227 \times 3$, according to model requirements. They used the harmonic inpainting technique for hair removal because this used less computational time than Mumford-shah and transport inpainting. Later, they proposed a method for black hole and circles removal in images. Many authors use image resizing regularly. In deep models, all pictures should have the same size. It produces the best results and cuts down in computation time. In [25], they prepare the images using a mean filter and histogram equalization. Summary of the existing preprocessing methods.

In [26], they reduce the noise from images with sharpening and smoothing filters. The skin image is also subjected to contrast limited adaptive histogram equalization (CLAHE) to obtain a better spatial image. In [27], the blur and noise-free images took using a Gaussian filter technique with a 2-D convolution operator. In [28], to reduce the artifacts, Victor et al. utilized the median filter. The color contrast of the lesion was improved using the histogram equalization approach. After this, the hairs eliminate by using morphological operators. Khan et al. [29] enhanced the contrast of images by using Local color-controlled histogram intensity values. They used a hybrid technique inspired by histogram equalization. First, compute the histogram of the image and multiply each pixel by variance. Then the resulting image gives to the histogram to refine it. Finally, adjust the contrast according to background and lesion intensities.

3 Segmentation

Lesion segmentation is the vital stage in automating skin cancer detection. It is an easy stage to recognize. The outcome of segmentation has a crucial influence on the performance of succeeding phases [30]. After enhancing, it is essential to segment the affected part of the images. If used better technique for segmentation, it improves the result of classification [31]. It is used in digital image processing for splitting and filtering out the desired information from the images [32]. The skin wound is isolated out of its origin (the skin) and some objects. Typically, the binary pitcher (AKA binary mask) creates, which marked the surrounding skin area to be removed from the tumors to be investigated further. The medical features only of divided lesion areas are segmented, revealing the majority of global features like imbalance and boundary anomaly. Numerous methods are utilized to segment the

skin lesions that are Otsu's thresholding [33], Fuzzy c-means, and K-means dependent Color Cluster, deep models (FCN, SegNet, U-Net) [34], etc. Hence, to section Skin lesions, detailed segmentation analysis techniques are discussed by the authors [35]. Autonomously or semi-automatically to separate skin lesions, many approaches have been developed. There are five different types of segmentation techniques. Histogram thresholding approaches aim to find a value that will allow the lesion to the segment from the surrounding area [36]. Unsupervised clustering algorithms use the RGB color space to identify homogenous regions in dermoscopy pictures [37]. The edge operator and various methods like region splitting and merging utilize region-based and edge-based techniques [38]. Active contour techniques use meta-heuristic algorithms, geodesic algorithms, genetic procedures, and gradient vector flow snake algorithms for the separation of the wound region [39]. The supervised segmentation algorithms are the last group. Decision trees (DT), ANN, and SVM divide the skin lesion by learning recognizers [40]. The most complete and recent evaluations of segmentation techniques used in skin lesions include more extensive information on these procedures [41]. Thresholding is the most widely and basic technique used for segmentation [42]. It turns the picture into a grayscale image for reduction of complexity. Then thresholding is implemented to get the binary pitcher. The main idea is that it divides the image on the basis of changes in intensity level [43]. Classification of the skin lesion is a complicated issue even for skilled physicians owing to the seamless separation between the lesion and the underlying tissue, and thus specifically segmentation is a daunting activity [44]. Otsu thresholding is another technique used for segmentation. It is directly applied to the grayscale histogram. It is a fast algorithm. In this, we must construct a thresholding score that minimizes within-class variance while maximizing between-class variation [45]. The most popular method used in literature is K-mean clustering [46]. It is an unsupervised learning algorithm for clustering. It is utilized to make clusters of given data in various matched groups. It is often utilized in segmentation to find region of interest (ROI) from images [21]. It works in 2 phases, (1) is to calculate the mean of each group, and (2) is to measure each group's distance to each point. Each point is added to a cluster that is near that point. Border detection, manual methods give faster and high performance rather than computer-assisted methods, according to several authors. Al-masni et al. [47] employed an full resolution convolutional network (FrCN) for lesion separation. They used available ISIC 2017 and PH2 datasets for experiments. They compare the proposed model results with deep learning models named U-Net, SegNet, and FCN. But they achieved a good result with FrCN. Ünver and Ayan [48] took advantage of a DCNN named YOLOv3 with the combination of the GrabCut Algorithm. They used YOLOv3 deep learning model to detect the skin lesion location in images. YOLOv3 marked the skin lesion with a rectangular box. Then Grab Cut algorithm was employed for the separation of the lesion from the surrounding. The graph is used to segment the resulting images. It is created to use a minimum cost reduction algorithm so that we can get the better results. In [49], they used self-generating neural network (SGNN) followed by Otsu's threshold for segmentation. They claimed that the SGNN gives good results than Otsu, Fuzzy c-means, and k-means under severe conditions. Watershed is a renowned tool for segmentation.

That has been utilized for skin lesions separation, border, and structural detection. Researchers have suggested several deep learning-based models [50]. These methods yield outstanding skin lesion segmentation results. These both are supervised and unsupervised approaches to image segmentation that rely on learning a system and studying previously collected data. ANN is a common intelligence-based segmentation model. Other models are genetic algorithm (GA) and fuzzy c-means (FCM) [51]. All of these methods rely on pixel-level characteristics at the low level. Deep learning-based approaches, particularly CNN, have achieved notable results in classification, segmentation, and object identification issues in recent years. The capacity of CNNs to learn hierarchical features and extract more high-level and powerful characteristics from basic data is the fundamental reason for their success [52]. FCN was used to build this architecture. It is a decoder-encoder system. Convolutional layers are used in the encoder as well as the decoder portions. Pooling layers and convolutional layers are present in the encoder part, while the decoder has the up-sampling layers. Between the encoder and decoder portion, it has a convenient skip link. It has been utilized for skin image segmentation by many scientists. In [53], they calculated a probability score for each point using the architecture during the segmentation. Vesal et al. [54] amended the network named SkinNet and employed dilate convolutions were used in the encoder's last layer. It consists of a set of pooling and convolutional layers. They used parallel integration for multi-stage FCN. The border of the segmented skin lesions was further enhanced using this PI technique. They attained futuristic results on ISBI 2016 skin images dataset. On the other hand, FCN models are prone to over-segmentation, which can result in rough image segmentation with a small training dataset. Al-masni et al. [47] altered the FCN model for the separation of the skin lesion named FrCN and took high accuracy. These networks are moderately ANN that use skip connections to leap over some convolutional layers to create a pyramidal structure. The majority of convolutional layers composed it. In [55], they suggested a two-step FCRN technique for the classification and segmentation of skin tumors that used this network. A network of higher than 50-layers had utilized for generating broader and much more discriminatory features. On ISBI 2016 dataset, the algorithm produces exact skin wound separation.

4 Hand-Crafted Feature Extraction and Selection Methods

The feature is a small part of an image. It has a significant role in classification problems. After preprocessing and segmentation, the subsequent stage is feature extraction from skin images [10, 56–64]. It is a hard mission to identify suitable attributes. Thousands of papers are published already conducted in this field. So that several features of skin lesions are defined. Skin-related attributes can be divided into various types. These types are color features, dermal features, ABCD rule features, and geometric features, histogram features [65], texture features, and contour features [66]. In image processing, local binary patterns (LBP) [67] are a complex image signifier generally utilized [68]. In [69], they used LBP with genetic programming (GP)

for features retrieval in dermoscopic images. Colors are a vital factor, have been kept to detect skin lesions. The proper color judgment and its relative diffusion are predominant for an accurate diagnosis. The essential aspects of the dermoscopic test inside the skin lesions have included color estimation, pigmentation degree, and color variation. The epidermis usually appears white in dermoscopic images. The color of melanin becomes most vital because it helps to identify the possible color and structural shapes [49]. The different distribution of pigmentation has been found in the various pigmented skin wounds. Based on the point of melanoma in distinct layers of the skin. Majumder and Ullah [70] used the ABCD rule to extract eight features from skin images and divided them into two groups are Shape features and lighting information. They extract one color feature and seven shape features that depend on the ABCD rule. This rule is an abbreviation of four terms: Asymmetry, Border, chromatic (Color), and Dimension (diameter). Xie et al. [49] retrieved 30 colors, 20 textures, and seven border features using gray level co-occurrence matrix (GLCM) in their research work. Hameed et al. [24] employed color histogram and GLCM to extract four textures and 36 color characteristics for skin lesion classification. In another proposed work, Hameed et al. [23] extracted color and texture characteristics using a neighborhood gray-tone difference matrix and GLCM. Both proposed methods achieved good results with these features. In [71], color and texture attributes had been derived from skin images. They produced statistical texture features utilizing GLCM. The texture is divided into the first, second, and higher-order features. First-order textures are directly calculated from images because there is no relationship in pixel neighboring. Using, GLCM the second-order statistical features are extracted from images. The relationship between two pixels is considered if found relationship then called neighbor pixels. The sum of gray levels in rows and columns in an image is identical in the GLCM is explained by the matrix. Several attributes are derived from the image dataset utilizing a GLCM entropy, dissimilarity, correlation, energy, etc. Victor et al. [28] used statistical features for skin lesion classification. They utilized statistical parameters that are area, standard deviation, mean, and variance. Khan et al. extracted Histogram Oriented Gradients (HOG) [72], Haralick features [73], and color features to identify skin wounds in [74]. The Histogram Oriented Gradients features are worked on object shape. It is also known as shape features. For color feature retrieval, different color channels named LAB, RGB, HSV, YCbCr, and HSI have been used. In [27], they used the LBP and GLCM as feature extractors in their proposed model. There was a total of 216 significant characteristics retrieved. They retrieved 13 statistical attributes named kurtosis, skewness, contrast, correlation, RMS, variance, energy, homogeneity, entropy, smoothness, mean, standard deviation utilizing the GLCM. In [75], they extracted color features from images using the color histogram. They converted color histograms into different color schemes such as Hue-Saturation-Value (HSV) and RGB. For each color space, 512 bins have been created that are used as deliberate single vector features. Afza et al. [76] retrieved OHOG, OCL, and GLCM features for the classification task. Before implementing the HOG descriptor, they resized the image. Then principal component analysis-controlled variance is applied to optimize them. For color features, they used two types of color spaces named HSV and RGB. From every color channel, four attributes

were extracted utilizing haze reduction. Later, characteristics were obtained from the binary image using GLCM. Hameed et al. [23] retrieved nine colors, four GLCM textures, and four NGTDM (neighborhood gray-tone difference matrix) features for the classification of dermoscopic images.

Feature selection or reduction is a critical phase in automated diagnosis systems. Many unnecessary attributes in the feature set may be insignificant [77]. In our problems, we always want to gain better results [78]. Therefore, we do not give all features to the machine learning algorithm. And let it decide which the best characteristics are for this [79, 80]. It is a procedure through which dominant features are selected or diminishing attributes from the input set. The best feature selection methods diminish the redundant features. And enhance the classification accuracy [81]. The execution of the presented process is also improved when eliminated the redundant features. Feature selection techniques use to delete these repetitive and meaningless attributes. These methods have been divided into three groups such as filtered methods, wrapper methods, and embedded methods. Filter methods have contained like Chi-Square and Pearson's correlation coefficient. It is also included mutual information-based feature selection (MIFS), Relief, and correlation-based feature selection (CFS) [82]. These techniques are generally quick and enable you to compare many different techniques together within an optimization system. Using statistical or clinical parameters techniques to minimize the number of possible variables is feasible and beneficial [83]. Wrapper methods include forward feature selection, backward features selection, and exhaustive features selection. Embedded methods have contained LASSO regression and RIDGE regression [84]. There are many benefits to selecting specific features from all features. Some of them are described here. It reduces overfitting and enables the algorithm to train faster. Choosing the best subset improves the efficiency of a proposed method [85]. It diminishes the complexity of a system and makes it easier to interpret. These use less storage. Rohrer et al. [86] proposed an analysis mainly focused on feature selection for melanoma detection and suggested that a small feature subset gave us better accuracy and observed that medium feature subsets show a tiny growth inaccuracy. The large feature subsets lead the identification rate to diminish. In [87], they used sequential backward floating search (SBFS), sequential forward floating search (SFFS) and described the best accuracy gain with a 10–15 feature subset. When they used it with 20 features subset, the accuracy degraded. Green et al. [88] demonstrated that the magnitude of a lesion is perhaps the essential element in their model by estimating correlation coefficients. Haim et al. [89] used principal component analysis (PCA) for feature selection. They fed 11 features to PCA, and PCA returns the five best features. Rob et al. [90] employ the sequential forward selection (SFS) algorithm to handle feature selection. They started with eighty-seven features measured from the clarity of lesions. They reduce the number to only five. Celebi et al. [91] demonstrated, using the correlation-based feature selection (CFS) algorithm and expressed that AUC peaks can be achieved only with eighteen features. Adding more features does not improve the classifier's efficiency significantly. In [92], they treated feature selection as a method of optimization and examined several algorithms, including heuristic techniques, greedy methods, and genetic algorithms. Xie et al. [49] used the PCA for feature selection.

A total number of 57 features, they choose two sets with 12 and 15 attributes. They obtained high results with 15. Ain et al. [93] also used genetic programming (GP) for attribute selection. They used ten individuals for this. Khan et al. [74] selected the best 200 features from 3780 HOG features, utilizing PCA. Then they used the entropy variance to choose the good features from color, Harlick, and HOG features. They selected 172 attributes out of 278. Khan et al. [58] utilized principal component analysis for feature selection after obtaining the kurtosis vector and got the best result. They used ResNet 50 and ResNet 101 for feature extraction and selected the best 2133 features. Oliveria et al. [94] utilized the greedy stepwise method with the CFS algorithm for feature selection. They chose 37 attributes by forwarding direction and 50 by backward direction. They compared this feature selection method with the best first search (BFS) and achieved good results with the greedy stepwise with the CFS algorithm. Khan et al. [29] used improved moth flame optimization (IMFO) algorithm to remove the redundant attributes from feature vectors. After applying this, a total number of 2088 features gained 1632 efficient features for experiment purposes. Summary of the existing features extraction/selection methods.

5 Deep Features Extraction Methods

Many researchers used deep learning models as a feature extractor for skin cancer classification, and they achieved good results than traditional methods. Transfer learning is an approach that allows you to reuse a pre-trained model on other although related tasks [95, 96]. In [97], they proposed a deep learning model deep convolutional neural network (DCNN) and compared it with ResNet, AlexNet, VGG-16, MobileNet, DenseNet. The proposed took less computational time than transfer learning. Khan et al. [29] used ResNet 101 and DenseNet to retrieve features. They employed transfer learning in the proposed method and achieved high accuracy. AlexNet has contained five convolutional and some pooling functions followed by three fully connected layers [98]. It is an easy and effective CNN architecture. The size in which it uses GPU for task and training execution is a benefit. It remains a popular baseline for deep neural network applications that are frequently utilized in CV and voice recognition. In [24, 99], they used the AlexNet architecture to extract the skin lesion features. Researchers from Oxford University's Visual Graphics Group proposed the VGG network. VGG's pyramidal shape distinguishes it. It is made up of convolutional layers accompanied by pooling layers, leading to the layer's narrower form [100]. The benefits include having a large design that is ideal for benchmarking any activity. VGG's network has been extensively utilized by researchers in everyday applications. However, it requires a vast number of computational assets and is very deliberate to learn, particularly when beginning from the scratch. Another network namely, GoogleNet is developed by Google scientists and is also labeled as Inception Network. It consists of twenty-two layers that make the structure. It can pool or convolve an input. Multiple inception components are piled on top of one another in this architecture. This layering permits for both joint and parallel training, aiding

the model in achieving quicker converge. Faster prepared with a smaller capacity is one of the benefits [101]. It does, has an Xception Network, which will raise the inception module's divergence speed. Extreme Inception architecture is a form of architecture that uses depth-wise separable convolution. To govern computational complexity, the initial inception block is widening, and several spatial dimensions (3×3 , 1×1 , and 5×5) are replaced with one dimension (5×5) followed by a 1×1 convolution. Through decoupling the spatial and feature-map networks, the network becomes more computationally efficient. In [102], they utilized five deep learning models and got the best results with the Xception model. The residual architecture's fundamental building block is the residual network, which is made up of several subsequent residual modules. These residual models are piled on top of one another to build a complete network [103]. It goes on high performance because it is the model that contains many layers. The residual blocks are a 152-layer deep CNN architecture. AlexNet and VGG are 20 and 8 times deeper, respectively [52]. It is less computationally demanding than other networks that have been proposed [104]. In [29], they utilized the improved version of ResNet 101 to extract the features from HAM 10000 dataset. In another study, they used the ResNet 50 and ResNet 101 for skin lesion classification. It was suggested that the vanishing gradient issue be solved in DenseNet and is similar to ResNet. DenseNet solves the problem by using cross-layer communication by connecting each previous layer feeds into the next layer in a feed-forward manner [105], while ResNet directly retains information by additive identity transformations but adds cost. It made use of dense squares, and all preceding layers function maps are utilized as inputs into the coming layers. In [29], they used the DenseNet 201 and skipped different layers. The attributes are combined in this architecture in a sequential sequence. Summary of the existing deep features extraction methods.

6 Classification

Many steps are required to identify this disease. Hence, choosing the best classifier is an important step. Different classifiers are present. Among these, SVM is often used for melanoma detection from benign images for classification. SVM are supervised learning techniques in machine learning. They are the most known classification methods. Responsibility for the information extracted. Many of them are clinical, while some are machine-assisted by many classification methods in the literature review [106]. The ABCD dermatoscopy rule [107], the 7-point checklist [108], the three-point checklist [109] the Menzies method [110], and the computer-aided pattern recognition process are all popular classification methods. In [102], they observed in the literature, as the categorization classes increase, the model's efficiency degrades. The scientists used various automated skin lesion classification methods for machine learning. Mainly used methods are the SVM, ANN, KNN, and decision tree. In statistical research, training and test paradigms are highly popular. The data is distributed in two different sets, according to this model. The testing and

training set will be statistically independent. The training set is used to develop and train the algorithm, while the test set utilizes to test the trained model efficiency. The typical rules for the efficiency of the system are precision, accuracy, F1-score and specificity. But alone accuracy has also been used in some cases. In [87], they described a system for automated skin cancer recognition. Noise and hair influence decreased by the grayscale closing operation of morphology and thresholding and color clustering algorithm employed for the fusion of the global threshold for skin lesions. A total of 122 features with shape and radiometric parameters were local and universal. The malignancy lesion is measured to define. It used the K-nearest neighbor algorithm for classification and achieved 73% accuracy. Rubegni et al. [111] evaluated the 588 images. The researcher analyzed 48 features that grouped into geometric groups, color, and texture. Different feature subsets are generated. This finding showed 13 attributes were enough to differentiate two lesion categories. The ANN was used as a classification algorithm for the identification of melanoma that achieved 94% accuracy. Lingala et al. [66] proposed image processing methods to examine different blue intensities. The training collection of 22 additional melanoma images was tested while creating the fuzzy set for various shades of blue color. The representation of the fuzzy set of colors. Hundred fifty characteristics that are contour, light, and texture were classified and derived into three groups. The SVM was used to classify the skin lesion images. They obtained 81.4% accuracy. Jain and Pise [3] described a method using digital image processing to detect melanoma. The presented work is divided into three main parts. The image was resized, and its brightness and contrast-enhanced during preprocessing. The Otsu threshold has been used for each channel (R, G, and B) in the image segmentation process. A lesion mask is created with the binary masks. For further segmentation, an edge detection technique had been applied. A segmented image has held several blobs the correct spot is picked. In the extraction step, geometric features like perimeter, area, circular index, and maximum diameter are gained. The classification stage used different predefined criteria to assign the data as melanoma or normal. Victor and Ghalib [28] used 1011 images to find the accuracy, four algorithms such as KNN, boosted tree, Decision tree, and SVM were used. They achieved 93.70% accuracy with SVM. In [23], they used several classifiers for skin cancer classification, but they gained a good result with quadratic SVM. They extracted 35 color and texture attributes using GLCM and NGTDM. Jinnai et al. [112] presented a method for brown to black clinical pigmented skin images. They took 120,000 clinical pigmented samples from the Department of Dermatologic Oncology (DDO) for the experiment. They have selected approximately six thousand images of 3551 patients. They chose 666 images for testing purposes, while others used for training purposes. They trained faster region-based convolutional neural network (FRCNN) on these samples and achieved 86.2% accuracy for six-class classification and got for two-classes (malignant and benign) 91.5%. They compare their results with ten board-certified dermatologists (BCDs) and ten dermatologic trainees (TRNs). Out of 20, only one dermatologist achieved good score than FRCNN. Hameed et al. [24] presented a computerized system for skin lesions categorization. Two approaches are described in this paper, first traditional and second, deep learning (DL). To remove artefacts and smooth the

images, they removed noise, resized and black frames removed using thresholding, and hair removed with the inpainting method. After this, the segmentation process is applied to the image dataset by the K-means algorithm. These 36 attributes are derived from the dataset to give the machine learning algorithm. In the deep learning section, they used the AlexNet model and got 96% accuracy. Chaturvedi et al. [102] utilized HAM 10000 dataset having seven classes of skin lesions, they used five deep learning models named InceptionResnetV2, Xception, ResNeXt101, InceptionV3, and NASNetLarge, 4 ensemble deep models named InceptionResNetV2 + Xception, InceptionV3 + Xception, InceptionResNetV2 + ResNeXt101 + Xception and InceptionResNetV2 + ResNeXt101. They get good results (93.20%) with ResNetXt101 and InceptionResNetV2. Khan et al. [29] described a computerized system for skin wound recognition. They employed HAM 10000 skin dataset for classification accuracy. First, they enhanced the images using local color-controlled histogram intensity values. They selected two deep learning models for feature extractors named ResNet 101, DenseNet 201 and took two feature vectors from them. An improved feature selection method was applied to improve these vectors. Lastly, these selected features are fed to the KELM classifier and gain 90.67% best results. Ali et al. [97] used a DCNN to recognize the skin lesions. The chosen HAM 10000 dataset. They compared it with other deep models named ResNet, AlexNet, MobileNet, VGG-16, and DenseNet. They achieved an accuracy of 91.43% highest results than these. This model can classify as skin lesion cancer even cancer is in an early stage. It took less computational time than other models. Alsaade et al. [27] used the ANN to classify the skin dataset named ISIC 2018 and PH2. They retrieved the 216 features by utilizing the LBP and GLCM. They obtained an accuracy of 98% for ISIC 2018 and 97% for PH2 datasets. They used transfer learning models which names are AlexNet and ResNet 50. They observed that the ANN gave good results than deep learning models.

7 Publicly Available Datasets

Benchmark datasets that are available online such as HAM 10000 [113], ISIC (2016) [114], ISIC (2017) [115], PH2 [116], ISIC (2018) [117], ISIC (2019) [113], ISIC (2020) [118], DermsQuest [119] and their detail description is mentioned in Table 1.

8 Challenges

Variation in skin images create problems to detect the skin lesions. The look of human skin color varies greatly, making skin identification a challenging and time-consuming task. Different variations are found in skin images. Below are some of the issues posed by the complex visual qualities of skin lesions images.

Table 1 Summary of the benchmark datasets

References	Datasets	Total no. of images	Classes	Year of release
[119]	DermsQuest	22,082	2	1999
[116]	PH2	200	3	2013
[114]	ISIC 2016	1279	2	2016
[113]	HAM 10000	10,015	7	2018
[115]	ISIC 2017	2750	3	2017
[117]	ISIC 2018	2594	7	2018
[113]	ISIC 2019	25,331	8	2019
[118]	ISIC 2020	33,126	8	2020

- i. The presence of noise and artifacts can make it hard to identify the skin lesion accurately.
- ii. The location and shape of lesions vary greatly.
- iii. Accurate segmentation of the lesion is the hard cause of the difference between the skin around the lesion and the lesion itself.
- iv. Some moles on the skin may never grow into cancer cells, but they make it difficult to diagnose skin cancer from images.
- v. Different sizes of images have been found in datasets. It is essential to resize the image in the proper size.
- vi. Skin lesions are complicated by the presence of fuzzy and uneven borders.
- vii. Many unnecessary features in the feature set may be insignificant.

9 Summary

Early melanoma detection can decrease mortality rates, according to the literature. The most recent techniques are discussed in this chapter. In which analyzed recent developments in various stages of computer diagnostics systems using traditional and deep learning approaches. These systems use several methods to perform preprocessing, segmentation, feature extraction, features selection, and classification. Much work has been done to improve the image quality such as contrast stretching, and image filtering methods. Most researchers widely utilized the Otsu thresholding technique and deep architecture for the detection of skin lesions. It was observed in the survey that nowadays, deep learning models in which ensemble and transfer learning methods with machine learning classifiers such as SVM, KNN are employed for skin lesions analysis. As per literature the precision rate of skin lesions detection is between the 80 and 98%.

References

1. Pacheco, A.G., Krohling, R.A.: Recent advances in deep learning applied to skin cancer detection. arXiv preprint [arXiv:1912.03280](https://arxiv.org/abs/1912.03280) (2019)
2. Hintz-Madsen, M.: A probabilistic framework for classification of dermatoscopic images. Citeseer (1998)
3. Jain, S., Pise, N.: Computer aided melanoma skin cancer detection using image processing. *Procedia Comput. Sci.* **48**, 735–740 (2015)
4. Seth, D., Cheldize, K., Brown, D., Freeman, E.E.: Global burden of skin disease: inequities and innovations. *Curr. Dermatol. Rep.* **6**(3), 204–210 (2017)
5. Hameed, N., Ruskin, A., Hassan, K.A., Hossain, M.A.: A comprehensive survey on image-based computer aided diagnosis systems for skin cancer. In: 2016 10th International Conference on Software, Knowledge, Information Management & Applications (SKIMA), pp. 205–214. IEEE (2016)
6. Sultana, A., Dumitrache, I., Vocurek, M., Ciuc, M.: Removal of artifacts from dermatoscopic images. In: 2014 10th International Conference on Communications (COMM), pp. 1–4. IEEE (2014)
7. Khan, M.A., Akram, T., Sharif, M., Javed, K., Rashid, M., Bukhari, S.A.C.: An integrated framework of skin lesion detection and recognition through saliency method and optimal deep neural network features selection. *Neural Comput. Appl.* **32**(20), 15929–15948 (2020)
8. Lee, T., Ng, V., Gallagher, R., Coldman, A., McLean, D.: Dullrazor®: a software approach to hair removal from images. *Comput. Biol. Med.* **27**(6), 533–543 (1997)
9. Amin, J., Sharif, M., Raza, M., Yasmin, M.: Detection of brain tumor based on features fusion and machine learning. *J. Ambient Intell. Hum. Comput.* 1–17 (2018)
10. Amin, J., Sharif, M., Raza, M., Saba, T., Anjum, M.A.: Brain tumor detection using statistical and machine learning method. *Comput. Methods Programs Biomed.* **177**, 69–79 (2019)
11. Celebi, M.E., Aslandogan, Y.A., Bergstresser, P.R.: Unsupervised border detection of skin lesion images. In: International Conference on Information Technology: Coding and Computing (ITCC'05)—Volume II, vol. 2, pp. 123–128. IEEE (2005)
12. Toossi, M.T.B., Pourreza, H.R., Zare, H., Sigari, M.H., Layegh, P., Azimi, A.: An effective hair removal algorithm for dermoscopy images. *Skin Res. Technol.* **19**(3), 230–235 (2013)
13. Church, J.C., Chen, Y., Rice, S.V.: A spatial median filter for noise removal in digital images. In: IEEE SoutheastCon 2008, pp. 618–623. IEEE (2008)
14. Amin, J., Sharif, M., Fernandes, S.L., Wang, S.H., Saba, T., Khan, A.R.: Breast microscopic cancer segmentation and classification using unique 4-qubit-quantum model. *Microsc. Res. Tech.* (2022)
15. Amin, J., Anjum, M.A., Sharif, A., Raza, M., Kadry, S., Nam, Y.: Malaria Parasite Detection Using a Quantum-Convolutional Network (2022)
16. Amin, J., Anjum, M.A., Sharif, M., Saba, T., Tariq, U.: An intelligence design for detection and classification of COVID19 using fusion of classical and convolutional neural network and improved microscopic features selection approach. *Microsc. Res. Tech.* **84**(10), 2254–2267 (2021)
17. Suganya, R.: An automated computer aided diagnosis of skin lesions detection and classification for dermoscopy images. In: 2016 International Conference on Recent Trends in Information Technology (ICRTIT), pp. 1–5. IEEE (2016)
18. Masood, A., Al-Jumaily, A.: Differential evolution based advised SVM for histopathological image analysis for skin cancer detection. In: 2015 37th Annual International Conference of the IEEE Engineering in Medicine and Biology Society (EMBC), pp. 781–784. IEEE (2015)
19. Abbas, Q., Celebi, M.E., García, I.F.: Hair removal methods: a comparative study for dermoscopy images. *Biomed. Signal Process. Control* **6**(4), 395–404 (2011)
20. Erkol, B., Moss, R.H., Joe Stanley, R., Stoecker, W.V., Hvatum, E.: Automatic lesion boundary detection in dermoscopy images using gradient vector flow snakes. *Skin Res. Technol.* **11**(1), 17–26 (2005)

21. Agarwal, A., Issac, A., Dutta, M.K.: A region growing based imaging method for lesion segmentation from dermoscopic images. In: 2017 4th IEEE Uttar Pradesh Section International Conference on Electrical, Computer and Electronics (UPCON), pp. 632–637. IEEE (2017)
22. Zakeri, A., Hokmabadi, A.: Improvement in the diagnosis of melanoma and dysplastic lesions by introducing ABCD-PDT features and a hybrid classifier. *Biocybern. Biomed. Eng.* **38**(3), 456–466 (2018)
23. Hameed, N., Hameed, F., Shabut, A., Khan, S., Cirstea, S., Hossain, A.: An intelligent computer-aided scheme for classifying multiple skin lesions. *Computers* **8**(3), 62 (2019)
24. Hameed, N., Shabut, A.M., Ghosh, M.K., Hossain, M.A.: Multi-class multi-level classification algorithm for skin lesions classification using machine learning techniques. *Expert Syst. Appl.* **141**, 112961 (2020)
25. Arivuselvam, B.: Skin cancer detection and classification using SVM classifier. *Turk. J. Comput. Math. Educ. (TURCOMAT)* **12**(13), 1863–1871 (2021)
26. Nyemeesha, V.: A systematic study and approach on detection of classification of skin cancer using back propagated artificial neural networks. *Turk. J. Comput. Math. Educ. (TURCOMAT)* **12**(11), 1737–1748 (2021)
27. Alsaade, F.W., Aldhyani, T.H., Al-Adhaileh, M.H.: Developing a recognition system for diagnosing melanoma skin lesions using artificial intelligence algorithms. *Comput. Math. Methods Med.* **2021** (2021)
28. Victor, A., Ghalib, M.: Automatic detection and classification of skin cancer. *Int. J. Intell. Eng. Syst.* **10**(3), 444–451 (2017)
29. Khan, M.A., Sharif, M., Akram, T., Damaševičius, R., Maskeliūnas, R.: Skin lesion segmentation and multiclass classification using deep learning features and improved moth flame optimization. *Diagnostics* **11**(5), 811 (2021)
30. Amin, J., et al.: An integrated design based on dual thresholding and features optimization for white blood cells detection. *IEEE Access* **9**, 151421–151433 (2021)
31. Sharif, M., Amin, J., Yasmin, M., Rehman, A.: Efficient hybrid approach to segment and classify exudates for DR prediction. *Multimed. Tools Appl.* **79**(15), 11107–11123 (2020)
32. Amin, J., Sharif, M., Anjum, M.A., Nam, Y., Kadry, S., Taniar, D.: Diagnosis of COVID-19 infection using three-dimensional semantic segmentation and classification of computed tomography images. *Comput. Mater. Contin.* **68**(2), 2451–2467 (2021)
33. Otsu, N.: A threshold selection method from gray-level histograms. *IEEE Trans. Syst. Man Cybern.* **9**(1), 62–66 (1979)
34. Amin, J., Sharif, M., Gul, E., Nayak, R.S.: 3D-semantic segmentation and classification of stomach infections using uncertainty aware deep neural networks. *Complex Intell. Syst.* 1–17 (2021)
35. Ali, A.-R.A., Deserno, T.M.: A systematic review of automated melanoma detection in dermatoscopic images and its ground truth data. In: Medical Imaging 2012: Image Perception, Observer Performance, and Technology Assessment, vol. 8318, p. 83181I. International Society for Optics and Photonics (2012)
36. Yüksel, M.E., Borlu, M.: Accurate segmentation of dermoscopic images by image thresholding based on type-2 fuzzy logic. *IEEE Trans. Fuzzy Syst.* **17**(4), 976–982 (2009)
37. Ashour, A.S., Hawas, A.R., Guo, Y., Wahba, M.A.: A novel optimized neutrosophic k-means using genetic algorithm for skin lesion detection in dermoscopy images. *SIViP* **12**(7), 1311–1318 (2018)
38. Abbas, Q., Celebi, M.E., Fondón García, I., Rashid, M.: Lesion border detection in dermoscopy images using dynamic programming. *Skin Res. Technol.* **17**(1), 91–100 (2011)
39. Mete, M., Sirakov, N.M.: Lesion detection in dermoscopy images with novel density-based and active contour approaches. *BMC Bioinform.* **11**(6), 1–13 (2010)
40. Xie, F., Bovik, A.C.: Automatic segmentation of dermoscopy images using self-generating neural networks seeded by genetic algorithm. *Pattern Recogn.* **46**(3), 1012–1019 (2013)
41. Celebi, M.E., Wen, Q., Iyatomi, H., Shimizu, K., Zhou, H., Schaefer, G.: A state-of-the-art survey on lesion border detection in dermoscopy images. *Dermosc. Image Anal.* **10**, 97–129 (2015)

42. Amin, J., Sharif, M., Yasmin, M., Saba, T., Anjum, M.A., Fernandes, S.L.: A new approach for brain tumor segmentation and classification based on score level fusion using transfer learning. *J. Med. Syst.* **43**(11), 1–16 (2019)
43. Kader, R.A., Chehade, W.E.H., Al-Zaart, A.: Segmenting skin images for cancer detection. In: 2018 International Conference on Computational Science and Computational Intelligence (CSCI), pp. 392–396. IEEE (2018)
44. Nachbar, F., et al.: The ABCD rule of dermatoscopy: high prospective value in the diagnosis of doubtful melanocytic skin lesions. *J. Am. Acad. Dermatol.* **30**(4), 551–559 (1994)
45. Gonzalez, R.C., Woods, R.E., Eddins, S.: Image segmentation. *Digit. image Process.* **2**, 331–390 (2002)
46. Celebi, M.E., Wen, Q., Hwang, S., Schaefer, G.: Color quantization of dermoscopy images using the k-means clustering algorithm. In: *Color Medical Image Analysis*, pp. 87–107. Springer (2013)
47. Al-Masni, M.A., Al-Antari, M.A., Choi, M.-T., Han, S.-M., Kim, T.-S.: Skin lesion segmentation in dermoscopy images via deep full resolution convolutional networks. *Comput. Methods Programs Biomed.* **162**, 221–231 (2018)
48. Ünver, H.M., Ayan, E.: Skin lesion segmentation in dermoscopic images with combination of YOLO and grabcut algorithm. *Diagnostics* **9**(3), 72 (2019)
49. Xie, F., Fan, H., Li, Y., Jiang, Z., Meng, R., Bovik, A.: Melanoma classification on dermoscopy images using a neural network ensemble model. *IEEE Trans. Med. Imaging* **36**(3), 849–858 (2016)
50. Saba, T., Mohamed, A.S., El-Affendi, M., Amin, J., Sharif, M.: Brain tumor detection using fusion of hand crafted and deep learning features. *Cogn. Syst. Res.* **59**, 221–230 (2020)
51. Mohamed, A.A.I., Ali, M.M., Nusrat, K., Rahebi, J., Sayiner, A., Kandemirli, F.: Melanoma skin cancer segmentation with image region growing based on fuzzy clustering mean. *Int. J. Eng. Innov. Res.* **6**(2), 91C95 (2017)
52. He, K., Zhang, X., Ren, S., Sun, J.: Deep residual learning for image recognition. In: *Proceedings of the IEEE Conference on Computer Vision and Pattern Recognition*, pp. 770–778 (2016)
53. Wen, H.: II-FCN for skin lesion analysis towards melanoma detection. arXiv preprint [arXiv: 1702.08699](https://arxiv.org/abs/1702.08699) (2017)
54. Vesal, S., Ravikumar, N., Maier, A.: Skinnet: a deep learning framework for skin lesion segmentation. In: 2018 IEEE Nuclear Science Symposium and Medical Imaging Conference Proceedings (NSS/MIC), pp. 1–3. IEEE (2018)
55. Yu, L., Chen, H., Dou, Q., Qin, J., Heng, P.-A.: Automated melanoma recognition in dermoscopy images via very deep residual networks. *IEEE Trans. Med. Imaging* **36**(4), 994–1004 (2016)
56. Nasir, M., Attique Khan, M., Sharif, M., Lali, I.U., Saba, T., Iqbal, T.: An improved strategy for skin lesion detection and classification using uniform segmentation and feature selection based approach. *Microsc. Res. Tech.* **81**(6), 528–543 (2018)
57. Khan, M.A., Sharif, M., Javed, M.Y., Akram, T., Yasmin, M., Saba, T.: License number plate recognition system using entropy-based features selection approach with SVM. *IET Image Proc.* **12**(2), 200–209 (2018)
58. Khan, M.A., Javed, M.Y., Sharif, M., Saba, T., Rehman, A.: Multi-model deep neural network based features extraction and optimal selection approach for skin lesion classification. In: *2019 International Conference on Computer and Information Sciences (ICCIS)*, pp. 1–7. IEEE (2019)
59. Mughal, B., Muhammad, N., Sharif, M., Rehman, A., Saba, T.: Removal of pectoral muscle based on topographic map and shape-shifting silhouette. *BMC Cancer* **18**(1), 1–14 (2018)
60. Mughal, B., Sharif, M., Muhammad, N., Saba, T.: A novel classification scheme to decline the mortality rate among women due to breast tumor. *Microsc. Res. Tech.* **81**(2), 171–180 (2018)
61. Khan, M.A., Sharif, M., Akram, T., Raza, M., Saba, T., Rehman, A.: Hand-crafted and deep convolutional neural network features fusion and selection strategy: an application to intelligent human action recognition. *Appl. Soft Comput.* **87**, 105986 (2020)

62. Saba, T., Rehman, A., Mehmood, Z., Kolivand, H., Sharif, M.: Image enhancement and segmentation techniques for detection of knee joint diseases: a survey. *Curr. Med. Imaging* **14**(5), 704–715 (2018)
63. Rehman, A., Abbas, N., Saba, T., Rahman, S.I.u., Mehmood, Z., Kolivand, H.: Classification of acute lymphoblastic leukemia using deep learning. *Microsc. Res. Tech.* **81**(11), 1310–1317 (2018)
64. Khan, M.A., et al.: Brain tumor detection and classification: a framework of marker-based watershed algorithm and multilevel priority features selection. *Microsc. Res. Tech.* **82**(6), 909–922 (2019)
65. Amin, J., Anjum, M.A., Sharif, M., Saba, T., Tariq, U.: An intelligence design for detection and classification of COVID19 using fusion of classical and convolutional neural network and improved microscopic features selection approach. *Microsc. Res. Tech.* (2021)
66. Lingala, M., et al.: Fuzzy logic color detection: blue areas in melanoma dermoscopy images. *Comput. Med. Imaging Graph.* **38**(5), 403–410 (2014)
67. Ojala, T., Pietikäinen, M., Harwood, D.: A comparative study of texture measures with classification based on featured distributions. *Pattern Recogn.* **29**(1), 51–59 (1996)
68. Sharif, M., Amin, J., Nisar, M.W., Anjum, M.A., Muhammad, N., Shad, S.A.: A unified patch based method for brain tumor detection using features fusion. *Cogn. Syst. Res.* **59**, 273–286 (2020)
69. Ain, Q.U., Xue, B., Al-Sahaf, H., Zhang, M.: Genetic programming for skin cancer detection in dermoscopic images. In: 2017 IEEE Congress on Evolutionary Computation (CEC), pp. 2420–2427. IEEE (2017)
70. Majumder, S., Ullah, M.A.: Feature extraction from dermoscopy images for an effective diagnosis of melanoma skin cancer. In: 2018 10th International Conference on Electrical and Computer Engineering (ICECE), pp. 185–188. IEEE (2018)
71. Kavitha, J., Suruliandi, A.: Texture and color feature extraction for classification of melanoma using SVM. In: 2016 International Conference on Computing Technologies and Intelligent Data Engineering (ICCTIDE'16), pp. 1–6. IEEE (2016)
72. Dalal, N., Triggs, B.: Histograms of oriented gradients for human detection. In: 2005 IEEE Computer Society Conference on Computer Vision and Pattern Recognition (CVPR'05), vol. 1, pp. 886–893. IEEE (2005)
73. Haralick, R.M., Shanmugam, K., Dinstein, I.H.: Textural features for image classification. *IEEE Trans. Syst. Man Cybern.* **6**, 610–621 (1973)
74. Khan, M.A., et al.: An implementation of normal distribution based segmentation and entropy controlled features selection for skin lesion detection and classification. *BMC Cancer* **18**(1), 1–20 (2018)
75. Nezhadian, F.K., Rashidi, S.: Melanoma skin cancer detection using color and new texture features. In: 2017 Artificial Intelligence and Signal Processing Conference (AISP), pp. 1–5. IEEE (2017)
76. Afza, F., Khan, M.A., Sharif, M., Rehman, A.: Microscopic skin laceration segmentation and classification: a framework of statistical normal distribution and optimal feature selection. *Microsc. Res. Tech.* **82**(9), 1471–1488 (2019)
77. Sharif, M., et al.: Recognition of different types of leukocytes using YOLOv2 and optimized bag-of-features. *IEEE Access* **8**, 167448–167459 (2020)
78. Khan, M.A., Sharif, M., Akram, T., Bukhari, S.A.C., Nayak, R.S.: Developed Newton-Raphson based deep features selection framework for skin lesion recognition. *Pattern Recogn. Lett.* **129**, 293–303 (2020)
79. Sharif, M., Tanvir, U., Munir, E.U., Khan, M.A., Yasmin, M.: Brain tumor segmentation and classification by improved binomial thresholding and multi-features selection. *J. Ambient Intell. Hum. Comput.* 1–20 (2018)
80. Khan, M.A., Arshad, H., Nisar, W., Javed, M.Y., Sharif, M.: An integrated design of fuzzy C-means and NCA-based multi-properties feature reduction for brain tumor recognition. In: *Signal and Image Processing Techniques for the Development of Intelligent Healthcare Systems*, pp. 1–28. Springer (2021)

81. Saleem, S., Amin, J., Sharif, M., Anjum, M.A., Iqbal, M., Wang, S.-H.: A deep network designed for segmentation and classification of leukemia using fusion of the transfer learning models. *Complex Intell. Syst.* 1–16 (2021)
82. Hall, M.A.: Correlation-based feature selection for machine learning (1999)
83. Harrell, F.E., Jr., Lee, K.L., Califff, R.M., Pryor, D.B., Rosati, R.A.: Regression modelling strategies for improved prognostic prediction. *Stat. Med.* **3**(2), 143–152 (1984)
84. Charfaoui, Y.: Hands-on with Feature Selection Techniques: Embedded Methods. Available at: <https://heartbeat.fritz.ai/hands-on-with-feature-selection-techniques-embedded-methods-84747e814dab> (2020)
85. Sharif, M., Khan, M.A., Iqbal, Z., Azam, M.F., Lali, M.I.U., Javed, M.Y.: Detection and classification of citrus diseases in agriculture based on optimized weighted segmentation and feature selection. *Comput. Electron. Agric.* **150**, 220–234 (2018)
86. Rohrer, R., Ganster, H., Pinz, A., Binder, M.: Feature selection in melanoma recognition. In: Proceedings. Fourteenth International Conference on Pattern Recognition (Cat. No. 98EX170), vol. 2, pp. 1668–1670. IEEE (1998)
87. Ganster, H., Pinz, P., Rohrer, R., Wildling, E., Binder, M., Kittler, H.: Automated melanoma recognition. *IEEE Trans. Med. Imaging* **20**(3), 233–239 (2001)
88. Green, A., Martin, N., Pfitzner, J., O'Rourke, M., Knight, N.: Computer image analysis in the diagnosis of melanoma. *J. Am. Acad. Dermatol.* **31**(6), 958–964 (1994)
89. Alquran, H., et al.: The melanoma skin cancer detection and classification using support vector machine. In: 2017 IEEE Jordan Conference on Applied Electrical Engineering and Computing Technologies (AEECT), pp. 1–5. IEEE (2017)
90. Roß, T., Handels, H., Kreusch, J., Busche, H., Wolf, H., Pöpll, S.J.: Automatic classification of skin tumours with high resolution surface profiles. In: International Conference on Computer Analysis of Images and Patterns, pp. 368–375. Springer (1995)
91. Celebi, M.E., et al.: A methodological approach to the classification of dermoscopy images. *Comput. Med. Imaging Graph.* **31**(6), 362–373 (2007)
92. Handels, H., Roß, T., Kreusch, J., Wolff, H.H., Poepll, S.J.: Feature selection for optimized skin tumor recognition using genetic algorithms. *Artif. Intell. Med.* **16**(3), 283–297 (1999)
93. Ain, Q.U., Xue, B., Al-Sahaf, H., Zhang, M.: Genetic programming for feature selection and feature construction in skin cancer image classification. In: Pacific Rim International Conference on Artificial Intelligence, pp. 732–745. Springer (2018)
94. Oliveira, R.B., Pereira, A.S., Tavares, J.M.R.: Computational diagnosis of skin lesions from dermoscopic images using combined features. *Neural Comput. Appl.* **31**(10), 6091–6111 (2019)
95. Umer, M.J., Amin, J., Sharif, M., Anjum, M.A., Azam, F., Shah, J.H.: An integrated framework for COVID-19 classification based on classical and quantum transfer learning from a chest radiograph. *Concurr. Comput.: Pract. Exp.* e6434 (2021)
96. Sharif, M.I., Li, J.P., Amin, J., Sharif, A.: An improved framework for brain tumor analysis using MRI based on YOLOv2 and convolutional neural network. *Complex Intell. Syst.* 1–14 (2021)
97. Ali, M.S., Miah, M.S., Haque, J., Rahman, M.M., Islam, M.K.: An enhanced technique of skin cancer classification using deep convolutional neural network with transfer learning models. *Mach. Learn. Appl.* **5**, 100036 (2021)
98. Krizhevsky, A., Sutskever, I., Hinton, G.E.: Imagenet classification with deep convolutional neural networks. *Adv. Neural Inf. Process. Syst.* **25**, 1097–1105 (2012)
99. Amin, J., et al.: Integrated design of deep features fusion for localization and classification of skin cancer. *Pattern Recogn. Lett.* **131**, 63–70 (2020)
100. Simonyan, K., Zisserman, A.: Very deep convolutional networks for large-scale image recognition. arXiv preprint [arXiv:1409.1556](https://arxiv.org/abs/1409.1556) (2014)
101. Szegedy, C., et al.: Going deeper with convolutions. In: Proceedings of the IEEE Conference on Computer Vision and Pattern Recognition, pp. 1–9 (2015)
102. Chaturvedi, S.S., Tembhurne, J.V., Diwan, T.: A multi-class skin cancer classification using deep convolutional neural networks. *Multimed. Tools Appl.* **79**(39), 28477–28498 (2020)

103. Wu, S., Zhong, S., Liu, Y.: Deep residual learning for image steganalysis. *Multimed. Tools Appl.* **77**(9), 10437–10453 (2018)
104. Khan, M.A., Zhang, Y.-D., Sharif, M., Akram, T.: Pixels to classes: intelligent learning framework for multiclass skin lesion localization and classification. *Comput. Electr. Eng.* **90**, 106956 (2021)
105. Iandola, F., Moskewicz, M., Karayev, S., Girshick, R., Darrell, T., Keutzer, K.: Densenet: implementing efficient convnet descriptor pyramids. *arXiv preprint arXiv:1404.1869* (2014)
106. Amin, J., Sharif, M., Haldorai, A., Yasmin, M., Nayak, R.S.: Brain tumor detection and classification using machine learning: a comprehensive survey. *Complex Intell. Syst.* 1–23 (2021)
107. Stoltz, W.: ABCD rule of dermatoscopy: a new practical method for early recognition of malignant melanoma. *Eur. J. Dermatol.* **4**, 521–527 (1994)
108. Betta, G., Di Leo, G., Fabbrocini, G., Paolillo, A., Scalvenzi, M.: Automated application of the “7-point checklist” diagnosis method for skin lesions: estimation of chromatic and shape parameters. In: 2005 IEEE Instrumentation and Measurement Technology Conference Proceedings, vol. 3, pp. 1818–1822. IEEE (2005)
109. Argenziano, G.: 3-point checklist of dermoscopy
110. Marcal, A.R., Mendonça, T., Silva, C.S., Pereira, M.A., Rozeira, J.: Evaluation of the Menzies method potential for automatic dermoscopic image analysis. *CompIMAGE* **2012**, 103–108 (2012)
111. Rubegni, P., et al.: Automated diagnosis of pigmented skin lesions. *Int. J. Cancer* **101**(6), 576–580 (2002)
112. Jinnai, S., Yamazaki, N., Hirano, Y., Sugawara, Y., Ohe, Y., Hamamoto, R.: The development of a skin cancer classification system for pigmented skin lesions using deep learning. *Biomolecules* **10**(8), 1123 (2020)
113. Combalia, M., et al.: BCN20000: dermoscopic lesions in the wild. *arXiv preprint arXiv:1908.02288* (2019)
114. Gutman, D., et al.: Skin lesion analysis toward melanoma detection: a challenge at the international symposium on biomedical imaging (ISBI) 2016, hosted by the international skin imaging collaboration (ISIC). *arXiv preprint arXiv:1605.01397* (2016)
115. Codella, N.C., et al.: Skin lesion analysis toward melanoma detection: a challenge at the 2017 international symposium on biomedical imaging (ISBI), hosted by the international skin imaging collaboration (ISIC). In: 2018 IEEE 15th International Symposium on Biomedical Imaging (ISBI 2018), pp. 168–172. IEEE (2018)
116. Mendonça, T., Ferreira, P.M., Marques, J.S., Marcal, A.R., Rozeira, J.: PH 2-A dermoscopic image database for research and benchmarking. In: 2013 35th Annual International Conference of the IEEE Engineering in Medicine and Biology Society (EMBC), pp. 5437–5440. IEEE (2013)
117. Codella, N., et al.: Skin lesion analysis toward melanoma detection 2018: a challenge hosted by the international skin imaging collaboration (ISIC). *arXiv preprint arXiv:1902.03368* (2019)
118. Rotemberg, V., et al.: A patient-centric dataset of images and metadata for identifying melanomas using clinical context. *arXiv preprint arXiv:2008.07360* (2020)
119. Boer, A., Nischal, K.: www.derm101.com: a growing online resource for learning dermatology and dermatopathology. *Indian J. Dermatol. Venereol. Leprol.* **73**(2), 138 (2007)

Improving Monitoring and Controlling Parameters for Alzheimer's Patients Based on IoMT



Mohsen Karimi , Majid Harouni , Elaheh Izadi Jazi , Afroz Nasr , and Nastaran Azizi

Abstract Today, the Internet has become an integral part of people's lives, so that it is impossible for some people to imagine life without the Internet. With the spread of the Internet, and the diversity of Internet use, a new type of Internet use called the Internet of Things (IoT) has emerged. In the Internet of Things, information is collected, managed, and communicated in the daily life of man through the Internet. In this chapter, an improved method Low power and Lossy Network is proposed to control and monitor the Alzheimer's patient in the cloud robot on the Internet of Things in smart homes. In the proposed method, load balancing in the routing protocol in LLN networks based on RPL is presented. The proposed method improves the structure of the P2P (pair-to-pair) path. Data packets are sent as RPL sorted and irregular. Paths sent in P2P mode have been improved to reduce computational overhead and balance load on the network. Elimination of control messages and load balancing in routing are among the advantages of the proposed method. The proposed method is compared with the RPL base car, and experiments based on a test environment will be performed in NS2 software. The results show that the ENRPL proposed in this study performs better in P2P communications and improves path construction in P2P and data transmission. It also affects the efficiency of MP2P point-to-point transmission of data. The results of the proposed method show that the proposed method is much more effective for sending data and creating load balance. The

M. Karimi ()

Department of Bioelectronics and Biomedical Engineering, School of Advanced Technologies in Medicine, Isfahan University of Medical Sciences, Isfahan, Iran

e-mail: Mohsen.karim25@gmail.com

M. Harouni

Department of Computer Engineering, Dolatabad Branch, Islamic Azad University, Isfahan, Iran

E. I. Jazi

Department of Computer Engineering, Ferdowsi University of Mashhad, Mashhad, Iran

A. Nasr

Department of Computer Engineering, Isfahan (Khorasgan) Branch, Islamic Azad University, Isfahan, Iran

N. Azizi

Sepahan Institute of Higher Education, Science and Technology, Isfahan, Iran

proposed ENRPL method, based on the removal and reduction of control messages, also shows a significant improvement over conventional RPL.

Keywords IOMT · Health · Low power and Lossy network · Alzheimer

1 Introduction

Health care or health care is the maintenance or improvement of health through the diagnosis, treatment, and prevention of disease, trauma, and other disabilities in humans. Health care is provided by people working in the field of medicine and health care in medical clinics, dentistry, midwifery, nursing, medicine, optometry, pharmacy, psychology, and other health sciences [1–3]. This care includes work done while providing primary, secondary, and tertiary care as well as public health [4, 5]. In the new definition of the World Health Organization, health not only means the normalization of human beings from various diseases, but also includes emotional, psychological, and social well-being [6]. Accordingly, the social factors determine health pay attention to the social conditions in which human beings live and work during their life cycle [5, 7–10]. One of the most challenging topics in the field of health, health care, and remote control is based on various patients including heart patients, epilepsy, and even Alzheimer's in a smart home environment [11].

The Internet of Things is a computational concept used to describe a future in which physical objects connect to the Internet one after another and interact with other objects. In this technology, everything is assigned a unique identifier as well as an IP that can send data to a specified database [12, 13]. Basically, IOMT can be considered as a connection of a wide network of application networks [14, 15]. Among all the issues related to active research in this field, special attention is paid to the fact that information is routed from one source node to the destination [16, 17]. Maintaining low-cost routing (in terms of energy and data loss) is still a major challenge and requires routing protocols. RPL is a routing protocol for use in low-power, high-waste networks such as networked objects and also in IOMT which is compatible with IEEE802.15.4 standard [18]. Ordinary smart objects have several kilobytes of memory, a small microcontroller, and a limited power source, but can form node networks that potentially consist of hundreds of thousands of nodes. The name LLN networks is derived from the serious limitation of energy and the expansion of these networks in unpredictable environments [19]. Low-power and high-voltage network equipment has limited resources such as processor, memory, battery, and unstable radio communication. The small size, low power, and low cost of producing equipment for such networks limit the resources in them, which provides mechanisms to direct the traffic of devices within the network to the central point or from the central point to other devices within the network [20]. RPL mainly includes criteria based on reliability or energy consumption. The RPL creates a directional graph called the DAG, in which each node selects one of its neighbors as the parent

and thus forms a graph. The basic structure in the RPL protocol is a destination-oriented round-robin graph rooted in boundary routers. Each router that is part of the DODAG graph sends DIO control messages and assigns its own rank within the graph, indicating its position within the network relative to the root. As soon as a DIO message is received, a node calculates its rank within the network, which must be greater than all its parents. DODAG must be built to energy standards [21].

In this study, we intend to introduce a new method for monitoring and controlling Alzheimer's patients by using intelligent health sensors and IOMT architecture. Obviously, many devices in the healthcare network around the world with the addition of simple network equipment have the ability to connect to an integrated network to send data from these devices to an online database. In this regard, it is appropriate to address the need to control and monitor the status of the disease, taking into account the features mentioned in the previous paragraph, and to provide integrated forms that are provided through databases. In the field of health care, a low-power sensor network will be proposed, according to which the relevant data will be collected for each patient, with any number of sensors, to be followed in the next steps in Internet-based remote monitoring and control. Objects to be used for Alzheimer's patients.

Usually in the IOMT context, WSN wireless network networks, IOMT, and CPS physical cyber systems, especially in the field of health care, all require low-power and high-loss LLNs [22]. This is required for all or part of the performance of these systems. These networks are classified as LLNs because nodes in such networks as well as the performance of nodes in these networks have limited resources and usually operate in environments, where there are losses in wireless data transmission. Communication, processing, and computing equipment are located in objects, and the process of placing this equipment inside objects is increasing day by day [23]. This placement in objects or in the environment will make it possible to feel in the network, and as a result, performance will be possible. Unlike older WSN networks, IOMT- and CPS-based networks require control, performance, and deployment as well as multiple decision making. Therefore, low-power devices and equipment not only need to be connected to the central nodes and central gates, but also need to be in direct contact with other equipment. The result is a type of connection called multi-point or MP2P, or point-to-point P2MP, or point-to-point or pair-to-pair P2P.

Due to limitations in energy sources exclusively batteries as well as communication limitations such as bandwidth, the equipment in the LLN may be connected directly to the gates or other equipment in a network [24]. But their cooperation with relays or data can be connected to several hubs or connected to the gate. Therefore, routing protocols are needed in which the data transmission in P2P or MP2P or P2MP is identified and routed. Given the limitations of the LLN, the IETF node standardized the routing of high-throughput and low-power ROLL networks, the LLN routing protocol, or RPL. RPL is a routing standard that supports MP2P, P2P, and P2MP. In fact, in MP2P, P2P, and P2MP, the path is identified and data are sent. The protocol also provides a general routing framework for LLNs. The RPL uses the concepts of the OF objective function. OF or the objective function monitors how the routes are constructed and the quality of the routes. An OF can be designed if the OFF

objective function is not defined in an RPL that does not meet the requirements of an LLN or does not meet the specific application requirements. In other words, OF design can be based on specific application. Designed and used OF, it has scalable flexibility and RPL compatibility. Based on these features, RPL has been introduced as a standard and is compatible and usable in many routing protocols such as IPv6 or 6LOWPAN networks. Considering the capabilities and features of RPL, several researches have been done on the use of RPL in low-power and wide-area networks in IOMT. Existing RPL methods have solved many of the challenges in LLNs, but some of the challenges still remain unresolved on the Internet of Things.

Optimization of the IOMT routing protocol is very important in low-power and high-loss RPL networks. In this chapter, by optimizing the RPL protocol, which is considered in IOMT routing, energy saving is attempted in these networks. In this research, without adding hardware parameters, and only using the parameters in the RPL protocol, this method has been improved. The proposed method will be reviewed in a smart home environment to improve control and monitoring of patients, especially Alzheimer's patients. The following contribution can be added to the theme:

- Collect and transfer health data to online databases with minimal human intervention.
- Ability to monitor patients online using sensors connected to the World Wide Web in the Internet of Things.
- Data integrity and availability of data collected in the same format (so that patient health can be assessed with the cooperation of physicians without geographical restrictions).

In the continuation of this article, it is divided as follows. Section 2 will introduce RPL networks. In Sect. 3, the proposed method for improving RPL networks will be introduced. In Sect. 4, the proposed method will be evaluated. Finally, in Sect. 5, conclusions will be presented.

2 RPL Routing Protocols

Ordinary smart objects have several kilobytes of memory, a small microcontroller, and a limited power source, but can form node networks that potentially consist of hundreds of thousands of nodes. Such networks are commonly known as low-power and high-loss networks, and this name is derived from the severe energy limitation and expansion of these networks in unpredictable environments. Low-power and high-bandwidth network equipment has limited resources such as processor, memory, battery, and unstable radio communication. The small size, low power, and low cost of production of equipment of such networks limit the resources in them. LLN devices are interconnected by a variety of communication links, such as Bluetooth 1, IEEE802.15.4, and low-power WiFi, where the use of IEEE 802.15.4 radio media is significantly more pervasive than other technologies. LLNs can also be used in

a variety of physical surveillance applications and environmental conditions [25]. LLNs are for low traffic applications. The radio media used by LLN equipment is short-range and highly prone to bit error. Communication is an intrinsic attribute of LLN, and given the greatness of the LLN topology, a new routing mechanism and protocol must be employed to adapt to their specific characteristics. The pervasive nature of LLNs has a significant impact on the design of their routing protocol [26]. Because link failure is frequent and usually transient, the routing protocol should not react strongly to network convergence due to temporary failure. For these reasons, one of the most challenging issues in LLNs is finding the best route for data delivery, which means the need for a highly efficient routing mechanism to find and keep track on the network. The routing mechanism pays particular attention to both the resource constraints of LLN equipment and the pervasive nature of LLN radio media.

RPL routing protocol

Low-power and high-loss networks face special conditions and limitations in the fields of computing, communication, and available energy resources, so in order to control and manage the mentioned limitations, advanced, efficient, and compatible routing mechanism. It is absolutely necessary in such networks. The IETF formed the ROLL Working Group to determine the most appropriate routing protocol for low-power and high-volume networks. The ROLL team conducted extensive research and testing on existing routing protocols and concluded that none of the existing routing protocols met all the needs and conditions of low-power and high-bandwidth networks, so the ROLL protocol group designed and standardized IPv6-based RPL routing [27].

RPL routing protocol is a range, distance, and lightweight protocol designed to meet the needs of low-power and high-throughput networks. In this protocol, the objective function is used to determine the quality of the path that each node provides to the gate. The specific needs of the intended application can also be incorporated into the routing using the objective function. RPL is also designed as a module, and new components can be added to meet the needs of special applications [18]. The RPL constructs a roundabout directional graph from network nodes and supports peer-to-peer, one-to-many, and multi-to-one traffic types. RPL is the best option in such networks, in which no effort has been made regarding load balancing, and also the route selection mechanism of this routing protocol itself causes the congestion of the network. The resulting congestion causes network latency, reduced throughput, and energy loss. In this research, using load balancing in RPL routing protocol, a new method in energy efficiency optimization is presented [28].

RPL routing protocol in LLN networks

The RPL routing protocol is modulated as much as possible according to the large set of different requirements. The main goal in RPL design is to achieve a fully modular protocol that can incorporate application requirements into the routing process and can easily add components that take into account application-specific requirements. Designed for use in LLN networks, which include equipment with limited resources and high-loss wired and wireless communication links. Many of the decisions made in

RPL design are based on the specific characteristics of these networks. The pervasive nature of LLN links is not the only feature that influences how RPL is designed. Since resources are also limited, control traffic should be reduced as much as possible. In such networks, data traffic is usually limited and control traffic needs to be reduced as much as possible in order to maintain bandwidth and energy. The use of fast query mechanisms, like other routing protocols, is not applicable here, and control traffic decreases as the network topology becomes stable [28]. RPL is a vector-distance protocol that builds DODAG network nodes so that paths are made from each node to the root of DODAG (Sync or LBR). One or more nodes are initially configured by the network administrator as DODAG roots. Defines neighbor detection operations using new ICMPv6 control messages [8] called DIO and DAO. The DIO message is used to advertise DODAG information such as objective function, DODAG ID, DODAG order, DODAG sequence number, and other DODAG parameters such as path criteria and constraints. When a node discovers multiple neighbors that have the potential to become a parent or child, it follows different rules in deciding to join DODAG. Adding nodes creates DODAG. When a node joins DODAG, it then has a path to the DODAG root to support multiple traffic to one of the leaf-to-root nodes (upward routing). RPL uses up and down directions. The upward direction is from the leaf to the root of DODAG and the downward direction is from the root to the leaf. The parent of a node in DODAG is the first node in DODAG in the upward path [29]. In order to send information downhill, a new mechanism is needed that also supports peer-to-peer traffic. For this purpose, RPL uses another ICMPv6 control message called DAO. The DAO message is to promote the downward trajectory. DAO carries information about the depth or cost of the route to the destination. In some cases, the DAO also stores information about visited nodes. A node that receives multiple DAOs from its children can aggregate their information using local policies to reduce the size of the routing table and the number of DAO messages [29].

- **How to form DODAG**

DODAG is a set of vertices that are connected by directional edges and there is no distance. The RPL creates a rounded directional graph that forms paths from each leaf to the root (border routing). Unlike tree topologies, DODAG allows plug-in paths. So if there is a node, there will always be more than one path between the leaf node and the root.

In the RPL distance vector routing protocol, nodes form a rounded directional graph (tree) called the DODAG, and the gateway or boundary router is rooted in the LLN that connects to the network backbone. The network administrator first configures one or more nodes as the root of DODAG. At the beginning of the DODAG construction operation, the root node broadcasts a control message called DIO, which contains information such as its identity and rank, as well as the target function that determines how the rank is calculated for the node. Of course, nodes can also request the sending of a DIO message from the surrounding nodes by sending a DIS message, in which case the recipient of the DIS message will send the DIO message immediately. Adjacent nodes receive the root of the DIO message from it and after processing, select the root as their parent because it has the lowest possible order.

The nodes that have become members of DODAG then, after calculating their rank and placing it in the DIO message, send the DIO messages in a diffused manner, and other nodes can receive them by receiving the DIO. Choose as a parent. Each node with the lowest rank (node providing the least expensive path to the root) chooses as its parent and puts the other nodes with the highest rank in its parent set and after calculation. In turn, it puts it in the DIO and sends it. This process will continue until all nodes have joined DODAG. Once the tree is formed and the route from nodes to the root is specified, the DAO message is sent by the nodes to the root to determine the route of traffic from the root to the nodes. Each node notifies its children by receiving a DAO message and updates its routing table. Figure 1 shows an example of how DODAG is formed step by step. The physical topology of the network is also shown in Fig. 1. The link criterion is the expected number of submissions and the route objective function specifies the minimum number of expected submissions. While the expected number of submissions is the total number of expected submissions of all links. The expected number of submissions for each link is specified, and in cases where it is not specified, it is equal to 1. The objective function also sets a limit on not selecting battery-powered nodes as a parent. In the first step, the DODAG root starts sending DIO messages. In the second step, nodes 11, 12, and 13 select the border router as their parent and then calculate their rank. Nodes 11 and 12 choose each other as twins because they have the same order to increase correlation. The third stage displays the DODAG obtained after another iteration, and the fourth stage shows the final DODAG. Since the objective function does not allow the selection of battery-powered nodes, node 46 does not select node 35 as the parent [29].

- **How to route in RPL**

RPL performance is divided into two main stages:

- Upward routing
- Downward routing.

- **Upward routing**

In order to route traffic upwards, only one parent is required for each node. So when a node wants to send depending on the root, it simply sends it to its parent. The parent also sends it to the parent of their choice, and this operation continues until it arrives depending on the root.

- **Downward routing**

The RPL routing protocol uses DAO messages to form a routing table for downstream traffic. Therefore, the node receives the packet and delivers it to the appropriate node according to the routing table. The DAO message can only be sent after the topology has been formed. The IP architecture proposed by ROLL separates the sending process from routing. The relay operator's task is to receive the packet and send it according to the destination address based on the routing table. The router is also responsible for creating and maintaining the routing table. After DODAG is

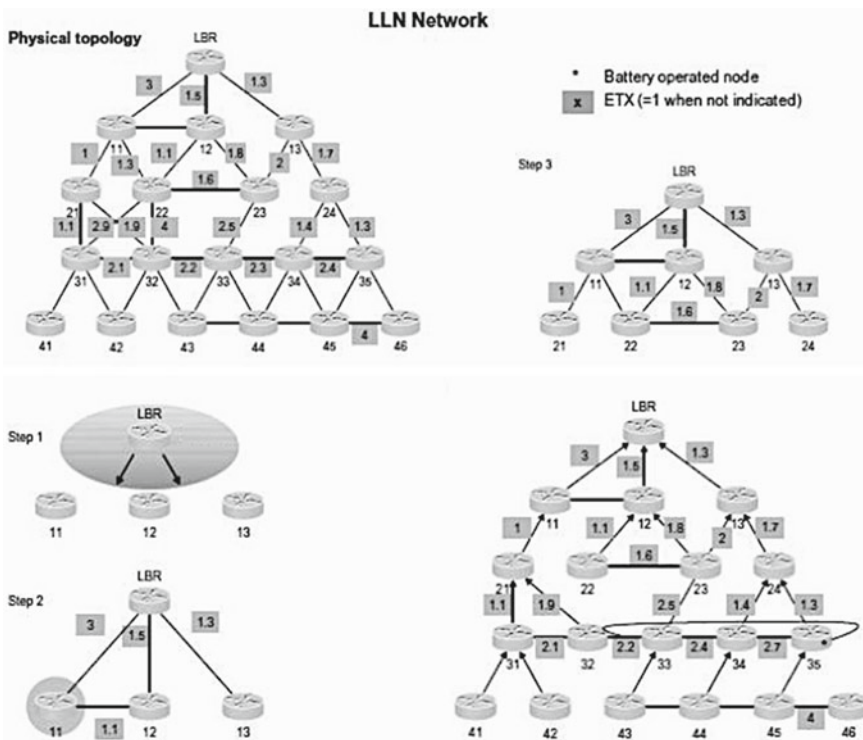


Fig. 1 An example of how DODAG is formed [29]

formed, each node sends a DAO message to the root, so the ancestors of each node are aware of its existence under their tree and update their routing table [30].

• RPL messages

The RPL routing protocol uses three types of control messages to create and maintain the RPL topology and routing table. These messages are: DIO, DAO, DIS.

• DIO message

The DIO message is used to form, maintain, and discover DODAG. Network nodes use this message to advertise DODAG and its attributes. When an LLN network is set up, the nodes start exchanging information about DODAG using the DIO message. DIO contains essential information. Some features in the DIO message are required. The following flags and fields are defined in the DIO.

Grounded (G)

This field indicates whether the DODAG root is connected to an IP-based network that is not an LLN. If DODAG is connected to an external IP-based network, it is called an interceptor. If DODAG is not grounded, it is called floating.

Destination Advertisement Trigger (T)

This bit is used to completely restore the paths in the downward direction.

Destination Advertisement Stored (S)

This bit is used to express the storage of the data extracted from the DIO message in the routing table of a non-root ancestor node.

DAODAG Sequence Number

The DODAG sequence number indicates the number of times the DAODAG fabrication operation is performed and is controlled and quantified exclusively by the DODAG root.

RPL Instance Identifier

The RPL sample identifier is used to identify the DODAG sample and is generated by the root node.

DAODAG ID

The DODAG ID is a 128-bit integer that is denoted by the root DODAG and identifies DODAG exclusively.

Order

The numeric order is 16-bit and specifies the relative position of the node in DODAG and is sent by the node using DIO. The order is calculated by the objective function [18].

- **DAO message**

An upward direction is used to propagate destination information during DODAG. The DAO message is used to propagate node-to-node IDs in downstream traffic support, and ancestor nodes can be used to form routing table elements to support one-to-many and similar traffic. Gives the peer [9]. The DAO message contains the following information:

DAO Sequence Number: A counter that is incremented by the DAO sender node for each new message.

RPL Sample ID: Indicates the sample topology constructed ID.

DAO rank: Specifies the rank of the DAO issuing node.

DAO Lifespan: DAO retention time is in seconds.

Path Label: An 8-bit integer used to label critical paths. It can be labeled to prioritize nodes in using a particular path.

- **DIS message**

The DIS message is similar to the router request messages in the IPv6 protocol and is used to detect DODAGs in the neighborhood and to request DIOs from nodes in

the neighborhood. This message is sent by the node if it does not receive the DIO after a predefined time interval [31].

- **Routing criteria**

Routing metrics are small values that are used to find the cost of a route and help select a route if there are multiple routes. In LLN networks, criteria are used to select the best route according to the objective function. Routing metrics are a critical component of a routing strategy. Many IP-based routing protocols, such as OSPF and IS-IS, typically use static (communication link bandwidth) metrics in common networks. But LLNs have a wide range of applications and limitations that are highly dependent on dynamic metrics. Unlike conventional networks, LLN considers node criteria separately from link criteria. Therefore, the criteria can be classified as node criteria and link criteria as follows [32]

Path Criteria Node Criteria: Node attributes and status, number of steps, node energy.

Node attributes and status: This criterion is used to report various information about node status and attributes. Nodes may appear in the role of traffic aggregator or have limitations that need to be communicated.

Number of steps: This criterion counts the number of intermediate nodes between the origin and destination. The number of steps 3 means that there are 3 nodes between the origin and the destination.

Node energy: Energy is a critical measure in LLNs. Power supply (battery or mains power), residual energy, and other energy-related attributes are defined in this case.

Link Criteria: Link Capacity, Link Delay, Expected Number of Posts of a Link, Link Quality Level, Link Rank.

Bonding power: Bonding power can indicate the maximum or minimum amount of bonding power along the path.

Link Delay: Link delay can represent the sum of link delays along the way or keep the maximum or minimum amount of link delay throughout the path.

Link Quality Level (LQL): Indicates link reliability using discrete values of 0–7. 0 indicates the degree of uncertainty of the link quality, 1 indicates the link with the highest level of quality and 7 indicates the lowest level of link quality.

Link color: In some cases, attributing color to the link in order to express a particular attribute can be useful. The link color is encoded by taking bits and the meaning of each color is up to the network administrator. For example, blue can be used to support cryptography at the link layer level.

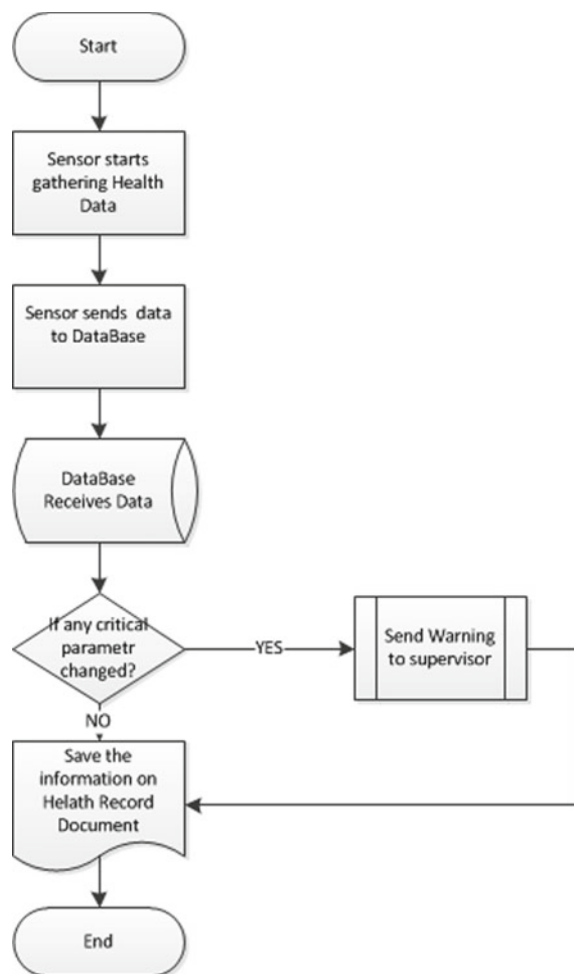
3 The Proposed Method

The proposed method, in simple terms, is that a set of sensors based on IOMT protocols are connected to the patient to monitor the patient's health status. These sensors continuously collect their data with a predetermined trickle and send it to the

address of the hospital service provider according to the schedule. Obviously, these sensors must have memory for situations to which the server does not respond in order to send their data as soon as the server is available. The server, while receiving the data and classifying it according to the device IDs, is a collection of data that can be analyzed by a fuzzy decision-based system or an artificial intelligence-based decision-making unit. If an indicator such as the number of beats per minute or body temperature in two consecutive monitoring exceeds the allowable level, this is important by sending a warning to the hospital staff or the patient's treating physician (who may not have been in the hospital at the time). Be) be informed. The flowchart in Fig. 2 simply shows the steps of the proposed method.

The proposed method has other innovative aspects which are:

Fig. 2 Flowchart proposed method for monitoring and controlling Alzheimer's patient



Online visit: This feature is one of the unique features for remote patient status analysis. If the patient is hospitalized in a hospital environment or in a smart home, the patient's condition can be monitored online at any time by monitoring the sensors remotely by the doctor and also by installing CCTV cameras. Also, if the patient is undergoing treatment at home, the patient can be visited by installing software on the patient's smartphone and also monitoring the sensors through the Internet portal.

Using the patient's medical record for research: Given that this method minimizes the written and handwritten correspondence and documents in the patient's health record, it is possible to have a large database of medical records according to characteristics such as the type of disease. Gender, age, place of residence, or health necessity are categorized according to the security protocols and privacy of the World Institute of Standards and Technology to be available to researchers around the world. Obviously, many diseases can be prevented by categorized study. Also, if necessary, the effects of different types of drugs on the patient's health can be stored in medical documents so that these documents will be available to researchers in the future.

Resource and Infrastructure Management: Using this method, the loss of resources and infrastructure can be greatly avoided. Also, with this method, much of the collected data can be authenticated to the legal aspects and aspects of legal responsibility of personnel. Protected and protected. For example, one of the main challenges in the field of handwritten health records occurs when an error occurs in the registration, while this error may have consequences for the patient's health, it is appropriate for future follow-up of all documents. It should be clear to the registrar that this is not possible in handwritten files as well as to avoid challenges in both online and offline handwriting recognition systems [33–37]. Therefore, a capability has been considered in this method to identify the human data storage agent with a unique identification code so that the related legal aspects can be traced. Also, if necessary, a printed physical version of the health record documents can be prepared.

Topology designed in the IOMT context

Considering the capabilities and features of RPL, several researches have been done on the use of RPL in low-power and wide-area networks in IOMT. Existing RPL methods have solved many of the challenges in LLNs, but some of the challenges still remain unresolved on the Internet of Things. Although RPL is flexible, some of the weaknesses in RPL can be summarized as follows. Weaknesses such as quasi-optimal path detection in P2P and data transmission, use of source routing for MP2P and P2MP, and P2P communication in stored mode of RPL performance. In this chapter of the dissertation in order to improve energy consumption and create load balance in LLN networks, load balance in RPL in stored and non-stored form with the approach of using the monitor and patient control in the smart home or in any. Another smart environment is in the field of health. In the proposed method, a filter

is designed based on which data packets are compressed to compress the length of the data packet.

This article focuses on analyzing and improving the RPL protocol in different scenarios. Interoperability between functional save and non-save modes, memory reduction required for memory functional mode, improved security, and discovery of data transmission paths in P2P mode are also considered. In this research, discovering the necessary path in P2P helps to control the computational overhead and reduce the required memory as well as the balance dimensions. In general, the innovations presented in this research are:

1. Improving P2P routing and sending data in RPL without using additional control messages and also with small changes in the protocol so that the necessary cooperation between the necessary standards of RPL implementation takes place.
2. Reduce computational overhead as well as create load balance in P2P, P2MP, and MP2P communications in stored operation mode.

Proposed routing protocol with load balancing

In this part of the research, an improved routing method and protocol for WSN wireless networks with low LLN capacity and power will be presented. The proposed method and protocol for RPL improvement consists of two parts.

- Improved routing in sending P2P data and creating load balancing
- Improve power consumption by balancing P2MP and MP2P routing.

Improve the proposed algorithm

To improve P2P path construction in RPL and packet-sending algorithms, the RPL protocol uses the objective function to improve data transmission and path routing when at least two nodes are in the immediate vicinity of each other or avoid the destination node, which is in the immediate vicinity of the source and the source node. The main goal is to improve the RPL algorithm in such a way as to avoid generating additional MDAO messages. There is also no change in RPL control messages in this protocol. Therefore, the features in the proposed solution-protocol can be easily implemented with existing RPLs.

The DIO control message is used by the RPL to create the MP2P and P2MP paths. Based on different DODAGs, DIO messages are propagated over the network. If a node is part of the DODAG notified in the DIO message, this node will propagate the corresponding DODAG message using the Trickle timer. If a node is not part of a DODAG, the node deletes the DIO message. The above description shows that in each case the nodes in a network are forced to process DIO messages. Regardless of whether or not a node connects to DODAG. Each node receives a DIO message emitted by its direct neighbors due to its wireless networking properties. A node can use its neighbor's DIO message to identify its direct neighbors, and it can also store this information in a table. Therefore, instead of using the MDAO message to

identify and maintain the data transmission table for neighboring nodes, it uses the DIO message directly to record this information and optimize. This process is done as follows.

If the DIO message is received by a node, that node extracts the publishing addresses from the DIO messages and then stores it in its send table. This step is done regardless of whether the node is interested in connecting to DODAG or not. If there is an entry to publish (in the submission table) or in other words, if there is node information in the table, it will only be updated and subsequent addresses will be equal to the publishing address. If a node has a packet to send, it will be sent to its destination in the table. If this address is present in the send table, the data packet will be sent to the next destination node or hop. Otherwise, it uses the data sending rules in RPL.

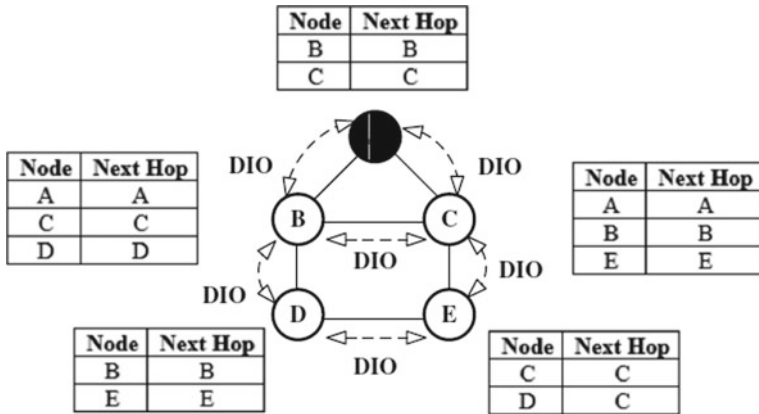
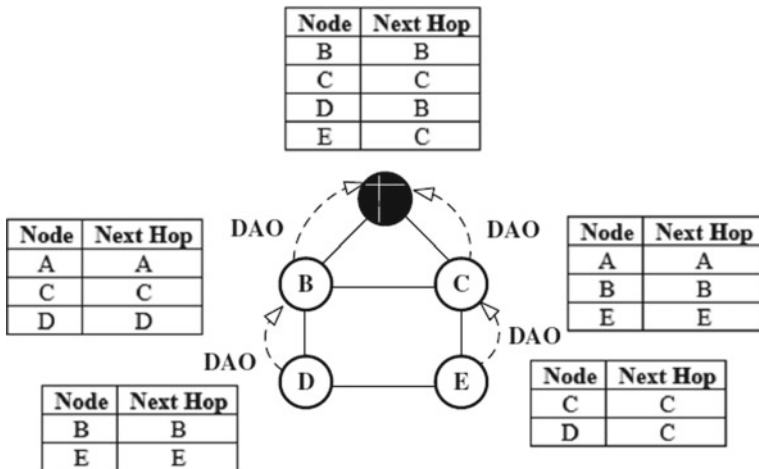
Improved algorithm in non-saved operation mode

The proposed ENRPL algorithm operates in regular storage mode, but nodes do not store data transmission tables in non-storage mode. In Irregular Mode, when the node receives the DIO message, it searches the IPv6neighborhood table. If the published message of the DIO node is not in the table, a new record is created for multiple nodes to be published and stored in the neighborhood table to provide local connection addresses. This forces the MAC layer to obtain the local connection address of the neighboring node before sending. In non-stored mode, another method can be used in which the address of the diffuser nodes is stored in the network layers. In the functional state expression, it is possible for a node to store only the addresses of direct neighboring nodes. If a node needs to send data and a data packet, the node searches for the addresses of the destination nodes. This search is performed on the addresses of the neighborhood table. Or the data structure holds addresses as well as the addresses of direct neighboring nodes. If there is a matching address, it will be sent depending on the destination node, otherwise the non-saved function mode in RPL will be used. They use resource routing when the roots send the packet, so this algorithm will work when resource routing is not used, for example when P2P data transmission is not obtained at the root.

The proposed ENRPL method uses the DIO message to store the information of the direct neighbors shown in Fig. 3. Similarly, the process of building the P2MP, P2P, and MP2P paths is shown in Fig. 4. These figures show that ENRPL can lead to load balancing.

Load balance in P2MP and MP2P routing

In the RPL protocol and in non-stored operation mode, RPL uses source routing for P2MP and MP2P communications. Resource routing results in large data packets can generate high processing latency. In addition, there are IEEE as IP addresses, or 802.15.4 MAC addresses for all nodes along the way to the destination in the data packet. In this method, it brings computational load as well as load imbalance in the path. Also, nodes in wireless networks that have limited power. Therefore, source routing in these networks requires high power consumption and thus reduces the life of the network.

**Fig. 3** Direct neighbor information storage for routing in P2P**Fig. 4** Storing direct neighbor information for routing in P2MP

To overcome this weakness in resource routing in RPL protocol in MP2P data transmission and P2MP data transmission protocol based on packet transmission in P2P will be superposed. In P2P mode, nodes use the DIO broadcast message to build tables and store addresses instead of using the DAO message. DIO messages are spread across the network, and each node updates the address tables and information about the nodes within it when it receives the DIO message. This feature will be used in sending data in P2MP and MP2P mode as a superposition or collection of works.

Send data packet in MP2P and P2MP mode

In MP2P and P2MP function mode, the address tables generated in P2P mode, which are generated by the propagation of the DIO message, will be used. When a node has

a packet to send to another node, it uses network topology information to construct the source path to the destination node. The node to send data in P2MP mode has the destination addresses available first. Is sent on the way to the destination nodes. Each path from the source node to each node is intentionally implemented independently based on the enhanced routing process in ENRPL in P2P. In other words, the P2P process in ENRPL for each node on the path to the destination node will be executed completely and independently of any other path. In the routing process, the packet node sends information to the next hop. If a node receives a packet path, it compares the address of the received packet with the address of the destination node; if both addresses are the same, it is sent depending on the transfer layer. Otherwise the node will use the desired neighborhood table to find the addresses of the nodes. If the retrieved address of the node is from the node that received the packet, the neighboring node will be deleted. This recovery is very important, because if the recovery and removal of the path is not done properly, the path loop will be created. In sending a data packet, if a node does not have direct access to the addresses of the target nodes, it will be routed through the neighbors, and if the desired path is not found, through the source routing provided in the RPL path to the sensor will be transferred. This routing through the source will be done only for the same single route, the rest of the routes will continue their routing process independently. For a complete and successful evaluation of this process, the MAC layers will pass from the layer containing the packet-sending node to the network layer address. The algorithm in Fig. 5 shows the routing process in P2MP mode.

To send data from MP2P, independent paths to the destination node will be created from the sending nodes based on P2P and with the help of DIO messages. Each path from the message-sending nodes to the destination node is created independently and based on the proposed improved ENRPL protocol. And the processes created in P2MP mode will be repeated in the same way. The algorithm in Fig. 6 shows the routing process in MP2P mode.

Steps	Executed process
1	Beginning
2	Spread the DIO message across the network
3	Update the address tables in each node based on the DIO message
4	Start sending messages from one sticker to several sensors
5	Number of destination sensors = M
6	Route construction based on the proposed ENRPL protocol
7	P2P routing independently on each path from the M path to the destination nodes
8	Has the message been delivered to the desired node?
9	If the message is delivered to the desired n node, the algorithm terminates
10	Send a message in the path leading to the node that did not receive the message via source routing in the RPL
11	Check receiving messages on M sensor
12	In case of termination of the algorithm, otherwise execution of step 10

Fig. 5 Routing process algorithm in P2MP operating mode

Steps	Executed process
1	Beginning
2	Spread the DIO message across the network
3	Update the address tables in each node based on the DIO message
4	Start sending messages from one sticker to several sensors
5	Number of source sensors to send the message = M
6	Route construction based on the proposed ENRPL protocol
7	P2P routing independently on each path of the M path from the source node to the destination node
8	Are the messages delivered from the source node to the target node?
9	If the message is delivered to the desired node from M different path based on P2P termination algorithm
10	Send message from the path of the node with an error leading to the destination node
11	Message through source routing in RPL
12	Check receiving messages from M sensor

Fig. 6 Routing process algorithm in MP2P mode

4 Results

To evaluate the proposed protocol in health control and monitoring called ENRPL, this method is performed on P2P routing protocol in sending data and on P2MP and MP2P in sending data. In summary, it can be stated that in terms of technical aspects, using the NS2 software (network simulator toolbox), the network status is examined and the behavior of the sensors during the sending and receiving of data is examined. For this purpose, the ENRPL method is introduced in this research. The necessary studies and relevant evaluations have been performed in [38].

The proposed method is designed and simulated in NS2 software. The proposed ENRPL method is based on routing in P2P, P2MP and MP2P. The objective function used in [20] is used in ENRPL. The space is intended to evaluate a hospital with 500 sensors. There is only one root in this network. Evaluations have been performed in different randomly selected topologies. The simulation parameters are generally shown in Table 1. The total simulation time is 30 minutes per second. Three parameters of reliability, latency, and energy consumption are considered. End-to-end latency of packets is used to evaluate the reliability of the PDR parameter, i.e., packet delivery rate, and to evaluate delay evaluation. Finally, for energy consumption, the total number of times the packets are resended will be taken into

Table 1 Simulation parameters

Parameter	Value
MAC layer	IEEE 802.15.4
MAC layer ACKS	Enable
Radio model	Single disk with path loss
Channel rate	250 k bps
MAC layer queue dimensions	10 frames
Node sending path length	M 50
The length of the knot carrier feel	M 100

account. The proposed ENRPL protocol is compared to the RPL. The experiments were performed using the saved working mode. This is because in the mode of operation, the nodes can deliver packets to the destination nodes without the need for a root node. As a result, by removing the roots, a lot of improvement will be achieved.

Generates packet data nodes to evaluate P2MP and MP2P communications. Nodes start generating data packets. Data generation will be in seconds and simulation, and packet production termination time will be in 1000 s. In P2MP and MP2P communications, the root of data generation starts in 20 s and the production of data packets ends in 1000 s. For each packet, the root of the destination node is randomly selected.

Similarly for P2P communication, each node starts the P2P connection in 20 s and ends in 1000 s. For each data packet, the nodes randomly select the destination node. This process is repeated in P2MP, MP2P, and P2P mode. Each node picks up information from its surroundings based on its mission. This information is collected continuously from the environment, but this information is sent to the target nodes or the target node at different time intervals. Package generation time will be 2, 4 and 8 s. And nodes are only allowed to send data to the destination node or nodes at these intervals.

Evaluation of ENRPL method with root located at the edge

The proposed ENRPL method is simulated on a fully connected stochastic topology. Also, two different sets of experiments have been performed to evaluate the effect of root position on protocol efficiency. For the first batch of experiments, the root is placed at each edge of the grid, and in the second batch, the root is placed in the center of the grid.

PDR evaluation of ENRPL method with root located at the edge

In the first set of tests, the root is placed on the edge and the desired evaluation criteria will be examined. In the next step, the proposed ENRPL method will be used to send P2P, P2MP and MP2P data. Tables 2, 3 and 4 show the results obtained in the PDR in the proposed ENRPL protocol at the time of data transmission of 2, 4 and 8 s. As can be seen from the results of Tables 3, 4 and 5, the rate of message delivery has also increased with increasing time interval. Because data production has decreased. To better evaluate the results of the numbers obtained in the pseudo-simulations, it is also shown in the form of a graph. In all cases, the proposed ENRPL method has a higher message delivery rate, which is mainly due to the reduction of the route in sending data and also the reduction of the possibility of producing loops in routing.

Table 2 Comparison of packet delivery rates in the proposed ENRPL method P2P data transmission mode by percentage

Time interval	2 s	4 s	8 s
RPL-P2P	41.25	69.32	87.85
ENRPL-P2P	45.71	87.14	95.19

Table 3 Comparison of package delivery rates in the proposed ENRPL method in P2MP mode with root-based roots in percentage

Time interval	2 s	4 s	8 s
RPL-P2MP	49.31	70.21	88.8
ENRPL-P2MP	58.17	78.91	96.17

Table 4 Comparison of package delivery rates in the proposed ENRPL method in MP2P mode by percentage

Time interval	2 s	4 s	8 s
RPL-MP2P	57.85	72.34	89.71
ENRPL-MP2P	65.17	79.65	96.85

Table 5 Comparison of end-to-end latency in the proposed ENRPL and RPL method in P2P with root-based roots in milliseconds

Time interval	2 s	4 s	8 s
RPL-P2P	3200	1610	1101
ENRPL-P2P	3120	1553	1005

Evaluate the results of end-to-end delays with roots located at the edge

The delay of delivery of message packets in P2P, P2MP, and MP2P communications is shown in Tables 5, 6 and 7 in the case of message generation intervals of 2, 4, and 8 s. By comparing the two protocols RPL and ENRPL in the proposed method, the results show a decrease in the delay in the proposed ENRPL compared to RPL. Also, the rate of latency has decreased with increasing data production time, which is mainly due to the reduction in the number of messages generated. For P2P, MP2P, and P2MP modes, the numbers indicate that the latency in the random topologies used in the simulation in packet generation modes decreases with increasing time. The ENRPL method was less delayed.

Evaluation of ENRPL method with center-based roots

The same experiments have been performed for the case where the root is in the center of the network, in other words, the evaluation of protocols in different topologies when the root is not in the center of the network is as follows.

Table 6 Comparison of end-to-end latency in the proposed ENRPL and RPL method in P2MP with root-based roots in milliseconds

Time interval	2 s	4 s	8 s
RPL-P2MP	3180	1591	1133
ENRPL-P2MP	3060	1541	954

Table 7 Comparison of end-to-end latency in the proposed ENRPL and RPL method in MP2P with root-based roots in milliseconds

Time interval	2 s	4 s	8 s
RPL-MP2P	3220	1607	1117
ENRPL-MP2P	3150	1545	905

Evaluate the root delivery rate of PDR messages located in the center

The process obtained in this case is shown in Tables 8, 9, and 10 with a message generation interval of 2, 4, and 8 s. The obtained process and the obtained results show that the same situation is repeated when the root is in the network. But a closer look reveals that the message delivery rate is slightly higher than when the root is at the edge. These results show that shorter paths in MP2P and P2MP mean DODAC and node have fewer nodes and shorter paths are created. In practice, longer routes reduce deliveries. In other words, nodes have to go a long way to create DODAC and send messages to destination nodes.

Compare end-to-end latency with center-based roots

In comparing the end-to-end latency when the root is in the center as well as when it is at the edge, a similar process is repeated. This means that in practice the delay in the ENRPL method proposed in this study has been reduced. This decrease is significantly reduced by increasing the number and time of production of the message packet. But compared to the case where the root is at the edge, when the root is in the center, this delay is reduced because the nodes travel a shorter path to send data to the root and destination. Tables 11, 12, and 13 are shown. The delay rate in ENRPL is much less than the original RPL.

Comparison of energy consumption with roots located at the edge

The load balance created in the proposed method and in the proposed ENRPL protocol leads to a reduction in energy consumption. This reduction in energy

Table 8 Comparison of message delivery rates in the proposed ENRPL method in P2P with centrally located root

Time interval	2 s	4 s	8 s
RP2-P2P	47.11	76.21	89.56
ENRPL-P2P	55.06	82.14	96.9

Table 9 Comparison of message delivery rates in the proposed ENRPL method in MP2P with centrally located root

Time interval	2 s	4 s	8 s
RPL-MP2P	46.91	76.12	91.15
ENRPL-P2P	56.15	81.91	98.01

Table 10 Comparison of message delivery rates in the proposed ENRPL method in P2MP with center-based root

Time interval	2 s	4 s	8 s
RPL-P2MP	46.39	75.98	90.01
ENRPL-P2MP	54.1	83.01	97.51

Table 11 Comparison of end-to-end latency in the proposed ENRPL method and RPL in R2P and root-based methods

Time interval	2 s	4 s	8 s
RPL-P2P	2517	1109	735
ENRPL-P2P	2412	1008	521

Table 12 Comparison of end-to-end latency in the proposed ENRPL and RPL methods in P2MP and center-based root

Time interval	2 s	4 s	8 s
RPL-P2MP	2491	1100	751
ENRPL-P2MP	2397	993	539

Table 13 Comparison of end-to-end latency in the proposed ENRPL and RPL methods in MP2P and root-based

Time interval	2 s	4 s	8 s
RPL-MP2P	2535	1059	769
ENRPL-P2P	2390	981	551

consumption is also consistent with the results obtained in the tables of successful package receipts. Since most of the energy in a wireless node network is consumed while sending or receiving data, it seems that the power consumption is reduced by reducing the number of packets sent in ENRPL compared to RPL in P2P, P2MP and MP2P. Tables 14, 15, and 16 show the reduction of energy consumption in the target network by placing the root at the edge. In general, the use of DIS messages, the reduction of the use of DAO control messages and also the reduction of the number of unsuccessful transmissions have been the reasons for the reduction of energy consumption.

Table 14 Comparison of energy consumption in the proposed ENRPL method and RPL in P2P with edge-based roots in millijoules

Time interval	2 s	4 s	8 s
RPL-P2P	4925	4621	4071
ENRPL-P2P	4075	3711	3279

Table 15 Comparison of energy consumption in the proposed ENRPL method and RPL in MP2P with root-based roots in millijoules

Time interval	2 s	4 s	8 s
RPL-MP2P	4885	4852	4036
ENRPL-MP2P	4021	3647	3199

Table 16 Comparison of energy consumption in the proposed ENRPL method and RPL in P2MP with root-based roots in millijoules

Time interval	2 s	4 s	8 s
RPL-P2MP	4896	4492	4050
ENRPL-P2MP	4041	3598	3208

Comparison of energy consumption with the root located in the center

By placing the root in the center of this energy consumption, although the process is the same as placing the root at the edge, but the reduction in energy consumption compared to the state where the root is at the edge is quite evident. Tables 17, 18, and 19 show the results of power consumption by the network in the case of P2P, P2MP, and MP2P. In general, the use of DIS messages, the reduction of the use of DAO control messages, and also the reduction of the number of unsuccessful transmissions have been the reasons for the reduction of energy consumption.

Table 17 Comparison of energy consumption in the proposed ENRPL method and RPL in P2P with centered root in millijoules

Time interval	2 s	4 s	8 s
RPL-P2P	3717	3025	2618
ENRPL-P2P	3100	2831	2017

Table 18 Comparison of energy consumption in the proposed ENRPL method and RPL in MP2P with centered root in millijoules

Time interval	2 s	4 s	8 s
RPL-MP2P	3697	2958	2555
ENRPL-MP2P	3058	2617	2019

Table 19 Comparison of energy consumption in the proposed ENRPL method and RPL in P2MP with the root located in millijoules

Time interval	2 s	4 s	8 s
RPL-P2MP	3649	3009	2601
ENRPL-P2MP	3068	2687	2005

5 Conclusion

To evaluate the proposed method in order to effectively deliver the data in the proposed method was evaluated. The proposed ENRPL or ENRPL method in routing in P2P, P2MP, and MP2P cases was evaluated from the perspective of PDR message delivery evaluation criteria as well as end-to-end delays in the control and monitoring of Alzheimer's patients in the health field. Nodes are allowed to send data packets at 2, 4, and 8 s. The simulations were performed in two modes. The root is located in the center, and the root is located in the heart. The results of the simulation showed that the proposed ENRPL method was able to achieve better results in the three criteria considered in this study, namely the amount of delivery, the end-to-end delay and the amount of energy consumed, so that the end-to-end delay is significantly reduced, compared to RPL. Also, the message delivery rate is more than 98% when the sensors send a message in 8 s, which shows the success of this algorithm in delivering messages on the Internet of Things in the field of health. Also, the energy consumption of the sensors in the proposed ENRPL method is much lower than RPL. This is due to the decrease in the number of messages sent and the increase in the number of messages received.

Conflicts of Interest There is no conflicts of interest in this chapter.

References

1. Yousaf, K., Mehmood, Z., Awan, I.A., Saba, T., Alharbey, R., Qadah, T., Alridge, M.A.: A comprehensive study of mobile-health based assistive technology for the healthcare of dementia and Alzheimer's disease (AD). *Health Care Manag. Sci.* 1–23 (2019)
2. Amin, J., Sharif, M., Raza, M., Saba, T., Rehman, A.: Brain tumor classification: feature fusion. In: 2019 International Conference on Computer and Information Sciences (ICCIS), pp. 1–6. IEEE (2019)
3. Iqbal, S., Khan, M.U.G., Saba, T., Mehmood, Z., Javaid, N., Rehman, A., Abbasi, R.: Deep learning model integrating features and novel classifiers fusion for brain tumor segmentation. *Microsc. Res. Tech.* **82**(8), 1302–1315 (2019). <https://doi.org/10.1002/jemt.23281>
4. Iftikhar, S., Fatima, K., Rehman, A., Almazyad, A.S., Saba, T.: An evolution based hybrid approach for heart diseases classification and associated risk factors identification. *Biomed. Res.* **28**(8), 3451–3455 (2017)
5. Karimi, M., Harouni, M., Nasr, A., Tavakoli, N.: Automatic lung infection segmentation of Covid-19 in CT scan images. *Intelligent Computing Applications for COVID-19*, pp. 235–253. CRC Press (2021)
6. Raftarai, A., Mahounaki, R.R., Harouni, M., Karimi, M., Olghoran, S.K.: Predictive models of hospital readmission rate using the improved AdaBoost in COVID-19. *Intelligent Computing Applications for COVID-19*, pp. 67–86. CRC Press (2021)
7. Saba, T.: Automated lung nodule detection and classification based on multiple classifiers voting. *Microsc. Res. Tech.* **82**(9), 1601–1609 (2019)
8. Karimi, M., Harouni, M., Rafieipour, S.: Automated medical image analysis in digital mammography. *Artificial Intelligence and Internet of Things*, pp. 85–116. CRC Press (2021)

9. Harouni, M., Karimi, M., Rafieipour, S.: Precise segmentation techniques in various medical images. *Artificial Intelligence and Internet of Things: Applications in Smart Healthcare*, vol. 117 (2021)
10. Rehman, A., Harouni, M., Karimi, M., Saba, T., Bahaj, S.A., Awan, M.J.: Microscopic retinal blood vessels detection and segmentation using support vector machine and K-nearest neighbors. *Microsc. Res. Tech.*
11. Sadad, T., Munir, A., Saba, T., Hussain, A.: Fuzzy C-means and region growing based classification of tumor from mammograms using hybrid texture feature. *J. Comput. Sci.* **29**, 34–45 (2018)
12. Yousaf, K., Mehmood, Z., Saba, T., Rehman, A., Munshi, A.M., Alharbey, R., Rashid, M.: Mobile-health applications for the efficient delivery of health care facility to people with dementia (PWD) and support to their carers: a survey. *Biomed. Res. Int.* **2019**, 1–26 (2019)
13. Aryanmehr, S., Karimi, M., Boroujeni, F.Z. (eds.): CVBL IRIS Gender Classification Database Image Processing and Biometric Research, Computer Vision and Biometric Laboratory (CVBL). 2018 IEEE 3rd International Conference on Image, Vision and Computing (ICIVC). IEEE (2018)
14. Saba, T., Haseeb, K., Ahmed, I., Rehman, A.: Secure and energy-efficient framework using Internet of Medical Things for e-healthcare. *J. Infect. Public Health* **13**(10), 1567–1575 (2020)
15. Khan, A.R., Doosti, F., Karimi, M., Harouni, M., Tariq, U., Fati, S.M., et al.: Authentication through gender classification from iris images using support vector machine. *Microsc. Res. Tech.* **84**(11), 2666–2676 (2021)
16. Ramzan, F., Khan, M.U.G., Rehmat, A., Iqbal, S., Saba, T., Rehman, A., Mehmood, Z.: A deep learning approach for automated diagnosis and multi-class classification of Alzheimer's disease stages using resting-state fMRI and residual neural networks. *J. Med. Syst.* **44**(2), 37 (2020)
17. Smys, S., Raj, J.S.: Internet of things and big data analytics for health care with cloud computing. *J. Inf. Technol.* **1**(01), 9–18 (2019)
18. Sobral, J.V., Rodrigues, J.J., Rabélo, R.A., Al-Muhtadi, J., Korotaev, V.: Routing protocols for low power and lossy networks in internet of things applications. *Sensors* **19**(9), 2144 (2019)
19. Sajjad, M., Ramzan, F., Khan, M.U.G., Rehman, A., Kolivand, M., Fati, S.M., Bahaj, S.A.: Deep convolutional generative adversarial network for Alzheimer's disease classification using positron emission tomography (PET) and synthetic data augmentation. *Microsc. Res. Tech.* **84**(12), 3023–3034 (2021). <https://doi.org/10.1002/jemt.23861>
20. Jamal, A., Hazim Alkawaz, M., Rehman, A., Saba, T.: Retinal imaging analysis based on vessel detection. *Microsc. Res. Tech.* **80**(7), 799–811 (2017)
21. Pham, M., Mengistu, Y., Do, H.M., Sheng, W. (eds.): Cloud-Based Smart Home Environment (CoSHE) for Home Healthcare. 2016 IEEE International Conference on Automation Science and Engineering (CASE). IEEE (2016)
22. Persson, H.L., Lyth, J., Lind, L.: The health diary telemonitoring and hospital-based home care improve quality of life among elderly multimorbid COPD and chronic heart failure subjects. *Int. J. Chron. Obstruct. Pulmon. Dis.* **15**, 527 (2020)
23. Lewis, K.E., Annandale, J.A., Warm, D.L., Hurlin, C., Lewis, M.J., Lewis, L.: Home tele-monitoring and quality of life in stable, optimised chronic obstructive pulmonary disease. *J. Telemed. Telecare* **16**(5), 253–259 (2010)
24. Ramzan, F., Khan, M.U.G., Iqbal, S., Saba, T., Rehman, A.: Volumetric segmentation of brain regions from MRI scans using 3D convolutional neural networks. *IEEE Access* **8**, 103697–103709 (2020)
25. Yaala, S.B., Bouallegue, R. (eds.): On MAC Layer Protocols Towards Internet of Things: From IEEE802.15.4 to IEEE802.15.4 e. 2016 24th International Conference on Software, Telecommunications and Computer Networks (SoftCOM). IEEE (2016)
26. Khan, F.I., Shon, T., Lee, T., Kim, K. (eds.): Wormhole Attack Prevention Mechanism for RPL Based LLN Network. 2013 Fifth International Conference on Ubiquitous and Future Networks (ICUFN). IEEE (2013)

27. Goyal, M., Baccelli, E., Philipp, M., Brandt, A., Martocci, J.: Reactive discovery of point-to-point routes in low power and lossy networks. Draft, IETF-ROLL (2011)
28. Bouaziz, M., Rachedi, A., Belghith, A., Berbineau, M., Al-Ahmadi, S.: EMA-RPL: energy and mobility aware routing for the Internet of Mobile Things. Future Gener. Comput. Syst. **97**, 247–258 (2019)
29. Sawada, H., Kuriyama, H., Yusa, N., Mizuno, T., Mineno, H. (eds.): Mutually Complementary Communication Protocol Based on Destination Oriented Directed Acyclic Graph. 2012 IEEE Consumer Communications and Networking Conference (CCNC). IEEE (2012)
30. Onwuegbuzie, I.U., Razak, S.A., Isnin, I.F.: Control messages overhead impact on destination oriented directed acyclic graph—a wireless sensor networks objective functions performance comparison. J. Comput. Theor. Nanosci. **17**(2–3), 1227–1235 (2020)
31. Farooq, M.O., Pesch, D.: Reduced overhead routing in short-range low-power and lossy wireless networks. Sensors **19**(5), 1240 (2019)
32. Gozuacik, N., Oktug, S.: Parent-aware routing for IoT networks. Internet of Things, Smart Spaces, and Next Generation Networks and Systems. pp. 23–33. Springer (2015)
33. Harouni, M., Mohamad, D., Rahim, M.S.M., Halawani, S.M.: Finding critical points of handwritten Persian/Arabic character. Int. J. Mach. Learn. Comput. **2**(5), 573 (2012)
34. Harouni, M., Mohamad, D., Rahim, M.S.M., Halawani, S.M., Afzali, M.: Handwritten Arabic character recognition based on minimal geometric features. Int. J. Mach. Learn. Comput. **2**(5), 578 (2012)
35. Harouni, M., Mohamad, D., Rasouli, A. (eds.): Deductive Method for Recognition of On-Line Handwritten Persian/Arabic Characters. 2010 The 2nd International Conference on Computer and Automation Engineering (ICCAE). IEEE (2010)
36. Harouni, M., Rahim, M., Al-Rodhaan, M., Saba, T., Rehman, A., Al-Dhelaan, A.: Online Persian/Arabic script classification without contextual information. Imaging Sci. J. **62**(8), 437–448 (2014)
37. Rehman, A., Harouni, M., Saba, T.: Cursive multilingual characters recognition based on hard geometric features. Int. J. Comput. Vis. Robot. **10**(3), 213–222 (2020)
38. Harouni, M., Baghmaleki, H.Y.: Color Image Segmentation Metrics. Encyclopedia of Image Processing, vol. 95 (2018)

A Novel Method for Lung Segmentation of Chest with Convolutional Neural Network



Muhammad Awais Malik, Mazhar Javed Awan, Muhammad Rehan Saleem, Amjad Rehman, and Jaber Alyami

Abstract Tuberculosis is a major health threat in many regions of the world. Opportunistic infections in immunocompromised HIV/AIDS patients and multi-drug-resistant bacterial strains have exacerbated the problem, while diagnosing tuberculosis remains challenging. Medical images have made a high impact on medicine, diagnosis, and treatment. The most important part of image processing is image segmentation. This chapter presents a novel X-ray of lungs segmentation method using the U-net model. First, we construct the U-net which combine the lungs and mask. Then, we convert to problem of positive and negative TB lungs into the segmentation of lungs, and extract the lungs by subtracting the chest from the radiography. In experiment, the proposed model achieves 97.62% on the public dataset of collection by Shenzhen Hospital, China and Montgomery County X-ray Set.

Keywords Computer-aided detection and diagnosis · Lung · Segmentation · Tuberculosis (TB) · X-ray imaging

M. A. Malik · M. J. Awan

Department of Software Engineering, School of System and Technology, Lahore 54770, Pakistan
e-mail: mazhar.awan@umt.edu.pk

M. R. Saleem

Department of Computer Science, School of System and Technology, Lahore 54770, Pakistan
e-mail: rehan.saleem@umt.edu.pk

A. Rehman (✉)

AIDA Lab CCIS, Prince Sultan University, Riyadh 11686, Saudi Arabia
e-mail: drrehman70@gmail.com

J. Alyami

Department of Diagnostic Radiology, Faculty of Applied Medical Sciences, King Abdulaziz University, Jeddah 21589, Saudi Arabia

Imaging Unit, King Fahd Medical Research Center, King Abdulaziz University, Jeddah 21589, Saudi Arabia

1 Introduction

Lungs are the two squidgy organs in chest. They look significantly different. The right side of lungs have three lobes and left lungs have two lobes. Both sides have the ribs. Below the lungs there is a big muscle [1]. The left lungs are divided into two section, and the lung on the right side contains three structures [2]. When we breathe in through the nose and/or mouth, the air enters and passes into the trachea or the windpipe at carina, and the trachea is divided into two bronchi than these branches into smaller bronchioles [3]. The CO₂ is exile from the body, and when it exhales, the lungs are thin membrane that protects and help them back and forth as we breathe. Both lungs connected to the small groups of immune systems of body cells called a lymph node.

1.1 X-Ray of Tuberculosis

X-ray [4] short-form is XR; XR technology utilizes high-energy beams that can pass through a definite person's body tissue and create an image vital to diagnosis and treatment. The X-ray machine is designed of an X-ray tube that carry a pair of electrodes called a cathode and an anode, the patient is placed between the films in the X-ray machine and a radiographic film is placed being the patient. The X-ray machine then focuses the energy beam at a particular area of the patient's body as the X-ray energy moves through the patient's body.

Information retrieval recommender system and information extraction aspect of the given chest X-ray the rotation and the media [5] end of clavicles equidistant from the espouse processes. The exposure of the image is it too dark or too bright. Other approaches are the ABCDE, A stands for Airways about the branches with the bronchi and the Airways trace it and looking both lung fields as well. B are lungs plus pleura the lung marking go all the way to the lateral or the side as back to the ribcage and to make sure there is no collections in the distal portion. C is the cardio mediastinum trace the outline of a heart, D is the disability of the bones and trace the bones of the clavicles, and E is the exposure (Fig. 1).

1.2 Magnetic Resonance Imaging (MRI)

A computer-aided medical diagnosis can perform fast and naturally with high robustness and steadfastness to reinforce the public health system. Medical images [6] help doctors get information about the body's internal parts. Nowadays, medical images are one of the most critical factors to detect the disease through which the patient gets well-treated and diagnosed. Most commonly, medical images are magnetic resonance images (MRI), X-ray, computed tomography (CT), and 3D/4D ultrasound images.

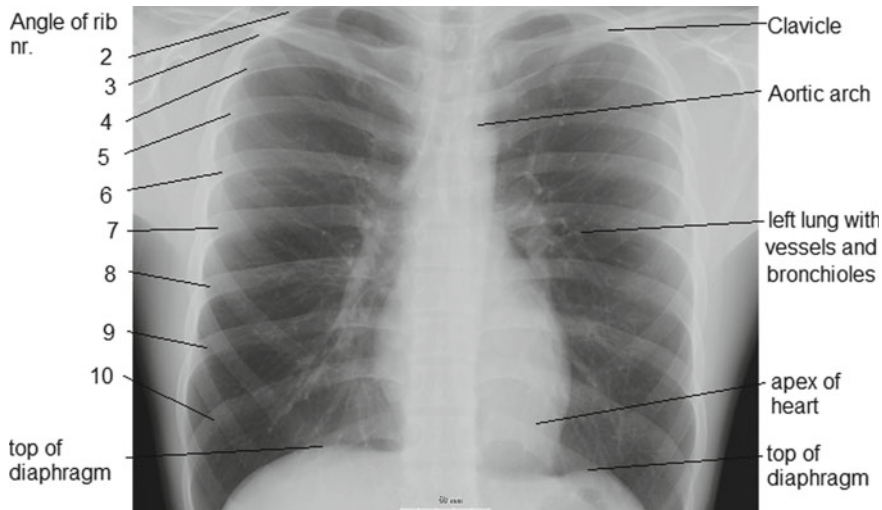


Fig. 1 Reading of a chest X-ray

The computed tomography scan uses X-ray, and magnetic resonance image uses radio waves to capture the image of the inside body. CT gives the general image of the body; on the other hand, MRI give the detailed image of body organ, tissue and soft ligaments. Doctors go through the medical images, numb the affected area, and describe the treatment process.

1.3 Method for the Cure of TB

There are longing that various disease by data mining models [7] and deep learning [8] enhance restorative image examination applications, image investigation, image segmentation, classification, and division and recovery. Some applications imply the deep learning [9] restorative image examination with the segmentation like disease location same as the machine learning to predict Covid-19 [10] and some machine learning which enhance the therapeutic image examination application.

1.4 Segmentation

In image segmentation, partition the image into multiple segments. This technique used to detect objects from the images to make decision association rule mining [11], by indicating different objects in a single image that separate different objects in a

single image. We call different object by different names on some properties. Sometimes, we use different marks on objects; some of them are useful and some osteoporosis [12], drug [13], of them are not useful. Foreground–background separation technique extracts the object from the image.

Segmentation of image is partitioning the image into multiple segments. Each segment identified is labeled, and it would be different from other segments. For example, an image cat and grass and sky would be the segmentation of three cat, grass, and sky labels. Likewise, image contains black and white color. So the segmentation of the image would be the first label of white color and the second would be the label of black color. Recently, machine learning models performed good result in various domains such as the decision of the two-stage classifier models [14] and fake news [15], suicide data mining [16], and pose estimation for active shape model [17] which categorize the segmentation of an image.

In general, a segmentation algorithm can better perform if the region's pixel is similar to the same characteristic. Otherwise, the manual segmentation could perform preprocessing and post-processing.

Edge detection [18] is trying to find out the regions of an image with a sharp change in intensity and a sharp change in color of a higher value which indicates a steep change and a low value which indicates a shallow change. A very common operator for doing this is a Sobel operator; it is an estimation to a derivative of an image. So, if we look at x direction of an image, the incline of an image in the direction equals to the operator. So, we have a kernel three by three which is small and quite quick. And we have the minus number on the left-hand side and positive number on the right-hand side, and we are sort preserving a little bit the center pixel because we have got these two values [19].

Thresholding is the segmentation technique that makes classes so that similar classes can be categorized. Threshold minimizes the error of mis-classifying to a point. For example, if you have image of light object and dark background, thresholding would be the best technique of image segmentation. The good threshold could be performed if mode peak in given threshold is tall, small, and symmetric and split up by deep valleys.

Thresholding refers to basic segmentation; it mostly applies to grayscale images. The threshold value applies many operations like if we apply some value on pixels and if the pixel value exceeds the threshold value, then the second set of operations applies to that practical value.

Some techniques of thresholding are:

- Basic Global thresholding
- Optimal Global Thresholding
- Otsu's Method for Global Thresholding
- Multiple Thresholds
- Variable Thresholding.

Dataset of osteoarthritic contains the large amount of data. Segmenting each data through semi-segmentation has sizable supervision. Automated segmentation became the hot topic of segmenting the data without user interaction. The large

amount of data of lungs [17] image could segment through automated segmentation. Texture analysis is used to identify of object classes. Texture analysis is a feature that classify the region of an image. Texture analysis is used to help in segmentation. There are two types of texture analysis; one is statistical approaches and another one is structural approaches. Big data analytics through machine learning models are performed well [5, 7, 20–29].

The ground truth labels the data [30] like image or video. Labeling is a tedious and time-consuming process, but it is necessary to create test data [31] to evaluate our perception algorithms. The ground truth label algorithms automate the labeling process. Region of interest label need defines of an image/video. There are apparent label and sub-label; the parent label is the object that need to be segmented, and sub-label in X-ray of chest would be the lungs or the heart. We can use ground truth like train classifiers and verify the operation of algorithms and search retrieve based on labels.

The application of support vector machine (SVM) is commonly used in face detection, text in hypertexts categorization classification of image, and bioinformatics. SVM [32] fits in machine learning very well. SVM fits in the biggest split in machine learning between supervised learning, and it can also train it into unsupervised learning, which make sense of data and reinforcement [33].

Medical imaging produces an expanded amount of data. The volume became too large for humans to grasp the doctors; generally, they are trained to spot the abnormalities through the medical image data. They need to focus and a good amount of time of focus on the part of body. They think which are critical to the patient's diagnosis [34], and they miss the important information that starts from other sections of the anatomy. The images [35] detect anomalies from missing image dataset.

Active shape model [36] is a different kind of object detection [37]. Its application is mostly used in face detection and face recognition [38]. It identifies the shape of object. These shapes are developed through the point distribution model with the labeled data. Profile model is commonly used in ASM which finds the strong edges for the point. ASM is widely used to detect through facial and medical images.

Graph cut algorithm cuts the graph [39] between two different areas, but they are linked. The graph cut would give the segmentation of the image [40], so there are algorithms [41] called min-cut algorithms, sometimes called max-flow because they are duels of each other. They are same that allow us to find that segmentation in relatively not too complex a matter. Min-cut by definition will try to pull out little segments that have as few connections as possible. Hence, it tends to pull off tiny segments. So these tinny segments only contact to a small number of other nodes. Finally, graph cut breaks the graph into segments.

2 Related Work

Felix Ambellan team propose the method of segmentation that is accurate as human being's result and combine the CNN with statistical shape knowledge process.

Zeynettin Akkus and his team present the state-of-the-art deep learning [50] and brain MRI segmentation.

Deep learning with segmentation is limited because the datasets are small and limited. Sometimes the larger dataset does not contain label data or the other approaches of large datasets; the training sets do not specify the required problem. The relatively small dataset methodologies could remain on the specific problem which transfers earning approaches.

The deep learning performance depends on several aspects such as preprocessing, post-processing, and initialization. Jordi Mennea and his team develop and train a convolutional neural network (CNN) for bone segmentation in CT scans. The automated convolutional neural network can efficiently segment the bone skull. Alireza Norouzi Sedeh proposes two main segmentation processes in his research thesis; first one is primary segmentation and the second one is graph cut map. The primary segmentation used iterative threshold to separate bones for future work, and it could be used to other medical images like CT.

Shape feature is used to detect five useful objects for future; it can be used in other bones like MRI images like T1-weighted (in this paper he used the T2-weighted) and used on other organs of the human body. Shape prior with graph cut is a famous method for using map; it can be useful for other part of body and also other medical images like CT. Some novel method are applied in 3D; it would be the best approaches if we used fixed shape model to guide the location of object to improve the segmentation or it can be producing the fixed shape model of knee bone.

Cem M. Deniz and his team presented a profound CNN for programmed proximal femur division from auxiliary MR images. The automatic segmentation [17] results show that the necessity of master learning on area determinations and time for segmentation of the proximal femur might be abstained from utilizing CNNs.

A deep CNN for programmed segmentation can help bringing the utilization of proximal femur [14] MRI estimations closer to clinical [51] practice, given that manual division of hip MR images can require around 1.5–2 h of exertion for high pixels of datasets.

Andrea Aprovitola and his team propose the literature review on the knee bone [12] segmentation in MRI. The classification techniques [21] are also identified in this paper. Some of the segmentation methods are adopted in this review. Some of the techniques [52] are the “Thresholding, region growing,” “Deformable Models,” [53] “Clustering methods,” and “Atlas guided approaches.” They identify the prior knowledge of segmentation process [54]. In this paper, the various automation steps can be performed by adopting various knee bone segmentation [55]. The virtual surgery procedure could be performed through the development of segmentation methods. By adopting hybrid approaches of segmentation, in this paper, the coarse segmentation approaches are adopted to more accurate segmentation steps and accuracy and efficient and fully automated segmentation approaches are adopted (Table 1).

Table 1 Related work of medical image segmentation

References	Type	Organ	Accuracy
Stefan Jaeger, Alexandros Karargyris	“Manual segmentation”	Ground truth lung segmentation	87–90%
Stefan Jaeger1, Alexandros Karargyris	Graph cut (HOG, LBP and EHD)	Lung region	
Stefan Jaeger, Alexandros Karargyris	Threshold 0.5 (Log Gabor mask)	Lung segmentation mask	83%
Bram van Ginneken and Bart M. ter Haar Romeny	“Automatic segmentation a new rule-based scheme”	Chest radiographs	94%
Bram van Ginneken a, Mikkel B. Stegmann, Marco Loog	“Active-shape models, active-appearance models and a multi-resolution pixel classification method”	Segmenting the lung field	Pixel classification perform well
Pragnya Maduskar, Laurens Hogeweg, Pim A. de Jong	“Supervised learning approaches”	Cavity contour segmentation	84%
Joao Otavio Bandeira Diniz, Pedro Henrique Bandeira Diniz	“Intrinsic manifold simple linear iterative clustering” (IMSLIC)	Spinal cord detection	92.87%
Rahul Hooda, Ajay Mittal	“Fully-convolutional network” that performs segmentation of lung fields	Automatic analysis of chest radiographs	95.88%
Ajay Mittal, Rahul Hooda	“Deep learning based fully convolutional encoder decoder network”	Segmentation of lung field	95.10%
Zhen Ma, João Manuel R. S. Tavares	“Threshold pattern recognition techniques”	Medical image segmentation	
Fabian Balsiger, Tiziano Ronchetti	“Random Forest”	Segmentation of the distal femur from magnetic resonance (MR)	91.57%
Dongyoun Kim, Jiyoung Lee	“Deformable model”	3D knee bones segmentation	0.927

3 Materials and Methodology

3.1 Dataset Details

Tuberculosis [47], or short-form TB, is one of the oldest and most common diseases affecting many developing countries. About 1/3rd of the world's population is

infected with tuberculosis [62]. Fortunately, only 5% of these infections progress to active this disease. While treatment is possible, it requires an accurate diagnosis. There are many X-ray machines available which provide low-cost projects. Still, the radiologist expert is often missing in my areas for assessing and accurately studying the medical images. Many algorithms are developed that can read images bitterly and quickly with cheap cost, and it could improve the ability to diagnose.

We have the dataset of 800 chest X-ray and about 704 manually mask the dataset. Positive tuberculosis [63] in the dataset are 394, and negative tuberculosis are 406. So, the total number of clinical readings are 800. Out of 800 images, 662 are from The Shezan set and 138 from Montgomery County X-ray set. We have a larger number of male patients, and the positive tuberculosis rate is also higher for male patients (51.4%) compared with a female (28.4%).

3.1.1 China Set—The Shenzhen Set—Chest X-Ray Database

The National Library makes the “standard computerized images” of database for the Tuberculosis of Prescription, Maryland, USA, in a joint effort with Shenzhen No. 3 Individuals’ Emergency clinic, Guangdong Medicinal School, Shenzhen, China. The Chest X-beams are from out-persistent facilities, and were caught as a major aspect of the day-by-day schedule utilizing Philips DR Computerized Analyze frameworks [48]. Number of XR are:

- 336 cases with positive of tuberculosis, and
- 326 normal cases.

3.1.2 Montgomery County X-Ray Set

Chest XR images in this informational collection have been gained from the TB [64] control program of the “Department of Health and Human Services of Montgomery County, MD, USA.” This set contains “138” back foremost XR images, of which 80 XR are negative TB and 58 XR are detected with signs of TB [65]. These images are de-distinguished and accessible through the DICOM format [66]. The set covers a wide scope of irregularities, including radiations and similar pattern.

3.2 Computational Neural Network

CNN is a part of neural network [42] which applies to image processing problems. It learns from images. A regular neural network contains three layers which are input layer, hidden layer, and output layer, respectively. The input layers have the inputs from different forms. The hidden layer performs the mathematics and statistic calculation on the inputs and delivers the outcome to the output layer.

A CNN has multiple layers; the first, convolutional layer, second, pooling layer, third, rectified linear unit layer and fully connected layer. The convolution layer is the important layer; function performs by placing a filter which make the convolved feature MAP [43]. Pooling layer downsizes the sample data of particular feature map, and it reduces the number of parameters. The RELU layer maintains the dimensionality of data and fully activates the classification on the dataset. CNN is the network that basically filter the data [44].

3.3 Acquainted with U-net Architecture

There are powerful architectural for image classification and segmentation in the field of machine learning, data science, and deep learning [45]. There are other approaches to many computers vision like:

- Alex Net
- VGG-16
- Inceptions Net
- Res Net
- GoogLeNet.

The parameter number, accuracy, and dice coefficient are nice because these networks act as a filter and learn feature specification through the input though convolutional neural network, which is applicable in some scenarios. Nonetheless, U-net contains the encoder–decoder network architecture which can generate accurate models [46]. It is one of the standard architectures for the classification because it segmented not only the whole image of a class, but also the segmented area of image by class. Google Colab cloud environment [38]. Recent work inspired deep learning [47], Fake news Bimodal now applied [48], transfer learning VGG19 attention malware detection [49]. It could also accommodate the small weight size of the model. It normalizes the weather to test the data, which is why it is significant for the noisy data (Fig. 2).

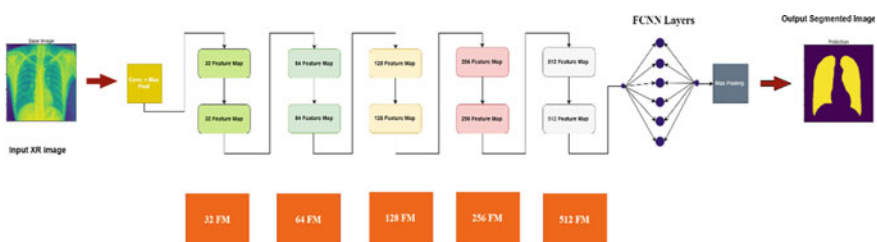


Fig. 2 U-net architecture of image segmentation

U-net is a deep convolutional neural network for segmentation of a bio-medical images [56]. It learned to segment the image, which means raw images enter the U-net model and output the segmented image. The main challenge is that we have few annotated images, and we need the object of the same class that need to be separated by the segmentation [57]. Like all other convolutional networks, it consists of many different operations embellish by the small arrows. The number of input images is entered to the network of U-net from the beginning. Then, the data propagate through the network all along with the possible path. In the end, the segmented images come out, and each of the blue box corresponds multichannel feature map. The x , y size and number of feature channel are noted on each layer. Most of the convolution follows ReLU activate function. The U-net architecture is synonymous with encoder [58] and decoder architectures [59]. The network architecture is shown in Fig. 3.

In 3×3 convolutional + ReLU, it uses the defined part in which convolution uses which mean the 3×3 of an image convolution of a one-pixel border is lost. This process allows to large image in individual tile. The next operation of the “u-net” is the max pooling [60] which reduces the $x-y$ size of the features map. The max pool operation expands its channel separately, and it cultivates the maximum activation from each 2×2 window to the next feature map. So after each of max pooling channel, it increases the number of features channel by factor of “2.”

The main challenge in bio-medical images is low number of training data. To teach the network desire to robust properties, we play random elastic deformation. The resulting image looks perfect like the original image. We participate at the dataset

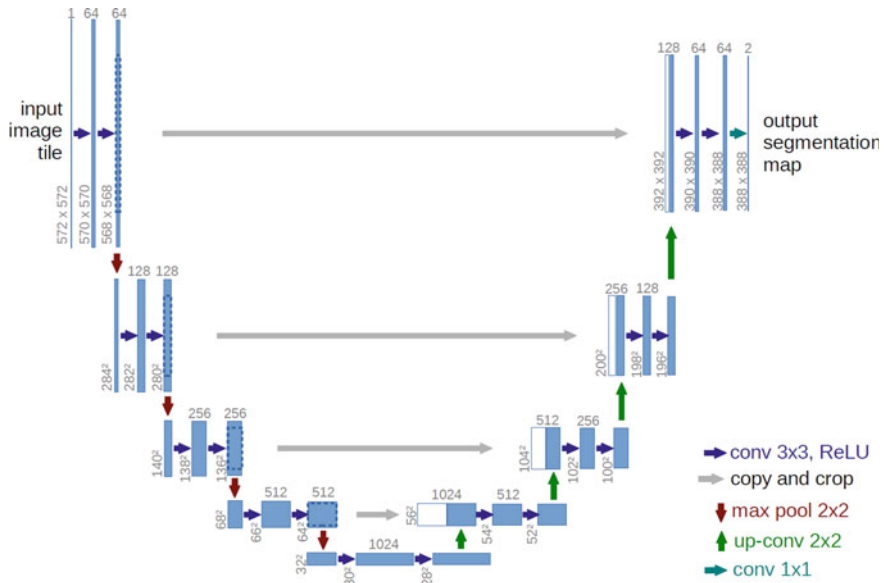


Fig. 3 U-net medical imaging architecture

of X-ray chest [61]. This dataset contains the lung segmentation with their manual mask of both lungs.

4 Model Training

4.1 Loss Function

The loss function takes the set of predictions given out by the network and ground truth labels and computes the loss by combining them together. In deep learning, loss function is used to measure the cost or the degree of model. Therefore, it is important to use the cost function based on the predicted task that need to solve. The best of the cost function that mostly used are accuracy and reduce error. The loss function evaluates each class prediction pixel individually and averages the overall pixel.

4.2 Dice Function

This method is used to train a pixel-wise segmentation model. In image segmentation, dice function is very popular in loss function. The dice function is measured between the two samples. In our method, the first element is prediction matrix and another is targeted matrix. The equation of dice function to train pixel-wise segmentation is:

$$2 * |X \cap Y| / |X| + |Y| \quad (1)$$

X belongs to prediction matrix and Y belongs to target metric. $|X|$ belongs to cardinality of sets X number of element in set, and this \cap belongs to the intersection between X and Y .

All of the convolution and max pooling operation sequences result in particular contraction where moderately increase the “What” and gradually “reduce the Where.” The U-net has an additional extension’s part to create high regulation segmentation map. The extensions part of up-convolutional and convolution 1×1 with sequentially concatenation of high resolution from the contraction path.

The up-convolutional uses alert kernel to alert each feature vector to the 2×2 pixel of the output window and again follow the nonlinear activation function. Again, the up-convolutional uses alert kernel to alert each feature vector to the 3×3 pixel output of the window and again follow the nonlinear activation functions. The output segmentation of the image has two channels, one for the foreground and one for the background class due to unpadded convolution. The map is much smaller than the image of the input. Figure 4 shows the max pooling up-sampling.

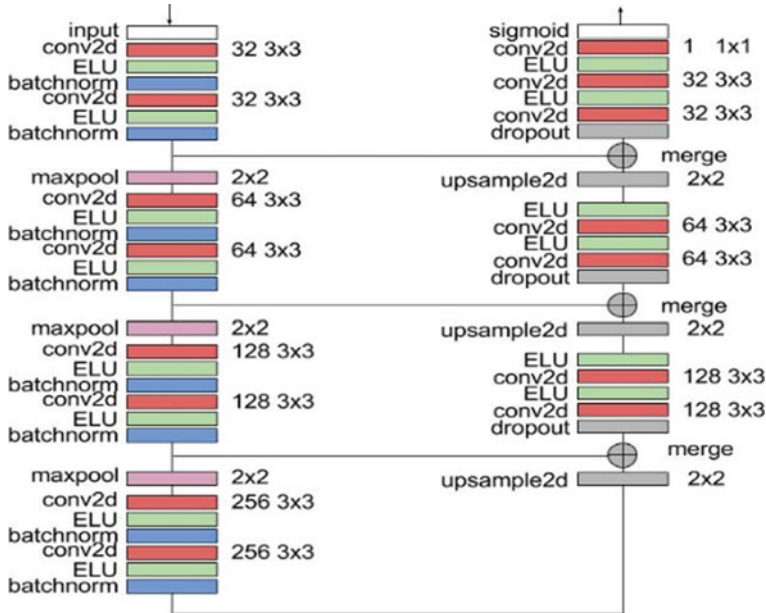


Fig. 4 Max pooling and up-sampling of each pixel of an image

5 Results

The following image gives quantitative map of lungs segmentation at each high point label. All these experiments of study is conducted under the Kaggle platform on workstation of GPU with 13 GB of RAM and 4.9 GB of disk space. The session time with each epoch is 9 h and 57 min. The results are achieved with 40 epochs, the output is shown in Fig. 5.

Figure 6 shows the training and test accuracy after 40 epochs.

Figure 7 shows the training and test dice coefficient after 40 epochs.

With the 40 epochs, the loss of the prediction is 0.9652, dice coefficient is 0.9652, binary accuracy is 0.9826, and validation loss is 0.9606.

The results are achieved with 50 epochs, as shown in Fig. 8.

Figure 9 shows the training and test accuracy after 50 epochs.

Figure 10 shows the training and test dice coefficient after 50 epochs.

With the 50 epochs, the prediction loss is 0.9681, dice coefficient is 0.9681, binary accuracy is 0.9839, and validation loss is 0.9648.

At last, we evaluated our results with 70 epochs as shown in Fig. 11.

Figure 12 shows the training and test accuracy after 70 epochs.

Figure 13 shows the training and test dice coefficient after 70 epochs.

With the 70 epochs, the loss of the prediction is 0.9728, dice coefficient is 0.9728, binary accuracy is 0.9863, and validation loss 0.964.

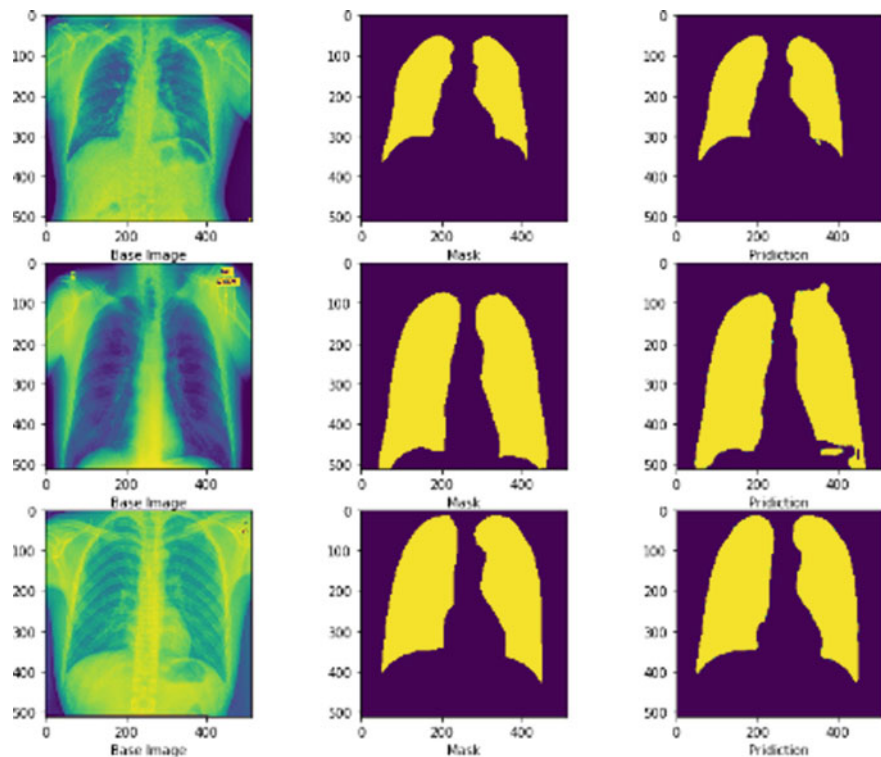


Fig. 5 Segmentation using U-net model with 40 epochs, basic image (left), mask image (middle), and prediction result (right)

The result is given in Table 2.

6 Conclusion

This chapter has presented the segmentation method to detect the abnormalities of lungs using the posterior–anterior X-ray with normal and abnormal manifestation of tuberculosis using the advance convolutional neural network. This research has included different stages such as data analysis of chest X-ray model training and model evaluations. The model implemented on medical image segmentation is known as the U-net model based on CNN and used for segmentation. We evaluate the advance technique for medical training images by given mask of each image. The dominant experimental approach presents the different results on different learning rates and iteration (epochs) of algorithms. The model dice function coefficient value and validation loss values nearly satisfy our approaches with best percentage values.

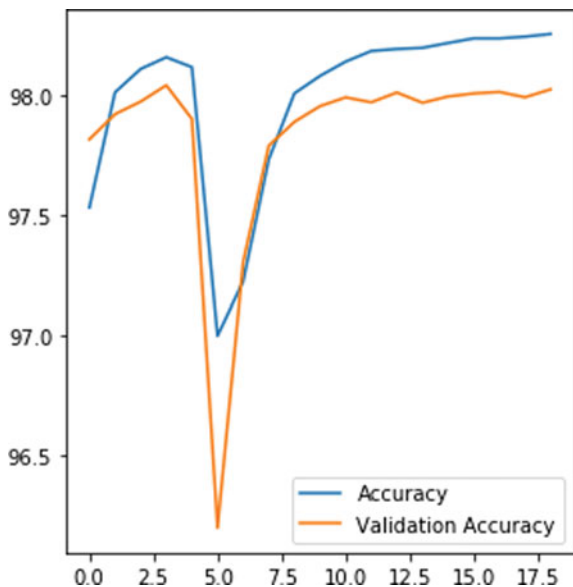


Fig. 6 Accuracy and validation accuracy of lung segmentation of 40 epochs

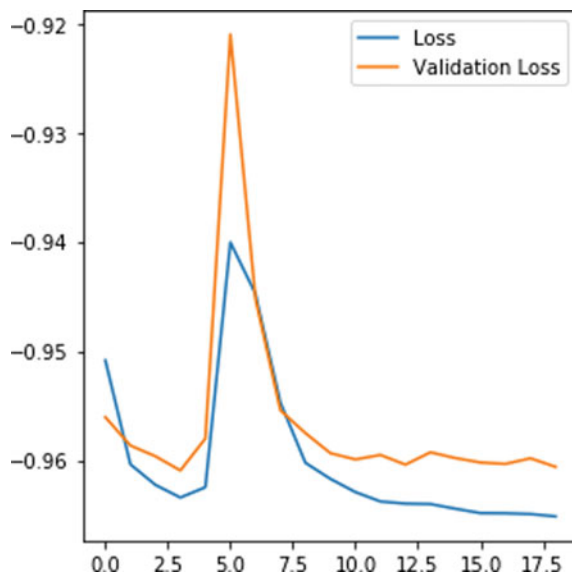


Fig. 7 Loss and validation loss of lung segmentation of 40 epochs

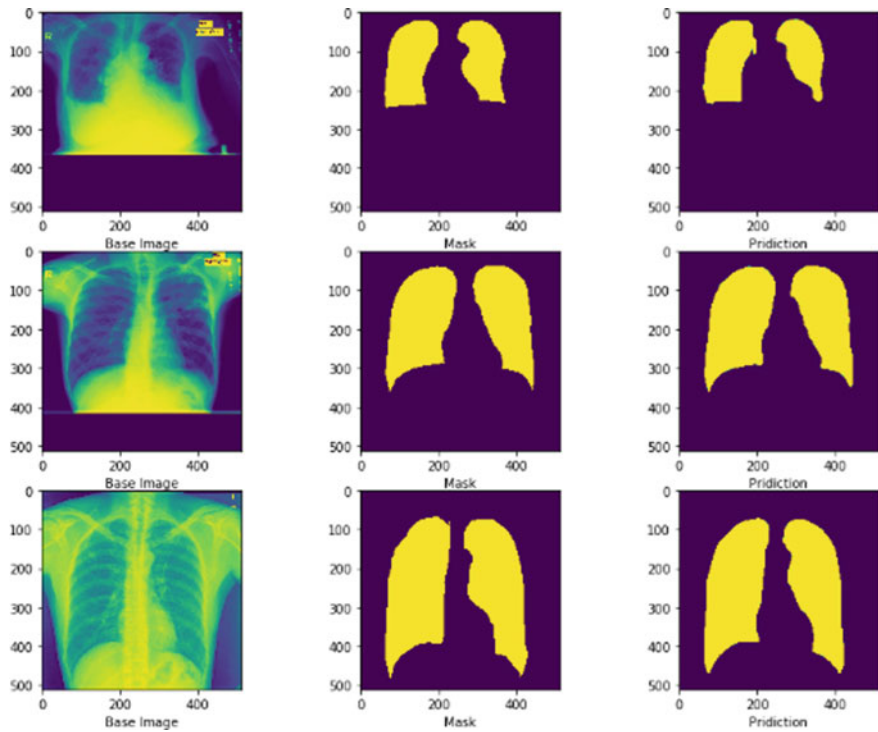


Fig. 8 Segmentation using U-net model with 50 epochs, basic image (left), mask image (middle), and prediction result (right)

With the good results achieved through the U-net architecture of lungs segmentation of chest XR, the number for good results needs to achieve different medical images like MRI and CT scan images and other diseases like cancer disease. Through U-net architecture, the number of high efficiencies could be achieved through the lung segmentation with the cancer disease. These techniques could improve the performance of a CNN.

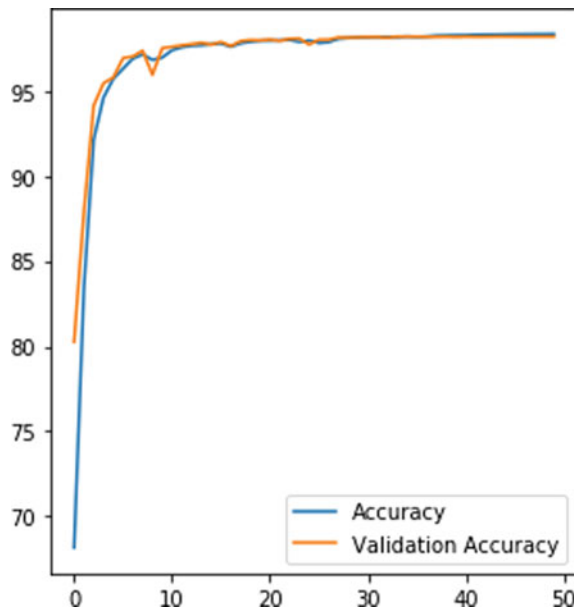


Fig. 9 Accuracy and validation accuracy of lung segmentation of 50 epochs

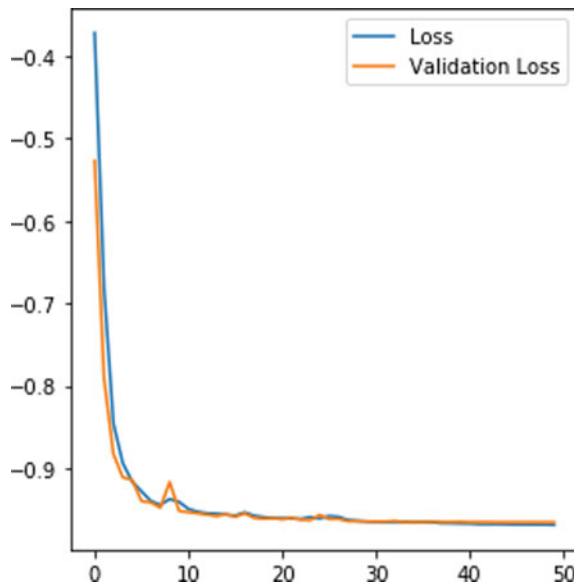


Fig. 10 Loss and validation loss of lung segmentation of 50 epochs

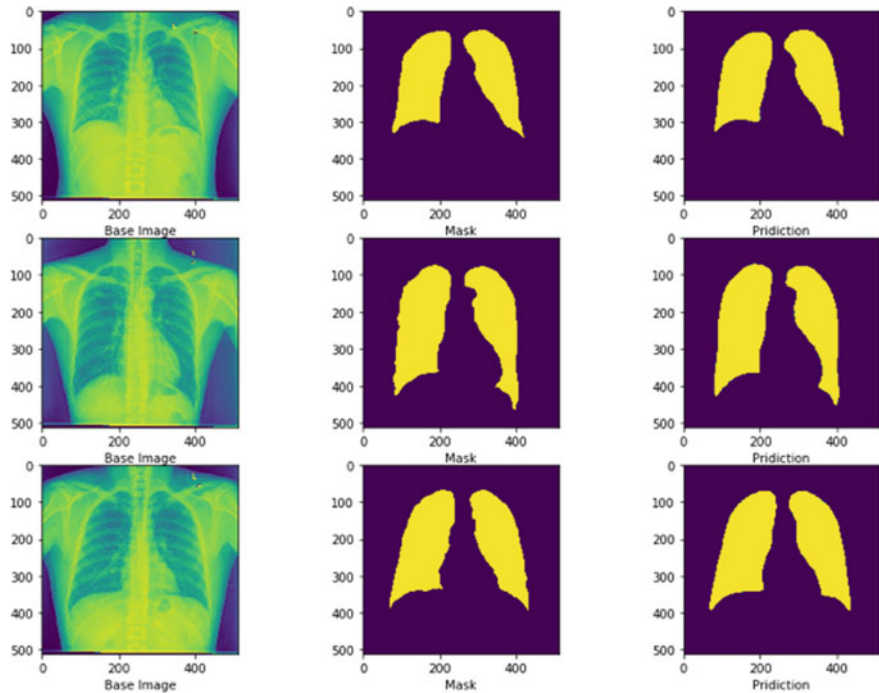


Fig. 11 Segmentation using U-net model with 70 epochs, basic image (left), mask image (middle), and prediction result (right)

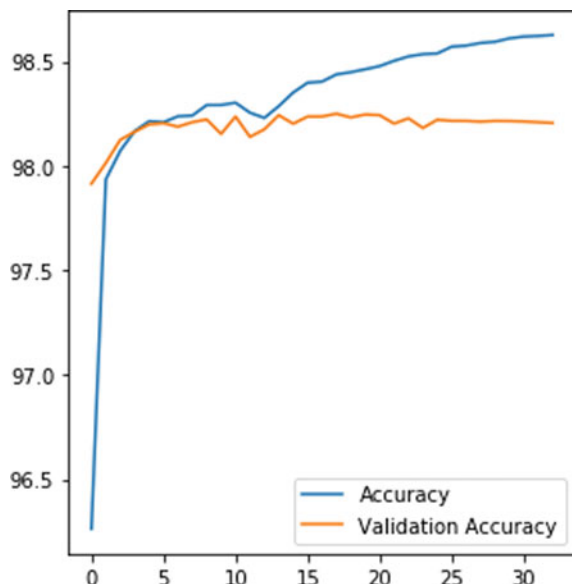


Fig. 12 Accuracy and validation accuracy of lung segmentation of 70 epochs

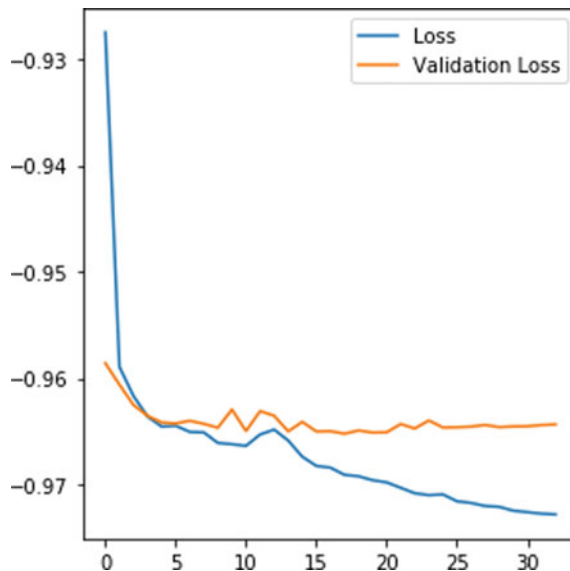


Fig. 13 Loss and validation loss of lung segmentation of 70 epochs

Table 2 Average accuracy of all the epochs is 0.9835

Number of epochs	Prediction loss	Dice coefficient	Binary accuracy	Validation loss
20	0.9627	0.9627	0.9813	0.9594
40	0.9652	0.9652	0.9826	0.9606
50	0.9681	0.9681	0.9839	0.9648
70	0.9728	0.9728	0.9863	0.964

References

1. Saba, T.: Automated lung nodule detection and classification based on multiple classifiers voting. *Microsc. Res. Tech.* **82**(9), 1601–1609 (2019)
2. Khan, S.A., Nazir, M., Khan, M.A., Saba, T., Javed, K., Rehman, A., Akram, T., Awais, M.: Lungs nodule detection framework from computed tomography images using support vector machine. *Microsc. Res. Tech.* **82**(8), 1256–1266 (2019)
3. Saba, T., Sameh, A., Khan, F., Shad, S.A., Sharif, M.: Lung nodule detection based on ensemble of hand crafted and deep features. *J. Med. Syst.* **43**(12), 332 (2019)
4. Abbas, N., Saba, T., Mohamad, D., Rehman, A., Almazyad, A.S., Al-Ghamdi, J.S.: Machine aided malaria parasitemia detection in Giemsa-stained thin blood smears. *Neural Comput. Appl.* **29**(3), 803–818 (2018)
5. Javed Awan, M., Shafry Mohd Rahim, M., Nobanee, H., Munawar, A., Yasin, A., Mohd Zain Azlanmz, A.: Social media and stock market prediction: a big data approach. *Comput. Mater. Contin.* **67**, 2569–2583 (2021). <https://doi.org/10.32604/cmc.2021.014253>
6. Jamal, A., Hazim Alkawaz, M., Rehman, A., Saba, T.: Retinal imaging analysis based on vessel detection. *Microsc. Res. Tech.* **80**(7), 799–811 (2017)

7. Nabeel, M., Majeed, S., Awan, M.J., Muslih-ud-Din, H., Wasique, M., Nasir, R.: Review on effective disease prediction through data mining techniques. *Int. J. Electr. Eng. Inform.* **13** (2021)
8. LeCun, Y., Bengio, Y., Hinton, G.: Deep learning. *Nature* **521**(7553), 436 (2015)
9. Mujahid, A., Awan, M.J., Yasin, A., Mohammed, M.A., Damaševičius, R., Maskeliūnas, R., Abdulkareem, K.H.: Real-time hand gesture recognition based on deep learning YOLOv3 model. *Appl. Sci.* **11** (2021). <https://doi.org/10.3390/app11094164>
10. Iqbal, S., Khan, M.U.G., Saba, T., Mahmood, Z., Javaid, N., Rehman, A., Abbasi, R.: Deep learning model integrating features and novel classifiers fusion for brain tumor segmentation. *Microsc. Res. Tech.* **82**(8), 1302–1315 (2019). <https://doi.org/10.1002/jemt.23281>
11. Iftikhar, S., Fatima, K., Rehman, A., Almazyad, A.S., Saba, T.: An evolution based hybrid approach for heart diseases classification and associated risk factors identification. *Biomed. Res.* **28**(8), 3451–3455 (2017)
12. Anam, M., a/p Ponnusamy, V., Hussain, M., Waqas Nadeem, M., Javed, M., Guan Goh, H., Qadeer, S.: Osteoporosis prediction for trabecular bone using machine learning: a review. *Comput. Mater. Contin.* **67**, 89–105 (2021). <https://doi.org/10.32604/cmc.2021.013159>
13. Javed, R., Saba, T., Humdullah, S., Jamail, N.S.M., Awan, M.J.: An efficient pattern recognition based method for drug-drug interaction diagnosis. In: Proceedings of the 2021 1st International Conference on Artificial Intelligence and Data Analytics (CAIDA), pp. 221–226 (2021)
14. Balsiger, F., Ronchetti, T., Pletscher, M.: Distal Femur Segmentation on MR Images Using Random Forests, pp. 1–6 (2016)
15. Awan, M.J., Yasin, A., Nobanee, H., Ali, A.A., Shahzad, Z., Nabeel, M., Zain, A.M., Shahzad, H.M.F.: Fake news data exploration and analytics. *Electronics* **10**, 2326 (2021)
16. Ferooz, F., Hassan, M.T., Awan, M.J., Nobanee, H., Kamal, M., Yasin, A., Zain, A.M.: Suicide bomb attack identification and analytics through data mining techniques. *Electronics* **10**, 2398 (2021)
17. Candemir, S., Jaeger, S., Palaniappan, K., Musco, J.P., Singh, R.K., Xue, Z., Karargyris, A., Antani, S., Thoma, G., McDonald, C.J.: Lung segmentation in chest radiographs using anatomical atlases with nonrigid registration. *IEEE Trans. Med. Imaging* **33**(2), 577–590 (2014). <https://doi.org/10.1109/TMI.2013.2290491>
18. Marr, D., Hildreth, E.: Theory of Edge Detection, pp. 187–217 (1980). <https://doi.org/10.1098/rspb.1980.0020>
19. Artaechevarria, X., Muñoz-barrutia, A., Ortiz-de-solórzano, C., Member, S.: Combination strategies in multi-atlas image segmentation: application to brain MR data. *IEEE Trans. Med. Imaging* **28**(8), 1266–1277 (2009)
20. Javed Awan, M., Shafry Mohd Rahim, M., Nobanee, H., Yasin, A., Ibrahim Khalaf, O., Ishfaq, U.: A big data approach to black friday sales. *Intell. Autom. Soft Comput.* **27**, 785–797 (2021). doi:<https://doi.org/10.32604/iasc.2021.014216>
21. Alam, T.M., Awan, M.J.: Domain analysis of information extraction techniques. *Int. J. Multidiscip. Sci. Eng.* **9**, 1–9 (2018)
22. Ahmed, H.M., Awan, M.J., Khan, N.S., Yasin, A., Shehzad, H.M.F.: Sentiment analysis of online food reviews using big data analytics. *Elem. Educ. Online* **20**, 827–836 (2021)
23. Chapman, H.N., Fromme, P., Barty, A., White, T.A., Kirian, R.A., Aquila, A., Fromme, R.: Femtosecond X-Ray Protein Nanocrystallography, pp. 3–8 (2011). <https://doi.org/10.1038/nature09750>
24. Gattinoni, L., Bombino, M., Pelosi, P., Lissoni, A., Pesenti, A., Fumagalli, R., Tagliabue, M.: Lung Structure and Function in Different Stages of Severe Adult Respiratory Distress Syndrome (2015)
25. Awan, M.J., Khan, R.A., Nobanee, H., Yasin, A., Anwar, S.M., Naseem, U., Singh, V.P.: A recommendation engine for predicting movie ratings using a big data approach. *Electronics* **10**, 1215 (2021). <https://doi.org/10.3390/electronics10101215>

26. Ali, Y., Farooq, A., Alam, T.M., Farooq, M.S., Awan, M.J., Baig, T.I.: Detection of schistosomiasis factors using association rule mining. *IEEE Access* **7**, 186108–186114 (2019). <https://doi.org/10.1109/access.2019.2956020>
27. Gupta, M., Jain, R., Arora, S., Gupta, A., Javed Awan, M., Chaudhary, G., Nobanee, H.: AI-enabled COVID-9 outbreak analysis and prediction: Indian states vs. union territories. *Comput. Mater. Contin.* **67**, 933–950 (2021). <https://doi.org/10.32604/cmc.2021.014221>
28. Awan, M., Rahim, M., Salim, N., Ismail, A., Shabbir, H.: Acceleration of knee MRI cancellous bone classification on google colaboratory using convolutional neural network. *Int. J. Adv. Trends Comput. Sci.* **8**, 83–88 (2019)
29. Awan, M.J., Gilani, S.A.H., Ramzan, H., Nobanee, H., Yasin, A., Zain, A.M., Javed, R.: Cricket match analytics using the big data approach. *Electronics* **10**, 2350 (2021)
30. Awan, M.J., Bilal, M.H., Yasin, A., Nobanee, H., Khan, N.S., Zain, A.M.: Detection of COVID-19 in chest X-ray images: a big data enabled deep learning approach. *Int. J. Environ. Res. Public Health* **18**, 10147 (2021)
31. Awan, M.J., Farooq, U., Babar, H.M.A., Yasin, A., Nobanee, H., Hussain, M., Hakeem, O., Zain, A.M.: Real-time DDoS attack detection system using big data approach. *Sustainability* **13**, 10743 (2021)
32. Burges, C.J.: A tutorial on support vector machines for pattern recognition. *Data Min. Knowl. Discovery* **2**, 121–167 (1998)
33. Haafza, L.A., Awan, M.J., Abid, A., Yasin, A., Nobanee, H., Farooq, M.S.: Big data COVID-19 systematic literature review: pandemic crisis. *Electronics* **10**, 3125 (2021)
34. Lee, C.H., Sharif, S.Z.: Primary breast tuberculosis (TB) in a patient with known invasive breast carcinoma: a case report. *Med. J. Malays.* **71**(3), 149–151 (2016)
35. Aftab, M.O., Awan, M.J., Khalid, S., Javed, R., Shabir, H.: Executing spark BigDL for leukemia detection from microscopic images using transfer learning. In: Proceedings of the 2021 1st International Conference on Artificial Intelligence and Data Analytics (CAIDA), pp. 216–220 (2021)
36. Abdullah, Awais, Y., Awan, M.J., Shehzad, M.F., Ashraf, M.: Fake news classification bimodal using convolutional neural network and long short-term memory. *Int. J. Emerg. Technol. Learn.* **11**, 209–212 (2020)
37. Penedo, M.G., Carreira, J., Mosquera, A., Cabello, D., Member, A.: Computer-aided diagnosis: a neural-network-based approach to lung nodule detection. *IEEE Trans. Med. Imaging* **17**(6), 872–880 (1998)
38. He, K., Sun, J.: Deep residual learning for image recognition. In: 2016 IEEE Conference on Computer Vision and Pattern Recognition (CVPR), pp. 770–778 (2016). <https://doi.org/10.1109/CVPR.2016.90>
39. Maška, M.: Segmentation of Touching Cell Nuclei Using a Two-Stage Graph Cut Model, pp. 410–419 (2009)
40. Liu, J., Li, M., Wang, J., Wu, F., Liu, T., Pan, Y.: A survey of MRI-based brain tumor segmentation methods. *Tsinghua Sci. Technol.* **19**(6), 578–595 (2014)
41. Rashid, M., Khan, M.A., Alhaisoni, M., Wang, S.H., Naqvi, S.R., Rehman, A., Saba, T.: A sustainable deep learning framework for object recognition using multi-layers deep features fusion and selection. *Sustainability* **12**(12), 5037 (2020)
42. Nawaz, M., Mehmood, Z., Nazir, T., Naqvi, R.A., Rehman, A., Iqbal, M., Saba, T.: Skin cancer detection from dermoscopic images using deep learning and fuzzy k-means clustering. *Microsc. Res. Tech.* **85**(1), 339–351 (2022)
43. Rehman, A., Khan, M.A., Saba, T., Mehmood, Z., Tariq, U., Ayesha, N.: Microscopic brain tumor detection and classification using 3D CNN and feature selection architecture. *Microsc. Res. Tech.* **84**(1), 133–149 (2021). <https://doi.org/10.1002/jemt.23597>
44. Rehman, A., Abbas, N., Saba, T., Mehmood, Z., Mahmood, T., Ahmed, K.T.: Microscopic malaria parasitemia diagnosis and grading on benchmark datasets. *Microsc. Res. Tech.* **81**(9), 1042–1058 (2018). <https://doi.org/10.1002/jemt.23071>

45. Awan, M.J., Rahim, M.S.M., Salim, N., Mohammed, M.A., Garcia-Zapirain, B., Abdulkareem, K.H.: Efficient detection of knee anterior cruciate ligament from magnetic resonance imaging using deep learning approach. *Diagnostics (Basel)* **11** (2021). <https://doi.org/10.3390/diagnostics1110105>
46. Vala, H.J., Baxi, P.A.: A review on Otsu image segmentation algorithm. *Int. J. Adv. Res. Comput. Eng. Technol.* **2**(2), 387–389 (2013)
47. Jaeger, S., Karargyris, A., Antani, S., Thoma, G.: Detecting Tuberculosis in Radiographs Using Combined Lung Masks, pp. 4978–4981 (2012)
48. Ali, S.F., Aslam, A.S., Awan, M.J., Yasin, A., Damaševičius, R.: Pose estimation of driver's head panning based on interpolation and motion vectors under a boosting framework. *Appl. Sci.* **11**, 11600 (2021)
49. Jaeger, S., Karargyris, A., Candemir, S., Siegelman, J., Folio, L., Antani, S., Thoma, G.: Automatic screening for tuberculosis in chest radiographs : a survey. *Quant Imaging Med Surg.* **3**(2), 89–99 (2013). <https://doi.org/10.3978/j.issn.2223-4292.2013.04.03>
50. Papandreou, G., Chen, L., Murphy, K.P., Yuille, A.L.: Weakly- and Semi-Supervised Learning of a Deep Convolutional Network for Semantic Image Segmentation, pp. 1742–1750 (n.d.)
51. Shepherd, F.A., Crowley, J., Houtte, P.V.: The International Association for the Study of Lung Cancer Lung Cancer Staging Project: Proposals Regarding the Clinical Staging of Small Cell Lung Cancer in the Forthcoming (Seventh) Edition of the Tumor, Node, Metastasis Classification for Lung Cancer. *JTO Acquis.* **2**(12), 1067–1077 (2007). <https://doi.org/10.1097/JTO.0b013e31815bdc0d>
52. Nagi, A.T., Awan, M.J., Javed, R., Ayesha, N.: A comparison of two-stage classifier algorithm with ensemble techniques on detection of diabetic retinopathy. In: Proceedings of the 2021 1st International Conference on Artificial Intelligence and Data Analytics (CAIDA), pp. 212–215 (2021)
53. Rehma, A.A., Awan, M.J., Butt, I.: Comparison and evaluation of information retrieval models. *VFAST Trans. Softw. Eng.* **6**, 7–14 (2018)
54. Bergouignan, L., Chupin, M., Czechowska, Y., Kinkingnéhun, S., Lemogne, C., Le Bastard, G., Lepage, M., Garnero, L., Colliot, O., Fossati, P.: Can voxel based morphometry, manual segmentation and automated segmentation equally detect hippocampal volume differences in acute depression? *NeuroImage* **45**(1), 29–37 (2009). <https://doi.org/10.1016/j.neuroimage.2008.11.006>
55. Awan, M.J., Rahim, M.S.M., Salim, N., Rehman, A., Nobanee, H., Shabir, H.: Improved deep convolutional neural network to classify osteoarthritis from anterior cruciate ligament tear using magnetic resonance imaging. *J. Pers. Med.* **11**, 1163 (2021)
56. Awan, M.J., Masood, O.A., Mohammed, M.A., Yasin, A., Zain, A.M., Damaševičius, R., Abdulkareem, K.H.: Image-based malware classification using VGG19 network and spatial convolutional attention. *Electronics* **10**, 2444 (2021)
57. Shi, J.: Normalized Cuts and Image Segmentation (2000)
58. Saidy, L., Lee, C.: Chest X-ray image segmentation using encoder-decoder convolutional network. In: 2018 IEEE International Conference on Consumer Electronics-Taiwan (ICCE-TW), pp. 1–2 (2018). <https://doi.org/10.1109/ICCE-China.2018.8448537>
59. Sahoo, P.K., Soltani, S.A.K.C., Wong, A.K.: A survey of thresholding techniques. *Comput. Vis. Graphics Image Process.* **41**(2), 233–260 (1988)
60. Cootes, T.F., Taylor, C.J. (1992)
61. Ginneken, B.V., Stegmann, M.B., Loog, M.: Segmentation of anatomical structures in chest radiographs using supervised methods: a comparative study on a public database. *Med. Image Anal.* **10**, 19–40 (2006). <https://doi.org/10.1016/j.media.2005.02.002>
62. Jaeger, S., Karargyris, A., Candemir, S., Siegelman, J., Folio, L., Antani, S., Thoma, G.: Automatic screening for tuberculosis in chest radiographs: a survey. *Quant Imaging Med Surg.* **3**(2), 89–99 (2013). <https://doi.org/10.3978/j.issn.2223-4292.2013.04.03>
63. Mitchell, B.A.: Tuberculosis Statistics and the McKeown Thesis: A Rebuttal to David Barnes (1992)

64. Pinheiro, M., Reis, S.: Liposomes as drug delivery systems for the treatment of TB. *Review* **6**, 1413–1428 (2011)
65. Pozniak, A.L., Coyne, K.M., Miller, R.F., Lipman, M.C.I., Freedman, A.R., Ormerod, L.P., Lucas, S.B.: British HIV Association guidelines for the treatment of TB / HIV coinfection 2011, pp. 517–524 (2011). <https://doi.org/10.1111/j.1468-1293.2011.00954.x>
66. Ronneberger, O., Fischer, P., Brox, T.: U-Net: Convolutional Networks for Biomedical, pp. 234–241 (2015). <https://doi.org/10.1007/978-3-319-24574-4>

Leukemia Detection Using Machine and Deep Learning Through Microscopic Images—A Review



Qurat Ul Ain, Shahzad Akbar, Sahar Gull, Muzammil Hussain, and Noor Ayesha

Abstract Leukemia is a blood malignancy that occurs due to neoplastic proliferation of bone marrow precursor cells resulting in impaired immunity, bleeding tendencies, and ineffective erythropoiesis. Therefore, several manual methods have been developed in the past to detect leukemia, but they have proven to be inaccurate and unreliable. The pathologist may recommend a bone marrow examination to confirm and identify the type of leukemia. This traditional method is time-consuming, and the medical professional's expertise in diagnosing leukemia may have inaccurate. In this chapter, it has been observed that there are numerous studies for the detection of acute leukemia, but there are only a few studies to detect chronic leukemia. Additionally, microscopic-based methods can be used to analyze microscopic smear images and detect the incidence of leukemia automatically and quickly. It also discusses the benefits, drawbacks, and limitations of a variety of traditional Artificial Intelligence-based approaches for detecting leukemia, such as machine learning and deep learning. Hence, this chapter aims to review the existing literature in the field of medical image processing of blood smear images, with a focus on automated leukemia detection. The analysis of various studies shows that deep learning techniques provide the best results compared to machine learning techniques. Hence, the major drawback in recent studies is that most of the research has been done on locally available datasets. Another weakness in the publicly available datasets is that they have a limited number of images. To solve these issues, research community should focus on large publicly available datasets.

Keywords Leukemia detection · Artificial intelligence · Red blood cells · White blood cells · Microscopic images

Qurat Ul Ain · S. Akbar (✉) · S. Gull

Riphah College of Computing, Riphah International University, Faisalabad Campus, Faisalabad, Pakistan

e-mail: shahzadakbarbz@gmail.com

M. Hussain

School of Systems and Technology, University of Management and Technology, Lahore, Pakistan
e-mail: muzammil.hussain1@umt.edu.pk

N. Ayesha

School of Clinical Medicine, Zhengzhou University, Zhengzhou, Henan, PR China

1 Introduction

The abnormal proliferation of leukocytes in the bone marrow and blood is known as leukemia. The presence of a large number of malignant immature white blood cells (WBCs), also known as blasts or blast cells, results in the number of normal blood cells being reduced. Leukocytes are substantially different for their specific roles, and they play a vital role in the immune system. Adolescent cells are unable to perform their normal functions, and the disease's malignancy ranges from non-malignant to extremely aggressive. Blasts or myeloid cells overproduce in the bone marrow, pushing out healthy immune cells and inhibiting normal hematopoiesis, making it more difficult to fight against infections, transport oxygen, and control bleeding. Leukemia is classified into chronic and acute leukemia based on how quickly the disease grows. Chronic leukemia develops slowly over time, unlike acute leukemia, which grows quickly and produces a large number of leukemic cells. Mature leukocytes can still perform some of their normal functions. Leukemia is further classified into myeloid and lymphoblastic cells based on what kind of damaged cell from which the malignancy originates [1].

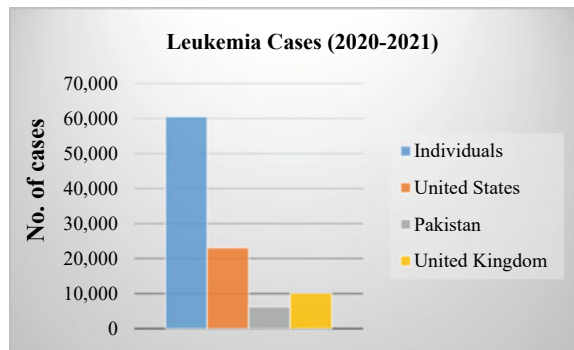
Whole blood is a combination of roughly 45% blood cells and 55% plasma that flows via arteries, veins, and tubes. Blood is roundabout 7–8% of our entire body. A male of typical size has around 12 pints of blood in his body, whereas a female of similar size has approximately nine pints. The highly regulated process of hematopoiesis, which begins with hematopoietic stem cells, generates blood cells in the bone marrow. These stem cells have been discovered in the blood and bone marrow of people of all ages and in the umbilical cords of newborn babies. Leukemia, lymphoma, bone marrow loss, and different immunological illnesses can all be treated using stem cells from any of these three sources [2]. Table 1 shows how hematopoietic stem cells can convert into WBCS, RBCS, and platelets.

In more detail, the risk of contracting this disease rises with age. People between the ages of 65 and 74 are the most prone to produce leukemia. Although leukemia is uncommon in children, it affects 30% of children and teens who are diagnosed with any type of cancer. In 2020, 60,530 persons were predicted to be detected with leukemia. According to Leukemia and Lymphoma Society, leukemia is predictable to kill 23,100 people (13,420 men and 9680 women) in the USA [2]. An estimation of the year-2020, 8305 persons were diagnosed with leukemia. In Pakistan, 6261 persons are predicted to die from leukemia [3]. Around 10,100 new cases of leukemia

Table 1 Hematopoietic stem cells

Types of cells	Purpose
Erythrocytes or red blood cells (RBCs)	Oxygen carries from the lungs to the human body
Leukocytes or white blood cells (WBCs)	It helps the immune system and fights infections
Thrombocytes, platelets	Assists in the clotting of blood

Fig. 1 Leukemia cases in different countries



are diagnosed in the United Kingdom each year [4]. Figure 1 indicates the leukemia cases from 2020 to 2021.

1.1 Types of Leukemia

There are two forms of leukemia: myeloid and lymphoid, as well as acute and chronic. Myeloid leukemia consists of two further sub-forms, AML (Acute Myeloid leukemia) and CML (Chronic Myeloid leukemia), while lymphocytic leukemia also consists of two subtypes, ALL (Acute Lymphoid leukemia) and CLL (Chronic lymphoid leukemia).

AML (Acute Myeloid Leukemia). This form of cancer develops due to a lack of development or a negative influence on the bone marrow. When WBCs grow fast, the bone marrow ability to function is severely harmed, resulting in cancer. Early diagnosis of such cancers in most situations can lead to effective treatment. A person suffering from this form of cancer may experience breathing difficulties, bleeding, and other symptoms, etc. AML symptoms are similar to those of an acute infection, including anemia, fever, granulocytic insufficiency, and mucous membrane ulcerations. A person suffering from this form of cancer may experience breathing difficulties, bleeding, and other symptoms [2, 5].

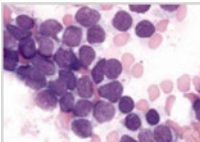
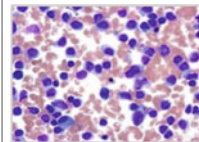
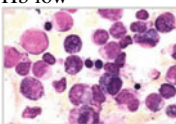
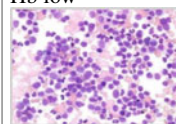
ALL (Acute Lymphocytic Leukemia). This form of malignancy is most common in children, and it is caused by the fast proliferation of WBCS. Viral infections, Radiation exposure, and transmitted disorders like Down syndrome are some of the causes linked to the current type of cancer. Children with this kind of leukemia have a higher remission rate than adults with this type of leukemia. ALL is divided into three categories: L1, L2, and L3. Fever, exhaustion, bleeding, leg discomfort, headache, nausea, and vomiting, etc., are common symptoms of this illness. Approximately 71% of childhood cases are L1, 27% are L2, and 2% are L3. L2 is the most prevalent ALL variation in adults [2, 5].

CML (Chronic Myeloid Leukemia). When the myeloid cells get a genetic mutation, this type of cancer develops. When cells undergo genetic change, the traditional cells cannot fight infections effectively. Adults are more likely to get this kind of leukemia, which is slow-growing cancer. The chronic phase accelerated and blast phases are the other three phases of CML malignancy. Cancer is in the early stages of development and progresses slowly. It becomes more potent in the second phase and begins to destroy blood cells, culminating in a blast cell. Patients with CML may have symptoms such as fever and night sweats when their spleen enlarges, and they begin to lose weight [2, 5].

CLL (Chronic Lymphocytic Leukemia). This kind of leukemia affects both blood cells and bone marrow. If someone were to have cancer, this could be the one with the highest chance of surviving. Adults are more likely to have it, whereas children are far less likely to have it. The clonal development and accumulation of leukemic cells with B-lymphocyte features define CLL. It might occur that persons diagnosed with chronic lymphoid leukemia may guide to the case of acute lymphoid leukemia. Weakness, weariness, anorexia, and weight loss are common signs of CLL, as are the enlarged lymph nodes. Small lymphocytes account for 80–90% of leukocytes, which are uniformly identical in appearance and seem normal in most cases [2, 5]. Table 2 shows the four primary kinds of leukemia.

Moreover, these types include ALL, AML, CLL, CML. ALL and AML are widely spread in human beings as compared to CLL and CML. AML is more frequent in older people, although it can strike anybody at any time. The majority of fatalities occur in persons between the ages of 65 and 84. The five-year relative survival rate is

Table 2 Types of leukemia

	Acute leukemia	Chronic leukemia
Myeloid leukemia	Acute myeloid leukemia Common 15 years above WBCs ($15\text{--}100 \times 10^9/\text{L}$) Palates low Hb low 	Chronic myeloid leukemia Common older person WBCs ($50\text{--}200 \times 10^9/\text{L}$) Palates low Hb low 
Lymphoid leukemia	Acute lymphoblastic leukemia Common children's WBCs ($15\text{--}100 \times 10^9/\text{L}$) Palates low Hb low 	Chronic lymphocytic leukemia Proliferation of myeloid cell WBCs ($50\text{--}500 \times 10^9/\text{L}$) Palates low Hb low 

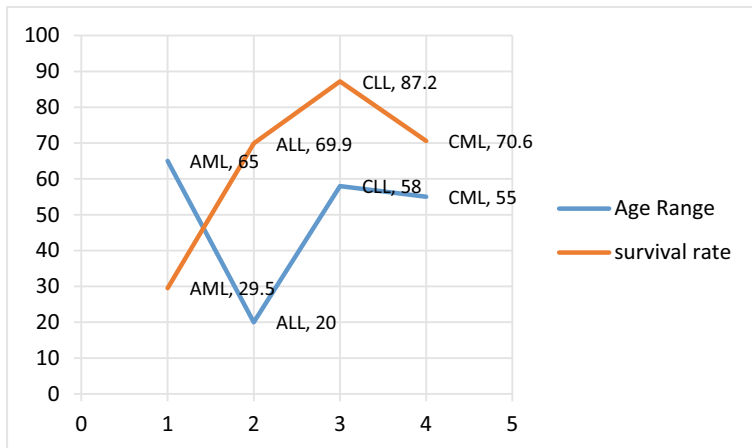


Fig. 2 Represent **a** age range, **b** survival rate

around 29.5% for people of all ages. ALL is a kind of leukemia that is most commonly diagnosed in persons under the age of 20. The typical age of those diagnosed with this kind of leukemia is 17, whereas the usual age of people who die from it is 58. Survival rates are quite consistent throughout all ages, with a relative survival rate of 69.9% for all ages. CLL is a kind of leukemia that primarily affects people over the age of 55. This kind of leukemia has a relative 5-year survival rate of 87.2% for patients of all ages. CML is also more common in people over the age of 55. This kind of leukemia has a five-year survival rate of around 70.6% for people of all ages, as indicated in Fig. 2 [6].

Leukemia can grow in people of any age. People over the age of 60 are the most likely to develop leukemia. AML and CLL are the most prevalent kinds in adults. Every year, around 3811 children are diagnosed with leukemia. The most frequent kind of leukemia in children is ALL. The word “risk factor” refers to something that increases a person’s chances of developing leukemia. The risk factors or possible causes of most kinds of leukemia are unknown. High-dose radiation treatment is also linked to an increased risk of ALL and CML. While CLL is uncommon, most families have several blood relatives who have the illness. Doctors are searching for why certain families have a higher CLL rate than others. Other potential risk factors for such four categories of leukemia are being researched all the time.

However, image processing is used to detect leukemia in microscopic images. Hematologists utilize microscopic analysis of human blood, which necessitates the use of procedures such as segmentation, microscopic color imaging, clustering, and classification to identify leukemia-affected peoples. Hematologists visualize tiny images, which is a time-consuming and tedious operation. The automatic image processing system is desperately needed and also can help overcome inspection process constraints. White blood cells (WBCS) are separated from other blood elements, while platelets and erythrocytes use statistical characteristics such as

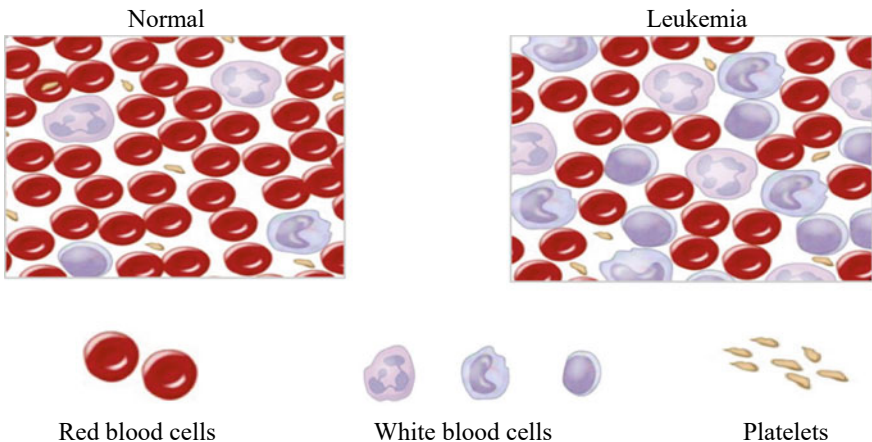


Fig. 3 Leukemia and normal image [7]

mean and standard deviation. Geometrical aspects of WBCS nuclei, such as area and perimeter, were investigated for Leukemia diagnostic prediction. The leukemia image and normal image are shown in Fig. 3.

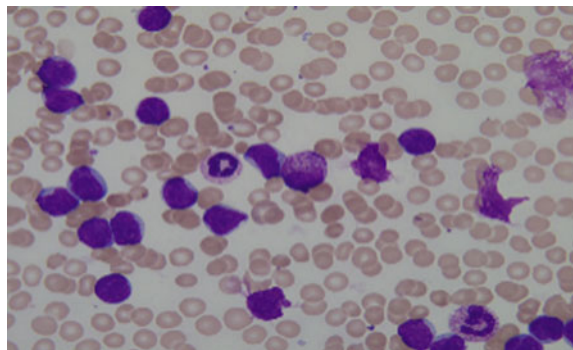
1.2 Publicly Available Datasets for the Detection of Leukemia

Reviewing the literature and comparing these research articles, it has been found that a variety of datasets have been used. This includes Private datasets retrieved from hospitals, clinics, and publicly available datasets (ALL-IDB1, ALL-IDB2, ASH, C-NMC 2019).

ALL-IDB 1. The ALL-IDB 1 is used to test algorithms segmentation capabilities as well as classification system accuracy. The dataset is made up of 108 photographs taken in September 2005. It contains around 39,000 blood particles, including lymphocytes identified by oncologists. In the ALL-IDB 1, there are 510 candidates lymphoblastic. Only the lymphoblastic in the images that are adequately described has been considered and classified. Example photographs from the ALL-IDB 1 are shown in Fig. 4. The image files in the ALL-IDB 1 database are named “ImXXX Y.jpg.” where XXX is a three-digit integer counter, and Y is a Boolean digit that is equal to 0 there is no blast cells present then equal to 0 if the image contains at least one blast cell then equal to 1. $Y = 0$ is a healthy person, and $Y = 1$ is an ALL patient.

ALL-IDB 2. This image dataset was invented to check the precision of classification approaches. ALL-IDB 2 dataset is a subcategory of the ALL-IDB 1 database that involves cropped parts of blast and normal cells. It accommodates 260 images, and the fifty-present images represent lymphoblastic. The gray-level possessions of the

Fig. 4 Leukemia image obtained from ALL-IDB 1



ALL-IDB 2 images are indistinguishable from the ALL-IDB 1 images. The database is free and publicly available. Figure 5 shows an example of the ALL-IDB 2. If the essential cell is a blast cell, the images of the ALL-IDB 2 database are called “ImXYZ 1.jpg” and “ImXYZ 0.jpg” in the other samples.

ASH. The American Society of Hematology Image Bank is a publicly available website that allows ASH members and the whole hematology community to search for high-quality, peer-reviewed hematologic images. The newly updated ASH Image Bank, which was introduced in March 2016, now has over 2100 pictures, with new images being added on a regular basis. New submissions to the Image Bank Editor are encouraged by ASH (Fig. 6).

C-NMC 2019. ALL (Acute lymphoblastic Leukemia) establishes about 25% of the pediatric malignancies. In general, distinguishing juvenile leukemic blasts cell from normal cells under the optical microscope is difficult since the two cells’ appearances are morphologically identical (Fig. 7).

Fig. 5 Leukemia-affected images obtained from ALL-IDB 2 dataset

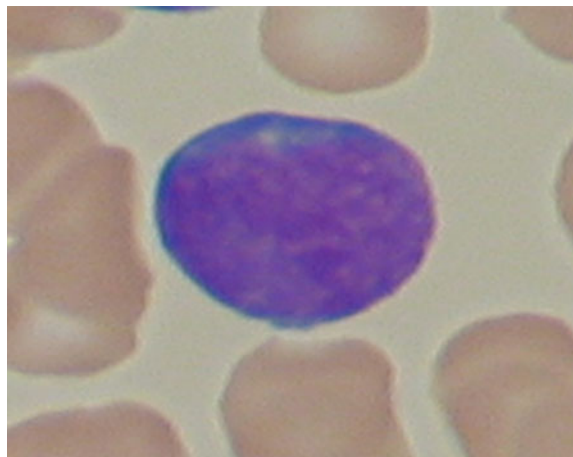


Fig. 6 Leukemia-affected image obtained from ASH dataset

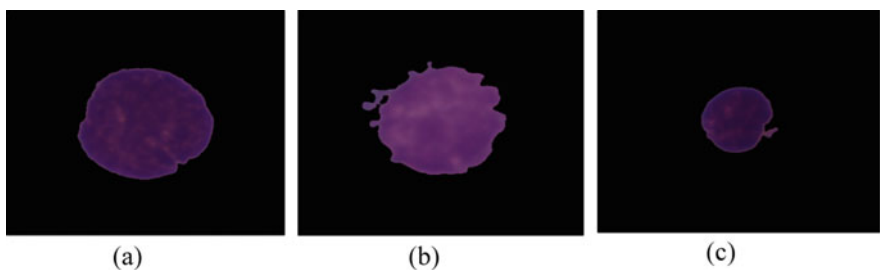
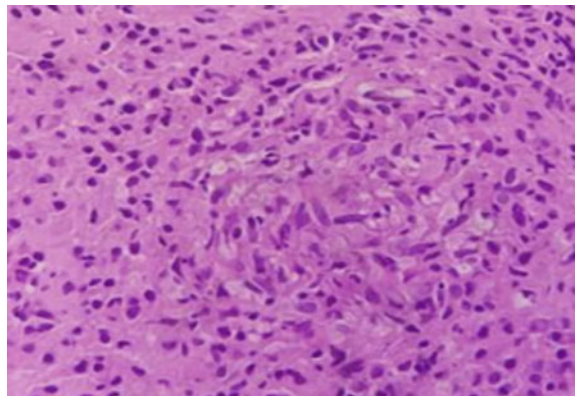


Fig. 7 C-NMC 2019 dataset. **a** Validation data, **b** training data, **c** testing data

2 Literature Review

A complete literature evaluation has been created in this area based on the steps below:

- Identify the advance and relevant article.
- Articles focus on the fundamental knowledge of research problems.
- A detailed search provides that identifies the research issue.
- Collection of necessary data from the research papers that have been chosen.
- Data visualization and readability are improved by presenting data in different way.

2.1 Artificial Intelligence (AI)

Artificial intelligence is a branch of computer science concerned with building smart machines that can perform tasks usually handled by humans. Training, validation, and testing are the three main aspects of using Artificial Intelligence (AI) to arrange

images. Machine Learning (ML) and Deep Learning (DL) are two of the most advanced artificial intelligence techniques (Fig. 8).

Machine Learning. Machine learning is an area of artificial intelligence (AI) and computer knowledge that focuses on data and algorithms to understand how humans learn to increase accuracy. In the field of studies, that gives the computer to capability to learn about without explicit programs. In addition, there are three stages to ML (Machine learning): supervised learning, unsupervised learning, and reinforcement learning. Predicting variables through a prearranged indicator (e.g., an objective function) simplifies the supervised learning process. Supervised learning techniques include Regression, Logistic Regression, KNN, Decision Trees, and Random Forests. In unsupervised learning, the goal is to predict a variable. The method is primarily used to fragment populations by dividing them into groups. Unsupervised learning is demonstrated by K-means and Apriorist algorithms. Reinforcement learning typically involves teaching the machine to sort and categorize explicit choices. There are different Classification Techniques for the Detection of Leukemia shown in Fig. 9.

Support Vector Machine (SVM). Support Vector Machine is a well-known and frequently utilized classification technique that is commonly applied for classification purposes. However, SVM is commonly used for classification problems. Each data element is planned as a point in n -dimensional space (where n denotes how many features you have), with each feature value being the value for a specific coordinate in the SVM algorithm. Then, attempt classification by categorizing the hyper-plane that clearly differentiates the two classes shown in Fig. 10.

Fig. 8 Artificial intelligence [8]

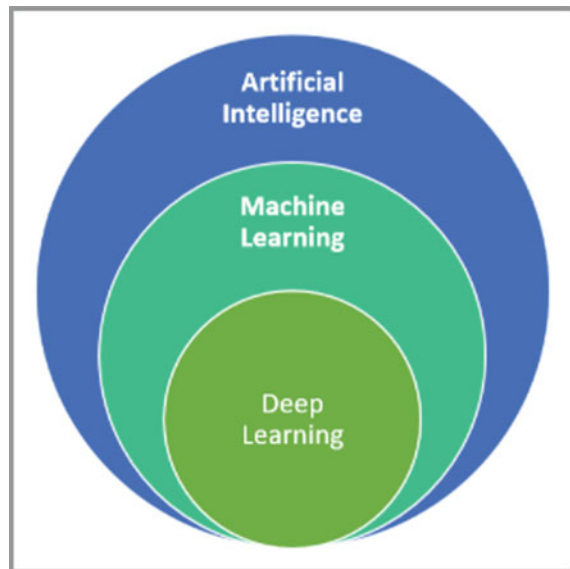


Fig. 9 Architecture of machine learning [9]

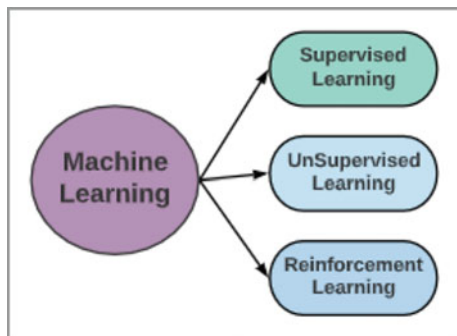
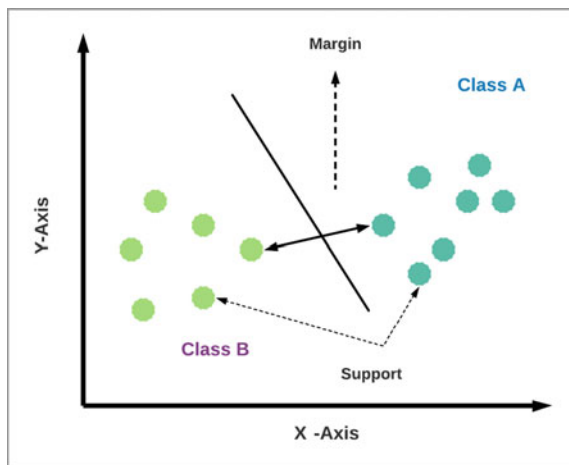


Fig. 10 Support vector machine [10]



2.2 Machine Learning Techniques for the Detection of Leukemia

Bodzad et al. [11] provided a method for automatically detecting acute lymphoblastic leukemia from blood smear pictures that were based on machine learning algorithms and image processing techniques. This system was trained and evaluated using a local dataset given by the University Hospital Ostrava's Department of Haematology. The ANN and SVM classifier were used as traditional machine learning classifiers. Both methods SVM, ANN were reached specificity 95.31%, sensitivity 98.25%, and accuracy 100%, respectively.

MoradiAmin et al. [12] put forward a method to Feature Reduction and Principal Component Analysis Improved Recognition of ALL. Cells in the image processing technique transformed pictures from RGB to HSV (Hue Saturation Value) color space, which lowered color channel correlation compared to RGB (Red, Green, Blue) and allowed the three Hue, Saturation, and Value channels to be treated individually.

They have added a histogram equalization pre-processing phase, which reduced the impact of changing lighting conditions. The authors collected five geometrical and 72 statistical variables after using the FCM clustering approach to segment the nucleus. Component analysis was used to decrease the dimensionality feature set to eight features, which was used for the SVM (support vector machine) classifier.

Mishra et al. [13] put forward a texture-based classification method to detect acute lymphoid leukemia using microscopic blood smear. This procedure implemented a two-dimensional unique orthonormal S transform for abstracting coarseness features from photographs obtained by a microscope. The vital part was providing the blend of AdaBoost and systematic jungle classifier to accomplish good quality. A free and publicly available dataset was used ALL IDB 1, which is employed scored a precision of 99.67%.

Acharya et al. [14] proposed a technique by considering the blood smear photographs predicted different stages of cancer. This process was completed by adopting two different ways. A novel approach was the first step to build the segmentalize the Cytoplasmic material of WBC (white blood cells) and nucleus. In the second step, A model was complete to collect cells' features and qualities and train the model. Atlas of Hematology, ALL-IDB Dataset, and more than 600 photographs were used during this experimentation. The given algorithm obtained 98.6% accuracy.

Vaghela et al. [15] proposed a method to recognize the number of leukemia cells. The author identified the shortcomings in the K-means clustering algorithm and watershed transform-based segmentation, linear contrast stretching, and edge checking by histogram equalizing technique. The photographs were changed priorly grayscale to binary by the threshold value. Borderline, Area, and other characteristics were calculated. Hybridizing and non-Hybridizing cells was distinguished by using a larger axis and smaller axis Value. Shape-dependent character finding was more precise than other methods for numbering the leukemia cells and obtained the most incredible accuracy of 97.8%.

Alireza et al. [16] proposed a method to indicate the WBCS from a Blood smear using the Color Conversion Model. The color space of the photograph was changed from RGB to CMYK. The author proved that the White blood cell's nucleus was more important in the opposite of the Y element. A threshold value was changed to binary computerized with the help of the Zack algorithm. Cytosol contents were lately counted by isolating the white blood cells nucleus from the whole leukocyte portion. The database associated with AS (Imam Reza) hospital in Mashhad comprised twenty-nine photographs of Blood cells and displayed a precision of 93%.

Ahsan et al. [17] put forward a process to detect the white blood cells from the blood smear images with the help of advanced morphologically closed and Watershed Transform operations. This process was capable of pointing out the WBC's Nucleus but does not deal with the splitting up the cytoplasm of WBC's. After the processing, the result showed an accuracy of 88.57%.

Shankar et al. [18] proposed a technique to identify the lymphoblastic cell, and the procedure offered good velocity, preciseness, and scope for detecting leukemia disease during at first stage. The input database comprised 108 samples

of photographs obtained by analyzing normal and abnormal patients' images by optical laboratory microscope and Canon PowerShot G5 Camera. This algorithm was applied in MATLAB. The accuracy was very poor in this article which was a major drawback.

Viswanathan et al. [19] proposed the process dependent upon detected Leukemia WBCs after a complete slide image helped the workflow have enervating and treadmill diagnosis of leukemia. Nucleus and leukemia departmentalization based on morphological processing contour was increased, giving righteous segmentation of White blood cells from the Blood micrographs. Given the precise evaluation of Leukemia cells, this was edited by Fuzzy C-mean average Classification accomplished with the obtained features row vector such as perimeter, compactness, and ratio from segmented nuclei with WBC. For the detection of leukemia, the database ALL-IDB used that were publicly available. The datasets obtained precision of 98% and contributed an effective, candid source of identifying Leukemia Cell varieties.

Agaiyan et al. [20] proposed the system, which displayed a technique for categorizing multi-nucleate Blood photographs. The writer transferred the pictures from RGB (red, green, blue) to the L * a * b color space and implied the K-mean clustering method. The selected character was color, Haar wavelet, GLCM, Shape, and Fractal dimension. As a classifier, they took the help of SVM. This system got an accuracy of 94% by using 98 images from ALL-IDB 1.

Shafique et al. [21] proposed a process, DCNN, that had implied a far intricate and complex artificial neural network for automatic identification of ALL and categorizing of subgroups into four types, i.e., L1, L2, L3, L4. They took the help of the All-Image dataset, a civilian dataset that could easily be reached and attained online. Dataset has been separated into two types. ALL-IDB 1 was composed of 108 pictures out of 59 images taken from normal people and 49 images obtained from leukemia patients. ALL use an ALL-IDB 2 dataset comprised of 260 unicellular pictures. Out of these, 130 images were taken from the disease-free patient, and the remaining 130 were from people affected by leukemia. For ALL verification, which accomplished a delicacy of 100%, accuracy value is 99.51%, and specificity of 98.12%, ALL subtypes categorize the value of sensitivity and specificity of 99.02%, sensitivity was 96.64%, and accurateness of 96.07% was obtained.

Patel et al. [22] put forward an automated detection to recognize leukemia cells with images of blood taken by a microscope. The whole procedure could be expanded into early processing, segment cutting, attribute abstraction, and categorization stages. During the first step, various filters were applied to reduce and eliminate the potential noises from the images. This process helps the cutting of segmented images. In contrast to all the previous work, the author did not alter the color space by RGB Color space. During the step of segmentation, the photographs were altered to grayscale. For this purpose, clustering algorithms K-means and Zack were implied. During the third step of feature abstraction, geometrical, coloring, texture, and statistical tools were used. In order to evaluate the whole process, ALL-IDB 1 is employed. Only 27 pictures were involved during the evaluation. The entire system accomplished an accuracy of 93.58% using SVM.

Sajjad et al. [23] proposed the smartphone-supported, cloud-backing, asset-aware skeleton for regulating the place of WBCs within blood smear microscopic images by using a trained multi-classed assemble categorization mechanism the cloud. SVM classifiers were used for the sake of multiclass categorization. Five tamper forms have been detected. Ensembled-based SVM classifier reduced the computational time with the help of reducing features from the images. Yet this had a prohibitive computational cost when used during a cloud scenario. White blood cells smear images dataset involved in the process is obtained from HMC. MATLAB was selected as a simulation tool during this future predicting system. The system obtained an accuracy of 98%.

Rawat et al. [24] proposed the computer-based network for leukemia detection and identification and applied SVM (support vector machine) for classification purposes. The Kernel-based techniques are used for grouping the cut of segments. This process had a high precision value. Using the ASH photobank dataset, priorly FAB ALL subframes were distinguished using GA with multiplayer perception Kernel (MLP) Function. The preciseness value thus obtained was 97.09%. Then, FAB AML subforums were determined using Genetic phenomenal with Gaussian Radial basis Kernel and got an accuracy value of 99.49%.

Moshavash et al. [25] proposed a booming declaration and decision-based process for reliable and authentic leukemia examination. From microscopic images of blood, ALL-IDB 1 and ALL-IDB 2 datasets were applied for All identification. The scheme involved during this process was using an SVM classifier. This process obtained an accuracy value of 89.82%.

Jothi et al. [26] put forward a process that introduces the rough set theory with the Jaya optimization to detect ALL. In a first step, leukemia photographs were subjected to cutting the segments with the help of BSA-supported clustering. During the second step, the Jaya method was employed along with a few localized classification methods like Support Vector Machine, linear discriminant evaluation, K-nearest neighbor, Naive Bayes, in concert with decision tree and random under-sampling blooming. Out of these, Jaya with SVM and decision tree brought improved results and accuracy. Results obtained from this procedure predict that the Jaya Algorithm enhanced classification accuracy when employed along with previously used categorization algorithms named as, Naive Bayes, Decision tree ensemble RUS Boost, and KNN. Results show that using the SVM classifier it provides best accuracy rate 99%.

Vogado et al. [27] represented a method for leukemia detection depending upon 377 images. The system has adapted the transfer learning technique and a CNN network to obtain the differential characters. That is followed by feature selection used to gain the information. At last, the Support vector machine founded classifiers done the classification. Alongside three different heterogeneous databases used for validity, the current method has attained the approximately 99% classification precision value.

Kazemi et al. [28] proposed an automated identification approach for AML and its most common subtypes, which included color correlation, nucleated cell segmentation, effective validation, and classification. By using a binary SVM classifier

with a tenfold cross-validation approach, pictures are identified as malignant or noncancerous. By using the selective median filtering in conjunction with changing the CIEL * a * b model, where perceived color difference is proportional to Cartesian distance. Sensitivity 95%, specificity 98%, and accuracy 96% of the binary SVM classifier, respectively. The accuracy of the multi-SVM classifier was found to be 87%.

Tahhan et al. [29] proposed an improved classification method for automatically identifying ALL subtypes. Different extracted characteristics for diagnostic accuracy were studied utilizing sophisticated classifiers such as K-nearest neighbor at various metric functions, support vector machine with multiple kernels, and artificial neural network. The ROC (receiver operating characteristic) curve and die-score/F1-score metrics were used to test the automated classification for Acute lymphoid leukemia and its subtypes based only on these two valuable characteristics. It has been verified that the approach is quite precise and saves time and effort in training.

Dasariraju et al. [30] proposed a technique using Random Forest methods, which detected and classified immature leukocytes to diagnose acute myeloid leukemia. The model efficiently detected immature leukocytes (WBCS) with 0.98 AUC-ROC and 93% accuracy.

Abdeldaim et al. [31] put forward a method for diagnosing Acute Lymphoblastic Leukemia using a computer-aided system based on the images analysis technique. All RGB (Red, Green, blue) colors changed to CMYK color model conversion, Zack method thresholding, histogram equalization, and background removal operations are included in this procedure. ALL-IDB 2 dataset used when evaluated with well-known classifiers, the current diagnosis system had reasonable accuracy; however, in this research article K-Nearest Neighbor had the most incredible classification accuracy.

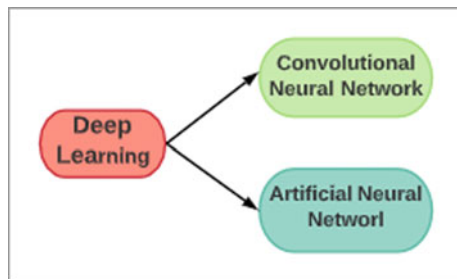
Khandekar et al. [32] proposed an automatic system that identifies blast cells quickly with the help of artificial intelligence (AI). This was done by using the ALL-IDB 1 dataset and the C-NMC-2019 dataset. ALL were classified depending upon cell energy characteristics by using SVM. This system acquired an efficiency of 96.17% and 98.8%, respectively.

2.3 Detection of Leukemia Through Deep Learning Techniques

In today's world, deep learning (DL) algorithms are commonly used for the identification and classification of images. Deep learning has a far higher classification accuracy than previous approaches, which is one of its most significant advantages. Below is a description of both CNN and ANN classifiers of deep learning (Fig. 11).

Convolutional Neural Network. CNN is the classifier of the Deep Learning technique that can take the images as input, assign importance (biases and learnable weights) to multiple objects/aspects in the image, and differentiate from one another.

Fig. 11 Deep learning architectures use in this literature



When compared to other classification methods, a Convolutional Neural Network requires less significant pre-processing. Convolutional Neural Networks can learn the filters/characteristics with enough training, whereas primitive approaches require hand-engineering filtering. The arrangement of the Visual Cortex, which is similar to the neuronal connection pattern in the human brain, inspired the creation of a CNN (Fig. 12).

Artificial Neural Network. Artificial Neural Networks is a method used for deep learning approach inspired by the human brain. That is, the ANN may learn from data and respond in the form of predictions or classifications, similar to how neurons in our nervous system can learn from previous data. The artificial neural network is a kind of AI (Artificial Intelligence). The ANN model must go between two phases: the first step is the training, and the second step is the testing phase. The first step involves training the model, and the second involves checking the model's performance. Many authors indicated that an artificial neural network might be a useful alternative for leukemia disease classification. An ANN used to identify leukemia illness generally has many processors working in parallel and organized in layers. The first layer, equivalent to the optic neurons in human visual processing, receives the raw data as an input. Each succeeding tier receives the outcome from the layer before it rather than the raw input, similar to how neurons further away from the optic nerve receive signals from those closest to it. The final layer generates the system's output (Fig. 13).

Vogado et al. [35] proposed a pre-trained Convolutional Neural Network for the character extraction and collective classifiers for grouping into various groups of

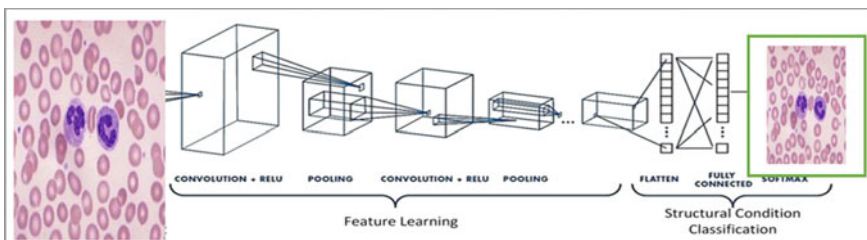


Fig. 12 Convolutional neural network architecture [33]

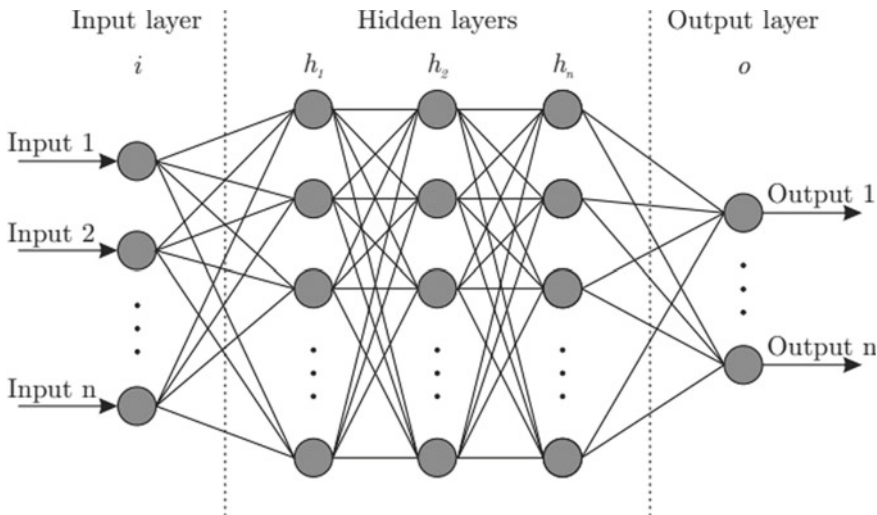


Fig. 13 Artificial neural network architecture [34]

normal and blast cells. In this practice, they applied Deep Convolutional Neural Network to recognize and classify the entire sub-forms frequently nullified in state-of-the-art methods. By defining its input and output parameters and including it as a component of the submodule to a completely automatic system and classifiers with a precision or accuracy rate of 100%, this method could be enhanced to a fully automatic system. This technique needs less processing duration than existing techniques, considering that it did not use the segmentation to get specific cell regions from microscopic images.

Nikitaev et al. [36] proposed a process supported by automatic blood smear image analysis to reveal blast cells. Blast cell tracking is connected with an unmasking for the informative narration of the featured used to separate blast cell and normal cells. Despite the component of a cell (18%) from the sampling being categorized wrong, the acquired result showed the method positively. Sample from normal cells was formed from cells morphologically similar to blast cells. The result was 82% correct identification that was appeasing despite these situations.

Li et al. [37] put forward the dual-threshold process for splitting up lymphocytes. They obtained reliable accuracy for splitting up lymphocyte segments. They brought an evolution in classical single-threshold procedure with the help of Golden section find to identify the best threshold value of lymphoid cells, optimal value $\text{thresh1} = 0.9$. Threshold value $2 = 220$ thus acquired. The given technique was evaluated on 130 Acute Lymphoid Leukemia images captured by ALL-IDB, a communal and chargeless database that obtained an accuracy value of 97.85. The $\text{DSC} \approx 0.98$ in consecutive lymphoblast categorization and ALL diagnosis.

Aftab et al. [38] hypothesized a technique for leukemia sensing by applying BigDL Apache spark publicly available library from the micrographs of human Blood cells

using Google Net deep transfer learning and Convolutional Neural Network. Using spark BigDL skeleton with Google-Net architecture, the given procedure got an accuracy of 97.33% during the training duration. And 94.78% of validity, respectively. In addition, they also compared their model in the absence of BigDL Google Network. Then, accuracy and validity values acquired were 96.42% and 92.68%, respectively.

Kumar Das et al. [39] proposed a swift and deep Convolution Neural Network architecture to extenuate that problem and produce extra precise Acute Lymphoblastic Leukemia detection. The Novel Chance-based weight factor was put forward that possesses a vital role in swiftly hybridization of Mobile Net V2 and ResNet18 along with upholding the profits of both techniques. Two randomly attainable datasets ALL-IDB 1, ALL-IDB 2, were used. The outcomes of these procedures show that these processes yield an accuracy of 30% by testing 70% by training. And in the ALL-IDB 91.39% while ALL-IDB 2 97.19% datasets, respectively. They also obtained better precision (50% by testing and 50% by training), and in ALL-IDB 1 97.93% while ALL-IDB 2 96.01% datasets.

Khobragade et al. [40] postulated a method to diagnose leukemia cells by ciphering different statistical and geometrical characters of the leucocytes. Although relatively better segmentation accuracy was achieved yet this model did not take under cogitation the computerizing of cytoplasmic contents, which play an important role in separating a normal cell from a blast cell. Applying the photograph processing algorithm in MATLAB displayed an accuracy of more than 91%.

Loey et al. [41] put forward the models that relied upon transfer learning and could differentiate among healthy and diseased blood smear images. First Model has adapted pre-trained CNN called Alex Net to get the scored features, and various other well-known classifiers like K-NN, LD, and SVM, DT were used for grouping. SVM classifiers have proven to be the best classifier practically. The second model has used Alex Net for Dual purposes, i.e., for feature extraction and classification. Practical was held on a database comprised of 2820 images providing, and the second model achieves maximum accuracy as compared to 1st model, as the second model acquired 100% classification accuracy.

Pansombut et al. [42] put forward different methods for grouping ALL and its subdirectories using the CNN network. Two standers random forest, multilayer perceptron (MLP) machine learning classifiers were used for equivalence checking. A dataset (ALL-IDB, ASH) of 364 images was used for analysis. As a result, 80% accuracy was obtained. Experimentally proven the superior performance of this technique compared to various other orthodox methods.

Uماماھےswari et al. [43] proposed an algorithm for better distribution of the nucleus region of WBCs that originate in smear images of stained blood intending to classify acute lymphoblastic leukemia. As a completely new approach, customized K-Nearest Neighbor ranks with the ALL-IDB 2 dataset, which achieves 96.25% accuracy, 95% sensitivity, and 97.50% specificity.

Jha et al. [44] put forward a chronological SCA-based Deep Convolutional Neural Network classifier and AA-IDB2 datasets and analyzed these by depending upon metrics, like True Positive Rate and True Negative Rate followed by comparison with various states-of-the-art methodologies. This given chronological SCA-depending

Deep CNN classifiers had a relatively enhanced output with an accuracy value of 98.8%. For futuristic plans, the Hybrid Optimization method would be formulated to train the Deep CNN. This method would increase the Classification outcomes.

Genovese et al. [45] put forward the first machine learning-dependent technique based on Deep learning to focus quality measurement, adopting un-sharpening and grouping acute lymphoblastic leukemia (ALL) blood samples. It was comparing both healthy and diseased cells. Practical on publicly available ALL dataset represents the Deep CNNs trained using the photographs unsharpened by the given methodology enhance the Lymphoblast diagnoses accuracy. The help of ALL-IDB 2 unsharp and VGG16 fine-tuned is allowed to get the immense classification precision value (96.6%) between the hypothesized tools. The futuristic program includes various DL architecture and datasets along with the increased number of samples.

Tuba et al. [46] proposed a method for detecting and classifying ALL using Generative Adversarial Optimization (GOA). The given technique for pointing out acute Lymphoblastic leukemia is contrasted with the Naive Bayes classifiers, K-Nearest Neighbor, reverse propagation neuron network and the SVM optimized by the Bare Bones fireworks System. For classification, five shape characters and six texture characters have been applied. Thus, the GAO-Based procedure acquired the classification accuracy of 93.85% dataset using ALL-IDB 2.

Boldú et al. [47] proposed an AL-Net method developed by two linearly inter-linked Convolutional networks. This method was suggested to help Clinical disease dealing scientists identify and remove Acute Lymphoblastic leukemia by analyzing White Blood cell smears. AL-Net could separate neoplastic and non-neoplastic leukemia cells, marking the leukemia lineage by the accuracy value of 94.43%. Sensitivity 100% and specificity values of 92.4%, respectively. For myeloid leukemia cells. Sensitivity value was obtained 89.01%, and the specification 100% along with preciseness value achieved 100%.

Thanh et al. [48] propose a method based on a Convolutional Neural Network to discern abnormal and normal blood cells in the images. The experimental results cover the initial classification step, representing an exceptional achievement in distinguishing between normal and abnormal cells. With the dataset (ALL-IDB) containing 1188 blood cells images, the suggested approach achieves an accuracy of up to 96.6%.

Al-jaboriy et al. [49] suggested a technique to cut the leukocyte cells' segments automatically. This process was acquainted depending upon the machine learning approach and micrograph evaluating methodology. This technique was examined with two other methods, i.e., Watershed and MBS technique, GA, ANN classifier and ALL IDB1 database was used. This process attained an accuracy of 97.06%.

Negm et al. [50] put forward a digital microscopic image-based decision support system to classify acute Leukemia K-means clustering and panel selection technique. They used a variety of public and benchmark databases and double-checked their research results with pathologists after investigation. When tested with this dataset, the algorithms obtained an overall accuracy of 99.517%, sensitivity 99.348%, and specificity of 99.529%.

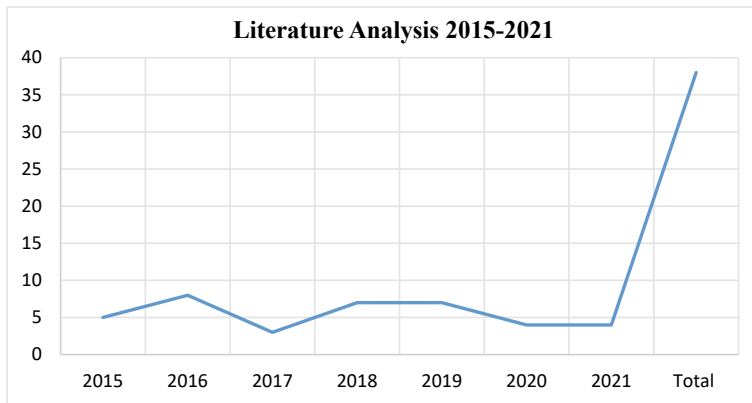


Fig. 14 Graphically representation of literature analysis in (2015 to 2021)

2.4 Literature Analysis

From 2015 to 2021, papers were assembled from Google scholar [51] and research gate [52], which included a variety of sources such as journals, book chapters, and conferences. Graphical information and statistical representation as shown in Table 5 (Fig. 14).

Technologies involving Artificial Intelligence have been rapidly integrating in our daily life. Moreover, many endeavors are being carried out in the realm of medical science and healthcare to incorporate the Artificial Intelligence advancements for run-time medical diagnosis and treatment [53–55].

The detection and diagnosis of retinal diseases such as hypertensive retinopathy. [56, 57], Papilledema [58, 59], Brain Tumor [60–62], Glaucoma [63–65], Melanoma [66, 67], Alzheimer's [68] and Central Serous Retinopathy [69, 70] can be performed through Machine Learning and Deep Learning methodologies using OCT and Fundus Images [71, 72].

3 Discussion

After reviewing 38 different research articles, it is concluded that numerous studies have been done on acute leukemia, and limited research on chronic leukemia using AI (Artificial Intelligence) methods along with microscopic/image processing techniques, as shown in Tables 3 and 4. Machine learning and Deep learning are two vital Artificial intelligence techniques implied during this research. Machine learning is comprised of three types named as supervised learning, unsupervised learning and reinforcement learning. Various classifiers employed during this research include SVM, Adaboost, K-NN, Random Forest. On the other hand, the deep learning

Table 3 Comparative analysis of machine learning

Refs.	Year	Authors	App. area	Methods	Classifiers	Datasets	Results
[11]	2020	Bodzdas et al.	ALL	Human visual perception-based automated diagnosed of ALL leukemia from microscopic images	SVM	The local dataset used, which was provides the Haemato-oncology Department Hospital Ostrava University Local datasets	Specificity 95.31%, Sensitivity 98.25, Accuracy 100%
[12]	2015	Morteza MoradiAmin et al.	ALL	Enhanced the recognition of ALL cells in microscopic images	SVM	—	—
[13]	2019	Sonal Mishra et al.	ALL	Classification of texture-based feature using microscopic images for the detection of ALL	Adaboost	ALL-IDB 1	Accuracy 99.67%
[14]	2019	Vasundhara Acharya et al.	ALL	Examine the various computer-assisted system strategies for segmenting the blood smear images	—	ALL-IDB	Accuracy 98.6%
[15]	2015	Hinali P Vaghela et al.	WBC	Digital image processing techniques	—	Private dataset	Accuracy 97.8%
[16]	2016	Zahra Khandan Khadem Alreza et al.	Leukemia	Using the machine vision systems to count WBC for leukemia classifications	—	Imam Reza (AS) hospital in Mashhad	Accuracy 93.0%
[17]	2016	Rakibull Ahasan et al.	WBC	Microscopic of a stretched peripheral blood smear produced during leukemia and in normal conditions	—	Private	Accuracy 88.57%

(continued)

Table 3 (continued)

Refs.	Year	Authors	App. area	Methods	Classifiers	Datasets	Results
[18]	2016	Vasuki Shankar et al.	Lymphoblastic leukemia	Image processing technique used for the detection and classification of acute lymphoblastic leukemia	–	ALL-IDB 1	–
[19]	2015	Viswanathan et al.	Fuzzy C means clustering	Fuzzy C means the use of morphological contour segmentation for leukemia detection	–	ALL-IDB	Accuracy 98%
[20]	2018	Sos Agaian et al.	Leukemia	Displayed as a technique for the categorization of multi-nucleate blood photographs	SVM	ALL-IDB 1	Accuracy 94%
[21]	2018	Sarmad Shafique et al.	ALL	DCNN used which had implied a fair intricate and complex ANN for automatic identification and classification for ALL and categorizing the subgroups into four types	SVM	ALL-IDB 1, ALL-IDB 2	Accuracy 99.50%
[22]	2015	Nimesh Patel et al.	Leukemia	Automated process for the recognition of leukemia with blood pictures taken by a microscope	SVM	ALL-IDB 1	Accuracy 93.58%

(continued)

Table 3 (continued)

Refs.	Year	Authors	App. area	Methods	Classifiers	Datasets	Results
[23]	2016	Muhammad Sajjad et al.	WBC	Smartphone-supported, cloud-backing, asset-aware skeleton for determining the place of white blood cells within blood smear microscopic	SVM	—	Accuracy 98.6%
[24]	2017	Jyoti Rawat et al.	ALL, AML	Computer-based network for leukemia identification and applying SVM for the classification	SVM	Government or private institutions or pathology labs	Accuracy 99.5%
[25]	2018	Zeinab Moshavash et al.	ALL	Booming declaration and decision-based process for reliable and authentic leukemia examination	SVM	ALL-IDB 1, ALL-IDB 2	Accuracy 89.82%
[26]	2018	G. Jothi et al.	ALL	For automated leukemia segmentation, approaches are used, followed by feature extraction and classification	—	ALL-IDB	Accuracy 99%
[27]	2018	Luis H. S. Vogado et al.	Leukemia	SVM, CNN classification, and transfer learning are used to diagnosis leukemia	SVM-based classifier	ALL-IDB 1, ALL-IDB 2	Accuracy 99%

(continued)

Table 3 (continued)

Refs.	Year	Authors	App. area	Methods	Classifiers	Datasets	Results
[28]	2016	Fatemeh Kazemi et al.	AML	Detection of acute myeloid leukemia through microscopic blood images using SVM classifier and k-mean clustering	SVM	—	Sensitivity 95%, Specificity 98%, Accuracy 96%
[29]	2020	F. E. Al-Tahhan et al.	ALL	A refined simple classification allows for accurate automated identification of acute lymphatic leukemia	SVM, KNN	—	—
[30]	2020	Satvik Dasariraju et al.	AML	A random forest algorithm was used to detect and classify immature leukocytes to the classification of Acute myeloid leukemia	Random Forest	—	Accuracy 93.45%
[31]	2018	A. M. Abdeldaim et al.	ALL	Image processing technique were used for the diagnosis of acute lymphoblastic leukemia	KNN	ALL-IDB 2	—
[32]	2021	Rohan Khande-kar et al.	ALL	Blast cell detection for the diagnosis of acute lymphoblastic leukemia using microscopic images	SVM	ALL-IDB 1, C_NMC_2019	ALL-IDB 1 Accuracy 96.06% C_NMC-2019 Accuracy 98.7%

Table 4 Comparative analysis of deep learning

Refs.	Year	Authors	App. area	Methods	Classifiers	Datasets	Results
[35]	2017	Luis H. S. Vogado et al.	Leukemia	CNN with ensemble classifiers	CNN	ALL-IDB 1, ALL-IDB 2	Accuracy 100%
[36]	2016	V. G. Nikitaev et al.	Leukemia	Blood smear images and dual-threshold method	—	—	Accuracy 82%
[37]	2016	Yan Li et al.	Segmentation of WBC	Dual-threshold process for splitting up lymphocytes	—	ALL-IDB 1, ALL-IDB 2	Accuracy 97.85% DSC \approx 0.98
[38]	2021	Muhammad Omer Aftab et al.	ALL, AML, CLL, CML	Detecting leukemia from microscopic images using transfer learning and Spark BigDL	CNN	—	Training accuracy 96.42% Validation accuracy 92.69%
[39]	2021	Pradeep Kumar Das et al.	ALL	Classification of acute lymphoblastic leukemia through microscopic images and deep CNN	CNN	ALL-IDB 1, ALL-IDB 2	—
[40]	2015	Shubhangi Khobragade et al.	ALL AML, CLL, CML	Microscopic WBC images use for leukemia detection	Neural network	Private dataset	Accuracy 91%
[41]	2020	Mohamed Loey et al.	Leukemia	Diagnosed of leukemia for using the transfer learning technique	—	—	Accuracy 100%
[42]	2019	Tatdow Pansombut et al.	ALL	CNN for lymphoblast cell recognition	CNN	ALL-IDB, ASH	Accuracy 80%

(continued)

Table 4 (continued)

Refs.	Year	Authors	App. area	Methods	Classifiers	Datasets	Results
[43]	2018	Duraiswamy Umanah-eswari et al.	ALL	Efficient architecture used to classification of acute lymphoblastic leukemia using KNN	C-KNN	ALL-IDB 2	Accuracy 96.25%, Sensitivity 95%, Specificity 97%
[44]	2019	Krishna Kumar Jha et al.	ALL	Hybrid-based model used for segmentation of acute lymphocytic leukemia	CNN	ALL-IDB 2	Accuracy 98.7%
[45]	2021	Angelo Genovese et al.	ALL	ALL based on adaptive un sharpening and DL	CNN	ALL-IDB	Accuracy 96.84%
[46]	2019	Tuba et al.	ALL	Generative adversarial optimization (GOA) for ALL detection	GAO	ALL-IDB 2	Accuracy 93.84%
[47]	2021	Laura Boldú et al.	Leukemia	(AL Net) deep learning for the analysis of acute leukemia	CNN	Core Laboratory, Hospital Clinic of Barcelona	Accuracy 94.43%. Sensitivity 100%, Specificity 92.4%
[48]	2018	T. T. P. Thanh et al.	Leukemia	CNN used for the classification of leukemia blood cell images	CNN	ALL-IDB 1	Accuracy 96.6%
[49]	2019	Saif S. Al-jaboriy et al.	ALL	Segmentation of ALL using local pixel information	ANN	ALL-IDB 1	Accuracy 97.07%
[50]	2018	Ahmed S. Negm et al.	Leukemia	Classification of acute leukemia using decision support system	ANN	—	Accuracy 99.517%, Sensitivity 99.348%, Specificity 99.529%

technique consists of two sub-forms named Qualitative learning and Quantitative learning. Classifiers hired during this deep learning were CNN, ANN, DenseNet-121, ResNet-34, GOA-based methods.

In contrast, the DL approach is useful for detecting leukemia, and its results are more accurate than classic ML. However, the results are highly dependent on the size of the datasets and the complexity of the algorithms. A qualitative and quantitative assessment of the algorithms in both categories is presented in this review (see Tables 3 and 4).

In this literature review, different types of datasets were used, such as (ALL-IDB1, ALL-IDB2, ASH image bank, C-NMC 2019) most of the research has been conducted on ALL-IDB 1 and ALL-IDB 2. The ALL-IDB 1 dataset has 108 images, and ALL-IDB 2 contains 260 leukemia-affected images. On the other hand, the ASH dataset contains 2400 images, and the CMN2019 dataset has several leukemia images. After the literature of various studies in machine and deep learning methods, it is concluded that ALL-IDB 1 and ALL-IDB 2 datasets are used in most research, as shown in Tables 3 and 4. The best results are contained through both ALL-IDB 1 and ALL-IDB 2 datasets.

The drawback of previous studies is that using small datasets provides best results, but it provides inaccurate results when a large dataset is used. There are some other problems, such as image resolution, image brightness, color fidelity, and not correctly detecting abnormal cells with high performance. Another major flaw in these ML and DL methods is that they were trained and tested on private datasets that are not available publicly. There are just a few datasets that are publicly available. Most of the methods are trained with private datasets collected from different clinics or hospitals. In further weakness, images were collected from a single medical center. As a result, the research community should have more public datasets to train and test their AI models. Hence, after studying various papers in Tables 3 and 4, a comparison graph of different classifiers with their accuracy rate is shown in Fig. 15 (Fig. 16 and Table 5).

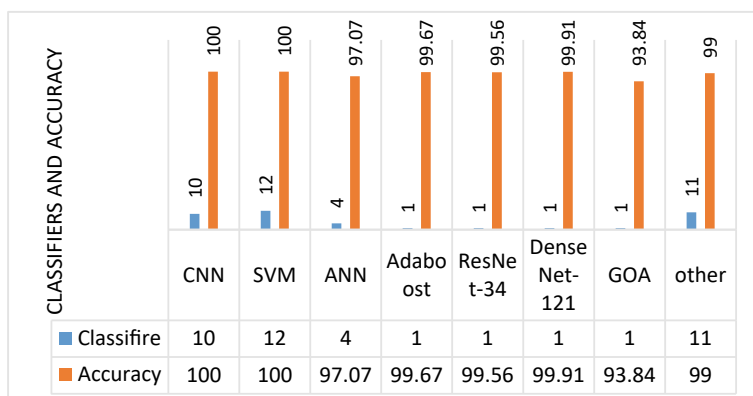


Fig. 15 Accuracy of different classifiers to detect leukemia

Fig. 16 Datasets used in this literature

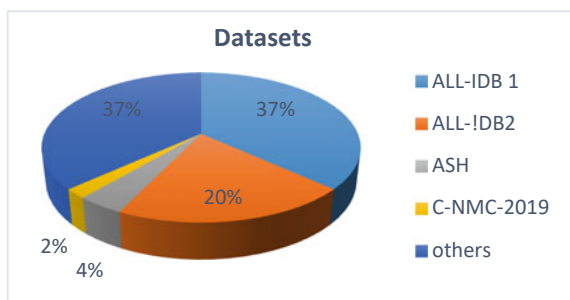


Table 5 Literature analysis per year

2015	2016	2017	2018	2019	2020	2021	Total
5	8	3	7	7	4	4	38

This chapter gives us an all-inclusive preview as compared to present ways to diagnose leukemia by Machine learning and Deep learning processes. A survey was also put forward for futuristic programming to build an open-source leukemia detecting framework depending upon ML/DL algorithms. A vast number of the advanced review article and research methodologies were analyzed, read, and evaluated to create a comparison among their algorithms, application of dataset and precision of their outcomes.

4 Conclusion

Various studies on leukemia diagnosis using microscopic images are presented in this paper. Most of the studies are available in this literature to automatically identify acute leukemia. But only a few studies are used for Chronic leukemia. The AI (Artificial Intelligence) methods used in this chapter are promised Machine and Deep learning methods. The use of ML and DL could assist in diagnosing leukemia at early stages. These methods could help to recognize dangerous blood cancer variants within a short time period and with maximum accuracy. In the machine learning methods, SVM, K-NN, Ad boost classifier achieved maximum accuracy, but in the case of deep learning methods used CNN architecture, ANN ResNet-34, denseNet-121 achieved more than higher accuracy as compared to the machine learning approach. Moreover, publicly (ALL-IDB 1, ALL-IDB 2, ASH, C-NMC 2019) and private (own private institutions) datasets are used in this literature for the research community to train and test AI (Artificial Intelligence) models. Furthermore, this article also penned down the drawbacks of those processes and algorithms. This paper is also offered for acceptance in order to overcome the drawbacks, to aid the population. The aim of this literature, research community and pathologist, each Machine Learning and

Deep Learning methodology are determined in order to perform a better analysis of leukemia detection.

Acknowledgements This study was supported by Riphah Artificial Intelligence Research (RAIR) Lab, Riphah International University, Faisalabad, Pakistan.

Conflict of Interest The authors of this chapter have no conflict of interest.

References

1. Salah, H.T. et al.: Machine learning applications in the diagnosis of leukemia: Current trends and future directions. *Int. J. Lab. Hematol.* **41**(6), 717–725 (2019)
2. Anilkumar, K., Manoj, V., Sagi, T.: A survey on image segmentation of blood and bone marrow smear images with emphasis to automated detection of Leukemia. *Biocybernetics Biomed. Eng.* (2020)
3. International agency for research on cancer. Available online at: <https://gco.iarc.fr/today/data/factsheets/populations/586-pakistan-fact-sheets.pdf>. Accessed on 31-10-2021
4. Cancer research UK. Available online at: <https://www.cancerresearchuk.org/health-professional/cancer-statistics/statistics-by-cancer-type/leukaemia/incidence#heading-One>. Accessed on 31-10-2021
5. Ratley, A., Minj, A., Patre, P.: Leukemia disease detection and classification using machine learning approaches: a review. In: 2020 First International Conference on Power, Control and Computing Technologies (ICPC2T). IEEE (2020)
6. Healthline statistics. Available online at: <https://www.healthline.com/health/leukemia/survival-rate-of-leukemia>. Accessed on 30-12-2021
7. Leukemia and noram images. Available online at: <https://orthoinfo.aaos.org/en/diseases--conditions/leukemia/>. Accessed on 31-10-2021
8. Simplilearn. Available online at: <https://www.simplilearn.com/tutorials/artificial-intelligence-tutorial/ai-vs-machine-learning-vs-deep-learning>. Accessed on 31-10-2021
9. Alpaydin, E.: Introduction to machine learning. MIT Press (2020)
10. Support Vector Machine (SVM). Available online at: https://www.tutorialspoint.com/machine_learning_with_python/classification_algorithms_support_vector_machine.htm. Accessed on 31-10-2021
11. Bodzas, A., Kodytek, P., Zidek J.: Automated detection of acute lymphoblastic leukemia from microscopic images based on human visual perception. *Fron. Bioeng. Biotechnol.* **8**, 1005 (2020)
12. MoradiAmin, M., et al.: Enhanced recognition of acute lymphoblastic leukemia cells in microscopic images based on feature reduction using principle component analysis. *Front. Biomed. Technol.* **2**(3), 128–136 (2015)
13. Mishra, S., Majhi, B., Sa, P.K.: Texture feature based classification on microscopic blood smear for acute lymphoblastic leukemia detection. *Biomed. Signal Proc. Control* **47**, 303–311 (2019)
14. Acharya, V., Kumar, P.: Detection of acute lymphoblastic leukemia using image segmentation and data mining algorithms. *Med. Biol. Eng. Comp.* **57**(8), 1783–1811 (2019)
15. Vaghela, H.P., et al.: Leukemia detection using digital image processing techniques. *Leukemia* **10**(1), 43–51 (2015)
16. Alreza, Z.K.K., Karimian, A.: Design a new algorithm to count white blood cells for classification leukemic blood image using machine vision system. In: 2016 6th International Conference on Computer and Knowledge Engineering (ICCKE). IEEE (2016)

17. Ahasan, R., Ratul, A.U., Bakibillah, A.: White blood cells nucleus segmentation from microscopic images of strained peripheral blood film during leukemia and normal condition. In: 2016 5th International Conference on Informatics, Electronics and Vision (ICIEV). IEEE (2016)
18. Shankar, V., et al.: Automatic detection of acute lymphoblastic leukemia using image processing. In: 2016 IEEE International Conference on Advances in Computer Applications (ICACA). IEEE (2016)
19. Viswanathan, P.: Fuzzy C means detection of leukemia based on morphological contour segmentation. *Procedia Comp. Sci.* **58**, 84–90 (2015)
20. Agaian, S., Madhukar, M., Chronopoulos, A.T.: A new acute leukaemia-automated classification system. *Comp. Methods Biomed. Eng. Imaging Visual.* **6**(3), 303–314 (2018)
21. Shafique, S., Tehsin, S.: Acute lymphoblastic leukemia detection and classification of its subtypes using pretrained deep convolutional neural networks. *Technol. Cancer Res. Treat.* **17**, 1533033818802789 (2018)
22. Patel, N., Mishra, A.: Automated leukaemia detection using microscopic images. *Procedia Comp. Sci.* **58**, 635–642 (2015)
23. Sajjad, M., et al.: Leukocytes classification and segmentation in microscopic blood smear: a resource-aware healthcare service in smart cities. *IEEE Access* **5**, 3475–3489 (2016)
24. Rawat, J., et al.: Computer assisted classification framework for prediction of acute lymphoblastic and acute myeloblastic leukemia. *Biocybernetics Biomed. Eng.* **37**(4), 637–654 (2017)
25. Moshavash, Z., Danyali, H., Helfroush, M.S.: An automatic and robust decision support system for accurate acute leukemia diagnosis from blood microscopic images. *J. Digital Imaging* **31**(5), 702–717 (2018)
26. Jothi, G., et al.: Rough set theory with Jaya optimization for acute lymphoblastic leukemia classification. *Neural Comput. Appl.* **31**(9), 5175–5194 (2019)
27. Vogado, L.H., et al.: Leukemia diagnosis in blood slides using transfer learning in CNNs and SVM for classification. *Eng. Appl. Artif. Intell.* **72**, 415–422 (2018)
28. Kazemi, F., Najafabadi, T.A., Araabi, B.N.: Automatic recognition of acute myelogenous leukemia in blood microscopic images using k-means clustering and support vector machine. *J Med. Signals Sensors* **6**(3), 183 (2016)
29. Al-Tahhan, F., et al.: Accurate automatic detection of acute lymphatic leukemia using a refined simple classification. *Microsc. Res. Tech.* **83**(10), 1178–1189 (2020)
30. Dasariraju, S., Huo, M., McCalla, S.: Detection and classification of immature leukocytes for diagnosis of acute myeloid leukemia using random forest algorithm. *Bioengineering* **7**(4), 120 (2020)
31. Abdeldaim, A.M., et al.: Computer-aided acute lymphoblastic leukemia diagnosis system based on image analysis. In: *Advances in Soft Computing and Machine Learning in Image Processing*, pp. 131–147. Springer (2018)
32. Khandekar, R., et al.: Automated blast cell detection for Acute Lymphoblastic Leukemia diagnosis. *Biomed. Signal. Proc. Control.* **68**, 102690 (2021)
33. Tabian, I., Fu, H., Sharif Khodaei, Z.: A convolutional neural network for impact detection and characterization of complex composite structures. *Sensors* **19**(22), 4933 (2019)
34. Bre, F., Gimenez, J.M., Fachinotti, V.D.: Prediction of wind pressure coefficients on building surfaces using artificial neural networks. *Energy Build.* **158**, 1429–1441 (2018)
35. Vogado, L.H., et al.: Diagnosing leukemia in blood smear images using an ensemble of classifiers and pre-trained convolutional neural networks. In: 2017 30th SIBGRAPI Conference on Graphics, Patterns and Images (SIBGRAPI). IEEE (2017)
36. Nikitaev, V., et al.: The blood smear image processing for the acute leukemia diagnostics. *Inter. J. Bio. Biomedic. Eng.* **10**, 109–114 (2016)
37. Li, Y., et al.: Segmentation of white blood cell from acute lymphoblastic leukemia images using dual-threshold method. *Comp. Math. Methods Med.* (2016)
38. Aftab, M.O., et al.: Executing Spark BigDL for Leukemia Detection from Microscopic Images using Transfer Learning. In: 2021 1st International Conference on Artificial Intelligence and Data Analytics (CAIDA). IEEE (2021)

39. Das, P.K., Meher, S.: An efficient deep Convolutional Neural Network based detection and classification of Acute Lymphoblastic Leukemia. *Expert Sys. Appl.* **115**:311 (2021)
40. Khobragade, S., Mor, D.D., Patil, C.: Detection of leukemia in microscopic white blood cell images. In: 2015 international conference on information processing (ICIP). IEEE (2015)
41. Loey, M., Naman, M., Zayed, H.: Deep transfer learning in diagnosing leukemia in blood cells. *Computers* **9**(2), 29 (2020)
42. Pansombut, T., et al.: Convolutional neural networks for recognition of lymphoblast cell images. *Comp. Intell. Neurosci.* (2019)
43. Umamaheswari, D., Geetha, S.: A framework for efficient recognition and classification of acute lymphoblastic leukemia with a novel customized-knn classifier. *J. Comput. Inf. Technol.* **26**(2), 131–140 (2018)
44. Jha, K.K., Dutta, H.S.: Mutual information based hybrid model and deep learning for acute lymphocytic leukemia detection in single cell blood smear images. *Comp. Methods Prog. Biomed.* **179**, (2019)
45. Genovese, A., et al.: Acute lymphoblastic leukemia detection based on adaptive unsharpening and deep learning. In: ICASSP 2021–2021 IEEE International Conference on Acoustics, Speech and Signal Processing (ICASSP). IEEE (2021)
46. Tuba, M., Tuba, E.: Generative adversarial optimization (GOA) for acute lymphocytic leukemia detection. *Stud. Inform. Control* **28**(3), 245–254 (2019)
47. Boldú, L., et al.: A deep learning model (ALNet) for the diagnosis of acute leukaemia lineage using peripheral blood cell images. *Comp. Methods and Prog. Biomed.* **202**, (2021)
48. Thanh, T., et al.: Leukemia blood cell image classification using convolutional neural network. *Int. J. Comp. Theory Eng.* **10**(2), 54–58 (2018)
49. Al-jaboriy, S.S., et al.: Acute lymphoblastic leukemia segmentation using local pixel information. *Pattern Recogn. Lett.* **125**, 85–90 (2019)
50. Negm, A.S., Hassan, O.A., Kandil, A.H.: A decision support system for Acute Leukaemia classification based on digital microscopic images. *Alexandria Eng. J.* **57**(4), 2319–2332 (2018)
51. Google Scholar. Available online at: <https://scholar.google.com/>. Accessed on 30-12-2021
52. Researchgate. Available online at: <https://www.researchgate.net/>. Accessed on 30-12-2021
53. Shoukat, A., Akbar, S.: Artificial intelligence techniques for glaucoma detection through retinal images. In: Applications in Smart Healthcare, Artificial Intelligence and Internet of Things, p. 209 (2021)
54. Gull, S., Akbar, S.: Artificial intelligence in brain tumor detection through MRI Scans. *Artif. Intell. Int. Things* 241–276 (2021)
55. Hassan, S.A., et al.: Artificial intelligence in coronavirus detection: Recent findings and future perspectives. *Intell. Comput. Appl. COVID-19*, 23–48 (2021)
56. Akbar, S., et al.: Arteriovenous ratio and papilledema based hybrid decision support system for detection and grading of hypertensive retinopathy. *Comp. Methods Prog. Biomed.* **154**
57. Akbar, S., et al.: Decision support system for detection of hypertensive retinopathy using arteriovenous ratio. *Artif. Intell. Med.* **90**, 15–24 (2018)
58. Akbar, S., et al.: Decision support system for detection of papilledema through fundus retinal images. *J. Med. Sys.* **41**(4), 66 (2017)
59. Saba, T., et al.: Automatic detection of papilledema through fundus retinal images using deep learning. *Microsc. Res. Tech.* **84**(12), 3066–3077 (2021)
60. Gull, S., Akbar, S., Khan, H.U.: Automated detection of brain tumor through magnetic resonance images using convolutional neural network. *BioMed. Res. Int.* **2021**, (2021)
61. Gull, S., Akbar, S., Safdar, K.: An interactive deep learning approach for brain tumor detection through 3D-magnetic resonance images. In: 18th International Conference on Frontiers of Information Technology (FIT). Islamabad, Pakistan (2021)
62. Gull, S., Akbar, S., Shoukat, I.A.: A deep transfer learning approach for automated detection of brain tumor through magnetic resonance imaging. In: 2021 International Conference on Innovative Computing (ICIC), pp. 1–6. (2021). <https://doi.org/10.1109/ICIC53490.2021.9692967>

63. Shoukat, A., Akbar, S., Hassan, S.A.E., Rehman, A., Ayesha, N.: Glaucoma diagnosis through convolutional neural network using fundus image. In: 18th International Conference on Frontiers of Information Technology (FIT). Islamabad, Pakistan (2021)
64. Shoukat, A., Akbar, S., Safdar, K.: A deep learning-based automatic method for early detection of the glaucoma using fundus images. In: 2021 International Conference on Innovative Computing (ICIC), pp. 1–6. (2021). <https://doi.org/10.1109/ICIC53490.2021.9693078>
65. Akbar, S., Hassan, S.A.E., Shoukat, A., Alyami, J., Bahaj, S.A.: Detection of microscopic glaucoma through fundus images using deep transfer learning approach. In: Microscopy Research and Technique (2022)
66. Safdar, K., Akbar, S., Gull, S.: An automated deep learning based ensemble approach for malignant melanoma detection using dermoscopy images. In: 18th International Conference on Frontiers of Information Technology (FIT). Islamabad, Pakistan (2021)
67. Safdar, K., Akbar, S., Shoukat, A.: A majority voting based ensemble approach of deep learning classifiers for automated melanoma detection. In: 2021 International Conference on Innovative Computing (ICIC), pp. 1–6. (2021). <https://doi.org/10.1109/ICIC53490.2021.9692915>
68. Ahmad, M.F., Akbar, S., Hassan, S.A.E., Rehman, A., Ayesha, N.: Deep learning approach to diagnose alzheimer's disease through magnetic resonance images. In: 2021 International Conference on Innovative Computing (ICIC), pp. 1–6. (2021). <https://doi.org/10.1109/ICIC53490.2021.9693041>
69. Hassan, S.A.E., et al.: Deep learning-based automatic detection of central serous retinopathy using optical coherence tomographic images. In: 2021 1st International Conference on Artificial Intelligence and Data Analytics (CAIDA). IEEE (2021)
70. Hassan, S.A., et al.: Recent developments in detection of central serous retinopathy through imaging and artificial intelligence techniques—a review. IEEE (2021)
71. Akram, M.U., et al.: Data on fundus images for vessels segmentation, detection of hypertensive retinopathy, diabetic retinopathy and papilledema. Data Brief **29**, 105282 (2020)
72. Akbar, S., et al.: AVRDB: annotated dataset for vessel segmentation and calculation of arteriovenous ratio. In: Proceedings of the 21th Int'l Conf on Image Processing, Computer Vision, & Pattern Recognition (IPCV'17). (2017)

A Review on Machine Learning-Based WBCs Analysis in Blood Smear Images: Key Challenges, Datasets, and Future Directions



Siraj Khan, Muhammad Sajjad, Naveed Abbas, and Amjad Rehman

Abstract In recent development of machine learning (ML)-based medical image analysis that have contributed to the prediction, planning, and early diagnostic process. Different chronic hermitic diseases like blood cancer/leukemia, AIDS, malaria, anemia and even COVID-19, all these are diagnoses via analyzing leucocytes or white blood cells (WBCs). Leucocytes analysis is the process of detection, localization, counting, analyzing WBCs, and it perform an active role in clinical hematology to assist health specialists in early stage disease diagnosing process. An automatic leucocytes analysis provide valuable diagnostics facts to doctors, via they can automatically detect, blood cancer, brain tumor and significantly improve the hematological, pathological activities. Manual Detection, counting and classification of WBCs is very slow, challenging and boring task due to having complex overlapping and morphological uneven structure. In this chapter, we provide a concise analysis of available ML techniques, to use these techniques for leucocytes analysis in microscopic images. The main aim of this chapter is to identify high performer and suitable ML algorithms for WBCs analysis using blood microscopic smear images. In the proposed review study, the recent and most relevant research papers are collected from IEEE, Science Direct, springer, and web of science (WoS) with the following keywords: ‘leucocytes detection’ or ‘leucocytes classification’. This study gives an extensive review of MIA but the research focuses more on the ML-based leucocytes/WBCs analysis in smear images. These techniques include traditional machine learning (TML), deep learning (DL), convolutional neural network (CNN) models,

S. Khan · M. Sajjad · N. Abbas (✉)

Digital Image Processing Lab, Department of Computer Science, Islamia College University Peshawar KPK, Peshawar 25000, Pakistan
e-mail: naveed.abbas@icp.edu.pk

S. Khan

e-mail: siraj.scholar@icp.edu.pk

M. Sajjad

e-mail: muhammad.sajjad@icp.edu.pk

A. Rehman

Artificial Intelligence and Data Analytics Lab (AIDA), CCIS Prince Sultan University, Riyadh, Saudi Arabia

hybrid learning, and attention learning-based techniques to analyze medical image modalities to detect and classify cells in smear images.

Keywords Blood microscopic images · Hematology · Medical imaging · Health care and Health risks · WBCs analysis · Machine learning · Deep learning

1 Introduction

Medical imaging allows us to process different images such as MRI, CT-Scan, blood smear to detect and classify hard tissues and soft tissues. The main aim of this process is to assist a doctor while diagnosis and treatment in terms of accuracy and efficiency of the treatment process. In medical image diagnostic, automatic or computer-aided diagnosis systems perform a crucial role in the process of timely diagnoses and speedup treatment process [1]. Further, recent advancements in technology (information technology (IT), hardware design, and computation capability) have a huge influence on automatic disease diagnoses systems. Formerly, the key application areas of ML techniques involve early detection and recognition of brain tumor in MR images, white and red blood cells segmentation, and categorization of microscopic blood images to diagnose various hematic diseases. The main objective of ML-based MIA, to assist doctors, and hematologists while diagnosing different diseases, i.e., tumors identification, blood cancer classification, malaria, and anemia robustly and efficiently. In addition it is realized that majority of the human diseases have been diagnosing from the blood cells for instance, leukocytes/WBCs [2]. In the last two decades, there are different automatic WBCs analysis techniques that can help medical experts in early disease diagnoses and speedup clinical treatment process. All the studies are reviewed in individual groups based on the methods used. These machine learning methods are mostly used by the research community for medical imaging and especially for leukocyte classification, i.e., SVM, ANN, Hybrids, and Ensembles models [1–4]. In the present study, we review different traditional ML approaches and DL approaches for the classification of WBCs in smear images. During reviewing the article, we found that both the approaches, i.e., ML have performed equally well with overall contributions in this field. It is also shown that analyzing MRI, CT, X-ray, Ultrasound images, and blood microscopic images incorporated ML techniques to deal with detection and classification problems [5–7]. In the current study, four out of the five techniques, SVM [8], ANN [2], Naïve Bayesian [4], CNN, and models CNNs are used to analyze smear images [9, 10]. However, manual WBCs analysis in smear images is difficult and time-consuming task, sometimes it is prone to errors [11]. The main focus of our survey is to conduct an extensive review of the involved research in the selected domain and also to identify the holes in existing work and provide future direction. In this book chapter, we have done a detail review on recent advancement of the ML methods, its impact and use of ML-based WBCs analysis using smear images. In view of MIA, there have been several surveys on ML-based diagnostics techniques [12–15]. The main focus

of the proposed research work is to provide a detailed review of the use of ML techniques for leucocytes analysis in smear images. The proposed study also identifies the massive popularity of DL methods in medical image analysis articles published from 2016 to 2021. This book chapter additionally contributes to identifying current challenges and future directions of ML-based leucocytes/WBCs analysis in smear images. This chapter provides important information and the state-of-the-art methods regarding ML and DL in the domain of hematology and WBCs analysis in smear images. In short words, the main purpose of this chapter is to provide a comprehensive review of ML technique in relation to WBCs/leucocytes analysis, the focus of study is not only in terms of current work, but also with emerge to the future direction of this chapter.

Following are some of the significant contributions of the proposed chapter;

- This study investigates different applications of ML methods for hematology image analysis.
- This study also targets, to find out the available datasets in this domain and its impact on ML, and contributions in the field of MIA.
- In this chapter, we also address the key challenges that the research community are facing, requirements and future directions for researcher MIA.

The remaining chapter organization includes, Sect. 2, gives a brief introduction about WBCs and its clinical significance in hematology. Section 3, include the details description and sources of commonly used datasets in the domain of leucocytes/WBCs analysis. Section 4 comprise ML-based LA in smear images, includes preprocessing, features extraction. Furthermore, leucocytes analysis using ML and deep learning techniques in smear images. Section 5, contain evaluations methods used in this domain. In Sect. 6 we address the key current challenges and requirements. Section 7 consist of discussion conclusion followed by future direction of the proposed review study.

2 Leucocytes/White Blood Cells

The stability of WBCs in human blood provides a pointer into the state of the immune system and any potential risks such as anemia, leukemia, AIDS, and malaria. Over-dramatic variation in the WBCs count and structure change relatively shows different disorders in your body. A deviation or variation in a specific type of WBCs usually correlates with a specific type of disease such as in lymphoblast leukemia only lymphocyte structure is affected. WBC play a crucial role in for proper functioning of human body and provide defensive system against various chronic diseases. The components of the blood cells can be broadly classified into RBCs, platelets, and WBCs [16]. WBCs are the primary component which is involved in the body's immune response and account for about 1% of the blood. WBC are produced in the bone marrow and are present in blood and lymph tissues [17]. They are further categorized into five subtypes; basophil, eosinophil, monocyte, lymphocyte, and

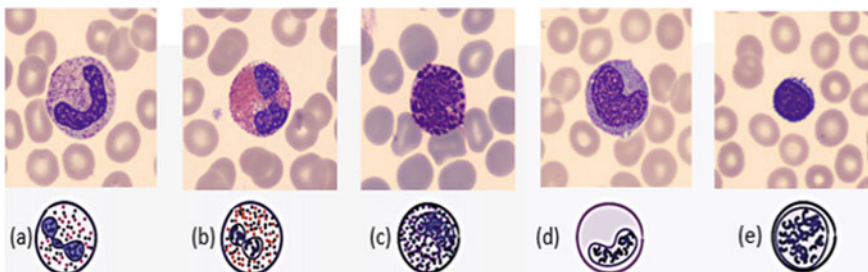


Fig. 1 WBCs; **a** neutrophil, **b** eosinophil, **c** basophil, **d** lymphocyte, and **e** monocyte

neutrophil (see Fig. 1). Each type of WBC has its own significance. Monocytes, breaks down any bacteria that enters the body and tend live longer than the rest of WBCs. Lymphocytes, creates antibodies to fight against viruses like COVID-19, bacteria or any other harmful invader to the human body [6]. Neutrophils are in larger number and are generally the first line of defense in the human body. They kill and digest bacteria and fungi, Eosinophil fights allergies, carcinogens, and parasites. The last type, Basophils are minute and less in number. The medical image analysis tools are used to detect and classify WBC to diagnose hematic diseases like leukemia, malaria, and AID [18]. In recent times, the outbreak of COVID-19 has created shock waves all over the world [19]. Immunity plays an important role in fighting this deadly virus.

Some clinical characteristics of COVID-19 involve WBC [20]. According to the studies conducted by Li et al. [21], and Zhang et al. [22] that a low lymphocyte count is common and in some cases severe. Low lymphocyte count also impacts the neutrophil to lymphocyte ratio with increased neutrophil percentage as a marker to observe. With the analysis of WBC having so much importance taking into account the severity of COVID-19, the need of giving the accurate results of total WBC concentration and the differential count is high. With the recent developments in ML, such as DL, the researcher's efforts to increase the efficiency, and accuracy of the WBCs analysis in blood smear images.

2.1 Clinical Significance of Leucocytes/WBC in Hematology

Computer-aided hematology is an important domain of automatic medical image analysis (MIA) that plays a vital role in the diagnosis of various diseases, i.e., brain tumor analysis, lung cancer, leukemia, and malaria. The structure, size, shape, color, and count of WBCs, all these are analyze by medical experts to identify different abnormality in the human body. The normal total count of WBC in a person is 4500–11,000 per micro liter of blood [20]. Variations in the count of WBCs and the concentration of different WBCs are analyzed to determine the presence of an infection. There are many factors which are responsible for variations in the WBC count.

A study conducted [23] shows that there is an increase in WBC among smokers. Numerous ML techniques are primarily used to detect these variations in WBC count and differential concentration. Conditions like ‘leukopenia’ where there is a decrease in total count of WBC can be diagnosed by observing the variation in total WBC count [24]. In recent times, the outbreak of COVID-19 has created shock waves all over the world. Immunity plays an important role in fighting this deadly virus. Some clinical characteristics of COVID-19 involve WBC. According to the studies conducted by, Li et al. [25], and Zhang et al. [22] that a low lymphocyte count is common and in some cases severe. Low lymphocyte count also impacts the neutrophil to lymphocyte ratio with increased neutrophil percentage as a marker to observe. With the analysis of WBC having so much importance taking into account the severity of COVID-19, the need of giving the accurate results of total WBC concentration and the differential count is high. With the recent developments in ML, such as DL, we are optimistic to improve the accuracy of the WBCs analysis, contribute toward digital hematology system, and clinical care.

3 Image Acquisition/Datasets Used in ML-Based WBC Analysis

In the field of medical image analysis and machine vision-based diagnostics systems, image acquisition/data collection plays significant role. In ML-based leucocytes analysis images or datasets are the first and most important element for diagnosing different hematic diseases. In clinical hematology, image acquisition using a special camera known as charged-couple device (CCD) is attached with hematology microscope to capture blood smear images from blood sample slide [26]. The image quality and quantity are equally important to trained a ML model for WBCs analysis using smear images. The quality of smear image is totally depends on the camera specification and hematological setting. Usually the hematology microscope with CCD camera, capture the image with 1000 magnifications and full $4\times$ optical zoom [27]. In the literature, most of the studies on ML-based leucocytes analysis have considered publically available datasets, i.e., PBC_dataset_normal_DIB, BCCD dataset, LISC database, All-IDB dataset, WBC multiclass dataset, Blood cell detection dataset, Blood cell detection dataset, and WBCs classification datasets of smear images; whereas some of the studies have collect their own datasets from different hospitals [8, 28–30]. Related datasets used in the literature in this domain are tabulated in Table 1. Where the table consists of three columns first column contains source or reference of the DB while the second and third columns contains name of the DB and number of images, respectively.

Table 1 Summary of commonly used datasets in ML-based WBCs analysis

Source	Name of dataset	No. of images
Acevedo et al. (2020) [31]	PBC_dataset_normal_DIB	17,092
Alam and Islam (2019) [32]	BCCD dataset	364
Jung et al. (2019) [33]	WBCs classification dataset	6562
Sarrafzadeh et al. (2014) [30]	Leukocytes (WBCs) and masks	262
Rezatofighi et al. (2011) [34]	LISC database	400
Labati et al. (2011) [35]	All-IDB dataset	368
https://www.kaggle.com/	Blood cells [36]	12,500
https://www.kaggle.com/	WBC multiclass dataset [37]	12,444
https://www.kaggle.com/	Blood cell detection dataset [38]	874
https://www.kaggle.com/	WBC images dataset [39]	4427
https://misp.mui.ac.ir/en/MISP DataBase	White blood cells (WBCs) [33]	198

4 ML-Based Leucocytes/WBCs Analysis

ML-based WBC analysis, is the process of WBCs counting, segmentation, and classification in smear images using ML algorithms. WBC size, morphological structure, color and count is play vital role in diagnosing hematic disease, i.e., COVID-19, blood cancer, AID, and Malaria. There different method available in the literature, for WBCs analysis in microscopic smear images. Khan et al. [40] represented a novel deep learning-based techniques, three different deep learning models with transfer learning are utilized to classify breast cancer cells cytology images. Iqbal et al. [41], used simple ML and deep learning-based approach human blood cells into normal and effected cells. And also conduct comparative analysis by and comparing the performance of ML and DL approaches. A systematic review have conducted by Khan et al. [12], to investigate the use of simple ML and DL for leucocytes analysis in smear images. And to find out deep CNN models, which are most advanced and suitable for analyzing WBCs in microscopic smear images. According to Patel et al. [42], in-depth learning approach, the interactive neural networks helps to analyze large medical datasets, extract rich features using CNN by enhancing the accuracy of leucocytes analysis in smear images. In the last two decades, ML and deep learning-based leucocytes analysis in smear images and its exponential growth as shown in Fig. 2.

In simple ML approaches, includes interconnected steps, (1) Preprocessing, (2) Segmenting ROI, (3) Extraction of features, (4) and (5) Classification. Numerous preprocessing methods are utilize to enhance the quality and increase data, however, low quality data effects the accuracy and efficiency of ML techniques [43]. The reason behind the size of data is, some deep learning models does not achieve the required accuracy and efficiency, due less amount of data. Both quality and quantity of data effects accuracy and efficiency of the model [44]. There are different ML methods used to segment region of interest (ROI), Zhao et al. [45] used a new

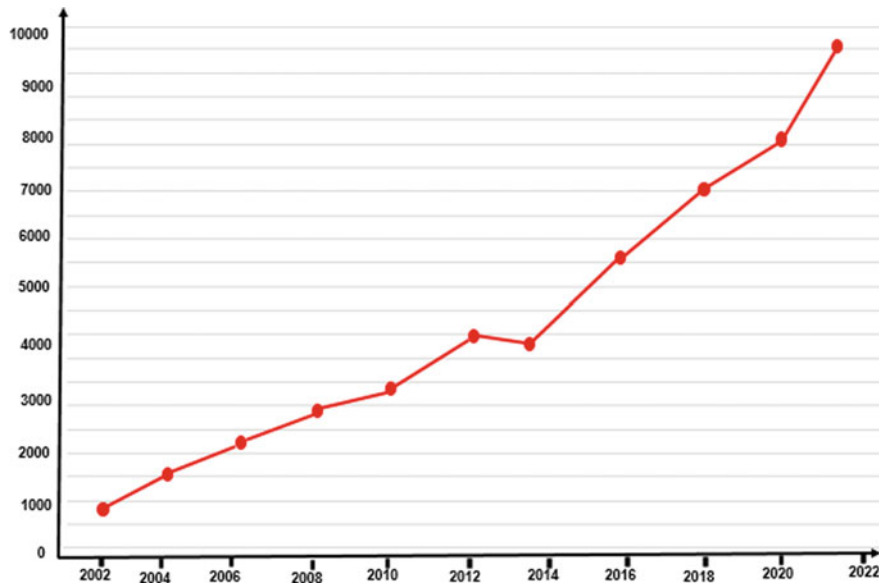


Fig. 2 Studies in the past two decades, ML-based leucocytes analysis in smear images [12]

approach named; Selective-Edge-Enhancement-based Nuclei Segmentation, it first divide the blood smear image into small ROIs via mathematical operator, exclude the repeated parts and extract nuclei as well. The features extraction and selection of the best feature extractor is a challenging task due to having different dynamics of features, i.e., geometric invariance, scale invariance, and photometric invariance [46]. Best features descriptor and best features selection leads to improve classifier accuracy and efficiency [47]. Image classification is the main domain of MIA, in which ML and DL play crucial role of analyzing WBCs in smear images. Image classification we passed the label data, training a ML and DL model to classify WBCs and diagnose several hematic diseases. Khan et al. [48], a CNN-based approach to classify WBC, into five sub-categories. Iftikhar et al.[4], used the technique named, Con-SVM model is used, in which the author first extracts features using CNN to categorize WBCs into five sub-categories. Yao et al.[49], proposed a novel technique weighted optimized deformable TWO-DCNN with transfer learning is deployed to analyze WBCs. General overview of ML-based WBCs analysis using blood smear images is shown in Fig. 3.

Simple ML approaches comprises of different steps, i.e., image requisition/collection of data, preprocessing, features extraction, and training of a classifier. In the recent developments in ML models some of the interconnected steps are excluded, deep learning, CNN, and attention-based models does not need preprocessing and separate features extractor workload. These models provide end-to-end learning capability to detect and identify WBCs using peripheral microscopic smear images. It involves of multiple layers, i.e., convolutional, pooling, fully

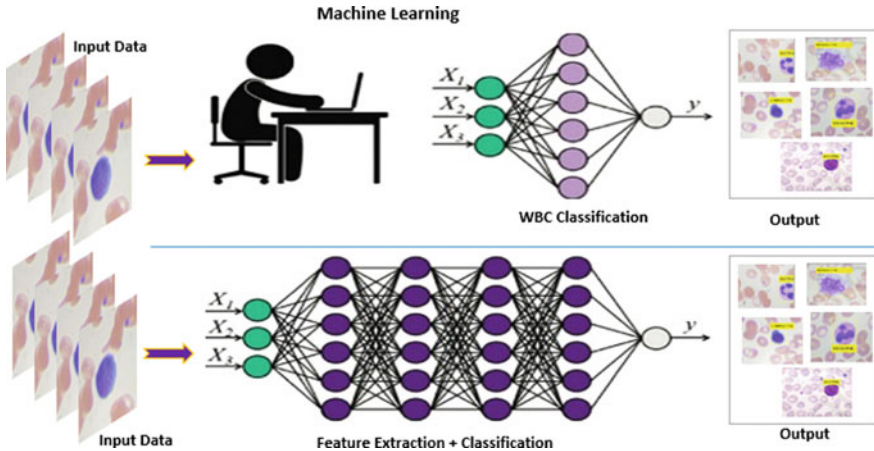


Fig. 3 General overview of ML-based WBCs analysis in smear images

connected or dense layers and activations functions sigmoid and Softmax, to classify WBCs/leucocytes in smear images (see Fig. 5). Deep learning models can fine-tuned and transfer learning approaches are also deployed to trained on less medical data, data augmentation techniques are also incorporated to increase the data [12].

4.1 Preprocessing

In ML-based leucocytes analysis, first the input data is processed using enhancement techniques. Several enhancement algorithm are available to increase and improve the quality of data, to achieve better classification accuracy and efficiency. In order to avoid under-fitting issue, due to lack of data, usually this issue is solve by using data augmentation techniques. Basic augmentation techniques like rotations and flips are employed for the classes which contain less training data. According to Hataya et al. [50] data augmentation approach can significantly increase image recognition and classification accuracy and efficiency. Training data can be doubles, triples times increased if you have less number of data. Further, one hot encoding is used to convert the categories into machine readable format.

4.2 Feature Extraction

Features are the basic and important properties through which we can describe the image in non-visual form. It is a crucial step toward image recognition and classification in computer vision and ML techniques. There are several ways to extract

image features, i.e., Texture, Geometric, Color features, these features are extracted via different ML techniques. Local Binary Patterns (LBP), Histogram Oriented Gradient's (HOG), SURF, SIFT, and CNN features descriptors are utilized to extract the above features from images [51]. Here is an example of how manual feature engineering is carried out in WBC analysis. In the paper, Sadad et al. [10] have used statistical and geometrical information extracted from the images used as input for the algorithm. A feature vector consisting of statistical features was extracted by calculating histogram values for each color band in the input image and geometrical features were extracted by computing the area, perimeter, radius, and other parameters by converting the input image into grayscale first. Two pre-trained semantic segmentation statistical morphological method, i.e., DarkNet-53 and ShuffleNet models are utilized for deep semantic analysis of leukemic cells in smear images [52]. The authors planned a study [53], in which they have discussed the properties of many ML methods, used for WBC analysis, moreover the authors emphasizes feature extraction for WBC classification and showcases the performance of different classification algorithms using the extracted feature set [54]. Another research study [10], CNN-based deep activation features are extracted via DCNN to classify WBCs in smear images.

4.3 ML-Based Segmentation of Leucocytes/WBCs

In the field of computer vision and ML, image segmentation can be explained as the process of dividing the image into different groups of pixels for the purpose to simplify the image. The segmentation of WBCs in smear images is a tedious task and sometime prone to error, due to its non-uniform color, size, and shape disparities. There are numerous unsupervised and supervise ML techniques available, such as, k-mean, Otsu thresholding, manual thresholding, watershed, fuzzy C mean. Anilkumar et al. [55], k-means algorithm is used segment the WBC from the blood smears. A typical blood sample contains a lot of other substances like red blood cells, platelets along with WBC. So in that case, it is very important to extract only the WBC and use it for classification. In this chapter, we includes the most significant and recent studies on the detection and classification of WBCs in smear images [12, 56, 57]. In the advancement of ML methods, a trend is reported that most of the machine learning techniques are to be hybrid and ensemble [58–60]. MIA played a vital role in computer-aided diagnosing (CAD), i.e., image-guided therapy, medical image annotation, tumor, breast cancer, and WBCs detection and classification. In ML-based classification depending on selecting features extractor and its classification algorithms [61]. This selection is one of the crucial step toward efficient ML-based system development. The big picture of ML system development process in Fig. 3 (Table 2).

Table 2 List of some notable research studies of ML for WBCs nuclei segmentation

References	Methods used and its remarks
Huang et al. [62]	Otsu thresholding-based WBCs segmentation and classification using an optimal threshold value
Manik et al. [63]	Adaptive thresholding-based intensity maxima technique is used for optimal segmentation of WBCs from other cells
Li et al. [64]	Dual-thresholding is used for WBCs segmentation and SVM algorithm is used for identification of segmented cells in hematology blood smear images
Ghosh et al. [65]	Author used fuzzy logics to segment WBCs, then various features are extracted such as statistical and geometric, followed supervise learning techniques to classify WBCs into their respective category
Wang et al. [66]	The spectral and morphologic extractor are used to extract various visual features and then a supervised learning (SL) model is employed to classify WBCs
Sajjad et al. [28, 67]	In the study the author proposed an automatic WBCs segmentation and classification scheme based on k-mean segmentation and SVM classification
Win et al. [68]	The k-mean region growing method is utilized to segment leukocytes nuclei from cytoplasm, and classify WBCs into five sub-categories
Negm et al. [69]	In this paper, the author used k-mean algorithm to segment, some rich statistical, geometric features were extracted. A binary classifier SVM is utilized to differentiate normal cells and leukemic cells
Marzuki et al. [70]	Snake or active contour model is used for leukocytes/WBCs detection via curve in smear images
Jha et al. [71]	Hybrid and Mutual Information (MI)-based models such as contour, fuzzy C means, and CNN are utilized to segment and then classify into blood microscopic visuals categories
Li et al. [72]	Image set if first converted from RGB to HSV color space then deep learning-based segmentation techniques UNet is utilized to segment WBCs
Lu et al. [73]	Deep learning model WBC-Net based on ResNet and UNet++ is incorporated to detect and classify WBCs in smear images
Roy et al. [53]	DeepLabv3 model is utilized with ResNet-50 for features extraction to segment WBCs in smear images
Reena et al. [74]	Deep learning-based Semantic segmentation of leukocytes followed by AlexNet with transfer learning to classify WBCs
Tran et al. [75]	Semantic segmentation is incorporated with cutting-edge technology to spate WBCs RBC in blood microscopic smear images
Marzuki et al. [70]	Snake or active contour model is used for leukocytes/WBCs detection via curve in followed by supervise learning technique to classify WBCs into five sub-classes
Win et al. [68]	The k-mean region growing method is utilized to segment leukocytes nuclei from cytoplasm for the purpose to classify WBCs into their respective sub-categories

(continued)

Table 2 (continued)

References	Methods used and its remarks
Fan et al. [76]	End-to-end WBCs localization techniques, Leucocyte-Mask is employed to segment WBCs from RBCs, platelets, and plasma

4.4 ML-Based Classification of Leukocytes/WBCs

There are numerous ML techniques exist in the field of hematology and MIA, to deal with WBCs analysis in smear images., i.e., SVM [8], ANN [2], Naïve Bayesian [4], and CNN models [9, 10]. There are also a number of research studies available, that have been applied ANN for leucocytes analysis. Many medical image analysis applications are using ANN, including brain tumor, breast cancer, and lung infections. Conceptual overview of ML-based WBCs analysis as shown in Fig. 4.

Iftikhar et al. [4] proposed a novel technique named Con-SVM model, in which the authors first extract CNN features then SVM classifier to categorized WBCs into five sub-classes. Furthermore, the proposed techniques achieved 85.96%. In the proposed techniques segmentation is done via morphological and color relation, WBCs, SVM classifier is trained with texture features to categorized WBCs into five

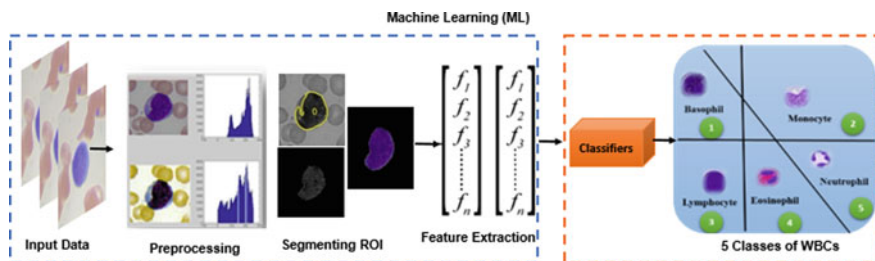


Fig. 4 Conceptual overview of ML-based WBCs analysis using blood smear images

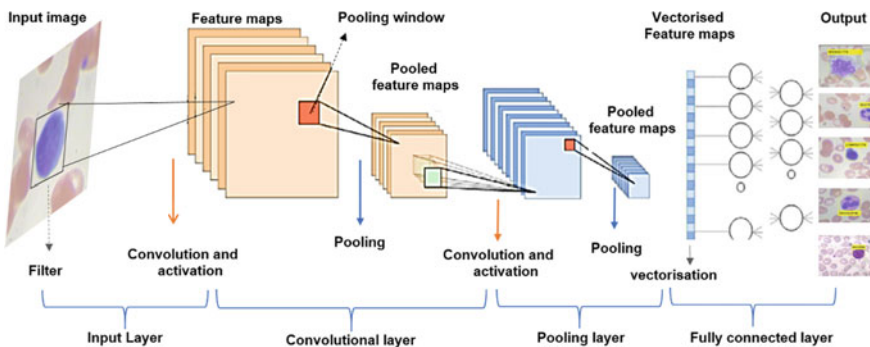


Fig. 5 Visualization of an example CNN architecture for WBC classification [7]

Table 3 Simple ML-based WBCs identification in hematology microscopic smear images

References	Noteworthy contributions
Duan et al. [78]	Supervise learning-based WBCs classification approach is used, first WBCs are segmented, geometric and statistical features were extracted for SVM classifier to classify WBCs in five sub-classes
Sajjad et al. [28, 67]	Cost-effective and resource aware cloud-based technique is utilized with SVM classifier to classify WBCs with better accuracy and efficiency
Amin et al. [58]	In this study, leucocytes are first segmented using k-mean clustering algorithm, some rich features are extracted, and then SVM predictor to distinguish leucocytes sub-categories using blood thick smear images
Agaian et al. [79]	An annotated segmentation approach is used, first the image is segmented and annotated with its proper label and then classify these label cells into two classes, i.e., leukemic and non-leukemic cells using SVM classifier
Zhao et al. [80]	Authors suggested a novel scheme, for WBCs detection and classification using R, B color relation along with image morphology, then WBCs are classified into its sub-categories using SVM classifier
Zheng et al. [81]	This study consist of hybrid segmentation approach, unsupervised and supervised segmentation, using k-mean and SVM to segment WBCs
Negm et al. [69]	The authors proposed, k-mean and SVM-based leucocytes segmentation and classification method, finally cells are classify into normal and leukemic cells using SVM
Sajjad et al. [28]	A resource aware cloud-assisted framework is employed to detect and classify leucocytes to promote smart healthcare services in smart cities

sub-categories [77]. Recurrent neural networks with CNN features, and Canonical Correlation Analysis (CCA) approach is used to avoid cell overlapping issues and reduce leukocytes/WBCs classification time [1]. A novel deep learning technique is proposed that is based on two-module CNN (TWO-DCNN) with transfer learning to classify WBCs [49]. Follows are some notable ML techniques and their contribution to WBCs analysis in smear images (Table 3).

4.5 *Hybrids Models-Based Leukocytes/WBCs Classification*

In the field of medical image diagnostics, there are significant contributions of hybrids and Ensembles ML models were used to detect and classify leukemia, AIDS, brain tumor, and lung cancer in different imaging modalities. In simple ML learning-based leucocytes classification demands depth knowledge of medical to analyze the hematology cells images, which is quite challenging and tiresome task. In the recent literature, there are hybrid and ensemble approaches were incorporated to detect and classify leucocytes in smear images. Sajjad et al. [69], suggested cloud-assisted computer-aided Ensemble multi-classifier-based leukocytes/WBCs analysis system, to contribute toward making smartphone-based healthcare and management system in smart cities. Vogado et al. [82], proposed a hybrid approach for leucocytes analysis

Table 4 Notable contributions of ensembles and hybrids models for leucocytes classification

References	Research contributions
Mondal et al. [83]	An ensemble of different deep CNNs models, better generalization, accuracy, and efficiency, different preprocessing techniques were utilized, to detect and classify ALL in smear images
Tantikitti et al. [84]	In this research a hybrid architecture, i.e., ResNet18 is used with SVM is employed to categorized leucocytes into five sub-categories using smear images
Nanglia et al. [85]	Three different techniques, i.e., KNN, SVM, and Decision Tree, heterogeneous ensemble ML approach is used to detect early stages breast cancer
Jha et al. [71]	Hybrid and Mutual Information (MI)-based models such as contour, fuzzy C means, and CNN are utilized to segment and then classify into blood microscopic visuals categories
Vogado et al. [82]	A hybrid CNN-based approach in which an SVM classifier is trained with CNN features with transfer learning to classify leucocytes
Pradeep et al. [86]	Ellipse fitting (EF)-based novel hybrid approach is used to categorized blood cells for detecting hematological disorders
Shankar et al. [87]	A hybrid Teaching Learning-Based Optimization (TLBO) approach with Salp swarm algorithm (SSA) known as TLBO-SSA, used and followed by ANN as a fitness function to detect breast cancer

using smear images, the authors extract CNN features with transfer learning to train the SVM classifier. And for more details of some notable hybrid approaches (see Table 4) as follows.

4.6 *CNN-Based Leucocytes/WBC Classification*

In deep learning techniques, there are different approaches that can be followed in field deep learning, depending on the data and requirements [88]. CNN are inspired by the neural networks in the human body and have been one of the most influential innovations in the field of computer science. When we see a dog and a cat, we interpret different features like paws, face, and so on to differentiate between the two animals. This interpretation is done with the help of our biological neural networks. In a similar way, the computer is able to perform this classification with the help of a CNN [89]. When the input is given to a CNN, it identifies low level features like edges and curves and when the input passes through its series of layers, and builds an abstract knowledge of unique features in the input. This is just an overview of the CNN. More specifics about the CNNs are discussed in the coming sections. CNN are hierarchical neural networks which extract localized features from input images by convolving over the image with a kernel. Typically, the CNN architecture comprises many layers. The input images are passed through the layers of the network like the image preprocessing layer, convolutional layer, pooling layer, and dense layers.

Figure 4 depicts the general architecture for leucocytes, during the training process [10].

The convolutional layers produce a feature map using filters. Filters (small squares) traverse over the input images. The element involved in convolutional operation is the kernel/filter [10]. Kernel and stride selection, the Kernel determines the height and width of the pixels for the feature extraction and strides determine the length of the next step in the image for the kernel to move. The kernel movement can be customize but generally it moves from left to right on the image. Çınar et al. [90] based on this paper reference is an example, in this study the kernel size chosen is (3, 3) and (5, 5). The pooling layer down samples the input image by factor K_x and K_y along each direction. This layer is useful to extract dominant information. Max pooling returns the maximum value of the pixels in the portion of the image covered by the kernel [10]. Dense layer, the layers before the dense layer are used for feature extraction. All the extracted features from the convolutional layers are then taken together in the dense layer into a 1D feature vector [10]. Dropout, this layer is used to tackle over-fitting. The hidden layer nodes are randomly set to zero for each new input, during training. The use of dropout with the fully connected and pooling layers are used for effectiveness of the model. Batch Size and Epochs, Batch size is selected to pass the images in batches to the network so that the network could handle it. Epoch is the number of times to run through training data while updating the weights, increasing batch size reflects efficient but effect accuracy (Table 5).

Deep learning and WBC analysis, the researcher try the same analysis using R-CNN, where the WBC image is divided into regions and then CNN is applied for each region, respectively [11]. This might help the network to learn more features and might improve the classification performance. Also, variants if RCNN like FAST RCNN can be used where CNN is applied first and then divided into regions [95]. This method is slightly faster than R-CNN. Other deep learning techniques like transfer learning where using a pre-trained model to classifying WBCs can also be explored.

5 Assessment Methods

The performance of the different ML approaches are assessed by plotting a confusion matrix [96]. These evaluation metrics are used to measure the accuracy performance a ML technique. In the literature, Sajjad et al. [28] used sensitivity, septicity, precision, and accuracy to measure the performance of the proposed technique. Rajaraman et al. [91] utilized different statistically evaluation methods to quantify the performance of their proposed approach, they used there measurements metrics, i.e., Matthews correlation coefficient (MCC), area under curve (AUC), sensitivity, septicity, F1-score, and accuracy. Confusion matrix basically based on these evaluation such as true positive ratio, true negative, false positive, and false native ratio. There is a confusion matrices for deep learning model DenseNet12 having batch sizes of 8, 16, 32, and 64, shown as follow in Fig. 5 [97]. In the following figure the diagonal boxes in dark blue color and the values in them represent the percentage of correct

Table 5 Noteworthy contributions of CNN models for WBCs analysis in smear images

References	Methods used and its remarks
Yao et al. [49]	In this paper, a two-module convolutional neural networks (TWO-DCNN) having weights optimizer with transfer learning approach is deployed to classify leucocytes
Iftikhar et al. [4]	In this research study, using a hybrid CNN model with SVM. Google net and Alexnet used to extract features, merged features vector is passed to SVM to analyze WBCs in smear images
Rajaraman et al. [91]	Pre-trained CNN with transfer learning method is employed to detect malaria parasite using thin blood smear images
Qin et al. [92]	A novel deep technique-based residual learning theory known as Fine-grained is incorporated to analyze leukocytes in smear images
Tiwari et al. [93]	Authors proposed, a fine-tuned CNN-based model to detect and classify leucocytes into subtypes in smear images
Hung et al. [94]	The author proposed, a two-stage-based DL concept is deployed to categorize RBCs, WBCs, and platelets and also recognize infected blood cells to diagnose leukemia
Imran et al. [56]	A deep learning technique, includes faster R-CNN, efficient extreme machine learning, and contour aware CNN is deployed to classify WBCs and RBCs using smear images
Zhao et al. [80]	An automatic CNN-based method is proposed, CNN features are extracted and random forest classifier to identify WBCs into respective sub-categories
Vogado et al. [82]	Author proposed a pre-trained CNN approach to extract features, followed by SVM first to extract WBCs and then classify it into normal and leukemic cell
Tobias et al. [95]	Faster R-CNN architecture is employed, to localize WBCs and RBCs and then classify them into their respective categories

classification/predictions whereas the light blue boxes and the white boxes represent the percentage of incorrect predictions. To explain the terminologies of a confusion matrix, let us take the example of WBC identification which consists of four classes, i.e., Eosinophil, Lymphocyte, monocyte, and Neutrophil. When an image from ‘singles’ is classified correctly under ‘Eosinophil’ then it is termed as true positive (TP) but if it is classified under ‘Lymphocyte’ it is termed as false negative (FN). When an image that does not belong to the class ‘Eosinophil’ and is not classified under the class ‘Eosinophil’, then it is termed as true negative (TN) but if classified under the class ‘Eosinophil’ then it is termed as false negative (FN) (Fig. 6).

Using the above-mentioned terminologies it is possible to evaluate the performance of the model. ‘Recall’ or ‘True positive rate’ or ‘Sensitivity’ is the ability of the model to find all the true positives. It is calculated as $\text{Recall} = \text{TP} = (\text{TP} + \text{FN})$. If recall indicates the rate of true positives in a model, ‘Precision’ represents the proportion of true positives that were actually true positives. It is calculated $\text{Precision} = \text{TP} = (\text{FP} + \text{TP})$. Another evaluated metrics F1-score, it is used to measure the model

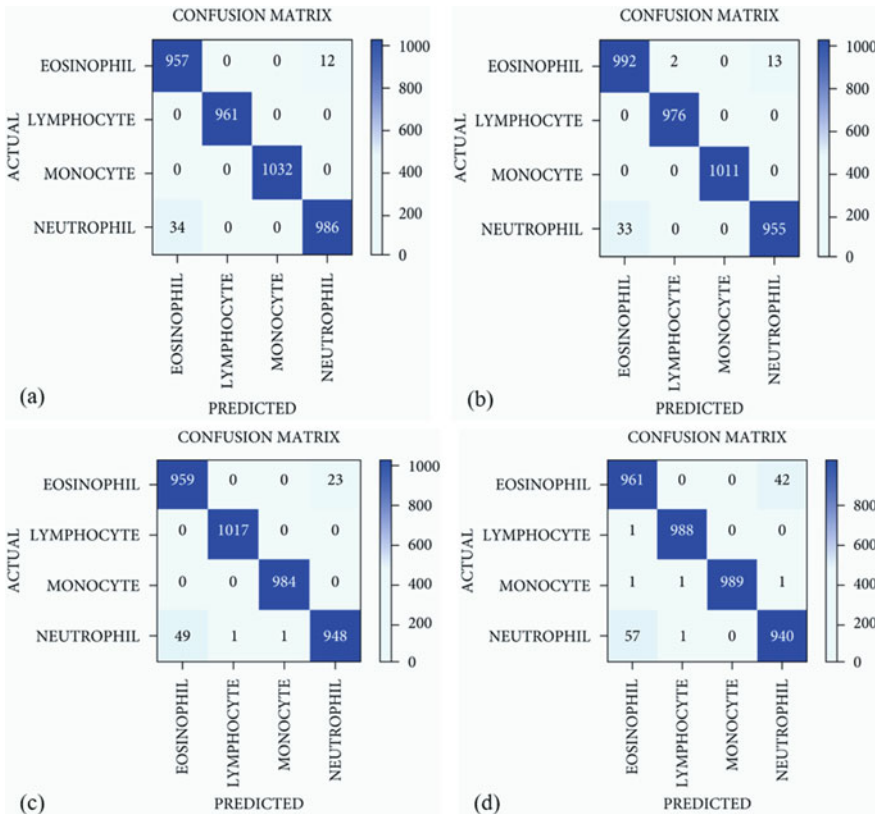


Fig. 6 WBCs analysis DenseNet121, batch sizes: **a** 8, **b** 16, **c** 32, and **d** 64 [97]

accuracy on a data set, the harmonic mean of recall and precision, mathematically it is calculated as $F1\text{-score} = 2 * (\text{Precision} * \text{Recall}) / (\text{Precision} + \text{Recall})$.

6 Current Barriers and Requirements

In this chapter, numerous important applications and advantages of ML-based LA, and its impact on medical diagnostics process. However, literature in the proposed review study perceived that there are still some barriers exist in ML-based leucocytes analysis that need to be addressed, some notable barriers/challenges are as follows; These challenges, include the unavailability publically available fully annotated and heterogeneous and large datasets for medical image analysis; There is no such resource and cost-effective models that can implement in real world clinical care system utilize for early diagnosing toolkits to assist medical experts; In the literature, we did not found any ML-based free trained hematological toolkits, which

can used by a hematologists for detecting hematic and other chronic diseases using smear images.

Observing the literature and from the above existing challenges in field of hematology and leucocytes or WBCs analysis in smear images. Based on the this review study, some notable recommendations are as follows.

World health community needs to put efforts on digitalizing hematological slides should continue and improve, also need to create larger, heterogeneous and annotated datasets of hematology and pathology. The acquired databases are make available researchers, developers publically; The developers are suggested to create such MIA toolkits, medical experts can easily utilize the developed toolkit for early diagnosis of various chronic diseases without having depth knowledge of ML tools; It is observed that most of the research work was focused only on the diagnostic accuracy of ML models; diagnostic accuracy is not the only advantage; improving healthcare efficiency, availability, cost and workflow is also a major advantage.

7 Conclusion and Future Work

In this chapter, we have provided an inclusive review of ML methods which were deployed in leukocytes analysis and MIA. In this study we followed a unique organization to find out the most relevant, recent and standard ML techniques used by the research community in the domain of hematology and WBCs classification. In medical image analysis, now a day's hematological microscopic image is an emerging domain, and it have had excessive attention by the researchers over the last two decades. In the literature, there are multiple research studies of ML tools have deployed to detect and identify WBCs in smear images. Some of recent research studies have claimed significant detection and classification accuracy. The scope of using deep learning techniques in hematology has a very wide range. Also, we have a strong belief that the ML methods could give convincing results if it is trained using different and quality images of a WBC rather than training with only grayscale images of WBC varying in focal length. Deep learning techniques can also be used to analyze other components of the blood or analyze all components in the blood to get the metrics of each component in the blood sample.

A promising future direction for researchers to develop such a cost-effective, lightweight, accurate, and efficient algorithms, in particular, DL models which can implement in real world digital hematology and clinical tools that will assist medical experts while diagnosing different chronic diseases; Further, narrowing down the future directions specifically, the researchers need to develop whole-slide imaging (WSI)-based computer-aided WBCs/leucocytes classification systems, in form of even app which are implementable at hematology laboratories, to assist the doctors, hematologist, and pathologists in early disease diagnosing. With the advancement in the field of hematology, it is possible to get access to numerous images related to blood and its components. In DL different techniques are design, CNNs are powerful tools at our disposal. By making good use of these models and we can make wonders

in the field of hematology or the healthcare sector on the whole. It can conclude that researchers should focus on the cost-effectiveness, efficiency, availability of ML model for MIA along with the classification accuracy.

References

1. Abbas, N., Saba, T., Rehman, A., Mehmood, Z., Kolivand, H., Uddin, M., Anjum, A.: Plasmodium life cycle stage classification based quantification of malaria parasitaemia in thin blood smears. *Microsc. Res. Tech.* (2018). <https://doi.org/10.1002/jemt.23170>
2. Iqbal, S., Khan, M.U.G., Saba, T., Mehmood, Z., Javaid, N., Rehman, A., Abbasi, R.: Deep learning model integrating features and novel classifiers fusion for brain tumor segmentation. *Microsc. Res. Tech.* **82**(8), 1302–1315 (2019). <https://doi.org/10.1002/jemt.23281>
3. Nazir, M., Khan, M.A., Saba, T., Rehman, A.: Brain tumor detection from MRI images using multi-level wavelets. In: 2019 International Conference on Computer and Information Sciences (ICCIS), pp. 1–5. IEEE (2019)
4. Iftikhar, S., Fatima, K., Rehman, A., Almazyad, A.S., Saba, T.: An evolution based hybrid approach for heart diseases classification and associated risk factors identification. *Biomed. Res.* **28**(8), 3451–3455 (2017)
5. Rehman, A., Khan, M.A., Saba, T., Mehmood, Z., Tariq, U., Ayesha, N.: Microscopic brain tumor detection and classification using 3D CNN and feature selection architecture. *Microsc. Res. Tech.* **84**(1), 133–149 (2021). <https://doi.org/10.1002/jemt.23597>
6. Khan, M.A., Kadry, S., Zhang, Y.D., Akram, T., Sharif, M., Rehman, A., Saba, T.: Prediction of COVID-19-pneumonia based on selected deep features and one class kernel extreme learning machine. *Comput. Electr. Eng.* **90**, 106960 (2021)
7. Jamal, A., Hazim Alkawaz, M., Rehman, A., Saba, T.: Retinal imaging analysis based on vessel detection. *Microsc. Res. Tech.* **80**(7), 799–811 (2017)
8. Rehman, A., et al.: Classification of acute lymphoblastic leukemia using deep learning. *Microsc. Res. Tech.* **81**(11), 1310–1317 (2018)
9. Saba, T., Haseeb, K., Ahmed, I., Rehman, A.: Secure and energy-efficient framework using Internet of Medical Things for e-healthcare. *J. Infect. Public Health* **13**(10), 1567–1575 (2020)
10. Sadad, T., Munir, A., Saba, T., Hussain, A.: Fuzzy C-means and region growing based classification of tumor from mammograms using hybrid texture feature. *J. Comput. Sci.* **29**, 34–45 (2018)
11. Saba, T., Rehman, A., Mehmood, Z., Kolivand, H., & Sharif, M.: Image enhancement and segmentation techniques for detection of knee joint diseases: a survey. *Curr. Med. Imaging Rev.* **14**(5), 704–715 (2018). <https://doi.org/10.2174/157340561366170912164546>
12. Khan, S., et al.: A review on traditional machine learning and deep learning models for WBCs classification in blood smear images. *IEEE Access* (2020)
13. Asadi, S., et al.: Understanding institutional repository in higher learning institutions: a systematic literature review and directions for future research. *IEEE Access* **7**, 35242–35263 (2019)
14. Jabeen, S., Mehmood, Z., Mahmood, T., Saba, T., Rehman, A., Mahmood, M.T.: An effective content-based image retrieval technique for image visual representation based on the bag-of-visual-words model. *PLoS ONE* **13**(4), e0194526 (2018)
15. Amin, J., Sharif, M., Raza, M., Saba, T., Rehman, A.: Brain tumor classification: feature fusion. In: 2019 International Conference on Computer and Information Sciences (ICCIS), pp. 1–6. IEEE (2019)
16. Abbas, A., Saba, T., Rehman, A., Mehmood, Z., Javaid, N., Tahir, M., Khan, N.U., Ahmed, K.T., Shah, R.: Plasmodium species aware based quantification of malaria, parasitemia in light microscopy thin blood smear. *Microsc. Res. Tech.* **82**(7), 1198–1214 (2019). <https://doi.org/10.1002/jemt.23269>

17. Abbas, N., Saba, T., Mohamad, D., Rehman, A., Almazyad, A.S., Al-Ghamdi, J.S.: Machine aided malaria parasitemia detection in Giemsa-stained thin blood smears. *Neural Comput. Appl.* **29**(3), 803–818 (2018). <https://doi.org/10.1007/s00521-016-2474-6>
18. Shah, A., et al.: Automated diagnosis of leukemia: a comprehensive review. *IEEE Access* (2021)
19. Amin, J., Anjum, M.A., Sharif, M., Rehman, A., Saba, T., Zahra, R.: Microscopic segmentation and classification of COVID-19 infection with ensemble convolutional neural network. *Microsc. Res. Tech.* (2021). <https://doi.org/10.1002/jemt.23913>
20. Haimed, A.M.A., Saba, T., Albasha, A., Rehman, A., Kolivand, M.: Viral reverse engineering using Artificial Intelligence and big data COVID-19 infection with Long Short-term Memory (LSTM). *Environ. Technol. Innov.* **22**, 1–20 (2021)
21. Li, J., et al.: Meta-analysis investigating the relationship between clinical features, outcomes, and severity of severe acute respiratory syndrome coronavirus 2 (SARS-CoV-2) pneumonia. *American Journal of Infection Control* **49**(1), 82–89 (2021)
22. Zhang, H., et al.: Clinical characteristics and outcomes of COVID-19-infected cancer patients: a systematic review and meta-analysis. *J. Natl. Cancer Inst.* **113**(4), 371–380 (2021)
23. Zare, S., et al.: miRNA96 expression level within red blood cells is probably associated with RSL indicators during the storage of red blood cell units. *Transfus. Apher. Sci.* **60**(3), 103122 (2021)
24. Abdulbari, H.A.: Lab-on-a-chip for analysis of blood. In: *Nanotechnology for Hematology, Blood Transfusion, and Artificial Blood*, pp. 265–283. Elsevier (2022)
25. Li, J., et al.: Epidemiology of COVID-19: a systematic review and meta-analysis of clinical characteristics, risk factors, and outcomes. *J. Med. Virol.* **93**(3), 1449–1458 (2021)
26. Abbas, N., Mohamad, D., Abdullah, A.H., Saba, T., Al-Rodhaan, M., Al-Dhelaan, A.: Nuclei segmentation of leukocytes in blood smear digital images. *Pak. J. Pharm. Sci.* **28**(5), 1801–1806 (2015)
27. Ganilova, Y.A., et al.: Optical digital microscopy for cyto-and hematological studies in vitro. *Opt. Spectrosc.* **115**(2), 212–217 (2013)
28. Sajjad, M., et al.: Leukocytes classification and segmentation in microscopic blood smear: a resource-aware healthcare service in smart cities. *IEEE Access* **5**, 3475–3489 (2016)
29. Mohamed, M., Far, B., Guaily, A.: An efficient technique for white blood cells nuclei automatic segmentation. In: *2012 IEEE International Conference on Systems, Man, and Cybernetics (SMC)*. IEEE (2012)
30. Sarrafzadeh, O., et al.: Selection of the best features for leukocytes classification in blood smear microscopic images. In: *Medical Imaging 2014: Digital Pathology*. 2014. International Society for Optics and Photonics
31. Acevedo, A., et al.: A dataset of microscopic peripheral blood cell images for development of automatic recognition systems. *Data Brief* (2020)
32. Alam, M.M., Islam, M.T.: Machine learning approach of automatic identification and counting of blood cells. *Healthc. Technol. Lett.* **6**(4), 103–108 (2019)
33. Jung, C., et al.: W-net: a CNN-based architecture for white blood cells image classification (2019)
34. Rezatofighi, S.H., Soltanian-Zadeh, H.: Automatic recognition of five types of white blood cells in peripheral blood. *Comput. Med. Imaging Graph.* **35**(4), 333–343 (2011)
35. Labati, R.D., Piuri, V., Scotti, F.: All-IDB: the acute lymphoblastic leukemia image database for image processing. In: *2011 18th IEEE International Conference on Image Processing*. IEEE (2011)
36. Baghel, N., et al.: WBCs-Net: type identification of white blood cells using convolutional neural network. *Multimed. Tools Appl.* 1–17 (2021)
37. Basnet, J., et al.: A novel solution of using deep learning for white blood cells classification: enhanced loss function with regularization and weighted loss (ELFRWL). *Neural Process. Lett.* **52**(2), 1517–1553 (2020)
38. Mohamed, E.H., et al.: Improved white blood cells classification based on pre-trained deep learning models. *J. Commun. Softw. Syst.* **16**(1), 37–45 (2020)

39. Sahlol, A.T., Kollmannsberger, P., Ewees, A.A.: Efficient classification of white blood cell leukemia with improved swarm optimization of deep features. *Sci. Rep.* **10**(1), 1–11 (2020)
40. Khan, S., et al.: A novel deep learning based framework for the detection and classification of breast cancer using transfer learning. *Pattern Recogn. Lett.* **125**, 1–6 (2019)
41. Iqbal, M.S., et al.: Deep learning recognition of diseased and normal cell representation. *Trans. Emerg. Telecommun. Technol.* **32**(7), e4017 (2021)
42. Patel, K.A., Gandhi, K.K., Vyas, A.S.: An effective approach to classify white blood cell using CNN. In: Proceedings of the International e-Conference on Intelligent Systems and Signal Processing. Springer (2022)
43. Nickolas, S., Shobha, K.: Efficient pre-processing techniques for improving classifiers performance. *J. Web Eng.* 203–228 (2022)
44. Kurup, R.V., Sowmya, V., Soman, K.: Effect of data pre-processing on brain tumor classification using capsulenet. In: International Conference on Intelligent Computing and Communication Technologies. Springer (2019)
45. Zhao, M., et al.: Seens: nuclei segmentation in pap smear images with selective edge enhancement. *Future Gener. Comput. Syst.* **114**, 185–194 (2021)
46. Mumuni, A., Mumuni, F.: CNN architectures for geometric transformation-invariant feature representation in computer vision: a review. *SN Comput. Sci.* **2**(5), 1–23 (2021)
47. Khan, M.A., et al.: Automated design for recognition of blood cells diseases from hematopathology using classical features selection and ELM. *Microsc. Res. Tech.* **84**(2), 202–216 (2021)
48. Khan, M.B., et al.: A CNN based deep learning approach for leukocytes classification in peripheral blood from microscopic smear blood images. In: Proceedings of International Joint Conference on Advances in Computational Intelligence. Springer (2021)
49. Yao, X., et al.: Classification of white blood cells using weighted optimized deformable convolutional neural networks. *Artif. Cells Nanomed. Biotechnol.* **49**(1), 147–155 (2021)
50. Hataya, R., et al.: Meta approach to data augmentation optimization. In: Proceedings of the IEEE/CVF Winter Conference on Applications of Computer Vision (2022)
51. Ramzan, F., Khan, M.U.G., Rehmat, A., Iqbal, S., Saba, T., Rehman, A., Mehmood, Z.: A deep learning approach for automated diagnosis and multi-class classification of Alzheimer's disease stages using resting-state fMRI and residual neural networks. *J. Med. Syst.* **44**(2), 37 (2020)
52. Yao, J., et al.: High-efficiency classification of white blood cells based on object detection. *J. Healthc. Eng.* **2021** (2021)
53. Roy, R.M., Ameer, P.M.: Segmentation of leukocyte by semantic segmentation model: a deep learning approach. *Biomed. Signal Process. Control* **65**, 102385 (2021)
54. Dhingra, S., Bansal, P.: Relative examination of texture feature extraction techniques in image retrieval systems by employing neural network: an experimental review. In: Proceedings of International Conference on Artificial Intelligence and Applications. Springer (2021)
55. Anilkumar, K., et al.: A survey on image segmentation of blood and bone marrow smear images with emphasis to automated detection of Leukemia. *Biocybern. Biomed. Eng.* (2020)
56. Imran Razzak, M., Naz, S.: Microscopic blood smear segmentation and classification using deep contour aware CNN and extreme machine learning. In: Proceedings of the IEEE Conference on Computer Vision and Pattern Recognition Workshops (2017)
57. Safuan, S.N.M., Tomari, M.R.M., Zakaria, W.N.W.: White blood cell (WBC) counting analysis in blood smear images using various color segmentation methods. *Measurement* **116**, 543–555 (2018)
58. Amin, M.M., et al.: Recognition of acute lymphoblastic leukemia cells in microscopic images using k-means clustering and support vector machine classifier. *J. Med. Signals Sens.* **5**(1), 49 (2015)
59. Sajjad, M., et al.: Leukocytes classification and segmentation in microscopic blood smear: a resource-aware healthcare service in smart cities. *IEEE Access* (2016)
60. Gautam, A., et al.: Automatic classification of leukocytes using morphological features and naïve Bayes classifier. In: 2016 IEEE Region 10 Conference (TENCON). IEEE (2016)

61. Kar, S., Das Sharma, K., Maitra, M.: Optimised feature selection for identification of carcinogenic leukocytes using weighted aggregation based transposition PSO. *IETE J. Res.* **1**–14 (2019)
62. Huang, D.-C., Hung, K.-D., Chan, Y.-K.: A computer assisted method for leukocyte nucleus segmentation and recognition in blood smear images. *J. Syst. Softw.* **85**(9), 2104–2118 (2012)
63. Manik, S., Saini, L.M., Vadhera, N.: Counting and classification of white blood cell using artificial neural network (ANN). In: 2016 IEEE 1st International Conference on Power Electronics, Intelligent Control and Energy Systems (ICPEICES). IEEE (2016)
64. Li, Y., et al.: Segmentation of white blood cell from acute lymphoblastic leukemia images using dual-threshold method. *Comput. Math. Methods Med.* **2016** (2016)
65. Ghosh, P., Bhattacharjee, D., Nasipuri, M.: Blood smear analyzer for white blood cell counting: a hybrid microscopic image analyzing technique. *Appl. Soft Comput.* **46**, 629–638 (2016)
66. Wang, Q., et al.: A spectral and morphologic method for white blood cell classification. *Opt. Laser Technol.* **84**, 144–148 (2016)
67. Sajjad, M., et al.: Computer aided system for leukocytes classification and segmentation in blood smear images. In: 2016 International Conference on Frontiers of Information Technology (FIT). IEEE (2016)
68. Win, K.Y., Choomchuay, S., Hamamoto, K.: K mean clustering based automated segmentation of overlapping cell nuclei in pleural effusion cytology images. In: 2017 International Conference on Advanced Technologies for Communications (ATC). IEEE (2017)
69. Negm, A.S., Hassan, O.A., Kandil, A.H.: A decision support system for Acute Leukaemia classification based on digital microscopic images. *Alex. Eng. J.* **57**(4), 2319–2332 (2018)
70. Marzuki, N.I.C., Mahmood, N.H., Razak, M.A.A.: Segmentation of white blood cell nucleus using active contour. *Jurnal teknologi* **74**(6), 115–118 (2015)
71. Jha, K.K., Dutta, H.S.: Mutual Information based hybrid model and deep learning for Acute Lymphocytic Leukemia detection in single cell blood smear images. *Comput. Methods Programs Biomed.* **179**, 104987 (2019)
72. Li, H., et al.: Color space transformation and multi-class weighted loss for adhesive white blood cell segmentation. *IEEE Access* **8**, 24808–24818 (2020)
73. Lu, Y., et al.: WBC-Net: a white blood cell segmentation network based on UNet++ and ResNet. *Appl. Soft Comput.* **101**, 107006 (2021)
74. Reena, M.R., Ameer, P.M.: Localization and recognition of leukocytes in peripheral blood: a deep learning approach. *Comput Biol. Med.* **126**, 104034 (2020)
75. Tran, T., et al.: Blood cell images segmentation using deep learning semantic segmentation. In: 2018 IEEE International Conference on Electronics and Communication Engineering (ICECE). IEEE (2018)
76. Fan, H., et al.: LeukocyteMask: an automated localization and segmentation method for leukocyte in blood smear images using deep neural networks. *J. Biophotonics* **12**(7), e201800488 (2019)
77. Varma, C.G., et al.: Astute segmentation and classification of leucocytes in blood microscopic smear images using titivated K-means clustering and robust SVM techniques. In: 2021 5th International Conference on Intelligent Computing and Control Systems (ICICCS). IEEE (2021)
78. Duan, Y., et al.: Leukocyte classification based on spatial and spectral features of microscopic hyperspectral images. *Opt. Laser Technol.* **112**, 530–538 (2019)
79. Agaian, S., Madhukar, M., Chronopoulos, A.T.: A new acute leukaemia-automated classification system. *Comput. Methods Biomed. Eng.: Imaging Vis.* **6**(3), 303–314 (2018)
80. Zhao, J., et al.: Automatic detection and classification of leukocytes using convolutional neural networks. *Med. Biol. Eng. Comput.* **55**(8), 1287–1301 (2017)
81. Zheng, X., et al.: Fast and robust segmentation of white blood cell images by self-supervised learning. *Micron* **107**, 55–71 (2018)
82. Vogado, L.H., et al.: Leukemia diagnosis in blood slides using transfer learning in CNNs and SVM for classification. *Eng. Appl. Artif. Intell.* **72**, 415–422 (2018)

83. Mondal, C., et al.: Acute Lymphoblastic Leukemia Detection from Microscopic Images Using Weighted Ensemble of Convolutional Neural Networks (2021)
84. Tantikitti, S., Tumswadi, S., Premchaiswadi, W.: Image processing for detection of dengue virus based on WBC classification and decision tree. In: 2015 13th International Conference on ICT and Knowledge Engineering (ICT & Knowledge Engineering 2015). IEEE (2015)
85. Nanglia, S., et al.: An enhanced predictive heterogeneous ensemble model for breast cancer prediction. *Biomed. Signal Process. Control* **72**, 103279 (2022)
86. Das, P.K., et al.: An efficient blood-cell segmentation for the detection of hematological disorders. *IEEE Trans. Cybern.* (2021)
87. Thawkar, S.: A hybrid model using teaching–learning-based optimization and Salp swarm algorithm for feature selection and classification in digital mammography. *J. Ambient Intell. Hum. Comput.* 1–16 (2021)
88. Rashid, M., Khan, M.A., Alhaisoni, M., Wang, S.H., Naqvi, S.R., Rehman, A., Saba, T.: A sustainable deep learning framework for object recognition using multi-layers deep features fusion and selection. *Sustainability* **12**(12), 5037 (2020)
89. Rehman, A., Khan, M. A., Saba, T., Mehmood, Z., Tariq, U., Ayesha, N.: Microscopic brain tumor detection and classification using 3D CNN and feature selection architecture. *Microsc. Res. Tech.* **84**(1), 133–149 (2021). <https://doi.org/10.1002/jemt.23597>
90. Çınar, A., Tuncer, S.A.: Classification of lymphocytes, monocytes, eosinophils, and neutrophils on white blood cells using hybrid Alexnet-GoogleNet-SVM. *SN Appl. Sci.* **3**(4), 1–11 (2021)
91. Rajaraman, S., et al.: Pre-trained convolutional neural networks as feature extractors toward improved malaria parasite detection in thin blood smear images. *PeerJ* **6**, e4568 (2018)
92. Qin, F., et al.: Fine-grained leukocyte classification with deep residual learning for microscopic images. *Comput. Methods Programs Biomed.* **162**, 243–252 (2018)
93. Tiwari, P., et al.: Detection of subtype blood cells using deep learning. *Cogn. Syst. Res.* **52**, 1036–1044 (2018)
94. Hung, J., Carpenter, A.: Applying faster R-CNN for object detection on malaria images. In: Proceedings of the IEEE Conference on Computer Vision and Pattern Recognition Workshops (2017)
95. Tobias, R.R., et al.: Faster R-CNN model with momentum optimizer for RBC and WBC variants classification. In: 2020 IEEE 2nd Global Conference on Life Sciences and Technologies (LifeTech). IEEE (2020)
96. Ullah, H., Saba, T., Islam, N., Abbas, N., Rehman, A., Mehmood, Z., Anjum, A.: An ensemble classification of exudates in color fundus images using an evolutionary algorithm based optimal features selection. *Microsc. Res. Tech.* **82**(4), 361–372 (2019). <https://doi.org/10.1002/jemt.23178>
97. Yu, W., et al.: Automatic classification of leukocytes using deep neural network. In: 2017 IEEE 12th International Conference on ASIC (ASICON). IEEE (2017)
98. Li, Q., Li, C., Chen, H.: Filter pruning via probabilistic model-based optimization for accelerating deep convolutional neural networks. In: Proceedings of the 14th ACM International Conference on Web Search and Data Mining (2021)

Automatic Detection of Liver Cancer Using Artificial Intelligence and Imaging Techniques—A Review



Zunaira Naaqvi, Shahzad Akbar, Syed Ale Hassan, Aima Khalid, and Muhammad Jawad Bashir

Abstract Millions of death cases have been occurring from liver cancer or hepatic cancer worldwide. This disease is most commonly caused by scarring or cirrhosis of the liver tissue. Therefore, the early detection of liver cancer is very important for timely treatment and saving the patient's life. However, it is challenging to detect and characterize liver cancer manually. Consequently, artificial intelligence (AI) techniques such as automated liver cancer detection services are now available in the medical field for the detection and treatment of this cancer. This review evaluates several types of researches and advanced technologies that can help to diagnose liver cancer automatically. Through this review of 26 relevant articles, the following synthesis of liver cancer detection techniques have been produced: (a) the use of machine learning (ML) and deep learning (DL) methods, and (b) the use of classical imaging technologies. Finally, it is found that the latest Deep Learning (DL) classifiers are capable of detecting liver cancer accurately, fastly, and reliably. However, a major problem with existing relevant articles is that there is a lack of publicly available datasets for the detection of liver cancer and the drawback of these datasets is that almost all have few images. Hence, further research should be performed on large publicly available datasets to improve the complexity of computation for reliable diagnosis of liver cancer. As a result, it serves mankind much better in efficiency and cost-effectiveness.

Keywords Liver cancer · Deep learning · CT imaging techniques · Machine learning · Magnetic resonance imaging (MRI)

Z. Naaqvi · S. Akbar (✉) · S. A. Hassan · A. Khalid

Riphah Collage of Computing, Riphah International University, Faisalabad Campus, Faisalabad 38000, Pakistan

e-mail: shahzadakbarbz@gmail.com

M. J. Bashir

School of Electrical Engineering and Computer Science, National University of Science and Technology (NUST), Islamabad, Pakistan

1 Introduction

The second major cause of death is cancer around the world. World Health Organization (WHO) statistics indicate that it caused 8.8 million deaths in 2015, out of which 788,000 deaths were due to liver cancer [1]. The human body is made up of two major metabolic systems: the liver is one of them which is the body's largest parenchymal organ [2]. The abnormal growth of liver cells in the liver is known as liver cancer or hepatic cancer. The fourth leading cause of death from cancer is liver cancer and the sixth most commonly diagnosed disease worldwide. Every year, almost 841,000 cases appear, which means 9.3 liver cancer per 100,000 people in a year, and almost 782,000 people die from liver cancer [3]. The most common cause of this illness is cirrhosis or scarring of the human liver tissue. This enzyme regulates metabolic processes and biochemical reactions. Bile is secreted by the human liver, which helps break down fat molecules into smaller ones. Bile travels through the bile duct to the small intestine during the digestive process as well as storing various nutrients like proteins, carbohydrates, fats, and vitamins (vitamins A and B). The liver produces substances that clot blood. These substances prevent even minor injuries from causing excessive bleeding. Additionally, it plays an important role in detoxification by removing harmful substances from the human body. Figure 1 shows two liver images (a) healthy liver and (b) cancerous liver image.

Liver cancer is classified into two main types. (i) Primary cancer (ii) Secondary cancer, below are descriptions of both types.

Primary liver cancer is also known as benign. These types of cancers are found in middle-aged and elderly individuals (over 60 years of age) who have liver cells present in their bodies. There are two major categories. First, primary liver cancer accounts for 75% of all cases, according to the origin of the tumor. Essentially every aspect of the liver functions is performed by cells called hepatocytes, which are the origin of hepatocellular carcinoma (HCC). As single or multiple tumors occur simultaneously, they may spread elsewhere in the liver. Most primary liver cancers arise from the linings of bile ducts. The bile flows into the gall bladder through the

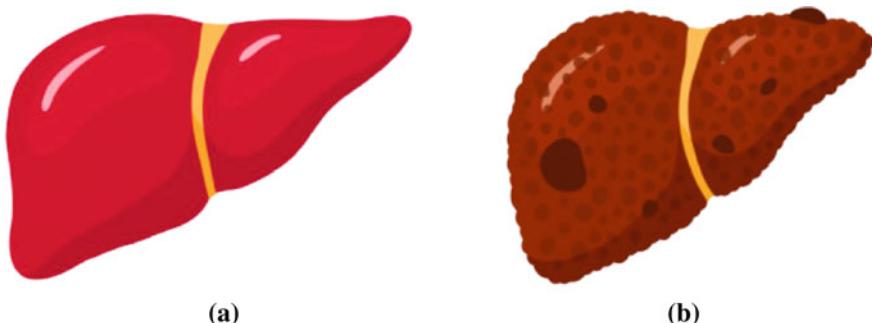


Fig. 1 Liver images **a** healthy liver **b** cancerous liver image [4]

bile duct. The cause of this type of cancer is thought to be intestinal inflammation and parasitic infection of the liver (liver fluke).

Secondary liver cancer is also known as malignant cancer. This type of cancer is very dangerous because it develops someplace else on the body before spreading to the liver; these include the stomach, colon, pancreas, lung, breast, or esophagus. The liver metastatic process of the cancer is also known as liver metastasis. It can occur at the time of the original diagnosis or later on when the primary tumor has been removed. To plan effective treatments, one needs to determine how extensive the disease is. The patient's survival rate can be enhanced through earlier diagnosis and treatment, which minimizes the treatment cost. The doctor suspects liver cancer based on changes in the abdominal organs such as the spleen, liver, or various other neighboring organs based on their size or shape when performing an abdominal examination. Any abnormal fluid collection in the abdomen can also be detected with this test. The whites of the eyes and the skin are also checked for yellowing and jaundice [5].

Cancer of the liver affects not only the liver but also the whole body. Hepatitis B and C frequently cause liver disease, so it is necessary to consider how to prevent them when addressing liver cancer countermeasures. There are four possible stages of liver tumors: benign, epithelial, malignant, and non-epithelial. Medical images can give accurate and independent information for liver disease diagnosis when accompanied by clinical symptoms and laboratory results. In addition, various diagnostic tests, such as computed tomography (CT) scans, ultrasound tests, blood tests, and angiography, magnetic resonance imaging (MRI), can be done to confirm the diagnosis. The liver may also be biopsied.

1.1 Methods for Liver Cancer Detection

Liver cancer can be diagnosed through various methods such as blood tests, angiography, and biopsies. Therefore, it's necessary to simplify and reduce the time required to detect liver cancer by implementing an efficient and effective approach. All these approaches are briefly defined below [6].

Blood Test. The liver can be examined with a blood test to determine how well it functions. An alpha-fetoprotein test is specialized for screening for tumor markers. The fetal liver secretes this protein. After birth, these levels stabilize. Cancers of the liver, ovary, and testis contain high protein levels, as tumors spread from other organs to the liver. AFP levels above 500 ng/ml are strongly associated with severe liver cancer. The AFP levels can also predict the outcome of treatment for liver cancer (they should fall after being successfully removed). Figure 2 shows blood test image for the detection of liver cancer.

Angiography. The X-ray is taken after a contrast agent is injected into a blood vessel. It allows non-surgical treatment and operation planning by showing the arteries supplying blood to cancer. Figure 3 shows liver with blood vessels.

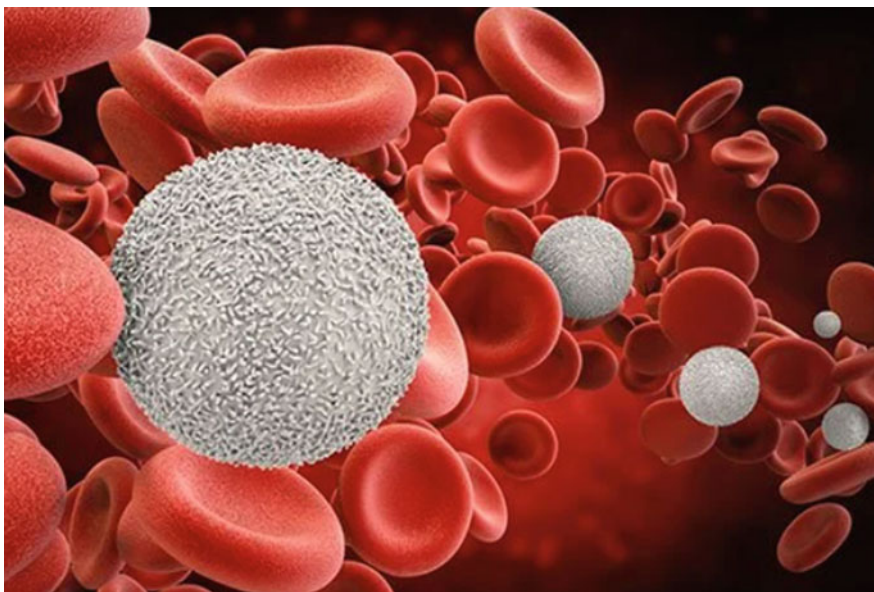
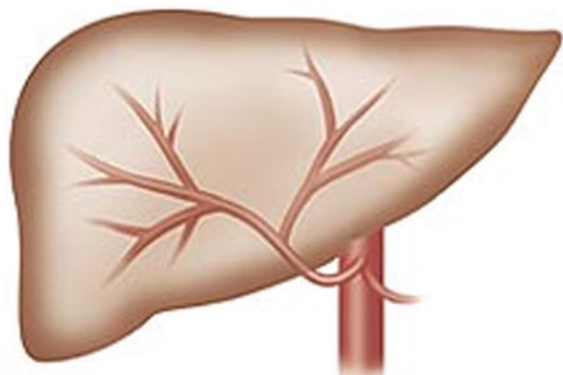


Fig. 2 Detection of liver cancer through blood test [7]

Fig. 3 Hepatic angiography
of liver [8]



Liver Biopsy. The diagnosis of liver cancer is determined by taking a small piece of tissue from the liver using a thin needle. Samples can sometimes be taken under CT or ultrasound guidance Fig. 4 shows liver biopsy for detection of liver cancer.

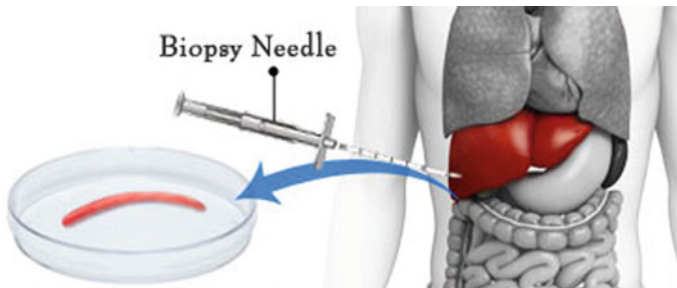


Fig. 4 Liver biopsy [9]

1.2 Liver Cancer Detection Through Imaging Techniques

There are several imaging technologies traditionally used to detect liver cancer, including computed tomography (CT), magnetic resonance imaging (MRI), and ultrasound (UL). Figure 5 depicts different imaging techniques to detect liver cancer.

Ultrasound (US). Ultrasound is the first medical imaging test ordered because it is safe, non-invasive, and relatively inexpensive as compared to other methods. The test can be taken to determine whether a tumor is present, the number of tumors (single or multiple), or how far the neighboring structures and blood vessels are involved. Ultrasound of normal liver has been taken for the detection of liver cancer in Fig. 6.

Computed Tomography (CT). A computed tomography (CT) scan can also diagnose liver cancer. A series of X-rays is used along with a computer to create 3D images of the liver. A CT scan is a non-invasive, painless way to capture the liver images through which radiologists can check liver conditions, abnormalities, and tumor. The image pre-processing techniques on CT images are used to enhance contrast

Fig. 5 Detection of liver cancer through (i) ultrasound (ii) computed tomography (iii) magnetic resonance imaging [2]

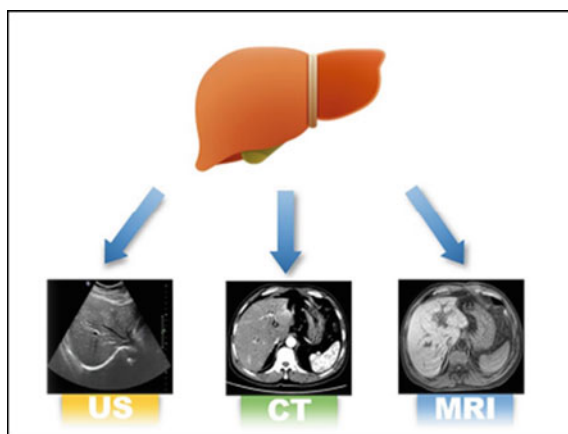


Fig. 6 Normal liver appear through ultrasound [10]



and reduce noise in the CT images. A thin slice of muscle, organ, or blood vessel is photographed so that healthcare providers can see the structures inside the body. X-rays are usually directed at a single point with traditional X-ray machines. Different tissues absorb X-rays in different amounts in the human body as they travel through them. Compared to a black background, higher density tissues create a whiter image. X-rays create a 2D image. For the detection of liver cancer Computed tomography (CT) image has been taken in Fig. 7.

Magnetic Resonance Imaging (MRI). MRI uses radiofrequency energy to produce an image that physicians can reconstruct and plan treatment. In addition, MRIs are useful for identifying malignant and benign tumors and verifying if the cancer has

Fig. 7 CT scan liver [11]



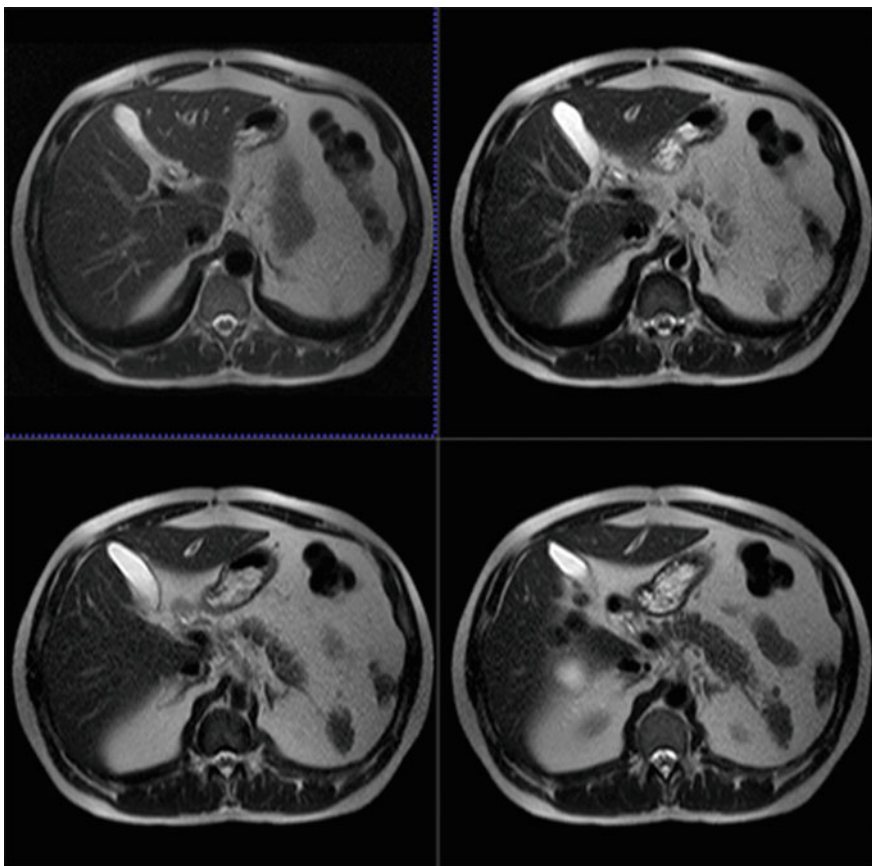


Fig. 8 Magnetic resonance imaging liver [12]

spread to other human organs. Magnetic resonance image has been taken for the detection of liver cancer in Fig. 8.

1.3 Publicly Available Datasets

Typical datasets contain various records, and these liver cancer datasets include CT and MRI images. Publicly available datasets can easily be utilized by researchers, which can be retrieved through their web links. These datasets are normally extracted to train new Machine and Deep Learning algorithms and models and test experimental studies. Here are the publicly available datasets in the following list and describe how users can access the data.

3D-IRCADb. The 3D-IRCADb database is an open-source 3D CT-scan imaging dataset available on the website [11]. These databases can be used for medical simulation or anatomical education. It consists of 3D CT scans of 20 images of liver tumors, 10 women and 10 men with liver tumors. You can download 20 different liver cancer patients report that are representing 20 different conditions. The images show liver in pixels of 512×512 , 0.56–0.87 mm in height and width. Slice thickness is 1–5 mm, pixel spacing 0.55–0.95 mm, and slice numbers 74–260 help determine the tumor's location. The tumor data is 75% out of 100%.

LiTS. The LiTs [13] is a publicly available dataset of CT scan images of Liver cancer-positive patients. The researchers developed an automated segmentation algorithm to isolate liver lesions in contrast CT images of enlarged abdomen. Medical analysis and diagnosis of treatable diseases have been based on the latest release of images. The LITS dataset contains 130 CT scan images with 70 test CT images [14]. The size of the images was 512×512 , with the slice thickness 0.7–5 mm. This chapter briefly explains how AI techniques can be incorporated into the detection and treatment of liver cancer.

The aim of this review article is to provide detailed review of various state-of-art technologies by using artificial intelligence (AI) algorithms to automatically detect liver cancer. There is discussion in this study about how most of these algorithms result in models that are trained on proprietary datasets. In hospitals, these models have assisted in the development of publicly available datasets designed to identify liver disease automatically. According to our knowledge, no such study exists in the literature for the summarization of such technologies for liver cancer detection.

The rest of this article describes a detailed literature review in Sect. 2. Furthermore, it discusses the criteria for determining which content should be included in the review article and which should be excluded. Additionally, it discusses AI techniques in imaging, utilizing machine learning and deep learning, as well as case studies. Section 3 discusses the literature review in an analytical manner and presents certain findings as well as open questions for further research. Lastly, the conclusion is presented in Sect. 4.

2 Literature Review

A systematic overview of the literature has been provided in this section which is based on these steps:

- Selection and evaluation of advanced and relevant articles.
- Emphasis on articles explaining the research problem in its simplest form.
- Identification of the research problem through an exhaustive search strategy.
- Selected research articles are mined for the desired information.
- The information is validated and fact-checked.
- A better way to visualize and read data.

2.1 Motive of the Review

This review shows the results of a specific and complete study of liver cancer for spontaneous separation in CT, US and MRI images are presented. This literature review aims to examine the development of liver cancer and the recognition of liver cancer. Diagnostic, treatment, and prevention can be achieved by analyzing optimistic algorithms. This review article presents new insights into the application of AI techniques to liver cancer. There is no comprehensive review of such technologies in the literature to our knowledge. This review presents recent approaches in pattern recognition based on pre-processing and segmentation techniques for CT, MRI, and US images that have already detected liver cancer.

2.2 Artificial Intelligence Based Liver Cancer Detection

There are three main parts to the arrangement of images using Artificial Intelligence (AI) such as training, validation, and testing. However, there are two advanced Artificial Intelligence techniques such as Machine Learning (ML) and Deep Learning (DL) [15]. The ML is further divided into three stages of supervised learning, unsupervised learning, and reinforcement learning. To simplify the supervised learning process, the variables are predicted based on a prearranged indicator (through an objective function). The advantage of a set of factors is that creating objective functions contributes to the expected goals [16]. This phase continues until the model reaches its optimal level of precision. Techniques such as Regression and Logistic Regression, KNN, Decision Tree, and Random Forest are examples of supervised learning [17]. Unsupervised learning involves predicting the objective or desired variable. Basically, it is a method of dividing populations into groups, widely used for fragmenting. K-means and Apriori algorithms are examples of unsupervised learning [18]. Normally, reinforcement learning involves training the machine to sort and categorize explicit choices. Through trial-and-error experimentation, it is programmed to learn from a certain situation and up-skill more efficiently [19]. As a result, the algorithm can learn and capture the ideal data to produce the perfect business decisions [20]. The framework of Artificial intelligence has been shown in Fig. 9.

Machine Learning (ML) Techniques for Liver Cancer Detection: A variety of medicinal applications use classification algorithms. The purpose of machine learning is to provide systems with the ability to automatically learn from experience without explicit programming. Below are a few types of ML techniques for liver cancer detection. Some of the best machine learning classifiers have been shown in Fig. 10.

Support Vector Machine (SVM). A SVM based calculation employs the learning structure, which utilizes an authentic learning approach, and they are widely used for game planning. In the SVM procedure, a hyperplane of two different sets in a vector

Fig. 9 Framework of artificial intelligence

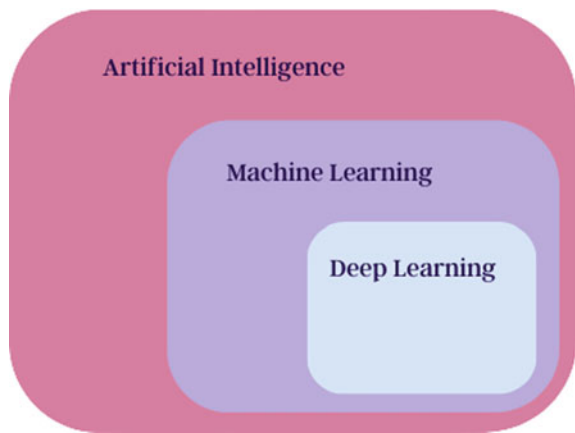
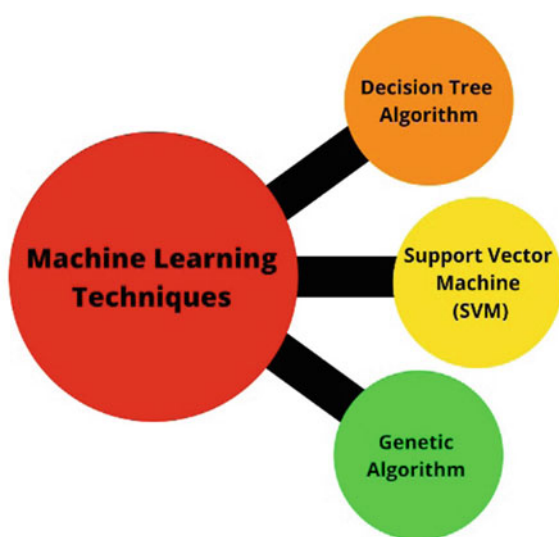


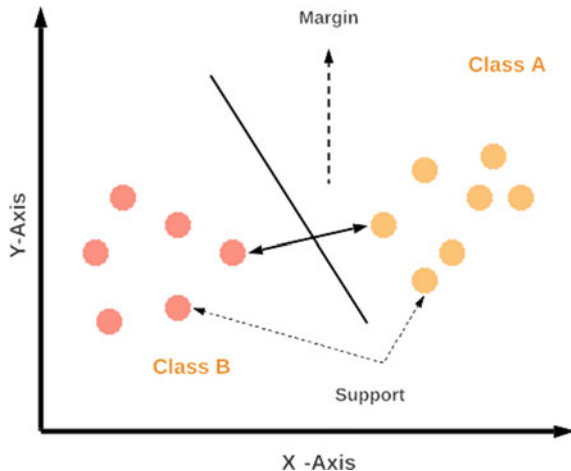
Fig. 10 Machine learning classifiers



space can be obtained by using the probabilistic dissemination of planning vectors in a set. In this hyperplane, in order to find the breaking point, vectors that are as close as possible to each other are moved away from one another. The vectors close to the hyperplane are called support vectors. There may be no disengaging hyperplane if the space is not legitimately separable. Piecework is used in this scenario. The piece works to assess the relationship between data and make an erratic division in the space [21]. The diagram of support vector machine (SVM) has been shown in Fig. 11.

Decision Tree. Decision trees are used in arrangement calculations. Building up the tree is based on a partition and overcome method. Cases are connected through an

Fig.11 Support vector machine (SVM)



array of attributes. The centers estimate a characteristic in a decision tree, while the leaves represent the class of events that satisfy the conditions. To avoid duplicates and trivial preconditions, tree pruning must be completed [22]. Decision tree has been graphically presented in Fig. 12.

Genetic Algorithm. Generic algorithm (GA) is a transformative and stochastic method for finding the optimal strategy for large and complex request spaces. Through innate exercises, such as crossover and change, a general population of encoded candidate game plans dubbed “chromosomes” is formed. At every age, the arrangements made

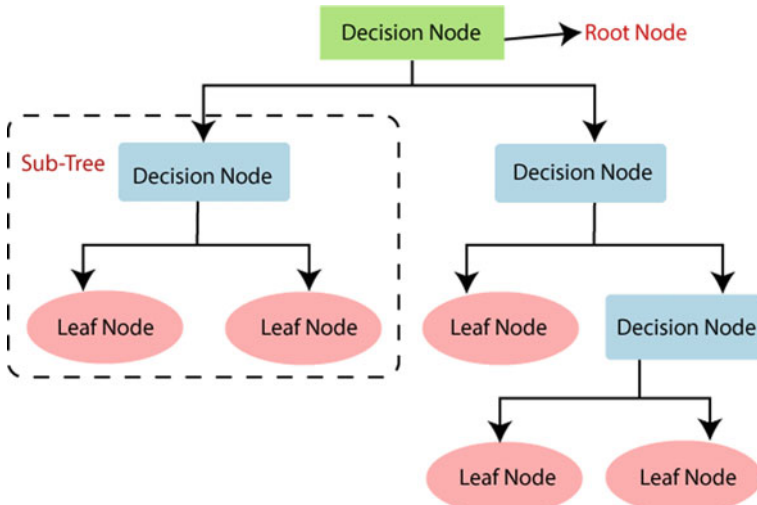


Fig. 12 Decision tree [23]

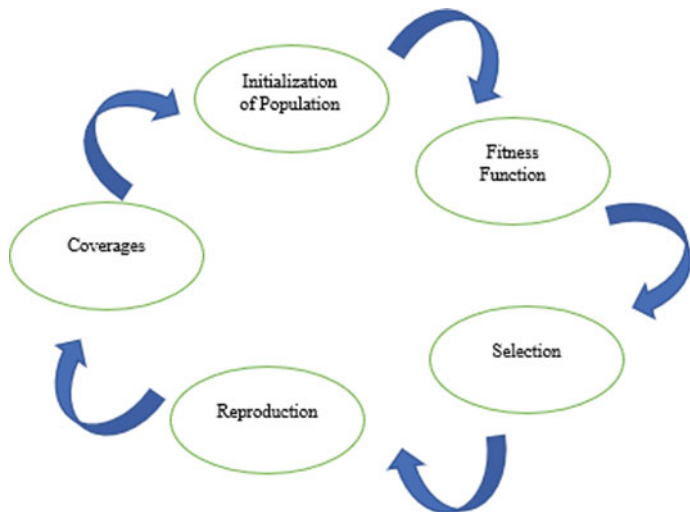


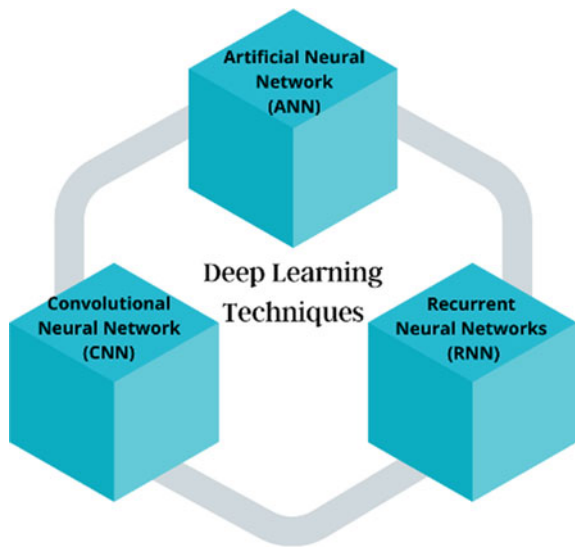
Fig. 13 Genetic algorithm

to produce posterity and produce the next generation are probabilistically determined by their welfare. Each applicant arrangement is evaluated against a wellness target work to improve the basic population. Objective work is defined in learning frameworks as the extent of a candidate's exactness over time [24]. Cyclic process of genetic algorithm has been shown in Fig. 13.

Deep Learning (DL): Deep Learning (DL) is an advanced version of Machine Learning (ML) based on instead of handcrafted feature filters, input data is exchanged using DL with non-linear transformation layer through various non-linear transformation layers. The input data features are learned and reconstructed through successive layers in the framework, which constructs the higher-level features from the lower-level ones. There are many architects of Deep Learning, and Auto-encoder (AE), recurrent Neural networks (RNN), and Deep Belief Networks (DBN). According to studies conducted recently, DL algorithms are broadly used by scientists and researchers in various fields, especially in automatic disease detection and image recognition [25]. For example, in Liver Cancer DL has been applied to detect the liver cancer, segment cancer, and the cancerous area of the liver. Three different classifiers of deep learning have been shown in Fig. 14 which are mostly used for the detection of liver cancer.

Artificial Neural Network (ANN). An artificial neural network uses learning algorithms to adjust itself independently as it receives new input. It consists of three or more layers. Its first layer is the input neurons. Next, the neurons send information to the deeper layers, sending the final output data to the final layer. The inner layers are hidden and composed of units that transform the information received from layer to layer through an adaptive process. Each layer acts as both an input and output

Fig. 14 Deep learning classifiers



layer, allowing the ANN to perceive more complex objects. Together, these layers are known as neural layers. By the information gathered according to the ANN's internal system, the units in the neural layer attempt to learn about the information gathered. Finally, a transformed result can be generated using these guidelines and sent to the next layer. ANNs can adjust their output results through backpropagation, which takes errors into account when adjusting the learning rules. Diagram of ANN with different layers has been shown in Fig. 15.

Convolutional Neural Network (CNN). The Convolutional Neural Networks (CNN) use deep learning (DL) to process unstructured data like scanned images, which include learning weights and biases assigned to various entities/viewpoints, as well

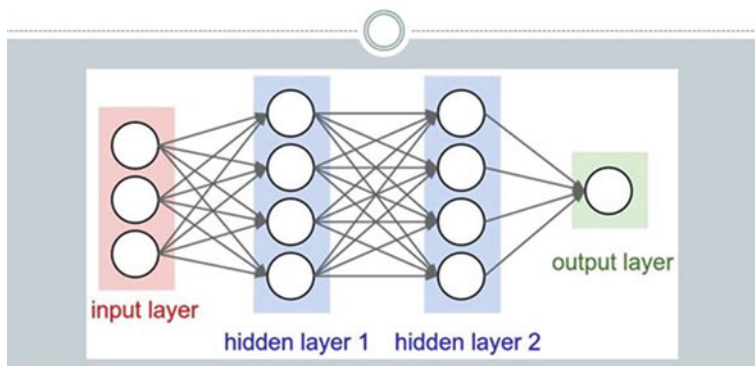


Fig. 15 Artificial neural network (ANN) [26]

as the ability to separate them by their significance. Images can be classified as best examples of CNN, with their outcomes easily linked to specific features anywhere on an image. Moreover, CNN models can represent feature maps of input data based on convolution kernels, pooling layers and rectilinear units, attached to both input and output layers. The convolutional algorithm is an average sliding convolution performed to obtain a feature map on an image. In the next step, the activation function is applied to increase the stability of the model and reduce the likelihood of the gradient vanishing simultaneously. Finally, the feature maps are pooled in pooling layers to accomplish compression and down sampling of features. A CNN model consists of these basic elements arranged in a repeating order. Gradient descent and backpropagation algorithms are used to self-optimize the parameters of the networks as they are trained. Hence, the fully convolutional network (FCN) replaces all the fully connected layers in the framework with convolution layers so the output can be any size. The FCN is used as a variant of CNN, it has become widely used in medical imaging. Using FCN, images are analyzed globally instead of using patch-based methods, and the key information of original images are restored. However, the U-Net architecture is the well-liked method of FCN. It consists of two parts, one of which compresses the pixel location information and the other unfolds the image features. CNN classifier has been shown with two layers in Fig. 16.

Recurrent neural networks (RNN). Recurrent neural networks (RNNs) are based on sequential or time-series data. Many of these deep learning algorithms have been incorporated into Siri, voice search, and Google Translate to solve ordinal or temporal problems, including language translation, natural language processing (NLP), speech recognition, and image captioning. Recurrent neural networks (RNNs) use training data to learn, like feedforward and convolutional neural networks (CNNs). The “memory” of such systems enables them to utilize information from prior inputs to influence the current input and output. However, a recurrent neural network’s output depends on the elements that preceded it within the sequence, whereas traditional deep neural networks assume inputs and outputs are independent. As a result,

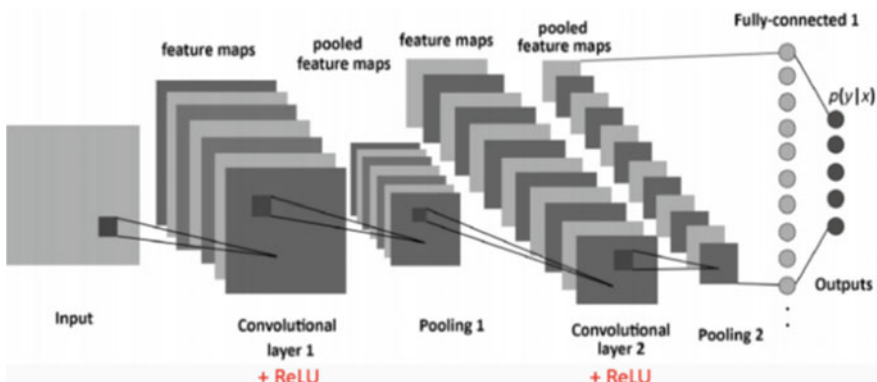


Fig. 16 Convolutional neural network (CNN) [27]

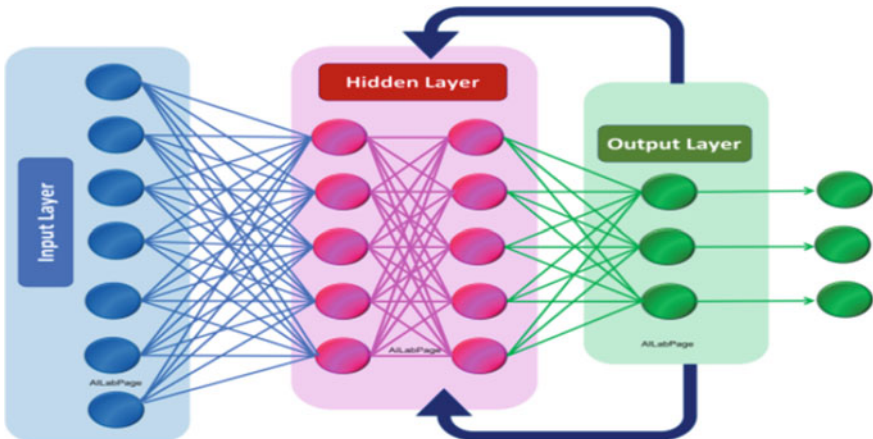


Fig. 17 Recurrent neural networks (RNN) [28]

unidirectional recurrent neural networks cannot incorporate future events into their predictions, even if they help determine a given sequence's output. Figure 17 shows the input layer, hidden layer, and output layer of the RNN classifier.

Detection of Liver Cancer Using Artificial Intelligence (AI)

Das et al. [29] proposed a technique that was the combination of two models for the detection of the cancer lesion accurately. The Watershed Gaussian Based Deep Learning (WGDL) technique was used to find the effective cancerous area in Computed Tomography (CT) images and Gaussian Mixture Model (GMM) algorithm was used to segment the cancer tissues. Using these models, extracted features were classified using the deep neural network (DNN) to control various liver tumors. The proposed method was tested on 255 CT images which consist of two stages Liver separation and cancer lesion detection, which showed the result after testing accuracy 99.38%, sensitivity 100%, specificity 99.09%.

Ayalew et al. [30] proposed a liver and tumor segmentation method from abdominal through CT images using deep learning (DL). Three different modified U-Net models were used for segmentation. The batch normalization normalizes the output of convolutional layers, and the dropout layer is used to deactivate neurons in hidden layers to eliminate the overfitting network issue. The dataset of 2346 CT images was used with data augmentation from scratch. In the pre-processing phase, the image's size was 512×512 , which was resized with 128×128 after the processing phase for better segmentation and good improvement, which showed the result after testing dice score 0.96, 0.74, and 0.63, an improvement of 0.01 and 0.11.

Ahn et al. [31] proposed a technique which was investigated an auto-segmentation application in liver cancer using a deep learning framework and demonstrated its performance improvement over atlas-based approaches. The MIM Maestro 6.5 (software) was used for auto segmentation with DCNN. The dataset of 70 patients was

used, and CT scan images were taken from the locally available dataset from South Korean liver cancer hospitals. Results showed that the deep learning-based segmentation is efficient and effective compared to atlas segmentation for (stomach, heart, Kidney, and liver) OARs in liver cancer with the maximum difference DSC 21.67, VOE 25.11%, and RVD 28.80%.

Hemalatha and Sundar [6] proposed an optimized technique that showed automatic detection of liver cancer in abdominal liver images. This technique was based on watershed and ROI algorithms. The algorithm worked on pre-processing stage, feature extraction through ROI and GLCM, and cancer classification from abdominal. The analysis of performance was performed by using entropy, accuracy, standard deviation, energy, mean, and elapsed time. The results showed dimensions about the normal and abnormal conditions of the liver's cancerous area, which enables the doctors to make a consistent treatment plan. Furthermore, to better identify tumors, statistical parameter-based segmentation, region-growing, and intensity-based thresholding can be used.

Kim et al. [32] proposed a deep learning (DL) based automatic model for the detection of hepatic malignancies through CT scan images. The technique was based on the Mask R-CNN multiphase CT images with the combination of both the multi-channel integration of multiphase CT scan images and auto segmentation of the liver. The dataset of 1086 patients were used with 1115 CT scan images. CT images were divided into different sets such as 586 training sets, 193 tuning scans, and 589 CT scan sets. After processing, the model showed 84.8% sensitivity in detecting hepatic malignancies with a 4.8 false positive CT scan on the test set. As a result, atypical enhancement patterns in HCC (71.7%) and segmentation/registration errors (42.7%) were the most frequent potential reason of false positives and false negative.

Twaisan et al. [33] proposed a method that was based on automatic segmentation of 2-D CT scan images of the liver using a watershed and thresholding algorithms. The Watershed algorithm and thresholding algorithm perform the segmentation of liver cancer. The two different scanners were used with the dataset of 44 liver images from the Radiology Department of Başkent University, Adana. The features were extracted through three different methods such as directional derivative (DD), the difference of the pixel with its neighborhood (DP) and local binary pattern (LBP). Moreover, a bilateral filter was used to enhance images and remove noise. The DP method of feature extraction yields 95.64% classification accuracy, while the DD method yields 98.8% accuracy.

Zheng et al. [34] proposed an automated method to separate cancer of liver from CT scan images. This method was used using FCN and NMF based models. The model contains 131 publicly available CT scan images such as “LiTs” and “3D-IRCADb”. The pre-processed training dataset FCN was trained for the semantic liver and liver tumor segmentation. Then, the surfaces of the tumor were refined using a 3D model, which was obtained from NMF and driven by LCSH. The CT images of these two datasets differ substantially among number, size of tumor, and level of contrast. The results showed robustness of this method to low noise, contrast, and heterogeneity, and the model achieves satisfactory results.

Al Sadeque et al. [35] proposed an automatic method for liver cancer or malignant tumor, which was based on the HOG-SVM algorithm. The method for detecting liver cancer consists of the step before image pre-processing, ROI selection, feature extraction using Histogram Oriented Gradients (HOG) with the CT images. Median and Gaussian filters were used to separate the noise in the images. For image segmentation and liver area extraction, thresholding and counteracting were used. For feature extraction ROI based Histogram Oriented Gradient (HOG) was used. The dataset of 27 confirmed liver cancer patients was contained, and results showed that the proposed methods have 94% classification accuracy using the SVM classifier of machine learning.

Masuda et al. [36] proposed a new method for the automatic liver tumor detection using adaptive contrast enhancement and EM/EMM algorithms. This method consists of steps, CT images, tumor detection, and segmentation of tumor region. For extraction of the liver region, EM/EMM algorithm was used that was based on Bayesian framework, for reducing the noise shape constraint was applied, for CT images enhancement from training data probability density function (PDFs) was used, Bayesian rules were applied to remove vessels. For the detection of segmentation of tumor region, a shape filter was used. The image contract was enhanced using the contrast enhancement with PDFs of tissue classes. Using the EM-EMM algorithm detection of tumor provide more accurate results, for future work will enhance the shape filter to handle large variations in liver tumor morphology.

Das et al. [22] proposed an automatic technique for the detection of cancerous regions on the liver using CT scan images that incorporate spatial fuzzy clustering and adaptive thresholding. The CT scan images of the public dataset were used. Initial segmentation was accomplished using adaptive thresholding, followed by spatial fuzzy clustering of lesions from the liver that have been affected by cancer. Informative features from the segmented cancerous region were extracted and classified into liver cancer types (HCC) and (MET). For the segmentation of the liver from the kidney and spleen, adaptive thresholding was used. Finally, automatic lesion segmentation process was achieved using the spatial fuzzy c-mean clustering, with two different decision tree classifiers, multilayer perceptron (MLP) and C4.5. Both methods effectively detect the lesion in the liver with 89.15% in MLP and 95.02% in C4.5 classifier. The C4.5 classifier provides the best and accurate results with LBP-HF texture descriptor compared to the MLP classifier.

Hong et al. [37] developed a method that was based on automatic segmentation of hepatic lesions and liver using 3D CT images. For the segmentation of liver and tumor the 3D U-net with dense connections and graph cut classifiers were used. The locally available datasets of liver cancer patients were used, with 1161 CT images across 294 liver cancer patients, and 100 images were used as testing datasets. The outcome showed that the algorithm got a mean Dice coefficient similarity of 73.6%. For the liver segmentation DSC 97.7%, RMSD 1.98%, ASD 0.174%, MSD 47.22%, and RVD 0.32% was accessed using proposed algorithm. For the tumor segmentation, DSC 73.6%, RMSD 1.82%, ASD 21.4%, MSD 81.02%, and RVD 6.49% were accessed of liver cancer cases on the local dataset.

Fan et al. [38] proposed a technique that was based on a deep learning (DL) classifier and the extraction of deep features through CT images for the detection of the liver and liver tumor. The dataset of publicly available 131 images were used images of CT of the liver. This study uses a self-attention mechanism and designs two blocks Position-wise Attention Block (PBA) to capture spatial dependences between Pixels and Multi-scale Fusion Attention Block (MFAB) to capture channel dependencies between features. The (MA-Net) model was used for the liver and tumor segmentation that was attained the best performance than other methods. The result showed that the liver's dice value was 0.960 ± 0.03 and tumor segmentation 0.749 ± 0 to identify liver tumors on the public dataset.

Das et al. [39] build a method that was based on a fuzzy clustering with the adaptive thresholding for liver segmentation and tumor region detection in CT scan images. The publicly available 45 CT images were used, which were collected from (MICCAI) database. The liver was separated with morphological operations and adaptive thresholding, and KFCM clustering was used for the cancerous region detection. ANN classifier was used to identify benign and malignant tumors based on GLCM and morphological features were extracted from the segmented image. The result showed that the accuracy of 97.82% of BPN, 95.74% of LVQ, and 98.82% was accessed with the PNN classifier. Improvement of the algorithm performance will be on the agenda for future research.

Alalwan et al. [40] proposed a method based on 3D Semantic segmentation of liver cancer with a deeper network and trainable parameters through CT images of the liver. For the detection of liver cancer, 3D-DenseUNet-569 algorithm were used, which utilizes the U-Net links and DenseNet connections and provides effective results with the preservation of low-level features. The publicly available dataset of 201 3D CT scan images was used, which was divided into two parts, 131 images for training and 70 for liver cancer testing. The result showed that the proposed method in liver segmentation analysis achieved an accuracy of 96.7%, DICE of 96.2% and DICE global score of 96.7%, and the tumor segmentation accuracy 80.7%, DICE of 69.6%, and DICE global score of 80.7% for the identification of liver cancer on the public dataset.

Sengun et al. [41] proposed an automated technique for the segmentation of liver cancer that was based on the deep learning architectures through images of CT scan of the liver. The model uses four different types of Deep Learning algorithms, U-net, Dense U-net, ResNet, and SegNet. The research purpose was to determine the most accurate and effective DL architecture for fully automatic liver segmentation. The public database of 125 images of CT scan of the liver was utilized for the experiments, and it was divided into 2 pieces (training, testing). The results demonstrated that the SegNet architecture has the more accurate and effective results in minimum time with the Training dataset Accuracy 0.9978%, Validation Accuracy 0.9944%, Training Dice Coefficient 0.9636%, Validation Dice Coefficient 0.8548% on the public dataset.

Dong et al. [42] proposed an automatic technique for the detection and segmentation of liver cancer using CT scan images. For the liver lesions detection and segmentation, the Hybridized Fully Convolutional Neural Network (HFCNN) was used. The

CNN was used for tumors segmentation as a voxel classifier. For the features extraction of patients with liver cancer, a 2D features map combined with residual and pre-trained weights was used. The CT scan image samples were contained that were locally available. The result showed that the proposed HFCNN method has 97.22% accuracy and 0.92 Dice coefficient on the local dataset.

Menegotto et al. [43] proposed a technique that was based on Machine Learning Computer-Aided Diagnosis algorithms for the automated classification and detection of liver cancer. The Discrete wavelet transform (DWT) model was used to attain accurate features. The features were extracted through the support vector machine (SVM) ML classifiers to classify the HCC liver cancer. The CT image samples were collected from the locally available dataset of HCC patients. The result showed that the SVM model attained the highest accuracy of 88.46% and the MLP model achieved the accuracy of 87.45% for the liver tumor diagnosis. Thus, the combination of lab markers and wavelet feature extraction was best to detect and classify HCC disease.

Meejaroen et al. [44] proposed an automatic method to recognize fibrosis in Biopsy images. The total of 34 locally available CT images were contained from Ramathibodi hospital, in which 24 images were used as test images, and 10 images were used to train the Bayesian classifier. The proposed technique updates the hidden gap between the liver tissue and the fibrosis zone. Subsequently, low-pass filters were applied to all concealed bands to reduce noise. An establishment domain, such as void slide location, excellent for regulating the degree of fibrosis against liver tissue in general. Next, image processing-based Bayesian classifiers were used to separate the fibrosis from liver tissue subjects to hide the information. In the end, to determine the degree of fibrosis in a tissue district, measure the thickness of the fibrosis zone. The results showed that the proposed method has 91.42% accuracy using a Bayesian classifier.

Ahmadi et al. [45] proposed a technique for automated segmentation of CT scan images in digital image processing. The segmentation process contains three steps such as pre-processing, image segmentation, and ROI classification. For the segmentation of the liver's blood vessels, FCM in conjunction with genetic algorithms (GA) was applied. The fuzzy C-mean method were used to involve clustering, feature analysis, and classifier design. After processing, results showed a sensitivity of 83.62%, an accuracy of 94%, and a specificity of 94.11%. During liver surgery, high desirable liver segmentation images are required. The fuzzy C-mean method is used to reach sensitivity and higher accuracy.

Todoroki et al. [46] proposed an automatic method of detecting liver cancer using a deep convolutional neural network (DCNN). The cancer detection method consists of two parts. First, a segmenting algorithm was used for segmentation of the liver from CT images. For calculating the probability of pixel, DCNN was used. Second, to extract features, convolution layers were used. For minimizing variations of features pooling layer was used, and for classification, the fully connected layer was used. The model uses multiphase CT scan images to detect five different types of liver cancer such as a hepatic tumor, FNH, CCC, HCC, Metastasis (Meta). Before contrast inject non-contrast (NC) was performed, Arterial (ART) and portal venous (PV) were used

after injection. After processing results showed, the DCNN method provides more accurate results compared to the Bayesian model.

Rozjan et al. [47] proposed a technique for the automated detection of liver cancer. 400 CT images were taken for the detection for cancer in liver. GGCM and gray scale histogram extracted the features. In addition, the dataset of 200 CT images of the GGCM classifier and 200 CT images of Grayscale histogram were contained from locally available hospitals. Finally, for feature selection and classification was performed according to hydatid liver cyst images through decision tree. The results showed that the proposed methods have for (GGCM) classifier 71% normal, single capsule 69%, and polycystic 69% Accuracy rate and for Grayscale histogram 74% normal, 63.5% single capsule, and 69% Polycystic Accuracy using a GGCM and grayscale classifiers on the local dataset.

Navaneethakrishnan et al. [48] proposed an AS-Jaya optimization algorithm based on pseudo-code for the detection of liver cancer. First, the pre-processing phase enhances the contrast by removing noise and redundancies in a medical image. Then, using the BHEFC, images were transformed into segmented. Finally, features were extracted through pixel values. The proposed method mimics the behavior of atomic motion, which inherits characteristic features from ASO & Jaya and updates classifier weight. The experimental results have shown that accuracy is 93.64%, specificity 96%, sensitivity 95%, and precision 94.88% by considering three features on the 80% training dataset. However, the proposed method has difficulties while operating in fictional computing and artificial computing platform. Further, through any other optimization algorithm performance of cancer detection will be enhanced.

Doll et al. [49] develop a technique for automatic detection of liver tumor using image segmentation and registration. The proposed algorithm for automatic liver cancer detection was based on concepts of neural network and fuzzy logic. The algorithm worked on the three phases: pre-processing phase, processing phase, and detection phase through the medical images for liver tumor detection. In experimenting, the research team used publicly available datasets of both CT and MRI images. This algorithm shows that Neuro-fuzzy (NF) systems are preferable to cover uncertainty found in extracting useful information from the images. In future, this algorithm will be applied to all kinds of cancers diagnosed through the medial images.

Table 1 summarizes the comparative study of AI detection methods applied with the efficiently obtained results. Both ML and DL technologies are used in this area to get the specific information about liver cancer.

There is a consensus that Convolutional Neural Networks (CNN) constitute the most popular digital imaging DL method that comprises multiple layers of convolutions. Its main advantage is that it offers end-to-end learning without the need for a hand-crafted engine. In the deep structure, layer 1 is convolutional, layer 2 is average or maximum pooling, layer 3 is nonlinear, layer 4 is batch normalization, layer 5 is fully connected, and layer 6 is SoftMax. In addition to boosting translational invariance, strengthening the network, and extracting classification parameters, these layers provide unique features.

Table 1 Summaries of liver cancer detection through artificial intelligence

S. No.	Authors	Years	Techniques	Datasets	Results
1	Das et al. [29]	2019	Watershed transform and Gaussian mixture model (GMM)	255 CT images of local dataset	Accuracy 99.38, sensitivity 100%, specificity 99.09%
2	Ayalew et al. [30]	2021	U-Net model, batch normalization, dropout layer	2346 CT scan Images	Dice score 0.96, 0.74, and 0.63, with the improvement of 0.01 and 0.11
3	Ahn et al. [31]	2019	MIM Maestro 6.5, and (DCNN)	70 CT scan images of local dataset	21.67% DSC 25.11% VOE 28.80% RVD
4	Hemalatha and Sundar [6]	2020	ROI, GLCM, and watershed algorithms	1115 CT scan images	84.8% sensitivity with a 4.8 false positive, enhancement in HCC (71.7%)
5	Kim et al. [32]	2021	Mask R-CNN		
6	Twaisan et al. [33]	2018	Watershed, a histogram thresholding algorithm	44 CT scan images	95.64% accuracy from sing pixels, 98.8% accuracy using histogram algorithm
7	Zheng et al. [34]	2019	FCN, NMF	131 CT images from publicly available MICCAI 2017 LiTS	
8	Al Sadeque et al. [35]	2019	HOG-SVM classifier	200 CT scan images	94% accuracy
9	Masuda et al. [36]	2011	EM/EPM algorithms		
10	Das et al. [22]	2019	Fuzzy clustering, MLP, and C4.5 classifiers	123 CT scan images of public dataset	89.15% in MLP, 95.02% in C4.5 lesion detection
11	Hong et al. [37]	2021	3D-Unet, graph cut	1161 CT scan images from local dataset	73.6% mean Dice coefficient similarity

(continued)

Table 1 (continued)

S. No.	Authors	Years	Techniques	Datasets	Results
12	Fan et al. [38]	2020	Multi-scale attention net (MA-Net)	131 CT images from publicly available MICCAI 2017 LiTS	Dice value 0.960 ± 0.03 Tumor segmentation 0.749 ± 0.08
13	Das et al. [39]	2018	GLCM, morphological/PNN, LVQ, BPN	45 CT scan images of a public dataset	Accuracy performance with respect to PNN 98.82%, LVQ 95.74%, BPN 97.82% classifiers
14	Alalwan et al. [40]	2020	3D-DenseUNet-569	201 3D CT scans from publicly available dataset	For liver segmentation accuracy 96.7%, DICE of 96.2% and DICE global score of 96.7% For tumor segmentation accuracy 80.7%, DICE of 69.6% and DICE global score of 80.7%
15	Sengun et al. [41]	2021	U-net, Dense U-net, ResNet, SegNet	125 3D CT scan images of a public dataset	SegNet architecture provide more accurate results with train accuracy 0.9978%, validation accuracy 0.9944%, train dice coefficient 0.9636, validation Dice coefficient 0.8548
16	Dong et al. [42]	2020	Hybridized fully convolutional neural network (HFCNN)	CT scan images	Dice coefficient 0.92 Accuracy 97.22%

(continued)

Table 1 (continued)

S. No.	Authors	Years	Techniques	Datasets	Results
17	Menegotto et al. [43]	2017	DWT, SVM, and MLP	CT images	88.45% SVM accuracy and 87.46% through MLP
18	Meejaroen et al. [44]	2015	Bayesian classifier	34 locally available CT images	91.42% accuracy
19	Ahmadi et al. [45]	2016	ROI, FCM, and fuzzy C-mean	20 CT scan image of public dataset	83.62% sensitivity, 94% accuracy, 94.11%, specificity
20	Todoroki et al. [46]	2017	DCNN, Bayesian model	225 CT scan images	
21	Rozjan et al. [47]	2018	Decision tree classifier (GGCM) and gray scale histogram	400 locally available CT images	For (GGCM) 71% normal, single capsule 69%, and polycystic 69% accuracy rate and for gray scale 74% normal, 63.5% single capsule, and 69% polycystic accuracy rate
22	Navaneethakrishnan et al. [48]	2020	AS-Jaya-based deep RNN	Publicly available dataset	Accuracy 93.64%, specificity 96%, sensitivity 95%, and precision 94.88%
23	Doll et al. [49]	2014	Fuzzy logic and neural network	Publicly available dataset of both CT and MRI images	Accuracy 93.64%, specificity 96%, sensitivity 95%, and precision 94.88%

Liver Cancer Detection Through Imaging Technologies. In this part, various imaging technologies for the detection of liver cancer are discussed. In every case study, the relevant information is observed, including their possible shortcomings and brief descriptions.

Ali et al. [50] proposed an intelligent Clinical Decision Support (CDS) framework to automate real-time image enhancement, segmentation, classification, and progression to diagnose cancer early. The authors used a total of 200 US images for training and testing purposes. For image normalization and enhancement, CLAHE and 2D Median Filters were used. For the region of interest segmentation, active counter models were used, and classification of objects LESH features was obtained to normalize ROI. On the LESH feature, various classifiers such as Multi-Layer Perception, KNN, SVM, Bayesian Logistic Regression, and J48graft were measured by WEKA explorer. The experimental results showed that SVM produced a maximum accuracy result with 95.29% and performed better among the ML algorithm tested. Future work predicts liver cancer using MRI and US images with cost-sensitive learning to improve the value of study and effectiveness.

Ruskó and Perényi [51] proposed a method that was based on multi-level geometric features for the automatic liver lesion detection using CT scan images. A multi-level segmentation approach was used for abnormal regions identification, and these regions were analyzed using basic geomatric features (compactness, asymmetry, or volume). The proposed method can be applied to various types of lesions in the liver which provide a counter of every single finding, and detection of cancer can be identified within half a minute. This method was trained on 55 cases with 120 lesions evaluated on a dataset of 30 images with 59 lesion types which were collected locally by physicians. The result showed 92% sensitivity at a low 1.7% false-positive rate. In the future, this method will work for MR and PET images.

Abd-Elaziz et al. [52] proposed an automated method for detecting liver cancer with the combination of region-growth, intensity analysis, and pre-processing for automatic segmentation of liver, as well as tumor segmentation with the use of CT images. The 15 CT scan images were contained from the department of Diagnostic Radiology. The results showed that the proposed region growth algorithm has 96.5 ± 0.62 sensitivity, $99.2 \pm 0.6\%$ specificity for liver segmentation and $92.6 \pm 0.33\%$ sensitivity, $99.8 \pm 0.1\%$ specificity for tumor segmentation on a public dataset. In Table 2, it is shown how the study employed and gained effectiveness in the segmentation of Imaging Technologies.

Liver Cancer can be segmented using imaging technologies, a process that would require considerable research efforts but is not yet widely available.

Artificial intelligence (AI) technologies are quickly becoming integrated into our daily lives. Furthermore, several efforts are being made in the fields of medical science and healthcare to include Artificial Intelligence developments for real-time medical diagnosis and treatment [53–55].

The detection and diagnosis of retinal diseases such as hypertensive retinopathy. [56, 57], 2 Papilledema [58, 59], 2 Brain Tumor [60–62], 3 Glaucoma [63–65], 3 Melanoma [66, 67], 2 Alzheimer's [68] 1 and Central Serous Retinopathy [69, 70]

Table 2 Summary of liver cancer detection through imaging technologies

S. No.	Authors	Years	Techniques	Datasets	Results
1.	Ali et al. [50]	2014	Clinical decision support CDS	Locally available dataset of 200 US images	Accuracy 95.29% using SVM classifier
2.	Ruskó and Perényi [51]	2013	Multi-level geometric features	30 CT scan images of public dataset	92% sensitivity at 1.7% false positive
3.	Abd-Elaziz et al. [52]	2014	Region growing, morphological image processing	15 CT scan images	For liver segmentation, sensitivity 96.5 ± 0.62 , specificity $99.2 \pm 0.6\%$ For tumor segmentation sensitivity $92.6 \pm 0.33\%$, specificity $99.8 \pm 0.1\%$

2 can be performed through Machine Learning and Deep Learning methodologies using OCT and Fundus Images [71, 72].

3 Discussion

Section 2 investigates several methods and algorithms for detecting liver cancer after the study of 26 relevant articles. This review consists of two parts (a) Liver cancer detection based on Machine/Deep Learning techniques (b) Liver cancer detection based on classic Imaging technologies. Tables 1 and 2 show the important information about the related publications about ML/DL and imaging technologies. This data includes the author's name, dataset size, results, and algorithms. This review mentions artificial intelligence (AI) techniques based on machine learning (ML) and deep learning (DL) techniques. In a comprehensive analysis, it can be decided that the classic ML approach to diagnosing liver cancer gives excellent results in both accuracy and reliability. Artificial intelligence has flourished over the past few years. Applying the ML/DL algorithm resulted in extraordinary advances in imageology. CNN-based methods for segmentation, classification, and other challenging issues have gained considerable attention in medical imaging of the liver. In the past, image processing techniques were mostly based on traditional methods. e.g., thresholding algorithm, graph cut method, and region growing algorithm.

This research is conducted on various classifiers such as CNN, ANN, FCNN, SVM, U-Net, Decision tree, and genetic algorithm. Figure 18 depicts the classifiers used in this literature review.

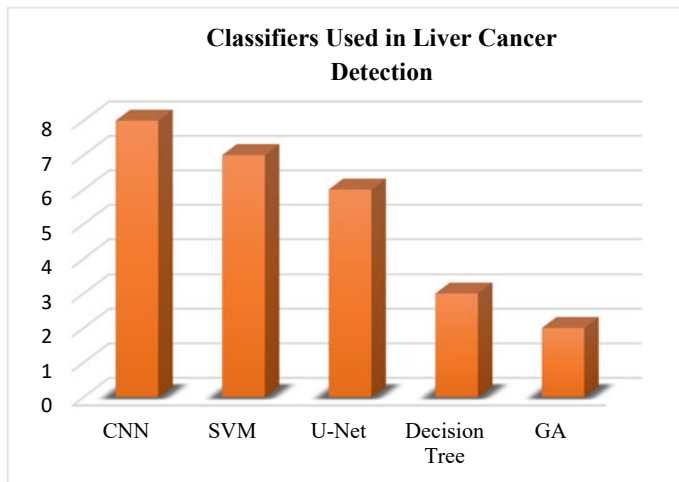


Fig. 18 Classifiers used in the literature for detection of liver cancer

In contrast, the DL technique provides more accurate results and is very helpful for image sorting procedures than the classical ML approach. A number of factors determine the results, including complexity of the underlying algorithm and the size of the datasets. The analysis of both qualitative and quantitative factors is presented in this review (check both Tables 1 and 2 for Summaries). Accurate description of the liver is a key step in most medical applications involving liver imaging. Radiologists can contour liver boundaries manually, but automated segmentation algorithms still prove the most time-efficient method and remove subjectivity.

After reading various literature, the conclusion is that segmentation, enhancement, feature extraction, and classification are generally used to identify and classify liver cancer. DL eliminates the need for inefficient models and hand-crafted feature filters to perform downstream tasks such as lesion detection and classification. Above discussed methods are more efficient, fast, and yield the best accuracy and analysis than the manual methods. In this review two different datasets are used for the validation, such as LiTS and 3D-IRCADb01.

However, in this review literature, three different types of imaging techniques are used such as CT, MRI, and the US. Figure 19 shows the total percentage of images used in the literature with respect to each imaging technique.

Moreover, this systematic review showed that Watershed Transform and Gaussian Mixture Model (GMM) classifier of machine learning has the highest accuracy 99.38%, sensitivity 100%, and specificity 99.09% results. On the other hand, in the DL Hybridized fully convolutional neural network (HFCNN) attained 97.22% accuracy.

Most ML/DL models have been trained and tested using proprietary datasets that are not publicly accessible, which is a major limitation. So, here's a vital question raises about the authenticity and integrity of these datasets. Publicly available datasets

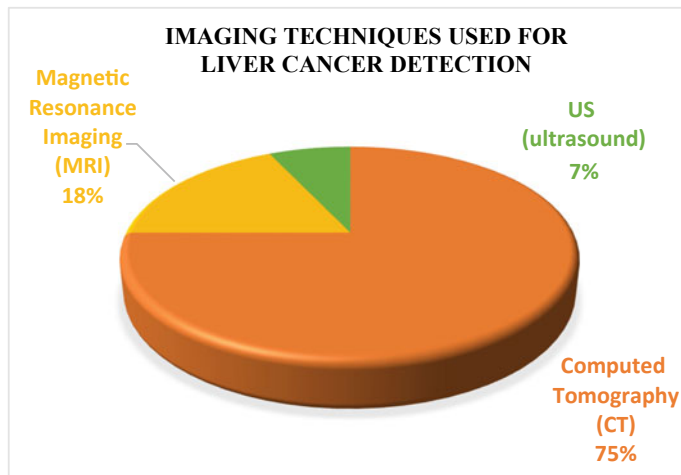


Fig. 19 Imaging technique used for the detection of liver cancer

are highly limited in number and if large datasets are available, they take a lot of computation time. To train and test the AI-based models, the research community should access more public datasets. Additionally, to make datasets more accessible to researchers, this practice will standardize the disease detection models for liver cancer. Thus, a generic detection model can be developed by the research community.

4 Conclusion

The symptoms of liver cancer are often not noticeable until the disease converts into the dangerous stage. The surface of the liver is covered by the visceral peritoneum (serosa), with a Glisson capsule underneath which makes it difficult to detect liver tumors. By the time tumor is felt, its size has increased. In people at average risk for liver cancer, there's no recommended screening test at this stage. However, the detection of liver cancer at an early stage is still a challenge for physicians. In this paper, various Artificial Intelligence (ML/DL) and image processing techniques are discussed to detect liver cancer. Recent researches find out that multiple algorithms are used on CT, MRI, and US images, and experts in segmentation procedures control this process. Researchers and physicians use these models to detect and diagnose liver cancer after testing and tuning automatically. These models are becoming increasingly accurate and reliable as time goes on. Through a review of various techniques used in artificial intelligence (AI) to detect liver cancer, this study provides a detailed review.

Computer-Aided Diagnosis (CAD) frameworks play an important role in the diagnosis of disease. It is emphasized that the ML and DL methods are important for the

research community to provide an excellent analysis of liver cancer. Many recent research articles have been analyzed and their algorithms, datasets, and results have been compared. According to a detailed analysis, advanced ML/DL models can be used to accurately, reliably, and quickly detect liver cancer. The data collection process is followed by pre-processing, in which noise is reduced and contrast is increased using different methods. To remove noise, filters are used. Different algorithms enhance images, segment them, and classify them. An automatic liver tumor identification helps doctors to treat patients better. It is essential to diagnose and treat liver cancer early to solve the treatment difficulties. However, a major problem with existing relevant articles is that there is a lack of publicly available datasets for the detection of liver cancer and the drawback of these datasets is that they have few images. If large datasets are available, it takes a lot of computation time. Even though the research shows promising results, more research is needed on publicly available datasets and improving the computational complexity. It is important to diagnose liver cancer early for the treatment of patients.

Acknowledgements This work was supported by Riphah Artificial Intelligence Research (RAIR) Lab, Riphah International University, Faisalabad Campus, Pakistan.

Conflict of Interest The authors of this literature review have no conflict.

References

1. Napte, K.M., Mahajan, A.: Liver segmentation and liver cancer detection based on deep convolutional neural network: a brief bibliometric survey. *Library Philosophy Pract.* 1–27 (2021)
2. Xiang, K., Jiang, B., Shang, D.: The overview of the deep learning integrated into the medical imaging of liver: a review. *Hep. Intl.* **15**(4), 868–880 (2021)
3. Dasgupta, P., et al.: Global trends in incidence rates of primary adult liver cancers: a systematic review and meta-analysis. *Front. Oncol.* **10**, 171 (2020)
4. Hepatocellular Cancer: Two Diseases in One online at: <https://www.narayanahealth.org/blog/hepatocellular-cancer-two-diseases-in-one/>. Accessed 27 Dec 2021
5. Liver cancer. Available at: <https://www.mayoclinic.org/diseases-conditions/liver-cancer/symptoms-causes/syc-20353659#:~:text=The%20most%20common%20form%20of,diaphragm%20and%20above%20your%20stomach>. Accessed 31 Oct 2021
6. Hemalatha, V., Sundar, C.: Automatic liver cancer detection in abdominal liver images using soft optimization techniques. *J. Ambient Intell. Hum. Comput.* **12**(5), 4765–4774 (2021)
7. Can Liver Cancer Be Diagnosed With a Blood Test online at: https://www.medicinenet.com/can_liver_cancer_be_diagnosed_with_a_blood_test/article.htm. Accessed 27 Dec 2021
8. Hepatic Angiography online at: <https://www.gastroconsultants.com/health-library/diagnostic-procedures/385511/angiography-hepatic>. Accessed 27 Dec 2021
9. Liver biopsy online at: <https://www.medindia.net/surgicalprocedures/liver-biopsy.htm>. Accessed 27 Dec 2021
10. Liver Ultrasound Abnormalities in Alcohol Use Disorder online at: <https://www.intechopen.com/chapters/66802>. Accessed 28 Dec 2021
11. Shu, X., Yang, Y., Wu, B.: Adaptive segmentation model for liver CT images based on neural network and level set method. *Neurocomputing* **453**, 438–452 (2021)

12. Magnetic Resonance Imaging Preparations—Liver with Spectroscopy online at: <https://www.cedars-sinai.org/programs/imaging-center/preparing-for-your-exam/mri-liver-spectroscopy.html>. Accessed 28 Dec 2021
13. Bilic, P., et al.: The liver tumor segmentation benchmark (LiTS). arXiv preprint [arXiv:1901.04056](https://arxiv.org/abs/1901.04056) (2019)
14. LiTS. Available online at: <https://competitions.codalab.org/competitions/17094>. Accessed 26 Dec 2021
15. Kingma, D.P., Ba, J.: Adam: a method for stochastic optimization. arXiv preprint [arXiv:1412.6980](https://arxiv.org/abs/1412.6980) (2014)
16. Kim, S., et al.: Effective liver cancer diagnosis method based on machine learning algorithm. In: 2014 7th International Conference on Biomedical Engineering and Informatics. 2014 (IEEE)
17. Patel, D., et al.: Implementation of artificial intelligence techniques for cancer detection. *Augment. Hum. Res.* **5**(1), 1–10 (2020)
18. Hwang, A., et al.: Supervised learning reveals circulating biomarker levels diagnostic of hepatocellular carcinoma in a clinically relevant model of non-alcoholic steatohepatitis; an OAD to NASH. *PLoS ONE* **13**(6), e0198937 (2018)
19. Goldstein, E., et al.: Optimal multiparametric set-up modelled for best survival outcomes in palliative treatment of liver malignancies: unsupervised machine learning and 3 PM recommendations. *EPMA J.* **11**(3), 505–515 (2020)
20. Xu, C., et al.: Synthesis of gadolinium-enhanced liver tumors on nonenhanced liver MR images using pixel-level graph reinforcement learning. *Med. Image Anal.* **69**, 101976 (2021)
21. Vadali, S., Deekshithulu, G., Murthy, J.: Analysis of liver cancer using data mining SVM algorithm in MATLAB. In: Soft Computing for Problem Solving, pp. 163–175. Springer (2019)
22. Das, A., et al.: Detection of liver cancer using modified fuzzy clustering and decision tree classifier in CT images. *Pattern Recognit. Image Anal.* **29**(2), 201–211 (2019)
23. Decision Tree Classification Algorithm online at: <https://www.javatpoint.com/machine-learning-decision-tree-classification-algorithm>. Accessed 29 Dec 2021
24. Maurya, B., Hirawal, S., Kumar, M.: A review on liver cancer detection techniques. In: 2020 5th IEEE International Conference on Recent Advances and Innovations in Engineering (ICRAIE). IEEE (2020)
25. Chen, M., et al.: Classification and mutation prediction based on histopathology H&E images in liver cancer using deep learning. *NPJ Precis. Oncol.* **4**(1), 1–7 (2020)
26. Artificial Neural Network (ANN) with practical implementation online at: <https://www.mediium.com/machine-learning-researcher/artificial-neural-network-ann-4481fa33d85a>. Accessed 29 Dec 2021
27. Simple Introduction to Convolutional Neural Networks online at: <https://towardsdatascience.com/simple-introduction-to-convolutional-neural-networks-cdf8d3077bac>. Accessed 20 Dec 2021
28. Recurrent Neural Networks online at: <https://www.ibm.com/cloud/learn/recurrent-neural-networks>. Accessed 29 Dec 2021
29. Das, A., et al.: Deep learning based liver cancer detection using watershed transform and Gaussian mixture model techniques. *Cogn. Syst. Res.* **54**, 165–175 (2019)
30. Ayalew, Y.A., Fante, K.A., Mohammed, M.A.: Modified U-Net for liver cancer segmentation from computed tomography images with a new class balancing method. *BMC Biomed. Eng.* **3**(1), 1–13 (2021)
31. Ahn, S.H., et al.: Comparative clinical evaluation of atlas and deep-learning-based auto-segmentation of organ structures in liver cancer. *Radiat. Oncol.* **14**(1), 1–13 (2019)
32. Kim, D.W., et al.: Deep learning-based algorithm to detect primary hepatic malignancy in multiphase CT of patients at high risk for HCC. *Eur. Radiol.* 1–11 (2021)
33. Twaisan, K.A.T.: MATLAB grafik arayüzü kullanıcı ile BT-karaciğer segmentasyonu için bir yazılım aracı. Fen Bilimleri Enstitüsü (2017)
34. Zheng, S., et al.: Automatic liver tumour segmentation in CT combining FCN and NMF-based deformable model. *Comput. Methods Biomech. Biomed. Eng.: Imaging Vis.* **8**(5), 468–477 (2020)

35. Al Sadeque, Z., et al.: Automated detection and classification of liver cancer from CT images using HOG-SVM model. In: 2019 5th International Conference on Advances in Electrical Engineering (ICAEE). IEEE (2019)
36. Masuda, Y., et al.: Liver tumor detection in CT images by adaptive contrast enhancement and the EM/MPM algorithm. In: 2011 18th IEEE International Conference on Image Processing. IEEE (2011)
37. Hong, Y., et al.: Automatic liver and tumor segmentation based on deep learning and globally optimized refinement. *Appl. Math. A J. Chin. Univ.* **36**(2), 304–316 (2021)
38. Fan, T., et al.: Ma-net: a multi-scale attention network for liver and tumor segmentation. *IEEE Access* **8**, 179656–179665 (2020)
39. Das, A., et al.: Adaptive fuzzy clustering-based texture analysis for classifying liver cancer in abdominal CT images. *Int. J. Comput. Biol. Drug Des.* **11**(3), 192–208 (2018)
40. Alalwan, N., et al.: Efficient 3d deep learning model for medical image semantic segmentation. *Alex. Eng. J.* **60**(1), 1231–1239 (2021)
41. Sengun, K., et al.: Automatic liver segmentation from CT images using deep learning algorithms: a comparative study. arXiv preprint [arXiv:2101.09987](https://arxiv.org/abs/2101.09987) (2021)
42. Dong, X., et al.: Liver cancer detection using hybridized fully convolutional neural network based on deep learning framework. *IEEE Access* **8**, 129889–129898 (2020)
43. Menegotto, A.B., Becker, C.D.L., Cazella, S.C.: Computer-aided hepatocarcinoma diagnosis using multimodal deep learning. In: International Symposium on Ambient Intelligence. Springer (2019)
44. Meejaroen, K., Chaweechan, C., Khodsiri, W., Khu-Smith, V., Watchareeruetai, U., Sornmagura, P., Kittiyakara, T.: Detection of fibrosis in liver biopsy images by using Bayesian classifier. In: 2015 7th International Conference on Knowledge and Smart Technology (KST), pp. 184–189. IEEE (2015, January)
45. Ahmadi, K., Karimi, A., Fouladi Nia, B.: New technique for automatic segmentation of blood vessels in CT scan images of liver based on optimized fuzzy-means method. *Comput. Math. Methods Med.* **2016** (2016)
46. Todoroki, Y., Han, X.H., Iwamoto, Y., Lin, L., Hu, H., Chen, Y.W.: Detection of liver tumor candidates from CT images using deep convolutional neural networks. In: Chen, Y.W., Tanaka, S., Howlett, R., Jain, L. (eds.) *Innovation in Medicine and Healthcare 2017. KES-InMed 2018 2017. Smart Innovation, Systems and Technologies*, vol. 71. Springer, Cham (2018). https://doi.org/10.1007/978-3-319-59397-5_15
47. Rozjan, A., et al.: Classification of computerized tomography images of endemic liver hydatid in Xinjiang based on decision tree. In: 2018 11th International Congress on Image and Signal Processing, BioMedical Engineering and Informatics (CISP-BMEI). IEEE (2018)
48. Navaneethakrishnan, M., et al.: Atom search-Jaya-based deep recurrent neural network for liver cancer detection. *IET Image Process.* (2021)
49. Doll, T.: Detection of tumor in liver using image segmentation and registration. https://www.academia.edu/download/43557982/Tumor_in_liver.pdf. Accessed 31 Oct 2021
50. Ali, L., et al.: Intelligent image processing techniques for cancer progression detection, recognition and prediction in the human liver. In: 2014 IEEE Symposium on Computational Intelligence in Healthcare and e-health (CICARE). IEEE (2014)
51. Ruskó, L., Perényi, Á.: Automated liver lesion detection in CT images based on multi-level geometric features. *Int. J. Comput. Assist. Radiol. Surg.* **9**(4), 577–593 (2014)
52. Abd-Elaziz, O.F., Sayed, M.S., Abdullah, M.I.: Liver tumors segmentation from abdominal CT images using region growing and morphological processing. In: 2014 International Conference on Engineering and Technology (ICET). IEEE (2014)
53. Shoukat, A., Akbar, S.: 8 Artificial intelligence techniques for glaucoma detection through retinal images. *Artificial Intelligence and Internet of Things: Applications in Smart Healthcare*, p. 209 (2021)
54. Gull, S., Akbar, S.: Artificial intelligence in brain tumor detection through MRI scans. *Artificial Intelligence Internet Things*, pp. 241–276 (2021)

55. Hassan, S.A., et al.: Artificial intelligence in coronavirus detection: recent findings and future perspectives. *Intelligent Computing Applications for COVID-19*, pp. 23–48 (2021)
56. Akbar, S., et al.: Arteriovenous ratio and papilledema based hybrid decision support system for detection and grading of hypertensive retinopathy. *Comput. Methods Programs Biomed.* **154**, 123–141 (2018)
57. Akbar, S., et al.: Decision support system for detection of hypertensive retinopathy using arteriovenous ratio. *Artif. Intell. Med.* **90**, 15–24 (2018)
58. Akbar, S., et al.: Decision support system for detection of papilledema through fundus retinal images. *J. Med. Syst.* **41**(4), 66 (2017)
59. Saba, T., et al.: Automatic detection of papilledema through fundus retinal images using deep learning. *Microsc. Res. Tech.* **84**(12), 3066–3077 (2021)
60. Gull, S., Akbar, S., Khan, H.U.: Automated detection of brain tumor through magnetic resonance images using convolutional neural network. *BioMed Res. Int.* **2021** (2021)
61. Gull, S., Akbar, S., Safdar, K.: An interactive deep learning approach for brain tumor detection through 3D-magnetic resonance images. In: 18th International Conference on Frontiers of Information Technology (FIT), Islamabad, Pakistan, 2021 (accepted)
62. Gull, S., Akbar, S., Shoukat, I.A.: A deep transfer learning approach for automated detection of brain tumor through magnetic resonance imaging. In: 2021 International Conference on Innovative Computing (ICIC), pp. 1–6 (2021). <https://doi.org/10.1109/ICIC53490.2021.969296>
63. Shoukat, A., Akbar, S., Hassan, S.A.E., Rehman, A., Ayesha, N.: Glaucoma diagnosis through convolutional neural network using fundus image. In: 18th International Conference on Frontiers of Information Technology (FIT), Islamabad, Pakistan, 2021 (accepted)
64. Shoukat, A., Akbar, S., Safdar, K.: A deep learning-based automatic method for early detection of the glaucoma using fundus images. In: 2021 International Conference on Innovative Computing (ICIC), pp. 1–6 (2021). <https://doi.org/10.1109/ICIC53490.2021.9693078>
65. . Akbar, S., Hassan, S.A., Shoukat, A., Alyami, J., Bahaj, S.A.: Detection of microscopic glaucoma through fundus images using deep transfer learning approach. In: *Microsc. Res. Tech.* (2022)
66. Safdar, K., Akbar, S., Gull, S.: An automated deep learning based ensemble approach for malignant melanoma detection using dermoscopy images. In: 18th International Conference on Frontiers of Information Technology (FIT), Islamabad, Pakistan (2021)
67. Safdar, K., Akbar, S., Shoukat, A.: A majority voting based ensemble approach of deep learning classifiers for automated melanoma detection. In: 2021 International Conference on Innovative Computing (ICIC), pp. 1–6 (2021). <https://doi.org/10.1109/ICIC53490.2021.9692915>
68. Ahmad, M.F., Akbar, S., Hassan, S.A.E., Rehman, A., Ayesha, N.: Deep learning approach to diagnose Alzheimer's disease through magnetic resonance images. In: 2021 International Conference on Innovative Computing (ICIC), pp. 1–6 (2021). <https://doi.org/10.1109/ICIC53490.2021.9693041>
69. Hassan, S.A.E., et al.: Deep learning-based automatic detection of central serous retinopathy using optical coherence tomographic images. In: 2021 1st International Conference on Artificial Intelligence and Data Analytics (CAIDA). IEEE (2021)
70. Hassan, S.A., et al.: Recent developments in detection of central serous retinopathy through imaging and artificial intelligence techniques—a review. *IEEE Access* (2021)
71. Akram, M.U., et al.: Data on fundus images for vessels segmentation, detection of hypertensive retinopathy, diabetic retinopathy and papilledema. *Data Brief* **29**, 105282 (2020)
72. Akbar, S., et al.: AVRDB: annotated dataset for vessel segmentation and calculation of arteriovenous ratio. In: Proceedings of the 21th International Conference on Image Processing, Computer Vision, & Pattern Recognition (IPCV'17) (2017)

Spot Filtering Adaptive Thresholding (SFAT) Method for Early Pigment Spot Detection on Iris Surface



Mohamad Faizal Ab Jabal, Suhardi Hamid, Nur Zuraifah Syazrah Othman, and Mohd Shafry Mohd Rahim

Abstract Iris pigment spot is a discrete pigmentation on the iris surface and can detect eye cancer. There are two types of iris spots, freckles and nevi. While freckles are usually harmless, nevi distort the stromal layer, and therefore, its existence is considered high potential for uveal melanoma, a type of cancer that can cause blindness. The features used to detect the uveal melanoma are size, shape, number of existences, spot of existence and the colour of the pigment spot on the iris surface. In image processing, feature extraction method typically extracts size, shape and colour. However, it is still challenging to produce an accurate extraction result for iris pigment spot. In this study, a threshold intensity value of colour is identified as the pigment spot feature used in the feature extraction process. Furthermore, Spot Filtering Adaptive Thresholding (SFAT) method has been developed to filter between pigment spot and iris surface feature. The proposed method extracted the pigment spot existence with an accuracy rate of 37.1%. This shows that the intensity of the saturation component has the potential to be used in the medical imaging analysis.

Keywords Medical imaging · Iris pigment spots · Iris image · Cancer detection · Image processing · Colour histogram · Feature extraction · Thresholding

M. F. Ab Jabal

Fakulti Sains Komputer dan Matematik, Universiti Teknologi MARA, Cawangan Johor Kampus Pasir Gudang, Masai, Johor, Malaysia

e-mail: m.faizal@uitm.edu.my

S. Hamid

Fakulti Sains Komputer dan Matematik, Universiti Teknologi MARA, Cawangan Kedah, Merbok, Kedah, Malaysia

e-mail: suhardi@uitm.edu.my

N. Z. S. Othman · M. S. M. Rahim (✉)

School of Computing, Faculty of Engineering, University Technology Malaysia, Skudai, Johor, Malaysia

e-mail: shafry@utm.my

N. Z. S. Othman

e-mail: zuraifah@utm.my

1 Introduction

In medical imaging, to take an image on parts of the human body for diagnosis, treatment procedures and examining disease purposes, various techniques and processes are involved. X-ray image, computed tomography (CT) scans, digital mammography, magnetic resonance imaging (MRI) and ultrasound are the types of images used as data in the medical imaging system [1, 2]. They are used to analyse the internal parts of human body. On the other hand, a high-resolution image is another type of image applicable to medical imaging [3, 4]. The high-resolution images can be used to analyse the external parts of human body. However, despite being external, in some instances, the parts can be very sensitive to touch or difficult to be observed, such as the iris. Hence, colour imaging is an alternative method to represent the parts for further analysis.

Uveal melanoma (UM) is an eye cancer that can cause blindness. The cancer is primarily driven by nevi spots, which are pigmentation spots on the iris surface that distort the stromal layer [5, 6]. In general, pigmentation on the iris surface, which can be either freckles or nevi, is a common trait in individuals of European ancestry. It is estimated that 50–60% of healthy adults have freckle spots on their iris surface. Freckle spots are pigmentation that do not distort the stromal layer and do not cause cancer.

On the other hand, around 4–6% of adults in Europe found to have nevi spots on their iris surface and are highly potential to get cancer [7]. Figure 1 shows the existence of pigment spots on the iris surface. The arrow points to one example from several pigment spots on the iris surface.

The pigment spots, either freckle or nevi, have similar topography but are extremely different ultra-structurally [7, 8]. In addition, there is no concrete method to differentiate between a freckle and nevi spots based on iris image. Therefore, the demand for a technique that can determine both spots based on the iris image has motivated this study. This will require two knowledge areas, digital image processing and medical expertise. There are stark differences between the two areas. For one thing, the medical field has trusted monochrome images (e.g. X-ray) for so long to

Fig. 1 Pigment spots exist on the iris surface



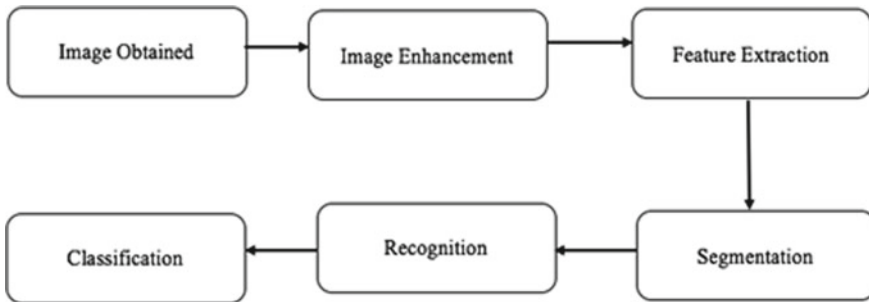


Fig. 2 Fundamental of image analysis process

perform analysis. However, the quality of digital images has increased tremendously, making it a viable option to be pursued [9, 10].

The development process is required in the image processing technology to analyse the obtained image. Typically, there are several steps involved, illustrated in Fig. 2. Feature extraction is vital in this process, where incorrect feature extraction will influence subsequent processes.

Based on the foregoing discussion, in this study, the main issues that need solution are the definition of the pigment spot features that can be used for the extraction process and the reliable extraction method to extract the pigment spot existence the iris surface. A filtering method is proposed to distinguish between the pigment spots and the iris surface colours during the extraction process. The application of the suitable filtering method in feature extraction can greatly increase the accuracy rate of the extraction output. The findings from this study are a reliable definition of the iris pigment spot feature and a robust feature extraction method [11, 12].

The structure of the paper is organised as follows. The discussion on the related work will be in Sect. 2: a literature review. The definition of the iris pigment spot feature and the proposed feature extraction method will be described in Sect. 3: methodology. The testing result, the evaluation of the accuracy performance and validation to the extraction result are explained in Sect. 4: result evaluation. Finally, Sect. 5: conclusion and future work will conclude the comprehensive study and present suggestions for future work.

2 Literature Review

The eyes are the window to the soul. There are so many things to study and discover on human eyes. Given the number of discoveries that researchers have accomplished merely by studying the eyes alone, it is fair to acknowledge that eyes are an extremely complex body part [13–15].

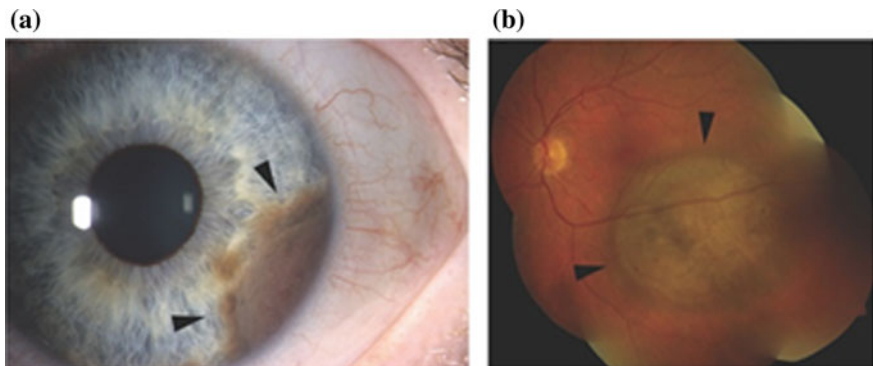


Fig. 3 Uveal melanoma—**a** Iris pigment spots arising had distorted the stromal layer (view from the iris surface). **b** Uveal melanoma arising from the choroidal component of the uveal tract normally known as tumour (view from the retina)

Edwards et al. in 2015 stated that it would be extremely useful to have a method of differentiating both freckle and nevi spots [7]. This is agreed in the work by Tarian, Field and Harbour in 2016 which also added that it could be extremely difficult to detect the uveal melanoma (UM) automatically [6]. Figure 3 presents the condition of the iris surface and the retina with the UM [6]. The complexity in detecting UM, among others, drives this research to be conducted. This research will look into different perspective that can possibly assist in advancing knowledge in this special area.

For this study, the area of interest is the pigment spots visible on the surface of iris. Pigment spots are defined as discrete areas of pigmentation on the iris surface and can be observed by the naked eye [7]. Man et al. in 2016 later concluded the pigment spot feature as a dynamic form of the pigmentation on the iris surface [3]. The dynamic form is referred to as the random shapes of the spots, random spot positions on the iris surface, random spot sizes and random number of the spot existence. The varying forms of the pigment spot features will make the feature extraction process arduous. However, based on Fig. 1, one feature is moderately consistent and possible to be used in the extraction process, which is the pigment spot colour. The colour of the pigment spots ranges from tan to dark brown [7, 16–18].

2.1 Iris Surface Feature

The discussion regarding the iris surface feature is divided into two perspectives. The first is from the biological or ophthalmology perspective, and the second is from the biometrics or image analysis perspective. In a biological or ophthalmology perspective, an iris surface feature contains a complex texture of visible particles of different sizes [1, 19, 20]. The particles are identified as freckles, furrows, stripes and

coronas. In different cases, the features that have been identified are Fuchs' crypts, Wolfflin nodules, pigment spots, contraction furrows and conjunctival melanosis [7]. However, based on these definitions, it is hard to develop the feature extraction method because the definition or forms of the feature cannot be recognised or understood by the computer. Furthermore, the form of the features, which are biologically constructed, is in unspecified and unpredictable forms [1, 20].

Looking from the biometrics or image analysis perspective, an iris surface feature is defined as a feature vector, binary feature, boundary feature and edge feature [2, 16, 19, 21, 22]. These features are commonly used in the iris biometrics recognition system or image analysis processing. Moreover, these features are recognised and understandable by the computer. Unfortunately, the random form of the pigment spots has made the feature construction process difficult. Therefore, the colour is also identified as a feature as an alternative.

According to Szeliski, the colour in the image contains significant information such as the boundary of the objects cited in [23]. However, the colour in the image is not directly recognised by the computer. Hence, the colour feature is used to help the computer to identify and recognise the existence of the colour in the image. Colour properties, the values of the colour components, the colour index values, intensity, mean, standard deviation and pixel intensities are the definition of the colour features [14, 24–30]. Based on the definition of the colour features, the computer can recognise the existence of the colour in the image during the image analysis process. Hence, a new definition is required for the iris pigment spot feature to perform the extraction process using a computer [31, 32].

2.2 Feature Extraction Approach

Generally, several feature extraction approaches have been developed either in the iris biometrics field or medical imaging [19, 21, 33]. Gradient-based edge detector is a method proposed by Wildes to detect the edges in the image. The information retrieved from the extracted edges is a boundary of the region of interest (ROI) cited in [23]. Next, wavelet analysis approach is another extraction method typically used by researchers. Patil and Patilkulkarni have utilised the method to extract the feature vector from the image. Then, the extracted vectors have been analysed and used to construct the ROI on the image cited in [34].

On the other hand, Gupta et al. applied the corner detection algorithm cited in [34]. The algorithm is used to extract the iris texture. The purpose is to find possible curves to be parameterised as the boundary. Nichal et al. in 2014 proposed and tested the zero crossings of differences between 1D discrete cosine transform (DCT) coefficient approach [34]. The approach extracted all ROI pixels along 45° lines in the image. In a different case, colour detection method was applied to extract the colour intensity [35]. The study aimed to classify the farmland based on environment information. Having seen the significance of these colour traits, Srivastava, Wadhvani and Gyanchandani in 2015 employed colour histogram intersection method [36].

The method is divided in two categories, which are local and global. The local is concerned with ROI and the spatial distribution of pixel, while the global is to analyse the image's colour frequency. The mainstream approach has always been the colour histogram and is commonly used to extract and segment the colour in the image [37, 38].

Next, Tiwari et al. in 2016 researched the colour segmentation technique to extract the colour density on the skin image to segment the ringworm psoriasis on the skin [8]. Prior to this, Othman in 2014 had used Hybrid Quantisation Dithering (HQD) algorithm [39]. The goal is to segment the colour based on the clothing image. The algorithm has successfully extracted the values of each colour component from the RGB colour model. Later, Michala in 2014 developed the colour-based segmentation approach [40]. The approach has extracted the colour intensity for every component in the RGB colour model. However, no publication regarding the developed approach has been published. However, the source code of the approach has been shared by the owner in the MATLAB website. Beran, Chmelar and Rejzek in 2016 continued research on colour detection threshold approach. The approach was executed in the RGB and HSV colour models [41]. The finding from the study shows that the HSV colour model is a more reliable colour model to be used for the image analysis processing compared to the RGB colour model, which is more suitable for display purposes. Another approach was developed by Image Analyst in 2016 using simple colour detection by hue in order to segment the object in the image [42–44]. The approach uses the maximum and minimum threshold intensity values to extract the pixel based on the intensity value held in each pixel. Every pixel containing the intensity values in a range of maximum and minimum threshold intensity values will be kept as the ROI, and the other pixel will be eliminated and labelled as irrelevant pixel.

2.3 *Challenge of the Study*

The main challenge of this study is to define the iris pigment spot feature to be used for extraction. In addition, pigment spot that has been defined still cannot be extracted accurately from the image as the existing extraction method cannot recognise between the pigment spot and iris surface colour. Therefore, the next challenge is to specify the pigment spot colour value to separate between the pigment spot and iris surface. Therefore, this study needs to develop a method in order to separate the pigment spot and iris surface colour.

The finding from the extensive literature study is that a reliable, suitable feature extraction approach that might use to evaluate the accuracy performance of the proposed feature extraction method is colour histogram. Moreover, the literature study has found that a reliable feature can be applied to extract pigment spots on the iris surface.

3 Methodology

3.1 Iris Pigment Spots Feature Definition

Iris pigment spot colour is moderately consistent with being used as a feature. However, there is no colour values that have been published related to pigment spot colour. This makes it difficult for this study to determine the true value of the pigment spot colour in order to define the pigment spot feature that is possible to be extracted. As stated earlier, the pigment spot colour is in a range of tan to dark brown. Still, this information is vague for the computer to perform an accurate extraction [45, 46]. Therefore, an investigation is conducted to discover a reliable feature that can be used for the extraction process.

Moreover, this study has considered the iris pigment spot as a region of interest (ROI). Thus, to extract the pigment spot, it is necessary to identify and extract the pigment spot feature in the ROI. Therefore, the first step is to identify the reliable feature to be used as a pigment spot feature in the ROI. Then, the process is continued to extract the feature in the ROI [47, 48].

Colour histogram method has been used in order to analyse the colour distribution and colour pattern. The testing was conducted using two common colour models: RGB and HSV colour models. The finding from the testing suggests that the HSV colour model is more reliable to be applied for the image analysis process. Figure 4 presents the sample of the colour distribution output. Figure 5 shows the HSV output.

Based on Fig. 5, the colour histogram method has been deployed to analyse the colour pattern for each colour component in the HSV colour model. The method is also used to discover the ROI on the iris surface. The sample output from the process is shown in Fig. 6. The finding from the analysis concludes that only the hue and saturation components are reliable to be applied in this study. Figure 7 presents the pixel value in 4 by 4 matrices for saturation components.

Figure 6 presents the colour histogram pattern of the HSV image. The red line in the histogram represents the hue component, the blue colour is saturation component, and the green colour is value component. The finding from Fig. 6 shows that most pixels in the image contain the hue colour value compared with the others. This information indicates the values contained in each pixel in the ROI. However, this finding is still not enough to determine the exact pixel values in the ROI. Hence, the next process is converting all the colour components as shown in Fig. 7. The process is to reduce the colour component into one colour scale: the grey scale.

Moreover, the value held in each pixel will be changed into one colour scale. Each value held in the pixel is known as a brightness or intensity. Based on Fig. 7, only hue and saturation components are reliable. However, after analysing the intensity values in each pixel within the ROI, it is found that the saturation component is much more reliable to be used because the range of intensity values in the ROI contrasts the intensity value of the non-ROI. Therefore, this study decides that the intensity value from the saturation component is a reliable feature to be extracted to recognise

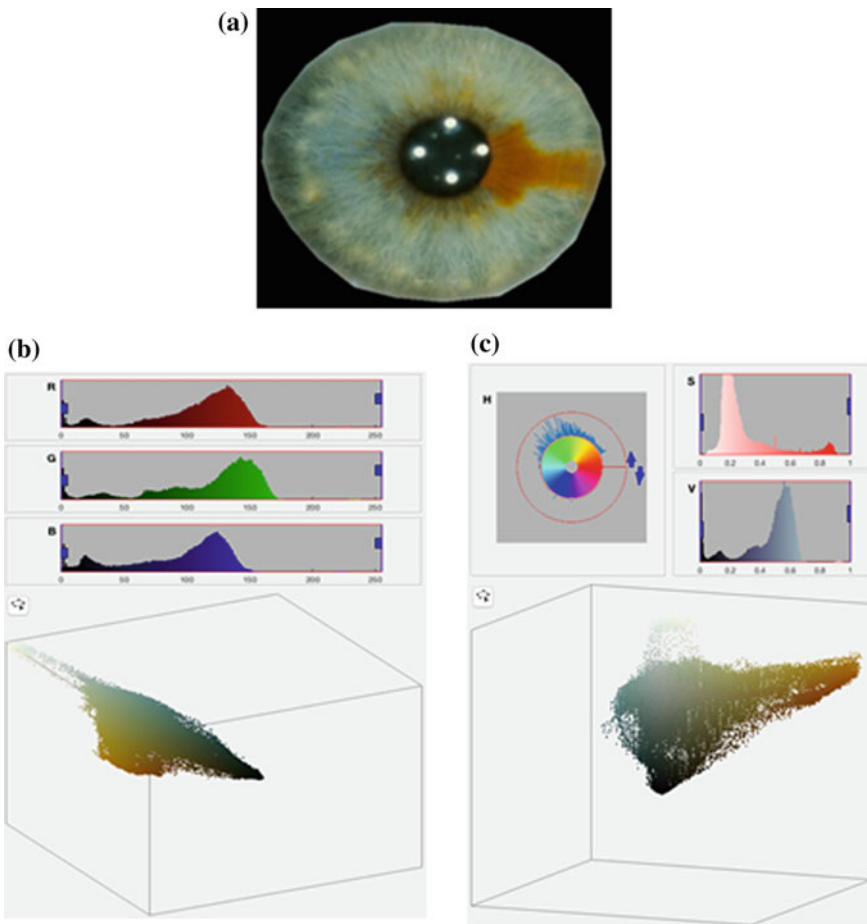


Fig. 4 Analysis of colour distribution by using colour histogram method. **a** Obtained image contains pigment spots on the iris surface. **b** Histogram of RGB colour model. **c** Histogram of HSV colour model

the existence of pigment spots on the iris surface. The range of the values is between 0.7 and 0.9.

To define the iris pigment spot feature that could be used for the extraction process and can be recognised by the computer, a hypothesis has been constructed as follows:

Case 1: Pigment spots on the iris surface can be defined through the feature of the spot such as the shape, the size of the spot, the position of the spot and the colour of the spot [7].

Case 2: The common features used in the image analysis are edge feature, shape feature, feature vector, boundary feature, binary feature and colour feature [23, 33, 37, 42].

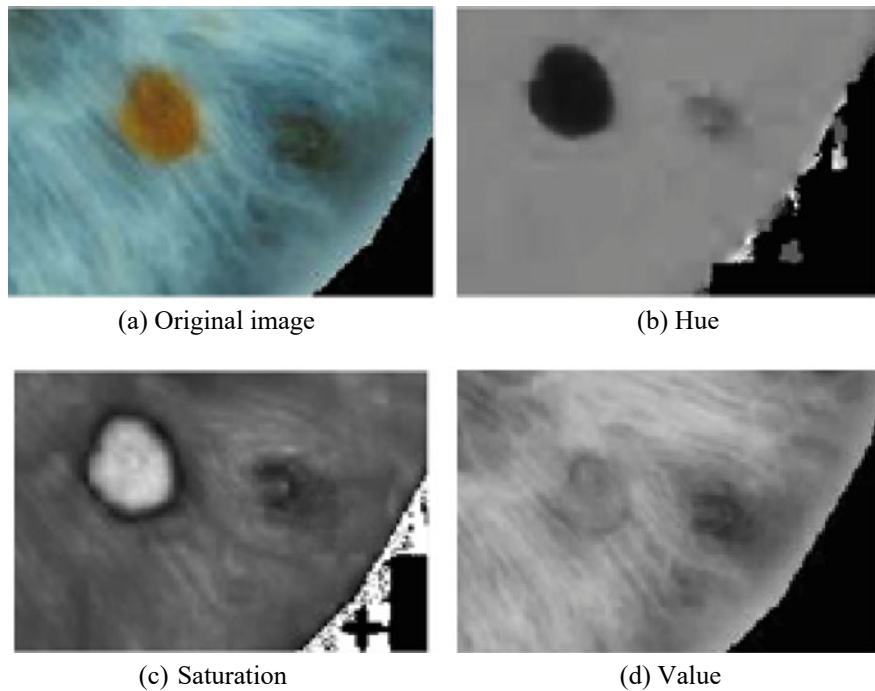


Fig. 5 The conversion process from RGB colour model to HSV colour model

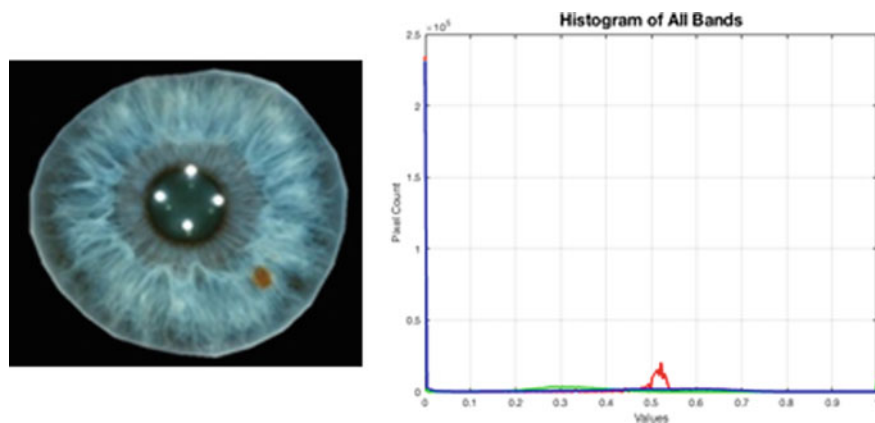


Fig. 6 Histogram of the HSV colour model



Fig. 7 Matrices 4 by 4 of saturation colour components

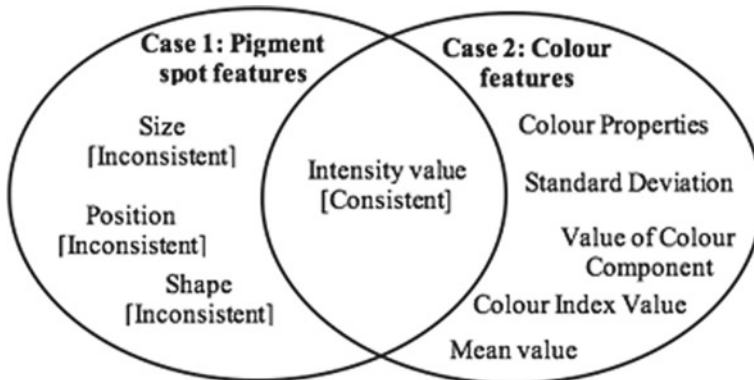


Fig. 8 Correlation between pigment spot colour and colour intensity value

Correlation: Based on the foregoing discussion, pigment spot colour is reliable to be used as an effective feature in the extraction process. The colour can be described by the computer based on the colour feature as described earlier. Furthermore, the finding from the study also concludes that the saturation intensity value highlighted the existence of the pigment spot in the image. Hence, this study's initial assumption shows that the saturation component's intensity value is reliable to be extracted as the pigment spot feature. Figure 8 illustrates the correlation between the pigment spot colour and the colour intensity value.

Hypothesis: Highlighted in Fig. 8, the colour intensity value intersects between two sets. This means that the colour intensity value is possible to meet the requirement from both sets. Hence, the colour intensity value from the pigment spot colour's saturation component can be defined as the iris pigment spot feature. Furthermore, this feature can be recognised by the computer and more reliable for image analysis.

3.2 Feature Extraction

This study proposes to deploy the colour histogram method to extract the colour feature. However, the current ability of the method is limited to distinguishing the pigment spot colour from iris surface colour. Therefore, thresholding method is

deployed and integrated in the colour histogram method. The role of the thresholding method is to filter the existence of the pigment spots on the iris surface. Hence, the pigment spots can be isolated from the iris surface accurately. The integration's impact has extended the colour histogram method's ability to distinguish between the pigment spot colour and the iris surface colour.

Moreover, the method can produce an accurate extraction output. This integration method has been named as Spot Filtering Adaptive Thresholding (SFAT) method. The development of the SFAT method consists of five steps including the pre-processing processes, which are noise elimination, conversion of colour model, thresholding, irrelevant pixel elimination and image enhancement.

3.3 Pre-processing

In the pre-processing phase, the noise in the image is eliminated. During data analysis, it is found that light reflection on the iris image does not bring any useful information to this study. Hence, these irrelevant pixels need to be eliminated to avoid jeopardising the following processes. The elimination process starts with converting the RGB image into the grey scale image. The process can be expressed in Eq. (1)

$$GI = 0.2989 * R_I + 0.5870 * G_I + 0.1140 * B_I \quad (1)$$

where GI is the grey scale image, which is the output of the conversion process, R_I is the red colour's value from the input image, G_I is the green colour value from the input image, and B_I is the value of the blue colour from the input image. In the next process, the GI is converted into binary image (BI) to detect the existence of the light reflection on the iris surface. The light reflection can be seen in the image as a white spot on the iris surface. All pixels that contain the threshold value greater than 220 will be changed to 1 which is the white colour on the BI and are known as holes. The remaining pixels that are less than the stated threshold value are changed to 0 which is black on the BI . The following process is dilation and fills the hole with new pixel value. The value is retrieved from the nearest neighbour pixels. The final step is to recombine the RGB colour. Figure 9 illustrates the pre-processing processes.

3.4 Spot Filtering Adaptive Thresholding (SFAT) Method

The following process is the pigment spot extraction. The process is performed using the proposed method called the Spot Filtering Adaptive Thresholding (SFAT) method. The process can be expressed in the algorithm form as follows:

Step 1: Obtain an iris image from the pre-processing output.

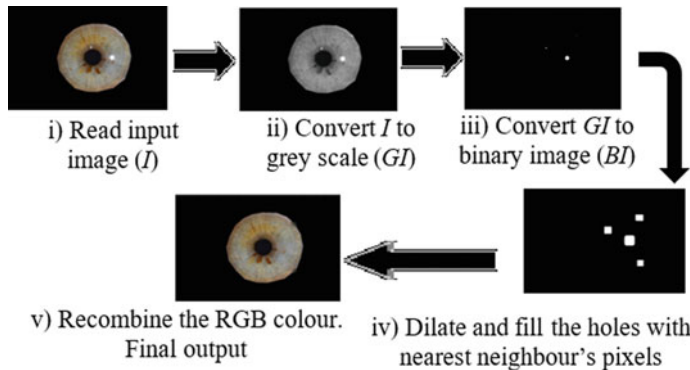


Fig. 9 Steps of image pre-processing

Step 2: Convert the RGB colour model into the HSV colour model.

Step 3: Threshold for each HSV colour component.

Step 4: Feature masking process.

Step 5: Irrelevant pixel elimination.

Step 6: Image Enhancement.

Figure 10 illustrates the algorithm and the process flow. Based on the algorithm, the extensive explanation for each step in the algorithm is discussed on the following paragraphs.

After the pre-processing, the generated output from the process is applied in the next step of the method. The subsequent process is conversion from the RGB colour model into the HSV colour model, which is the second step in the algorithm. The conversion process can be expressed using Eqs. (2), (3), (4) and (5).

$$R_n = \frac{R}{2^b}; \quad G_n = \frac{G}{2^b}; \quad B_n = \frac{B}{2^b} \quad (2)$$

where R_n , G_n and B_n are normalised RGB components, and the result ranges from 0 to 1, while b is a length for each colour component.

$$C_{\max} = \max(R_n, G_n, B_n) \quad (3)$$

$$C_{\min} = \min(R_n, G_n, B_n) \quad (4)$$

$$\Delta = C_{\max} - C_{\min} \quad (5)$$

where C_{\max} is the maximum value from normalised RGB component and C_{\min} is the minimum value from normalised RGB components.

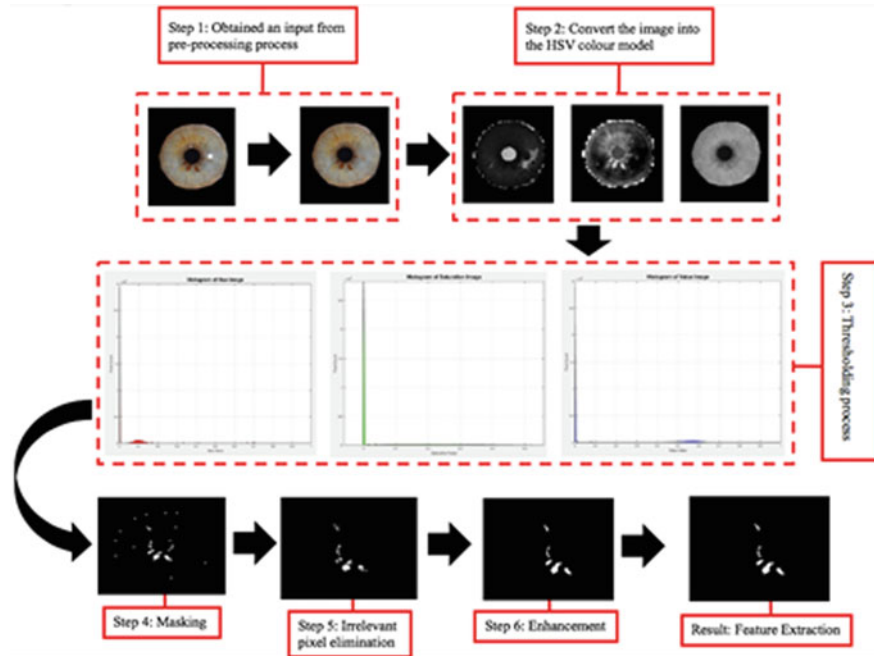


Fig. 10 Spot Filtering Adaptive Thresholding (SFAT) method algorithm

$$\text{Hue} = \begin{cases} 0^\circ & \text{if } \Delta = 0 \\ 60^\circ \Delta \left(\frac{G_n - B_n}{\Delta} \bmod 6 \right) & \text{if } C_{\max} = R_n \\ 60^\circ \Delta \left(\frac{B_n - R_n}{\Delta} + 2 \right) & \text{if } C_{\max} = G_n \\ 60^\circ \Delta \left(\frac{R_n - G_n}{\Delta} + 4 \right) & \text{if } C_{\max} = B_n \end{cases} \quad (6)$$

$$\text{Saturation} = \begin{cases} 0 & \text{if } C_{\max} = 0 \\ \frac{\Delta}{C_{\max}} & \text{if } C_{\max} \neq 0 \end{cases} \quad (7)$$

$$\text{Value} = C_{\max} \quad (8)$$

The output from the conversion process is a set of individual images, which are hue, saturation and value images as presented in Fig. 11. The purpose of the process is to remove the irrelevant colour on the image such as the iris surface colour. Moreover, it is to limit the colour on the image from the combination of the RGB colour component to the grey scale colour component. Based on Fig. 11, the saturation component has highlighted the existence of the pigment spots on the iris surface.

Then, the process continues with the step 3 in the algorithm, which is the thresholding process. The process aims to get the binary image for all three images. In this process, new thresholding intensity values are introduced. The thresholding process

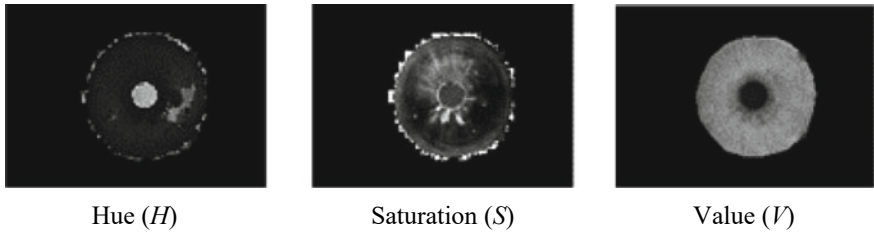


Fig. 11 The output from the conversion process

Table 1 Proposed value for thresholding intensity colour value

k	m	n	q
0.01	0.90	0.70	0.01

has been conducted to all images individually. The process can be expressed in the following algorithm as shown in Eq. (9). The algorithm assigns low and high threshold intensity values for each colour band. The minimum and maximum values for every low and high threshold for each colour band are in the range of 0 to 1. The low and high threshold values influence the colour intensity values.

$$f(x) = \begin{cases} \alpha_k \\ \beta_n^m \\ \gamma_q \end{cases} \quad (9)$$

where x is the function for set of the thresholds; α is the hue image; β is the saturation image; γ is the value image; and k, m, n and q are the proposed values by this study as presented in Table 1.

The fourth step in the algorithm is called the extraction process. The process starts by masking the image to differentiate between the intensity value in the ROI area and the non-ROI area from the saturation image. Then, only the relevant intensity value will be selected. The process can be expressed in the following algorithms from Eqs. (10) to (12).

$$f(\alpha_\Delta) = (\alpha_i > \alpha_k) \quad (10)$$

$$f(\beta_\Delta) = (\beta_i \geq \beta_n) \cap (\beta_i \leq \beta_m) \quad (11)$$

$$f(\gamma_\Delta) = (\gamma_i > \gamma_q) \quad (12)$$

where α is the hue, β is the saturation, γ is the value, Δ is the mask, and i is the image. The output from the process is shown in Fig. 12.

Fig. 12 Output from the masking process



Proceeding to step 5 of the algorithm is eliminating the irrelevant pixels. Only the masked saturation image will be used because the image contains critical information, which is pigment spot colour. The process eliminates the pixel size less than 20, which this study considers irrelevant pixels. The process can be expressed in the arithmetic equation as shown in Eqs. (13) and (14),

$$f(y) = (x_i, k) \quad (13)$$

where

$$x_i = (\alpha_\Delta \cap \beta_\Delta \cap \gamma_\Delta) \quad (14)$$

and $f(y)$ is the function to eliminate the small pixels less than 20-pixel size. x_i is the mask of the colour object, α is the hue, β is the saturation, γ is the value, Δ is the mask, and k is the pixel size that will be eliminated. Figure 13 shows the output after the elimination process and the output is also known as the extraction output, where the pigment spots have been successfully isolated from the iris surface.

Fig. 13 Pigment spots extraction output



Fig. 14 Output from the enhancement process



The final step in the algorithm is image enhancement. The enhancement is conducted by tidying up all borders of the detected areas in the image. The process implements a morphological closing operation function. Then, the process continues with filling up of any holes found in the image by changing the pixel value with 0. Figure 14 presents the output from the process.

3.5 Datasets

The conducted testing has used images downloaded from Miles Research datasets [49, 50]. The dataset can be downloaded freely at the website under the menu sample iris photos: <http://milesresearch.com> [42, 51]. The images are 1749 by 1184 pixels in size with a resolution of 256 dpi. The images have been stored in Joint Photographic Experts Group (jpeg) format, 24-bit RGB colour model.

Furthermore, the dataset has been obtained in order to study an individual psychology and interpersonal dynamics based on the iris pattern [42]. These iris images have been prepared by the company with clear and high-resolution iris pattern. They were evidently meant for different purpose. In spite of that, the quality of the images is very reliable to be used in this study. In addition, Edwards have used the same device used by the Miles Research company in order to acquire the iris image, where he put on more focus on ophthalmology perspective. The dataset obtained by the Edwards et al. is confidential and has not been shared by the authors [5]. Based on this situation, this study has decided that the iris images prepared by Miles Research company are relevant to be used because they have used the same device to acquire the iris image. Figure 15 presents the sample of the iris images from the dataset. The images have been categorised into two manually before the testing is run. The first category is non-pigment spots and, second category is containing pigment spots.

The total number of images from the dataset is 256, in which 125 images are from non-pigment spots category and 131 images contain pigment spots. The result of testing is summarised in Table 2.

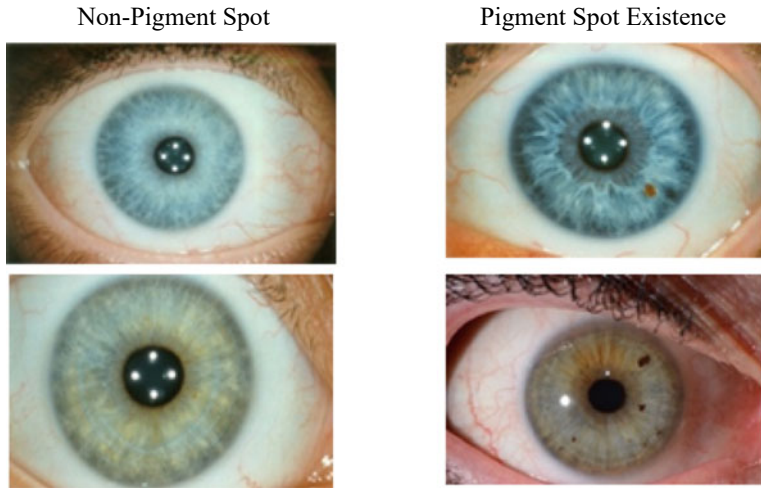


Fig. 15 Sample of iris images from the dataset

Table 2 Result

Non-pigment spots		Contain pigment spots	
Correct extraction	Incorrect extraction	Correct extraction	Incorrect extraction
56 images	69 images	102 images	29 images

Based on Table 2, a total of 158 images have been successfully extracted with a total of 98 images incorrectly extracted. The sample output from the testing is presented in Table 3.

4 Evaluation

4.1 Results

The evaluation of the accuracy performance to the SFAT method is based on the standard of the iris biometrics recognition system. Since the definition to the parameters of the metrics will be re-defined, it will be aligned to the ophthalmology perspective. The validation to the results will be compared to the results from the medical experts.

Table 4 presents the standard performance metrics used in this study to evaluate the accuracy performance of the SFAT method. Figure 16 presents the comparative study with selected extraction methods proposed by other researchers.

The equations for all standard performance metrics are presented as shown in (15)–(17).

Table 3 Sample output from the extraction process

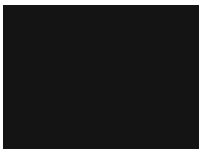
Contain pigment spots	
Correct extraction	Incorrect extraction
Obtained image 	Obtained image 
Output image 	Output image 

Table 4 The standard performance metrics

Standard performance metrics	Description
False acceptance rate (FAR)	Incorrect amount of pigment spots detected from the image that contains pigment spots
False rejection rate (FRR)	Do not detect the pigment spots from the image that contains pigment spots (or) Pigment spots detected from the image that does not contain pigment spots
Detection rate (DR)	Correct detection of pigment spots from the image that contains pigment spots (or) Correct detection of no pigment spot from the image that does not contain pigment spots

$$\text{FAR} = \frac{\text{No. of Incorrect Pigment Spots Detection}}{\text{Total Tested Images}} \times 100\% \quad (15)$$

$$\text{FRR} = \frac{\text{No. of Pigment Spots Detection Error}}{\text{Total Tested Images}} \times 100\% \quad (16)$$

$$\text{DR} = \frac{\text{No. of Accurate Pigment Spots Detection}}{\text{Total Tested Images}} \times 100\% \quad (17)$$

Proceeding with the discussion, Table 5 presents the sample of the output from all test methods.

Based on Table 5 and Fig. 16, the accuracy rate is according to DR. Hence, the SFAT has performed greatly with better accuracy rate than the other two methods, which are 37.1%, where the increment is 8.6% from colour-based segmentation

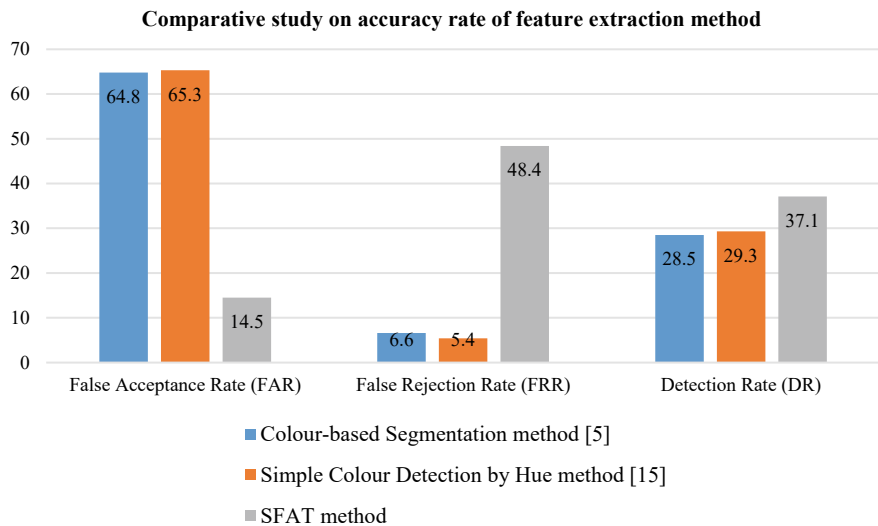


Fig. 16 Comparative study of the accuracy performance between the methods

Table 5 Sample output

	Colour-based segmentation [41]	Simple colour detection by Hue [42]	SFAT method
FAR			
FRR			
DR			

method [41] and 7.8% from simple colour detection by Hue method [42]. Furthermore, the processing time per image is approximately less than 8 s. In addition, the SFAT method has accurately extracted the pigment spots compared with the other two methods as presented in DR row in the Table 5. However, the SFAT method has leading the percentage of the FRR, which is at 48.4% as opposed to 41.8% from

colour-based segmentation method [41] and 43% from simple colour detection by Hue method [42]. In other words, the percentage of the FAR and FRR show the opportunity for improvement in the future in order to increase the accuracy rate.

4.2 Contribution

Based on the discussion in Sects. 3 and 4, the main contribution of this study is the definition of the iris pigment spot. The definition is reliable to be used to the iris pigment spot in order to automate the iris pigment spot recognition process. Next contribution is the pigment spot colour values. The values can be used to extract the pigment spot accurately. Furthermore, the values are the contribution to the image processing field of study, which is previously the exact values for the iris pigment spot and is hard to find from the literature.

5 Conclusion and Future Work

Conducting the study on the iris pigment spot feature is a challenging process. Unidentified pigment spot feature is the main challenge that needs to be addressed. Furthermore, distinguishing the pigment spot colour from the iris surface colour is another challenge to this study. The existing colour histogram method has a limitation to perform the process. Hence, an improvement was needed in order to solve the issue. These two challenges were successfully answered in this study. The intensity of the saturation component from the HSV colour model has been defined as a pigment spot feature in order to extract the pigment spots. Afterwards, the SFAT has been proposed in order to extract the feature. The SFAT method was developed based on the integration of the colour histogram method and the thresholding method. The method has been successful to distinguish the iris pigment spot colour from the iris surface colour.

Moreover, the method has accurately extracted and isolated the pigment spots from the iris surface. The percentage of the accuracy is at 37.1%. The complexity in order to deploy the method is low based on the processing time per image, with the time of approximately less than 8 s. In conclusion, this study has successfully achieved all the objectives by solving all the problems discovered at the initial stage of the study. The finding from the study is that the intensity of the saturation component from the HSV colour model has a very high potential to be applied in the medical imaging analysis. The contribution from this study is the definition of the pigment spot feature, which is not a main concern in image analysis field. Furthermore, the improvement on the ability of the colour histogram method in order to extract the coloured object from the uncondusive background image is profound. The recommendation to the future work regarding the accuracy performance is highly welcome. This has been

highlighted in the evaluation and validation section that an opportunity to improve the accuracy performance of the method.

Acknowledgements This study was supported by the Geran Lepasan Ph.D. MyRA, grant no.: 600-RMC/GPM LPHD 5/3 (167/2021). The authors would like to thank all their colleagues at Universiti Teknologi MARA (UiTM), ViCubeLab Research Group, Universiti Teknologi Malaysia (UTM) and Universiti Malaysia Terengganu (UMT).

References

1. Rad, A.E., Rahim, M.S.M., Rehman, A., Altameem, A., Saba, T.: Evaluation of current dental radiographs segmentation approaches in computer-aided applications IETE Tech. Rev. **30**(3), 210–222 (2013)
2. Rehman, A.: Light microscopic iris classification using ensemble multi-class support vector machine. Microsc. Res. Techn. **84**(5), 982–991 (2021)
3. Man, M., Ab Jabal, M.F., Rahim, M.S.M., Ahmad, I.: Implementation of geodesic active contour approach for pigment spots segmentation on the iris surface. J. Comput. Sci. **12**(11), 564–571 (2016). <https://doi.org/10.3844/jcssp.2016.564.571>
4. Mitra, A., Banerjee, P.S., Roy, S., Roy, S., Setua, S.K.: The region of interest localization for glaucoma analysis from retinal fundus image using deep learning. Comput. Methods Programs Biomed. **165**, 25–35 (2018). <https://doi.org/10.1016/j.cmpb.2018.08.003>. Epub 8 Aug 2018. PMID: 30337079
5. Javed, R., Rahim, M.S.M., Saba, T., Rehman, A.: A comparative study of features selection for skin lesion detection from dermoscopic images. Netw. Model. Anal. Health Inform. Bioinform. **9**(1), 1–13 (2020)
6. Tiwari, A., Marathe, A., Mondhe, P., Vashishth, S., Pawar, S.J.: Skin disease detection system. In: International Online Conference on Advance Research and Development in Engineering and Technology (IO-CARDET 2016) (2016). Retrieved from <http://www.iejrd.com/index.php/ /article/view/458>
7. Edwards, M.: The genetic architecture of iris colour and surface feature variation in populations diverse ancestry. Unpublished Dissertation in Partial Fulfilment of the Requirements for the Degree of Doctor of Philosophy, University of Toronto, Canada (2016)
8. Chaudhry, H., Rahim, M.S.M., Saba, T., Rehman, A.: Crowd region detection in outdoor scenes using color spaces. Int. J. Model. Simul. Sci. Comput. **9**(2), 1–15 (2018). <https://doi.org/10.1142/S1793962318500125>
9. Rahim, M.S.M., Rehman, A., Kumoi, R., Abdullah, N., Saba, T.: FiLeDI framework for measuring fish length from digital images. Int. J. Phys. Sci. **7**(4), 607–618 (2012)
10. Ejaz, K., Rahim, M.S.M., Rehman, A., Chaudhry, H., Saba, T., Ejaz, A.: Segmentation method for pathological brain tumor and accurate detection using MRI. Int. J. Adv. Comput. Sci. Appl. **9**(8), 394–401 (2018)
11. Ebrahim, A.Y., Kolivand, H., Rehman, A., Rahim, M.S.M., Saba, T.: Features selection for offline handwritten signature verification: state of the art. Int. J. Comput. Vis. Robot. **8**(6), 606–620 (2018)
12. Ejaz, K., Rahim, M.S.M., Bajwa, U.I., Chaudhry, H., Rehman, A., Ejaz, F.: Hybrid segmentation method with confidence region detection for tumor identification. IEEE Access **9**, 35256–35278 (2021). <https://doi.org/10.1109/ACCESS.2020.3016627>
13. Amin, J., Sharif, M., Raza, M., Saba, T., Rehman, A.: Brain tumor classification: feature fusion. In: 2019 International Conference on Computer and Information Sciences (ICCIS), pp. 1–6. IEEE (2019)

14. Roy, S., Mitra, A., Roy, S., et al.: Blood vessel segmentation of retinal image using Clifford matched filter and Clifford convolution. *Multimed. Tools Appl.* **78**, 34839–34865 (2019). <https://doi.org/10.1007/s11042-019-08111-0>
15. Rahim, M.S.M., Isa, S.A.M., Rehman, A., Saba, T.: Evaluation of adaptive subdivision method on mobile device. *3D Res.* **4**(4), 1–10 (2013). [https://doi.org/10.1007/3DRes.02\(2013\)](https://doi.org/10.1007/3DRes.02(2013)). Ejaz, K., Rahim, M.S.M., Bajwa, U.I., Rana, N., Rehman, A.: An unsupervised learning with feature approach for brain tumor segmentation using magnetic resonance imaging. In: Proceedings of the 2019 9th International Conference on Bioscience, Biochemistry and Bioinformatics, pp. 1–7 (2019)
16. Clark, A.D., Kulp, S.A., Herron, I.H., Ross, A.A.: A theoretical model for describing iris dynamics. In: Burge, M., Bowyer, K. (eds.) *Handbook of Iris Recognition. Advances in Computer Vision and Pattern Recognition*. Springer, London, pp. 129–150. (2013) https://doi.org/10.1007/978-1-4471-4402-1_7
17. Husain, N.A., Rahim, M.S.M., Khan, A.R., Al-Rodhaan, M., Al-Dhelaan, A., Saba, T.: Iterative adaptive subdivision surface approach to reduce memory consumption in rendering process (IteAS). *J. Intell. Fuzzy Syst.* **28**(1), 337–344 (2015). <https://doi.org/10.3233/IFS-14130>
18. Javed, R., Shafry, M., Saba, T., Fati, S.M., Rehman, A., et al.: Statistical histogram decision based contrast categorization of skin lesion datasets dermoscopic images. *Comput. Mater. Cont.* **67**(2), 2337–2352 (2021)
19. Rahim, M.S.M., Norouzi, A., Rehman, A., Saba, T.: 3D bones segmentation based on CT images visualization. *Biomed. Res.* **28**(8), 3641–3644 (2017)
20. Javed, R., Rahim, M.S.M., Saba, T., Rashid, M.: Region-based active contour JSEG fusion technique for skin lesion segmentation from dermoscopic images. *Biomed. Res.* **30**(6), 1–10 (2019)
21. Iftikhar, S., Fatima, K., Rehman, A., Almazyad, A.S., Saba, T.: An evolution based hybrid approach for heart diseases classification and associated risk factors identification. *Biomed. Res.* **28**(8), 3451–3455 (2017)
22. Johnson, D. (1984). *What the Eye Reveals: An Introduction to the Rayid Method of Iris Interpretation*. 1st edn. Rayid Model Publications, Goleta, CA. ISBN: 0917197011
23. Mary, J.S., Magneta, S.C.: Content based image retrieval using colour, multi-dimensional texture and edge orientation. *Int. J. Sci. Technol. Eng. (IJSTE)* **2**(10), 110–115 (2016)
24. Bobeldyk, D., Ross, A.: Predicting eye colour from near infrared iris images. In: *International Conference on Biometrics*, pp. 104–110. IEEE, Gold Coast, QLD, Australia (2018)
25. Khan, M.A., Sharif, M.I., Raza, M., Anjum, A., Saba, T., Shad, S.A.: Skin lesion segmentation and classification: a unified framework of deep neural network features fusion and selection. *Exp. Syst.*, e12497 (2019)
26. Image Analyst: Simple Colour Detection by Hue. MathWorks (2016). <https://www.mathworks.com/matlabcentral/fileexchange/28512-simplecolordetectionbyhue>. Accessed on 26 Apr 2017
27. Man, M., Jabal, M.F.A., Rahim, M.S.M.: A comparative study on Hough transform segmentation approach for outlier iris image. In: Kim, K., Joukov, N. (eds.) *Information Science and Applications (ICISA). Lecture Notes in Electrical Engineering*, vol. 376, pp. 409–419. Springer, Singapore (2016). https://doi.org/10.1007/978-981-10-0557-2_41
28. Roy, S., Bhattacharyya, D., Bandyopadhyay, S.K., Kim, T.H.: An effective method for computerized prediction and segmentation of multiple sclerosis lesions in brain MRI. *Comput. Methods Program. Biomed.* **140**, 307–320 (2017). <https://doi.org/10.1016/j.cmpb.2017.01.003>. Epub 10 Jan 2017. PMID: 28254088
29. Mitra, A., Roy, S., Roy, S., Setua, S.K.: Enhancement and restoration of non-uniform illuminated Fundus Image of Retina obtained through thin layer of cataract. *Comput. Methods Programs. Biomed.* **156**, 169–178 (2018). <https://doi.org/10.1016/j.cmpb.2018.01.001>. Epub 10 Jan 2018. PMID: 29428069
30. Adnan, M.M., Rahim, M.S.M., Rehman, A., Mehmood, Z., Saba, T., Naqvi, R.A.: Automatic image annotation based on deep learning models: a systematic review and future challenges. *IEEE Access* **9**, 50253–50264 (2021)

31. Norouzi, A., Rahim, M.S.M., Altameem, A., Saba, T., Rad, A.E., Rehman, A., Uddin, M.: Medical image segmentation methods, algorithms, and applications. *IETE Tech. Rev.* **31**(3), 199–213 (2014)
32. Javed, R., Rahim, M.S.M., Saba, T.: An improved framework by mapping salient features for skin lesion detection and classification using the optimized hybrid features. *Int. J. Adv. Tr. Comput. Sci. Eng.* **8**(1), 95–101 (2019)
33. Bastys, A., Kranauskas, J., Krüger, V.: Iris recognition with taylor expansion features. In: Burge, M., Bowyer, K. (eds.), *Handbook of Iris Recognition. Advances in Computer Vision and Pattern Recognition*, 1st edn., vol. 1, pp. 103–127. Springer Publishing Company, pp. 103–127 (2013). https://doi.org/10.1007/978-1-4471-4402-1_6
34. Nixon, M., Aguado, A.: *Feature Extraction and Image Processing for Computer Vision*, 3rd edn. Academic Press (2012). ISBN: 978-0123965493.
35. Michala: Colour-Based Segmentation. MathWorks (2014). <https://ww2.mathworks.cn/matlabcentral/fileexchange/45679-colour-based-segmentation>. Accessed on 12 June 2016
36. Sutojo, T., Tirajani, P.S., Ignatius Moses Setiadi, D.R., Sari, C.A., Rachmawanto, E.H.: CBIR for classification of cow types using GLCM and colour features extraction. In: 2017 2nd International conferences on Information Technology, Information Systems and Electrical Engineering (ICITISEE), pp. 182–187. <https://doi.org/10.1109/ICITISEE.2017.8285491>
37. Nazir, M., Khan, M.A., Saba, T., Rehman, A.: Brain tumor detection from MRI images using multi-level wavelets. In: 2019 International Conference on Computer and Information Sciences (ICCIS), pp. 1–5. IEEE (2019)
38. Kolivand, H., Fern, B.M., Saba, T., Rahim, M.S.M., Rehman, A.: A new leaf venation detection technique for plant species classification. *Arab. J. Sci. Eng.* **44**(4), 3315–3327 (2019)
39. Nawaz, M., Mehmood, Z., Nazir, T., Naqvi, R.A., Rehman, A., Iqbal, M., Saba, T.: Skin cancer detection from dermoscopic images using deep learning and fuzzy k -means clustering. *Microsc. Res. Tech.* **85**(1), 339–351 (2022)
40. Miles Research: Miles Research (2013). <http://www.milesresearch.com>. Accessed on 5 May 2014
41. Iqbal, S., Khan, M.U.G., Saba, T., Mehmood, Z., Javaid, N., Rehman, A., Abbasi, R.: Deep learning model integrating features and novel classifiers fusion for brain tumor segmentation. *Microsc. Res. Tech.* **82**(8), 1302–1315 (2019). <https://doi.org/10.1002/jemt.23281>
42. Jillela, R., Ross, A.A.: Methods for iris segmentation. In: Bowyer, K., Burge, M. (eds.) *Handbook of Iris Recognition. Advances in Computer Vision and Pattern Recognition*, pp. 15–54. Springer, London (2016). https://doi.org/10.1007/978-1-4471-6784-6_7
43. Javed, R., Saba, T., Shafry, M., Rahim, M.: An intelligent saliency segmentation technique and classification of low contrast skin lesion dermoscopic images based on histogram decision. In: 2019 12th International Conference on Developments in eSystems Engineering (DeSE), pp. 164–169 (2020)
44. Rahim, M.S.M., Rehman, A., Kurniawan, F., Saba, T.: Ear biometrics for human classification based on region features mining. *Biomed. Res.* **28**(10), 4660–4664 (2017)
45. Rahim, M.S.M., Razzali, N., Sunar, M.S., Abdullah, A.A., Rehman, A.: Curve interpolation model for visualising disjointed neural elements. *Neural Regen. Res.* **7**(21), 1637–1644 (2012). <https://doi.org/10.3969/j.issn.1673-5374.2012.21.006>
46. Saba, T., Bashardoust, M., Kolivand, H., Rahim, M.S.M., Rehman, A., Khan, M.A.: Enhancing fragility of zero-based text watermarking utilizing effective characters list. *Multimed. Tools Appl.* **79**(1), 341–354 (2020)
47. Harouni, M., Rahim, M.S.M., Al-Rodhaan, M., Saba, T., Rehman, A., Al-Dhelaan, A.: Online Persian/Arabic script classification without contextual information. *Imag. Sci. J.* **62**(8), 437–448 (2014). <https://doi.org/10.1179/1743131X14Y.0000000083>
48. Lung, J.W.J., Salam, M.S.H., Rehman, A., Rahim, M.S.M., Saba, T.: Fuzzy phoneme classification using multi-speaker vocal tract length normalization. *IETE Tech. Rev.* **31**(2):128–136. <https://doi.org/10.1080/02564602.2014.892669>
49. Kumar, E.B., Thiagarasu, V.: Colour channel extraction in RGB images for segmentation. In: 2nd International Conference on Communication and Electronics Systems (ICCES), pp. 234–239. IEEE, Coimbatore, India (2017)

50. Nichal, A., Jadhav, P., Nikam, V., Hipparkar, V.: DCT based iris feature extraction and recognition for security system. *Int. J. Adv. Res. Comput. Commun. Eng.* **3**(5):6490–6494. ISSN (Online): 2278–1021 (2014)
51. Khan, M.A., Kadry, S., Zhang, Y.D., Akram, T., Sharif, M., Rehman, A., Saba, T.: Prediction of COVID-19-pneumonia based on selected deep features and one class kernel extreme learning machine. *Comput. Electr. Eng.* **90**, 106960 (2021)
52. Jamal, A., Hazim Alkawaz, M., Rehman, A., Saba, T.: Retinal imaging analysis based on vessel detection. *Microsc. Res. Tech.* **80**(7), 799–811 (2017)

A Big Survey on Biometrics for Human Identification



Zahra Karimi , Somayeh Arab Najafabadi ,
Aliakbar Rabbani Nezhad , and Farnaz Ahmadi

Abstract Biometrics are a branch of science that is used to identify as well as authenticate. Biometrics are basically of two types: behavioral biometrics and physiological biometrics. Characteristics and biometrics are fundamentally fixed and unique, allowing individuals to distinguish one from another. Biometric authentication systems have received more attention in recent years than other traditional authentication methods such as passwords or signatures. All human biological traits are unique as biometrics such as fingerprints, palms, irises, palm blood vessels and fingerprint blood vessels, and other biometrics. Biometric identification systems basically have a complex structure that consists of different parts. Biometric-based authentication systems and authentication methods, along with other authentication systems, can improve the security aspects of authentication systems. Identification methods and tools are used in many important and essential applications such as surveillance processes, security investigations, fraud detection technologies, and access controls. Biometric-based identification methods in machine learning consist mainly of preprocessing, feature extraction, feature selection, classification, and finally evaluation. These systems can also be based on one biometric or based on several biometrics together. In this chapter, we examine the methods of identifying identity information with the help of various biometrics, highlight the challenges in each biometrics, and introduce the solutions that have been proposed to overcome this challenge.

Keywords Identification · Biometric · Pattern identification

Z. Karimi ()

Department of Bioelectronics and Biomedical Engineering, School of Advanced Technologies in Medicine, Isfahan University of Medical Sciences, Isfahan, Iran
e-mail: zkaimi286@gmail.com

S. A. Najafabadi

Department of Computer Engineering, Islamic Azad University, Najafabad Branch, Isfahan, Iran

A. R. Nezhad

Department of Electrical Engineering, Isfahan University of Technology, Isfahan, Iran

F. Ahmadi

Department of Electrical Engineering, Tabriz University, Azerbaijan, Iran

1 Introduction

Biometrics are a branch of science that is used to identify as well as authenticate. Biometrics are basically of two types: behavioral biometrics and physiological biometrics. Characteristics and biometrics are fundamentally fixed and unique and with the help of which individuals can identify with each other [1]. Biometric identification systems basically have a complex structure that consists of different parts. Biometric-based authentication systems and authentication methods, along with other authentication systems, can improve the security aspects of authentication systems. Identification methods and tools are used in many important and essential applications such as surveillance processes, security investigations, fraud detection technologies, and access controls. Biometric-based identification methods in machine learning consist mainly of preprocessing, feature extraction, feature selection, classification, and finally evaluation. Also, these systems can be based on one biometric or based on several biometrics with each other [2].

Biometric systems are systems that identify individuals based on one or more biometrics of the person in question. Biometrics are unique characteristics of every human being that are fixed over time or have the least change. These biometrics are of two categories: behavioral biometrics and physiological biometrics. The best behavioral biometrics include walking, typing, and signing. He also mentioned biometrics of the iris, face, fingerprints, and retinal and finger blood vessels [3, 4]. As stated, the basis of these systems is based on the principle that these biometrics are generally fixed. And they do not change over time [5]. Physiological biometrics or physiological characteristics such as palm, fingerprint, ear, face pattern, retinal blood vessels of the palm as well as fingerprint blood vessels and other biometrics, such as cardiac ECG and sound signals, fall into this category. These biometrics are widely used because they are stable, collectible, and unique [6]. Behavioral biometrics describe each person's behavior and performance, like the type of walking, signing, talking, and handwriting [7].

Conventional detection methods to identify individuals using passwords, cards, etc., are no longer very reliable, and the need to replace them with new methods is increasingly felt. This is because of the sheer volume of passwords and different cards required for different applications. The possibility of forgetting, getting lost, and being used illegally are other reasons why it is necessary to use safer and more efficient methods. Today, there is a significant need for reliable, fast, and noninvasive tools to automatically identify individuals. Computer techniques used to identify the characteristics of individuals such as face, fingerprints, retina, voice, palm geometry, and eyes have many applications in the fields of security, surveillance, and ownership. But many existing methods have limited capabilities in identifying features in practical and real cases; some methods require contact with a person's body, some are aggressive, some methods require final adjustment by a person, and some of them are expensive. One method that has recently received more attention than other methods is the identification of individuals based on the characteristics of their iris. Iris-based

identification of individuals is expected to extend to a wide range of applications in which identification of individuals should be established or validated [8, 9].

Humans have long used the biometric features of others, such as face, voice, or handwriting, to identify themselves. Identification of people has become very important today, especially when it comes to security issues. In today's society, with the rapid advancement of technology, we have many tools needed to achieve this goal, one of these tools, both in terms of performance and security, given its long history, is the image of the vessels of the fingers. Patterns of finger arteries can be somewhat unique to each individual due to the texture they have. According to research conducted since the 1990s, the iris image of each individual has features that can not only be used to identify, but can also be used to identify gender and ethnicity [10, 11].

With the advancement of technology and the production of large volumes of information and assets, the need to protect and control access to this information is felt more and more, and the best response to this need is the use of biometric-based systems. But of the various biometrics that have been proposed so far, many are capable of alteration, forgery, or error. These include faces and fingerprints that can be easily forged and changed. Therefore, to meet this challenge, biometrics must be used inside the body, such as the iris, retina, palm arteries, and fingerprint vessels. But there is still criticism of these biometrics. For example, imaging of the retina is very sensitive and difficult. The use of hand and finger arteries may not have a good scientific and economic justification. But the irreplaceable iris image can also be used without the need for cooperation. In line with the above, a lot of research has been done to identify the iris, sometimes with a low identification rate and a high response time, or a high identification rate and a low response time. For this reason, presenting a method with features such as high detection rate and low computational complexity is very much felt [12, 13].

Identification is one of the most important and sensitive branches of technology, and this importance has led to extensive research to improve these systems. The main contribution of this study is

1. big survey on of identification methods using various biometrics
2. comprehensive review of the research literature on authentication systems and algorithms
3. discussed on the advantages and disadvantages of methods
4. classification done on different types of biometrics
5. comparing these biometrics
6. providing a review of biometric identification research.

In the continuation of this article, it is divided as follows. In Sect. 2, different types of biometrics will be introduced and compared in different aspects. Then, in Sect. 3, the pattern methodology in identification will be examined. In Sect. 4, research on identification in various modern biometrics will be reviewed. Finally, in Sect. 5, conclusions will be presented.

2 Biometrics

Various biometrics for identification have been discussed by researchers. Biometrics of the face, iris, retina, and blood vessels of the palms of the hands, and fingerprints and ears are among the most common biometrics that will be examined below. With the rapid advancement of technology in the field of e-commerce and Internet commerce, the need for security and identification of different people is felt more. Biometric systems are a reliable method that can overcome the limitations of older automated authentication systems [14–17]. The ear is now introduced as a new type of biometric. Today, human identification from biometric images is one of the most important issues in the field of machine vision and pattern recognition [18].

Face Biometric

Face has long been one of the first biometric identifiers, both through technology and visually, and has been the only way to identify individuals with these biometrics. Facial hair growth, nose size, cheek delicacy, and lips were the parameters used to identify. But with the advent of technology instead of human life, these features were used in the form of parameters of identification algorithms and visual identification criteria became the criteria of descriptors and classifiers. Figure 1 shows an example of facial biometrics [19].

Face biometric identification is one of the most challenging areas of biometric identification. Because the face can be affected by many changes such as changing facial expressions, changing the amount of light on the face, and covering the face with glasses and other changes. Therefore, the study of these challenges in research related to face biometric identification is very important and increases the efficiency and performance of face biometric identification system.

The Iris

The iris consists of the colored part of the eye that lies beneath the cornea and the pupil in the center. The iris is a combination of a kind of circular muscle with a series of radial, layered, or mesh-like lines that start from the three months of the fetus until the eight months of the developmental process. The muscle tissue as well as the pigments in the iris of the eye can change in the early years of the baby, but after

Fig. 1 Example of face biometrics



that, until death, it changes almost nothing. This muscle contains a set of patterns such as lines, rings, holes, grooves, threads, and spots that have the ability to identify and distinguish gender for identification systems. Because the iris muscle patterns are unique to each person, the degree of similarity between members of a family is very low. Figure 2 shows examples of iris images [6].

Retina

Cone receptors, of which there are about 6 million, help us see different colors, and rod receptors, of which there are approximately 125 million, help us see at night and in the environment. This is the pattern of blood vessels in the retina through which identification is made. Figure 3 shows the position of the retina. As can be seen, the cornea is located in front of the eye and the retina is located at the end of the eye. Because the retina is located in a place inside the eye and not in front of the environment outside the eye, it is considered as a method of stable identification [20].

Figure 4 shows a close-up of the pattern of blood vessels inside the eye. The red lines indicate the blood vessels, and the yellow line indicates the location of the optic disk (the place where the optic nerve connects to the retina and where information is sent from the eye to the brain). The circle in the figure is the location scanned by the device to extract the feature.

Fingerprint and Palm Blood Vessels

Fingerprints and palm blood vessels are one of the physiological biometrics that have different patterns in different people. Fingerprint blood vessel images are captured by infrared cameras with wavelengths between 700 and 1000 nm. Infrared light is absorbed by red blood cells or hemoglobin but is easily passed through other parts of



Fig. 2 Example of iris images

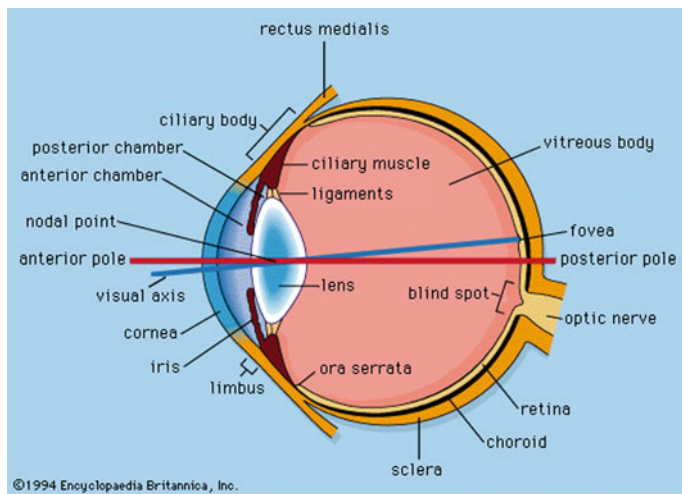
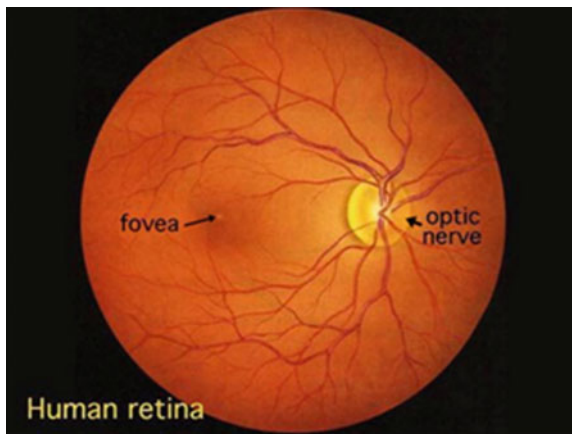


Fig. 3 Retinal position

Fig. 4 Close-up of the pattern of blood vessels inside the eye



the fingerprint and is not absorbed. As a result of this process, patterns of blood vessels are easily formed. Fingerprint and palm blood vessels, as a biometric, have unique features such as amplitude and ubiquity. This means that all people have patterns of blood vessels, and they have a high ability to differentiate. They are also highly acceptable and durable and also have a major advantage over other biometrics such as face, gait, or even other biometrics [21]. These biometrics can only be used by living people. People who have died can easily have their faces, fingerprints, or even their palms faked. It is also very difficult and practically impossible to forge this type of biometrics in living people. Although these two major advantages have attracted the use of this biometrics, these biometrics are highly influenced by body temperature.

And if a person's body temperature changes, these patterns may change as well [22]. The use of near-infrared images was proposed to increase security and to improve the efficiency of person identification systems. Such images have a high efficiency in indoor environments and provide useful information even in very low light and dark. Infrared spectroscopy images also have many applications in individual identification systems. For example in fingerprint identification systems based on fingerprints, close fingerprint imaging of blood vessels in the infrared spectrum extracts vascular pattern, which is a unique feature comes. As a result, the use of near-infrared images was proposed to overcome the problems of visible spectrum images. Light reflection or light absorption can be used to capture images of fingerprints and palm blood vessels. The main difference between the two methods is the position of the infrared light. In the light reflection method, infrared light is placed near the palm of the hand. But in the light absorption method, it is placed on the back of the hand. Figure 5 shows these two types of records. Comparing the two forms of light absorption method in infrared light emission records images with higher accuracy and quality. Examples of images recorded from fingerprint blood vessels are shown in Fig. 6. Figures 7 and 8 also show recorded images of the blood vessels in the palm of the hand [23].

Ear

Identification with the help of ear images among different biometrics is one of the active branches. In other words, identification with the help of ear images has received a lot of attention in recent years. The ability to record ear images from a distance as well as covert behavior in ear biometrics has made these biometrics highly regarded for surveillance and security processes. Much research has been done in recent years, but there are still many challenges in identifying with the help of the ear. Ear images are used in automatic identification systems based on face profiles as well as video

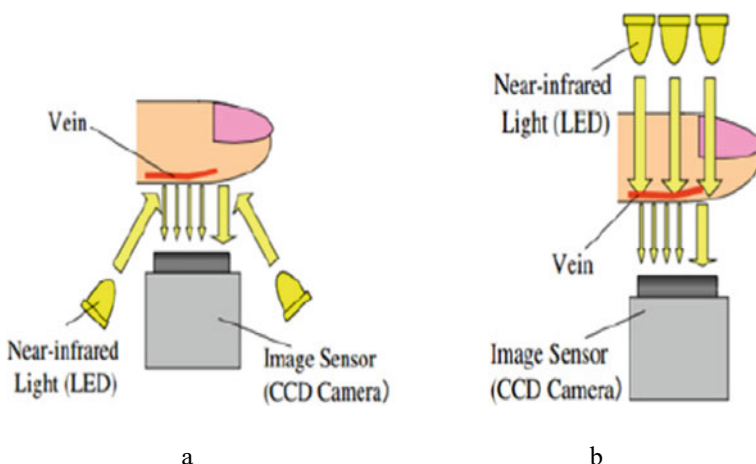


Fig. 5 Two types of recording fingerprint blood vessel patterns. **a** Light transmission. **b** Light reflection [23]

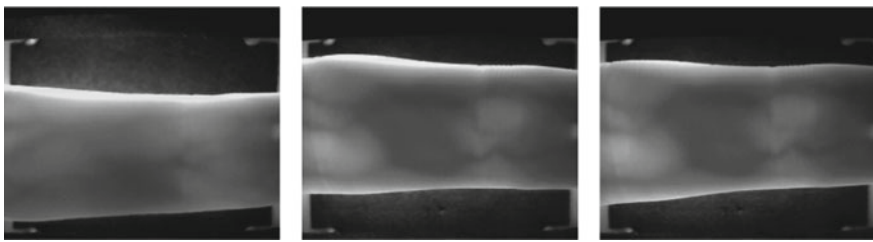


Fig. 6 Examples of images recorded by fingerprint sensors [24]

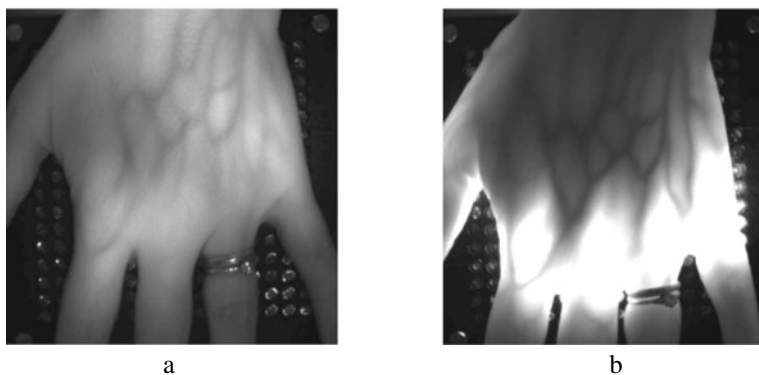


Fig. 7 Two types of recording of blood vessel patterns in the palm of the hand. **a** Light transmission. **b** Light reflection [23]

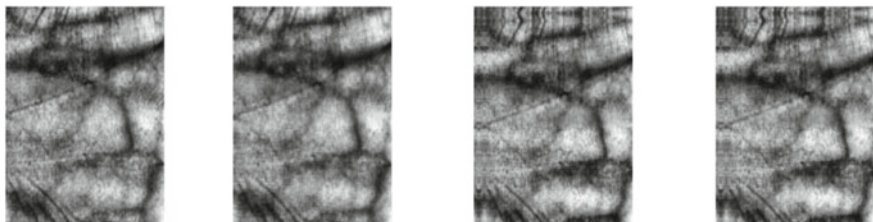
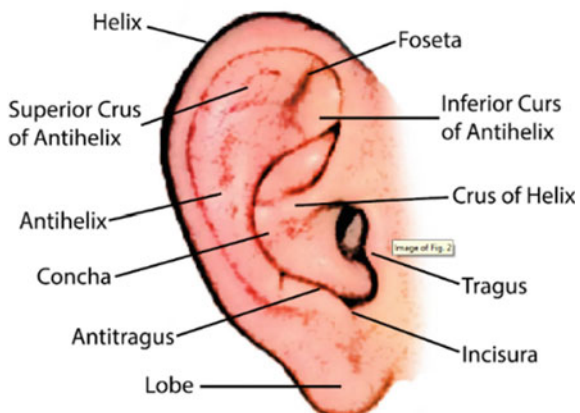


Fig. 8 Examples of images recorded by palm blood vessel sensors [24]

images. The process of recording the image of the ear is non-contact, noninvasive, and non-subduing, the person in question does not need to cooperate with the surveillance camera in recording this image, and the desired image is recorded without feeling this recognition. Although these benefits are similar to those of other biometrics, such as the face, the lack of change in the shape and size of the ears between the ages of 8 and 70 has attracted the attention of researchers. Ear images, or ear biometrics, can also be used to complement and improve authentication alongside other biometrics such as fingerprints. If a biometric card is not very reliable, these biometrics can be

Fig. 9 Structure of the earlobe



used as a supplement. For example, when identifying a face profile, using ear features along with other related face profile features can improve performance accuracy. The human ear is formed in the early stages of pregnancy in the mother's womb and is completed in its true form at birth. The ear is the element that identifies the sense of hearing and, of course, its main organ, and it can be said that this form is different for every human being. The external shape of the ear and its organs is shown in Fig. 9 [25].

Comparison of Biometrics

Biometrics are compared from different angles. Comparisons of biometrics are compared in terms of stability, uniqueness, reliability, security, as well as the type of application [8]. Table 1 provides a comparison of these biometrics in two categories: behavioral and physiological. The type of use of biometrics is also presented in this table.

Each of the behavioral or physiological biometrics is suitable for a specific application. The use of a biometric in an authentication system depends on the type of application, the sensitivity, the cost, and the conditions of use. For example, in highly sensitive security systems, the gait type cannot be used for authentication. In the banking system, however, the use of fingerprints and signatures is sufficient [26]. For an ideal identification system, the criteria for assessing the FER error rate and the FAR error acceptance rate should not be more than 0.1. Various parameters affect the choice of a biometric system, which are distinguishing capability, stability and durability, collectability, efficiency, fraud and counterfeiting rate, and system speed and costs [27]. Table 2 compares these criteria.

Reliability Check

Although biometric-based authentication systems have a significant advantage over similar systems such as password-based systems, they are still not immune to some attacks. Direct and indirect attacks are made on these systems. Direct attacks involve

Table 1 Comparison of biometrics in terms of capabilities and type of use [19]

Biometric type	Important features and characteristics	Applications
Fingerprint	<p>Advantage</p> <ul style="list-style-type: none"> • Safe, reliable, cheap as well as high accuracy • Fast adaptation process • Requires little memory <p>Disadvantages</p> <ul style="list-style-type: none"> • Can be stolen and changed with factors such as cutting, dust and also cutting • Requires physical contact 	<ul style="list-style-type: none"> • Identification and authentication on the phone • Low importance applications • Passport and visa authentication • Access control not so important
Face	<p>Advantages</p> <ul style="list-style-type: none"> • No need for physical contact • Easy template storage • Low processing complexity and fast detection <p>Disadvantages</p> <ul style="list-style-type: none"> • Variable with time and even emotional states of people • Is affected by environmental conditions • Light as well as coatings change it 	<ul style="list-style-type: none"> • Authentication in access control • Human-computer interactions • Monitoring and investigation • Identification and criminology
Retina	<p>Advantages</p> <ul style="list-style-type: none"> • Non-theft • No change and high uniqueness and no similarity between two people, even twins • High accuracy—high reliability <p>Disadvantages</p> <ul style="list-style-type: none"> • It is difficult to access, expensive to use, affected by diabetes 	<ul style="list-style-type: none"> • Security agencies like NASA, spy agencies
Ear	<p>Advantages</p> <ul style="list-style-type: none"> • High stability and high computational complexity • Fast calculation speeds <p>Disadvantages</p> <ul style="list-style-type: none"> • Influenced by hairstyles, cosmetics, and decorations 	<ul style="list-style-type: none"> • Supervised processes • Criminological processes

(continued)

Table 1 (continued)

Biometric type	Important features and characteristics	Applications
The iris	<p>Advantages</p> <ul style="list-style-type: none"> • High scalability, high accuracy, and protected and non-theft • Small size and low processing cost but expensive to use <p>Disadvantages</p> <ul style="list-style-type: none"> • High randomness • No need for individual cooperation to register • Do not use over long distances • It is affected by diseases 	<ul style="list-style-type: none"> • Identification at the airport • Access control • International and national institutions and maritime transport
Hand geometry	<p>Advantages</p> <ul style="list-style-type: none"> • High usability • Small mold dimensions • Low processing cost <p>Disadvantages</p> <p>Affected by hand injuries and cuts and amputation of fingers</p>	<ul style="list-style-type: none"> • Identify a specific identity • Medical diagnosis • Blood-related determination • Athlete selection
Blood vessels of the hands	<p>Advantages</p> <ul style="list-style-type: none"> • Noninvasive as well as high reliability • High accuracy and non-forgery • Very unique and dissimilar <p>Disadvantages</p> <ul style="list-style-type: none"> • It is affected by body temperature • Requires thermal and infrared identification systems 	<ul style="list-style-type: none"> • Security systems input to organizations • Banking systems • Transportation, visa, and passport • Registries
Voice	<p>Advantages</p> <ul style="list-style-type: none"> • Simple and easy to use • Cheap and easy to use <p>Disadvantages</p> <ul style="list-style-type: none"> • Dependence on microphone quality • Ability to forge • Is affected by the disease 	<ul style="list-style-type: none"> • Diagnosis of diseases • Gender verification
Type of walking	<p>Advantage</p> <ul style="list-style-type: none"> • Ability to remotely record and shoot without individual cooperation <p>Disadvantages</p> <ul style="list-style-type: none"> • Very low detection accuracy and high forging capability 	<ul style="list-style-type: none"> • Identity recognition systems • Monitoring and investigation

(continued)

Table 1 (continued)

Biometric type	Important features and characteristics	Applications
Signature	Advantage <ul style="list-style-type: none"> • Simple and cheap usability Disadvantages <ul style="list-style-type: none"> • Low reliability and counterfeit 	<ul style="list-style-type: none"> • Banking system

Table 2 Comparison of biometrics from different aspects

Biometric	Extent	Distinctive	Durability	Collectability	Efficiency	Processing capability
Ear	Top	Medium	Top	Medium	Medium	Top
Face	Top	Down	medium	Top	Down	Top
Fingerprint	Medium	Top	Top	medium	Top	Medium
Gaiting	Medium	Down	Down	Top	Top	Medium
Facial expression	Top	Top	Down	Top	Medium	Top
The iris	Top	Top	Top	Medium	Medium	Down
Retina	Top	Top	Medium	Down	Top	Down
Signature	Down	Down	Down	Top	Down	Top
Blood vessels	Medium	Medium	Medium	Medium	Medium	Medium

attacks on the system without any knowledge of system performance [22]. The performance of identification systems includes feature extraction methods and machine learning methods. Direct attacks are also called sensor attacks. But direct attacks, which are even more dangerous, must have sufficient information from the internal information of the systems, for example, the attacker must have the necessary and sufficient information of the feature extraction algorithm as well as the machine learning algorithm. These attacks are also called response attacks. To further check the reliability, other parameters are also checked, which are as follows:

1. Biometric forgery: In this type, forged biometrics enter the system, and as a result, the wrong output will be produced. These types of forgeries are easily seen in systems and biometrics such as signatures or fingerprints.
2. Use of pre-recorded data: In this case, the desired biometric signal or image of the person is pre-recorded and is identified to the system at the time of authentication.
3. Disruption of the detection process: In this case, the attacker interferes with the detection algorithm [5].

Security and Privacy in Biometrics

There are different aspects of security and privacy in biometric technology. Since attacks and forgeries are common in these systems, control systems as well as mechanisms for monitoring the performance of biometrics are necessary. The following can be used to maintain security and privacy:

Biometrics is not a secret technology.

- Biometrics can be easily forged and used by a second or third party.
- People may not even know about smart biometric data.

Biometric data is not altered or reconstructed [28].

3 Identification by Pattern Recognition

Identification systems generally follow a common structure, which includes imaging, biometric image zoning, feature extraction, and identification and evaluation [29].

Image enrollment: In this stage, the biometric imaging operation is performed with the help of a camera, such as an infrared camera, and a two-dimensional image of the biometrics is prepared.

Preprocessing: In this stage, the range of biometric space is separated from other parts of it [30, 31].

Feature extraction and reduction: In this step, an attribute extraction procedure is used to generate a distinct attribute vector for the images of each class. After generating attribute vectors, these vectors are stored in a database called attribute databases to match the test images.

Identification unit: In this section, the test images are matched with the attribute vectors in the attribute database by going through the training and production steps of attribute vectors, and the identification operation is performed. Figure 10 shows the general block diagram of an authentication system using biometric images.

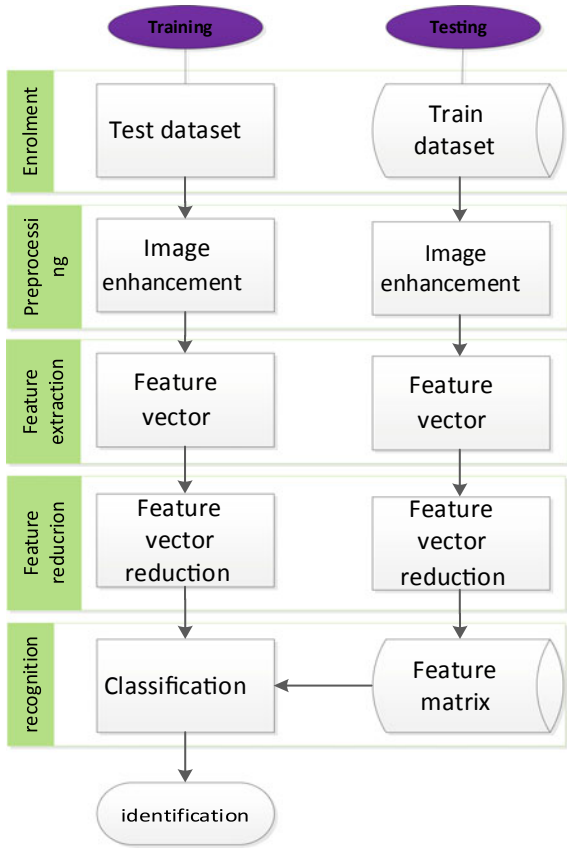
Methods Based on Pattern Recognition

The proposed algorithms based on pattern recognition are mostly automated methods on which classification and identification are based. Pattern recognition-based methods are divided into two categories: supervised and unsupervised methods. Supervised methods use learning information such as tagged images to classify a pixel, but unsupervised methods classify pixels without any prior knowledge.

Supervised Methods

In supervised methods, the main rule is used to extract a feature from the iris using a learning algorithm based on training sets that are usually manually segmented and known as the gold standard. Gold images, background images, or GT are segmented

Fig. 10 General diagram of identification systems with multiple biometrics



by a specialist. In general, surveillance methods must be GT image imaging base. Usually, the results of methods based on monitoring methods in identification are better than other methods because they use educational data [32, 33].

Unsupervised Methods

Unsupervised methods of classification seek to find the intrinsic patterns in the iris to identify differences between irises. Labeled data or training data is not used directly to identify the iris. Among the unsupervised methods, we can mention the types of clusters [11], for example, in fuzzy clustering methods, based on finding the appropriate membership distribution. In this method, the space around the iris is removed, and then the iris location and features are clustered. One FCM-based tracking method works by selecting the initial regions that are selected by fuzzy distribution and then adding other points and pixels that are similar during a repetitive fuzzy clustering process [34]. To provide a suitable background in iris identification, the latest research in this field was reviewed and evaluated to identify the weaknesses and needs of the day in this area of research. Although several studies have been conducted to identify

with the help of the iris, here is a selection of methods of identification with the help of this unique biometrics.

4 Research Background

Face

Heisele et al. [35], in his article, compare a component-based method and two global methods for face recognition. In this study, the robustness of these methods against facial changes is evaluated. In the component-based method, after extracting the feature from the face images, these features are combined with each other and finally classified by the backup vector machine. In the first global system, a support vector machine classifier is used to classify images, and in the second global system, a classifier is used next to a cluster for classification. From the results of this paper, it can be concluded that the component-based method has the best efficiency, followed by the global method of classification and clustering, and finally the classification method has the lowest efficiency.

Günther et al. in 2009 [36], in a study called face recognition and identification, worked on Gabor graphs using maximum likelihood classification. In this paper, a maximum probability estimate (ml) with Gabor diagram for face recognition on a variable scale and in rotation mode is presented by Bayesian classifier, which operates based on graph similarities for face recognition. In this paper, a variety of similarity functions have been used, and the detection rate in the rotation mode was 90.5% in the best case and 95.8% in the scaling mode. This algorithm has been tested on the Cassia-Pet base.

Yu et al. in 2010 [37] in a study entitled “Presenting a method for identification using facial images using Gabor texture and general model and Gaussian gamma” have been presented. In this paper, two Gabor strategies based on texture display phase and Gabor based on texture display size are presented. The size-based strategy used gamma density, and the phase-based strategy used Gaussian density to model the Gabor large distribution. The above strategies have been tested on ORL, YALE, and FERET databases, which have obtained the highest value for the ORL database, which is 93.67. It should be noted, however, that all three of the listed databases have no specific face states for these databases, and these values are insignificant for evaluating the external state of these databases.

Farokhi et al. in 2015 [38] in a study entitled “Identification of Infrared Images of the Face” using the properties of Zernik moments and the Hermit core filter, a new method for identification was presented. In this research, features are extracted from images in two phases, local and global, and each image is produced by combining the extracted features in the feature vectors. To identify each image in this method, the image property vector is generated by the method, then this vector is compared with the database image property vector, under the equation specified in the article, and the image that the property vector has the most similarity and is identified as the target image. Farrokhi et al.’s method is identified with an accuracy of nearly 87%,

but the criticism that can be made of this article is that it has a high processing time, which will be evaluated in the proposed method and will try to process the processing time and have less than this research.

Lukas et al. in 2016 [39] in a study entitled “Identification” with the help of the implementation of discrete wavelet transform and cosine transform using a neural network of radial basis function, a new method of identification has been proposed. In the paper presented by this team, images of 41 students with 131 images were used, and, on these images, discrete cosine transformation and discrete wavelet tidying were applied and the detection process was performed using radial base function neural networks. The test results show that the best values for the radial bases function. Recognition rate in this study is 98% which is acceptable.

Banerjee et al. in 2016 [40], in his paper, present a short-range correlation filter in the frequency range for face recognition functions in different lighting conditions. The essence of the proposed Gabor intermediate filter is a combination of a high-pass filter and a discrete wavelet filter, and an optimal range of scales is selected for the mentioned wavelet filter. The performance of the proposed method by evaluating the YalaB and Cumple images on the light noise challenges shows that the proposed method is more efficient than many similar filters and has a low detection rate.

Li et al. in 2017 [41], in an article, used machine learning techniques to solve the problem of unbalanced light on the face. This method is based on Gabor filter, basic component analysis, and SVM classification. In this research, to solve the problem of light in the face, the histogram matching method and Gaussian low-pass filter have been used. Then, Gabor wavelets were used to extract the feature, and finally, to reduce the dimension of feature vectors, principal component analysis was used to classify the feature vector machines, and the detection rate in the proposed method was less than 95%.

Paria et al. in 2017 [42] have used a set of techniques based on logarithm conversion, histogram matching, and cosine conversion to solve the problem of unbalanced light in the face. In a way, combining these three techniques together is a kind of preprocessing to solve the imbalance of light in the face. The image containing light is subjected to the three mentioned algorithms and combined with each other, and finally a normalized image is produced. Finally, the feature is extracted from the image, and the classification is performed using the SVM classifier. The proposed method is implemented on ATT data, and its detection rate is set at 93%.

Tu et al. in 2017 [43] in an article propose a framework for normalizing facial light with the idea of the term in areas with large-scale components (areas with frequencies). In this method, first, a logarithmic periodicity is used to identify areas with large and small components. The following two hypotheses have been proposed: (1) Those large-scale components are affected by light and (2) that they are inherently an area with a large-scale component. Based on these hypotheses, a framework for reducing energy from the area of large-scale components has been proposed. The proposed method is implemented on the CMVPIE and CAS_PEAL databases, and the results are close to 95%.

Wang et al. in 2017 [44], in an article, presented a new method to solve the problem of changing the angle of the face and the presence of light in the face.

This method is implemented based on matched local binary patterns and multiple directional gradient histograms, and finally, after extracting the feature from each block, it is weighted to each of the face blocks using entropy information. At the end, the feature vector each image generated is finally classified into feature vectors with four methods: neural networks, RE, backup vector machine, and WSRC. The proposed method is implemented on the ORL database, and the detection rate is 96%.

Fang et al. in 2017, [45] in a study called multilayer detection to identify identity, reviewed all the research conducted in this challenge. In this article, researchers have reviewed and compared all the predispositions, feature extraction, and categories in light challenge research. The only drawback of this review article is this, which has examined only one challenge, but the strength of this work is that it has almost comprehensive research on the light challenge and can be a good guide for exploring and discovering ideas in other challenges.

Woo et al. in 2017 [46] introduced new dimensions of the light challenge into face recognition through images. In this study, in order to obtain dissociation information from image reconstruction errors, both linear synthesis coefficient and reconstruction error are combined with the ℓ_1 -Norm algorithm, which does not allow distortion of outgoing data. Then, using similar transformations, the parameters are calculated in a linear system. This method has been evaluated on the extended Yale B and AR face databases, which of course can be deduced from the results obtained. The proposed method has not been able to achieve good results, but the important point is that this research can be considered a step to start research with different challenges.

Satanj et al. in 2017 [47] presented a new method for face recognition in a study entitled combination of Gabor extractors and Zernik torques. In this research, first, using Gabor filter, 40 sub-images of the original images with 5 scale and 8 direction change are produced. Then four Zernik properties are extracted from each sub-image, and the results are classified by the nearest neighbor classifier. The detection rate in this study was 89.23%, which cannot be acceptable. But in the database produced by this research team, the identification rate has reached 98.5%.

Nakada et al. in 2017 [48] in a study entitled identification with facial images using the cannulation neural network have proposed a new way to identify with different images of the face. The images used in this study are such that the faces of people are photographed from different angles to explore a new challenge in identifying with the help of face images. In this research, two identification and control modules have been used. In this paper, the properties extracted by convolutional neural networks are classified by a K classifier nearest neighbor. The results of the study of identification in different angles (90° to -90°) show that only in the angle of 0° , the identification was 100% and more angles of identification were minimized. But it should be noted that even at high angles such as 90° , acceptable results are provided.

In 2017, Fan et al. [49] proposed a fuzzy Gabor-based method for extracting features from face images with the feature of stability against light changes. In this research, first, the light intensity in the face is reduced by a normalization. In the second stage, a set of Gabor violets is used in different directions to deform the images, and then the multiple Gabor coefficients are combined with each other to

obtain the spectrum and phase. Finally, stability is obtained against light changes after the feature stage. In this research, two databases, YalaB and Cumple, have been used to evaluate the proposed method, the identification rate of the proposed method has been 96%, and this method has an important criticism, and that is the computational and temporal complexity of using Gabor violet. Eventually, it has led to a drop in the detection rate.

McLaughlin et al. in 2018 [50] introduced a new approach to face recognition with three combined challenges: inadequate lighting, covering part of the face with glasses or scarves, etc., reducing training data, and emphasizing recognition based on finding the largest area that can be matching are provided anywhere on the face. In this method, a transient filter is used to preprocess and reduce the effects of light on the face, and Fourier magnitude is used to extract the feature. Finally, the cosine similarity criterion is used to measure the similarity of the feature vectors [51]. The LEW database was used to evaluate the proposed method, and the detection rate obtained from this method for light challenge is between 94 and 96%, which is not a significant rate.

The Iris

The iris has been used as a biometric for many years as a research goal. In this section, some of these studies have been studied. Iris segmentation is a necessary and difficult step in iris detection systems. Differential integral operators and Huff transmissions are widely used to segment the iris tissue of images. Both algorithms offer good segmentation efficiency but have high computational complexity.

Tajbakhsh et al. [52] in 2010 proposed an authentication system based on iris detection by reducing the error rate. The main sources of rising error rates are decreasing factors in iris tissue. To reduce the error rate, a robust feature extraction method based on local and global variables in iris tissue is proposed. This method is designed to work on blurred and decentralized iris images. Global changes extract a general presentation of texture, while local changes encode texture details that rely least on image quality. In the adaptation phase, a backup vector machine will be combined with similar values of local and global characteristics. Performance evaluations of this method have been compared with CASIA Ver.1 and UBIRIS databases. The result is a significant reduction in the error rate.

However, a large part of the computational time will be spent determining the primary centers of the circular borders of the iris and pupil. In 2012, Radman et al. [53] proposed a simple solution to this problem by locating the primary center of the pupil. The Gabor circular filter will be used to locate the initial center of the pupil. The evaluation of the efficiency of this method has been done by the UBIRIS.v1 image database. The results show an increase in segmentation efficiency in this method.

In 2015, Raja et al. introduced a new segmentation method for smartphones based on visible iris images to estimate iris radius and obtain a strong segmentation. In the proposed method, the particle efficiency improvement with OSIRISv4.1 standard is about 85, which includes 15 errors and a high rate. This paper also presents a method based on scattered filters to achieve strong results in infinite iris images and uses a new database of iris images. The VISSIRIS database is used on both the iPhone 5S

and Nokia Lumia 1020 smartphones. Biometric efficiency is based on an equal error rate. An error rate of 1.62 was obtained under this database, which is an improvement over other two databases [54].

In 2015, Jillela et al. used iris tissue for biometric identification in mobile devices. One of the main parts of an iris recognition system is its segmentation module that separates the iris from the rest of the eye image. Because cell phones take color photos from the eye, this article deals with the automatic division of the iris into the visible spectrum so that color spectrum images can be segmented efficiently. The identification steps are not discussed in this article [55].

Liu et al. in 2015 a method for noise images and noise images of test and most that one side is noisy and the other side is not and in the preprocessing stage to reduce noise and using Gabor filter and standard deviation of this method is presented is a feature selection. Among the disadvantages of this method is that it does not compare with other methods and only examines the noise problem and that it does not introduce Gabor parameters and the number of filters and the directions in which these filters are used, and among the advantages of this, the method can be used for the first time using Gabor filter and standard deviation [56].

Lee et al. worked in 2015 on tissue analysis with LBP, which works on tissue and is a binary model. In this method, each area is compared with the central area. If that area is smaller than the central area, we set the number to zero, and if it is larger, we set the number one to NBP. This method solves the network problem. The Casia database does the job and then uses NBP to extract the attribute and then compares it by clockwise comparing each area with all its neighbors. If it is larger, we set it to one, and if it is smaller, we set it to zero. This method solves the rotation problem well and has high accuracy [57].

In their 2016 study, Salvi et al. introduced a new method of using eyebrows to determine gender. They used shape-based eyebrow features under non-ideal imaging conditions for biometric detection and identification. In this study, three different methods of gender determination have been compared with each other: These three methods include (1) identification using the least distance, (2) identification using linear separator analysis, and (3) gender determination using backup machine vector. These methods have been tested on images from two existing face image databases, such as the multiple biometric large challenge database and the large face recognition challenge database. The biometric detection rate of this algorithm is 90 when it uses multiple biometric databases and 75 when it uses FRGC database. Also, the sex detection rates for these two databases are 96 and 97, respectively [58].

Suciati et al. in 2016 improved the image quality by using radon and wavelet transforms and also increased the accuracy of image recognition. The feature extraction step uses discuss sinusoidal and wavelet transform, the main purpose of which is to improve the quality of images. By combining DCT and DWT, useful features can be extracted from these images and the accuracy of identifying individuals can be increased. He pointed out that it does not find proper accuracy compared to other methods. The most important advantage of this method is that it has worked on popular databases such as phoenix and IITD [59].

In 2017, Trokielewicz et al. [60] conducted an analysis of the impact of iris detection by ocular diseases and a database with 2996 iris images out of 230 separate images. Images were taken near radiation and visible light inside an ophthalmology equipment laboratory. In the experiments, four independent iris detection algorithms (MIRLIN VeriEye, OSIRIS, and IriCore) were used, and different results were obtained. Initially, the registration process is very sensitive to those eye conditions that interfere with the iris or cause geometric distortion. Second, even conditions that do not produce visible changes in the structure of the iris may cause heterogeneity between specimens of the same eye. Third, eye conditions may differ in the geometric location or structure of the iris tissue in images taken by one eye. Fourth, for diseased eyes, the effect of the disease on the diagnosis of the iris is to create segmentation errors.

In 2017, Umer et al. [61] proposed a new iris detection method based on the efficiency of various feature learning techniques such as (1) word bag, (2) thin programming, and (3) space-limited linear programming. Here, the second technique along with pyramidal spatial mapping is used to calculate the properties of the iris pattern, which has better results than the others. The proposed method has a high execution time despite its high accuracy.

Rai et al. in 2018, using matching graphs and Gabor feature conversion algorithm, have used a method for noise image accuracy. This article has done its work on Casia and UBIRIS databases. In this article, hough transform to segment the area. He used his eyes and studied the noise images and came to the conclusion that he had a high accuracy compared to the noise images. He also compared the proposed method of his work with the work done in recent years to conclude which one has higher accuracy and better [62].

Liano et al. in 2018 at first, the iris image is normalized and its challenges compared to when the irises in our database for training are different from our test, and different imaging is done and tries to capture this image. Improve and filter images in different background bands using different sigmas and with Gaussian and Laplace in filters to determine the position of each pixel. This method uses EL, LP, and MLP feature extraction operations and normalizes images. This method is more powerful than images taken with different sensors, and one of the advantages is that it examines the challenge that most articles differ from and pays no attention to the fact that databases are different. Disadvantages of this method Inaccurate and complete feature extraction step can be noted [63].

In 2019, loan et al. used the extraction of various key points and the SIFT algorithm to identify iris images and pointed out that most methods cannot work well for rotation, but in this article we present a method that is very strong compared to rotation. First, it extracts a band related to the iris of the eye, then using the SIFT algorithm, the feature extraction operation is performed, and this method is fixed compared to rotation. The disadvantage is that other challenges have not been addressed [64].

Choudhary et al. studies in 2019 are exactly the same as the article done by Levan et al., and it has solved the problem of rotating images [65].

In 2020, Abiram et al. developed a system for identifying the complete image of the iris. In this research, by integrating power-based display and hybrid learning

algorithms, the part-based identification method (PBGR) using the image from the front and from the back angle has been proposed with an accuracy of 76.0. This method is resistant to small irregularities in the iris [66].

In 2020, Abdo et al. determined identification based on the appearance characteristics extracted from the iris. In this experiment, they chose the CASIA database. The results of their study show that gait characteristics help to improve the accuracy of identification [67].

Khozani et al. in 2020 according to the different parts of feature extraction from the iris, identification through the iris can be divided into two methods of local feature extraction and global feature extraction. The local feature extraction method extracts feature from specific points of the iris, while the global feature extraction method extracts feature from the entire iris. In this study, it was proved that local features, while having high accuracy, can perform authentication with more optimal time [68].

Fingerprint Blood Vessels

In [69], using the image manipulation distance classifier to identify and authenticate the images of finger blood vessels reached 94.80% accuracy. The preprocessing processes used include Mornazer area detection for ROI vessels as well as the use of feature extraction and zoning improvements in these orthogonal neighborhood images and the manual learning of ONPP maintenance injections. Although the accuracy obtained is remarkable, it has a high computational cost.

In [70], simultaneous precedence and segmentation of the desired ROI area in the preprocessing section are used. Steerable filters have been used to extract the feature, and finally the nearest neighbor classification has been used, which has an accuracy of 94.73%. Like many traditional methods, it has a high computational cost despite its high efficiency.

In [71], a complex process for preprocessing NIR images of fingerprint blood vessels has been proposed. In the proposed method, after the ROI is generated, the proximity of the filters is used to remove Gaussian and salt pepper noise. After the filtering process is done, zoning is done and noise is eliminated. Blood vessels are then extracted and normalized for assimilation in feature extraction. To extract the feature, the 2LDA 2D weighted directional algorithm is used, the initial vectors are generated, and finally, the Hamming distance is used for classification. Identification accuracy is 94.69%. Despite the great complexity of the preprocessing process, good accuracy has not been achieved.

In [72] suggested the Hemingway HD distance for classification and authentication in this type of biometrics. Although the simple preprocessing process of Gaussian high-pass filters has been used, and for simple feature extraction, duplication and binary processing, as well as local binary LBP patterns, the result has not been a good detection rate of 89% for the system. Authentication cannot be numerically appropriate at all.

In [73] again, with a complex process, including preprocessing as well as feature extraction as well as classification, they have reached 100% accuracy. The complex algorithm proposed in the classification step uses pattern matching, which is very complex. Also, after heavy preprocessing processes such as background extraction

and foreground separation, noise cancelation and image quality improvement, size normalization, and image brightening, they have used a combination of four powerful feature extractors. Feature extractors used include local dynamic thresholding, intermediate filters, morphological actuators, and reducing the direction and position of vessels globally.

In [74], LLBP linear local binary patterns are used for feature extraction, although the simple Hamming distance classifier is used, and despite the improved Gaussian filter preprocessing process, the detection accuracy is 89%, which is not very good for the system. Authentication is not efficient.

In [75], after ROI extraction, limited adaptive adaptation of CLAHE contrast and normalization in the preprocessing stage were used by analyzing the entropy components of the KECA linear kernel. Complex mathematical processes in the preprocessing and feature extraction stages combine with the Euclidean distance classification, resulting in 96% identification accuracy. Although the result is acceptable, this algorithm is very complex.

In [76], the complex K classifier used the nearest weighted central neighborhood WKNCN along with the PCA kernel feature extractor. The accuracy of the proposed method is 99.7%, which is remarkable. It should be noted that ROI extraction preprocessing processes, image sizing, and Gaussian high-pass filters have been used in preprocessing. The computational time presented is very high which is the main disadvantage of the proposed method. In the sophisticated algorithm, adaptation is used to classify the features of the best personal record map. In the proposed method, gray surface processing jump images are proposed for ROI extraction and normalized in size and gray surfaces. The accuracy obtained is 95%. Compared to other methods, this method is less complicated, but the obtained number is not a good evaluation.

In [77], the classifications used Violet transform and entropy properties. The obtained accuracy is 95% reported. In the proposed method, fractal dimensions and wavelet conversion have been proposed as feature extractors, and also simple cubic interpolation and histogram analysis and equivalence processes have been used. This method has good accuracy, and of course, complex algorithms have been used.

In [78] again, the complex adaptation algorithm is used for classification in the proposed method. Also in the proposed preprocessing process, ROI is extracted, and then normalization takes place. The 100% accuracy reported in this study is a bit thought provoking, and at the same time, the extractors of local directional code features at zero and 45° angles are used as features. The processing cost of the proposed method is very high.

In the method proposed in [79], the accuracy has reached 99.85%. The method proposed in this paper, while very smart, has a high processing cost and computational time. Anisotropic methods and non-diffusion transfer maps with Gabor have been proposed for preprocessing, which is significant in terms of computational volume. Feature extraction is done by directional filtering method, and the phase correlation strategy is used in the classification.

In [80] have proposed LLBP local line binary patterns with pulse width modulation for classification as well as LLBP for feature extraction. In the proposed method,

after extracting the ROI and improving the image quality, the dimensions and color in the image are normalized. Despite the simplicity of the proposed method, the result is 99.67% significant. In this study, edge finding and ROI extraction along with softener filtering were proposed in the preprocessing stage. PBBM best personal bit mapping algorithms are categorized for cross-correlation adaptation. The proposed method is very complicated and at the same time slow. But the results are very interesting. 97.56% is registered for this algorithm.

In [81], the hard adaptation algorithm was used for classification, but in the preprocessing phase only the ROI is extracted and the feature extractor used in this method is only the competitive Gabor HCGR response histogram, which in turn is a new method. The obtained accuracy is 98.1%. The proposed method is simpler than other methods, but there still seems to be room for research to simplify.

In [82], they used a complex and complex pattern matching algorithm for classification in the proposed method. The proposed methods are complex in the preprocessing as well as feature extraction stages. The preprocessing area after ROI extraction as well as normalization of light and brightness of infrared images near Mumford Shah has been used for minimization. More interestingly, in the extraction step, the local entropy threshold feature of morphological refusal and morphological filtering is proposed, and with all the complexity of the proposed method, the accuracy is 90.9%, which creates a question mark in the mind of the reader. Despite the high computational cost and processing time, the result is not acceptable.

In [83], different classifications have been used to result in authentication using finger blood vessel images. The classification of the sum of squares of differences is first presented by this research. Modification methods have been used for feature extraction, while in the preprocessing stage after ROI extraction, multi-comparison filtering and linear search have been proposed. The obtained accuracy is 93.11%. Although the proposed method is relatively simple in terms of calculation, but this result is far from reaching the desired point.

In [84] used machine learning algorithms to authenticate fingerprint images. In the preprocessing stage, after extracting the area, the images are also sized. Appropriate features are then extracted by principal component analysis (PCA) as well as LDA linear separator and finally classified by SVM. The accuracy of the proposed method is 98.1%, which is appropriate due to the simplicity of the proposed numerical method. But the classifier used is very sensitive to noise.

In [85] after the same preprocessing process, only PLA is used to enter the properties into ANFIS-based fuzzy classifier. The fuzzy classifier is less sensitive to noise and is inherent in the nature of biometric data. But the results are satisfactory, and the reported accuracy is 99%.

In [86], various preprocessing processes were used to improve the quality of IR infrared images. These methods include ROI extraction and then intermediate filtering and histogram equivalence. Morphological operators and maximum points of the curve have been used as extracted features for classification using multilayer perceptron neural network. The proposed method is very simple to implement, and the results are impressive. However, it seems that multilayer progesterone neural

networks are deficient in nonlinear data separation and will have problems with classification efficiency noise.

In [87], only Gaussian adaptive filter has been used to improve the image quality and in the preprocessing stage, and feature extraction is performed with the help of variance of practical LBPV binary patterns. The proposed classification is based on global compliance as well as SVM. The proposed method is more complex than other methods in identifying finger blood vessels, and the results obtained are not very suitable for an authentication system. 89.71% accuracy has been obtained.

In [88], the complex preprocessing process includes histogram equalization, contrast enhancement, intermediate filtering, and Gabor filters, and finally the extracted features include global thresholding as well as Gabor filters. The classifier used is also SVM. In general, the proposed method is very complex, and the results obtained are also desirable.

In [89], convolutional neural networks have been used to classify images of finger blood vessels. Convulsive neural networks are one of the deep learning methods that has recently attracted the attention of many researchers. In this method, the feature no longer needs to be extracted, and CNN classifies by creating a data pool from the image. 98.1% accuracy can be a good result.

Although the algorithms of identification presented by the researchers have been able to overcome many challenges such as low image quality, and several methods have been proposed, in the field of fingerprint identification using a lot of research has not taken place. In research, complex computational methods are needed to identify because of these changes, which are mostly nonlinear. These methods mainly have low detection rate and low detection speed.

Blood Vessels in the Palm of the Hand

Humans have long and naturally used the biometric features of others, such as face, voice, or handwriting, to identify themselves. In today's society, identity identification has become very important, especially in security issues. Today, with the rapid advancement of technology, many tools are needed to achieve this goal. One of these tools is much more efficient in terms of security than the other. The tools are the arteries of the palm. According to researchers, fingerprint has a unique property for each person in the world and also has advantages such as no change in life and the possibility of copying and so on. In the last two decades, several methods have been proposed to identify the palm.

In 2020, using the image manipulation distance classifier to identify and authenticate the images of the blood vessels in the palm of the hand reached 97.80% accuracy. The preprocessing processes used include Mornazer area detection for ROI vessels as well as the use of feature extraction and zoning improvements in these orthogonal neighborhood images and the manual learning of ONPP maintenance injections. Although the accuracy obtained is remarkable, it has a high computational cost [90].

In 2020, simultaneous priority and segmentation of the desired ROI area in the preprocessing section have been used. Guided filters have been used to extract the feature, and finally the nearest neighbor classification has been used, which has an

accuracy of 97.73%. Like many traditional methods, despite its high efficiency, it has a high computational cost [91].

In 2019, a complex process has been proposed for the preprocessing of NIR blood vessel floor images. In the proposed method, after the ROI is generated, the proximity of the filters is used to remove Gaussian and salt pepper noise. After the filtering process is done, zoning is done and noise is eliminated. Blood vessels are then extracted and normalized for assimilation in feature extraction. To extract the feature, the 2LDA 2D weighted directional algorithm is used, the initial vectors are generated, and finally the Hamming distance is used for classification. Identification accuracy is 94.69%. Despite the high complexity of the preprocessing process, good accuracy has not been achieved [92].

Improved alignment histogram correction was implemented by [93], which identified the edges of the vessel more efficiently and thus improved the overall contrast of the image. This article uses a separator binary code. In the first step, a graph is designed to identify the relationship between objects. Based on this graph, a binary format is then used to describe the vascular properties of objects. Also, converting this graph to an analytical optimization problem can be invoked by the resolution of binary formats. There are also a number of Gabor filters based on FVR techniques.

In [94], multidirectional Gabor was used to extract the vascular pattern. In this method, first the general variance normalization is used to decompose the initial image into an image including structure and noise. A local binary pattern descriptor is then used to encode both image patterns. Finally, a backup vector machine is used to classify and identify the true pattern of arteries from the fake pattern.

In 2017, [95] introduced a new method for extracting an interesting area of an image in which less information is lost from the image. For this purpose, he used external rectangle methods and a modified sliding window. Improper selection of the interesting area can cause the destruction of parts of the image, including the arteries of the hand, and reduce the accuracy of the system, so he used a sliding window instead of a fixed window to reduce possible problems in the interesting area and speedup processing.

In [96], the PolyU database introduced an advanced method of custom localized linear binary pattern in which the reduction of image information is eliminated, and the local distinguishing features in the image are increased and the identification time of the identification system is greatly reduced. Experimental results show that the recognition method of the proposed method is better compared to LLBP-based methods.

In 2018, after preparing the images, they did preprocessing to remove the noise. The proposed method was tested on the CASIA database with images of 100 people, which in the best case provided 96.5% accuracy. The proposed method is not stable for image rotation and transfer [97].

In 2018, they used the dual-channel network method for fingerprint verification, which extracted the smallest ROI of the original image. The proposed method on the MMCBNU database includes palm images of 100 people [98].

Hufng et al. minimized the instability against image quality degradation by minimizing the DNN verification error on the fingerprint using the p -SVM support vector in order to improve the quality assessment performance [99].

In 2017, Cancian et al. proposed a method for identifying palm arteries based on biometric characteristics. In this method, after preparing the images, the features were extracted using Gabor filter. The proposed method was tested on a database containing palm images of 21 people, which achieved high accuracy and speed. But the challenge of inappropriate alignment has not been considered [100].

Kumar et al. [12] used multidirectional Gabor to extract the vascular pattern. In this method, first the general variance normalization is used to decompose the initial image into an image including structure and noise. A local binary pattern descriptor is then used to encode both image patterns. Finally, a backup vector machine is used to classify and identify the true pattern of arteries from the fake pattern. The Gabor filter and the edge detector were combined by Kaud et al. [101], thereby improving the image of the finger vein and removing noise from the image. In fact, noise is a very effective factor in reducing the image recognition rate, and as a result, this method greatly increases the accuracy of the system. The image consists of the finger area, and its vessels include two general parts. One part is the background of the image, which does not contain the vessels, and the next part of the area contains the vessel, which must be analyzed and information extracted from it. Therefore, an important phase in identification is the extraction of an interesting area or ROI from the image, so that studies are limited to this area of the image and the rest of the image is omitted [102].

In 2014, Wang and colleagues proposed a way to identify the arteries of the palm. In this method, the vascular pattern of the palm is used as a biometric feature and also the Gabor wavelet is used as a feature extractor to identify individuals. Although this method was able to achieve a very high detection accuracy of 98.8%, this accuracy was achieved in conditions where the images are normal, in other words, the images used in this study have conventional challenges in palm vessel detection systems. It is not as inappropriate as alignment [103].

In 2013, Kuang-Shyr Wu et al. proposed a way to improve security in palm vascular-based infrared detection systems. In this method, a two-dimensional Gaussian filter is used to extract the properties. The high accuracy of this method, which is more than 99%, has made this method a practical, effective, and noise-resistant method for detecting palm arteries, but none of the challenges in palm artery recognition systems, such as rotation, transfer, and scaling challenges are not considered [104].

In 2013, Bayoumi et al. [105] developed a method for identifying individuals based on vascular palm images in the near-infrared spectrum. The proposed method achieved an identification accuracy of 85%, which is not very accurate compared to other methods presented in this field, and the images used in it were normal and non-challenging images.

In 2012, Hahn and colleagues developed a way to identify people based on the arteries of the palm. In this method, the palm vessels obtained in the near-infrared image spectrum are used as biometric features and the Gabor filter is used to extract

the feature. The features of this method include high adaptation speed, high accuracy, and increased efficiency compared to similar methods. Jalili et al. [106] used a four-layer neural network and a combination of local Gabor histograms to increase the accuracy of the fingerprint recognition system in 2015 to teach complete images of the palmar arteries, in which no interesting area of the image is extracted.

In 2015, Minaei and Wang [107] used a two-layer deep scattered neural network to identify the vessels in the palm of the hand. Scattered networks are similar to torsional neural networks, except that they use violet conversion filters instead of data-based learning filters. It is noticeable in the images.

Dayan et al. [106] used the interesting area and the Hausdorff distance to match the patterns. The use of a scattered network and descriptor SIFT and principal component analysis and an identification rate of over 99% were one of their achievements.

Chai et al. [108] used torsional neural networks to identify left and right hands and key points in the palmar arteries to extract the area of interest, which had an error rate equal to EER compared to the robust methods introduced.

5 Conclusion

For many years, identification using biometrics as an attractive field of research has been considered by researchers and craftsmen. Extensive research has also been done in this regard, but a lot of effort is needed to achieve very good results. But one thing that can be pointed out as a weakness in this research is that it does not take into account all the challenges and problems of these systems in the real world. Problems such as errors in identifying the correct location of biometric patterns lead to the production of an image that is inconsistent with the image in question, or disruption of the image scanning system and the production of high-noise images and other problems that can occur. A review of the research background revealed that so far, no comprehensive research has been presented considering all of these problems. Therefore, this study aims to provide a complete overview of these challenges and biometrics.

Conflicts of Interest There is no conflicts of interest in this paper.

References

1. Rahim, M.S.M., Rehman, A., Kurniawan, F., Saba, T.: Ear biometrics for human classification based on region features mining. *Biomed. Res.* **28**(10), 4660–4664 (2017)
2. Jabeen, S., Mehmood, Z., Mahmood, T., Saba, T., Rehman, A., Mahmood, M.T.: An effective content-based image retrieval technique for image visual representation based on the bag-of-visual-words model. *PLoS ONE* **13**(4), e0194526 (2018)

3. Abbas, N., Saba, T., Mohamad, D., Rehman, A., Almazyad, A.S., Al-Ghamdi, J.S.: Machine aided malaria parasitemia detection in Giemsa-stained thin blood smears. *Neural Comput. Appl.* **29**(3), 803–818 (2018)
4. Rehman, A., Harouni, M., Karimi, M., Saba, T., Bahaj, S.A., Awan, M.J.: Microscopic retinal blood vessels detection and segmentation using support vector machine and K -nearest neighbors. *Microsc. Res. Tech.* **85**(5), 1899–1914 (2022)
5. Amin, J., Sharif, M., Raza, M., Saba, T., Rehman, A.: Brain tumor classification: feature fusion. In: 2019 International Conference on Computer and Information Sciences (ICCIS), pp. 1–6. IEEE (2019)
6. Khan, A.R., Doosti, F., Karimi, M., Harouni, M., Tariq, U., Fati, S.M., et al.: Authentication through gender classification from iris images using support vector machine. *Microsc. Res. Tech.* **84**(11), 2666–2676 (2021)
7. Saba, T., Rehman, A., Altameem, A., Uddin, M.: Annotated comparisons of proposed preprocessing techniques for script recognition. *Neural Comput. Appl.* **25**(6), 1337–1347 (2014). <https://doi.org/10.1007/s00521-014-1618-9>
8. Shaheed, K., Mao, A., Qureshi, I., Kumar, M., Abbas, Q., Ullah, I., et al.: A systematic review on physiological-based biometric recognition systems: current and future trends. *Arch. Comput. Methods Eng.*, 1–44 (2021)
9. Harouni, M., Karimi, M., Rafieipour, S.: Precise segmentation techniques in various medical images. In: Artificial Intelligence and Internet of Things: Applications in Smart Healthcare, p. 117 (2021)
10. Iqbal, S., Khan, M.U.G., Saba, T., Mehmood, Z., Javaid, N., Rehman, A., Abbasi, R.: Deep learning model integrating features and novel classifiers fusion for brain tumor segmentation. *Microsc. Res. Tech.* **82**(8), 1302–1315 (2019). <https://doi.org/10.1002/jemt.23281>
11. Karimi, M., Harouni, M., Nasr, A., Tavakoli, N.: Automatic lung infection segmentation of covid-19 in CT scan images. In: Intelligent Computing Applications for COVID-19, pp. 235–253. CRC Press (2021)
12. Patua, R., Muchhal, T., Basu, S.: Gait-based person identification, gender classification, and age estimation: a review. In: Progress in Advanced Computing and Intelligent Engineering, pp. 62–74 (2021)
13. Karimi, M., Harouni, M., Rafieipour, S.: Automated medical image analysis in digital mammography. In: Artificial Intelligence and Internet of Things, pp. 85–116. CRC Press (2021)
14. Harouni, M., Mohamad, D., Rasouli, A. (eds.): Deductive method for recognition of online handwritten Persian/Arabic characters. In: 2010 the 2nd International Conference on Computer and Automation Engineering (ICCAE). IEEE (2010)
15. Harouni, M., Rahim, M., Al-Rodhaan, M., Saba, T., Rehman, A., Al-Dhelaan, A.: Online Persian/Arabic script classification without contextual information. *Imag. Sci. J.* **62**(8), 437–448 (2014)
16. Mohammadi Dashti, M., Harouni, M.: Smile and laugh expressions detection based on local minimum key points. *Sig. Data Process.* **15**(2), 69–88 (2018)
17. Rehman, A., Harouni, M., Karchegani, N.H.S., Saba, T., Bahaj, S.A., Roy, S.: Identity verification using palm print microscopic images based on median robust extended local binary pattern features and k -nearest neighbor classifier. *Microsc. Res. Tech.* **85**(4), 1224–1237 (2021).
18. Khan, M.Z., Jabeen, S., Khan, M.U.G., Saba, T., Rehmat, A., Rehman, A., Tariq, U.: A realistic image generation of face from text description using the fully trained generative adversarial networks. *IEEE Access* **9**, 1250–1260 (2020)
19. Meethongjan, K., Dzulkifli, M., Rehman, A., Altameem, A., Saba, T.: An intelligent fused approach for face recognition. *J. Intell. Syst.* **22**(2), 197–212 (2013). <https://doi.org/10.1515/jisy-2013-0010>
20. Amin, J., Sharif, M., Rehman, A., Raza, M., Mufti, M.R.: Diabetic retinopathy detection and classification using hybrid feature set. *Microsc. Res. Tech.* **81**(9), 990–996 (2018)
21. Iftikhar, S., Fatima, K., Rehman, A., Almazyad, A.S., Saba, T.: An evolution based hybrid approach for heart diseases classification and associated risk factors identification. *Biomed. Res.* **28**(8), 3451–3455 (2017)

22. Qayoom, I., Naaz, S.: Review on secure and authentic identification system using finger veins. *Int. J. Adv. Res. Comput. Sci.* **8**(5) (2017)
23. Rehman, A., Sadad, T., Saba, T., Hussain, A., Tariq, U.: Real-time diagnosis system of COVID-19 using X-ray images and deep learning. *IEEE IT Prof.* **23**(4), 57–62 (2021). <https://doi.org/10.1109/MITP.2020.3042379>
24. Singh, A., Singh, D.: Palm vein recognition technology: a literature survey. *Int. J. Solid State Mater.* **5**(1), 46–51 (2019)
25. Aurangzeb, K., Haider, I., Khan, M.A., Saba, T., Javed, K., Iqbal, T., Rehman, A., Ali, H., Sarfraz, M.S.: Human behavior analysis based on multi-types features fusion and Von Nauman entropy based features reduction. *J. Med. Imag. Health Inf.* **9**(4), 662–669 (2019)
26. Mughal, B., Muhammad, N., Sharif, M., Saba, T., Rehman, A.: Extraction of breast border and removal of pectoral muscle in wavelet domain. *Biomed. Res.* **28**(11), 5041–5043 (2017)
27. Yang, W., Wang, S., Hu, J., Zheng, G., Valli, C.: Security and accuracy of fingerprint-based biometrics: a review. *Symmetry* **11**(2), 141 (2019)
28. Kavati, I., Prasad, M.V., Bhagvati, C.: Search space reduction in biometric databases: a review. In: *Computer Vision: Concepts, Methodologies, Tools, and Applications*, pp. 1600–1626. IGI Global (2018)
29. Sharif, M., Naz, F., Yasmin, M., Shahid, M.A., Rehman, A.: Face recognition: a survey. *J. Eng. Sci. Technol. Rev.* **10**(2), 166–177 (2017)
30. Perveen, S., Shahbaz, M., Saba, T., Keshavjee, K., Rehman, A., Guergachi, A.: Handling irregularly sampled longitudinal data and prognostic modeling of diabetes using machine learning technique. *IEEE Access* **8**, 21875–21885 (2020)
31. Khan, A.R., Khan, S., Harouni, M., Abbasi, R., Iqbal, S., Mehmood, Z.: Brain tumor segmentation using K -means clustering and deep learning with synthetic data augmentation for classification. *Microsc. Res. Tech.* **84**(7):1389–1399 (2021)
32. Adapa, D., Joseph Raj, A.N., Alisetti, S.N., Zhuang, Z., Naik, G.: A supervised blood vessel segmentation technique for digital Fundus images using Zernike moment based features. *PLoS ONE* **15**(3), e0229831 (2020)
33. Raftarai, A., Mahounaki, R.R., Harouni, M., Karimi, M., Olghoran, S.K.: Predictive models of hospital readmission rate using the improved AdaBoost in COVID-19. In: *Intelligent Computing Applications for COVID-19*, pp. 67–86. CRC Press (2021)
34. Mughal, B., Sharif, M., Muhammad, N., Saba, T.: A novel classification scheme to decline the mortality rate among women due to breast tumor. *Microsc. Res. Tech.* **81**(2), 171–180 (2018). <https://doi.org/10.1002/jemt.22961>
35. Heisele, B., Ho, P., Poggio, T. (eds.): Face recognition with support vector machines: global versus component-based approach. In: *Proceedings Eighth IEEE International Conference on Computer Vision, 2001. ICCV 2001*. IEEE (2001)
36. Günther, M., Würtz, R.P.: Face detection and recognition using maximum likelihood classifiers on Gabor graphs. *Int. J. Pattern Recognit. Artif. Intell.* **23**(03), 433–461 (2009)
37. Yu, L., He, Z., Cao, Q.: Gabor texture representation method for face recognition using the Gamma and generalized Gaussian models. *Image Vis. Comput.* **28**(1), 177–187 (2010)
38. Farokhi, S., Sheikh, U.U., Flusser, J., Yang, B.: Near infrared face recognition using Zernike moments and Hermite kernels. *Inf. Sci.* **316**, 234–245 (2015)
39. Lukas, S., Mitra, A.R., Desanti, R.I., Krishnadi, D.: Implementing discrete wavelet and discrete cosine transform with radial basis function neural network in facial image recognition. *J. Image Graph.* **4**(1) (2016).
40. Banerjee, P.K., Datta, A.K.: Band-pass correlation filter for illumination-and noise-tolerant face recognition. *SIViP* **11**(1), 9–16 (2017)
41. Li, M., Yu, X., Ryu, K.H., Lee, S., Theera-Umpon, N.: Face recognition technology development with Gabor, PCA and SVM methodology under illumination normalization condition. *Clust. Comput.*, 1–10 (2017)
42. Paria, E., Cardenas, R., Gutierrez, J., Galdos, J. (eds.): An improved face recognition based on illumination normalization techniques and elastic bunch graph matching. In: *Proceedings of the International Conference on Compute and Data Analysis*. ACM (2017)

43. Tu, X., Gao, J., Xie, M., Qi, J., Ma, Z.: Illumination normalization based on correction of large-scale components for face recognition. *Neurocomputing* **266**, 465–476 (2017)
44. Wang, K., Chen, Z., Wu, Q.J., Liu, C.: Illumination and pose variable face recognition via adaptively weighted ULBP_MHOG and WSRC. *Sig. Process. Image Commun.* **58**, 175–186 (2017)
45. Yu, Y.-F., Dai, D.-Q., Ren, C.-X., Huang, K.-K.: Discriminative multi-layer illumination-robust feature extraction for face recognition. *Pattern Recogn.* **67**, 201–212 (2017)
46. Wu, X., Fang, B., Tang, Y.Y., Zeng, X., Xing, C.: Reconstructed error and linear representation coefficients restricted by ℓ_1 -minimization for face recognition under different illumination and occlusion. *Math. Probl. Eng.* **2017**, 1–16 (2017)
47. Satange, D., Alsubari, A., Ramteke, R. (eds.): Composite feature extraction based on Gabor and Zernike moments for face recognition. In: IOSR-JCE, International Conference on Recent Advance in Computer Science, Engineering and Technology, Aurangabad (2017)
48. Nakada, M., Wang, H., Terzopoulos, D. (eds.): AcFR: active face recognition using convolutional neural networks. In: 2017 IEEE Conference on Computer Vision and Pattern Recognition Workshops (CVPRW). IEEE (2017)
49. Fan, C., Wang, S., Zhang, H.: Efficient Gabor phase based illumination invariant for face recognition. In: Advances in Multimedia (2017)
50. McLaughlin, N., Ming, J., Crookes, D.: Largest matching areas for illumination and occlusion robust face recognition. *IEEE Trans. Cybernet.* **47**(3), 796–808 (2017)
51. Harouni, M., Baghmaleki, H.Y.: Color image segmentation metrics. In: Encyclopedia of Image Processing, p. 95 (2018)
52. Tajbakhsh, N., Araabi, B., Soltanian-Zadeh, H.: Robust iris verification based on local and global variations. *EURASIP J. Adv. Sig. Process.* **2010**(1), 979058 (2010)
53. Radman, A., Jumari, K., Zainal, N.: Iris segmentation in visible wavelength environment. *Proc. Eng.* **41**, 743–748 (2012)
54. Raja, K.B., Raghavendra, R., Vemuri, V.K., Busch, C.: Smartphone based visible iris recognition using deep sparse filtering. *Pattern Recogn. Lett.* **57**, 33–42 (2015)
55. Jillela, R.R., Ross, A.: Segmenting iris images in the visible spectrum with applications in mobile biometrics. *Pattern Recogn. Lett.* **57**, 4–16 (2015)
56. Liu, Y., He, F., Zhu, X., Liu, Z., Chen, Y., Han, Y., et al.: The improved characteristics of bionic Gabor representations by combining with sift key-points for iris recognition. *J. Bionic Eng.* **12**(3), 504–517 (2015)
57. Li, C., Zhou, W., Yuan, S.: Iris recognition based on a novel variation of local binary pattern. *Vis. Comput.* **31**(10), 1419–1429 (2015)
58. Salve, S.S., Narote, S. (eds.): Iris recognition using SVM and ANN. In: 2016 International Conference on Wireless Communications, Signal Processing and Networking (WiSPNET). IEEE (2016)
59. Suciati, N., Anugrah, A.B., Faticah, C., Tjandrasa, H., Arifin, A.Z., Purwitasari, D., et al. (eds.): Feature extraction using statistical moments of wavelet transform for iris recognition. In: 2016 International Conference on Information and Communication Technology and Systems (ICTS). IEEE (2016)
60. Trokielewicz, M., Czajka, A., Maciejewicz, P.: Implications of ocular pathologies for iris recognition reliability. *Image Vis. Comput.* **58**, 158–167 (2017)
61. Umer, S., Dhara, B.C., Chanda, B.: A novel cancelable iris recognition system based on feature learning techniques. *Inf. Sci.* **406**, 102–118 (2017)
62. Ray, A., Mahapatra, N., Das, S.S., Mishra, A.: Iris recognition using Gabor filter and SURF feature detection technique. *IUP J. Inf. Tech.* **14**(2), 53–61 (2018)
63. Llano, E.G., Vázquez, M.S.G., Vargas, J.M.C., Fuentes, L.M.Z., Acosta, A.A.R.: Optimized robust multi-sensor scheme for simultaneous video and image iris recognition. *Pattern Recogn. Lett.* **101**, 44–51 (2018)
64. Păvăloiu, I., Niță, C.D., Lazăr, L.C. (eds.): Novel matching method for automatic iris recognition using SIFT features. In: 2019 International Symposium on Signals, Circuits and Systems (ISSCS). IEEE (2019)

65. Choudhary, M., Tiwari, V., Venkanna, U.: Enhancing human iris recognition performance in unconstrained environment using ensemble of convolutional and residual deep neural network models. *Soft Comput.* **24**(15), 1–15 (2019)
66. Abirami, M., Vasavi, J.: A qualitative performance comparison of supervised machine learning algorithms for iris recognition. *Eur. J. Mol. Clin. Med.* **7**(6), 1937–1946 (2020)
67. Abdo, A.A., Lawgali, A., Zohdy, A.K. (eds.): Iris recognition based on histogram equalization and discrete cosine transform. In: Proceedings of the 6th International Conference on Engineering and MIS 2020 (2020)
68. Khuzani, A.Z., Mashhadi, N., Heidari, M., Khaledyan, D.: An approach to human iris recognition using quantitative analysis of image features and machine learning. arXiv preprint arXiv:200905880 (2020)
69. Liu, Z., Yin, Y., Wang, H., Song, S., Li, Q.: Finger vein recognition with manifold learning. *J. Netw. Comput. Appl.* **33**(3), 275–282 (2010)
70. Yang, J., Li, X. (ed.) Efficient finger vein localization and recognition. In: 2010 International Conference on Pattern Recognition. IEEE (2010)
71. Guan, F., Wang, K., Yang, Q. (eds.): A study of two direction weighted (2D) 2 LDA for finger vein recognition. In: 2011 4th International Congress on Image and Signal Processing (CISP). IEEE (2011)
72. Lee, E.C., Jung, H., Kim, D.: New finger biometric method using near infrared imaging. *Sensors* **11**(3), 2319–2333 (2011)
73. Yang, W., Rao, Q., Liao, Q. (eds.): Personal identification for single sample using finger vein location and direction coding. In: 2011 International Conference on Hand-Based Biometrics (ICHB). IEEE (2011)
74. Rosdi, B.A., Shing, C.W., Suandi, S.A.: Finger vein recognition using local line binary pattern. *Sensors* **11**(12), 11357–11371 (2011)
75. Damavandinejadmonfared, S. (ed.): Finger vein recognition using linear kernel entropy component analysis. In: 2012 IEEE International Conference on Intelligent Computer Communication and Processing (ICCP). IEEE (2012)
76. Mobarakeh, A.K., Rizi, S.M., Khaniabadi, S.M., Bagheri, M.A., Nazari, S. (eds.): Applying weighted K -nearest centroid neighbor as classifier to improve the finger vein recognition performance. In: 2012 IEEE International Conference on Control System, Computing and Engineering (ICCSCE). IEEE (2012)
77. Harsha, P., Subashini, C. (eds.): A real time embedded novel finger-vein recognition system for authenticated on teller machine. In: 2012 International Conference on Emerging Trends in Electrical Engineering and Energy Management (ICETEEEM). IEEE (2012)
78. Meng, X., Yang, G., Yin, Y., Xiao, R.: Finger vein recognition based on local directional code. *Sensors* **12**(11), 14937–14952 (2012)
79. Yang, J., Shi, Y.: Towards finger-vein image restoration and enhancement for finger-vein recognition. *Inf. Sci.* **268**, 33–52 (2014)
80. Yang, G., Xiao, R., Yin, Y., Yang, L.: Finger vein recognition based on personalized weight maps. *Sensors* **13**(9), 12093–12112 (2013)
81. Lu, Y., Yoon, S., Xie, S.J., Yang, J., Wang, Z., Park, D.S. (eds.): Finger vein recognition using histogram of competitive Gabor responses. In: 2014 22nd International Conference on Pattern Recognition (ICPR). IEEE (2014)
82. Vlachos, M., Dermatas, E.: Finger vein segmentation from infrared images based on a modified separable Mumford Shah model and local entropy thresholding. *Comput. Math. Methods Med.* (2015)
83. Gupta, P., Gupta, P.: An accurate finger vein based verification system. *Digital Signal Process.* **38**, 43–52 (2015)
84. Wu, J.-D., Liu, C.-T.: Finger-vein pattern identification using SVM and neural network technique. *Expert Syst. Appl.* **38**(11), 14284–14289 (2011)
85. Wu, J.-D., Liu, C.-T.: Finger-vein pattern identification using principal component analysis and the neural network technique. *Expert Syst. Appl.* **38**(5), 5423–5427 (2011)

86. Hoshyar, A.N., Sulaiman, R., Houshyar, A.N.: Smart access control with finger vein authentication and neural network. *J Am. Sci.* **7**(9) (2011)
87. Wang, K.-Q., Khisa, A.S., Wu, X.-Q., Zhao, Q.-S. (eds.): Finger vein recognition using LBP variance with global matching. In: 2012 International Conference on Wavelet Analysis and Pattern Recognition (ICWAPR). IEEE (2012)
88. Khellat-Kihel, S., Cardoso, N., Monteiro, J., Benyettou, M. (eds.): Finger vein recognition using Gabor filter and support vector machine. In: 2014 First International Image Processing, Applications and Systems Conference (IPAS). IEEE (2014)
89. Radzi, S.A., Hani, M.K., Bakhteri, R.: Finger-vein biometric identification using convolutional neural network. *Turk. J. Electr. Eng. Comput. Sci.* **24**(3), 1863–1878 (2016)
90. Mitica-Valentin, M., Ana-Maria, T., Ciprian, R.: Biometric security: recognition according to the pattern of palm veins. *Sci. Bull. “Mircea cel Batran” Nav. Acad.* **23**(1), 257–262 (2020)
91. Hussein, I.S., Sahibuddin, S.B., Nordin, M.J., Sjarif, N.N.B.A.: Multimodal recognition system based on high-resolution palmprints. *IEEE Access* **8**, 56113–56123 (2020)
92. Yang, L., Yang, G., Wang, K., Liu, H., Xi, X., Yin, Y.: Point grouping method for finger vein recognition. *IEEE Access* **7**, 28185–28195 (2019)
93. Xi, X., Yang, L., Yin, Y.: Learning discriminative binary codes for finger vein recognition. *Pattern Recogn.* **66**, 26–33 (2017)
94. Qiu, X., Kang, W., Tian, S., Jia, W., Huang, Z.: Finger vein presentation attack detection using total variation decomposition. *IEEE Trans. Inf. Forensics Secur.* **13**(2), 465–477 (2017)
95. Wang, M., Tang, D.: Region of interest extraction for finger vein images with less information losses. *Multimed. Tools Appl.* **76**(13), 14937–14949 (2017)
96. Liu, H., Song, L., Yang, G., Yang, L., Yin, Y. (eds.): Customized local line binary pattern method for finger vein recognition. In: Chinese Conference on Biometric Recognition Springer (2017).
97. Soh, S.C., Ibrahim, M., Yakno, M.B., Mulvaney, D.J.: Palm vein recognition using scale invariant feature transform with RANSAC mismatching removal. In: IT Convergence and Security 2017, pp. 202–209. Springer (2018)
98. Fang, Y., Wu, Q., Kang, W.: A novel finger vein verification system based on two-stream convolutional network learning. *Neurocomputing* **290**, 100–107 (2018)
99. Qin, H., El-Yacoubi, M.A.: Deep representation for finger-vein image-quality assessment. *IEEE Trans. Circuits Syst. Video Technol.* **28**(8), 1677–1693 (2017)
100. Cancian, P., Di Donato, G.W., Rana, V., Santambrogio, M.D. (eds.): An embedded Gabor-based palm vein recognition system. In: 2017 IEEE EMBS International Conference on Biomedical and Health Informatics (BHI). IEEE (2017)
101. Akintoye, K.A., Shafry, M.R.M., Abdullah, A.H.: A novel approach for finger vein pattern enhancement using Gabor and Canney edge detector. *Int. J. Comput. Appl.* **157**(2) (2017)
102. Brindha, S.: Finger vein recognition. *Int. J. Renew. Energy Technol.* **4**, 1298–1300 (2017)
103. Wang, R., Wang, G., Chen, Z., Zeng, Z., Wang, Y.: A palm vein identification system based on Gabor wavelet features. *Neural Comput. Appl.* **24**(1), 161–168 (2014)
104. Wu, K.-S., Lee, J.-C., Lo, T.-M., Chang, K.-C., Chang, C.-P.: A secure palm vein recognition system. *J. Syst. Softw.* **86**(11), 2870–2876 (2013)
105. Bayoumi, S., Al-Zahrani, S., Sheikh, A., Al-Sebayel, G., Al-Magooshi, S., Al-Sayigh, S. (eds.): PCA-based palm vein authentication system. In: 2013 International Conference on Information Science and Applications (ICISA), 24–26 June 2013
106. Han, W.-Y., Lee, J.-C.: Palm vein recognition using adaptive Gabor filter. *Expert Syst. Appl.* **39**(18), 13225–13234 (2012)
107. Jalali, A., Mallipeddi, R., Lee, M. (eds.): Deformation invariant and contactless palmprint recognition using convolutional neural network. In: Proceedings of the 3rd International Conference on Human-Agent Interaction (2015)
108. Chai, T., Prasad, S., Wang, S.: Boosting palmprint identification with gender information using DeepNet. *Futur. Gener. Comput. Syst.* **99**, 41–53 (2019)

Computer-Aided Diagnosis of Pneumothorax Through X-Ray Images Using Deep Learning—A Review



Farwa Urooj, Shahzad Akbar, Syed Ale Hassan, Saba Firdous, and Muhammad Jawad Bashir

Abstract A pneumothorax is a severe ailment that can result in mortality in humans due to shortness of breath. Due to its complicated features and poor contrast of the disease areas, pneumothorax is a life-threatening but simple thoracic ailment that is hard to detect using chest X-ray imaging. The automated diagnosis of pneumothorax in health surveillance is difficult for radiologists. Early detection of a pneumothorax is crucial for improving treatment outcomes and patient survival. In the medical field, the identification of pneumothorax through image processing is a tricky task. Recently, a rise of interest has been noticed in employing deep learning algorithms to aid pneumothorax detection. Nowadays, different medical imaging tools are available to detect specific diseases. Chest radiographs are widely used to diagnose pneumothorax. Detection of pneumothorax at early stages can overcome the treatment difficulties. This chapter evaluates several innovative technologies and research that could help detect pneumothorax automatically. Artificial intelligence (AI) provides a significant result for automated pneumothorax (PTX) detection. Research has been done to see pneumothorax disease automatically through the chest radiograph. This article abstracts previous articles for detecting PTX from CXRs through machine and deep learning and also discusses different publicly available datasets. This study provides a detailed overview and discusses the existing literature's goodness and limitation. This literature chapter helps the researchers to find an optimal way to solve this problem and gives direction on which technique provides a better result.

Keywords Machine learning · Chest radiographs · Deep learning · Chest X-ray datasets · Pneumothorax diagnosis

F. Urooj · S. Akbar (✉) · S. A. Hassan · S. Firdous

Riphah College of Computing, Riphah International University, Faisalabad Campus, Faisalabad, Pakistan

e-mail: shahzadakbarbz@gmail.com

M. J. Bashir

School of Electrical Engineering and Computer Science, National University of Science and Technology (NUST), Islamabad, Pakistan

1 Introduction

Pneumothorax, often known as collapsed lung, is a condition in which air seeps into the pleural cavity [1]. The pressure in this breath causes the lungs to burst. Shortness of breath and abrupt and intense tightness in the chest are the most prevalent symptoms. It can develop for various reasons, including a chest injury or other lung diseases, but it can also arise for no apparent reason. The length of the pneumothorax-affected region varies significantly, and the extent of the collapsed lung determines the treatment. Furthermore, the intricate intersecting positions of the thoracic cavity and different parts and areas in patients make it challenging to identify the disease (Fig. 1).

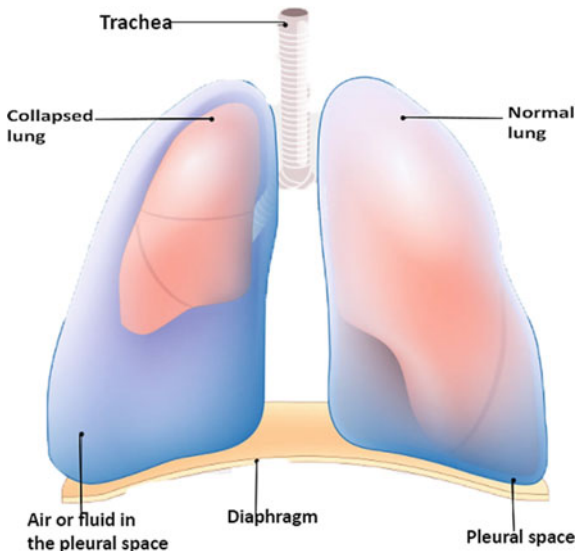
1.1 Types of Pneumothorax

There are some basic types of pneumothorax: The first one is traumatic and the second one is non-traumatic (spontaneous pneumothorax) [2].

Traumatic Pneumothorax. When the chest or lung wall has been traumatized or wounded, traumatic pneumothorax ensues. It could be minor or significant harm. Trauma can cause tissue destruction in the chest. Furthermore, it permits air to enter the pleural cavity [2].

Non-traumatic Pneumothorax. This type of pneumothorax does not occur as a result of an injury. Instead, it occurs spontaneously, given the nickname “spontaneous

Fig. 1 Pneumothorax anatomy [1]



pneumothorax". This type is future divided into two subtypes, namely primary and secondary spontaneous pneumothorax [3].

Primary Spontaneous Pneumothorax (PSP). PSP affects tall and skinny youngsters and arises in patients with no established lung illness. Some factors increase the risk of primary SP, such as smoking and weather change atmospheric pressure, and mainly occur in male between 10 and 30 ages. High chest pains and a slow plus rate are symptoms of a pneumothorax in these patients (tachycardia). It is necessary to get early recognition of the proper ailment since it is essential to rule out other, more life-threatening disorders with similar problems, such as a heart problem.

Secondary Spontaneous Pneumothorax (SSP). SSP mainly affects the old age patient with already known lungs problems. Underlying pulmonary disorders can cause pneumothoraxes such as "emphysema, COPD, tuberculosis, and cystic fibrosis". SSPs are severe than elementary lung disease that already weakens the patient's critical functions. The prevalence rate of both types is the same. In SSP, the exact location of pneumothorax is challenging to find.

Tension Pneumothorax. A tension pneumothorax can occur when the air around the lung increases in pressure for any reason. A tension pneumothorax is a common trauma consequence that needs prompt medical treatment.

1.2 Symptoms of Pneumothorax

When a pneumothorax arises due to trauma, the symptoms appear almost soon after the damage. Indication of a spontaneous PTX might occur when a patient is stable. A short episode of chest pain is typically the initial symptom, more complex chest pain, fast heart rate, shortness of breathing, and low blood pressure. An echoing sound will be heard if you tap your chest on one side [3].

1.3 Diagnosis and Treatment of Pneumothorax

The treatment depends upon the size and sensitivity of the pneumothorax. A few treatments are discussed [4].

Monitoring. If you have a small pneumothorax, your doctor may monitor you for signs of heart or breathing difficulties. A follow-up appointment with your provider will be scheduled.

Additional Oxygen. If you have a little pneumothorax but are experiencing pain, your doctor might recommend you more oxygen. Your clinician will watch and you ensure that your situation remains stable.

Needle Aspiration. A syringe is used to remove part of the oxygen out from thoracic region by a clinician. Percutaneous chest tube evacuation may be used after that.

Drainage of the Chest Tube. Your doctor may place a breathing cylinder into the chest to drain the air from the pulmonary area if you have had a severe pneumothorax. The lung swells and heals itself as the pressurization drops. This tube can be remained in position for several days or even weeks.

Chemical Pleurodesis. A physician can use pleurodesis with chemicals to keep the lung from collapsing again. Your physician makes an incision through which a tube is placed. The lung is then bound to the chest cavity with medications like doxycycline or talc, removing the additional space in the chest cavity.

1.4 Imaging Technology

Over the last two decades, medical imaging technology has led to a significant increase in medical testing for the early detection, diagnosis, and treatment of diseases. In health care, imaging plays an increasingly important role, and most patient care paths rely on a well-functioning radiology service to achieve the best results [5]. Pneumothorax is typically detected with a chest X-ray. In some cases, a computed tomography (CT) scanning might well be needed to provide more detailed images. Moreover, ultrasound imaging can also be used to diagnose a pneumothorax.

Computer Tomography. Disorders and damages can be diagnosed with a computed tomography (CT) scan. It uses a series of X-rays and a computer to build a 3D image of soft tissues and bones. CT scans, which are fast and non-invasive, can be used by your healthcare professional to detect ailments. A CT scan can be done in hospitals or imaging centers [6]. Chest CT scan is the most reliable imaging study for diagnosing pneumothorax. It is not suggested for frequent usage in pneumothorax. CT scan is used for tin PTX [7] (Fig. 2).

Ultrasound. Lung ultrasonography has a number of advantages, including the ease with which it can be used in an emergency situation, notably in patients within intensive care unit. As a result, instead of X-rays and CT scans, chest ultrasonography can also be used to identify the extent of a pneumothorax and monitor its progress in critical patients and patients with regular plain films who have a strong suspicion of pneumothorax [8] (Fig. 3).

Chest X-ray. One of most common imaging modalities is chest X-rays, which are used in millions of examinations each year across the world [9]. Because of its greater availability, inexpensive, non-invasive nature, accessibility, and ease of use, it is an appealing first choice for detecting a broad spectrum of thoracic disorders [9, 10].

The number of digital X-ray machines accessible in various parts of the world vastly outnumbers the number of specialists who can interpret and report on

Fig. 2 CT scan of pneumothorax [7]

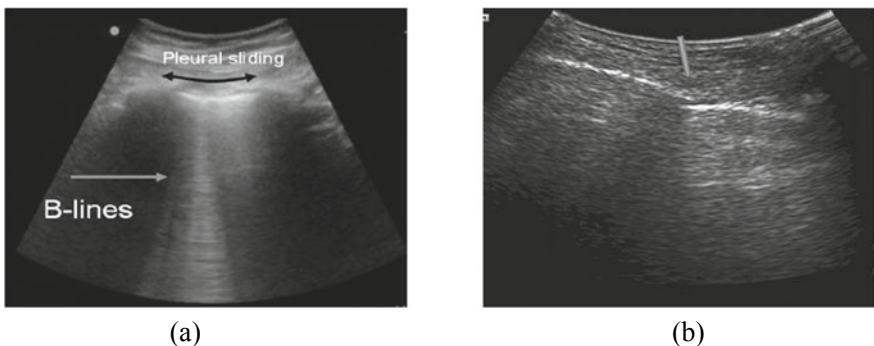
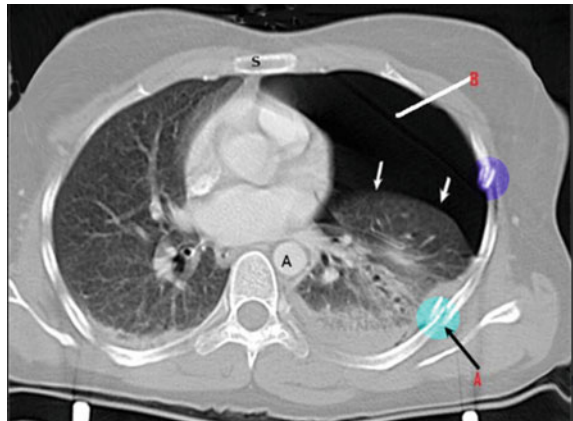


Fig. 3 Lungs ultrasound (a) normal and (b) pneumothorax [3]

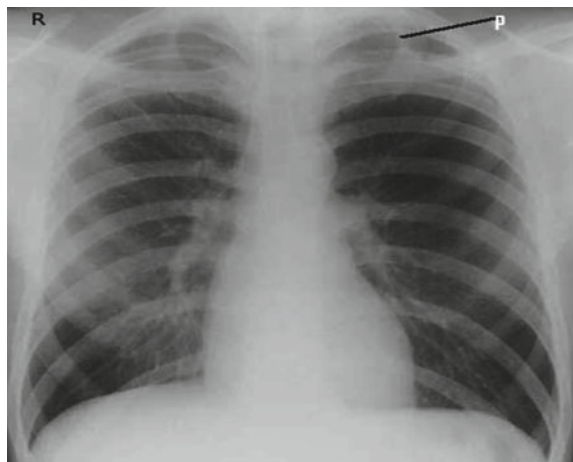
them. Backlogs, delayed diagnosis, fatigue-related diagnostic inaccuracies, and poor patient care are all consequences of personnel shortages in radiology (Fig. 4).

1.5 Publicly Available Dataset for Pneumothorax

This section discusses the publicly available dataset most commonly used for automatic pneumothorax detection. In short, only datasets with images labeled for a pneumothorax are significant to us. To learn the ultimate difference between healthy lungs and lungs with a pneumothorax, we would prefer to train on healthy lungs versus lungs with a pneumothorax.

NIH: ChestX-Ray14 Dataset. An exceptionally colossal chest X-Ray14 dataset comprising information from the national institutes of clinical health centers was introduced by Wang in 2017 [11]. The database includes 112,120 front-facing chest

Fig. 4 Chest X-ray of pneumothorax [9]



X-ray images of 30,805 patients. The NIH clinics' picture archiving and communication systems (PACS) were utilized to get the CXRs [12]. This dataset contained eight thoracic diseases, later expanded to 14. These 14 chest disease names are “pneumothorax, pneumonia, atelectasis, edema, union, emphysema, cardiomegaly, emanation, mass, fibrosis, penetration, hernia, pleural thickening, and knob”. A total of 60,412 CXRs out of 112,120 have no pathology, whereas 51,708 CXRs contain at least one disease. There are 5298 CXRs with pneumothorax in the whole dataset. Each CXR in this dataset has a resolution of 1024-by-1024 pixels. Aside from the CXR images, information such as the patient's sexual orientation, age, and CXR view location is also available. The chest radiography gives us more information about a patient's sexual orientation, age, and location of the pneumothorax is likewise accessible. The samples are separated so that CXRs out of the same individual were assigned to either the training or validating lists in this dataset (Fig. 5).

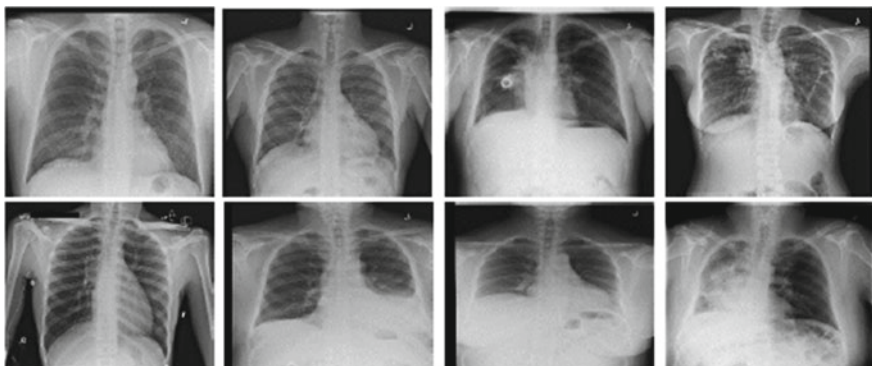


Fig. 5 NIH chest X-ray dataset sample [12]

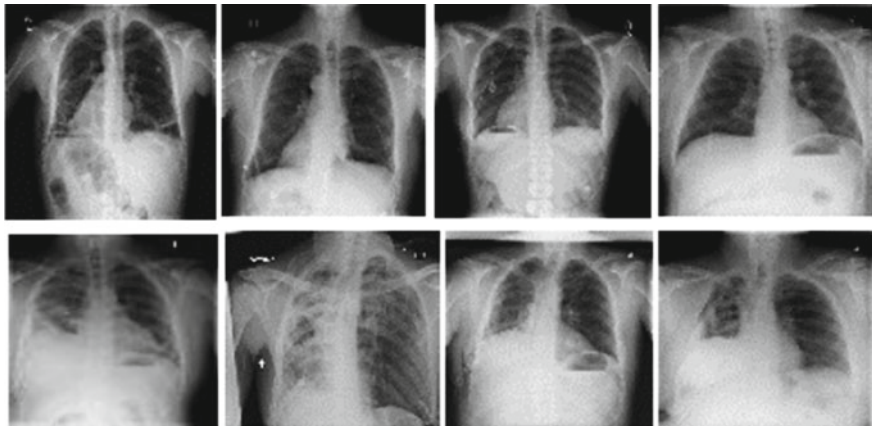


Fig. 6 SIIM-ACR chest X-ray dataset sample [14]

SIIM-ACR Dataset. The Society for Informatics in Medicine (SIIM) developed a new dataset in 2019. The images were taken from the NIH ChestX-Ray14 collection and then labeled at the pixel level with AI algorithms before being checked out by experienced radiologists [13]. The dataset is accessible on Cloud Healthcare, including CXR pictures in DICOM layout and matching masks in Run-Length Encoding (RLE) format for each image [14].

Moreover, there are two stages. In the first stage, 10,675 images (8296 X-rays are non-PTX and 2379 are PTX) are used for training purposes and 1372 for testing. In the second stage, samples are increased, 12,047 (2669 pneumothorax and 9378 images non-pneumothorax) images are used for training, and 3205 are used for testing (Fig. 6).

CheXpert Dataset. We use public datasets from various hospitals to develop a robust pneumothorax diagnosis system. The most commonly used dataset is CheXpert, presented by the Stanford ML in 2019 [15]. Its entire dataset comprises 224,316 CXRs from 65,420 people collected at Stanford Hospital between 2002 and 2017 [16]. In this dataset, each chest X-ray size is typically 320×320 . Other than ChestX-ray14, the Stanford ML group needed a high-quality dataset, so they released a dataset with many skilled labels. The dataset consists of 14 different chest diseases: “cardiomegaly, edema, fracture, lung opacity, pneumonia, consolidation, pleural effusion, pneumothorax, pleural other, atelectasis, enlarged cardiomom, and lung lesion, no finding, and support devices”.

This dataset is different because it includes an uncertainty label for each disease. There are 207,689 CXRs in the dataset consisting of at least one pathology and the remaining 16,627 X-ray images with no pathology. The dataset contains 17,313 confirmed pneumothorax images; 2663 X-ray images are not (Fig. 7).

MIMIC-CXR-JPG Dataset. The 2019 publicly accessible chest X-ray dataset consists of 377,110 CXRs images linked to 227,827 radiologic tests and span 14

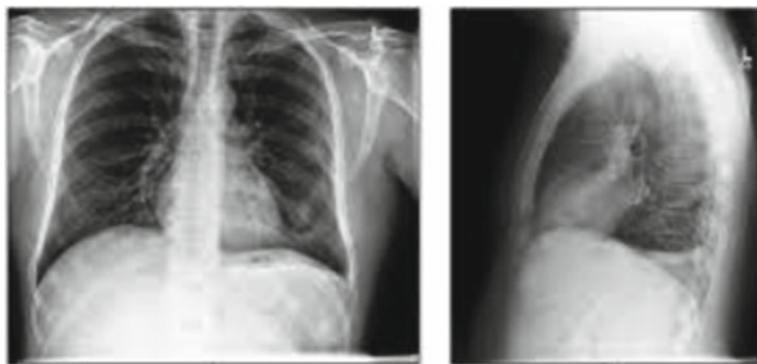


Fig. 7 CheXpert chest X-ray dataset sample [16]

different chest illnesses. These chest diseases are “lung lesion, fracture, lung opacity, no finding, atelectasis, pleural effusion, pneumothorax, pneumonia, cardiomegaly, edema, consolidation pleural, and support devices” [17]. There are 301,947 CXRs in the dataset consisting of at least one pathology and the remaining 75163 X-ray images with no pathology. The chest X-rays were obtained over five years from Beth Israel Deaconess Medical Centre (Massachusetts, USA) (2011 to 2016) (Fig. 8).

NIH Chest X-Ray Dataset (RS-NIH). RS-NIH is publically available on Kaggle that consists of 5% samples from the total dataset [18]. The data were chosen so that the percentage of the occurrence of each disease matches that of the NIH CXR14. This dataset contains 5606 CXR, covers the 14 different chest diseases, and contains a sample of no pathology. A total of 3044 CXRs are healthy, while the other 2562 CXRs are associated with one or more pathologies. Each CXR in this dataset has a

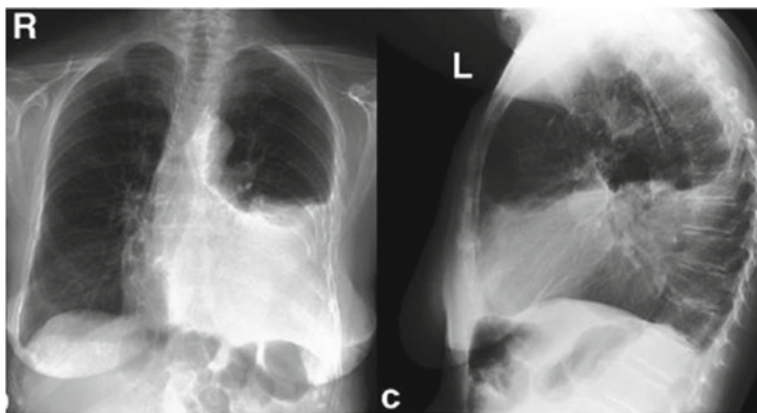


Fig. 8 MIMI-CXR chest X-ray dataset sample [17]

resolution of 1024-by-1024 pixels. In this, datasets 271 are confirmed pneumothorax images (Fig. 9).

In Fig. 10, the chart shows only pneumothorax images in each dataset, i.e.,

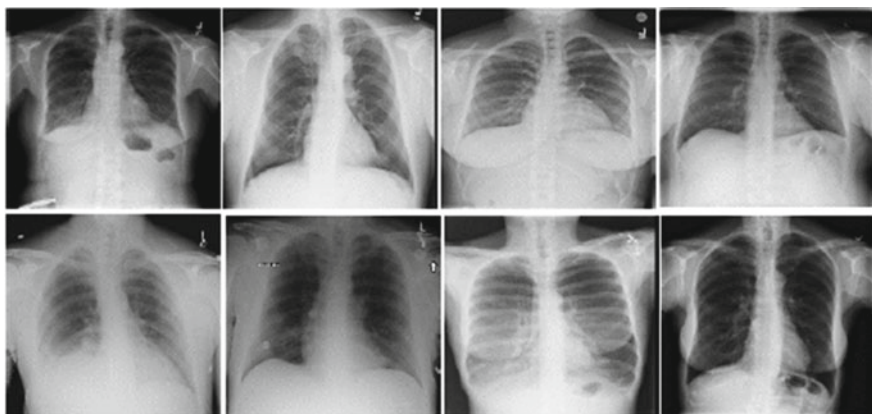


Fig. 9 RS-NIH chest X-ray dataset sample [12]

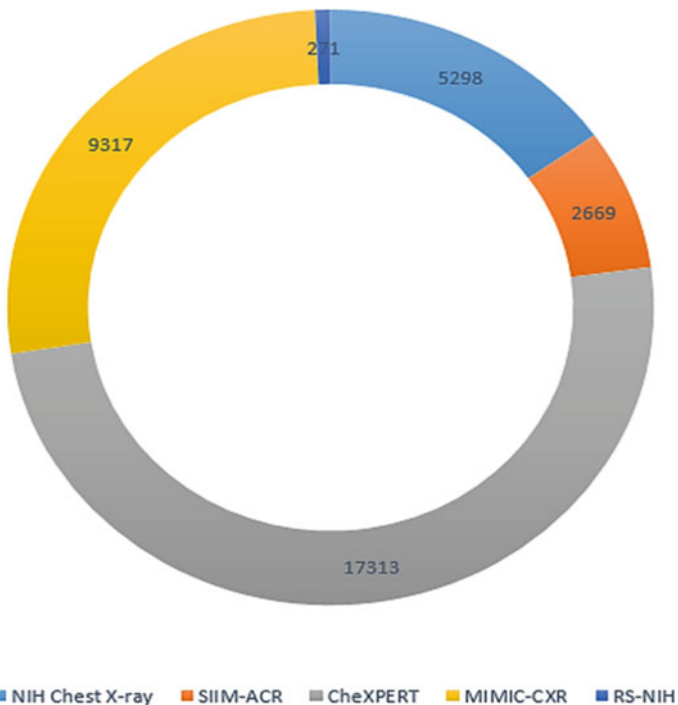


Fig. 10 Graphical representation of PTX images in each dataset

the CheXpert dataset consists of 224,316 images, of which 17,313 images are pneumothorax.

1.6 Goal of the Study

The results of a comprehensive study of PTX for the automatic detection procedure using chest X-ray images are presented in this chapter. This chapter aims to analyze the classification and localization of the PTX. Diagnostic, treatment and prevention can be achieved by analyzing optimistic algorithms. This chapter presents new insights into applying AI techniques to PTX. There is no comprehensive review of such technologies in the literature to our knowledge. This chapter presents recent approaches in pattern recognition based on pre-processing and segmentation techniques for CXRs that have already detected PTX.

2 Literature Review

A complete literature evaluation has been created in this area based on the methods given in the following:

- Locating advanced research items that are appropriate.
- Articles that focus on fundamental knowledge of the research problem (RP).
- A particular search strategy that pinpoints the research issue.
- Extraction the required data from the selected paper.
- Verification of and analyzing the information gathered (Fig. 11).

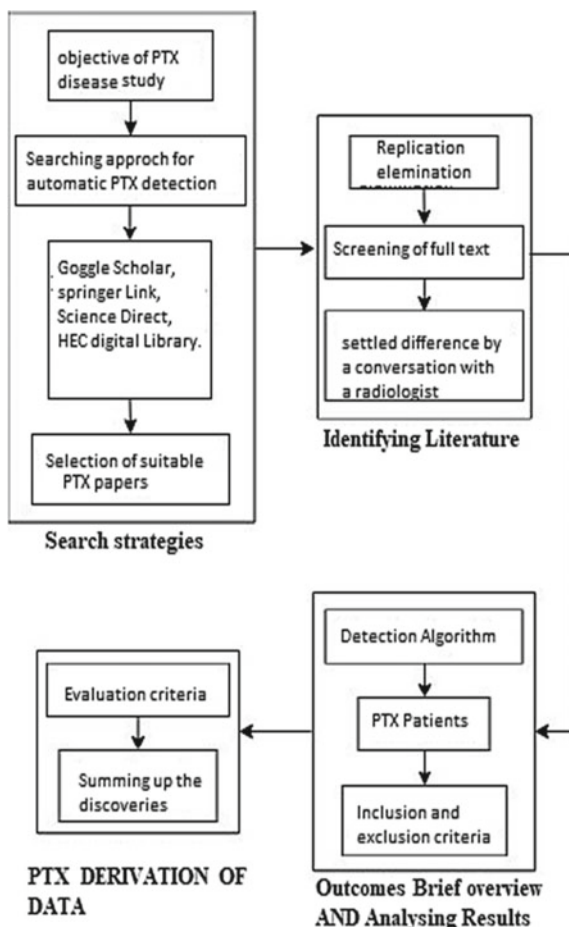
2.1 Search Strategies

The goal of the PTX disease study is defined and explained in this phase. In this selection for automatic PTX detection, many relevant research articles have already been chosen for additional analysis.

2.2 Identifying Literature

After providing a detailed search of PTX, the next step was to identify the prized articles for this study. In the review of each article, a chest radiologist was consulted to resolve any discrepancies and better understand the PTX.

Fig. 11 Flowchart of review process



2.3 PTX Derivation of Data

Throughout this phase, a variety of sophisticated PTX detection algorithms consisting of artificial intelligence, machine learning, and deep learning have been researched and analyzed. Moreover, a collection of cutting-edge algorithms emerged because of this process. Additionally, the results, advantages and drawbacks of these state-of-art methodologies have been mentioned in this chapter.

Finally, all of the findings were summarized after assessing the content quality. The following subsections provide an in-depth analysis of various technologies based on the latest PTX articles. After that, the journal selection criteria are briefly described, followed by the study's goal.

2.4 Standards Holistic Approach Data

The sign indication for the literature search is “Detection of PTX through CXR images using artificial intelligence”. The research prompt and facts were checked in each article’s abstracts, titles, and methodologies. We chose articles with a clear research domain for identifying and detecting PTX using chest X-ray scans. Additional parameter was created to assess the usage of bioinformatics and artificial intelligence to detect PTX disease.

2.5 Content Prohibiting Principles

The goal of this study is to bring together the methods and strategies that are used to segment PTX using chest X-ray images. However, the irrelevant algorithms about PTX disease were not considered in this chapter. The articles were also chosen based on the journal’s reputation and impact factor. Another factor was the number of references and institutional affiliations of the articles.

2.6 Journal Articles Selection

After a thorough investigation, the research publications were chosen for evaluation and prohibition standards. Initially, the papers that were chosen were copied and saved to the system library. Afterward, the title, publishing year, publisher, and author’s first and last initials were utilized to limit papers; this description aided in the selection of journal research articles. The references from many papers were collected and saved in the EndNote reference library. A database of documents was created drew on the above-mentioned selection criteria and including papers about the fundamental concepts of retinal ailments formed on human anatomy studies, the PTX disease and its subtypes, as well as recent research toward the application of AI algorithms to detect PTX automatically. These studies are examined in depth in the following sections.

2.7 Areas of This Analysis

The results of a detailed and comprehensive study of PTX algorithms for automatic segmentation of PTX from CXRs are presented in this chapter. The chapter’s primary goal is to evolve PTX algorithms and detect PTX from CXRs. Optimistic algorithms for diagnosis, treatment, and prevention have some clinical benefits. This chapter

offers new perspectives on applying AI techniques to PTX. There is no comprehensive review of such technologies in the literature as far as we know. The goal of this research is to look at current trend identification techniques that have successfully recognized PTX using pre-processing and segmentation strategies from chest X-ray images.

2.8 *Pneumothorax Detection Techniques Base on AI*

Training, validation, and testing are the three phases of artificial intelligence (AI) systems for image categorization. AI technique includes ML and DL. AI and deep learning are revolutionary technologies that have accelerated from a futuristic promise to a contemporary reality at an unfathomable rate. AI and ML (machine learning) have started to penetrate all areas of life, and they are now being used in health care. ML is divided into supervised, unsupervised, and reinforcement learning. A variety of medical applications use classification algorithms. There are a few types of machine learning algorithms for detecting PTX. Example of ML techniques is SVM (support vector machine), KNN (*K*-nearest neighbors), regression, and decision tree.

In this section, the existing valuable literature encompassing detection pneumothorax is presented for PTX detection, and different DL/ML techniques are described. The quality research studies are highlighted in each case, along with brief explanations and any flaws. There is a discussion of all conceivable PTX categories, including classification, localization, and combining them both. In classification, articles describe chest X-ray images as PTX or normal? Only the area of PTX was discussed in localization papers.

Antonio Sze et al. [19] proposed a method to use Auto Thorax-Net, a feature generator. The suggested structure involves three essential steps: (1) deep feature tagging (all X-ray images add the database into a pre-trained network for features extract); (2) image finding; and (3) categorization. Three large public datasets (MIMIC-CXR, CheXpert, ChestX-ray14) were used in this experiment. The experiment's major goal is to test the efficiency of image search using deep feature matching. On an extensive archive of X-ray images, Auto Thorax-Net can provide a clear and more consistent result rather than CheXNet. Auto Thorax-Net has achieved the highest AUC (92%) and specificity of 84%. CheXNet delivers AUC (88%) and specificity of 70%. The results showed that Auto Thorax-Net improves classification performance better than traditional principle component analysis (PCA).

Li et al. [20] proposed a method that uses two deep learning classifiers to differentiate between normal and PTX on chest CT. CNN and SVM classifier is used to detect pneumothoraces on chest CT rapidly. Eighty chest CTs were used to train an eight-layer convolutional neural network (CNN) utilizing constant-size (36 * 36 pixels) 2D image patches. SVM (support vector machine) was used to train for classification. CNN generates the heat map. The heart maps were further described by (1) the size of the pneumothorax, (2) the region's relative position to the lung wall, and

(3) a shape feature based on regional anisotropy. The proposed technique provided a 100% sensitivity (all 160/160 pneumothoraxes detection) and specificity as 82.5% (true negative 33/40).

Wang et al. [21] proposed a CNN method used for pneumothorax segmentation, called CheXLocNet. CheXLocNet generates a high-quality segmentation mask and accurate classification results for pneumothorax. The dataset was obtained from SIIM-ACR pneumothorax used for training and validation. CheXLocNet is trained on six different hyperparameters. Six CheXLocNet datasets were trained and tested individually first. The two CheXLocNet datasets with the best sensitivity or specificity were combined to make an ensemble model. CheXLocNet trained dataset to consist of 2079 radiography with annotated and evaluated on (1082 non-pneumothorax images and 290 pneumothorax radiographs). The proposed method CheXLocNet provides the best sensitivity and provides an accuracy of 0.87% and a specificity of 0.78%.

Chan et al. [22] presented a framework which mainly used LBP, SVM, Sobel edge detection, and multi-scale intensity texture. SVM was used to recognize common pneumothorax—the first strategy LBP (“local binary pattern”) is used for feature extraction from lung images. Classification is done through SVM. The second automatic PTX prediction approach relies on multi-scale intensity texture segmentation, which eliminates the backdrop and other distracting elements from chest images. The rib limits are quickly impacted; Sobel edge diagnosis was used to identify it. The proposed method provided different accuracy on different patch sizes. Ten normal and 32 traumatic pneumothorax CXRs were used in this study. The proposed method provided 85.8% accuracy, 83.6% precision, and sensitivity 87.4% on 5 * 5 patch size.

In Lindsey et al. [23,] the proposed method shows how deep neural networks can provide accurate chest photographs and video interpretations. Processing techniques are used to achieve this result. Many deep neural network architecture models (CNN, Visual Geometry Group (VGG16), VGG19, ResNet50, Bayesian) are used to be examined to identify reliable designs for our application. Pre-trained CNN models have been used for large datasets; for example, ImageNet contains one million images. Porcine clinical ultrasonography data sources for lung health were provided by the United States AISR Institute. Dataset PTX category binary labels with ground-truth 404 Mmode (209 BMP, 195jpg) and 420 B-mode mp4 video clips. In this proposed method, two modes are used M-mode and B-model. They provide binary categorization validation AUCs of 98.3% for M-model images and B-mode video frames with 99.8%.

Andrew et al. [24] put forward a framework to identify the significant and moderate PTX on CXRs images. These algorithms trained on a large set of positive and negative chest X-rays. Firstly, I trained the algorithm labeled each image for the non-appearance of PTX and the idea of pneumothorax size. This method works well on large and moderate pneumothorax rather than small. A total of 13,292 frontal chest X-rays are used for the dataset on a ratio of 70:30. Multiple network models were trained and evaluated on ChestX-ray14. Validation is done at two levels (internal and external). The algorithm outperformed with a sensitivity of 0.84% and a specificity of 0.97% on a dataset.

Park et al. [25] proposed a method to calculate the performance of the convolutional neural network (CNN) to detect the symptom of PTX from the chest radiographs. PTNB is mainly used for the detection of pulmonary lesions. The dataset came from two tertiary referral hospitals composed of PACs (picture archiving and communication system). It consisted of 1343 PTX images arbitrarily fragmented at a 9:1 ratio into validation and training data. For internal validation, 250 standard images and 253 disease CXRs are used. The specificity and sensitivity of pneumothorax detection were 96.4% (241/250) and 89.7% (227/253), respectively, and AUC was 0.984.

Sebastian et al. [26] developed a deep residual U-Net model for automatically detecting pneumothorax on chest CT (computed tomography). PTX accuracy is graded at two levels, namely volume level and pixel level. A PTX is present or not in volume-level labeled images. Classification is at the level of the pixel (quantification and segmentation of pneumothorax). This method obtained an AUC of 0.98, an average precision of 0.97, and a DSC of 0.94. The volume-level accuracy of 567 chest CT scans was tested, with 167 images containing pneumothorax and 400 normal images. And the AUC was 0.98, with an average precision of 0.95. A DSC of 0.92 performance segmentation was similar to the inter-rater segmentation at the pixel level.

Geva et al. [27] proposed automatically detecting pneumothorax abnormality in CXRs. The developed method consists of two main stages: texture analysis and global image representation. Local abnormalities detected through the texture analysis process for this purpose used two states of the art: (1) LBP and (2) MRF (“maximum response filters”). The global representation is used to detect and train the image-level abnormalities. The unique features of PTX are mainly focused. The supervised training method is used to train the system at both stages. Dataset used in this research consists of 108 upright CXRs in which 48 images are pneumothorax, 19 images have one or more of the following pathologies but do not contain pneumothorax, but 41 remaining images are healthy lungs. This method yielded a sensitivity of 81% and a specificity of 87%.

Rajpurkar et al. [28] presented an automated technique to utilizing CheXNeXt framework. The goal of this study is to compare CheXNeXt’s performance on the elevation of pathologies in CXRs to that of practicing radiologists. The CheXNeXt incidentally predicts the appearance of 14 different pathologies, including “pneumothorax, pneumonia, hernia, cardiomegaly, atelectasis pulmonary masses, pleural effusion, and nodules” in frontal-view CXRs. It is trained on the ChestX-ray80 dataset, and validation consists of 420 images; at least 50 cases are required for each original pathology label. CheXNeXt did not obtain radiologist-level performance on three pathologies and obtained on other 11 pathologies. CheXNeXt achieves better performance in detecting atelectasis rather than a radiologist. The radiologist achieved AUC on cardiomegaly, hernia, and emphysema: 0.888 (0.863 to 0.910), 0.985 (0.974 to 0.991), and 0.911 (95% CI 0.866–0.947), respectively.

Pranav et al. [29] proposed a 121-layer CNN architecture called CheXNet to diagnose 14 diseases from chest radiographs. CheXNet is trained on ChestX-ray14 containing over 100,000 frontal-view X-ray. CheXNet was first present to diagnose

pneumonia, but it was later expanded to include different thoracic disorders. The trained model created a binary labeled vector with a length equal to all classes in the classification task that is 14. In order to conduct the task of pneumonia evaluation, authors inconstantly went through the process of data splitting in such a manner that 70% (28,744 patients, 98,637 images) was used for training and 10% for validation (1672 patients, 6351 images) and the remaining 20% (389 patients, 420 images) was declared as the test set. Before entering the image in the network resolution of 224×224 , there is no subject crossover here between groups. The proposed model achieves performance on AUC of 88.87% for pneumothorax.

Cho et al., [30] proposed a method to identify the performance of small artificial neural networks (ANNs) for the automatic exact location of PTX from the X-ray images. The Kim-Monte Carlo algorithm is used to identify the place of PTX. This study examines the comparison between the two DL methods, namely ANNs (“artificial neural networks”) and CNNs (“convolutional neural networks”). The original pixel resolution of X-ray images (512×512) was reduced to 20×20 , 30×30 , 40×40 , 60×60 , and 80×80 pixels in the ANN model. CNN applies to the same dataset with a different input pixel resolution of 256×256 . The performance of CNN is less than fully connected small ANN. The National Institutes of Health (NIH) pneumothorax dataset was used for this research. A total of 1000 chest X-ray images were casually selected. Every X-ray image with PTX was spilled into 49 boxes for PTX localization. Each box contained ROC’s test set, sensitivity was 80.6%, specificity was 83.0%, and AUC was 0.882. ANN accurately detects the location, reduces pneumothorax’s diagnosing time, and increases effectiveness.

Xu et al. [31] put forward a framework utilizing chest X-ray images in order to detect multiple lesions. This paper presents an improved classification model using a CNN, LSTM (long short-term memory), association mining, an attention mechanism for identifying multiple lesions on CXRs. CNN-ATTENTION-LSTM (CAL) network takes advantage of the diagnosis of multiple types of data. The chest X-ray14 dataset used in this research is the largest accessible chest X-ray image. There are a total of 112,120 labeled chest X-ray images in ChestX-ray14 dataset, in which 51,759 images are labeled with lesion and other remaining (60,361) chest X-ray images are lesion-free.

Abiyev et al. [32] presented a CNN framework to diagnose chest diseases; architecture and design principles of CNN are discussed. CNN is evaluating to classify 12 common diseases, i.e., pneumonia, pneumothorax, consolidation, edema, emphysema, atelectasis, cardiomegaly, effusion, infiltration, mass, nodule, and fibrosis. Competitive neural networks (CPNNs) and backpropagation networks (BPNNs) diagnose chest diseases through chest X-ray images for comparative analysis. In both competitive and backpropagation networks, a pixel size of 32×32 was set as input to achieve a high recognition rate and performance. The data obtained 120,120 images from NIH (National Institutes of Health—Clinical Centre), and CNN used 70% data for training and 30% for testing. CNN achieves a high recognition rate rather than other networks. The three models (CNN, BPNN, and CPNN) achieved 92.4%, 80.04%, and 89.57% accuracy, respectively.

Wang et al. [33] presented a robust chest radiograph database (Chest-ray8)-based research to locate and classify several diseases through X-ray scans. The database consists of 108,948 frontal-view X-ray images, of which 24,636 images contain multiple pathologies and other remaining (84,312) are normal images. Eight different diseases (“infiltration, mass, nodule, pneumonia, pneumothorax, atelectasis, cardiomegaly, effusion”) images are involved in this database. The proposed method uses a CNN deep learning classifier; 70% of data were used for training and the rest of the 30% images were used for testing. Different CNN architecture (AlexNet, GoogleNet, ResNet50, and VGG16) is used for multiple-label pathologies. ResNet50 model achieves the best result on pneumothorax ($AUC = 0.7891$) and cardiomegaly ($AUC = 0.8141$) compared with others. Deep convolutional neural networks (DCNNs) are used to detect one or many diseases that are present in each X-ray image.

Hieu et al. [10] developed a framework for analyzing and diagnosing 14 typical lung disorders from hundreds of CXR images using a trained multi-label classification framework based on CNN. The proposed method considers on CheXpert dataset that is the largest and openly available. CheXpert dataset consists of 224,316 CXRs, in which 65,240 unique patients are labeled for the existence of 14 everyday CXR observations. The whole dataset (224,316) was used for the training set, and a testing set consists of 200 scans. The experiment consisted of 14 common chest diseases. CheXpert dataset achieves an AUC of 0.940 in evaluating four diseases (pleural effusion, cardiomegaly, atelectasis, and edema) from the validation set. LSR (label smoothing regularization) is used for the better handling of uncertain samples. Geographical variation is the limitation of this model.

Andre et al. [34] proposed three different deep learning techniques for automatic prediction and localization of PTX. The dataset obtained from UWMC (University of Washington Medical Centre) contains 1003 CXRs, 437 images with pneumothorax and 566 with different or no abnormalities. The first deep learning (DL) approach includes CNN that is most widely used for classification task. The second deep learning technique is MIL (multiple instance Learning), which was utilized for both classification and localization. The third is FCN (fully convolutional network) technique allowing for semantic segmentation. A pre-trained ResNet50 architecture with a resolution of 448×448 was precisely trained for convolutional neural network (CNN) on single-channel input. For FCN (fully convolutional network), the position of PTX was determined using a U-Net model. The AUC of the CNN models was 0.96, and that of the other two models was 0.93 and 0.92, respectively. In this proposed method, FCN and MIL perform well for detecting the location purpose, and CCN achieves the best result for the classification of pneumothorax. In this way, internal rather than extremal dataset is validated.

Karan et al. [35] designed a U-Net approach for the rapid and precise identification of pneumothorax. A segmentation model was presented to correctly assess the lung region influenced by PTX. To assist the clinicians in determining the position and extent of the pneumothorax, a binary mask was created. The classic encoder portion was put back with the ResNet architecture, which utilized the U-Net architecture.

U-Net architecture provides effective results in medical image segmentation. In addition to shrinking the input photographs from 1024×1024 to 256×256 , contrast correction was performed to ensure that the image had a uniform color spectrum. The SIIM PTX dataset, which contains 12,047 chest radiographic images, was used for the investigation. Performance of the model was evaluated on two metrics, namely IoU (intersection over union) 82.6% result and DSC (dice coefficient score) 84.3%.

In Qingfeng et al. [36], in a novel segmentation architecture for diagnosis, the residence of PTX was proposed. Pixel-wise-level supervised network is used to identify pneumothorax and automatic segmentation. The proposed framework combines three modules: fully convolutional DenseNet, multi-scale module, and scSE. In this study, single-channel images with a resolution of 256×256 were used. The dataset utilized in this study was employed from PACs. The trained model achieved a DSC of 92.0% and mean pixel accuracy of 93.01%.

In Ecem et al. [37], architecture for automatically segmenting pathology regions was proposed. For segmentation, the main goal of this architecture was to reduce the reliance on pixel-level annotation. There was a deep learning-based architecture proposal for autonomously segmenting pathological regions. This framework's primary purpose was to lessen segmentation's dependency on PL ("pixel-level") annotations. The initial step was to train an image-level classifier that detected the CXR picture class and created attention masks that provided a rough approximation of the disease region. The spatial label smoothing regularization (SLSR) technique was used to rectify several flaws in these masks. That is, (i) the classifier was tested employing numerous well-annotated pixel-level pictures and masks generated by the image level classifier. The SLSR technique was used to correct some errors in these masks. (ii) Well-annotated images at the pixel level were used for training the segmentation model, as well as the masks created by the image-level classifier. The ResNet101 model was used for image-level classification, and the guided attention inference network (GAIN) was used to obtain the weakly annotated masks. Three different frameworks, including U-Net, Link-Net, and Tiramisu, are used for segmentation (FCDenseNet67).

Tae et al. [38] proposed an ensemble-based framework for distinguishing between normal and PTX chest radiography. The cooperative model was built from three identical convolutional neural network architectures trained on different size inputs. Rescaling an image with numerous sizes, such as 512×512 , 384×384 , and 256×256 , can help to preserve lost information during the resizing process. Based on each image-sized input, three ResNet models are trained. The best classification result is computed using the average softmax outputs of the three models—ImageNet weights used for model initialization. Publically available dataset chest X-ray was used in this experiment. A total of 100,000 CXRs images are used in technique: 59,156 healthy images and 5225 disease images were used. A total of 64,381 CXRs images were inconstantly split into 8:2 ratios for training and testing, respectively; rather than using the probability from the softmax layer directly, a split value was chosen to increase the total of specificity and sensitivity in the ROC curve and minimize class imbalance. The ensemble model had an area under the curve of 91.1% for PTX prediction when evaluated on the testing set.

Lan et al. [39] propose a method to predict the abnormality of chest radiography; the primary purpose of this research is to figure out the effective and efficient CNN (conventional neural network). Two datasets are used in this research: a National Institute of Health and Rhode Island Hospital (RIH-CXR). The model was trained on two different CNN architectures, namely Net and Mobile Net V2, and they categorize the chest radiography into standard and diseases images. The NIH-CXR models were also used to recognize 14 other pathological features. There seems to be no external data validation for disease diagnoses because the data from Rhode Island Hospital only supplied healthy/unhealthy designations. On PTX prediction, MobileNetV2 and DenseNet get AUROC (“area under the receiver operating characteristic curves”) of 0.883 and 0.898, correspondingly. This lightweight network like MobileNetV2 can nonetheless deliver good results. They conclude that networks trained on one dataset perform well on other datasets, except with poorer efficiency for normal/abnormal predictions.

Blumenfeld et al. [40] proposed a method to use CNN for pixel classification. Four key steps are involved in this framework: (1) lungs field segmentation; (2) image extraction; (3) classification; and (4) decision making. The primary purpose of the experiment is to verify the performance of image search using deep feature matching. Dataset was obtained from the “Diagnostic Imaging Department of Sheba Medical Centre (Tel-Hashomer, Israel)”. The dataset was divided into two sets: training and testing. A total of 203 posteroanterior images were composed in which 117 images were used in training and 86 images were used in testing. CNN has achieved an AUC of 0.95, a specificity of 80.6%, and a sensitivity of 95.4%. The results showed that CNN improves classification performance better than others.

Crosby et al. [41] proposed a VGG19 neural network to detect and local PTX. This model helps to distinguish between images that have or have not PTX. CXRs are split into two apex images in this method and extract 256×256 input size patches from apex images. Two network models are used: the first one for apex images and the second one for used 256×256 pixels patches. The network was fine-tuned with 240 CXR consisting of PTX. This network provided AUROC = 0.80 accuracy on fine-tuned apex images, and high-resolution 256×256 pixel patches provided AUROC = 0.73.

Wang et al. [42] designed a segmentation framework in order to detect pneumothorax in CXRs. The proposed deep learning method consists of two main stages. The first stage used multiple modified U-Net models to classify the image having PTX or not. The second stage includes several U-Net-like models, i.e., SE-Resnext50, SE-Resnext101, and EfficientNet-B5, as well as one deeplabv3+ model enabling reliable segmentation of PTX region. During the first stage, multitask networks provide an excellent classification performance rather than training a single model. For PTX-positive images, the segmentation task employs detailed annotated data that aids classifier targets on other more relevant regions in achieving higher classification accuracy. In both stages, the supervised learning technique was employed to train the system. The model validation is done on the SIIM-ACR challenges dataset. This method provided a Dice score of 0.8883 and an AUC of 0.9795.

Yimer et al. [43] proposed a method that used a state-of-the-art Xception model of CNN to classify various lung illnesses. The dataset was obtained from two different places for model training validation and testing. The publically available NIH (National Institute of Health) dataset used 11,716 label X-ray images and 443 images were obtained from local JUMC (Jimma University Medical Centre). The model was classified on five lung diseases (PTX, pneumonia, tuberculosis, lung cancer, COPD). A total of 2038 PTX images were taken from the NIH dataset, and 19 PTX images were obtained from JUMC. The Xception model provides a sensitivity on PTX of 97.3, a specificity of 98.9%, and an accuracy of 97.3%.

Wang et al. [44] presented a framework that used a DCNN (deep convolutional neural network) to detect pneumothorax. The ResNet101 deep residual network was adjusted via transfer learning. The dataset was obtained from NIH pneumothorax used to train and validate. A total of 5302 PTX images were used from this dataset. For train, the system images are divided into positive and negative categories. Images are divided randomly in 70% and 30% ratios. The proposed model ResNet101 provides the sensitivity of 85.8% and produced an AUC of 86.3% and a specificity of 86.7%. 92.13% accuracy achieves on ROC.

Groza and Kuzin [45] proposed a segmentation pipeline method for PTX detection through CXR images that consisted of post-processing conditioned, which used a three Link-Net networks. The dataset was obtained from a publicly available SIIM-ACR PTX segmentation dataset [46–48]. This dataset consists of two stages; in the first stage, 10,675 images are used for training, and both stages are used for the testing. They convert DICOM images into 8-bit PNG format for reduced the CPU load. The proposed model provides a Dice score of 0.881 at stage 1 and 0.861 at stage 2 [49–51].

Artificial intelligence (AI) technologies are quickly integrating into our daily lives. Nevertheless, numerous attempts are being taken in the field of healthcare science and medicine to include artificial intelligence developments for real-time medical diagnosis and treatment [52–54].

The detection and diagnosis of retinal diseases such as hypertensive retinopathy [55, 56], papilledema [57, 58], brain tumor [59–61], glaucoma [62–64], melanoma [65, 66], Alzheimer's [67] and central serous retinopathy [68, 69] can be performed through machine learning and deep learning methodologies using OCT and fundus images [70, 71] (Table 1).

3 Discussion

The review of different research papers shows that pneumothorax, often known as a collapsed lung, is a life-threatening medical condition. Pneumothorax is unpleasant and dangerous; thus, it must be treated as soon as possible. After reading the various articles on pneumothorax, we can see the different datasets, methodologies, and algorithms. Automated and semi-automatic models for pneumothorax identification

Table 1 Summary of pneumothorax detection based on machine/deep learning

References	Year	Authors	Techniques	Datasets	Results
[27]	2015	Geva, Ofir, Zimmerman-Moreno	LBP, texture analysis, KNN	Sheba Medical Center	Sensitivity = 81% Specificity = 87%
[11]	2017	Xiaosong Wang	CNN, DCNN	ChestX-ray8	<i>Classification</i> AUC = 0.7891
[38]	2017	Tae Joon Jun	50-layer ResNet, CNN	ChestX-ray	<i>Localization</i> Accuracy = 0.1836 On T(IoBB) = 0.5
[29]	2017	Pranav Rajpurkar	CheXNet DenseNet	ChestX-ray14	AUC = 0.911 AUC = 88.87
[22]	2018	Yuan-Hao Chan	SVM, LBP, Sobel edge, multi-scale intensity texture	CSMU Hospital, Taiwan	Accuracy 85.8%, Precision = 83.6%, Sensitivity = 87.4% on 5 * 5 patch
[24]	2018	Andrew G. Taylor	Multiple network model	NIH ChestX-ray14	Sensitivity = 0.84% Specificity = 0.97%
[28]	2018	Pranav Rajpurkar, Jeremy IrvinID	CheXNeXt algorithm		AUC on Cardiomegaly = 0.888 Hernia = 0.985, emphysema = 0.911
[32]	2018	Rahib H. Abiyev	CNN	NIH	Accuracy = 92.4
[40]	2018	Blumenfeld	CNN	Sheba Medical Center (Tel-Hashomer, Israel)	AUC = 0.95 Specificity = 80.6 Sensitivity = 9.54
[20]	2019	Xiang Li*, James H. Thrall	Eight-layer CNN, heat map, SVM		Sensitivity = 100% Specificity = 82.5%
[23]	2019	Tony Lindsey	CNN, VGG16, VGG19, ResNet50, Bayesian	US Army Institute of Surgical Research	Validation accuracies M-model = 98.3% B-model = 99.8%

(continued)

Table 1 (continued)

References	Year	Authors	Techniques	Datasets	Results
[25]	2019	Sohee Park, Sang Min Lea	CNN PTNB	PACs	Sensitivity = 89.7% Specificity = 96.4% AUC = 0.984
[10]	2019	Hieu H. Pham	Multi-label classification CNN, LSR	CheXpert	AUC = 0.940
[34]	2019	Andre Goen	CNN, FCN, MIL, U-Net	University of Washington Medical Centre	Performance evaluates on CNN AUC = 0.96 FCN AUC = 0.92 MIL AUC = 0.93
[35]	2019	Karan Jakhar	ResNet, U-Net	SIM	IoU = 82.6 DCS = 84.3
[36]	2019	Qingfeng Wang	DenseNet, scSE, multi-scale module	PACs	DCS = 92.01 MPA = 93.01
[39]	2019	Lan Pan	DenseNet-121 MobileNetV2	Chest-X-ray14	0.898 and 0.883
[21]	2020	Hongyu Wang	CheXLocNet	SIM_ACR	With best sensitivity (AUC = 0.87 Specificity = 0.78 Sensitivity = 0.78) With best specificity (AUC = 0.79 Specificity = 0.46 Sensitivity = 0.92
[26]	2020	Sebastian Röhricht, Thomas Schlegl	U-Net	Medical University of Vienna	AUC = 0.98% Average precision = 0.97% DSC = 0.94%

(continued)

Table 1 (continued)

References	Year	Authors	Techniques	Datasets	Results
[31]	2020	Shuaiping Xu, Junqi Guo	LSTM, CNN-ATTENTION-LSTM (CAL), CLA	ChestX-ray14	AUC = 0.791 Accuracy 85.4%
[41]	2020	Jennie Crosby	VGG19; Apex-based network	ChestX-ray8	AUROC = 0.80 AUROC = 0.73
[45]	2020	Vladimir Groza et al. [45]	Se-resnext50, se-resnext101 and SENet154	SIM-ACR	Dice score = 86%
[19]	2021	Antonio Sze-To	Auto Thorax-Net	MIMIC-CXR, CheXpert, ChestX-ray14	AUC = 92% Specificity = 84%
[30]	2021	Yongil Cho, Jong Soo Kim	ANN, Kim-Monte Carlo	NIH	Sensitivity = 80.6 Specificity = 83.0 AUC = 0.882
[37]	2021	Ecem Sogancioglu	SLSR, ResNet101, GAIN U-Net, linkNet	ChestX-ray14	
[42]	2021	Xiyue Wang	U-Net (SE-Resnext50, SE-Resnext101, EfficientNet-B5), deeplabv3+	SIM-ACR	Dice score of 0.88883 and AUC of 0.9795
[43]	2021	Fethya Seid	Xception model	NIH and Jimma University Medical Center	Sensitivity = 97.3 Specificity = 98.9% Accuracy = 97.3%
[44]	2021	Ziqi Wang	DCNN ResNet-101	NIH	Sensitivity = 85.8% Specificity = 86.7% Accuracy = 86.3% AUC = 92.13%

have already been developed, combining traditional image analysis techniques with ML/DL methodologies.

Deep learning provides efficient results to diagnose thoracic disease rather than machine learning. The scale of the databases and the expertise of the algorithms, on the other hand, have a considerable impact on the results. This capacity analyzes a descriptive and analytical review of the techniques in both categories (see tables and summary).

Figure 12 shows the accuracy comparisons between different classifiers. Moreover, this meta-analysis of earlier investigations discovered numerous approaches, including CNN, U-Net, KNN, ANN, and SVM algorithms. The results' accuracy, sensitivity, and specificity are all described. Auto Thorax-Net, CNN, and ANN algorithms provide an excellent development for detecting pneumothorax, and mostly, ChestX-ray14, NIH, and SIIM-ACR datasets are used.

We have analyzed different PTX detection techniques and methodologies after reviewing 28 relevant papers. The table shows the key information about ML/DL technologies related to the publications. These data include the author's name, year, key techniques, dataset, and results. The machine learning technique is divided into three main sections: supervised learning, unsupervised learning, and reinforcement learning. In a comprehensive analysis, it can be determined that the classic DL approach to diagnosing PTX gives excellent results in both accuracy and reliability. AI has flourished over the past few years. Applying the ML/DL algorithm resulted in extraordinary advances in imagology. Most work is done on DL. Traditional machine learning techniques were limited by the difficult feature engineering, considerable domain knowledge, and data processing expertise necessary to extract the core discriminative features needed to train non-deep learning models. Deep

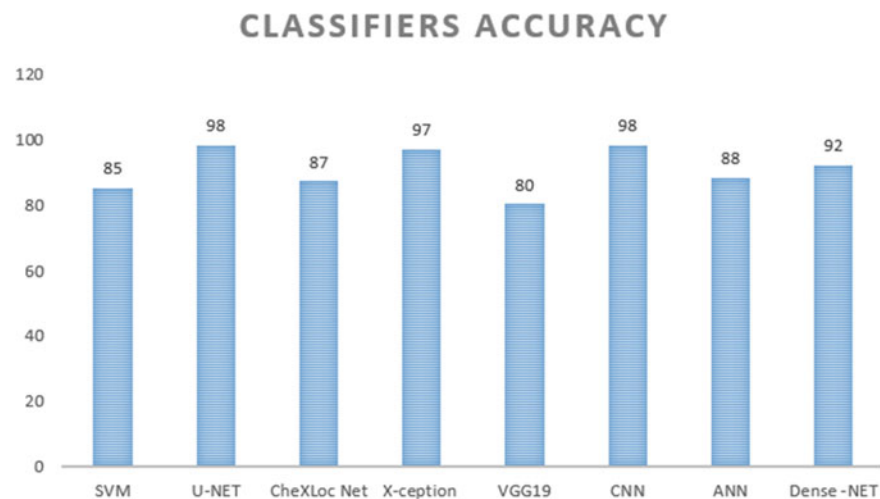
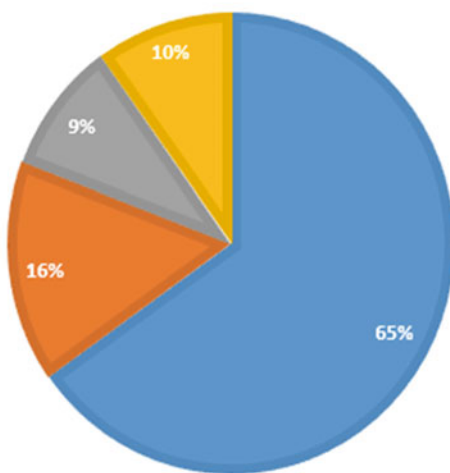


Fig. 12 Comparison of different classifiers accuracy

Fig. 13 Classifiers used in pneumothorax detection

CLASSIFIERS USED IN PTX DETECTION

CNN U-NET SVM KNN&ANN



learning systems, on the other hand, can automate the feature extraction and classification phases, thereby moving a load of feature engineering away from humans. CNN-based methods are most commonly used for PTX segmentation and classification. According to the literature review, 65% of work is done on CNN classifiers and 16% is done on U-Net for PTX diagnosis and localization. However, few works are done on machine learning. In the bar chart, you can see that most of the studies are based on the CNN architectures (“VGG19 VGG16, ResNet, DenseNet”) compared with others (Fig. 13).

The deep learning technique, on the other hand, is significantly more useful for image processing methods and produces more precise findings than that of the traditional machine learning approaches. The result is determined by the size of the databases and the complexities of the algorithm. This chapter provides both a descriptive and analytical assessment for both categories.

The table shows that very little effort was already made for integrated classification and localization of the injured area for pneumothorax identification. Earlier, the SIIM-ACR dataset was extensively used by researchers, who used the NIH chest X-ray14, which contains the common 14 thoracic disorders. Furthermore, other datasets such as CheXpert and MIMIC-CXR-JPG concentrate on image-level labeling rather than pixel-level annotation. Achieving pixel-level labeling is difficult; yet, the localization of a disease, particularly pneumothorax, is critical because the size of the pneumothorax determines the treatment. This limitation can be overcome by providing localization solutions that limit pixel-level annotation for training and later prediction of the affected lung area. Measures to remedy this issue have been undertaken, but there is still considerable room for improvement.

Although enormous quantities of data are used for training, some research use very small test sets for model assessment. However, it should be performed on as many samples as feasible to improve the validity and reliability of the analysis.

4 Conclusion

Chest radiography is a relatively inexpensive and straightforward diagnostic method for numerous chest diseases, including PTX. The success of DL methodologies in health care influences the researchers to come up with the automation of the diagnosis procedure utilizing chest radiographs. As a result, some frameworks based on diverse ML and, specifically, DL algorithms have been presented. Yet, there is no summary of the previous studies for pneumothorax detection. This article offers an inclusive review of studies from the last decade that used chest radiographs to detect pneumothorax automatically, as well as a discussion of research gaps. It will assist researchers in contributing to the closure of such gaps and selecting the optimal method for additional investigation.

Imaging technology and computer-aided techniques are used to identify pneumothorax. Nevertheless, this remains a contentious issue, and the studies that have been published thus far rely on old methodology and are unconstrained. The patient may die if PTX is not recognized and diagnosed. Although studies have given positive results, further research on publicly available datasets is needed to improve computing complexity. As a result, further research is required to address the problem and enhance patient care.

This article gives us a more extensive analysis than the previous review papers for identifying PTX using machine learning and deep learning techniques. The limitations of these approaches have also been investigated, and important ideas for dealing with the constraints for the benefit of the research community. Furthermore, developing an interactive pneumothorax diagnosis frameworks based on deep learning technology that the research community may test on their own private or publicly available datasets could be an interesting subject for future research.

Acknowledgements This study was supported by Riphah Artificial Intelligence Research (RAIR) Lab, Riphah International University, Faisalabad, Pakistan.

Conflict of Interest The authors declare that they have no conflict of interest.

References

1. Pneumothorax Detection: AI for Health. <https://ictsg.com.sg/pneumothorax/>. Accessed 31 Oct 2021
2. Zarogoulidis, P., et al.: Pneumothorax: from definition to diagnosis and treatment. *J. Thorac. Dis.* **6**(Suppl 4), S372–S376 (2014). <https://doi.org/10.3978/j.issn.2072-1439.2014.09.24>

3. Pneumothorax (Collapsed Lung): Symptoms, Causes, and More. Healthline. 12 Oct 2021. <https://www.healthline.com/health/collapsed-lung>. Accessed 31 Oct 2021
4. Collapsed Lung (Pneumothorax): Symptoms, Causes and Treatment. Cleveland Clinic. <https://my.clevelandclinic.org/health/diseases/15304-collapsed-lung-pneumothorax>. Accessed 03 Jan 2022
5. Subotic-Kerry, M., King, C., O'Moore, K., Achilles, M., O'Dea, B.: General practitioners' attitudes toward a web-based mental health service for adolescents: implications for service design and delivery. *JMIR Hum. Factors* **5**(1), e12 (2018). <https://doi.org/10.2196/humanfactors.8913>
6. CT Scan (Computed Tomography): What is It, Preparation and Test Details. Cleveland Clinic. <https://my.clevelandclinic.org/health/diagnostics/4808-ct-computed-tomography-scan>. Accessed 03 Jan 2022
7. Pneumothorax CT Scan. <https://www.ncbi.nlm.nih.gov/books/NBK441885/figure/article-27370.image.f3/?report=objectonly>. Accessed 31 Oct 2021
8. Pneumothorax (Collapsed Lung): Symptoms, Causes, and More. Healthline. [https://www.eji-nme.com/article/S0953-6205\(20\)30455-6/fulltext](https://www.eji-nme.com/article/S0953-6205(20)30455-6/fulltext). Accessed 31 Oct 2021
9. Pneumothorax Chest X-ray scan. <https://www.ncbi.nlm.nih.gov/books/NBK538316/figure/article-27372.image.f1/>. Accessed 31 Oct 2021
10. Pham, H.H., Le, T.T., Tran, D.Q., Ngo, D.T., Nguyen, H.Q.: Interpreting chest X-rays via CNNs that exploit hierarchical disease dependencies and uncertainty labels. *Neurocomputing* **437**, 186–194 (2021). <https://doi.org/10.1016/j.neucom.2020.03.127>
11. Wang, X., Peng, Y., Lu, L., Lu, Z., Bagheri, M., Summers, R.M.: ChestX-ray8: hospital-scale chest X-ray database and benchmarks on weakly-supervised classification and localization of common thorax diseases. In: 2017 IEEE Conference on Computer Vision and Pattern Recognition, pp. 3462–3471. CVPR, 2017. <https://doi.org/10.1109/CVPR.2017.369>
12. NIH Chest X-ray Dataset for 14 Common Thorax Disease Categories. <https://academicjournals.com/details/557481faacd824c83fbf57def7b6da9383b3235a>. Accessed 31 Oct 2021
13. Filice, R.W., et al.: Crowdsourcing pneumothorax annotations using machine learning annotations on the NIH chest X-ray dataset. *J. Digit. Imaging* **33**(2), 490–496 (2020). <https://doi.org/10.1007/s10278-019-00299-9>
14. SIM-ARC Chest X-ray Dataset. <https://www.kaggle.com/c/siim-acr-pneumothorax-segmentation>. Accessed 31 Oct 2021
15. CheXpert chest X-ray dataset sample. <https://aimi.stanford.edu/chexpert-chest-x-rays>. Accessed 31 Oct 2021
16. CheXpert: Chest X-Rays. Center for Artificial Intelligence in Medicine and Imaging. <https://aimi.stanford.edu/chexpert-chest-x-rays>. Accessed 31 Oct 2021
17. Johnson, A.E.W., et al.: MIMIC-CXR-JPG, a large publicly available database of labeled chest radiographs. ArXiv 190107042 Cs Eess, Nov 2019. Accessed: 31 Oct 2021 [Online]. Available: <http://arxiv.org/abs/1901.07042>
18. Random Sample of NIH Chest X-Ray Dataset. <https://kaggle.com/nih-chest-xrays/sample>. Accessed 31 Oct 2021
19. Sze-To, A., Riasatian, A., Tizhoosh, H.R.: Searching for pneumothorax in X-ray images using autoencoded deep features. *Sci. Rep.* **11**(1), 9817 (2021). <https://doi.org/10.1038/s41598-021-89194-4>
20. Li, X., et al.: Deep learning-enabled system for rapid pneumothorax screening on chest CT. *Eur. J. Radiol.* **120**, 108692 (2019). <https://doi.org/10.1016/j.ejrad.2019.108692>
21. Wang, H., Gu, H., Qin, P., Wang, J.: CheXLocNet: automatic localization of pneumothorax in chest radiographs using deep convolutional neural networks. *PLoS ONE* **15**(11), e0242013 (2020). <https://doi.org/10.1371/journal.pone.0242013>
22. Chan, Y.-H., Zeng, Y.-Z., Wu, H.-C., Wu, M.-C., Sun, H.-M.: Effective pneumothorax detection for chest X-ray images using local binary pattern and support vector machine. *J. Healthc. Eng.* **2018**, e2908517 (2018). <https://doi.org/10.1155/2018/2908517>
23. Lindsey, T., Lee, R., Grisell, R., Vega, S., Veazey, S.: Automated pneumothorax diagnosis using deep neural networks. In: Iberoamerican congress on pattern recognition (pp. 723–731). Springer, Cham

24. Taylor, A.G., Mielke, C., Mongan, J.: Automated detection of moderate and large pneumothorax on frontal chest X-rays using deep convolutional neural networks: a retrospective study. *PLoS Med.* **15**(11), e1002697 (2018). <https://doi.org/10.1371/journal.pmed.1002697>
25. Park, S., et al.: Application of deep learning-based computer-aided detection system: detecting pneumothorax on chest radiograph after biopsy. *Eur. Radiol.* **29**(10), 5341–5348 (2019). <https://doi.org/10.1007/s00330-019-06130-x>
26. Röhrrich, S., Schlegl, T., Bardach, C., Prosch, H., Langs, G.: Deep learning detection and quantification of pneumothorax in heterogeneous routine chest computed tomography. *Eur. Radiol. Exp.* **4**, 26 (2020). <https://doi.org/10.1186/s41747-020-00152-7>
27. Geva, O., Zimmerman-Moreno, G., Lieberman, S., Konen, E., Greenspan, H.: Pneumothorax detection in chest radiographs using local and global texture signatures. In: Medical Imaging 2015: Computer-Aided Diagnosis, vol. 9414, pp. 448–454 (2015). <https://doi.org/10.1117/12.2083128>
28. Rajpurkar, P., et al.: Deep learning for chest radiograph diagnosis: a retrospective comparison of the CheXNeXt algorithm to practicing radiologists. *PLOS Med.* **15**(11), e1002686 (2018). <https://doi.org/10.1371/journal.pmed.1002686>
29. Rajpurkar, P., et al.: CheXNet: Radiologist-Level Pneumonia Detection on Chest X-Rays with Deep Learning. *ArXiv* 171105225 Cs Stat, Dec 2017. Accessed: 02 Oct 2021 [Online]. Available: <http://arxiv.org/abs/1711.05225>
30. Cho, Y., Kim, J.S., Lim, T.H., Lee, I., Choi, J.: Detection of the location of pneumothorax in chest X-rays using small artificial neural networks and a simple training process. *Sci. Rep.* **11**(1), 13054 (2021). <https://doi.org/10.1038/s41598-021-92523-2>
31. Xu, S., Guo, J., Zhang, G., Bie, R.: Automated detection of multiple lesions on chest X-ray images: classification using a neural network technique with association-specific contexts. *Appl. Sci.* **10**(5) (2020). Art. no. 5. <https://doi.org/10.3390/app10051742>
32. Abiyev, R.H., Ma'aitah, M.K.S.: Deep convolutional neural networks for chest diseases detection. *J. Healthc. Eng.* **2018**, e4168538 (2018). <https://doi.org/10.1155/2018/4168538>
33. Wang, X., Peng, Y., Lu, L., Lu, Z., Bagheri, M., Summers, R.: ChestX-Ray8: hospital-scale chest X-ray database and benchmarks on weakly-supervised classification and localization of common thorax diseases. In: 2017 IEEE Conference on Computer Vision and Pattern Recognition. CVPR, 2017. <https://doi.org/10.1109/CVPR.2017.369>
34. Goosßen, A., et al.: Pneumothorax Detection and Localization in Chest Radiographs: A Comparison of Deep Learning Approaches (2019)
35. Jakhar, K., Kaur, A., Gupta, D.M.: Pneumothorax Segmentation: Deep Learning Image Segmentation to predict Pneumothorax. *ArXiv* 191207329 Cs, Apr 2021. Accessed: 02 Oct 2021 [Online]. Available: <http://arxiv.org/abs/1912.07329>
36. Wang, Q., et al.: Automated segmentation and diagnosis of pneumothorax on chest X-rays with fully convolutional multi-scale ScSE-DenseNet: a retrospective study. *BMC Med. Inform. Decis. Mak.* **20**(14), 317 (2020). <https://doi.org/10.1186/s12911-020-01325-5>
37. Sogancioglu, E., Çallı, E., van Ginneken, B., van Leeuwen, K.G., Murphy, K.: Deep learning for chest X-ray analysis: a survey. *Med. Image Anal.* **72**, 102125 (2021). <https://doi.org/10.1016/j.media.2021.102125>
38. Jun, T.J., Kim, D., Kim, D.: Automated Diagnosis of Pneumothorax Using an Ensemble of Convolutional Neural Networks with Multi-Sized Chest Radiography Images, p. 18
39. Pan, I., Agarwal, S., Merck, D.: Generalizable inter-institutional classification of abnormal chest radiographs using efficient convolutional neural networks. *J. Digit. Imaging* **32**(5), 888–896 (2019). <https://doi.org/10.1007/s10278-019-00180-9>
40. Blumenfeld, A., Konen, E., Greenspan, H.: Pneumothorax detection in chest radiographs using convolutional neural networks. In: Medical Imaging 2018: Computer-Aided Diagnosis, vol. 10575, p. 1057504 (2018). Proc. SPIE. Accessed 27 February 2018. <https://doi.org/10.1117/12.2292540>
41. Crosby, J., Rhines, T., Li, F., MacMahon, H., Giger, M.: Deep learning for pneumothorax detection and localization using networks fine-tuned with multiple institutional datasets. In: Medical Imaging 2020: Computer-Aided Diagnosis, vol. 11314, pp. 70–74 (2020). <https://doi.org/10.1117/12.2549709>

42. Wang, X., et al.: Automatic segmentation of pneumothorax in chest radiographs based on a two-stage deep learning method. *IEEE Trans. Cogn. Dev. Syst.*, **14**, 1 (2020). <https://doi.org/10.1109/TCDS.2020.3035572>
43. Yimer, F., Tessema, A.W., Simegn, G.L.: Multiple Lung Diseases Classification from Chest X-Ray Images using Deep Learning Approach. https://www.researchgate.net/publication/355203166_Multiple_Lung_Diseases_Classification_from_Chest_X-Ray_Images_using_Deep_Learning_approach. Accessed 22 Dec 2021
44. Wang, Z., Haddad, R.J.: Automated diagnosis of pneumothorax X-ray images utilizing deep convolutional neural network. In: 2020 SoutheastCon, pp. 1–2 (2020). <https://doi.org/10.1109/SoutheastCon44009.2020.9249683>
45. Groza, V., Kuzin, A.: Pneumothorax segmentation with effective conditioned post-processing in chest X-ray. In: IEEE Conference Publication. IEEE Xplore. <https://ieeexplore.ieee.org/document/9153444>. Accessed 22 Dec 2021
46. Neri, E., et al.: What the radiologist should know about artificial intelligence—an ESR white paper. *Insights Imaging* **10**(1), 44 (2019). <https://doi.org/10.1186/s13244-019-0738-2>
47. Montagnon, E., et al.: Deep learning workflow in radiology: a primer. *Insights Imaging* **11**(1), 22 (2020). <https://doi.org/10.1186/s13244-019-0832-5>
48. Chan, H.-P., Samala, R.K., Hadjiiski, L.M., Zhou, C.: Deep learning in medical image analysis. *Adv. Exp. Med. Biol.* **1213**, 3–21 (2020). https://doi.org/10.1007/978-3-030-33128-3_1
49. Viniasvkyi, O., Dobko, M., Dobosevych, O.: Weakly-Supervised Segmentation for Disease Localization in Chest X-Ray Images. ArXiv 200700748 Cs, July 2020. Accessed: 27 Dec 2021 [Online]. Available: <http://arxiv.org/abs/2007.00748>
50. Yao, L., Prosky, J., Poblenz, E., Covington, B., Lyman, K.: Weakly Supervised Medical Diagnosis and Localization from Multiple Resolutions. ArXiv 180307703 Cs, Mar 2018. Accessed: 27 Dec 2021 [Online]. Available: <http://arxiv.org/abs/1803.07703>
51. Salehinejad, H., Valaei, S., Dowdell, T., Colak, E., Barfett, J.: Generalization of Deep Neural Networks for Chest Pathology Classification in X-Rays Using Generative Adversarial Networks. ArXiv 171201636 Cs, Feb 2018. Accessed: 27 Dec 2021 [Online]. Available: <http://arxiv.org/abs/1712.01636>
52. Shoukat, A., Akbar, S.: Artificial Intelligence Techniques for Glaucoma Detection Through Retinal Images. *Artificial Intelligence and Internet of Things: Applications in Smart Healthcare*, p. 209 (2021)
53. Gull, S., Akbar, S.: Artificial intelligence in brain tumor detection through MRI scans. *Artif. Intell. Internet Things*, 241–276 (2021)
54. Hassan, S.A., et al.: Artificial intelligence in coronavirus detection: recent findings and future perspectives. In: *Intelligent Computing Applications for COVID-19*, pp. 23–48 (2021)
55. Akbar, S., et al.: Arteriovenous ratio and papilledema based hybrid decision support system for detection and grading of hypertensive retinopathy. *Comput. Methods Programs Biomed.* **154**, 123–141 (2018)
56. Akbar, S., et al.: Decision support system for detection of hypertensive retinopathy using arteriovenous ratio. *Artif. Intell. Med.* **90**, 15–24 (2018)
57. Akbar, S., et al.: Decision support system for detection of papilledema through fundus retinal images. *J. Med. Syst.* **41**(4), 66 (2017)
58. Saba, T., et al.: Automatic detection of papilledema through fundus retinal images using deep learning. *Microsc. Res. Tech.* **84**(12), 3066–3077 (2021)
59. Gull, S., Akbar, S., Khan, H.U.: Automated detection of brain tumor through magnetic resonance images using convolutional neural network. *BioMed Res. Int.* (2021)
60. Gull, S., Akbar, S., Safdar, K.: An interactive deep learning approach for brain tumor detection through 3D-magnetic resonance images. In: Accepted in 18th International Conference on Frontiers of Information Technology (FIT), Islamabad, Pakistan (2021)
61. Gull, S., Akbar, S., Shoukat, I.A.: A deep transfer learning approach for automated detection of brain tumor through magnetic resonance imaging. In: 2021 International Conference on Innovative Computing (ICIC), pp. 1–6 (2021). <https://doi.org/10.1109/ICIC53490.2021.9692967>

62. Shoukat, A., Akbar, S., Hassan, S.A.E., Rehman, A., Ayesha, N.: Glaucoma diagnosis through convolutional neural network using fundus image. In: Accepted in 18th International Conference on Frontiers of Information Technology (FIT), Islamabad, Pakistan (2021)
63. Shoukat, A., Akbar, S., Safdar, K.: A deep learning-based automatic method for early detection of the glaucoma using fundus images. In: 2021 International Conference on Innovative Computing (ICIC), pp. 1–6 (2021). <https://doi.org/10.1109/ICIC53490.2021.9693078>
64. Akbar, S., Hassan, S.A.E., Shoukat, A., Alyami, J., Bahaj, S.A.: Detection of microscopic glaucoma through fundus images using deep transfer learning approach. In: Accepted in Microscopy Research and Technique, 27 Jan 2022
65. Safdar, K., Akbar, S., Gull, S.: An automated deep learning based ensemble approach for malignant melanoma detection using dermoscopy images. In: Accepted in 18th International Conference on Frontiers of Information Technology (FIT), Islamabad, Pakistan (2021)
66. Safdar, K., Akbar, S., Shoukat, A.: A majority voting based ensemble approach of deep learning classifiers for automated melanoma detection. In: 2021 International Conference on Innovative Computing (ICIC), pp. 1–6 (2021). <https://doi.org/10.1109/ICIC53490.2021.9692915>
67. Ahmad, M.F., Akbar, S., Hassan, S.A.E., Rehman, A., Ayesha, N.: Deep learning approach to diagnose Alzheimer's disease through magnetic resonance images. In: 2021 International Conference on Innovative Computing (ICIC), pp. 1–6 (2021). <https://doi.org/10.1109/ICIC53490.2021.9693041>
68. Hassan, S.A.E., et al.: Deep learning-based automatic detection of central serous retinopathy using optical coherence tomographic images. In: 2021 1st International Conference on Artificial Intelligence and Data Analytics (CAIDA). IEEE (2021)
69. Hassan, S.A., et al.: Recent developments in detection of central serous retinopathy through imaging and artificial intelligence techniques—a review. IEEE Access (2021)
70. Akram, M.U., et al.: Data on fundus images for vessels segmentation, detection of hypertensive retinopathy, diabetic retinopathy and papilledema. Data Brief **29**, 105282 (2020)
71. Akbar, S., et al.: AVRDB: annotated dataset for vessel segmentation and calculation of arteriovenous ratio. In: Proceedings of the 21th International Conference on Image Processing, Computer Vision, and Pattern Recognition (IPCV'17) (2017)

ML and DL Architectures Comparisons for the Classification of COVID-19 Using Chest X-Ray Images



Erum Afzal, Tanzila Saba, Haris Ali, Adnan Karim, and Kashif Javed

Abstract Pandemic COVID-19 ranked as one of the world's worst pandemics ever witnessed in history. It has affected every country by spreading this disease with an increase in mortality at alarming rates despite the technologically advanced era of medicine. AI/ML is one of the strong wings in the medical field so while fighting the battle to control and diagnose the best medicine for the outbreak COVID-19 disease. Automated and AI-based prediction models for COVID-19 are the main attraction for the scientist hoping to support some good medical decisions at this difficult time. However, mostly classical image processing methods have been implemented to detect COVID-19 cases resultant in low accuracy. In this chapter, multiple naïve machine and deep learning architectures are implied to evaluate the performance of the models for the classification of COVID-19 using a dataset comprising of chest x-ray images of, i.e., COVID-19 patients and normal (non-infected) individuals. The analysis looks at three machine learning architectures including Logistic Regression, Decision Tree (DT) Classifier, and support vector machine (SVM), and four deep learning architectures, namely: Convolutional neural networks (CNNs), VGG19, ResNet50, and AlexNet. The dataset has been divided into train, test and validation set and the same data have been used for the training, testing, and validation of all the architectures. The result analysis shows that AlexNet provides the best performance out of all the architectures. It can be seen that the AlexNet model achieved 98.05% accuracy (ACC), 97.40% recall, 98.03% F1-score, 98.68% precision, and 98.05% area under the curve (AUC) score.

Keywords COVID-19 · Transfer learning · Machine learning · Healthcare · Public health

E. Afzal · H. Ali · A. Karim · K. Javed
National University of Sciences and Technology, Islamabad, Pakistan

T. Saba (✉)
Artificial Intelligence and Data Analytics Lab CCIS, Prince Sultan University, Riyadh 11586,
Saudi Arabia
e-mail: tsaba@psu.edu.sa

1 Introduction

As the world strives to free itself from the shackles of COVID-19, new variants of the disease, some being more contagious than the previous ones, keep surfacing [1]. One of the methods to detect the disease is examining Chest X-Ray (CXR). However, it takes relatively longer time and a radiologist on the scene, to examine the CXR and identify the infectious lesions on the X-ray image associated with presence of corona. In addition, the limited number of radiologists in front of the swarm of patients make it very difficult to detect COVID-19, as opposed to the need for faster detection [2].

Hence, there has been a need for automatically detecting the disease without much help from a radiologist, just using the CXR. Many researchers and machine and deep learning experts have used multiple methods to distinguish and detect COVID-19 from other diseases and have achieved significant results. Every study is executed considering different aspects; some had access to a large amount of input data, while others tried to maximize performance with a relatively limited dataset. Many deep/transfer machine learning models have previously been administered in computer vision to classify and detect different diseases, including breast cancer [3] and colon cancer [4].

This study has been done to use naïve and well-known machine and deep learning architectures in their raw states, to analyze the results they provide on the dataset fed. In total, three machine learning architectures have been used in the study. The first one is the Decision Tree Classifier (DT), the second one being Logistic Regression following support vector machine (SVM). Whereas four deep learning and few pre-trained architectures have been implemented for classification. The first one is a classical convolutional neural network (CNN) build from scratch, while the other three architectures are well-known pre-developed models, namely: VGG19, ResNet50, and AlexNet. The three of these models have been used as feature extractors from the image dataset added as input to the pre-trained weights from the dataset of ImageNet. The extracted features were later fed as input to the self-defined fully connected layers, which gives the resultant output.

1.1 Data Collection

The data used for the models has been obtained from Kaggle comprising of image X-rays of chest of the categories: COVID-19 Pneumonia infected, COVID-19 infected and normal [5]. In this research only COVID-19 infected and normal images have been used as input to models. In the original dataset, sample of CXR has been collected from different resource because there is no large dataset available at one data archival repository for concert analysis. In this regard 1401 sample of COVID-19 infected were taken from GitHub repository [6, 7], SIRM; an Italian Society of SIRM [8] and Radiopaedia; an open-source platform providing educational radiology dataset for experiments [9] and data repository website for COVID-19 analysis by

fig share [10, 11]. The augmented dataset was also collected from Mendeley [12] and lastly 2313 normal images of Chest X-rays were taken from Kaggle [5, 13].

Since the dataset is pre-augmented, further augmentation has not been performed so the dataset is taken as is for input to the models. Figure 1 the chest X-ray images of the COVID-19 infected patients and normal persons. As seen by the naked eye, the corona infected CXR have blurry patches and the lungs' opacity is different from the normal CXR. The normal and infected images through machine and deep learning models will try to distinguish between corona and normal CXR majorly exploiting these features of the CXR. The dataset is also a balanced data, i.e., equal number of images (2313) are present for both category (Fig. 2).

Fig. 1 a–e Chest X-ray images of Corona infected patient. f–j Chest X-rays image of normal individuals

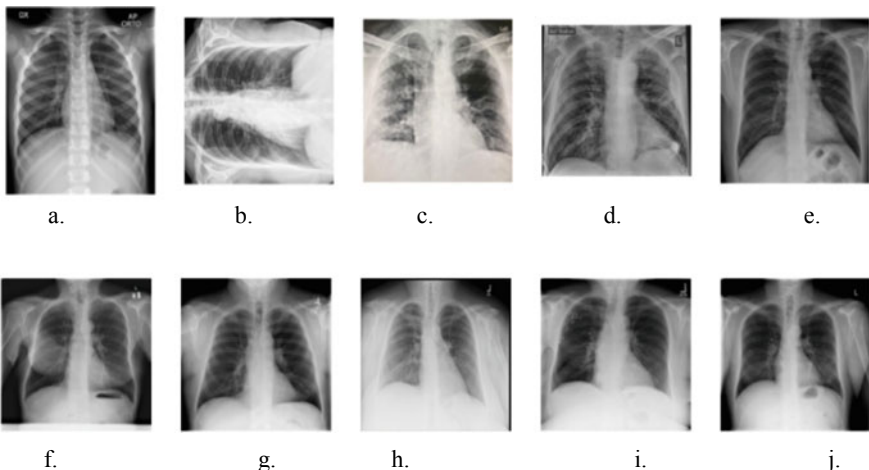
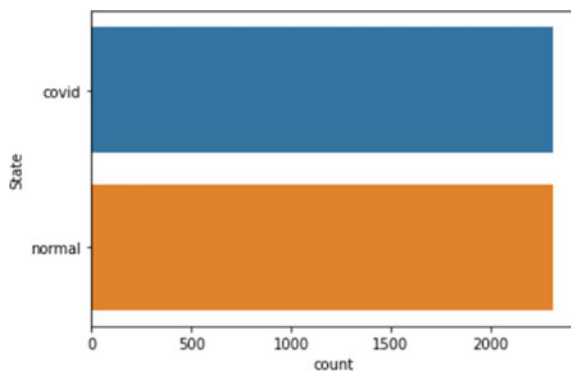


Fig. 2 Count of the images of each category in the dataset (blue = COVID-19, orange = Normal)

1.2 Related Work

COVID-19 led numerous researchers in the field to work for the automatic detection/diagnostic of the corona disease. The works include studies based on either image dataset of chest X-ray, computed tomography (CT) scans for corona classification versus several possible infections including pneumonia. In [14] multiple deep learning architectures have been used, some in an ensemble manner, of lung cancer, pneumonia, and corona cases for multi-classification. The dataset includes a combination of images of chest X-ray and CT scans. The architectures used include ResNet152V2, VGG19 with CNN, ResNet152v2 with Gated Recurrent Unit (GRU), and ResNet152V2 with Bidirectional GRU. The VGG19 accomplished best performance with CNN model, it achieved an accuracy of 98.05%, recall of the model was 98.05% following precision of the model was 98.43, whereas area under the curve was 99.66%.

In [15] a total of seven classification algorithms were used to construct a majority voting ensemble classifier to classify normal, suspected and corona infected patients, based on chest X-ray images. The seven selected models include support vector machine (SVM), Decision Tree (DT), Naïve Bayes (NB), K -nearest neighbor (KNN), artificial neural networks (ANN), the SVM model was implemented with linear kernel, radial basis function (RBF) kernel and polynomial kernel, respectively. The dataset included equal number (696) of images of chest X-ray for normal, pneumonia, and corona infected patients for training and testing and 86 images of each category for validation. Model was trained in two phases and recorded the results for each. The accuracy of Phase1 was observed as 98.062% and 95.6% area under the curve following accuracy of 91.33% and 0.81 area under the curve in Phase 11.

Referring to [16], DarkNet-19 inspired model, called DarkCovidNet, was used for classification before implementing real-time object detection through You Only Look Once (YOLO) algorithm. The model was used for binary classification, i.e., corona infected versus normal patient and multi-classification corona infected patients versus Pneumonia versus normal patients (no COVID-19). The dataset comprises only chest X-ray images with 127 CXR images diagnosed with COVID-19 positive. The model implemented 17 convolutional layers with different filtering methods on each layer. The accuracy of the model for binary classification is 98.08%, while it achieved an accuracy score of 87.02% for multiclass classification.

In [17] a different take is adopted, a deep transfer learning method by using a pre-trained model ResNet50, the model was trained on the dataset of ImageNet [18], and then propose a convolutional neural network on top of the feature map extracted from the ResNet50 pre-trained model as a means of transfer learning of the optimized parameters. The convolutional neural network is then tasked with outputting the classified result as COVID-19+ or COVID-19-. They have also used a dataset comprising of only CT images of the chest instead of CXR or a mixture of both. The accuracy of the proposed model was 96.22% with a precision score of 97.78%, a sensitivity of 94.96%, and a specificity of 97.61%.

Similarly, authors in [19] also use a pre-trained model to extract the feature as a means for deep transfer learning. They also used CT images as their dataset for training the model. The study uses the DenseNet201 for feature extraction from the image dataset of CT scans using the pre-trained model on the ImageNet dataset [18]. The resulting feature map is then input to a top level artificial neural network, also called as dense layers, to get an output regarding the classification of the disease. The model consisted of a dataset comprising a total of 2492 CT images. From these images 68% were used for training. Out of the remaining 32%, 17% were used for validation purpose while the other 15% were used for testing purpose. Furthermore, the initial model was trained for the epochs of 300. The performance was captured as of 97% area under the curve, an accuracy of 97.48% of validation dataset whereas the accuracy of 96.25% on test dataset.

Another approach taken by [20] implemented an Adaptive Feature Selection guided Deep Forest (AFS-DF) for features extraction from image dataset of CT scans and training the deep forest architecture to classify corona infected patients versus the community acquires pneumonia (CAP). The dataset included 1495 images from confirmed corona cases and 1027 images of the community acquires pneumonia patients. The model evaluation was done by dividing the model under fivefold cross-validation on the present CT images. The dataset was divided into 5 random subsets with 504 images in each of the first four subsets while 506 in the final subset. Each subset in sequence wise selection used as test dataset, whereas 4 subsets were selected as the train dataset. Each layer of AFS-DF had many independent random forests and selection of feature unit, each of the random forest having a different feature importance and the overall feature importance was calculated at the end. The AFS-DF model achieved an accuracy of about 91.79%, sensitivity of 93.05%, a precision of 93.10%, and an area under the curve of 96.35%.

Several models in the literature with performances have been listed in Table 1. In this research, we analyze the base machine learning architectures directly provided the dataset, and some deep learning architectures, majority of which are based on deep learning and transfer learning, to see and analyze the performance in the actual architecture on the dataset of image dataset of chest X-ray for the classification of corona infected cases.

2 Materials and Methods

The diagnosing of corona infection is performed by radiologists using both CT and CXR images. The use of CXR images of the patients to identify the infection of COVID-19 is an effective method for diagnosing the disease. In this study, we have analyzed multiple machine learning and deep learning models for the classification of corona infection versus normal patients using CXR images as input. The evaluation of the architectures is based on the performance as used in the raw form architecture for the classification of the disease. All the models are structured to output the binary value of the decision that is 1 (COVID-19+) or 0 (COVID-19-).

Table 1 Similar research work with evaluation metrics

Research	Dataset	Architecture	Accuracy	Precision	Area under curve (AUC)
[14]	CXR + CT	VGG19 + CNN, ResNet152V2, ResNet152V2 + GRU, ResNet152V2 + BiGRU	98.05	98.43	99.66
[15]	CXR	SVM (linear kernel), SVM (RBF kernel), SVM (polynomial kernel), DT, NB, KNN, and ANN,	98.062 (phase-I), 91.329 (phase-II)	-	95.6 (phase-I), 83.1 (phase-II)
[16]	CXR	DarkCovidNet	98.08 (binary classification), 87.02 (multiclass classification)	98.03 (binary classification), 89.96 (multiclass classification)	-
[17]	CXR + CT	ResNet50 + CNN	96.22	97.77	-
[19]	CT	DenseNet201	97.4 (validation), 96.25 (testing)	-	97
[20]	CT	AFS-DF	97.79	93.05	96.35
[21]	CXR	DeTrac with VGG19 as pre-trained backbone	97.35	-	96.54
[22]	CXR	VGG, InceptionV3, ResNet, MobileNet, DenseNet, NasNetMobile	98.69 (from DenseNet121)	-	-
[23]	CXR	Ensemble ResNet34, ResNet50, ResNet152, VGG16	90.3	-	96
[24]	CXR	AlexNet, GoogleNet, SqueezeNet	96.46 (AN), 96.20 (GN), 96.25 (SN)	98.11(AN), 98.44(GN), 96.01(SN)	99.8 (AN), 99.8 (GN), 99.8 (SN)

Figure 3 is explaining overall general approach of our work is executed in the following manners: the first and foremost was the data collection phase and it has been accomplished as explained in Sect. 1.1. The next stage is the preparation of the data. The preparation includes preprocessing steps implied on the data before inputting it to the model for training, testing, and validation. The preprocessing includes any kind of resizing, normalization, and splitting of the data. Since the data is already augmented, no further augmentation was required to be performed. After the preprocessing, the next part is to develop the model that is to be used to train on the given dataset. The models are instantiated and passed to the training phase. In the training phase we input the prepared dataset to the constructed model and train the model on the given dataset for a specific number of epochs. The validation is done parallel to the training to evaluate the runtime performance of the model while training. After the model was trained, it was moved to the testing phase. In the testing phase, the model was evaluated on a data it has not seen during the training process, so it helps to evaluate how the model would behave given new data to output a prediction.

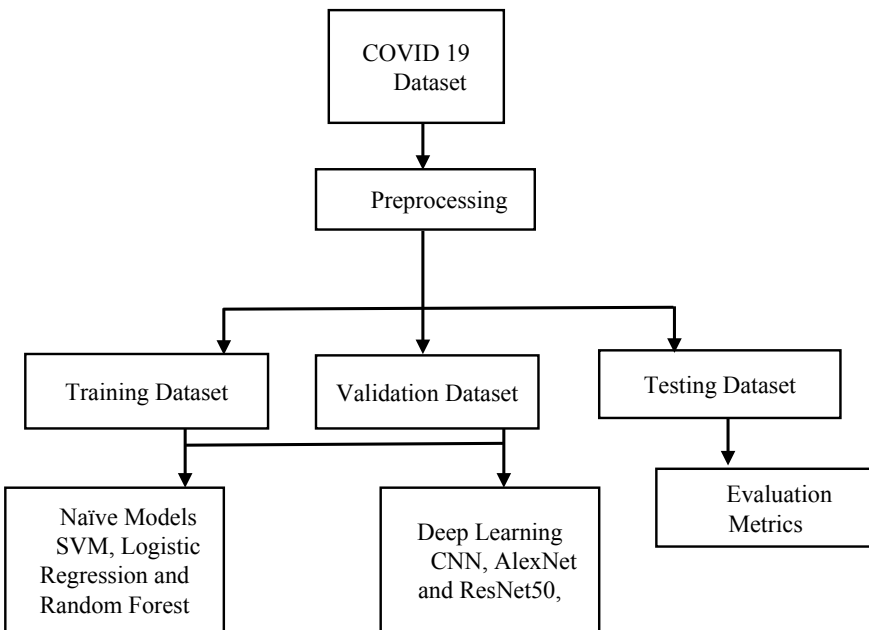


Fig. 3 The architecture the classification framework

2.1 Data Preparation

The data preparation is the part where the input data is preprocessed to be taken as input by the model. The preprocessing includes all tweaks to the input data before the training like resizing, cropping, splitting, and augmenting the data [25, 26]. For the present study, a total of 4626 CXR images are present in the dataset. Each class that is COVID-19 infected and normal patient, is equally represented by the dataset. Equal number of CXR images, 2313, belong to each class.

For evaluation purposes, the dataset has been split into training, testing, and validation data. The split ratio of training versus evaluation is 80/20 that is, 80% of the data is reserved for training while the other 20% has been reserved for evaluation. The evaluation data is further equally split into validation set and testing set. Hence, from the total data, 10% has been set for testing and 10% has been set for validation purposes.

Each of these datasets contain equal representation of both classes. Figure 4 shows the data distribution for the set containing the training data. While Fig. 5 represent the datasets for testing and validation.

The dataset contains images that is a mixture of RGB, or 3-channel, and grayscale, 2-channel. For the model to receive the images as input, the size of the images should be consistent. Hence all the images were resized to have only three channels to turn into grayscale images. Moreover, the images in the dataset were inconsistent in sizes, so all the images were resized to have a consistent size of $224 \times 224 \times 3$. Finally, all the images were normalized after resized. For the implementation of naïve machine learning models, dataset was converted into two-dimensional image array from three dimensions.

To input data to the three machine learning models, the images must be in two-dimensional arrays, instead of three dimensional. Hence, for the naïve machine

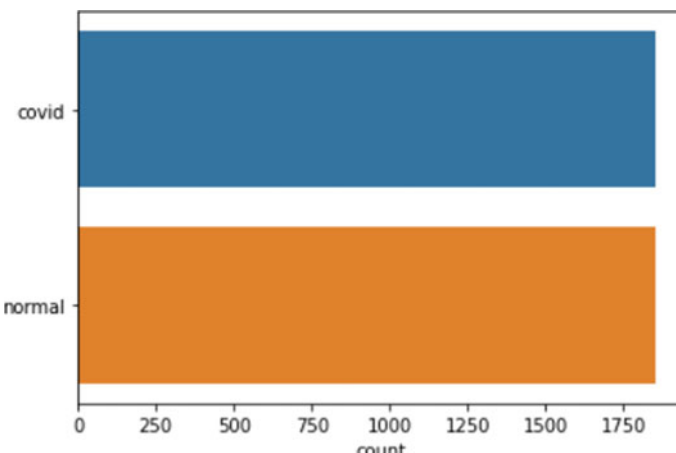


Fig. 4 Training set data distribution

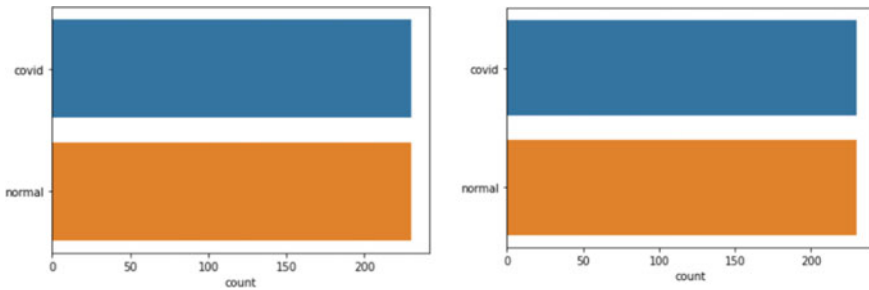


Fig. 5 **a** Testing set data distribution. **b** Validation set data distribution

learning-based models, images were transformed to a single channel with shape 50,176 (224×224). After the transformation, the whole data was fed to the model as input; for training having the shape (3700, 50,176), where the 3700 represents the total number of images in the dataset.

2.2 Model Building

For this study, three machine learning architectures were analyzed, namely: Decision Tree (DT) classifier, Logistic Regression, and support vector machine (SVM) [27–29]. On the other hand, four deep learning architectures were used to make the predictions. These include a classical convolutional neural network (CNN) and three pre-trained deep learning models used for deep transfer learning (DTL). These pre-trained models are VGG19, ResNet50 and AlexNet [30, 31]. The sections below describe each model in detail.

Decision tree: The decision tree algorithm is one of the most widely known algorithm for both binary and multiclass classification. It has a flowchart-like structure where internal nodes represent a specific test done on the input data attribute(s). The branches represent the result of the tests on the nodes and the leaf node represent the label of the class that is predicted after the tests [32]. The training dataset was input to the developed model to train itself at the attributes of the input data. When the model was trained, it was evaluated by using it to make predictions based on the validation and test datasets.

Logistic regression: Logistic regression is one of the most basic classification algorithms in machine learning. Like DT, it can also be used for both binary and multiclass classification. It uses a hypothesis function to be used as a predictor with adjustable weights. A loss function to converge to a global (or local) minimum by adjusting the weights of the hypothesis function. Minimizing the loss function ensures better prediction and an accurate model [33, 34]. Like the DT classifier, the logistic regression model takes the input dataset for the training. The ‘liblinear’ solver used for

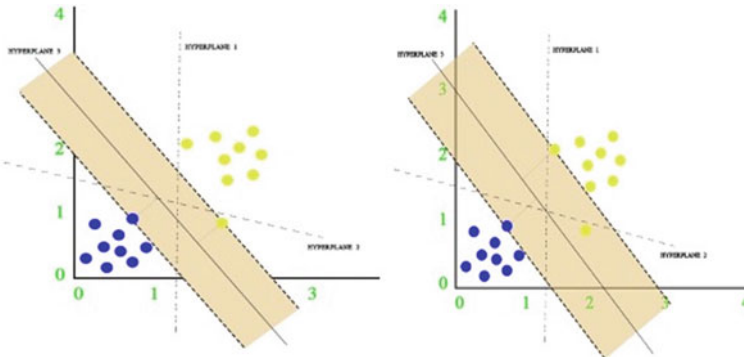


Fig. 6 SVM with hard margin (a) and soft margin (b)

the model as it performs approximate minimizations along coordinate hyperplanes using the coordinate descent algorithm. After the training, the model was tested by taking predictions using the validation and the test datasets.

Support Vector Machine: SVM is one of the most effective machine learning algorithms developed. It can be used for both regression and classification purposes. At the basic level it finds hyperplanes to separate classes with highest possible margin. In case of binary classification, it finds the hyperplane that gives the highest possible margin from both the classes. There are two types of margins available for the classification purposes. The first one is called the soft margin where the classes are not perfectly distinguishable, so SVM allows some of the datapoints to be misclassified. And the other one being the hard margin, where the classes are perfectly distinguished from each other. Figure 6 shows the difference between a hard and soft margin graphically using a set of two-dimensional data points. When the classes are not linearly separable, SVM use a kernel, which transforms non-separable classes into separable classes in higher dimensions [35, 36]. The model used for this research used Radial Basis Function (RBF) kernel.

Like the models discussed earlier, the next steps were same to evaluate the model. The dataset was input to SVM classifier for training and evaluate the trained model by making the predictions for the validation and test datasets.

Convolutional Neural Network (CNN): CNNs have contributed a significant impact toward the problems of machine learning especially ones that involve image data, hence it has brought major ground breaks in the field of computer vision. CNNs are not only known to reduce the number of parameters but also have features that are spatially independent. CNNs also tend to learn abstract features as the convolutional layers go deeper [37–39].

The created model for the classification purposes was made to evaluate the power of convolutional neural networks. The model comprises 8 convolutional layers and 3 dense layers, with max pooling, batch normalization, dropout and nonlinearity in between. All the convolutional layers contain stride and padding of 1 and a kernel

size of 3×3 . The convolutional layers are followed by the LeakyReLU nonlinearity. LeakyReLU is used to avoid the vanishing gradient problem. Four LeakyReLU layer was then followed by a max pooling layer with stride of 2 and a kernel size of 2×2 . The final linear layer is followed by the sigmoid nonlinearity to output a binary prediction. The total parameters of the model are 103,784,714 where all of the parameters are trainable. Figure 7 shows the constructed CNN model. Table 2 shows the convolutional network with input and output shapes related with each layer.

VGG19: VGG has been a very effective and frequently used architecture for computer vision applications. The architecture used for classification in VGG19 [40], a 19 layers deep architecture, the depth of the layer's ranges from 11 to 19. VGG19 is used as a feature extractor model with weights pre-trained on the ImageNet dataset. The top fully connected layers are removed from the pre-trained model. The feature map extracted from the input images is passed to a flatten layer and then to the dense layer manually added on top of the pre-trained model. Five dense layers are manually added on top of the pre-trained model [41, 42]. Each of the first four layers

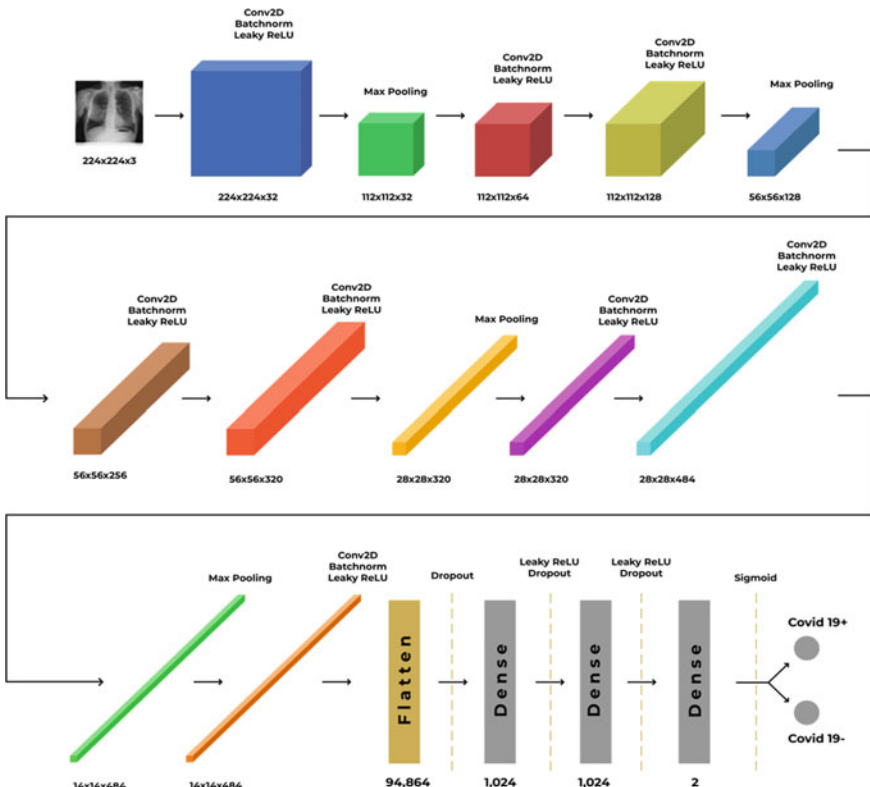


Fig. 7 Proposed CNN architecture

Table 2 CNN model layers with their respective input and output shape

Layer	Input shape	Output shape
Conv2d	(3, 224, 224)	(32, 224, 224)
Batchnorm2d	(32, 224, 224)	(32, 224, 224)
LeakyReLU	(32, 224, 224)	(32, 224, 224)
MaxPool2D	(32, 224, 224)	(32, 112, 112)
Conv2d	(32, 112, 112)	(64, 112, 112)
Batchnorm2d	(64, 112, 112)	(64, 112, 112)
LeakyReLU	(64, 112, 112)	(64, 112, 112)
Conv2d	(64, 112, 112)	(128, 112, 112)
Batchnorm2d	(128, 112, 112)	(128, 112, 112)
LeakyReLU	(128, 112, 112)	(128, 112, 112)
MaxPool2d	(128, 112, 112)	(128, 56, 56)
Conv2d	(128, 56, 56)	(256, 56, 56)
Batchnorm2d	(256, 56, 56)	(256, 56, 56)
LeakyReLU	(256, 56, 56)	(256, 56, 56)
Conv2d	(256, 56, 56)	(320, 56, 56)
Batchnorm2d	(320, 56, 56)	(320, 56, 56)
LeakyReLU	(320, 56, 56)	(320, 56, 56)
MaxPool2d	(320, 28, 28)	(320, 28, 28)
Conv2d	(320, 28, 28)	(320, 28, 28)
Batchnorm2d	(320, 28, 28)	(320, 28, 28)
LeakyReLU	(320, 28, 28)	(320, 28, 28)
Conv2d	(320, 28, 28)	(484, 28, 28)
Batchnorm2d	(484, 28, 28)	(484, 28, 28)
LeakyReLU	(484 28, 28)	(484, 28, 28)
MaxPool2d	(484, 28, 28)	(484, 14, 14)
Conv2d	(484, 14, 14)	(484, 14, 14)
Batchnorm2d	(484, 14, 14)	(484, 14, 14)
LeakyReLU	(484 14, 14)	(484, 14, 14)
Flatten	(484, 14, 14)	(1, 94,864)
Linear	(1, 94,864)	(1, 1024)
Dropout (0.5)	(1, 94,864)	(1, 94,864)
Linear	(1, 94,864)	(1,1024)
LeakyReLU	(1, 1024)	(1, 1024)
Dropout (0.5)	(1, 1024)	(1, 1024)
Linear	(1, 1024)	(1, 1024)
LeakyReLU	(1, 1024)	(1, 1024)
Linear	(1, 1024)	(1, 2)
Sigmoid	(1, 2)	(1, 2)

are followed by the LeakyReLU nonlinearity, while the final layer is followed by the sigmoid nonlinearity.

The total parameters of the model are 46,015,010 out of the total number of parameters, the trainable parameters are 25,990,626 while the number of non-trainable parameters is 20,024,384. Figure 8 shows the developed model using the VGG19 feature extractor. Table 3 shows the dense layers on top of the feature extractor and the input and output shapes corresponding to each layer.

ResNet50: The ResNet50 model was used as a feature extractor using the pre-trained weights from the ImageNet dataset. The original ResNet architecture, introduced in [43], comprises deep layers ranging from 50 to 152. Like the model discussed earlier, the model was used to extract the features from the input image. The top fully connected layers were removed from the model and a new set of fully connected layers were added to make a prediction for the required number of classes.

Six fully connected layers are added on top of the feature extractor. The first five layers are each followed by the LeakyReLU nonlinearity while the final dense layer

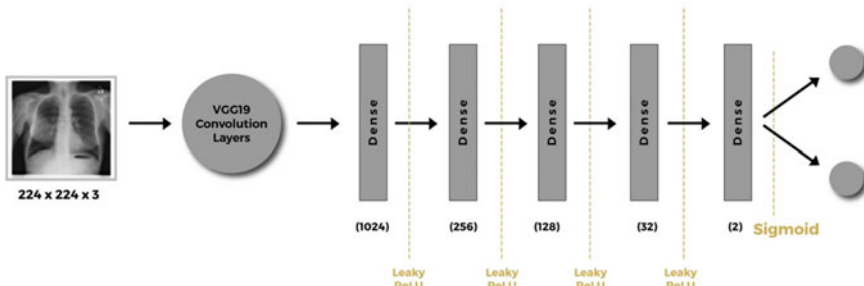


Fig. 8 Pre-trained VGG19 used as a feature extractor and top dense layers

Table 3 Pre-trained VGG19 with fully connected layers

Layer	Input shape	Output shape
VGG19	(3, 224, 224)	(512, 7, 7)
Linear	(1, 25,088)	(1, 1024)
LeakyReLU	(1, 1024)	(1, 1024)
Linear	(1, 1024)	(1, 256)
LeakyReLU	(1, 256)	(1, 256)
Linear	(1, 256)	(1, 128)
LeakyReLU	(1, 128)	(1, 128)
Linear	(1, 128)	(1, 32)
LeakyReLU	(1, 32)	(1, 32)
Linear	(1, 32)	(1, 2)
Sigmoid	(1, 2)	(1, 2)

is followed by a sigmoid nonlinearity. The total number of parameters in the model are 26,279,858. Out of these parameters 2,771,826 were trainable parameters, while 23,508,032 were non-trainable parameters. Figure 9 shows the developed model using the ResNet50 feature extractor. Table 4 shows the dense layers on top of the feature extractor and the input and output shapes corresponding to each layer.

AlexNet: Next architecture used for the model is AlexNet, proposed in [44] in 2012, won the ImageNet contest of 2012. AlexNet is relatively smaller network compared to VGG16 and ResNet50. This architecture is also used as a feature extractor. Like the previous transfer learning models, the top fully connected layers were removed, and new ones were added to output the required predictions [45].

Four fully connected layers are added on top of the convolutional layers. The first three layers are each followed by a LeakyReLU nonlinearity, while the final layer is followed by a sigmoid. The total number of parameters in the model were 12,178,594. Out of these total parameters, the number of trainable parameters were 9,708,898

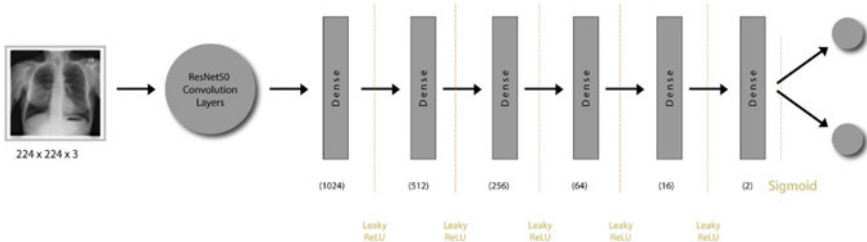


Fig. 9 ResNet50 used as a feature extractor and top dense layers

Table 4 ResNet50 with fully connected layers, corresponding input and output shapes

Layer	Input shape	Output shape
ResNet50	(3, 256, 256)	(2048, 1, 1)
Linear	(1, 2048)	(1, 1024)
LeakyReLU	(1, 1024)	(1, 1024)
Linear	(1, 1024)	(1, 512)
LeakyReLU	(1, 512)	(1, 512)
Linear	(1, 512)	(1, 256)
LeakyReLU	(1, 256)	(1, 256)
Linear	(1, 256)	(1, 64)
LeakyReLU	(1, 64)	(1, 64)
Linear	(1, 64)	(1, 16)
LeakyReLU	(1, 16)	(1, 16)
Linear	(1, 16)	(1, 2)
Sigmoid	(1, 2)	(1, 2)

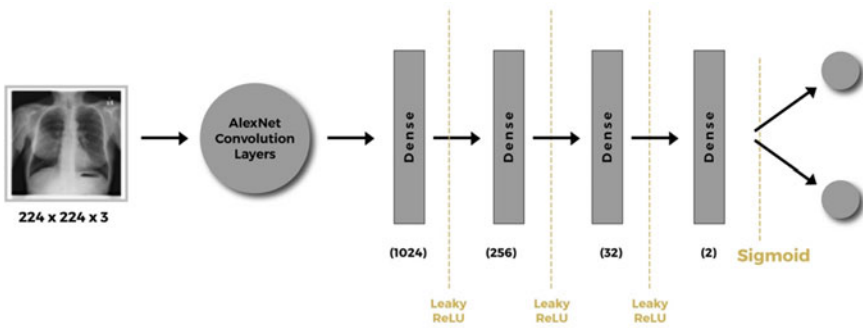


Fig. 10 Pre-trained AlexNet used as a feature extractor and top dense layers

Table 5 AlexNet with connected layers corresponding input and output shapes

Layer	Input shape	Output shape
AlexNet	(3, 256, 256)	(256, 7, 7)
Linear	(1, 9216)	(1, 1024)
LeakyReLU	(1, 1024)	(1, 1024)
Linear	(1, 1024)	(1, 256)
LeakyReLU	(1, 256)	(1, 256)
Linear	(1, 256)	(1, 32)
LeakyReLU	(1, 32)	(1, 32)
Linear	(1, 32)	(1, 2)
Sigmoid	(1, 2)	(1, 2)

and non-trainable parameters were 2,469,696. Figure 10 shows the developed model using the ResNet50 feature extractor. Table 5 shows the dense layers on top of the feature extractor and the input and output shapes corresponding to each layer.

3 Results

3.1 Evaluation Metrics

The models created for the classification were all written in Python 3. The machine learning models were applied using the sklearn library [46]. The deep learning models were created using the PyTorch library [47]. The codes were run on Google Colab with an Nvidia k80 GPU with 12 GB memory. The dataset is input to the DataLoader utility of PyTorch. The optimizer used for the deep transfer learning models is Adam [48] and the loss function used is the Cross Entropy loss. The training process, for

Table 6 Transfer learning models with the corresponding optimizer and learning rate

Model	Optimizer	Learning rate
CNN	Adam	0.0001
VGG19		0.0005
ResNet50		0.0005
AlexNet		0.0005

each deep transfer learning model, ran for 50 epochs and the trained model with the least validation loss is saved as the final model. The saved model is then tested by using it to make predictions for the data in the test set. The models with their learning rate (LR) and optimizer used are listed in Table 6.

The results obtained from the models can be evaluated based on several metrics. In this research, the models built are evaluated through five metrics, namely: accuracy, precision, recall, F1-score, and area under curve (AUC). The mathematical formulas for the metrics are shown in Eqs. (1), (2), (3), (4) and (5) [49]. In the predictions of our models, ‘tp’ refers to the true positives, ‘tn’ refers to true negatives. Similarly, ‘fp’ refers to false positives and ‘fn’ refers to false negatives. For the expression (5), for the AUC, S_p is the sum of all positive examples ranked, while n_p and n_n denote the number of positive and negative examples [50].

$$\text{Accuracy (acc)} = \frac{\text{tp} + \text{tn}}{\text{tp} + \text{fp} + \text{tn} + \text{fn}} \quad (1)$$

$$\text{Precision (p)} = \frac{\text{tp}}{\text{tp} + \text{fp}} \quad (2)$$

$$\text{recall (r)} = \frac{\text{tp}}{\text{tp} + \text{fn}} \quad (3)$$

$$F\text{-measure (FM)} = \frac{2 * p * r}{p + r} \quad (4)$$

$$\text{Area under curve (AUC)} = \frac{S_p - n_p(n_n + 1)/2}{n_p n_n} \quad (5)$$

3.2 Experimental Parameters

The models created for the classification were all written in Python 3. The machine learning models were applied using the sklearn library [46]. The deep learning models were created using the PyTorch library [47]. The codes were run on Google Colab with an Nvidia k80 GPU with 12 GB memory. The dataset is input to the DataLoader

utility of PyTorch. The optimizer used for the deep transfer learning models is Adam [48] and the loss function used is the Cross Entropy loss. The training process, for each deep transfer learning model, ran for 50 epochs and the trained model with the least validation loss is saved as the final model. The saved model is then tested by using it to make predictions for the data in the test set. The models with their learning rate (LR) and optimizer used are listed in Table 6.

3.3 Model Results and Discussion

This section includes the results obtained from training the models with analysis and discussion regarding the results obtained from the various models used in this study. The confusion matrix for each of the proposed model is to be plotted to aid evaluation purposes. Table 7 shows each model used with its confusion matrix plotted for testing set. Table 8 shows the CNN and deep transfer learning models with their corresponding loss values plotted opposite to the number of epochs while both the training and the validation phase. Table 9 shows the values of the evaluation metrics corresponding to each of the model used.

Seeing both the confusion matrices and the values of the evaluation metrics, it can be concluded that AlexNet gives the best predictions and is the best architecture out of all, in the study, for the prediction of COVID-19 using CXR images. The AlexNet model gives an accuracy of 98.05%, an AUC score of 98.05%, a precision of 98.68%, a recall of 97.40%, and an F1-score of 98.03%. Decision tree algorithm proved to be the least efficient model in its pre-trained state, giving an accuracy of 86.82%, AUC score of 86.81%, a precision of 88.63%, a recall of 84.41%, and an F1-score of 86.47% despite multiple attempts of fine tuning without adding convolutional layers on top of the pre-trained architecture. Figure 11 gives the plot of the values of the evaluation metrics of all the 7 models used, both machine and deep learning, in the study. Where we can visually see that that SVM proves to be the most efficient model.

3.4 Sample Heading (Third Level)

Only two levels of headings should be numbered. Lower-level headings remain unnumbered; they are formatted as run-in headings.

Sample Heading (Forth Level). The contribution should contain no more than four levels of headings. The following Table 10 gives a summary of all heading levels.

Displayed equations are centered and set on a separate line.

$$x + y = z \quad (6)$$

Table 7 Models used with the corresponding confusion matrix plot and values

Model	Confusion matrix plot	Confusion matrix values
		$[[TP \ TN \ FP \ FN]]$
Decision tree	<p style="text-align: center;">Confusion matrix</p> <p>True labels</p> <p>Predicted labels</p>	$[[207 \ 25 \ 36 \ 195]]$
Logistic regression	<p style="text-align: center;">Confusion matrix</p> <p>True labels</p> <p>Predicted labels</p>	$[[207 \ 25 \ 25 \ 206]]$
SVM	<p style="text-align: center;">Confusion matrix</p> <p>True labels</p> <p>Predicted labels</p>	$[[216 \ 16 \ 13 \ 218]]$

(continued)

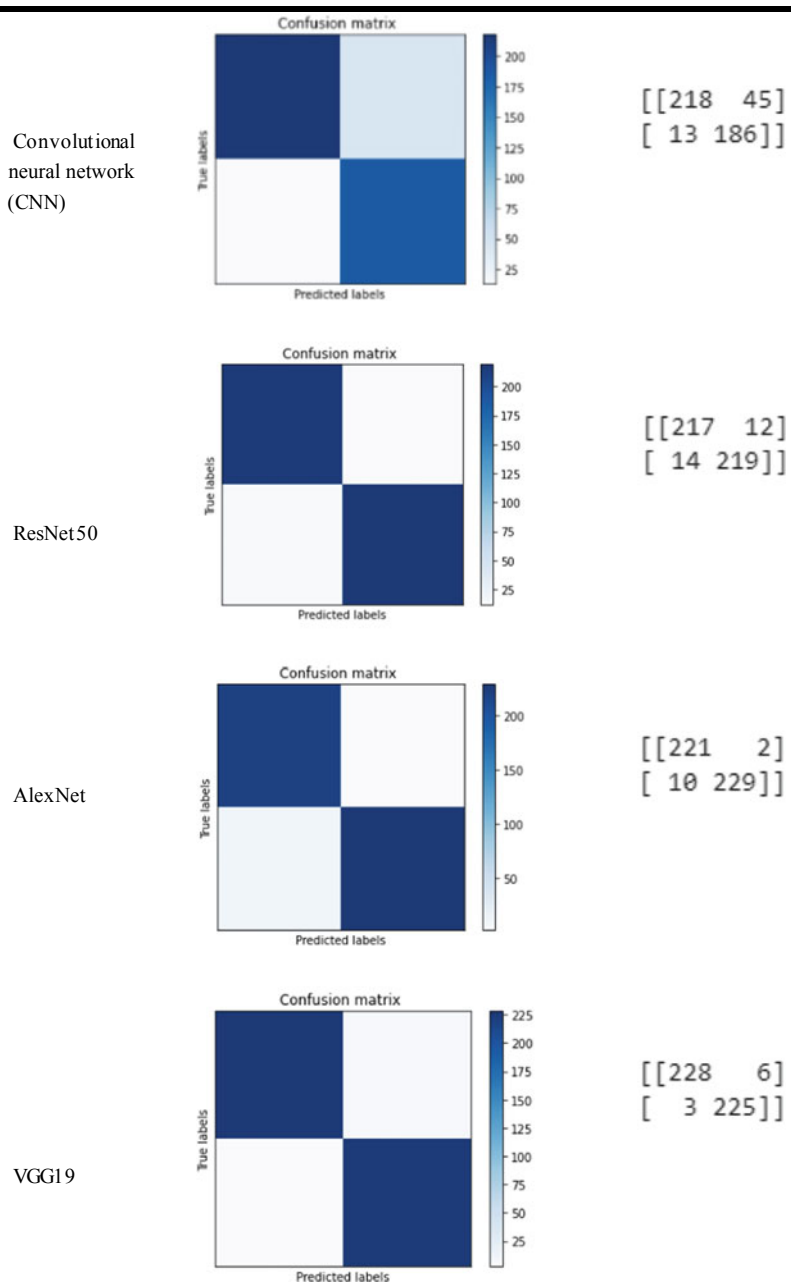
Table 7 (continued)

Table 8 CNN and deep learning models used with the corresponding loss value plots for training and validation

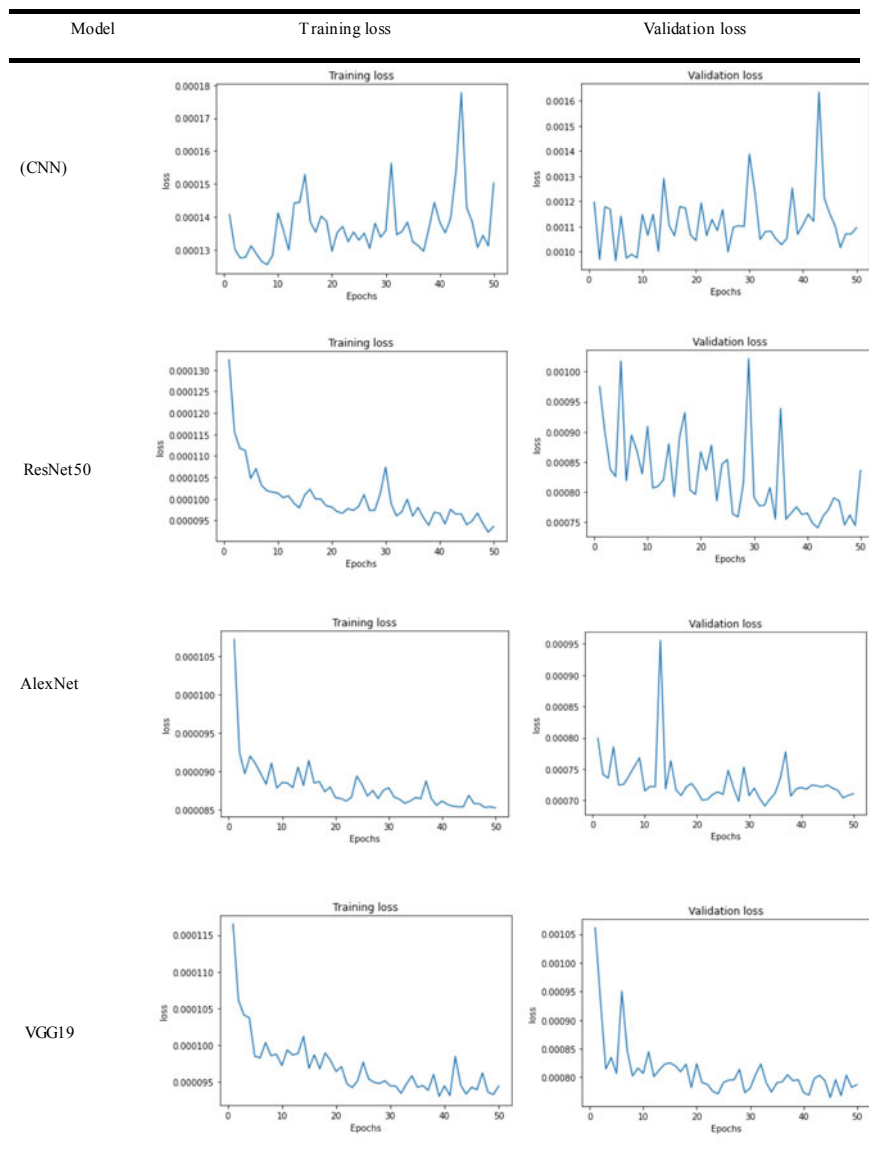
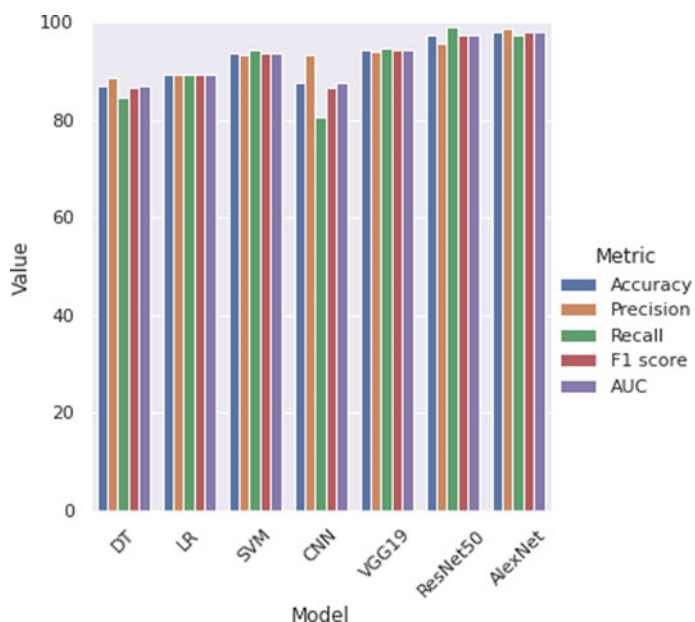


Table 9 Values of accuracy, precision, recall, F1-score, and area under curve for all the models used

Model	Accuracy (%)	Precision (%)	Recall (%)	F1-measure (%)	Area under curve (AUC) (%)
Decision tree	86.82	88.63	84.41	86.47	86.81
Logistic regression	89.20	89.17	89.17	89.17	89.20
Support vector machine	93.73	93.16	94.37	93.76	93.73
CNN	87.44	93.47	80.5	86.51	87.44
VGG19	94.37	93.99	94.80	94.39	94.37
ResNet50	97.40	95.81	99.13	97.44	97.40
AlexNet	98.05	98.68	97.40	98.03	98.05

**Fig. 11** Comparison plot of the models based on the evaluation metrics

Please try to avoid rasterized images for line-art diagrams and schemas. Whenever possible, use vector graphics instead depicted in Fig. 12.

Table 10 Table captions should be placed above the tables

Heading level	Example	Font size and style
Title (centered)	Lecture Notes	14 point, bold
1st-level heading	1 Introduction	12 point, bold
2nd-level heading	2.1 Printing area	10 point, bold
3rd-level heading	Run-in heading in bold. Text follows	10 point, bold
4th-level heading	<i>Lowest level heading.</i> Text follows	10 point, italic

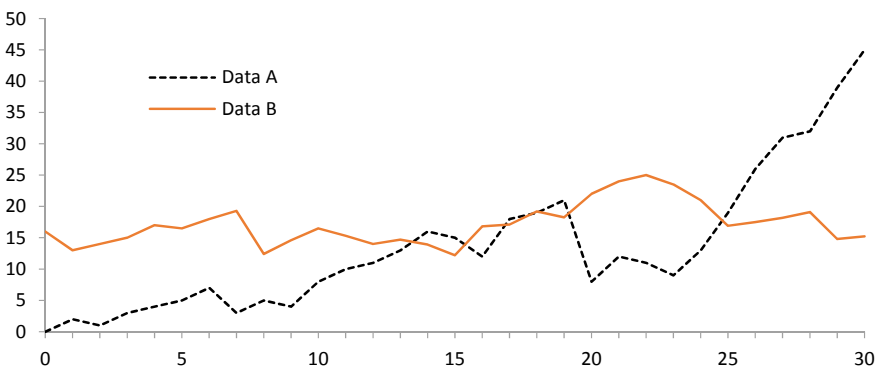


Fig. 12 A figure caption is always placed below the illustration. Short captions are centered, while long ones are justified. The macro button chooses the correct format automatically

4 Conclusion and Future Work

X-ray and CT scan can play an effective role in early diagnosing of diseases even before passing through a tedious process of comment by radiologist and medical expert team. We implemented 3 naïve machine learning models and four deep learning models to classify X-ray images in two categories: COVID-19+ and COVID-19-, respectively. We applied Naïve models with their default architecture whereas for deep learnings we opted CNN with default architecture and transfer learning algorithms VGG19, ResNet50, and AlexNet were implemented with little tweaking. The models were used for classes classification and feature extraction through an FC layer. The results of the experiments show AlexNet outperformed overall in 7 algorithms. The key takeaways as conclusion are that performance of deep learning models is better as compared to basic machine learning classification. Furthermore, machine learning can assist the doctor to triage patient of COVID-19 by automatic detection of COVID-19 through X-ray samples directly instead of going through tedious routine process of X-ray examination. Furthermore, the result of X-ray classification can be combined with patient history of chronological diseases to get better picture of

disease history by triangulating recovery rate and severity of the COVID-19 impact on overall health of the patient. The same model architecture can be used to classify X-rays from other diseases including lungs infection, pulmonary dieses on other hand same architecture be testes with CT scan and MRI dataset as well.

Acknowledgements This research is supported by Artificial Intelligence & Data Analytics Lab (AIDA) CCIS Prince Sultan University, Riyadh, Saudi Arabia, Authors are thankful for the support.

Declaration Authors declare no conflict for this research.

Funding No specific funding received for this research.

References

1. Khan, M.A., Kadry, S., Zhang, Y.D., Akram, T., Sharif, M., Rehman, A., Saba, T.: Prediction of COVID-19-pneumonia based on selected deep features and one class kernel extreme learning machine. *Comput. Electr. Eng.* **90**, 106960 (2021)
2. Amin, J., Anjum, M.A., Sharif, M., Rehman, A., Saba, T., Zahra, R.: Microscopic segmentation and classification of COVID-19 infection with ensemble convolutional neural network. *Microsc. Res. Tech.* (2021). <https://doi.org/10.1002/jemt.23913>
3. Saba, T.: Recent advancement in cancer detection using machine learning: systematic survey of decades, comparisons and challenges. *J. Infect. Public Health* **13**(9), 1274–1289 (2020)
4. Pacal, I., Karaboga, D., Basturk, A., Akay, B., Nalbantoglu, U.: A comprehensive review of deep learning in colon cancer. *Comput. Biol. Med.* **104003** (2020)
5. COVID19_Pneumonia_Normal_Chest_Xray_PA_Dataset: <https://www.kaggle.com/amanolahasraf/covid19-pneumonia-normal-chest-xray-pa-dataset>. Last accessed 10 Aug 2020
6. COVID-19 Image Data Collection: <https://arxiv.org/abs/2003.11597>. Last accessed 20 Aug 2020
7. Github: <https://github.com/agchung>. Last accessed 15 Aug 2020
8. <https://www.sirm.org/en/category/articles/covid-19-database/>. Last accessed 20 Aug 2020
9. Radiopaedia: <https://radiopaedia.org/?lang=gb>. Last accessed 10 Aug 2020
10. Figshare: <https://figshare.com/articles/COVID-19ChestX-RayImageRepository/12580328/2>. Last accessed 09 Aug 2020
11. Figshare: <https://figshare.com/articles/COVID-19ImageRepository/12275009/1>. Last accessed 05 Aug 2020
12. <https://data.mendeley.com/datasets/2fxz4px6d8/4>
13. <https://www.kaggle.com/nih-chest-xrays/data>. Last accessed 20 Aug 2020
14. Haimed, A.M.A., Saba, T., Albashta, A., Rehman, A., Kolivand, M.: Viral reverse engineering using artificial intelligence and big data COVID-19 infection with long short-term memory (LSTM). *Environ. Technol. Innov.* **22**, 1–20 (2021)
15. Chandra, T.B., Verma, K., Singh, B.K., Jain, D., Netam, S.S.: Coronavirus disease (COVID-19) detection in chest X-ray images using majority voting based classifier ensemble. *Expert Syst. Appl.* **165**, 113909 (2021). <https://doi.org/10.1016/j.eswa.2020.113909>
16. Ozturk, T., Talo, M., Yildirim, E.A., Baloglu, U.B., Yildirim, O., Rajendra, A.U.: Automated detection of COVID-19 cases using deep neural networks with X-ray images. *Comput. Biol. Med.* **121**, 103792 (2020). <https://doi.org/10.1016/j.combiomed.2020.103792>
17. Pathak, Y., Shukla, P.K., Tiwari, A., Stalin, S., Singh, S., Shukla, P.K.: Deep transfer learning based classification model for COVID-19 disease. *IRBM* (2020). ISSN 1959-0318

18. Deng, J., Dong, W., Socher, R., Li, L.-J., Li, K., Fei-Fei, L.: Imagenet: a large-scale hierarchical image database. In: 2009 IEEE Conference on Computer Vision and Pattern Recognition, pp. 248–255 (2009)
19. Jaiswal, A., Gianchandani, N., Singh, D., Kumar, V., Kaur, M.: Classification of the COVID-19 infected patients using DenseNet201 based deep transfer learning. *J. Biomol. Struct. Dyn.* (2020). <https://doi.org/10.1080/07391102.2020.1788642>
20. Sun, L., et al.: Adaptive feature selection guided deep forest for COVID-19 classification with chest CT. *IEEE J. Biomed. Health Inform.* **24**(10), 2798–2805 (2020). <https://doi.org/10.1109/JBHI.2020.3019505>
21. Abbas, A., Abdelsamea, M.M., Gaber, M.M.: Classification of COVID-19 in chest X-ray images using DeTraC deep convolutional neural network. *Appl. Intell.* **51**, 854–864 (2021). <https://doi.org/10.1007/s10489-020-01829-7>
22. Kamal, K.C., Yin, Z., Wu, M., et al.: Evaluation of deep learning-based approaches for COVID-19 classification based on chest X-ray images. *SIViP* **15**, 959–966 (2021). <https://doi.org/10.1007/s11760-020-01820-2>
23. Keidar, D., Yaron, D., Goldstein, E., et al.: COVID-19 classification of X-ray images using deep neural networks. *Eur. Radiol.* (2021). <https://doi.org/10.1007/s00330-021-08050-1>
24. Pham, T.D.: Classification of COVID-19 chest X-rays with deep learning: new models or fine tuning? *Health Inf. Sci. Syst.* **9**, 2 (2021). <https://doi.org/10.1007/s13755-020-00135-3>
25. Meethongjan, K., Dzulkifli, M., Rehman, A., Altameem, A., Saba, T.: An intelligent fused approach for face recognition. *J. Intell. Syst.* **22**(2), 197–212 (2013). <https://doi.org/10.1515/jisys-2013-0010>. Lung, J.W.J., Salam, M.S.H., Rehman, A., Rahim, M.S.M., Saba, T.: Fuzzy phoneme classification using multi-speaker vocal tract length normalization, *IETE Tech. Rev.* **31**(2), 128–136 (2014). <https://doi.org/10.1080/02564602.2014.892669>
26. Saba, T., Rehman, A., Sulong, G.: Improved statistical features for cursive character recognition. *Int. J. Innov. Comput. Inf. Control (IJICIC)* **7**(9), 5211–5224 (2011). Sadad, T., Munir, A., Saba, T., Hussain, A.: Fuzzy C-means and region growing based classification of tumor from mammograms using hybrid texture feature. *J. Comput. Sci.* **29**, 34–45 (2018)
27. Jabeen, S., Mehmood, Z., Mahmood, T., Saba, T., Rehman, A., Mahmood, M.T.: An effective content-based image retrieval technique for image visual representation based on the bag-of-visual-words model. *PLoS ONE* **13**(4), e0194526 (2018)
28. Abbas, N., Saba, T., Mohamad, D., Rehman, A., Almazyad, A.S., Al-Ghamdi, J.S.: Machine aided malaria parasitemia detection in Giemsa-stained thin blood smears. *Neural Comput. Appl.* **29**(3), 803–818 (2018)
29. Amin, J., Sharif, M., Raza, M., Saba, T., Rehman, A.: Brain tumor classification: feature fusion. In: 2019 International Conference on Computer and Information Sciences (ICCIS), pp. 1–6. IEEE (2019)
30. Iqbal, S., Khan, M.U.G., Saba, T., Mehmood, Z., Javaid, N., Rehman, A., Abbasi, R.: Deep learning model integrating features and novel classifiers fusion for brain tumor segmentation. *Microsc. Res. Tech.* **82**(8), 1302–1315 (2019). <https://doi.org/10.1002/jemt.23281>
31. Iftikhar, S., Fatima, K., Rehman, A., Almazyad, A.S., Saba, T.: An evolution based hybrid approach for heart diseases classification and associated risk factors identification. *Biomed. Res.* **28**(8), 3451–3455 (2017)
32. https://en.wikipedia.org/wiki/Decision_tree
33. Khan, M.A., Sharif, M.I., Raza, M., Anjum, A., Saba, T., Shad, S.A.: Skin lesion segmentation and classification: a unified framework of deep neural network features fusion and selection. *Exp. Syst.* e12497 (2019)
34. Jamal, A., Hazim Alkawaz, M., Rehman, A., Saba, T.: Retinal imaging analysis based on vessel detection. *Microsc. Res. Tech.* **80**(7), 799–811 (2017)
35. Nazir, M., Khan, M.A., Saba, T., Rehman, A.: Brain tumor detection from MRI images using multi-level wavelets. In: 2019 International Conference on Computer and Information Sciences (ICCIS), pp. 1–5. IEEE (2019)
36. Nawaz, M., Mehmood, Z., Nazir, T., Naqvi, R.A., Rehman, A., Iqbal, M., Saba, T.: Skin cancer detection from dermoscopic images using deep learning and fuzzy k-means clustering. *Microsc. Res. Tech.* **85**(1), 339–351 (2022)

37. Albawi, S., Mohammed, T.A., Al-Zawi, S.: Understanding of a convolutional neural network. In: 2017 International Conference on Engineering and Technology (ICET), pp. 1–6 (2017). <https://doi.org/10.1109/ICEngTechnol.2017.8308186>
38. Rahim, M.S.M., Norouzi, A., Rehman, A., Saba, T.: 3D bones segmentation based on CT images visualization. *Biomed. Res.* **28**(8), 3641–3644 (2017)
39. Rashid, M., Khan, M.A., Alhaisoni, M., Wang, S.H., Naqvi, S.R., Rehman, A., Saba, T.: A sustainable deep learning framework for object recognition using multi-layers deep features fusion and selection. *Sustainability* **12**(12), 5037 (2020)
40. Simonyan, K., Zisserman, A.: Very Deep Convolutional Networks for Large-Scale Image Recognition (2015). 1409.1556, arXiv, cs.CV
41. Rehman, A., Khan, M.A., Saba, T., Mehmood, Z., Tariq, U., Ayesha, N.: Microscopic brain tumor detection and classification using 3D CNN and feature selection architecture. *Microsc. Res. Tech.* **84**(1), 133–149 (2021). <https://doi.org/10.1002/jemt.23597>
42. Rehman, A., Abbas, N., Saba, T., Mehmood, Z., Mahmood, T., Ahmed, K.T.: Microscopic malaria parasitemia diagnosis and grading on benchmark datasets. *Microsc. Res. Tech.* **81**(9), 1042–1058 (2018). <https://doi.org/10.1002/jemt.23071>
43. He, K., Zhang, X., Ren, S., Sun, J.: Deep Residual Learning for Image Recognition (2015). 1512.03385, arXiv, cs.CV
44. Krizhevsky, A., Sutskever, I., Hinton, G.: ImageNet classification with deep convolutional neural networks. *Neural Inf. Process. Syst.* **25** (2012). <https://doi.org/10.1145/3065386>
45. Ullah, H., Saba, T., Islam, N., Abbas, N., Rehman, A., Mehmood, Z., Anjum, A.: An ensemble classification of exudates in color fundus images using an evolutionary algorithm based optimal features selection. *Microsc. Res. Tech.* **82**(4), 361–372 (2019). <https://doi.org/10.1002/jemt.23178>
46. Pedregosa, F., et al.: Scikit-learn: machine learning in python. *JMLR* **12**, 2825–2830 (2011). Last accessed 15 Sept 2020
47. Paszke, A., Gross, S., Massa, F., Lerer, A., Bradbury, J., Chanan, G., Killeen, T., Lin, Z., Gimelshein, N., Antiga, L., Desmaison, A., Kopf, A., Yang, E., DeVito, Z., Raison, M., Tejani, A., Chilamkurthy, S., Steiner, B., Fang, L., Bai, J., Chintala, S.: PyTorch: An Imperative Style, High-Performance Deep Learning Library, *Advances in Neural Information Processing Systems*, vol. 32, pp. 8024–8035. Curran Associates, Inc. (2019). <http://papers.neurips.cc/paper/9015-pytorch-an-imperative-style-high-performance-deep-learning-library.pdf>
48. Roy, S., Shoghi, K.I.: Computer-aided tumor segmentation from T2-weighted MR images of patient-derived tumor Xenografts. In: Karay, F., Campilho, A., Yu, A. (eds.) *Image Analysis and Recognition. ICIAR 2019. Lecture Notes in Computer Science*, vol. 11663. Springer, Cham (2019). https://doi.org/10.1007/978-3-030-27272-2_14
49. Hossin, M., Sulaiman, M. N.: A review on evaluation metrics for data classification evaluations. *Int. J. Data Min. Knowl. Manag. Process* **5**(2), 01–11 (2015). <https://doi.org/10.5121/IJDKP.2015.5201>
50. Saba, T., Bokhari, S.T.F., Sharif, M., Yasmin, M., Raza, M.: Fundus image classification methods for the detection of glaucoma: a review. *Microsc. Res. Tech.* (2018). <https://doi.org/10.1002/jemt.23094>

Data Mining in Medical Laboratory Service Improves Disease Surveillance and Quality Healthcare



Uchejeso Mark Obeta , Obiora Reginald Ejinaka,
and Nkereuwem Sunday Etukudoh

Abstract Day in day out, data are turned out in various medical laboratories which are adequately documented and used for surveillance in various diseases of concern in public health. Though data mining seems to be new in healthcare, medical laboratory services as very important component of healthcare need serious data mining for diagnosis of ailments and numerous public health diseases. This chapter was carried out based on review of literatures and practices available in Nigeria which contributes to healthcare quality improvement. The chapter examined origin, basic principles, advantages and disadvantages, uses, and challenges of data mining in relation to medical laboratory information management system (MLIMS) while looking at data management from hard to soft copies, possible applications, ethico-legal perspectives, implications of data mining, disease surveillance, and data mining toward quality improvement as used in medical laboratories. It is evident that most of decisions taken in healthcare and public health are based on information provided by data mining from medical laboratory services based on the diseases of interest. Data mining in medical laboratory services is a tool that aids in monitoring trends in the diagnosis of cancer, HIV, COVID-19, malaria, diabetes, and other diseases based on various parameters of assessment with all demographic variables well documented and analyzed. The interested agencies or ministries may apply data mining techniques based on medical laboratory results to find trends in disease outbreaks or deaths, per hospital, state, region, or country through which policies could be formulated and implemented toward surveillance and quality healthcare improvement.

Keywords Data mining · MLIMS · Medical laboratory services · Disease surveillance · Quality laboratory · Quality healthcare

U. M. Obeta · O. R. Ejinaka · N. S. Etukudoh

Department of Medical Laboratory Management, Federal School of Medical Laboratory Science, Jos, Nigeria

e-mail: mark.obeta.pg00014@unn.edu.ng

1 Introduction

The practice of medical laboratory science cannot be complete without contact with numerous data. It is stated that 70–75% decisions in healthcare are based on results and data presented by the medical laboratory findings. In the clinic, admissions and discharge of patients are depending on such data results [1, 2]. The medical laboratory science practice across the globe may have different nomenclatures [3] like Biomedical Science, Medical Technology, Medical Laboratory Technology, and Clinical Laboratory Science but in the end means same practice of analysis of patients' samples to generate numerous data/results for the use in the management of the patient [1].

Data mining has given an impetus to strong medical decisions, disease surveillance, pandemic epidemiology and control, policy formulations, and patients' responses and satisfaction to medical treatment. Data mining remains a gold mine in medical laboratory science as all disease conditions are associated with medical laboratory findings. This chapter discusses data mining in healthcare with special interest in medical laboratory science which has numerous data that are used to determine the scientific bases of medical care.

Several terms (Fig. 1) have been used in data mining historical perspectives comprising of databases, information retrieval, statistics, algorithms, and machine

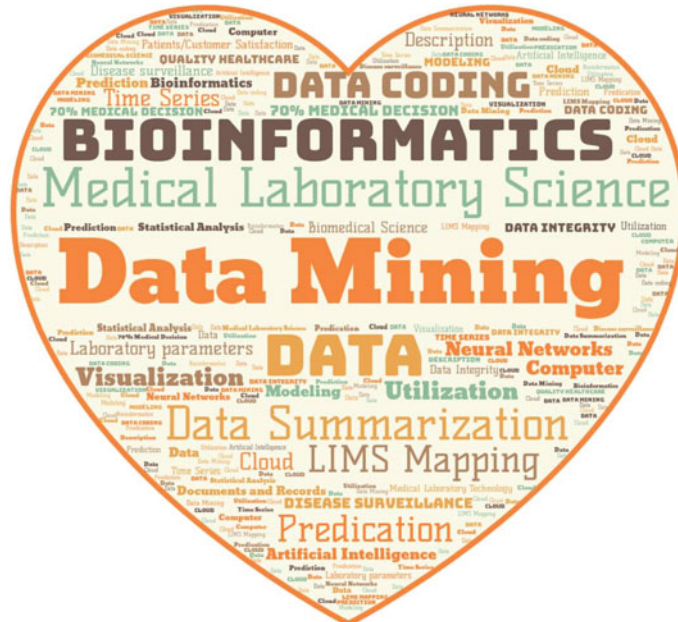


Fig. 1 Data mining in medical laboratory science word cloud. Image credited to Obeta Uchejeso who developed it using Google WordCloud App

learning. Data mining can be described as process of extracting knowledge from data and no wonder it can be called knowledge discovery in databases (KDD) with the aid of useful information using algorithms [4–6].

This chapter is organized in such a way that it discusses the origin, principles, and techniques of data mining in healthcare with special reference to medical laboratory science, viz-a-viz the advantages, uses, and importance. It X-rayed the sources of data with medical laboratory information management system, challenges, and ethico-legal issues. The chapter finally discussed the implications for disease surveillance with quality improvement perspectives.

2 Origin of Data Mining

Data mining is as old as data itself. The data mining historical trend and developmental components (Fig. 2) cannot be completed without tracing it back to era of statistics laced with Bayes theorem in 1763 and regression in 1805. The statistics age was followed by computer age which had turing in 1936, neural networks in 1943, evolutional computation in 1965, and databases in 1970s with algorithms in 1975. It was John Snow who described medical laboratory science as evidence-based medicine when he employed data mining in 1854 to discover Cholera epidemiology from a particular water source [4–8]. However, the recent developed data mining using some methodology and technology started as noted in 1990s [8–10] with knowledge discovery in database (KDD) in 1989 and support vector machine (SVM) in 1992. Subsequently, data science and moneyball started in 2001 and 2003,

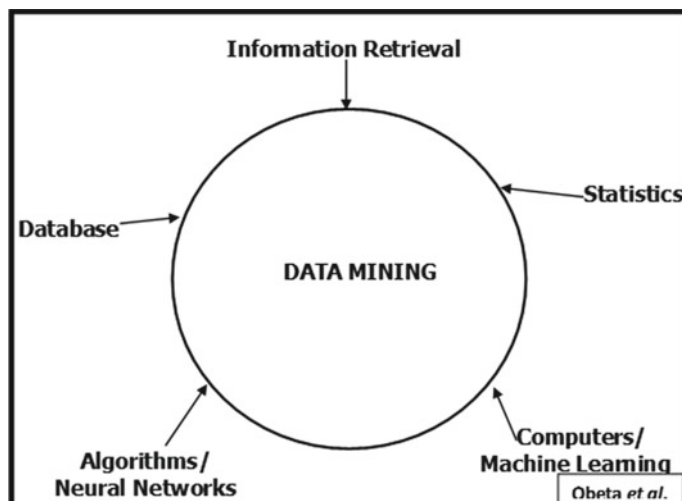


Fig. 2 Data mining historical trend and developmental components

respectively. Data mining is aimed at identifying potential useful, valid, novel, and understandable correlations with patterns in a given detailed large sets of data that could be seen as complex for humans to detect ordinarily.

Data mining has been applied in supermarkets in relation to customer transactions data for optimum value of customers, in credit card companies data warehouse for fraud detection among customer transactions, in hotel establishments survey databases to track good customer attributes, in semiconductor fabrication engineering companies for crosschecking yield problems, in television stations for predicting audience in their programs and advert surveillance, and in hospitals for cancer patient predictions and management [11, 12].

3 Basic Principles and Techniques in Data Mining

The medical laboratory mining techniques involve complex analysis of data and determination data connections in a given large database. Basically, two approaches to medical data mining involve machine learning algorithms and statistics. The processes could be classified into descriptive and predictive data mining techniques (Fig. 3). While descriptive mining is interested in general data properties, the predictive mining makes inferences on the available data for predictions.

Data mining techniques could be effective and predictive in nature based on Lashari et al. [4] following reasons:

- i. User friendly in predicting past circumstances
- ii. Operates very well by using past data to learn
- iii. Manages large data from various sources of required data
- iv. Have a models that is easily updated by relearning from old information in order to change trends.

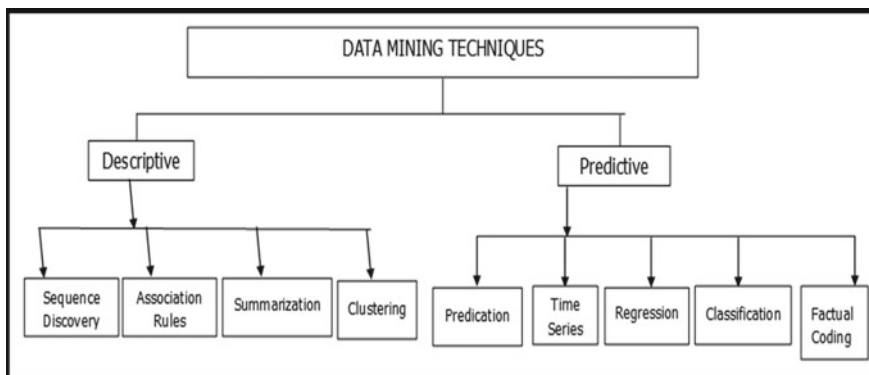


Fig. 3 Classification of data mining processes

4 Data Mining in Healthcare

Data mining is gaining grounds in healthcare after a huge success in marketing and business organizations. Studies have shown the use of data mining techniques, while employing decision tree, random forest, Naive Bayes, and logistic regression, for cancer, brain tumor, hypertension and infectious diseases detection, using algorithms, and machine learning on the standard databases [4, 13].

Just as data mining is done in other aspects of life, in health, the processes are equally followed including sampling and registration, exploration and visualization, modification and manipulation, modeling and prediction, and assessment of accuracy (Fig. 4). It may be in biomedical/medical laboratory samples analysis for various parameters including DNA studies.

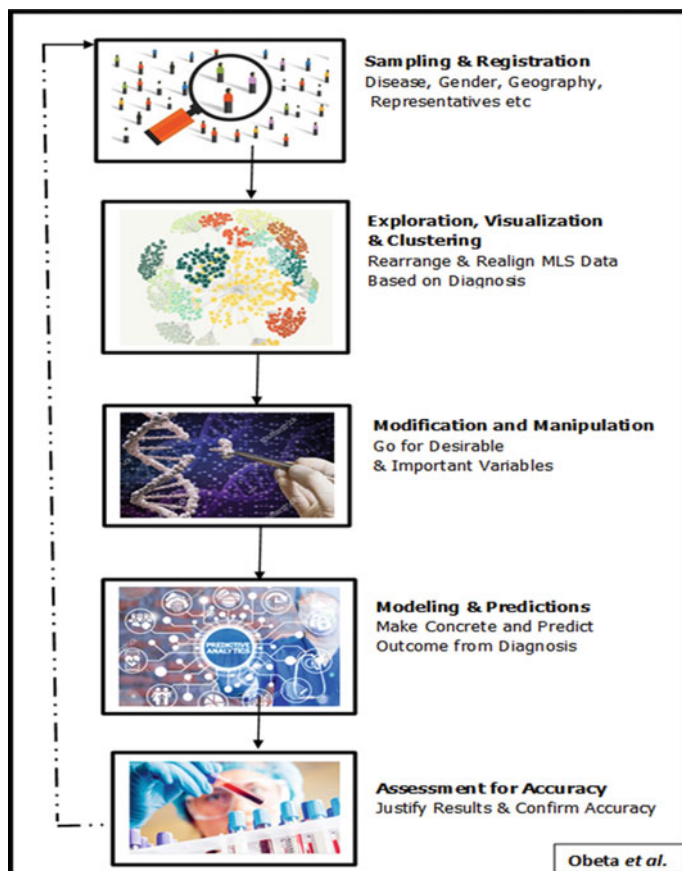


Fig. 4 Processes of data mining in medical laboratory services

The data mining in healthcare has not failed to mention the aspect of evidence-based medicine called the medical laboratory aspect of health services [4, 14]. This, therefore, conforms the role of medical laboratory services in clinical decisions and policy making in healthcare.

4.1 Data Mining in Medical Laboratory Science

If up to 70% decisions in healthcare are based on the medical laboratory diagnosis results as posited by some researchers, then it implies that medical laboratories have majority of the databases generated in healthcare. Therefore, the knowledge discovery in database (KDD) in health and medical practice is mostly based on the outcomes of data mining in the medical laboratory services in stand-alone or hospital-based laboratories for any given disease condition.

Such knowledge (KDD) Fig. 5 as illustrated in medical laboratory science could be gotten following a sequential step. Such steps are further explained [4] as follows:

Data Collection and Cleaning: Data collection is gotten from the reception benches and testing benches in various medical laboratories. Data cleaning is represent the elimination of any data collected, that is, random, irrelevant, or missing in values from the benches. There are cases where clients refuse to disclose their age, thereby creating for a room to use adult (Ad) to connote age. In this case, there is need for data cleaning in order to eliminate the Ad as inputted in the database.

Data Integration: Data integration combining a filtered data into a meaningful and useful data for the study for the knowledge ahead.

Data Selection: Data selection is where a data are made relevant for the analysis based on the data selection and kind of data in question.

Data Transformation: Data transformation is the conversion of data into the required forms for performing different mining analysis and operations including smoothing, aggregation, and normalization.

Data Mining: Data mining is the process of data analysis using patterns or rules that are useful for the new knowledge.

Pattern Evaluation: Pattern data evaluation is identification of patterns through which knowledge is obtained based on given acceptable measures within data mining process.

Knowledge Representation: Knowledge (KDD) is the outcome of data mining stages after employing all the tools, and techniques including visualization tools to create a different picture from the already existing results of such study.

The various data mining techniques applicable in healthcare data mining are used to turn raw medical laboratory data into some useful forms for new knowledge and

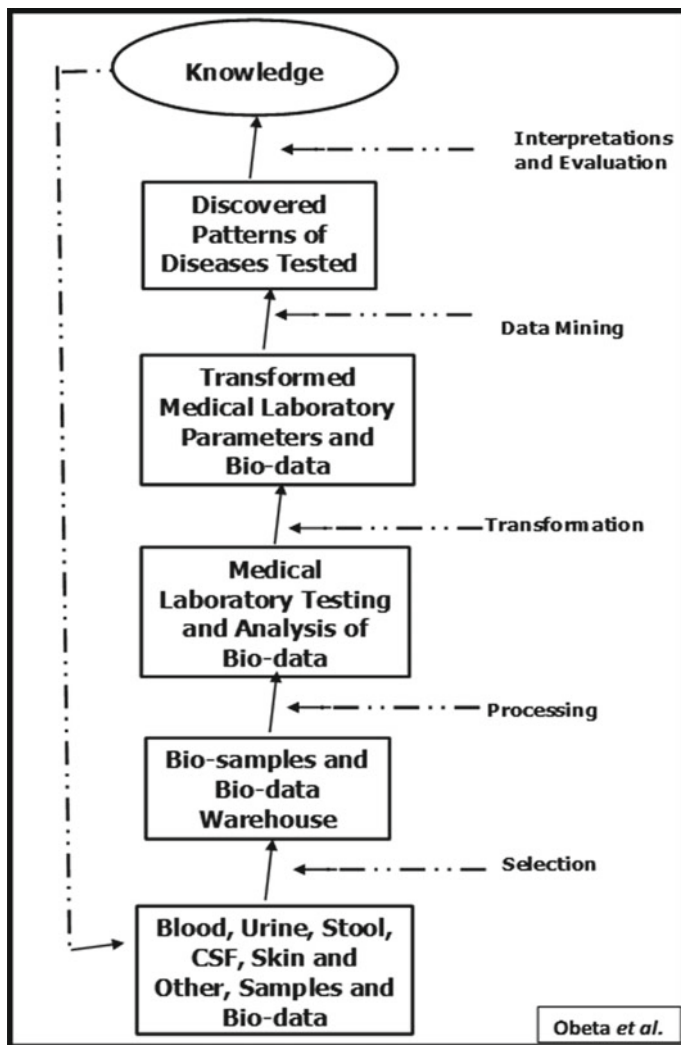


Fig. 5 Knowledge discovery in database from medical laboratory samples

possible policy formulation. Such applicable techniques in data mining for medical laboratory services are

Classification: Classification represents a data mining technique that requires to collect various of information and data for their attributes in order to be analyzed. Once the attributes have been identified, the data can be further categorized and managed.

Clustering: Clustering as used in data mining technique is the identification of data that relates with considerations in their differences and similarities. Visual approach is mostly used to show the distribution of data in relations. Take for instance, Hepatitis B testing in a giving sample population in terms of clustering shall identify the relations and similarities existing among the positive and negative subjects.

Regression: Regression techniques involve identifying and analyzing the relationship between variables in a data set. Regression is a technique in data modeling showing relationship between variables various instances.

Outlier detection: Outlier detection is another way to express anomaly detection in a giving data set. It consist of observing data items which does not match (anomaly) when certain behaviors are assessed. An identification of an anomaly creates room for root cause identification and prevention.

Sequential Pattern: Sequential pattern is a technique t discovering similar patterns and consistency in databases. This technique uncovers deviation in the databases at regular intervals over a study time.

Prediction: Prediction simply involves analyzing a retrospective testing scenario to predict future occurrences. Historical and genealogical data when used for examination and analysis to gain some insight are a useful data mining process to predict what will happen to the samples in future.

Association Rules: Association rules are a data mining technique that relates to statistics. It searches and indicates certain data for association that may linked together between two data set for discovering a hidden pattern.

There is a need for all medical laboratory service providers to procure a medical LIMS that has capacity to do data mining and sharing. Such systems should ensure security of entry (Fig. 10) such that these functions are present:

Client/Patient Registration: This is to permit clients/patients to register themselves or are registered by the medical laboratory receptionist or ICT staff in the case of first time visit where they are provided opportunity for username and password the system.

Client/Patient Login: Client/patients or their authorized persons would be able to login into the system with their username and password for follow up and possibly their results.

Viewing Details: Healthcare providers and all clients [15] of medical laboratories should have an opportunity to view there details where necessary to familiarize laboratory and clinical service providers.

Disease Prediction: There should be an opportunity predict or evaluate the illness/diseases that the client is trying to test or diagnose by going through corresponding questions, answers, and results of data mining to pinpoint the disease accurately based on result outcomes and underlying symptoms.

Search Options: Clients, doctors, and medical laboratory scientists/staff patients should have an opportunity to search for one another according to their interest, diseases, and tests results available for references.

Providing Feedbacks: Clients should be able to provide feedback to the medical laboratory for satisfaction, payment, or other additional information to improve or validate quality.

Adding Diseases Symptoms and Possible Tests Required: Medical laboratory administrators/managers may add diseases' symptoms and possible tests needed into the system for all clients to examine and make request where possible.

Doctor/Healthcare Providers Login: Doctors and other healthcare providers are required to login with their username and password to use the medical LIMS and other information systems.

Doctor/Healthcare Provider Registration: Administrators (admin) could add and register a new doctor or other healthcare providers into the system with adequate username and password.

Administrator/Director Medical Laboratory Services Login: Administrator/director medical laboratory services are equally expected to login with their username and password to use the system at any instance for security and confidentiality purposes.

View Diseases Testing Parameters: Medical laboratory administrators and clients can view various disease testing parameters stored in the database for easy data mining in the system.

Sharing Information: There should be a link for data sharing opportunity patients or to another healthcare provider that is approved to receive the information. Medical laboratory scientists could share information of a disease test result parameters to another professional for input in the diagnosis or for verification. This is where data mining comes in for tele-medical laboratory service (TMLS), mobile medical laboratory service (MoMLS), and Internet of things in medical laboratory science (IoTMLS).

4.2 Advantages of Data Mining in Medical Laboratory Science

Latest technologies and improvement in equipment installations and interconnectivities (Figs. 6 and 7) in medical laboratory services have improved services and open opportunities for better data mining in medical laboratory science. The advantages of data mining in this context are as follows:



Fig. 6 Medical laboratory equipment incorporated in laboratory information management systems for easy data mining in medical laboratories. Image credited to Abims Fertility and Garmete Banking Services, Lagos-Nigeria

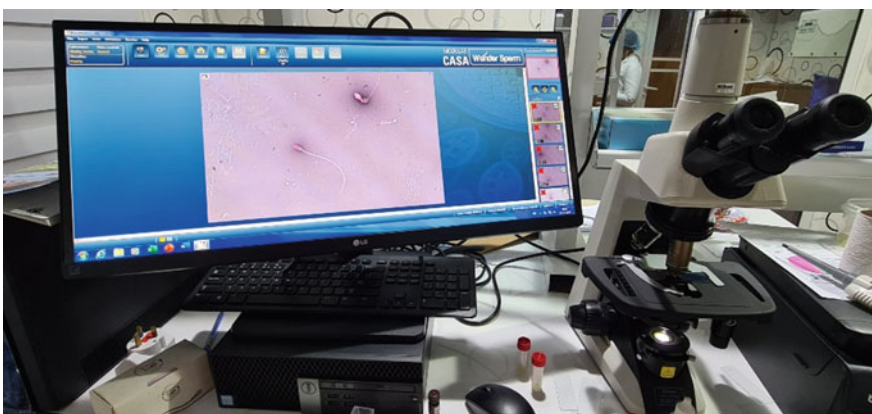


Fig. 7 Semen analysis in medical laboratory information management systems incorporated microscope. Image credited to Abims Fertility and Garmete Banking Services, Lagos-Nigeria

- i. Data mining provides an organizational agility even if it is a small medical laboratory to compete with laboratory or health giants due to workflow automation and data management systems that provide the needed reliable results.
- ii. Data mining provides reduction in time and effort put by the medical scientist and that of the request healthcare provider.

- iii. The system integration and technology algorithms create ability of LIMS to examine multiple areas and large data simultaneously as needed.
- iv. There is a very high decrease in potential human error.
- v. There is an adequate presentation of data in an appealing and correct format as expected by the end user.
- vi. There is an opportunity to access medical laboratory data anytime and anywhere in the world with system linkages and improved technologies.

4.3 Uses and Importance of Data Mining in Medical Laboratory

Data mining deals with a large medical laboratory data. Take for instance, hormonal data in Abims Fertility and Garmetes Banking Services, Lagos-Nigeria where various hormonal profiles are found. Data mining in such a laboratory helps to establishing reference intervals (RIs). The RIs may be direct or indirect. Having used international RIs for long in Nigeria, the COVID-19 pandemic has taught Africans a major lesson that what happens in Europe may be different in Nigeria.

With aid of artificial intelligence, data mining could assist the medical laboratory in diagnostic/testing or prognostic modeling. This is because machine learning technology can aid to combine measurements derived from multiple blood parameters to develop disease diagnostic and prognostic models with an avalanche of data.

Data mining aids in epidemiological investigation and disease surveillance. This is evident with the happenings in the current ravaging COVID-19 [16] where real-time world data are shared and managed in accurate, reliable, and timely manner with follow up on isolation, treatments, discharge, and death. This measure can equally be adopted in malaria, diabetes, cancer, and other health challenges and diseases using real-world big-data studies (RWBDS).

The data mining helps in proper laboratory management with aid of LMIS. This goes a long way to do a retrospective study on the laboratory quality indicators, including inappropriate requests, misidentification errors, test transcription errors, testing processes, and result issuing challenges.

There is no doubt that data mining is used in analysis of sources of variations medical laboratory parameters. There is exploration of the data distribution of parameters so as to compare whether differences exist in their distributions.

Data mining aids in internal and external quality assessment (EQA) programs. This can help to overcome sources of errors to the barest minimum.

Patient data-based real-time quality control (PBRTQC) has been well organized and carried out using data mining for internal quality control (IQC).

Data mining employs auto-verification models based on algorithms and decision trees to automatically review test results.

It is very important to know that there is data overload in medical laboratory services found in standing alone or hospital-based facilities. Therefore, automated systems using data mining use databases/data warehouses/data marts therein to

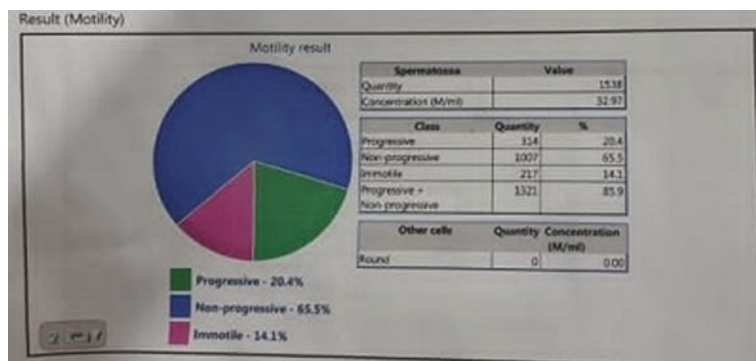


Fig. 8 Computer-assisted semen analysis (CASA) result that is data mining compliant. Image credited to Abims Fertility and Garmete Banking Services, Lagos-Nigeria

provide wealth of new knowledge for better healthcare for a human being to do this.

Data mining can help patients and medical laboratory clients to have more value for money and cost savings. Data mining can equally be used to discover financial and practice fraud in in medical laboratories and health systems.

Data mining can also aid in introducing non-invasive medical laboratory testing and decision support toward some laboratory procedures that are invasive, costly, or painful to patients and clients like biopsy in women cervical cancer diagnosis. Computer-aided diagnosis (CAD) is an advice as a result of data mining in cancer testing. This is also like CASA in Fig. 8 as seen in fertility laboratory.

Data mining is useful in new discoveries in medical laboratory diagnosis. This has helped in change or update on the medical laboratory policies and policies of government and useful agencies especially in infectious diseases and pandemic control.

5 Source of Data and Medical Laboratory Information Management Systems (MLIMS)

Sources of data toward a successful data mining in medical laboratory science practice can be gotten from:

- i. Medical laboratory request forms
- ii. Medical laboratory general registration books
- iii. Medical laboratory bench registers
- iv. Medical laboratory disease/parameters results books
- v. Medical laboratory/hospital records linked to systems
- vi. Equipment systems linked storage devices.

There is no doubt that these record books contain various data such as names, addresses/locations, gender, age, marriage status, previous medical records, educational levels, work stations, risk behaviors, and some environmental factors. Also, data such as sample identification number, collection date and time, and type of sample: for example, urine, stool, throat, cerebrospinal fluid, etc., tests to be performed, name of ordering healthcare provider or physician, location of patient such as ward, clinic, outpatient, medical laboratory test results, and time and date results are reported.

Medical laboratory information management system (MLIMS) otherwise called laboratory information management system (LIMS) and customer care are essentials of a quality management system and process control of a good medical laboratory practice. These information can be in hard or soft copies and stored adequately in line with the laboratory policies as seen in the laboratory hand books. Considering the large flow of clients and medical/biological samples daily in the medical laboratories, large data are generated, and there is germane need to employ good LIMS for improvement and policy generation when needed with aid of data mining [1, 17].

MLIMS could be described as a process that integrates all medical laboratory workflow, instrumentation, testing, and analysis of samples and result reporting [17, 18] as seen in Fig. 9 which is the movement from a paper work to software and applications. The input including personnel and output are put together toward eliminating errors and improving quality and providing regulatory compliance.

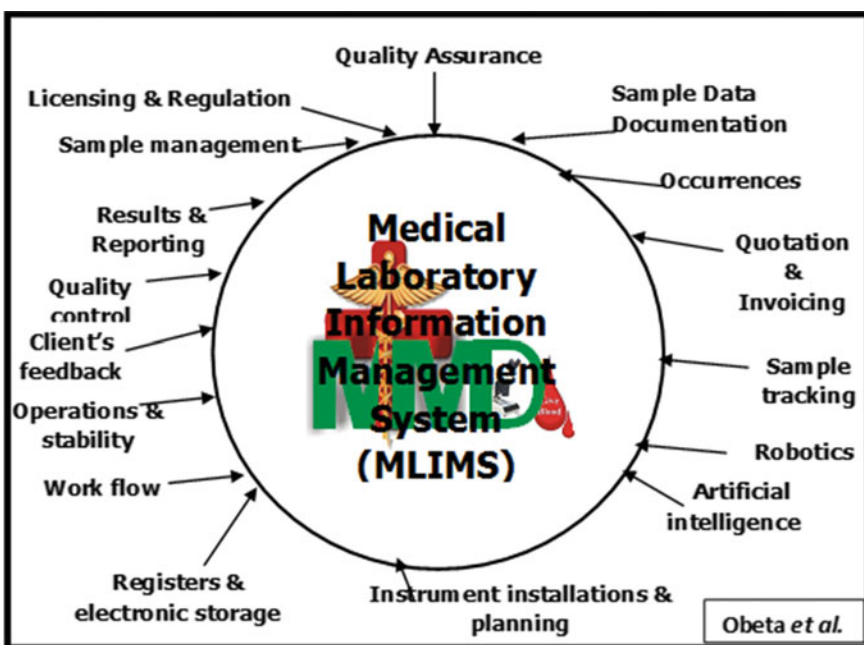


Fig. 9 Medical laboratory information management system (MLIMS) in data mining age

ROLES	DMLS	ADMIN	PATH	MLS	MLT	MLA	C.CARE	DISABLE	CHANGE
								MLIMSO	ICTO
GENERAL SETTINGS									
ALL ABILITIES	<input checked="" type="checkbox"/>	<input checked="" type="checkbox"/>	<input type="checkbox"/>	<input checked="" type="checkbox"/>	<input type="checkbox"/>	<input type="checkbox"/>	<input type="checkbox"/>	<input checked="" type="checkbox"/>	<input checked="" type="checkbox"/>
ACCOUNT ENTRY SETTINGS									
FULL ACCESS	<input checked="" type="checkbox"/>	<input type="checkbox"/>	<input checked="" type="checkbox"/>	<input checked="" type="checkbox"/>					
LIST	<input checked="" type="checkbox"/>								
VIEW	<input checked="" type="checkbox"/>								
CREATE	<input checked="" type="checkbox"/>	<input checked="" type="checkbox"/>	<input checked="" type="checkbox"/>	<input checked="" type="checkbox"/>	<input type="checkbox"/>	<input type="checkbox"/>	<input checked="" type="checkbox"/>	<input checked="" type="checkbox"/>	<input checked="" type="checkbox"/>
EDIT	<input checked="" type="checkbox"/>	<input checked="" type="checkbox"/>	<input type="checkbox"/>	<input checked="" type="checkbox"/>	<input type="checkbox"/>	<input type="checkbox"/>	<input type="checkbox"/>	<input type="checkbox"/>	<input type="checkbox"/>
DELETE	<input checked="" type="checkbox"/>	<input checked="" type="checkbox"/>	<input type="checkbox"/>	<input checked="" type="checkbox"/>	<input type="checkbox"/>	<input type="checkbox"/>	<input type="checkbox"/>	<input type="checkbox"/>	<input type="checkbox"/>
SEND FOR REVIEW	<input checked="" type="checkbox"/>	<input type="checkbox"/>	<input checked="" type="checkbox"/>	<input checked="" type="checkbox"/>	<input checked="" type="checkbox"/>				
FINALIZE	<input checked="" type="checkbox"/>	<input checked="" type="checkbox"/>	<input checked="" type="checkbox"/>	<input checked="" type="checkbox"/>	<input type="checkbox"/>	<input type="checkbox"/>	<input type="checkbox"/>	<input checked="" type="checkbox"/>	<input type="checkbox"/>
SENT TO TT	<input checked="" type="checkbox"/>	<input type="checkbox"/>	<input type="checkbox"/>	<input checked="" type="checkbox"/>	<input checked="" type="checkbox"/>				
SEND FOR COMPLIANCE	<input checked="" type="checkbox"/>	<input checked="" type="checkbox"/>	<input checked="" type="checkbox"/>	<input checked="" type="checkbox"/>	<input type="checkbox"/>	<input type="checkbox"/>	<input type="checkbox"/>	<input checked="" type="checkbox"/>	<input type="checkbox"/>
SEND TO CLIENT	<input checked="" type="checkbox"/>	<input checked="" type="checkbox"/>	<input type="checkbox"/>	<input checked="" type="checkbox"/>	<input type="checkbox"/>	<input type="checkbox"/>	<input checked="" type="checkbox"/>	<input checked="" type="checkbox"/>	<input type="checkbox"/>
PUBLISH	<input checked="" type="checkbox"/>	<input checked="" type="checkbox"/>	<input type="checkbox"/>	<input checked="" type="checkbox"/>	<input type="checkbox"/>	<input type="checkbox"/>	<input type="checkbox"/>	<input checked="" type="checkbox"/>	<input checked="" type="checkbox"/>
TT-Track & Trace, C.Care-Customer Care, DMLS-Director Medical Laboratory Services, ADMIN-Administrator, PATH-Pathologist, MLS-Medical Laboratory Scientist, MLT-Medical Laboratory Technician, MLA-Medical Laboratory Assistant, MLIMSO-Medical Laboratory Information Management System Officer, ICTO-Information Communication Technology Officer									
Obeta et al									

Fig. 10 Security roles for a chart account entry setting for data mining compliant systems access in a medical laboratory establishment

MLIMS uses online transactional processing (OLTP) and online analytical processing (OLAP) systems in the storage and management of medical laboratory data.

The MLIMS must have these basic functions in line with Association of Public Health Laboratories (APHL) [19]:

- i. A well-defined specimen inventory management,
- ii. Quality management reports,
- iii. A good reagent and equipment inventory management,
- iv. Quality training, education, and human resource management
- v. Standard laboratory policies and operating procedures,
- vi. Good laboratory mutual assistance and disaster management,
- vii. Quality assurance (QA) and quality control mechanisms
- viii. Acceptable external quality assurance/proficiency testing (EQA/PT)
- ix. A very good storage, analytical, and retrieval system with rooms for improvement based on improved technologies.

With digital world new order, so many LIMS systems and applications have been developed that makes LIMS practice easier in medical laboratories.

There are so many applications including: AQ Manager LIMS, Autoscribe, CloudLIMS, Dx ONE, eLab Journal, eLabInventory, Illumina, LabwareLIMS, Labwise™-XD, LockboxLIMS, Maqsimalab⁺, NEXUSPro, QReserve, ampleManagerLIMS, Sysmex, WeLIMS, and a few to mention. All these applications and their uses can be found on their various Websites.

Most importantly, MLIMS applications can be customized based on the needs and facility. This action should align with Boyar et al. [17] specifications such as

- i. Categories and nature of medical laboratory data and the samples and clients identification.
- ii. The use of medical laboratory data by clients, laboratory managers, public health, and policy makers.
- iii. Ability to meet quality, regulatory, and accreditation criteria.
- iv. Medical laboratory size, personnel, and services.
- v. The complexity sample size, unique services, and data expected.
- vi. Other functions the medical laboratory may wish to incorporate.

6 Data Management from Hard to Soft Copies

Data management has been solely in hard copies before the arrival of computers. Hard copies for the storage off data to a greater extent are still in use in Nigeria for instance especially in government health institutions and medical laboratories. The reason may be due to poor technical know-how and poor budgetary provisions toward systems upgrade and interest in data mining.

With the digital age laced with new era after COVID-19, there is an urgent need to move all hard copies in medical laboratories to soft copies with adequate applications for LIMS [19–21]. This shall provide an adequate platform (possibly with use of any LIMS app mentioned above) for good medical laboratory data mining in the world and Nigeria in particular. This practice shall lead medical laboratory services to tele-medical laboratory service (TMLS), mobile medical laboratory service (MoMLS), and Internet of things in medical laboratory science (IoTMLS).

Data mining cannot be judiciously carried out with soft copies found in various algorithms-based LIMS. The challenges notwithstanding, various medical laboratory managers and administrators should as a matter of urgency upgrade from hard copies to better medical laboratory science information management systems.

7 Data Mining and Possible Applications Used in Medical Laboratories

There are various tools, software, and algorithms that can be employed in data mining in medical laboratories. The common available ones according to Sen and Khandelwal [22] are

Orange: This is “component-based data mining and machine learning software suite written in the Python language”.

R: This is a programming language and software environment for computation in statistics, graphics, and data mining.

Rapid Miner: This is machine learning and data mining in laboratory and experimental environment.

SCaViS: This is a Java cross-platform developed by Argonne National Laboratory for data analysis framework.

SenticNet API: This is “semantic and affective resource for opinion mining and sentiment analysis”.

UIMA: “The unstructured information management architecture (UIMA) is a component framework for analyzing unstructured content such as text, audio, and video—originally developed by IBM”.

Weka: This is a “suite of machine learning software applications written in the Java programming language”.

Considering that there are various algorithms in existence and upcoming ones, choosing the type of an algorithm to be used is very important in medical laboratories based on their types:

Classification algorithms: This algorithm predicts one or more discrete variables based on their attributes, e.g., support vector machines (SVMs) and C4.5.

Regression algorithms: This predicts discrete variables and continuous variables, e.g., AdaBoost and Naïve Bayes.

Association algorithms: This is useful in determining the associations between various attributes in a data set, e.g., Apriori algorithm.

Segmentation algorithms: This is useful in slicing the data into groups or clusters, e.g. Microsoft clustering algorithm.

Sequence analysis algorithms: This summarize frequent sequences or episodes in data, such as a Web path flow, e.g., CART algorithm.

Notably, Mittal et al. [21] provided three main data mining techniques with examples to include association rule mining (ARM)—Apriori, FP growth, and ECLAT; classification—C4.5, ID3, CART, SVM, perceptron, nearest neighbor, and clustering— K -means, BIRCH, EM, DBSCAN, FCM, CLIQUE, and O-cluster.

Zhang and Segall [23] extensively listed some selected software for data mining, text mining, supercomputing data mining, and Web mining in their book chapter as arranged “selected software for data mining are SAS Enterprise MinerTM, Megaputer PolyAnalyst 5.0, PASW (formerly SPSS Clementine), IBM Intelligent Miner, and BioDiscovery GeneSight. The selected software for text mining is SAS Text Miner and Megaputer PolyAnalyst 5.0. The selected software for Web mining are Megaputer PolyAnalyst and SPSS Clementine. The software for supercomputing is Avizo by Visualization Science Group and JMP Genomics from SAS Institute. Avizo is 3D visualization software for scientific and industrial data that can process very large data sets at interactive speed. JMP Genomics from SAS is used for discovering the biological patterns in genomics data”. These software are not available for free to those in need of them.

New applications are possible and every medical laboratory service provider not minding the challenges in data mining [24], should key into data mining by engaging any of the applications that might suit their purpose [25–27].

8 Challenges of Data Mining in Medical Laboratory Services

Numerous challenges ranging from lack of computers, LIMS, digital equipment, and poor technical knowledge among medical laboratory staff in developing and low-income countries like Nigeria [24]. Other challenges and militating factors [23] are below.

Medical laboratory researches are based on hypothesis but data mining may start without hypothesis.

Ordinarily, traditional data mining is all about data patterns and trends medical laboratory science, data mining lay much emphasis on the errors, and conformance to the standard. This is because the sample analysis of the patient represents the patient's life or death [28, 29]. Reporting high concentration of glucose in non-diabetic patient may put the patient in danger of administering diabetes drugs on the subject which may lead to serious complications and death and vice versa.

There is difficulty in medical laboratory professionals and other medical professionals who use laboratory data to adapt to change based on data mining results even when credible based on old practice and knowledge. There is delay in change of laboratory policies until after a long time. It is possible to miss out or lose some lives as a result of error and delay in correction.

The ethics of informed consent, non-disclosure of information, and privacy of medical laboratory information and result records of patients' information is a big challenge in medical laboratory data mining. There is no authorization to use medical laboratory data even when they are large and available though, the data mining outcome could save a generation.

There is also security challenge of authorization to access of information in database or MLIMS. This could be controlled through creating access passcodes for all who have access to the system as described in Fig. 10 where access is marked based on medical laboratory staff functions.

9 Ethico-Legal Perspectives of Data Mining in Medical Laboratory Services

Data mining technology in medical laboratory science involves large volumes of data toward useful knowledge discovery. There are social, ethical, and legal issues that may arise considering that in most cases, there are lack of informed consent from individual clients that their data could be shared with third parties or medical laboratory data miners [30].

The major issues are that of confidentiality and informed consent. It is currently the practice that ethical clearance be gotten from relevant ethical review institutions for any data mining leading to search for knowledge. However, one would ask, would that clearance be enough? It is suggestive to include informed consent for individual clients during sample collection that such data or results could be used for data mining as used for surveillance, epidemiological studies, and other research. This to some extent provides soft landing though individual informed consent may add cost to the system [31].

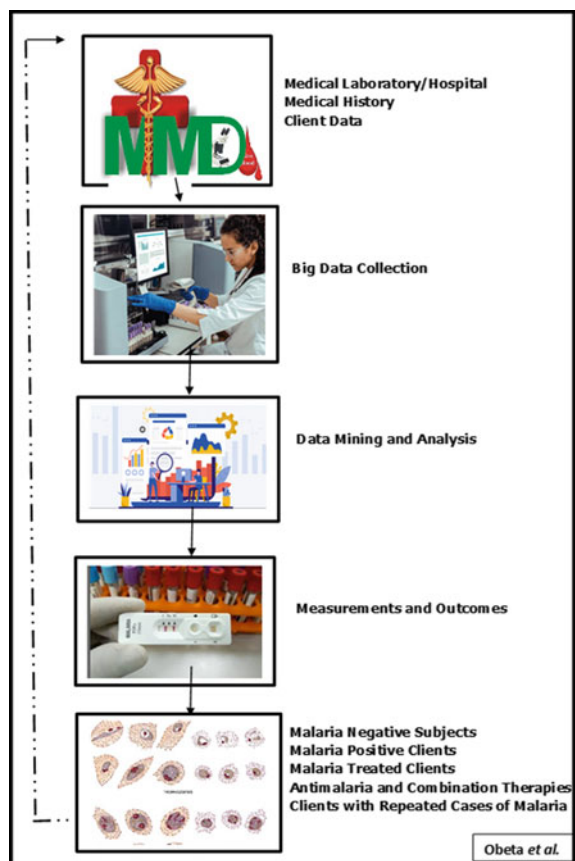
Due to issues of confidentiality, researchers and data miners in the medical laboratories should ensure total conceal of identities or the likes even when there is data linkage. Also, strong data integrity practices should be done in medical laboratory data mining as data evidence is admissible in court [32].

10 Implications of Data Mining Toward Disease Surveillance in Medical Laboratories

COVID-19 has taught the world a very big lesson as all spheres of life was affected. COVID-19 brought a new era where online learning and training become a norm. Most importantly, the data mining technology reached it great height considering the minute by minute global disease update of coronavirus using various platforms and applications. The COVID-19 can come up with malaria question toward surveillance and quality knowledge (Fig. 11) for data mining practice that would cause eradication of malaria in Africa and the world.

Data mining in an instance of malaria gave the global hot spots as shown in red in Fig. 12 and in Nigeria as seen in Fig. 13. The COVID-19 example if employed in malaria shall lead to policies that would free the world of malaria. Data mining can adequately predict diseases situations at all levels of surveillance [33–35]

Fig. 11 Analysis of data mining strategy for malaria testing and treatment



Obeta et al.

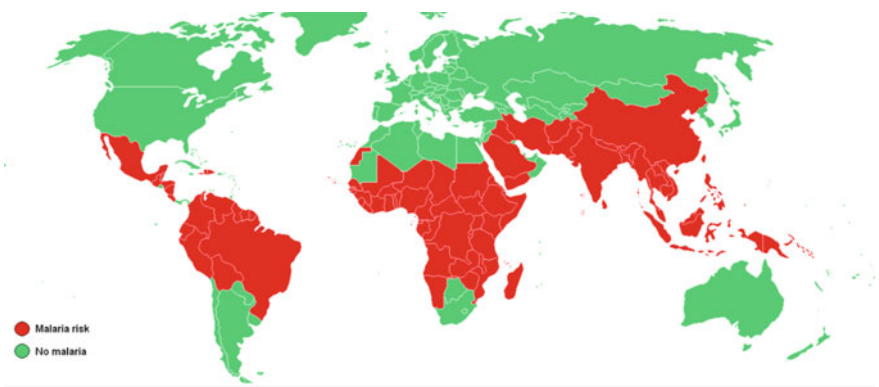


Fig. 12 Global malaria hot spots based on medical laboratory data



Fig. 13 Nigerian hot spots for anopheles mosquito and malaria endemicity

This chapter has no option than to agree with Mittal et al. [21] that “data mining is an inevitable task in most of the emerging computing technologies as it debilitates the complexity of data sets by rendering a better insight” as seen in the sophistications coming up in medical laboratory services with robotics, heavy, and system linked equipment used in diagnosis and diseases surveillance. The future of medical laboratory science based on digital technology including data mining is here [36, 37].

11 Data Mining Toward Quality Improvement of Medical Laboratory Services

Data mining in the aspect of error detection and analysis provides data and outcomes on the causes, effects, remedies, and prevention [38]. This no doubt would affect laboratory policies and cause improvement. The data mining (DM) process do not neglect the MLIMS. This depicts that there is synergy between DM and MLIMS. From COVID-19 point of view, Nigeria experienced quality improvement in terms of equipment, training, testing services, and medical laboratory structural improvement. No wonder researchers called the medical laboratory services in Nigeria during COVID-19 from grass to grace [39]. This is because data mining in medical laboratory services is at its peak and speaks volume daily about COVID-19 pandemic.

It is recommendable that such improvement experienced in COVID-19 should be extended to all diseases and infectious diseases starting with malaria testing and surveillance for quality outcome and total eradication.

This chapter has explored various possibilities related to data mining in medical laboratory. However, it is challenged by the fact that there is paucity of materials in the area of medical laboratory data mining of which the chapter is available to fill the gaps. On the other hand, the chapter has contributed as follows:

- i. That medical laboratory service generates majority of the data in use in healthcare and can adequately predict diseases conditions and management.
- ii. That adequate data mining in medical laboratory science provides immense disease surveillance in pandemic and other diseases of public health importance.
- iii. That data mining in medical laboratory science helps to improve healthcare quality based on clients' assessment and analytics.

12 Conclusions

Data mining has come to stay in medical laboratory science just like medical laboratory information management system. Data mining does a lot of disease surveillance and epidemiological studies and in turn help in detection of equipment and human errors in medical laboratory diagnosis.

This chapter suggests that for future direction, all medical laboratories, both stand-alone and hospital-based ones, are discouraged from hard copy paper works alone, to acquire medical laboratory information management systems and data mining compliant machines so as to meet up with the digital trend of the new era. This would make data mining for integrative and networks in medical laboratory services possible so as to lift the status to national and international linkage for better disease surveillance and quality analytics and reporting. In the end, the laboratory services do not miss any data that is helpful in adequate healthcare, disease surveillance, and quality improvement in health service.

The knowledge gotten from data mining causes change and improvement toward quality diagnosis and results for a better medical laboratory component of public health. This data mining approach in medical laboratory services builds up from one center to the other until it is globally linked for surveillance and management of diseases outbreaks and pandemics.

Acknowledgements We acknowledge MLS Wojuade Kehinde, the MD/CEO of Abims Fertility and Garmete Banking Services, Lagos-Nigeria for providing us with some pictures to be used in the chapter.

Funding None.

Competing Interest None.

References

1. Obeta, M.U., Maduka, K.M., Ofor, I.B., Ofojekwu, N.M.: Improving quality and cost diminution in modern healthcare delivery: the role of the medical laboratory scientists in Nigeria. *Int. J. Bus. Manage. Invent. (IJBMI)* **08**(03), 8–19 (2019)
2. Etukudoh, N.S., Nelson, A.B., Obeta, M.U., Ejinaka, O.R., Ibanga, I.E., Nwapi, L.L., Samuel, P.: Health care delivery business and the role of medical laboratory scientists. *IAR J. Med. Sci.* **2**(4), 76–80 (2021)
3. Obeta, M.U., Eze, E.M., Ofojekwu, M.N., Jwanse, R.I., Maduka, M.K.: Organogram for medical laboratory services in Nigerian public health institutions. *North Am. Acad. Res.* **2**(6), 69–75 (2019). <https://doi.org/10.5281/zenodo.3246909>
4. Lashari, S.A., Ibrahim, R., Senan, N., Taujuddin, N.S.A.M.: Application of data mining techniques for medical data classification: a review. In: *MATEC Web of Conferences*, vol. 150, p. 06003. *MUCET 2017* (2018). <https://doi.org/10.1051/matecconf/201815006003>
5. Nabeel, M., Majeed, S., Awan, M.J., Muslih-ud-Din, H., Wasique, M., Rabia Nasir, R.: Review on effective disease prediction through data mining techniques. *Int. J. Electr. Eng. Inf.* **13**(3) (2021)
6. Toivonen, H., Gross, O.: Data Mining and Machine Learning in Computational Creativity. *Interdisc. Rev.* (2015)
7. Wibamanto, W., Das, D., Chelliah, S.A.L.: Smart health prediction system with data mining. In: *4th Global Conference on Computing and Media Technology* (2020)
8. Ks, D., Kamath, A.: Survey on techniques of data mining and its applications. *Int. J. Emerg. Res. Manag. Technol.* **6**(2) (2017). <https://pdfs.semanticscholar.org/b738/3df4705133a132f58104b514b80555fc78cb.pdf>
9. Illhoi, Y., Alafaireet, P., Marinov, M., Pena-Hernandez, K., Gopidi, R., Jia-Fu, C., Lei Hua, L.: Data mining in healthcare and biomedicine: a survey of the literature. *J. Med. Syst.* **36**(4), 2431–2448 (2012)
10. Kolling, M.L., Furstenau, L.B., Sott, M.K., Rabaioli, B., Ulmi, P.H., Bragazzi, N.L., Tedesco, L.P.C.: Data mining in healthcare: applying strategic intelligence techniques to depict 25 years of research development. *Int. J. Environ. Res. Public Health* **18**, 3099 (2021). <https://doi.org/10.3390/ijerph18063099>
11. Tulsi, B.B.: Big data mining. In: *Business Management* (2016). <https://www.labmanager.com/author/bernard-b-tulsi>
12. Sun, W., Cai, Z., Li, Y., Liu, F., Fang, S., Wang, G.: Data processing and text mining technologies on electronic medical records: a review *Healthcare. J. Eng. Healthc. Eng.* (2018). <https://doi.org/10.1155/2018/4302425>
13. Rehman, A., Haseeb, K., Saba, T., Lloret, J., Tariq, U.: Secured big data analytics for decision-oriented medical system using internet of things. *Electronics* **10**, 1273 (2021). <https://doi.org/10.3390/electronics10111273>
14. Soni, N., Gandhi, C.: Application of data mining to health care. *Int. J. Comput. Sci. Appl.* 245–248 (2014)
15. Etukudoh, N.S., Obeta, M.U.: Patients' (clients) satisfaction with medical laboratory services contributes to health and quality improvement. In: Agrawal, A. (ed.) *Healthcare Access*. IntechOpen (2021). <https://doi.org/10.5772/intechopen.99290>
16. Rajesh, G., Karthika, S., Ashwinth, J., Shanmugapriya, R., Mercilin-Raajini, X.: An investigation on COVID 19 using big data analytics and artificial intelligence. In: Khosla, P.K., et al. (eds.) *Predictive and Preventive Measures for Covid-19 Pandemic*, Algorithms for Intelligent Systems, pp. 231–250 (2020). https://doi.org/10.1007/978-981-33-4236-1_13
17. Boyar, K., Pham, A., Swantek, S., Ward, G., Herman, G.: Laboratory information management systems (LIMS). In: Opie, S.R. (ed.) *Cannabis Laboratory Fundamentals*. Springer, Switzerland (2021). https://doi.org/10.1007/978-3-030-62716-4_7
18. Ramanadhan, S., Revette, A.C., Lee, R.M., Aveling, E.L.: Pragmatic approaches to analyzing qualitative data for implementation science: an introduction. *Implement. Sci. Commun.* **2**, 70 (2021). <https://doi.org/10.1186/s43058-021-00174-1>

19. APHL. Laboratory Information Systems Project Management: A Guidebook for International Implementations (2018)
20. Rehman, A., Saba, T., Haseeb, K., Marie-Sainte, S.L., Lloret, J.: Energy-efficient IoT e-health using artificial intelligence model with homomorphic secret sharing. *Energies* **14**, 6414 (2021). <https://doi.org/10.3390/en1419641>
21. Mittal, M., Goyal, L.M., Hemanth, J.D., Sethi, J.K.: Clustering approaches for high-dimensional databases: a review. *Adv. Rev.* (2018). <https://doi.org/10.1002/widm.1300>
22. Sen, I., Khandelwal, K.: Data Mining in Healthcare. Texas State University, Spring (2014)
23. Zhang, Q., Segall, R.S.: Commercial Data Mining Software Book Chapter (2010). https://doi.org/10.1007/978-0-387-09823-4_65
24. Singh, H., Sharma, A.: Challenges of internet of things: development and application of conceptual framework. *Int. J. Rec. Technol. Eng.* **8**(3), 2277–3878 (2019)
25. Jovičić, S.: Smartphone applications for laboratory medicine—are they ready-to-use? AACC (2019)
26. Pharma, I.Q., Dotmatics: Unlocking the Value of Data and Workflow Automation in the Lab. <https://www.dotmatics.com/>
27. Stoyanov, S.R., Hides, L., Kavanagh, D.J., Zelenko, O., Tjodronegoro, D., Mani, M.: Mobile app rating scale: a new tool for assessing the quality of health mobile apps. *JMIR mHealth Uhealth* **3**(1), e27 (2015). <https://doi.org/10.2196/mhealth.3422>
28. Krasowski, M.D.: Data Mining to Improve Laboratory Utilization and Patient Care. <https://academic.oup.com/criticalvalues/article-abstract/9/1/24/1802322>
29. Cervinski, M.: The Transformative Power of Big Data in Laboratory Medicine. AACC (2020)
30. Wasan, S.K., Bhatnagar, B., Kaur, H.: The impact of data mining techniques on medical diagnostics. *Data Sci. J.* **5**, 119–125 (2006)
31. Ashwinkumar, U.M., Anandakumar, K.R.: Ethical and legal issues for medical data mining. *Int. J. Comput. Appl.* **1**(28) (2010)
32. Okur, M.C.: On ethical and legal aspects of data mining. *J. Yasar Univ.* **3**(11), 1455–1461 (2008)
33. Kirubha, V., Priya, S.: Survey on data mining algorithms in disease prediction. *Int. J. Comput. Trends Technol. (IJCTT)* **38**(3), 24–128 (2016). <https://pdfs.semanticscholar.org/0d05/05b5b057333888de85043ae9b41259f07d85.pdf>
34. Witten, I.H., Eibe, F., Mark, A.H., Christopher, J.P.: Data Mining: Practical Machine Learning Tools and Techniques. Morgan Kaufmann (2016)
35. Kanakaraddi, S.G., Gull, K.C., Bali, J., Chikaraddi, A.K., Giraddi, S.: Disease prediction using data mining and machine learning techniques. In: Roy, S., Lalit Goyal, L.M., Mittal, M. (eds.) Advanced Prognostic Predictive Modelling in Healthcare Data Analytics, pp. 71–92. Springer. https://doi.org/10.1007/978-981-16-0538-3_4
36. Desiere, F., Kolwalik, K., Fassbind, C., Asaad, R.S., Fuzery, A.K., Gruson, D., Heydlauf, M., Kotani, K., Nichols, J.H., Uygun, Z.O., Gouget, B.: Digital diagnostics and mobile health in laboratory medicine: an international federation of clinical chemistry and laboratory medicine survey on current practice and future perspectives. *J. Appl. Lab. Med.* **6**(4) (2021). <https://doi.org/10.1093/jalm/ifab026>
37. Htun, P.W.: Telemedicine and M-health in developing nations—at present and in the future. *EC Emerg. Med. Crit. Care* **5**(8), 30–34 (2021)
38. Plebani, M.: Quality indicators to detect pre-analytical errors in laboratory testing. *Clin. Biochem. Rev.* **33**I, 85–88 (2012)
39. Obeta, M.U., Nkereuwem, S.E., Okoli, C.C.: Nigerian medical laboratory diagnosis of COVID-19; from grass to grace. In: Saba, T., Khan, A.R. (ed.), Intelligent Computing Applications for COVID-19: Predictions, Diagnosis, and Prevention, pp. 84–93 (2021). CRC Press Tailor and Francis Group (Chapter 5). <https://doi.org/10.1201/9781003141105-5>

Deep Learning-Based Lung Infection Detection Using Radiology Modalities and Comparisons on Benchmark Datasets in COVID-19 Pandemic



Jaber Alyami

Abstract The SARS-CoV-2 (severe acute respiratory syndrome coronavirus) pandemic, also known as COVID-19 (coronavirus 2019), impacted humanity worldwide and significantly impacted the healthcare community. COVID-19 infection and transmission have resulted in several international issues, including health hazards. Sore throat, trouble breathing, cough, fever, weariness, and other clinical signs have been described. In SARS-CoV-2 patients, the most common infections are in the lungs and the gastric intestine. Lung infections may be caused by viral or bacterial infections, physical trauma, or inhalation of harmful particles. This research presents deep learning-based approaches for COVID-19 infection detection based on radiological images, prevention and therapy based on benchmark publicly available datasets. Finally, the analysis and findings explore evidence-based methodologies and modalities, leading to a conclusion and possible future healthcare planning.

Keywords Lung infection · COVID-19 · Deep learning techniques · Radiology · Radiography · Treatments · WHO · Computed tomography · Ultrasound

1 Introduction

Novel pneumonia infected case was reported in Wuhan, Hubei Province, China, in late December 2019 lately called SARS-CoV-2 or COVID-19. The primary origin of COVID-19 was several cases reported from Huanan Seafood Wholesale Market and closed for public on December 31, 2019. World Health Organization (WHO) declared the SARS-CoV-2 as COVID-19 or coronavirus pandemic globally on March 11, 2020 [1, 2].

J. Alyami (✉)

Department of Diagnostic Radiology, Faculty of Applied Medical Sciences, King Abdulaziz University, Jeddah 21589, Saudi Arabia
e-mail: jalyami@kau.edu.sa

Imaging Unit, King Fahd Medical Research Center, King Abdulaziz University, Jeddah 21589, Saudi Arabia

Smart Medical Imaging Research Group, King Abdulaziz University, Jeddah 21589, Saudi Arabia

The clinical manifestation of infected patients from bronchoalveolar lavage samples reported SARS-CoV-2 as a serious threat. The research studies provide that COVID-19 associated 88% similarity with bat-related (bat-SL-CoVZC21 and bat-SL-CoVZC45) coronaviruses, possibly natural host. The COVID-19 transmission is yet unknown whether it occurs from bats directly or another host [3, 4]. Human spread may occur through contact, direct or aerial transmission (cough, sneeze, droplet inhalation). Medical staff and flight attenders were also reported in close contact with COVID-19 patients. It mainly infects and initiates lung disease in humans, leading to serious respiratory infections. There have been around 61,299,371 confirmed COVID-19 cases including 1,439,784 deaths were reported till November 28, 2020 [5, 6].

The virus affected people slightly while some aged and old have comorbidities such as pneumonia, ARDS, and multi-organ dysfunction. The predicted fatality rate is 2–3%. Distinct molecular assessments are undergone during diagnosis for the virus in respiratory secretions. Imaging modalities such as CT (Computed Tomography), CXR (Chest X-Ray), US (ultrasound) were used during the diagnosis procedures by examining the nasopharyngeal swab, bronchoalveolar lavage, or tracheal aspirate samples and possible contact history. The key symbol of SARS-COV2 is the GGO (ground-glass opacities) two-sided distribution by or deprived of consolidation in lungs. The analysis of CT imaging of lung injury related infections due to COVID-19, several features were observed such as crazy paving pattern, airway variations, reversed halo sign and others for precise diagnosis [1, 7].

Researchers implemented numerous procedures and techniques for COVID-19 detection and diagnosing earlier with accurate classification [8, 9]. Several medical screening modalities such as Chest X-ray, CT scans (Computer Tomography), LUS (Lung ultrasound) and more were used for COVID-19 detection and diagnosing. The analysis reported that CT scan modality is more effective due to virus detection from patients' images. CAD (Computer-Aided Diagnosis) procedures development started having efficient performance and assisting doctors in examination process during 1980. Numerous ML (Machine Learning) Models were developed and reported efficacy in medical imaging such as SVM (support vector machine), NB (naive Bayes), KNN (K-nearest neighbors), decision trees and more [10, 11]. On the other hand, DL (Deep Learning) techniques such as NN (Neural Networks), CNN (Convolutional Neural Networks) and more were developed reported better performance than ML techniques and in case of big data. In this chapter, lung infection occurrence was analyzed and discussed comprehensively due to COVID-19, evaluated over deep learning techniques [12–14].

2 Lung Infections Overview

The computed tomography reported the variations in lung-related irregularities in patients with a history of fever, respiratory indications, or both while faintness,

headache, nausea, vomiting and diarrhea are reported as common low symptoms [15–17].

COVID-19 infects any organ due to ACE2 receptor existence in human body. Mainly ACE2 receptor showed in lungs gut enterocytes and alveolar epithelial (type II) cells. ACE2 amino acid transport function is associated with gastrointestinal (GI) tract gut infections and SARS-COV2, may ease infect through microbiota. Superfluous lung indications in the GI tract exposed in some COVID-19 patients.

Explicit microbial development occurred due to severe variations inside lung pathology. Plenty of *Porphyromonas*, *Neisseria*, *Haemophilus* and *Fusobacterium* were revealed in case of lung infection, asthma, bronchoscopy samples [18]. Previous indications reported minor asthma allergic irritation due to microbiota management oral or intranasal. In addition, several bacteria were observed such as *Achromobactin*, *Pseudomonas* and more indifferent lung diseases and lung cancer. The reports also showed lung microbiota and pneumonia connection. Lung disease pneumonia activated by fungi, bacteria or others by alveoli infection in the lung is as exhibited in Fig. 1.

CS (Cytokine storm) is identified due to patients' other positive coronavirus disease collaboration. In COVID-19, respiratory failure, C-reactive protein (CRP) and IL-6 association have also been reported in [19]. During COVID-19 disease, IL-6 plays a significant role in lung injury activation. Constant boost of IL-6 leads to immune facilitated lung injury and MAS (macrophage activation syndrome) in patients possibly connected with coronavirus [20]. The comparison reports between lung ultrasound and CT based on pleural and parenchymal regions detection and screening capacity of different treatments showed lung ultrasound better due to fast detection and diagnosing of influenza during the A(H7N9) (avian influenza) epidemic in 2013. The disease was reported in a big geographic area in China with



Fig. 1 General structure of healthy and severe lungs **a** healthy lungs, **b** early-stage infected lungs, **c** advanced stage lungs, **d** severe stage lungs

40% mortality rate. Lung ultrasound also helps in COVID-19 disease detection and diagnosis. It is better than CT in detecting deep lung features in infected patients. In COVID-19 infection detection and diagnosing processes in patients, air bronchograms, lung inner and outer regions, B-lines, inaccurate pleural lines, consolidations and more were screened through ultrasound [21, 22]. Whereas more features are required for severe pneumonia variations, just like CT was frequently unsuccessful for lung injury detection throughout A (H1N1) (influenza) epidemic in 2009. The patients become worsened fast into complex pneumonia. The average sensitivity, specificity, PPV, NPV of 94%, 89%, 86% and 96%, respectively, were reported for lung ultrasound effective than CT [23].

COVID-19 infected 62 patients, including 39 males and 23 females with a mean age of 52.8 (ranging from 30 to 77), were studied by analyzing medical and CT data from China. The spread, CT lesions indications and degree of CT contribution score were assessed and evaluated by two radiologists through the Mann-Whitney U test. Early CT indications and complex coronavirus infection association were evaluated by chi-square test. The results reported lymphocyte amount reduction, improved erythrocyte sedimentation rate and high sensitivity C-reactive protein level evaluation and more. CT results in infected patients showed GGO, consolidation, fibrotic streaks, vacuolar sign, GGO+reticular pattern of 40.3%, 33.9%, 56.5%, 54.8%, 62.9% and more like bronchus distortion and air bronchogram, 72.6% and 17.7% respectively [24]. CT modality plays a crucial role in early COVID-19 recognition and screening during the evolution of health issues globally. The study of COVID-19 infected patients from three different China hospitals was analyzed and reported GGO, crazy-paving pattern, infection fringe spread, healthy CT and morphology opacities of 57%, 19%, 33%, 14% and 33%, respectively. The lymphadenopathy, pleural declarations, lung nodules and lung cavitation were not found. The CT scans were recorded in supine situation of entire infected patients. The patients were described as confirmed COVID-19 patients due to the oropharyngeal swab, endotracheal aspirate, bronchoalveolar lavage, nasopharyngeal swab samples lab evaluations [25].

The results reported the consecutive CT images assessment of coronavirus infected patients and showed low development in virus in non-pregnant patients. The clinical manifestation evolutions reported CT is important commodity in SARS-COV2 detection. It is widely used for any type of lung infection either in mild cases or severe cases. In addition, the report evidenced the ultrasound screening commodity used mostly in pregnant women for SARS-COV2 detection due to its safe and lack of radiations nature [26]. Lung cancer (LC) individuals were expressively affected in coronavirus outbreak due to fast evolution and death rate. The COVID-19 influence and on lung cancer and progression were examined in South Korea due to lack of diagnosing and preventive procedures. Based on results, the comparison between new and previous three-years LC identified patients' history from three different hospitals. The study reported lung cancer detected in 612 patients for three years. 16% reduction has been reported than preceding year in patients in term of lung treatment in hospital during COVID-19 outbreak [27–29]. The isolation wards were created for infected patients' treatment. Several detections and preemptive procedures were executed, LC diagnosis suspension was reduced and patients were protected from coronavirus

infection from hospital acquaintance. The expressive growth was recorded in advance NSCLC (non-small-cell lung cancer) stage percentage during these three years and diagnostic percentage are similar [30].

The experiments showed worsened lung function in patients having pragmatic deficient breathing assistance during early days of pandemic. There is no strong medical or scientific evidence for affection for P-SILI (Patient self-inflicted lung injury). The lack of sympathetic investigations reported that P-SILI affect lungs due to local, different stress and high respiration. The ARDS and remote respiratory abnormalities evaluation is complex during SARS-COV2 lung injury. Hypoxemia is occasionally the main source of lung injury. However, COVID-19 infection might spread into multiple organs than lungs such as kidney, liver and more. The study has distinctly limited due to lack of breathing infections detection during the SAR-COV2 lung injury and P-SILI examination processes not yet provided that P-SILI is cause of lung infection evolution [31].

CXR (portable chest radiography) is usually used to screen and detect lung infections due to several preventive CT-associated problems, such as CT accessibility locally or globally, CT room sanitization inadequacies, and more. In addition, CXR might reduce cross-infection threat due to the CT distillation subsequently infected cases that disorder accessibility of radiological facility reported by ACR (American College of Radiology). The CT and CXR detect lung infection in any doubt created in some diagnosed patients. Distinctive redundancy of symptoms i.e.; reticular, hazy, irregular, GGO and more were reported in infected or non-infected patients on CXR [32]. Lung infections occur by oral viruses through inferior respiratory area. Cough, fever, deprived oral sterility, abnormal respiration, MV (mechanical ventilation) and deprived oral sterility aspects cause lung diseases. Oral microbiota-initiated anaerobes and facilitation by SARS-COV2 indications and lung hypoxia. Lung infection might worsen due to the COVID-19 and microbiota relationship through variations in T-cell retorts, cytokines, and possessions of host situations. The precautions for controlling lung infections based on oral in SARS-COV2 infected individuals are essential due to COVID-19 and oral microbiome relationship [33].

Current examinations present the efficacy of lung ultrasound for SARS-COV2 detection but there is lack of infected children lung ultrasound-based data. In Rome hospitals, 10 positive infected children were reported sequentially. Ultrasound was used for infection detection from lungs. The results reported 10%, 60%, 70% and 10% white lung regions, pleural abnormalities, vertical portions and subpleural consolidations, respectively, in patients and pleural declarations were not created in any of patients. The results showed monotonous usage of lung ultrasound in coronavirus or non-coronavirus infected children screening due to radiation-free, safety and spread [34].

MV (Mechanical Ventilation) usage is reported in ARDS infection while excessive death rate is 39% approx. were recorded. When MV used inadequately, the death rate in ARDS individuals will grow. The inflated local lung stress, mostly alveolar variability regions issue to tidal conscription or de-conscription and stress variation trigger VILI (Ventilation-Induced Lung Injury) is recommended by current research. The VILI and local active strain reduction will occur when ventilation approach keep

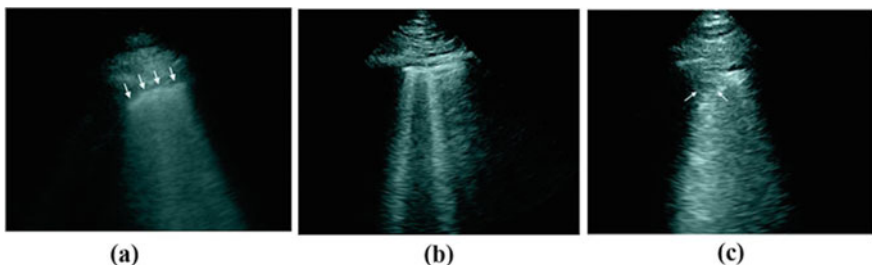


Fig. 2 Lung ultrasound for COVID-19 infection detection **a** pleural line abnormalities, **b** confluent B lines, **c** subpleural consolidation

lung extravagant constant and similar. TCAV (Time-Controlled Adaptive Ventilation) technique proposed that reduced active alveolar stress through breath regulation conferring automatic lung features. The result showed that a normal and healthy lung decreases local strain and has better lung safety. ARDS infections were reported in over 3 million patients worldwide, including 10% of ICU patients. The death rate is 75 k while 2 million identified having ARDS infection annually in US [35, 36].

According to the state-of-the-art analysis reports pulmonary fibrosis occurs in infected COVID-19 patients due to old age, the severity of disease, prolonged staying intensive care unit and ventilation, smoking and alcohol consumption [37, 38]. Lung prevalence and protection recommended for other infections due to lack of pulmonary fibrosis procedures. Some features in patients might lead to augmented danger like lung damage, death or pulmonary fibrosis [39]. Figure 2 presents lung ultrasound results in COVID-19 detection stages.

3 Diagnostics

A novel pandemic SARS-CoV-2 named as COVID-19 emerged in late December 2019 worldwide [40]. For decades, the research studies of influenza, tuberculosis, and pneumonia have shown that lung infections are fatal diseases worldwide. In addition, the clinical symptoms such as cough, fever, tiredness, myalgia and dyspnea are common in COVID-19 patients [41, 42].

The study of eight patients reported examining bronchoalveolar lavage samples from COVID-19 infectious lung through microbial composition and occupied by oral and upper respiratory tract bacteria like traditional pneumonia. The analysis recognized the acute respiratory distress syndrome might be predicted through microbial signs and antiviral immunity improvement by gut microbiota [3, 43]. The cause of Lung infection is typically an external offence, damaged tissue or immune syndrome. The COVID-19 caused pandemic since December 2019 when the early infected cases were reported from China and its basics and origin has still been unknown [44, 45].

A study of COVID-19 infected patient (age—72 years) with cough, fever, diabetes and hypertension history. The reports presented COVID-19 through early examination of throat and pharyngeal swabs samples. After the necessary therapies, using imaging modalities such as CT scans analysis obtained samples from lungs various parts. The patient died and the study has several limitations, even with antidote therapies, the breath shortness sustained. The incapability to acquire larger tissue samples and solve the sample issues using autopsy or thoracoscopic lung biopsy [46]. COVID-19 was detected during two cases' adenocarcinoma (lung lobectomies) operation. Although the patients didn't have any symptoms of fever or pneumonia before or at operation time, it signifies that the early COVID-19 procedures vary due to investigations reporting lungs oedema, multinucleated giant cells, and irregular seditious cellular penetration and proteinaceous exudate in patients [47].

The innovative automated segmentation pipeline technique was proposed for limited datasets (overfitting) issues by considering modified datasets. The method uses numerous preprocessing image techniques before training. Neural network-based 3D U-Net model executed for additional overfitting reduction. The model validated on 20 COVID-19 infected CT scans resulted in 0.956 and 0.761 dice similarity coefficients for lungs and COVID-19, respectively which was accurate and robust in case of limited datasets deprived of overfitting issue for coronavirus and lung [48].

Machine learning and deep learning techniques such as neural networks-based CNN and more mainly used for automatic diagnosis of medical imaging [49, 50]. There are two methodologies segmentation and classification, used along with these techniques. The segmentation purpose is to extract features (ROIs) from each pixel of an image and label it. At the same time, classification is used for whole labeling images and categorizing it a distinct group. Deep learning techniques such as U-Net, VB-Net and other U-Net modifiers are used for segmentation while DenseNet, ResNet and Inception-v3 used for classification, which accomplished better performance than humans [51, 52].

POI (percentage of infection) used for inclusive prediction of infection registration and imagining whereas better and accurate data extraction through various lung parts and infections segmentation is required for analysis. COVID-19 infection also diagnosed in some of lung transplant individuals [53]. The study has been limited due to the following issues: data recorded for analysis was only from China, more data essential such as more regions, countries or worldwide for in-depth analysis of SARS-CoV2. In addition, the data and clinical reports about COVID-19 were limited at the time of analysis [54, 55].

A prognostic model was proposed using lung ultrasound imagining and medical features for COVID-19. The study analyzed 100 patients, while 31 out of 100 confirmed COVID-19 infected patients through RT-PCR. COVID-19 infected examination autonomously related to fast organs injury serial wise, consolidation and lower site hard pleura [56–58]. The statistical analysis reported 0.82, 97%, 62%, 54% and 98% of ROC, sensitivity, specificity, PPV (positive predictive value) and NPV (negative predictive value). This study is limited due the following limitations: the proposed technique is not more effective due the misclassification of infected

patients recorded in some sensitivity tests. And lung ultrasound examination distinguishes other pulmonary and cardiac diseases but couldn't distinguish the pneumonia type and influenza, but it differentiates in COVID-19 variations. The research aimed to examine more regions of lungs to improve the model's performance [59, 60].

Youssef et al. [61] reported that RT PCR effectiveness during immediate SARS-COV2 disease diagnosis while CT and X-ray are better in COVID-19 analysis have some limitations. LUS ((Lung Ultrasound) only detect features deeply and imagine next to pleura. It can't detect any other infections like tumors and others. LUS depends on skilled sonographers with sophisticated analytical accurateness. It also depends on patient, if overweight the examination will be complex because the breadth of soft tissues. The performance is not effective than CT scans. LUS is recommended for COVID-19 patients due to its visualization of pneumonia signs, which distinguishes lung infection in COVID-19 [40, 62, 63].

Trauer et al. [64] review-based study analyzed 33 research studies after large explorations of database search for lung ultrasound imaging modality efficacy during COVID-19 outbreak. The study reported different outcomes and limitations. It shows that LUS is better in sensitivity and specificity in COVID-19 diagnosis than other imaging modalities that varies based on many features such as history of lung infections, virus occurrence and others and aimed for future research to be explored. Sensitivity and specificity of 92% and 93%, respectively, were reported for 5 K patients in 2018 based on lung ultrasound for pneumonia cases [64–66].

Shan et al. [67] implemented VB-Net neural network for infected regions automatic segmentation from COVID-19 patients CT images based on deep learning. The study evaluated 249 infected patients for training model, 300 images were used for testing. The model analysis reported 91.6%, 10.0% dice similarity coefficients for both automatic and manual segmentation and 0.3% POI and accurate. This research study is limited due to lack of evaluated data, it is obtained from one hospital not from big hospitals or more regions. Moreover, this system was implemented only for infections evaluation not specifically for any type of severe infection like pneumonia. The study aimed to extend it to multiple regions and centers for severity of pneumonia infections detection [68, 69].

Lack of literature research studies based on autopsy COVID-19 patient's analysis than deaths because of severe infectious and unavailability of accurate methods and procedures for treatment conduction. Clinical manifestations during diagnostic procedures reported that COVID-19 lead to infections or injury to many tissues and organs such as lungs and more. It occurs and infect animals and humans both spreading through respiratory, hepatic, bowel, neurologic and renal [70–72]. Several procedures and techniques were evaluated to treat viral, immune system and lung infections during COVID-19 [73, 74]. Table 1 presents treatments against lung and COVID-19 infection.

Table 1 List of treatments against lung and COVID-19 infection

Treatments	Treatment Category	Status
Lopinavir/ritonavir	HIV protease inhibitor	FDA approved
Pembrolizumab	Anti-viral drug	FDA approved
Vedolizumab	Anti-viral drug	FDA approved
Favipiravir	Nucleoside equivalent	Under trial
Nivolumab and Iplimumab variation	Anti-viral drug	FDA approved
Infliximab	Anti-viral drug	FDA approved

4 Deep Learning Methodology

CAD (Computer-Aided Diagnosis) systems were developed for misclassification and false-negative rates reduction. It assists the doctors in automatic detecting and diagnosing the infections explicitly and in early stages from CT images [75, 76]. Deep neural network based on deep learning has lately grown extensive attention of researchers in medical imaging and the capability of deep feature understanding. Recently, several deep learning models implementations and big data development reported significant performance effectiveness [77, 78].

Deep learning techniques are based on primarily two categories, one is supervised learning (consists of neural networks NN, convolutional networks CNN, Recurrent neural networks RNN and others), while second is unsupervised learning (consists of Auto-encoders AEs, stacked auto-encoders SAEs, deep belief networks DBNs and more). CNN (Convolutional Neural Network) based on deep learning techniques result in high-performance accuracy and improved performance in the case of medicinal imaging. Numerous models developed in state of the art based on CNN such as AlexNet [79], ResNet [80], DenseNet [68], Inception [81] and more [69, 82].

Deep learning techniques include the following basic steps followed during the entire process: pre-processing, segmentation, feature extraction & selection and finally classification.

4.1 Datasets

The dataset section aimed to collect and provide an overview of a different publicly available dataset that might be useful for future research during COVID-19 or any other severe disease [80].

The COVIDx dataset was created by collecting chest radiography images data from five publicly available databases: 1-COVID-19 Image Data Collection, 2-COVID-19 Chest X-ray Dataset Initiative, 3-ActualMed COVID-19 Chest X-ray Dataset Initiative, 4-RSNA Pneumonia Detection Challenge dataset and 5-COVID-19 radiography database. The whole dataset contains CXR images and cases of

13,970 and 13,870, respectively. The COVID-19 X-ray images dataset is collected from three different datasets that contain 381 images of COVID-19, pneumonia and normal patients divided equally. The dataset was created by amalgamating two datasets of 100 images of COVID-19 infected and healthy patients [83]. The collection of 20 COVID-19 CT scans was labeled by and verified by two radiologists as left and right lung, named COVID-19 CT Lung and Infection Segmentation Dataset [84]. The dataset prepared by images labeling from 64 videos simultaneously consists of 1103 lung ultrasound patient images comprising COVID-19, bacterial pneumonia, and healthy of images of 654, 277 and 172 images, respectively [85].

The dataset is collecting Twitter tweets regarding COVID-19 of different countries and languages since Jan 22, 2020 simultaneously through API and hashtags (virus, coronavirus and more) when infected patients reported <600 globally Lopez et al. (2020). The dataset called NAIST COVID (Multilingual COVID-19 Twitter and Weibo Dataset) contains multilanguage Twitter and Weibo of more than 20 million microblogs since Jan 20–March 24, 2020. In addition, it comprises related microblog IDs, timestamps and keywords [86, 87]. In addition, Weibo-COV dataset was found to consist of more than 40 million Twitter tweets from Dec 1, 2019–April 30, 2020 containing tweets variations, retweet data and more [88, 89].

The dataset CoAID (COVID-19 Healthcare Information Dataset) consist of 183,564 user related engagements from 516 social platform posts and 1,896 news and labels. The data was collected after evaluating fact-based strategy for fake and true news confirmation of articles, post and websites, and users' social signals Cui et al. [90]. The dataset based on Instagram collected the English language data of over posts, likes and comments of 5.3 k, 329 k and 18.5 k, respectively of 2.5 publisher distribution from Jan 5–March 30, 2020 using (COVID-19, virus, corona and more) hashtags. It is categorized into post content, features, comments and publisher data [91]. The dataset based on online questions were collected from 13 sources such as google, yahoo, Quora and more of 1690 questions about COVID-19. It is labeled into 207 classes and 15 groups. Wei et al., [92]. The city of Wuhan China was evacuated from 2666 foreigners after isolation and monitored their healthiness for any infection, 12 COVID-19 infected individuals were reported. The data was named as evacuee dataset Zhou et al. [93]. Table 2 presents different datasets access links for experiments.

4.2 Preprocessing

Preprocessing is an important stage of DL techniques for medical image examinations. The process comprises noise removal (like images undesirable and unnecessary parts exclusion) and improved image quality. It also used for labeling, tagging the desired classes [94, 95].

Table 2 Datasets with access links

Dataset	Access Links
COVID19_Tweets	https://github.com/lopezbec/COVID19_Tweets_Dataset
LUNA16	https://luna16.grand-challenge.org/
COVID19	https://github.com/socioicom/covid19_dataset
LIDC/IDRI	https://wiki.cancerimagingarchive.net/display/Public/LIDC-IDRI
COVId19 Pocus Ultrasound	https://github.com/jannisborn/covid19_pocus_ultrasound
COVID-19-InstaPostIDs	https://github.com/kooshazarei/COVID-19-InstaPostIDs
ChestX-ray14	https://academictorrents.com/details/557481faacd824c83fbf57dcf7b6da9383b3235a
CoAID	https://github.com/cuilimeng/CoAID
COVID-Net	https://github.com/lindawangg/COVID-Net
Convid19-X-rays	https://www.Kaggle.com/andrewmvd/convid19-X-rays
COVID-19 lung and infection segmentation	https://zenodo.org/record/3757476#.XxKOkgzbIU
Weibo public-opinion	https://github.com/nghuyong/weibo-public-opinion-datasets
Evacuees from Wuhan	https://figshare.com/articles/Evacuees_from_Wuhan/11859207/1
COVID-Q	https://github.com/JerryWei03/COVID-Q
Chest Xray pneumonia	https://www.kaggle.com/paultimothymooney/chest-xray-pneumonia
Lung1	https://wiki.cancerimagingarchive.net/display/Public/NSCLC-Radiomics

4.3 Segmentation

The segmentation process is the most substantial, critical and complex task of image processing due to the results that depends on these features. After noise contrast removal and others enhancements. It divides images into parts for analysis. Several techniques are implemented, such as edge, region, thresholding, and clustering for segmentation. Numerous methods are used for image segmentation such as ANN (artificial neural network), Gaussian mixture model, Gaussian kernel FCM and more. Whereas, no inclusive segmentation technique was reported that validates effectiveness in case of image types and for a specific medical imaging modality [96–98].

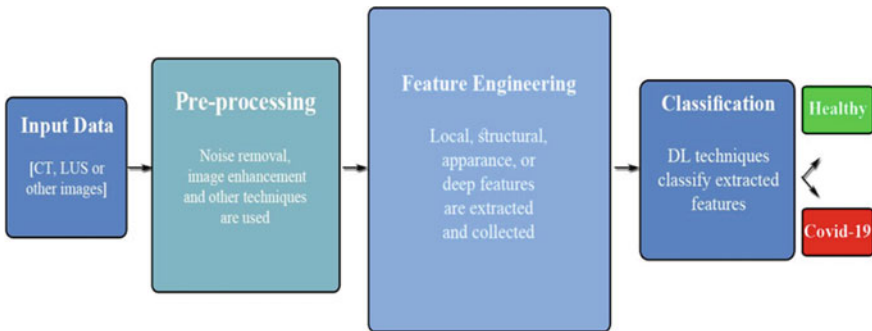


Fig. 3 General CAD architecture for COVID-19 detection

4.4 *Feature Extraction and Selection*

In this step the features are extracted from medical images for infections of disease diagnosis. This section categories many local, texture and statistical features from patients' images. Several techniques are used such as LBP (Local Binary Pattern), CS-LBP (Center Symmetric Local Binary Pattern), SIFT (Scale Invariant Feature Transform) and more for feature extraction [99, 100].

4.5 *Classification*

The final step of deep learning techniques is classification. It assists the researcher build an effective model for diagnosis based on feature vector created during the feature extraction and selection processes. The classification section is used to classify patients' images through healthy or infected labels. Several techniques are used for classification such as CNN, ResNet, AlexNet, DensNet and more [101, 102]. Figure 3 exhibits general CAD architecture for COVID-19 detection.

5 Analysis and Findings

COVID-19 is a newly emerged pandemic that originated in December 2019. The mortality rate is very high globally and a severe threat to the health community. There were no specific treatment procedures and guidelines were available. Chest CT modality was mainly used for infection detection and diagnosing to assist doctors in controlling the virus. Analysis of lung infection and COVID-19 detection and diagnosis based on different deep learning techniques through different performance measures such as AUC (Areas Under the Curve), ROC (receiver operating characteristic), Accuracy and more were presented [103–105].

The SARS-CoV-2 cause ARDS due to considered lung inflammation risk. ARDS is considered a result of classified COVID-19 lung injury. The analysis is still not accurate that severe hypoxemia is associated with an insignificant reduction in lung acquiescence and recommended supplementary procedures for hypoxia contribution than parenchymal damage procedures. The analysis of COVID-19 patient's lungs reports presented that monocytes polymorphonuclear neutrophils and other leukocytes conscription follow-on due to activation of pro-inflammatory intermediaries and paracrine and autocrine cytokine proclamation [19, 106]. In COVID-19, preference is given to lung ultrasound in diagnosis over CT and X-ray due to history of past epidemics, affordable cost, low virus spread threat and easy usages as it assists the doctors in distinguishing pneumonia and dyspnea and also recommended where lack of molecular examinations [23, 107, 108].

In treatment procedure, the patients require oxygen assessment due to severe infected people almost 15–20% while some people have common infection [109, 110]. Proinflammatory cytokines released due to lung epithelial cells and alveolar macrophages initiation in some infected lung patients. The DL-based algorithm's performance reported 94.4%, 11% and 5% of AUC, false positives and negatives, respectively for NLST images. The algorithm Mask-RCNN and Cancer ROI detection technique applied on LIDC, NLST and LUNA datasets [111] sensitivity and specificity of 94% and 91% were reported in case of LIDC-IDRI and LUNA16 datasets evaluated by CMixNet, faster R-CNN and gradient boosting machine techniques [112]. 3D U-Net and CapNets examined the effectiveness of lung nodule data. The method resulted in accuracy, sensitivity, specificity and AUC of 84.5%, 92.9%, 0.84 and 70%. The specificity is low because of benign samples extravagance. The performance is limited due to less data size.

In children's, fever FR (frequency rate) was low (92.8%, 95%CI 89.4–96.2%) whereas high in adults (43.9%, 95% CI 28.2–59.6%) [113]. The clinical manifestations examined and evaluated more than having 11,950 COVID-19 infected patients from 24 studies that reported fever, cough and fatigue of 77%, 60% and 38%, respectively. The study is limited due to the lack of lab results variations, full data access, patients with various sickness stages, and poor treatment procedures [114]. Chest CT procedure was reported effective and fast during COVID-19 diagnosing. COVIDx dataset consists of CXR (Chest X-ray) images of COVID-19 patients that was created and evaluated through a proposed COVID-Net deep CNN which resulted in 91%, 98.9% sensitivity and high PPV (positive predicted value), respectively. Low false positive COVID-19 detection was reported due to misclassification of 1 normal patient CT image as COVID-19 [109].

Lack of throat swab samples and detection procedure, 30–60% sensitivity was recorded for RT-PCR. Negative RT-PCR resulted due to positive CT outcomes. When pneumonia diagnoses through CT scans, RT-PCR must require for COVID-19 patients having lung infections, cough, fever or related history (Liu et al., 2020). 97% CT sensitivity and 90% patients were diagnosed and analyzed for COVID-19 having different CT results [109]). PPR (positive probability ratio), NPN (negative probability ratio), specificity and sensitivity 1.17, 0.48; 25% and 88% were reported for CT [115]. 64 patients were studied containing 56 years old 26 male patients

at baseline Chest radiography. 91% (58), 69% (44) and 59% (38) patients were reported infected for COVID-19 and abnormal respectively by diagnosing through RT-PCR. 69% sensitivity was recorded for the proposed method despite some limitations: the diagnostic and treatment procedures were not followed accordingly. The effectiveness during the process probably changed due to the interruption of CT and RT-PCR diagnosis. The lack of radiologists also affects specificity and sensitivity [109]. COVID-19 associated irregular results and variables 19% leucopenia, 13% lymphocytes, body temperature is high and 31% creatine kinase MB (high level) and 17% procalcitonin was expressively reduced [116]. Performance measures such as accuracy, ROC, AUC, sensitivity of different research studies is presented and compared in Table 3.

6 Conclusions and Future Challenges

A novel coronavirus named COVID-19 by WHO is the biggest threat due to its fast spread globally for the health community. The most common symptom such as fever, cough, tiredness and others reported initially for SAR-COV2. Individuals who have prior contact or travel history to coronavirus epidemic areas must follow clinical procedures, guidelines and protection through lab tests. Effective vaccine is not yet developed to control virus spread and death rate among community. Many effective deep learning techniques were developed to detect and diagnose COVID-19 using different radiology modalities with better efficacy. However, this research paper reviewed and analyzed lung infection due to COVID-19 based on deep learning techniques including overview of COVID-19 diagnosis and public dataset. This study aimed for future to resolve the complicated association of lung microbiome, immunity and COVID-19 virus and their difficulties. Still, no vaccine is available for equally applicable to COVID-19 all variants treatment but research on chloroquine and remdesivir medications is in trial in the US and China companies. However, COVID-19 vaccine evolution discussion is out of scope of this research.

Coronavirus and its variants affected humanity globally and left the world to face many future challenges. Many researchers studied and analyzed future challenges and possible solutions for COVID-19: GDP, economic and unemployment crisis due to lockdown globally. Air contamination growth and the medical waste of infected patients controlling requires fast policies and strategies. Medical nursing needs protection during patient assistance, new challenges during lockdown for orthopedic patients, doctor's communication, arthroscopic surgery or fractures monitoring.

Table 3 Performance measures based on deep learning techniques

Author	Techniques	Database	AUC	Accuracy	Sensitivity	Specificity	F1 score	PPV	NPV
Wang et al. [117]	prognostic model	Ultrasound images	N/A	97%	62%	N/A	54%	98%	N/A
Liu et al. [73]	FCONet model (ResNet-50)	CT (COVID-19 pneumonia)	99%	98.67%	97.39%	99.64%	N/A	N/A	N/A
Fang et al. [118]	PNAIDS	Lung CT Images	76.5%	N/A	63%	75.3%	N/A	N/A	N/A
Huang et al. [119]	CMixNe+RCNN	LUNA16 LIDC-IDRI	N/A	N/A	94%	91%	N/A	N/A	N/A
Kermany et al. [120]	DenseNet121	CT	90.30%	82.50%		83.90%	80.10%	N/A	N/A
Liu et al. [121]	3D U-Net+CapNets integration	LIDC-IDRI	0.84	84.50%	92.90%	70.00%	N/A	N/A	N/A
He et al. [122]	(DECAPS)	CT images	96.10%	87.60%	N/A	N/A	N/A	N/A	N/A

References

1. Rehman, A., Sadad, T., Saba, T., Hussain A., Tariq, U.: Real-time diagnosis system of COVID-19 using X-ray images and deep learning. *IEEE IT Prof.* **23**(4), 57–62 (2021). <https://doi.org/10.1109/MITP.2020.3042379>
2. Saba, T., Abunadi, I., Shahzad, M.N., Khan, A.R.: Machine learning techniques to detect and forecast the daily total COVID-19 infected and deaths cases under different lockdown types. *Microsc. Res. Tech.* **84**(7), 1462–1474 (2021)
3. Khan, M.A., Kadry, S., Zhang, Y.D., Akram, T., Sharif, M., et al.: Prediction of COVID-19-pneumonia based on selected deep features and one class kernel extreme learning machine. *Comput. Electr. Eng.* **90**, 106960 (2021)
4. Amin, J., Anjum, M.A., Sharif, M., Rehman, A., Saba, T., Zahra, R.: Microscopic segmentation and classification of COVID-19 infection with ensemble convolutional neural network. *Microsc. Res. Tech.* <https://doi.org/10.1002/jemt.23913>
5. Haimed, A.M.A., Saba, T., AlBasha, A., Rehman, A., Kolivand, M.: Viral reverse engineering using artificial intelligence and big data COVID-19 infection with long short-term memory (LSTM). *Environ. Technol. Innov.* **22**, 1–20 (2021)
6. Khan, M.Z., Khan, M.U.G., Saba, T., Razzak, I., Rehman, A., Bahaj, S.A.: Hot-Spot zone detection to tackle COVID19 spread by fusing the traditional machine learning and deep learning approaches of computer vision. *IEEE Access* **9**, 100040–100049 (2021)
7. Rehman, A., Saba, T., Tariq, U., Ayesha, N.: Deep learning-based COVID-19 detection using CT and X-ray images: current analytics and comparisons. *IT Prof.* **23**(3), 63–68 (2021)
8. Dawood, S., Dawood, A., Alaskar, H., Saba, T.: COVID-19 artificial intelligence based surveillance applications in the kingdom of Saudi Arabia. In: 2021 1st International Conference on Artificial Intelligence and Data Analytics (CAIDA), pp. 200–205. IEEE (2021)
9. Saba, T., and Khan, A. R. (Eds.). (2021). Intelligent computing applications for COVID-19: predictions, diagnosis, and prevention. CRC Press.
10. Neamah, K., Mohamad, D., Saba, T., Rehman, A.: Discriminative features mining for offline handwritten signature verification. *3D Res.* **5**(2), 1–6. <https://doi.org/10.1007/s13319-013-0002-3>
11. Ramzan, F., Khan, M.U.G., Iqbal, S., Saba, T., Rehman, A.: Volumetric segmentation of brain regions from MRI scans using 3D convolutional neural networks. *IEEE Access* **8**, 103697–103709 (2020)
12. Rahim, M.S.M., Norouzi, A., Rehman, A., Saba, T.: 3D bones segmentation based on CT images visualization. *Biomed. Res.* **28**(8), 3641–3644 (2017)
13. Rashid, M., Khan, M.A., Alhaisoni, M., Wang, S.H., Naqvi, S.R., et al.: A sustainable deep learning framework for object recognition using multi-layers deep features fusion and selection. *Sustainability* **12**(12), 5037 (2020)
14. Rehman, A., Khan, M.A., Saba, T., Mehmood, Z., Tariq, U., Ayesha, N.: Microscopic brain tumor detection and classification using 3D CNN and feature selection architecture. *Microsc. Res. Tech.* **84**(1), 133–149 (2021). <https://doi.org/10.1002/jemt.23597>
15. Sadad, T., Khan, A.R., Hussain, A., Tariq, U., Fati, S.M., Bahaj, S.A., Munir, A.: Internet of medical things embedding deep learning with data augmentation for mammogram density classification. *Microsc. Res. Tech.* (2021)
16. Rehman, A., Abbas, N., Saba, T., Mehmood, Z., Mahmood, T., Ahmed, K.T.: Microscopic malaria parasitemia diagnosis and grading on benchmark datasets. *Microsc. Res. Tech.* **81**(9), 1042–1058 (2018). <https://doi.org/10.1002/jemt.23071>
17. Rehman, A., Saba, T.: (2021) Performance analysis of character segmentation approach for cursive script recognition on benchmark database. *Digit. Sig. Proc.* **21**(3), 486–490 (2021). <https://doi.org/10.1016/j.dsp.2011.01.016>
18. Ahlawat, S., Sharma, K.K.: Immunological co-ordination between gut and lungs in SARS-CoV-2 infection. *Virus Res.* 198103 (2020)

19. Polidoro, R.B., Hagan, R.S., de Santis Santiago, R., Schmidt, N.W.: Overview: Systemic inflammatory response derived from lung injury caused by SARS-CoV-2 infection explains severe outcomes in COVID-19. *Front. Immunol.* **11**, 1626 (2020)
20. Mayor-Ibarguren, A., Robles-Marhuenda, Á.: A hypothesis for the possible role of zinc in the immunological pathways related to COVID-19 Infection. *Front. Immunol.* **11**, 1736 (2020)
21. Rehman, A., Alqahtani, S., Altameem, A., Saba, T.: Virtual machine security challenges: case studies. *Int. J. Mach. Learn. Cybern.* **5**(5), 729–742 (2014)
22. Alyami, J., Khan, A.R., Bahaj, S.A., Fati, S.M.: Microscopic handcrafted features selection from computed tomography scans for early stage lungs cancer diagnosis using hybrid classifiers. *Microsc. Res. Tech.*
23. Convissar, D., Gibson, L.E., Berra, L., Bittner, E.A., Chang, M.G.: Application of lung ultrasound during the coronavirus disease 2019 pandemic: a narrative review. *Anesth. Analg.*
24. Zhou, S., Wang, Y., Zhu, T., Xia, L.: CT features of coronavirus disease 2019 (COVID-19) pneumonia in 62 patients in Wuhan China. *Am. J. Roentgenol.* **214**(6), 1287–1294 (2020)
25. Chung, M., Bernheim, A., Mei, X., Zhang, N., Huang, M., Zeng, X., Cui, J., Xu, W., Yang, Y., Fayad, Z.A., Jacobi, A.: CT imaging features of 2019 novel coronavirus (2019-nCoV). *Radiology* **295**(1), 202–207 (2020)
26. Buonsenso, D., Raffaelli, F., Tamburini, E., Biasucci, D.G., Salvi, S., Smargiassi, A., Inchigolo, R., Scambia, G., Lanzone, A., Testa, A.C., Moro, F.: Clinical role of lung ultrasound for the diagnosis and monitoring of COVID-19 pneumonia in pregnant women. *Ultrasound Obstet. Gynecol.* (2020)
27. Abbas, N., Saba, T., Mohamad, D., Rehman, A., Almazyad, A.S., Al-Ghamdi, J.S.: Machine aided malaria parasitemia detection in Giemsa-stained thin blood smears. *Neural Comput. Appl.* **29**(3), 803–818 (2018)
28. Amin, J., Sharif, M., Raza, M., Saba, T., Rehman, A.: Brain tumor classification: feature fusion. In: 2019 International Conference on Computer and Information Sciences (ICCIS), pp. 1–6. IEEE (2019)
29. Iqbal, S., Khan,M.U.G., Saba, T. Mehmood, Z. Javaid,N., Rehman,A., Abbasi, R.: Deep learning model integrating features and novel classifiers fusion for brain tumor segmentation. *Microsc. Res. Tech.* **82**(8), 1302–1315 (2019). <https://doi.org/10.1002/jemt.23281>
30. Park, J.Y., Lee, Y.J., Kim, T., Lee, C.Y., Kim, H.I., Kim, J.H., Park, S., Hwang, Y.I., Jung, K.S., Jang, S.H.: Collateral effects of the coronavirus disease 2019 pandemic on lung cancer diagnosis in Korea. *BMC Cancer* **20**(1), 1–8 (2020)
31. Cruces, P., Retamal, J., Hurtado, D.E., Erranz, B., Iturrieta, P., González, C., Díaz, F.: A physiological approach to understand the role of respiratory effort in the progression of lung injury in SARS-CoV-2 infection. *Crit. Care* **24**(1), 1–10 (2020)
32. Jacobi, A., Chung, M., Bernheim, A., Eber, C.: Portable chest X-ray in coronavirus disease-19 (COVID-19): a pictorial review. *Clin. Imaging*
33. Bao, L., Zhang, C., Dong, J., Zhao, L., Li, Y., Sun, J.: Oral microbiome and SARS-CoV-2: beware of lung co-infection. *Front. Microbiol.* **11**, 1840 (2020)
34. Musolino, A.M., Supino, M.C., Buonsenso, D., Ferro, V., Valentini, P., Magistrelli, A., Lombardi, M.H., Romani, L., D'Argenio, P., Campana, A.: Lung ultrasound in children with COVID-19: preliminary findings. *Ultrasound Med. Biol.*
35. Nieman, G.F., Gatto, L.A., Andrews, P., Satalin, J., Camporota, L., Daxon, B., Blair, S.J., Al-Khalisy, H., Madden, M., Kollisch-Singule, M., Aiash, H.: Prevention and treatment of acute lung injury with time-controlled adaptive ventilation: physiologically informed modification of airway pressure release ventilation. *Ann. Intensive Care* **10**(1), 1–16 (2020)
36. Nawaz, M., Mehmood, Z., Nazir, T., Naqvi, R.A., Rehman, A., Iqbal, M., Saba, T.: Skin cancer detection from dermoscopic images using deep learning and fuzzy k-means clustering. *Microsc. Res. Tech.* **85**(1), 339–351 (2022)
37. Rehman, A.: Ulcer recognition based on 6-Layers deep convolutional neural network. In: Proceedings of the 2020, 9th international conference on software and information engineering (ICSIE), pp. 97–101. Cairo Egypt (2020)

38. Safdar, A., Khan, M.A., Shah, J.H., Sharif, M., Saba, T., Rehman, A., Javed, K., Khan, J.A.: Intelligent microscopic approach for identification and recognition of citrus deformities. *Microsc. Res. Tech.* **82**(9), 1542–1556 (2019)
39. Ojo, A.S., Balogun, S.A., Williams, O.T., Ojo, O.S.: Pulmonary fibrosis in COVID-19 survivors: predictive factors and risk reduction strategies. *Pulm. Med* 2020
40. Fu, L., Wang, B., Yuan, T., Chen, X., Ao, Y., Fitzpatrick, T., Li, P., Zhou, Y., Lin, Y.F., Duan, Q., Luo, G.: Clinical characteristics of coronavirus disease 2019 (COVID-19) in China: a systematic review and meta-analysis. *J. Infect.*
41. Iftikhar, S., Fatima, K., Rehman, A., Almazyad, A.S., Saba, T.: An evolution based hybrid approach for heart diseases classification and associated risk factors identification. *Biomed. Res.* **28**(8), 3451–3455 (2017)
42. Meethongjan, K., Dzulkifli, M., Rehman, A., Altameem, A., Saba, T.: An intelligent fused approach for face recognition. *J. Intell. Syst.* **22**(2), 197–212 (2013). <https://doi.org/10.1515/jisy-2013-0010>
43. Lung, J.W.J., Salam, M.S.H., Rehman, A., Rahim, M.S.M., Saba, T.: Fuzzy phoneme classification using multi-speaker vocal tract length normalization. *IETE Tech. Rev.* **31**(2), 128–136 (2014). <https://doi.org/10.1080/02564602.2014.892669>
44. Minucci, S.B., Heise, R.L., Reynolds, A.M.: Review of mathematical modeling of the inflammatory response in lung infections and injuries. *Front. Appl. Math. Stat.* **6**, 36 (2020)
45. Khan, M.A., Sharif, M.I., Raza, M., Anjum, A., Saba, T., Shad, S.A.: Skin lesion segmentation and classification: a unified framework of deep neural network features fusion and selection. *Expert Syst.* e12497 (2019)
46. Zhang, G., Hu, C., Luo, L., Fang, F., Chen, Y., Li, J., Peng, Z., Pan, H.: Clinical features and short-term outcomes of 221 patients with COVID-19 in Wuhan, China. *J. Clin. Virol.* 104364 (2020)
47. Tian, S., Hu, W., Niu, L., Liu, H., Xu, H., Xiao, S.Y.: Pulmonary pathology of early phase 2019 novel coronavirus (COVID-19) pneumonia in two patients with lung cancer. *J. Thorac. Oncol.* (2020)
48. Müller, D., Rey, I.S., Kramer, F.: Automated chest CT image segmentation of COVID-19 Lung Infection based on 3D U-Net. *arXiv preprint arXiv:2007.04774* (2020)
49. Javed, R., Rahim, M.S.M., Saba, T., Rehman, A.: A comparative study of features selection for skin lesion detection from dermoscopic images. *Netw. Model. Anal. Health Inform. Bioinf.* **9**(1), 1–13 (2020)
50. Jamal, A., Hazim Alkawaz, M., Rehman, A., Saba, T.: Retinal imaging analysis based on vessel detection. *Microsc. Res. Tech.* **80**(7), 799–811 (2017)
51. Nazir, M., Khan, M.A., Saba, T., Rehman, A.: Brain tumor detection from MRI images using multi-level wavelets. In: 2019 International Conference on Computer and Information Sciences (ICCIS), pp. 1–5. IEEE (2019)
52. Saba, T., Bokhari, S.T.F., Sharif, M., Yasmin, M., Raza, M.: Fundus image classification methods for the detection of glaucoma: a review. *Microsc. Res. Tech.* (2018). <https://doi.org/10.1002/jemt.23094>
53. Ronneberger, O., Fischer, P., Brox, T.: U-net: convolutional networks for biomedical image segmentation. In: International Conference on Medical Image Computing and Computer-Assisted Intervention, pp. 234–241. Springer, Cham (2015)
54. Saba, T., Rehman, A., Sulong, G.: Improved statistical features for cursive character recognition” International Journal of Innovative Computing. Information and Control (IJICIC) **7**(9), 5211–5224 (2011)
55. Saba, T., Haseeb, K., Ahmed, I., Rehman, A.: Secure and energy-efficient framework using Internet of Medical Things for e-healthcare. *J. Infect. Public Health* **13**(10), 1567–1575 (2020)
56. Sadad, T., Munir, A., Saba, T., Hussain, A.: Fuzzy C-means and region growing based classification of tumor from mammograms using hybrid texture feature. *Journal of Computational Science* **29**, 34–45 (2018)

57. Ullah,H., Saba,T. Islam, N. Abbas, N. Rehman, A., Mehmood, Z. Anjum, A. (2019) An ensemble classification of exudates in color fundus images using an evolutionary algorithm based optimal features selection, Microscopy research and technique, 82(4), 361-372. doi.org/<https://doi.org/10.1002/jemt.23178>
58. Sharif, U., Mehmood, Z., Mahmood, T., Javid, M.A., et al.: Scene analysis and search using local features and support vector machine for effective content-based image retrieval. Artif. Intell. Rev. **52**(2), 901–925 (2019)
59. Bar, S., Lecourtois, A., Diouf, M., Goldberg, E., Bourbon, C., Arnaud, E., ... & Gosset, P. (2020). The association of lung ultrasound images with COVID-19 infection in an emergency room cohort. Anaesthesia.
60. Sajjad, M., Ramzan, F., Khan, M.U.G., Rehman, A., Kolivand, M., Fati, S.M., Bahaj, S.A.: Deep convolutional generative adversarial network for Alzheimer's disease classification using positron emission tomography (PET) and synthetic data augmentation. Microsc. Res. Tech. **84**(12), 3023–3034 (2021). <https://doi.org/10.1002/jemt.23861>
61. Youssef, A., Cavalera, M., Azzarone, C., Serra, C., Brunelli, E., Casadio, P., Pilu, G.: The use of lung ultrasound during the COVID-19 pandemic: A narrative review with specific focus on its role in pregnancy. J. Popul. Ther. Clin. Pharmacol. **27**(SP1), e64–e75 (2020)
62. Yousaf, K., Mehmood, Z., Saba, T., Rehman, A., Munshi, A.M., Alharbey, R., Rashid, M.: Mobile-health applications for the efficient delivery of health care facility to people with dementia (PWD) and support to their carers: A survey. Biomed. Res. Int. **2019**, 1–26 (2019)
63. Saba, T., Javed, R., Shafry, M., Rehman, A., Bahaj, S.A.: IoMT Enabled Melanoma Detection Using Improved Region Growing Lesion Boundary Extraction. CMC-Computers, Materials & Continua **71**(3), 6219–6237 (2022)
64. Trauer, M. M., Matthies, A., Mani, N., McDermott, C., & Jarman, R. (2020). The utility of lung ultrasound in COVID-19: A systematic scoping review. Ultrasound, 1742271X20950779.
65. Saleem, S., Usman, M., Saba, T., Abunadi, I., Rehman, A., et al.: Efficient Facial Recognition Authentication Using Edge and Density Variant Sketch Generator. CMC-Computers, Materials & Continua **70**(1), 505–521 (2022)
66. Shahzad, M.N., Ali, H., Saba, T., Rehman, A., Kolivand, H., Bahaj, S.A.: Identifying patients with PTSD utilizing resting-state fMRI data and neural network approach. IEEE Access **9**, 107941–107954 (2021)
67. Shan, F., Gao, Y., Wang, J., Shi, W., Shi, N., Han, M., ... & Shi, Y. (2020). Lung infection quantification of COVID-19 in CT images with deep learning. arXiv preprint [arXiv:2003.04655](https://arxiv.org/abs/2003.04655).
68. Sharif, M., Attique, M., Tahir, M.Z., Yasmin, M., Saba, T., Tanik, U.J.: A Machine Learning Method with Threshold Based Parallel Feature Fusion and Feature Selection for Automated Gait Recognition. Journal of Organizational and End User Computing (JOEUC) **32**(2), 67–92 (2020)
69. Sharif, M. Khan, M.A Akram, T. Javed, M.Y. Saba,T. Rehman, A (2017) A framework of human detection and action recognition based on uniform segmentation and combination of Euclidean distance and joint entropy-based features selection, EURASIP Journal on Image and Video Processing 2017 (1), 89, pp.1–18
70. Wan, Y., Shang, J., Graham, R., Baric, R. S., & Li, F. (2020). Receptor recognition by the novel coronavirus from Wuhan: an analysis based on decade-long structural studies of SARS coronavirus. Journal of virology, 94(7).
71. Sharif, M., Naz, F., Yasmin, M., Shahid, M.A., Rehman, A.: Face Recognition: A Survey. Journal of Engineering Science & Technology Review **10**(2), 166–177 (2017)
72. Soleimanizadeh, S., Mohamad, D., Saba, T., Rehman, A. (2015) Recognition of partially occluded objects based on the three different color spaces (RGB, YCbCr, HSV) 3D Research, Vol. 6 (3), 1–10, doi. <https://doi.org/10.1007/s13319-015-0052-9>.
73. Liu, J., Zheng, X., Tong, Q., Li, W., Wang, B., Sutter, K., ... & Yang, D. (2020). Overlapping and discrete aspects of the pathology and pathogenesis of the emerging human pathogenic coronaviruses SARS-CoV, MERS-CoV, and 2019-nCoV. Journal of medical virology, 92(5), 491–494.

74. Sulong, G., Rehman, A., Saba, T.: Improved offline connected script recognition based on hybrid strategy. *Int. J. Eng. Sci. Technol.* **2**(6), 1603–1611 (2010)
75. Tahir, B., Iqbal, S., Khan, M.U.G., Saba, T., Mehmood, Z., Anjum, A., Mahmood, T.: Feature enhancement framework for brain tumor segmentation and classification. *Microsc. Res. Tech.* **82**(6), 803–811 (2019)
76. Waheed, S.R., Alkawaz, M.H., Rehman, A., Almazyad, A.S., Saba, T.: Multifocus watermarking approach based on discrete cosine transform. *Microsc. Res. Tech.* **79**(5), 431–437 (2016)
77. Yaseen, S., Abbas, S. M. A., Anjum, A., Saba, T., Khan, A., Malik, S. U. R., ... & Bashir, A. K. (2018). Improved generalization for secure data publishing. *IEEE Access*, 6, 27156–27165.
78. Yousaf, K., Mehmood, Z., Awan, I. A., Saba, T., Alharbey, R., Qadah, T., & Alridge, M. A. (2019). A comprehensive study of mobile-health based assistive technology for the healthcare of dementia and Alzheimer's disease (AD). *Health Care Management Science*, 1–23.
79. Krizhevsky, A., Sutskever, I. and Hinton, G.E., 2012. Imagenet classification with deep convolutional neural networks. In *Advances in neural information processing systems* (pp. 1097–1105).
80. Sharif, M., Khan, S., Saba, T., Raza, M., & Rehman, A. (2019, April). Improved Video Stabilization using SIFT-Log Polar Technique for Unmanned Aerial Vehicles. In *2019 International Conference on Computer and Information Sciences (ICCIS)* (pp. 1–7). IEEE.
81. Szegedy, C., Liu, W., Jia, Y., Sermanet, P., Reed, S., Anguelov, D., Erhan, D., Vanhoucke, V. and Rabinovich, A., 2015. Going deeper with convolutions. In *Proceedings of the IEEE conference on computer vision and pattern recognition* (pp. 1–9).
82. Ausawalaithong, W., Thirach, A., Marukatat, S. and Wilairasitporn, T., 2018, November. Automatic lung cancer prediction from chest X-ray images using the deep learning approach. In *2018 11th Biomedical Engineering International Conference (BMEICON)* (pp. 1–5). IEEE.
83. <https://www.kaggle.com/tawsifurrahman/covid19-radiography-database>
84. Shuja, J., Alanazi, E., Alasmary, W. and Alashaikh, A., 2020. COVID-19 Datasets: A Survey and Future Challenges. *medRxiv*.
85. Born, J., Brändle, G., Cossio, M., Disdier, M., Goulet, J., Roulin, J. and Wiedemann, N., 2020. POCOVID-Net: automatic detection of COVID-19 from a new lung ultrasound imaging dataset (POCUS). *arXiv preprint arXiv:2004.12084*.
86. Gao, Z., Yada, S., Wakamiya, S. and Aramaki, E., 2020. Naist covid: Multilingual COVID-19 twitter and weibo dataset. *arXiv preprint arXiv:2004.08145*.
87. Qureshi,I. Khan,MA., Sharif, M., Saba, T., Ma, J. (2020) Detection of glaucoma based on cup-to-disc ratio using fundus images *International Journal of Intelligent Systems Technologies and Applications*, Vol.19(1), pp.1 - 16, <https://doi.org/10.1504/IJISTA.2020.105172>
88. Hu, Y., Huang, H., Chen, A. and Mao, X.L., 2020. Weibo-COV: A Large-Scale COVID-19 Social Media Dataset from Weibo. *arXiv*, pp. arXiv-2005.
89. Perveen, S., Shahbaz, M., Saba, T., Keshavjee, K., Rehman, A., Guergachi, A.: Handling irregularly sampled longitudinal data and prognostic modeling of diabetes using machine learning technique. *IEEE Access* **8**, 21875–21885 (2020)
90. Cui, L. and Lee, D., 2020. CoAID: COVID-19 Healthcare Misinformation Dataset. *arXiv preprint arXiv:2006.00885*.
91. Zarei, K., Farahbakhsh, R., Crespi, N. and Tyson, G., 2020. A first Instagram dataset on COVID-19. *arXiv preprint arXiv:2004.12226*.
92. Wei, J., Huang, C., Vosoughi, S. and Wei, J., 2020. What Are People Asking About COVID-19? A Question Classification Dataset. *arXiv preprint arXiv:2005.12522*.
93. Zhou, C., 2020. Evaluating new evidence in the early dynamics of the novel coronavirus COVID-19 outbreak in Wuhan, China with real time domestic traffic and potential asymptomatic transmissions. *medRxiv*.
94. Rahim, M.S.M., Rehman, A., Kurniawan, F., Saba, T.: Ear biometrics for human classification based on region features mining. *Biomed. Res.* **28**(10), 4660–4664 (2017)
95. Ramzan, F., Khan, M.U.G., Rehmat, A., Iqbal, S., Saba, T., Rehman, A., Mehmood, Z.: A Deep Learning Approach for Automated Diagnosis and Multi-Class Classification of Alzheimer's

- Disease Stages Using Resting-State fMRI and Residual Neural Networks. *J. Med. Syst.* **44**(2), 37 (2020)
- 96. Raza, M., Sharif, M., Yasmin, M., Khan, M.A., Saba, T., Fernandes, S.L.: Appearance based pedestrians' gender recognition by employing stacked auto encoders in deep learning. *Futur. Gener. Comput. Syst.* **88**, 28–39 (2018)
 - 97. Rehman, A.A., Saba, N., Mahmood, T., Kolivand, T., H.: Rouleaux red blood cells splitting in microscopic thin blood smear images via local maxima, circles drawing, and mapping with original RBCs. *Microscopic research and technique* **81**(7), 737–744 (2018). <https://doi.org/10.1002/jemt.23030>
 - 98. Rehman, A.: Light microscopic iris classification using ensemble multi-class support vector machine. *Microsc. Res. Tech.* **84**(5), 982–991 (2021)
 - 99. Rao, C.S.: Exploration and evaluation of efficient preprocessing and segmentation technique for breast cancer diagnosis based on mammograms. *International Journal of Research in Pharmaceutical Sciences* **10**(3), 2071–2081 (2019)
 - 100. Saba, T., Rehman, A., Mahmood, Z., Kolivand, H., Sharif, M.: Image enhancement and segmentation techniques for detection of knee joint diseases: A survey. *Current Medical Imaging* **14**(5), 704–715 (2018)
 - 101. Nasir, M., Khan, M.A., Sharif, M., Javed, M.Y., Saba, T., Ali, H., Tariq, J.: Melanoma detection and classification using computerized analysis of dermoscopic systems: a review. *Current Medical Imaging* **16**(7), 794–822 (2020)
 - 102. Naz, A., Javed, M.U., Javaid, N., Saba, T., Alhussein, M., Aurangzeb, K.: Short-term electric load and price forecasting using enhanced extreme learning machine optimization in smart grids. *Energies* **12**(5), 1–30 (2019)
 - 103. Nazir, M., Khan, M.A., Saba, T., & Rehman, A. (2019). Brain Tumor Detection from MRI images using Multi-level Wavelets. In 2019, IEEE International Conference on Computer and Information Sciences (ICCIS) (pp. 1–5).
 - 104. Nodehi, A., Sulong, G., Al-Rodhaan, M., Al-Dhelaan, A., Rehman, A. and Saba, T., (2014). Intelligent fuzzy approach for fast fractal image compression. *EURASIP Journal on Advances in Signal Processing*, 2014(1), p.1–9, doi. <https://doi.org/10.1186/1687-6180-2014-112>.
 - 105. Norouzi, A., Rahim, M.S.M., Altameem, A., Saba, T., Rad, A.E., Rehman, A., Uddin, M.: Medical image segmentation methods, algorithms, and applications. *IETE Tech. Rev.* **31**(3), 199–213 (2014)
 - 106. Mughal, B., Muhammad, N., Sharif, M., Rehman, A., Saba, T.: Removal of pectoral muscle based on topographic map and shape-shifting silhouette. *BMC Cancer* **18**(1), 778 (2018). <https://doi.org/10.1186/s12885-018-4638-5>
 - 107. Mughal, B. Muhammad, N. Sharif, M. Saba, T. Rehman, A. (2017) Extraction of breast border and removal of pectoral muscle in wavelet, domain Biomedical Research, vol.28(11), 5041–5043.
 - 108. Mughal, B. Sharif, M. Muhammad, N. Saba, T. (2018). “A novel classification scheme to decline the mortality rate among women due to breast tumor,” *Microscopy Research and Technique*, 81(2), 171–180, doi. <https://doi.org/10.1002/jemt.22961>.
 - 109. Wang, H., Wei, R., Rao, G., Zhu, J., & Song, B. (2020). Characteristic CT findings distinguishing 2019 novel coronavirus disease (COVID-19) from influenza pneumonia. *European Radiology*, 1.
 - 110. Saba, T., Rehman, A., Altameem, A., Uddin, M. (2014) Annotated comparisons of proposed preprocessing techniques for script recognition, *Neural Computing and Applications* Vol. 25(6), pp. 1337–1347, doi. <https://doi.org/10.1007/s00521-014-1618-9>
 - 111. Harouni, M., Rahim, M.S.M., Al-Rodhaan, M., Saba, T., Rehman, A., Al-Dhelaan, A.: Online Persian/Arabic script classification without contextual information. *The Imaging Science Journal* **62**(8), 437–448 (2014)
 - 112. Saba, T., Al-Zahrani, S., Rehman, A.: Expert system for offline clinical guidelines and treatment *Life Sci Journal* **9**(4), 2639–2658 (2012)
 - 113. Rodriguez-Morales, A. J., Cardona-Ospina, J. A., Gutiérrez-Ocampo, E., Villamizar-Peña, R., et al., (2020). Clinical, laboratory and imaging features of COVID-19: A systematic review and meta-analysis. *Travel medicine and infectious disease*, 101623.

114. Ebrahimi, M., Saki Malehi, A. and Rahim, F., 2020. COVID-19 Infection in Medical Staffs versus Patients: A Systematic Review and Meta-analysis of Laboratory Findings, Comorbidities, and Clinical Outcome. Fakher, COVID-19 Infection in Medical Staffs versus Patients: A Systematic Review and Meta-analysis of Laboratory Findings, Comorbidities, and Clinical Outcome (April 20, 2020).
115. Siordia Jr, J. A. (2020). Epidemiology and clinical features of COVID-19: A review of current literature. *Journal of Clinical Virology*, 104357.
116. Ahmad, A.M., Sulong, G., Rehman, A., Alkawaz, M.H., Saba, T.: Data hiding based on improved exploiting modification direction method and Huffman coding. *J. Intell. Syst.* **23**(4), 451–459 (2014)
117. Wang, D., Hu, B., Hu, C., Zhu, F., Liu, X., Zhang, J., ... & Zhao, Y. (2020). Clinical characteristics of 138 hospitalized patients with 2019 novel coronavirus–infected pneumonia in Wuhan, China. *Jama*, 323(11), 1061-1069.
118. Saba, T., Rehman, A., Al-Dhelaan, A., Al-Rodhaan, M.: Evaluation of current documents image denoising techniques: a comparative study. *Appl. Artif. Intell.* **28**(9), 879–887 (2014)
119. Huang, C., Wang, Y., Li, X., Ren, L., Zhao, J., Hu, Y., ... & Cheng, Z. (2020). Clinical features of patients infected with 2019 novel coronavirus in Wuhan, China. *The lancet*, 395(10223), 497-506.
120. Saba, T.: Automated lung nodule detection and classification based on multiple classifiers voting. *Microsc. Res. Tech.* **82**(9), 1601–1609 (2019)
121. Liu, T., Hu, J., Kang, M., Lin, L., Zhong, H., Xiao, J., He, G., Song, T., Huang, Q., Rong, Z. and Deng, A., 2020. Transmission dynamics of 2019 novel coronavirus (2019-nCoV).
122. He, K., Zhang, X., Ren, S. and Sun, J., 2016. Deep residual learning for image recognition. In Proceedings of the IEEE conference on computer vision and pattern recognition (pp. 770–778).